PETROLEUM GEOCHEMISTRY, SOURCE ROCK EVALUATION AND MODELLING OF HYDROCARBON GENERATION IN THE SOUTHERN TAROOM TROUGH

WITH PARTICULAR REFERENCE TO THE TRIASSIC SNAKE CREEK MUDSTONE

KHALED R. AL-AROURI
B.Sc. (Geology and Environmental Sciences)
M.Sc. (Geology and Organic Geochemistry)

Thesis submitted for the degree of
DOCTOR OF PHILOSOPHY
in
The Department of Geology and Geophysics
and
The National Centre for Petroleum Geology and Geophysics

AUGUST 1996

The University of Adelaide

STATEMENT OF ORIGINALITY

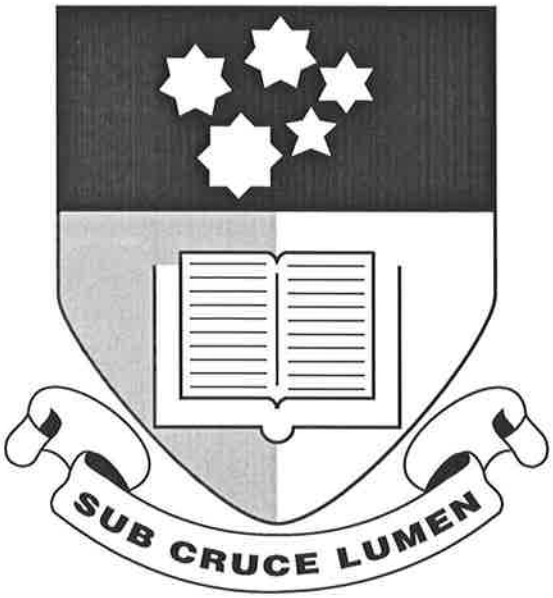

To the best of my knowledge and belief, and except where reference is made herein, this thesis contains no material previously published or written by another person, nor any material that has been accepted for the award of any other degree or diploma in any university. I give consent to my thesis, when deposited in the University Library, being available for photocopying and loan.

Khaled Al Arouri

August 1996

DEDICATE

To my parents,
my wife Lama and my beloved sons Laith and Yazan

ABSTRACT

Whether or not Triassic source rocks have contributed to the known petroleum reserves of the Bowen and Surat Basins is still unknown. In order to assess the relative contributions of Triassic and Permian hydrocarbons, a comprehensive geochemical study was made of oils and potential source rocks from the southern Taroom Trough. The study employed total organic carbon, Rock-Eval pyrolysis, organic petrography, extractable bitumen, biomarker and isotopic analyses, the latter including compound-specific isotope analysis (CSIA) of individual *n*-alkanes in extracts, pyrolysates and oils. Petroleum generation was also modelled, using first-order reaction kinetics and the BasinMod program, in order to predict the timing and amount of hydrocarbon generation and to explain the observed distribution of oil *versus* gas in the petroleum systems of the Bowen and Surat Basins.

In the Taroom Trough, the major potential source rocks are marine mudstones in the lower part of the Permian section (Back Creek Group, BCG), and coals and carbonaceous shales in its upper part (Blackwater Group, BWG). Both Permian marine and nonmarine lithofacies are organic-rich and have attained sufficient maturity for oil and gas generation. However, using molecular and isotopic data, the major source of petroleum was shown to be the BWG. A previously unrecognised subsidiary source was identified - the Triassic Snake Creek Mudstone (SCM) - and this lacustrine unit became the focus of further detailed investigation. Two SCM lacustrine environments are distinguished by their diagnostic molecular fingerprints. An oxygenated freshwater setting was widely distributed across the southern Taroom Trough, whereas a brackish suboxic environment developed locally in different parts of the basin. Evidence of a marine influence on the Snake Creek palaeolake is confined to the northwest and southeast margins of the southern Taroom Trough.

Artificial and natural maturation of the Taroom Trough source rocks reveals that biomarker maturity parameters can be affected by variations in kerogen type as well as mineralogy. Whereas rearranged drimanes are a characteristic feature of argillaceous petroleum source rocks, abundant homodrimanes and methylhomodrimanes are a diagnostic peculiarity of calcareous mudstones deposited under less oxic, and probably more saline, conditions. A comparison of the relative abundance of 16α(H)- and 16β(H)-phyllocladane with other maturity data revealed a 'reversal' in the trend of increasing β/(α+β) values at maturities higher than those corresponding to the onset of oil generation. The present study sheds light on the previously undocumented behaviour of the phyllocladanes during the late stage of catagenesis. The proportion of 16β(H)-phyllocladane β/(α+β) increases quickly with increasing maturation to a maximum value of ~0.88 at about the oil generation threshold, and then declines steadily from 0.88 to 0.65 through the oil window, eventually attaining equilibrium at 0.6 within the zone of dry gas generation.

The Permo-Triassic sequence in the southern Taroom Trough attained its maximum palaeotemperatures during the Late Cretaceous as a result of deep burial (in the south), or a combination of Cretaceous (± Triassic) burial and a thermal episode (in the north). This differential uplift and erosion has resulted in different effective periods of maturation and thus different prospectivities along the basin. The SCM in the south entered the oil window in the latest Early Cretaceous, whereas the underlying Permian section started generating hydrocarbons during the Jurassic. These hydrocarbons migrated updip to the east and west where structural-stratigraphic traps had formed in response to Triassic compressional deformation. Kinetic modelling proved that the oil and gas currently produced from sandstone reservoirs were sourced mainly from the BWG, with a lesser contribution from the BCG. Although the contribution of hydrocarbons from the SCM source rock was minor, it was sufficient to form a second petroleum system. In the north of the study area, early (Triassic) generation of hydrocarbons and subsequent (Jurassic-Cretaceous) burial left an overmature Permian section, at present able to generate only dry gas. The bulk of its hydrocarbons have, most likely, migrated to the south and west where oil and gas currently are being produced. High prospectivity is indicated for the southern region where generation and migration of hydrocarbons (Jurassic-Cretaceous) post-dated trap formation (Triassic), whereas in the north the bulk of generated hydrocarbons were expelled before the main deformation. Therefore, the considerable volumes of hydrocarbons generated in the north must have been lost as no traps or seals were in place.

Two petroleum systems can be identified in the southern Taroom Trough. The Triassic 'SCM-Showgrounds' petroleum system involves Triassic source and reservoir rocks in a very localised area of the southwestern part of the trough. It encompasses Family 1 oils produced from the Roswin North, Rednook and Merroombile petroleum pools (reservoired in the Showgrounds Sandstone), and the SCM source rock in the vicinity of Inglestone-1 and the adjacent deeper parts of the trough where the unit has its highest hydrocarbon-generating potential and shows microscopic evidence of active hydrocarbon generation. Hydrous pyrolysis of SCM kerogens and CSIA of the SCM extracts and kerogen pyrolysates suggest that its expelled oils are derived primarily from free lipids, with a minor contribution by hydrocarbons released catagenetically from the kerogen. The Blackwater-Precipice petroleum system (Permian-sourced), on the other hand, is of wider areal and stratigraphic extent. It includes the source rocks of the Back Creek and Blackwater Groups, which are mature to overmature throughout much of the Taroom Trough, and all related Family 2 hydrocarbons produced from reservoirs of Permian to Jurassic age along the southeastern and southwestern margins of the trough.

ACKNOWLEDGEMENTS

This research project was carried out with the assistance of an Overseas Postgraduate Research Scholarship, complemented by a University of Adelaide Postgraduate Research Scholarship. This financial support enabled me to undertake my doctorate studies in Australia and is highly appreciated.

I am extremely grateful to my mentor, Associate Professor David M. McKirdy, for his keen supervision and constant support and guidance throughout my research. His critical reading and corrections of the manuscript often left him 'burning the midnight oil'.

I would like to extend my deep appreciation and gratitude to Dr. Chris J. Boreham (Australian Geological Survey Organisation, Canberra) for his supervision, fruitful discussions and careful review of my thesis. His hospitality, encouragement and support with experimental work assisted in the completion of this project. I am also very thankful to Dr. Roger Summons and Dr. Chris Boreham for their co-operation in making available their organic geochemistry facilities. I consider myself very fortunate that I have had the opportunity to work alongside these distinguished scientists. Technical assistance was cheerfully provided by the AGSO's staff Zarko Roksandic, Janet Hope and Zoltan Horvath. Andrew Murray is also thanked for help with the GCMS analysis on selected aromatic fractions.

I gratefully appreciate the help provided by the staff of the Department of Geology and Geophysics and the National Centre for Petroleum Geology and Geophysics. Some people, however, deserve a special mention. Dr. Nick Lemon is thanked for reviewing the manuscript and funding the kinetic analysis performed at Geotech, Perth. Special thanks also go to Dr. Peter Tingate for many stimulating discussions about the thermal history of the Bowen/Surat Basins, for his help with BasinMod computing and for critically reviewing parts of this thesis. Further, I would like to express my thanks to Dr. Keith Turnbull for help with the carbon isotope analysis, Ms Sherry Proferes for help with computer drafting and Sophia Craddock for friendly secretarial assistance. A close friendship with my Jordanian crony Ghazi Kraishan, and my Tanzanian chum Meshack Kagya provided much encouragement.

I also extend my acknowledgement to Peter Green and David Carmichael of the Geological Survey of Queensland for source rock samples and fruitful discussions and

suggestions. Crude oil samples were supplied by Bridge Petroleum Ltd., Command Petroleum Holdings N.L. and Oil Company of Australia N.L.

Sincere thanks are due to my friend and former supervisor Associate Professor Lloyd Hamilton (Queensland University of Technology, Brisbane) who, through his encouragement and enthusiasm, made my first days in Australia 'easy going'. He is very much thanked for his concern for my well-being.

Finally, I would like to express my sincere appreciation to my family for their support and kind wishes, my kids Laith and Yazan for tolerating the absence of their dad and especially to Lama, my wonderful wife, for her encouragement, help, patience and understanding.

TABLE OF CONTENTS

LIST OF FIGURES

LIST OF TABLES

PLATES.....

CHAPTER ONE

INTRODUCTION

1.1 Rationale, aims and scope of the thesis

The first commercial discovery of hydrocarbon resources in Australia was at Roma in the Surat Basin (Elliott and Brown, 1989). The Surat and Bowen Basins are two of Australia's more prospective petroleum basins and both are important producers of oil and gas. The Bowen Basin also supplies most of Queensland's export coal which is largely used in electricity generation. Natural gas from the Surat Basin is piped to Brisbane and other regional centres. Thus, much of Queensland's local and exported energy supplies come from these two basins.

Currently, much interest is being shown in these basins by the federal Government and companies who are exploring for petroleum and gas. As part of the National Geoscience Mapping Accord, a project entitled "Sedimentary Basins of Eastern Australia (SBEA)" is being conducted jointly by the Australian Geological Survey Organisation (AGSO, formerly BMR), the Department of Resource Industries of the Geological Survey of Queensland (GSQ) and the New South Wales Department of Mineral Resources (Geological Survey and Coal Geology branches), with co-operation from CSIRO, universities and industry. The Bowen and Surat Basins (Fig. 1.1) are logical candidates for inclusion in this project.

The research presented in this thesis forms part of the SBEA program aimed at assessing the hydrocarbon generation potential of the Surat and Bowen Basins. The first phase of the program involved delineation of regional maturation trends using vitrinite reflectance data and assessment of source-rock potential by Rock-Eval pyrolysis. Isoreflectance maps for selected stratigraphic horizons are being produced using reflectance data already stored in the Queensland Petroleum Exploration Database (QPED).

The major source rock units in the Taroom Trough and their contributions to the oils reservoired in the Bowen and Surat Basins have been identified by AGSO and GSQ researchers, and a considerable part of this work has been recently published (Hawkins et al., 1992; Boreham, 1995; Carmichael and Boreham, 1996). In the latter paper, the Triassic Moolayember Formation is considered a potential source rock for petroleum. However, the lacustrine Snake Creek Mudstone (SCM), a member of the Middle Triassic Moolayember Formation, is better known as a laterally-continuous seal which

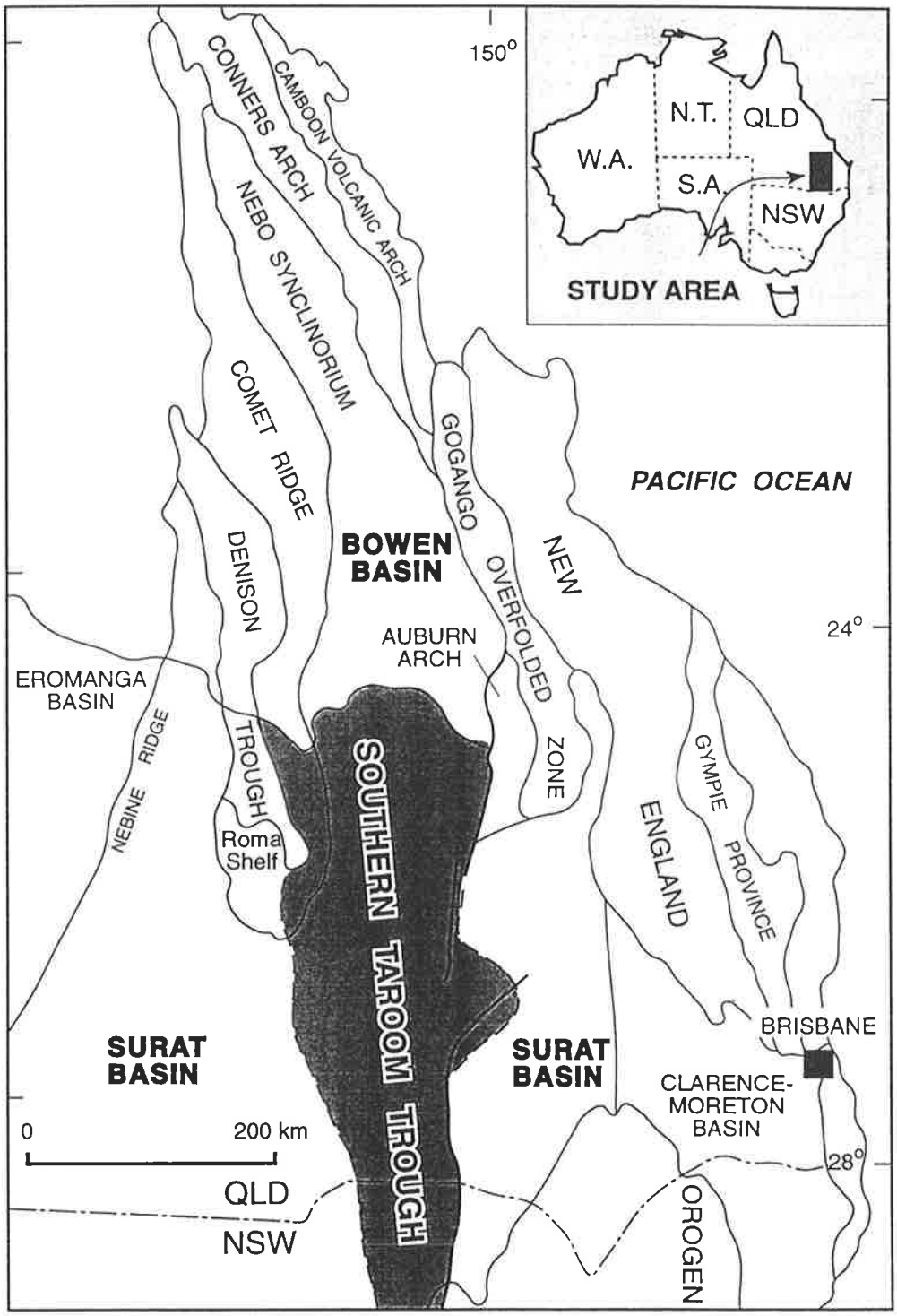

Figure 1.1 Location of the southern Taroom Trough (shaded) within the Bowen and Surat Basins.

effectively forms a barrier to vertical migration from established Permian source rocks. Hydrocarbon accumulations in the overlying Triassic and Jurassic formations suggest the existence of a source (or sources) other than Permian, as long lateral and vertical migration paths have traditionally been considered unlikely. The SCM is the most mature of the possible alternative sources. Where juxtaposed with carrier and reservoir rocks, the SCM might have contributed to the oil found in the underlying Showgrounds Sandstone.

The present research project has two main aims, firstly to better assess the contribution from Triassic source rocks in the southern Taroom Trough to the oil reserves of the Bowen/Surat Basin; and, secondly, to reconstruct the thermal history of the trough in order to establish the timing and amount of hydrocarbons generated from its Permo-Triassic organic facies. By relating generation to the timing of structural development, migration pathways can be delineated and the observed distribution of oil and gas in the region explained.

To achieve the first objective, an extensive investigation of the Snake Creek Mudstone was undertaken, based on organic petrography, total organic carbon, Rock-Eval pyrolysis, extract and biomarker analyses of representative samples from 40 exploration wells (Fig. 1.2). Sealed-tube hydrous pyrolysis was also carried out on kerogens representative of the end-member SCM facies and the resulting pyrolysates were compared with the extracts in terms of their biomarker and isotopic compositions. Eleven oils and one condensate were sampled and analysed chemically and isotopically for the purpose of oil-source correlation. The latter exercise included use of state of the art 'compound-specific isotope analysis' of individual *n*-alkanes in the SCM extracts and pyrolysates. Finally, for the sake of completeness, the major source units of the Permian section were also sampled in four deep exploration wells.

The second objective, that of modelling petroleum generation in the southern Taroom Trough, was addressed using the BasinMod® computer program. Input data were acquired from current knowledge of the trough's stratigraphic and tectonic evolution and new source rock kinetic analyses of selected Triassic and Permian organic facies.

The overall aim of this study was to help explain the observed distribution of oil and gas throughout the Taroom Trough, with a view to delineating those areas most prospective for further discoveries.

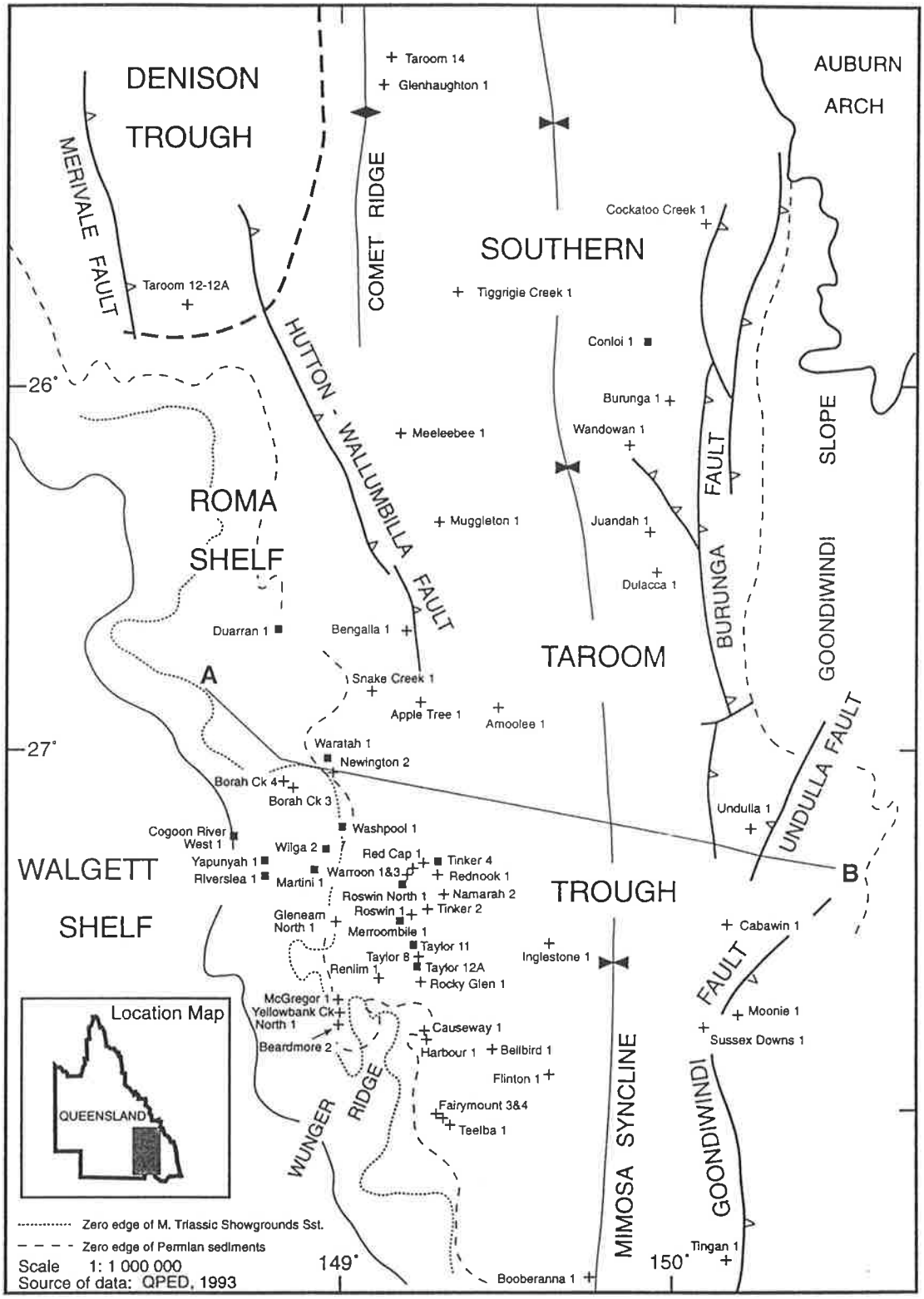

Figure 1.2 The wells sampled for source rock (+) and oil (▪) in the southern Taroom Trough of the Bowen and Surat Basins.

1.2 Location and geological setting of the Taroom Trough

The Taroom Trough is an asymmetric, near-meridional, depocentre which forms the eastern part of the Bowen Basin (Fig. 1.1) where the thickest (up to 9 km) Permo-Triassic section is preserved. The Permo-Triassic sequence comprises shallow marine and terrestrial sediments, including thick deposits of black coal. Another depocentre, the Denison Trough, lies to the west beyond the Comet Ridge (Fig. 1.1). The southern portions of the Denison Trough and the Taroom Trough are unconformably overlain by the Jurassic-Cretaceous succession of the Surat Basin. The southern Taroom Trough covers an area of ca. 50 000 km^2 between latitudes 25°S and 29°S.

The western margin of the southern Taroom Trough is identified by wedging out of the Permo-Triassic section over the Walgett Shelf and Roma Shelf, whereas an extremely complex fault zone (Burunga-Leichhardt-Moonie-Goondiwindi Fault System) defines the eastern boundary (Fig. 1.2). This fault system has been variously interpreted as a major normal fault with downthrow to the west (Power and Devine, 1970); a thrust or high-angle reverse fault (Exon, 1976); extensional and listric faults (Wake-Dyster et al., 1987); and faults created by duplexing and backthrusting (Korsch et al., 1990; Totterdell et al., 1992). Both the Permian succession [Back Creek Group (BCG); Gyranda Formation; and Blackwater Group (BWG)] and the Triassic sequence (Rewan Group; Clematis Group; and Moolayember Formation, including its SCM member) (Fig. 1.3) thicken eastwards off the Comet Ridge (Totterdell et al., 1992) and attain their maximum thicknesses in the central part of the southern Taroom Trough along its N-S axis (Fig. 1.2). The thickest Surat Basin succession is preserved along the Mimosa Syncline (a Late Triassic structural element that parallels the underlying N-S axis of the Taroom Trough: Fig. 1.2) where it comprises more than 2.7 km of fluvio-lacustrine to shallow marine sediments. Late Jurassic and mid-Tertiary movements caused broad tilting to the south and west (Exon, 1974), leading to the preserved Surat Basin succession increasing in thickness southward in the direction of the Mimosa Syncline (Totterdell et al., 1992).

A major angular unconformity (dipping up to 30° to the west) is recognised between the Surat Basin sequence and the underlying Bowen Basin succession (Elliott, 1993) (Fig. 1.4). This unconformity might have resulted from a depositional hiatus or differential uplift and erosion. Late Triassic erosion appears to have been minimal along the trough axis and most extensive in the vicinity of the Auburn Arch where the whole Triassic section is removed. A recent seismic survey conducted by the Australian Geological Survey Organisation (Totterdell et al., 1992) produced evidence for erosional loss of up to 4.4 km of the Bowen Basin succession in the Taroom region (near the Burunga-1 well: Fig. 1.2). In the Cockatoo Creek-1 area, the remnant Triassic section is

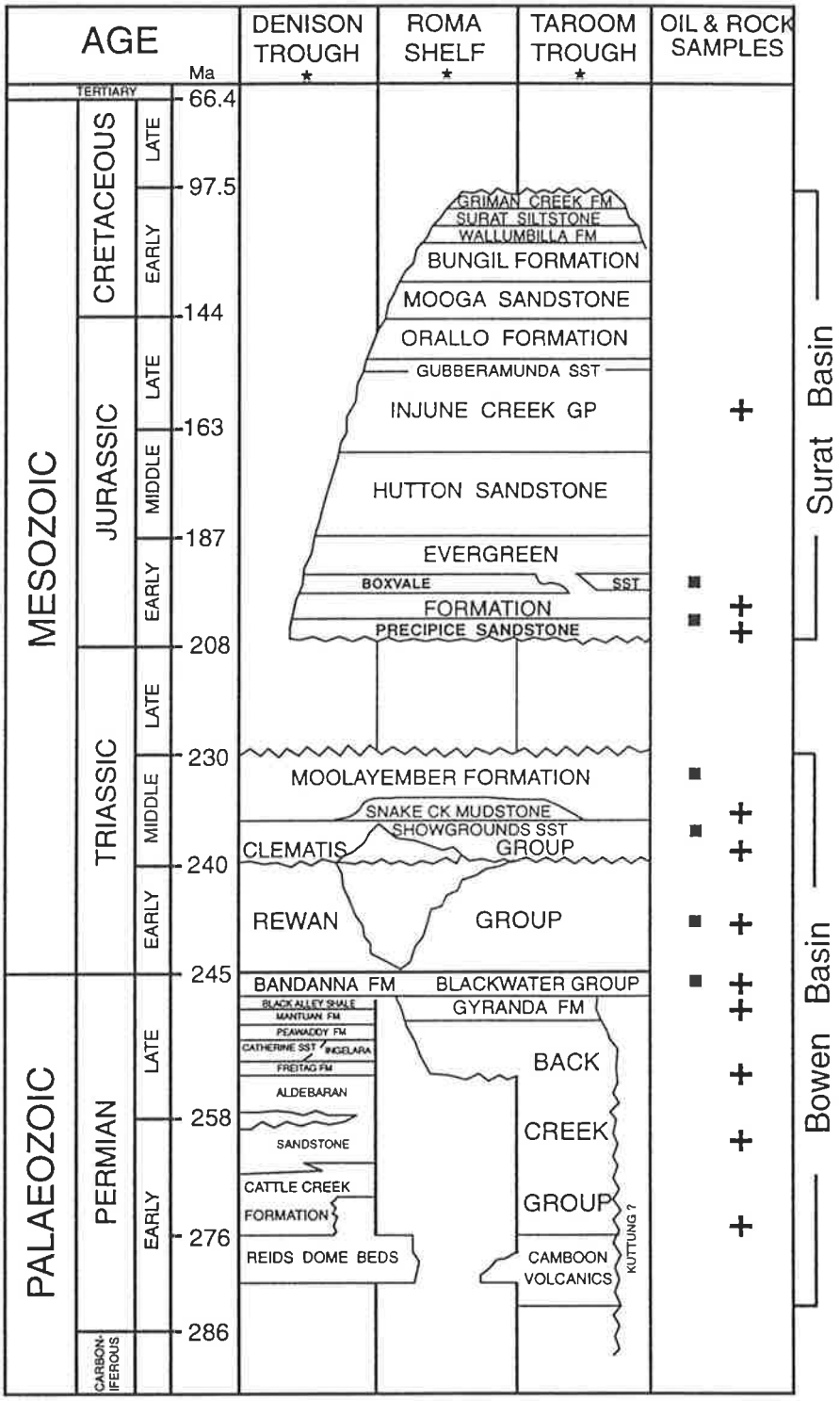

* Stratigraphy adapted from Elliott (1993)

Figure 1.3 Stratigraphic table showing the formations in the southern Taroom Trough sampled for source rocks (+) and the reservoirs sampled for oil (▪).

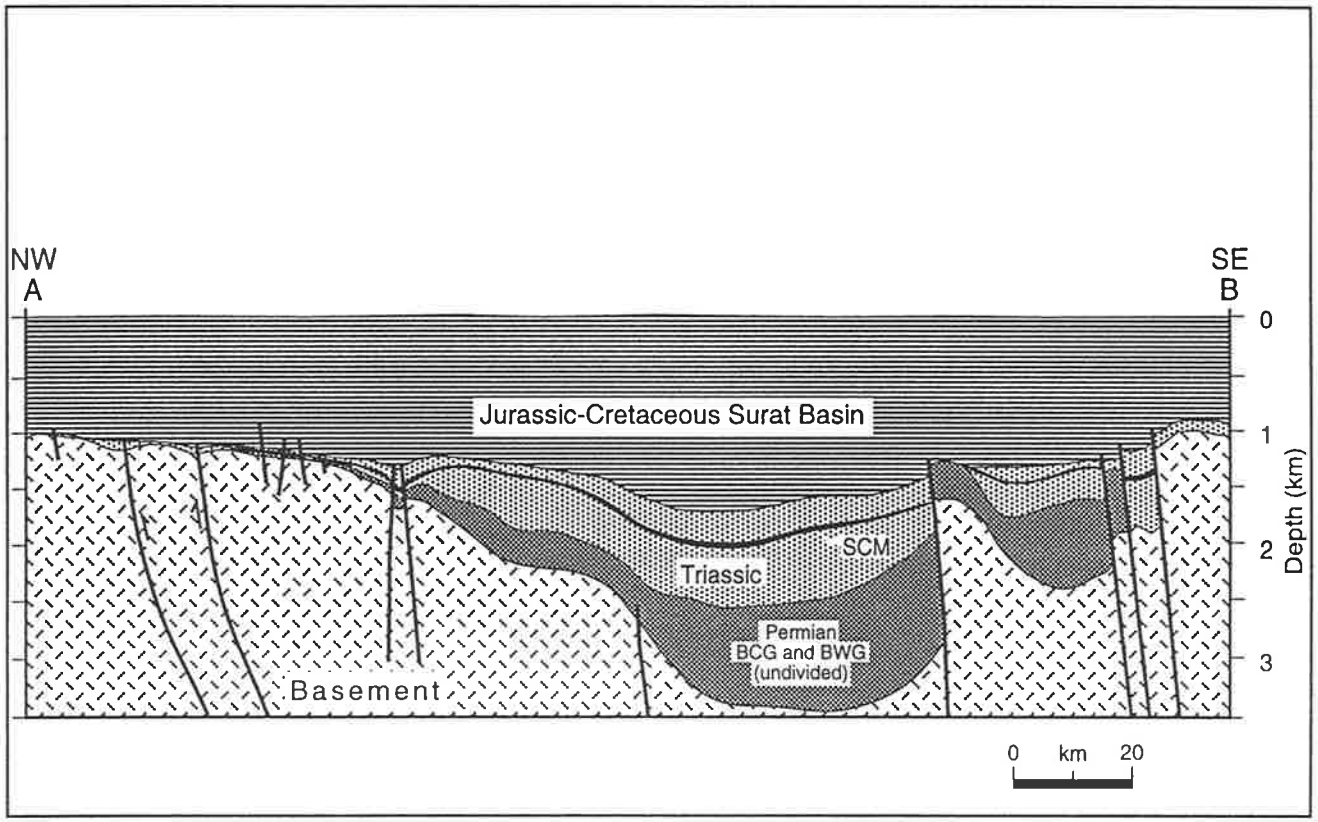

Figure 1.4 NW-SE cross section of the central area of the southern Taroom Trough (redrawn from seismic section after Elliott and Brown, 1989), showing the main petroleum source rock formations (Permian Back Creek 'BCG' and Blackwater 'BWG' Groups, and Triassic Snake Creek Mudstone 'SCM'). See Figure 1.2 for location of cross section.

approximately 470 m thick and composed entirely of the Rewan Group which is directly overlain by the Precipice Sandstone.

1.3 Basin development

The dating of certain tectonic events in the Taroom Trough is still controversial. A synopsis of the models proposed for the evolution of the Bowen and Surat Basins is presented below.

In the latest Carboniferous or Early Permian (Artinskian), volcanism was active and the Bowen Basin was initiated during back-arc crustal (intracratonic) extension and thinning associated with subduction along the continental margin (Camboon Volcanic Arch) (Hammond, 1987; Mallett et al., 1988; Middleton and Hunt, 1989; Murray, 1990). This rift phase produced an extensional trough in the west (Denison Trough), whereas to the east, a foreland basin (Taroom Trough) was formed in response to a compressive force accompanying the subduction. Elliott (1993) emphasizes that the Taroom Trough was unlikely to have been initiated as a deep rift.

Cooling and thermal relaxation of the lithosphere followed the extensional phase. Slow initial subsidence spanned the late Early and early Late Permian, continuing for 10 m.y. (280-270 Ma) in the east (e.g., Cockatoo Creek-1, Burunga-1), and for 20 m.y. in the west (e.g., Glenhaughton-1, Tiggrigie Creek-1). However, Murray (1985) and Fielding et al. (1990) suggested that the initial subsidence was due to loading of the crust by volcanic and plutonic rocks of the adjacent Camboon Volcanic Arch. After this slow subsidence, a phase of rapid subsidence started at about 270-260 Ma and continued until the Middle Triassic, resulting in the deposition of 7 km of sediment in the central Taroom Trough (Totterdell et al., 1992). The BCG attained a thickness of up to 3 km, comprising shallow marine to paralic carbonates and clastic-volcaniclastic sediments (Fielding et al., 1990). Along the southeastern Taroom Trough, these sediments and volcanics are intermixed and undifferentiated. A late Permian marine transgression led to deposition of the Gyranda Formation. The bulk of the BWG was deposited during a regression when sediments, shed from the orogen, accumulated in alluvial plain, deltaic and paralic environments, forming extensive coal measures (Totterdell et al., 1992). Over 4 km of Permian section accumulated in the north near Taroom (Thomas et al., 1982).

Compression and, hence, westward thrusting and inversion east of the Bowen Basin caused rapid subsidence in front of the thrust sheets, particularly over the eastern Bowen Basin, with subsidence diminishing to the west. This deformation was initiated during the late Early - early Late Permian and culminated in the Middle Triassic during

deposition of the Moolayember Formation. In the latest Early Triassic, after deposition of the Rewan Group (fine-grained terrestrial red beds), compression caused thrust faulting along the eastern margin of the trough (Elliott, 1993). This faulting cuts the Permian section and Rewan Group but not the overlying Middle Triassic Clematis Group. About 300 m of the Rewan Group were eroded on the upthrown side of the fault. Thrusting along the Burunga-Leichhardt Fault continued in the Middle Triassic, while fluvial, lacustrine and deltaic sediments of the Showgrounds Sandstone, Snake Creek Mudstone, and Moolayember Formation were deposited. By the end of the Middle Triassic, an asymmetric basin with about 9 km fill (of which up to 5 km is Triassic) had formed in the northern Taroom Trough.

Uplift, attributed by Harrington and Korsch (1985) to accretion of the Gympie Province along the eastern margin of the Australian continent, led to cessation of sediment accumulation in the Bowen Basin after the deposition of the Moolayember Formation. This compressional event occurred during the Late Triassic. The unconformity between the Bowen and Surat Basins represents an erosional episode which lasted for approximately 40 m.y. (Totterdell et al., 1992). The amount of erosion is variable but estimated to be in excess of 4 km of section along the eastern margin.

During the Jurassic and Early Cretaceous, renewed subsidence was driven by thermal relaxation (due to cooling of the lithosphere) and led to the accumulation of the Surat Basin sequence (Fig. 1.3) (Elliott, 1993). Sedimentation started in the Early Jurassic with deposition of the fluvial Precipice Sandstone across the peneplaned Bowen Basin. The next unit, the Evergreen Formation, was deposited in fluvial and fluvio-lacustrine environments (subject to episodic marine incursions). It was overlain by the fluvial Hutton Sandstone. Coal swamps developed in the Middle Jurassic and resulted in the Walloon Coal Measures (within the Injune Creek Group). A widespread marine transgression in the Early Cretaceous led to deposition of Bungil Formation, Wallumbilla Formation, Surat Siltstone and Griman Creek Formation (Elliott, 1993). By the time deposition ceased in the Late Albian or Early Cenomanian, up to 2.7 km of marine and continental sediments had accumulated in the central Surat Basin (Thomas et al., 1982).

Erosion caused by regional uplift and southward tilting of the area in the Mid- to Late Cretaceous shifted the northern preservational edge of the Surat Basin to the south. Moreover, Elliott (1993) attributed the erosional loss of 2 - 3 km of Triassic and Permian section to the emplacement of a thrust sheet along the Gogango Overfolded Zone (Fig. 1.1). In the Mid-Tertiary, tilting to the southwest resumed and was accompanied by widespread volcanic eruption in the north and east of the Surat Basin (Thomas et al., 1982). Structural control of Surat Basin deposition was mainly the result

of reactivation of Permo-Triassic faults (Elliott, 1993). Strike-slip movement on some of these faults is also evident (Cosgrove and Mogg, 1985). Erosion started again in the Late Tertiary and continued to the present, particularly in the northeastern part of the basin (Thomas et al., 1982).

1.4 Previous studies of hydrocarbon genesis in the Bowen/Surat Basin

1.4.1 Source rock and petroleum geochemistry

Over one hundred oil and gas discoveries have been made in the Bowen and Surat Basins, most of them located along the eastern and western margins of the southern Taroom Trough (Elliott and Brown, 1989; Hawkins et al., 1992). The origin of these petroleum occurrences has been of interest to local explorers for more than 30 years, and is still being debated. Some scientists favour a marine source, others a non-marine shale or coal source. Some consider the likely source beds to be of Permian age, whereas others favour source rocks of Triassic or Jurassic age. Many of the later studies agree that the principal source is coal or carbonaceous shale containing a mixture of land plant, algal and bacterial remains that were deposited in a predominantly oxic environment. Organic-rich source rocks which fulfill these criteria occur throughout the entire Permian to Jurassic succession, with Type III kerogen being the most common variety of organic matter (Hawkins et al., 1992; Boreham, 1995). Indeed, there may be more than one source rock in the sequence. Some of the oils display evidence of alteration by water washing and biodegradation (McKirdy, 1984; Boreham, 1995). Thus, it is important to find out how many oil families exist and how many 'effective', as distinct from 'potential', source rocks there are.

Thomas et al. (1982) concluded that the Permian section is the major, and probably only, source for the oils discovered in the region. These Permian rocks are known to contain abundant Type III kerogen, although appreciable amounts of Type II kerogen occur in the latest Permian BWG (Hawkins et al., 1992). To the west, in the Denison Trough, hydrocarbon discoveries are exclusively gas (an exception is the small Merivale oil field). Here, the Early Permian Reids Dome Beds and the Cattle Creek Formation, which contain abundant Type III kerogen, are considered the most favourable source rocks (Jackson et al., 1980; Draper and Beeston, 1985). However, detailed examination of organic matter revealed abundant liptinite throughout the Permian succession (Beeston, 1987), suggesting good potential for yet undiscovered liquid petroleum, particularly in the southern part of the Denison Trough. These sediments range from marginally mature/mature in the south and southeast to overmature in the north (Jackson et al., 1980).

Organic-rich Triassic and Jurassic sediments are precluded from being effective sources because of their immaturity throughout much of the Taroom Trough (Thomas et al., 1982), although they commonly contain enough liptinite to be oil-prone. If and where these rocks attain sufficient maturity in the deeper parts of the trough, they would be effective contributors of hydrocarbons (Thomas et al., 1982; Philp and Gilbert, 1986). Elliott (1989) considers the Evergreen Formation to be the source of Jurassic-reservoired hydrocarbons. In his comprehensive geochemical study of 31 oils and condensates from the Bowen and Surat Basins, McKirdy (1984) recognised four discrete oil families which he tentatively ascribed to four different sources, the Permian BCG and BWG, the Middle Triassic Moolayember Formation and the Early Jurassic Evergreen Formation. Oil from Moonie, the largest field on the eastern side of the Taroom Trough, has been variously attributed to nonmarine Jurassic shales (Moran and Gussow, 1963; de Jersey and Allen, 1966) and to the marine intervals of the BCG (Traves, 1965). Later work (Philp et al., 1982) supported a nonmarine origin for the Moonie crude, which exhibits very similar characteristics to the oil from Alton, but showed the Conloi oil to have a different source. Out of the 12 oils analysed by Philp and Gilbert (1986), only oil (Cabawin) was thought to have its source in the marine BCG. However, when analysed by Boreham (1995), the Cabawin oil displayed no evidence of any marine input. Boreham's biomarker and isotopic study of petroleum in the Surat and Bowen Basins found that most of it was of Permian nonmarine origin, with minor contributions to certain fields from the marine-influenced BCG section. Finally, based on its light carbon isotopic composition, the Rednook oil appears to have a Triassic source affinity (Boreham, 1995).

The Middle Triassic lacustrine SCM is the next most mature alternative source rock (Fig. 1.3). This unit is better known as a laterally continuous seal which effectively forms a barrier to vertical migration from the underlying Permian source rocks (Golin and Smyth, 1986). The hydrocarbon-generating potential of this potential source rock has not yet been adequately evaluated. Petrographic analysis of 38 SCM samples from ATP 145P, which forms the southwestern part of the study area, revealed that the mudstone contains dispersed organic matter (DOM) with a liptinite content high enough to be oil-prone (average 30% liptinite, 20% vitrinite and 50% inertinite: Golin and Smyth, 1986; Smyth, 1988; Smyth and Mastalerz, 1991). The SCM has its highest source potential in the vicinity of Roswin-1, where DOM constitutes about 4-5 vol.%, of which 1-2 vol.% is reworked coal.

1.4.2 Thermal maturity modelling of the Bowen Basin

The cause(s) of coalification in the Bowen Basin are clouded by controversy. Isoreflectance maps drawn by Thomas et al. (1982) and Beeston (1986) show that the Permian section is within the oil window ($0.7\% < R_O < 1.3\%$) over much of the Taroom Trough, with thermal maturity increasing from the western and eastern margins of the trough towards its axis. A steady northerly increase in reflectance is also evident such that the whole Permian section is overmature ($R_O > 1.3\%$: Thomas et al., 1982) over the major part of the northern Taroom Trough. Beeston (1986) noticed a general parallelism between the depth contours and isoreflectance trends across most of the southern Taroom Trough, which strongly suggests that variations in thermal maturity are controlled solely by burial. Higher vitrinite reflectance values in the Permian and Triassic sections in the northern part of the Taroom Trough are coincident with the plunge of the trough in that direction. However, the northwestern edge of the southern Taroom Trough (which has no, or only very thin, Jurassic overburden) exhibits relatively high reflectance values at or near the surface ($\geq 0.5\%$ R_O) thereby providing evidence of considerable uplift after initial subsidence. Triassic formations in the Taroom Trough have similar isopach patterns, with local modification caused by uplift and erosion on the eastern side of the basin (Totterdell et al., 1992). Hence, maximum reflectance values may be expected along the axial region of the trough.

Shiboaka and Bennett (1976) suggested that coalification in the northern and central parts of the basin (~ between 20° and 24°S) is a function of depth of burial, with a critical erosional event (resulting in the removal of up to 3 km of cover) during the Triassic. Beeston (1981, 1986) supported this view and further suggested that a higher Permo-Triassic heat flow was an important element. Middleton (1982, 1983) and Middleton and Hunt (1989) argued that the major cause for the observed rank is depth of burial prior to Triassic uplift and erosion. Local areas of high rank were attributed to igneous intrusives in the northernmost part of the basin (Conners Arch and Nebo Synclinorium) or overthrusting along the eastern margin of the basin, closer to the Gogango Overfolded Zone (Fig. 1.1). Totterdell et al. (1992) suggested that in excess of 4 km of sediments may have been eroded in the vicinity of Cockatoo Creek-1, based on the nearest non-eroded section immediately to the west. Faraj et al. (1996) found that illitization in the Upper Permian Baralaba/Rangal Coal Measures in the northern Bowen Basin took place during the Triassic (244-212 Ma). This observation, supported by K/Ar radiogenic isotope dating, suggests that Triassic burial was a critical event in the thermal history of this exposed part of the Taroom Trough (Faraj et al., 1996). Emplacement of igneous intrusions during the Early Cretaceous (Beeston, 1986; Mallett et al., 1990) might have had a role in increasing the heat flow particularly in the northern

Bowen Basin. This is strongly supported by apatite-fission-track-annealing studies (Marshallsea, 1988; Raza et al., 1995) which concluded that the sediments in this area attained their maximum temperature during the Early Cretaceous, although Beeston (1981, 1986) argues for a high heat flow during the Permo-Triassic. Thermal pulses are associated with major rifting (McKenzie, 1978), after which heat flow decays exponentially. However, Elliott (1993) opposes the idea that the Taroom Trough was initiated during a rift phase. The proposed alternative heating models will be evaluated as part of the present study.

CHAPTER TWO

PETROLEUM BIOMARKERS AS TOOLS IN BASIN ANALYSIS

2.1 Introduction

Biomarkers, or biological markers, are molecular fossils of bacteria, plants and animals. These complex organic compounds, composed of carbon, hydrogen and other elements, are found in sediments, sedimentary rocks, coals and petroleums (Brassell, 1992). They are useful in assessing the original organic matter inputs to sediments and the source rocks from which oils are derived. Some biomarkers can be used to infer the lithology and depositional environment of petroleum source rocks whereas others are sensitive thermal maturity indicators. Their usage in the petroleum industry has assisted oil and gas exploration, especially in frontier or sparsely explored basins, by providing important information about the origin of crude oils and their possible migration pathways. When biomarkers are employed in conjunction with thermal and kinetic modelling, the timing and extent of petroleum generation in sedimentary basins can be inferred. The names and structures of the main classes of biomarkers identified in the present study, and their uses in basin analysis are summarised in this chapter. As a general rule, a single biomarker cannot be used as definitive proof of organic matter type, source rock lithology or depositional environment. Instead, wherever possible, multiple biomarker parameters should be employed and interpreted in the light of the available isotopic, geochemical and geological data.

2.2 Nomenclature and structures

The following diverse assemblage of saturated and aromatic hydrocarbons was identified in the oils and source rocks of the southern Taroom Trough. The structures of these compounds are presented in Figures 2.1 - 2.4.

2.2.1 Normal alkanes and acyclic isoprenoids

The normal alkanes (*n*-alkanes or *n*-paraffins) are saturated hydrocarbons containing 12 - 35 or more carbon atoms arranged in straight chains, whereas the isoprenoids are branched alkanes composed of isoprene units. Pristane (i-C_{19}) and phytane (i-C_{20}) are the most common acyclic isoprenoids (Fig. 2.1).

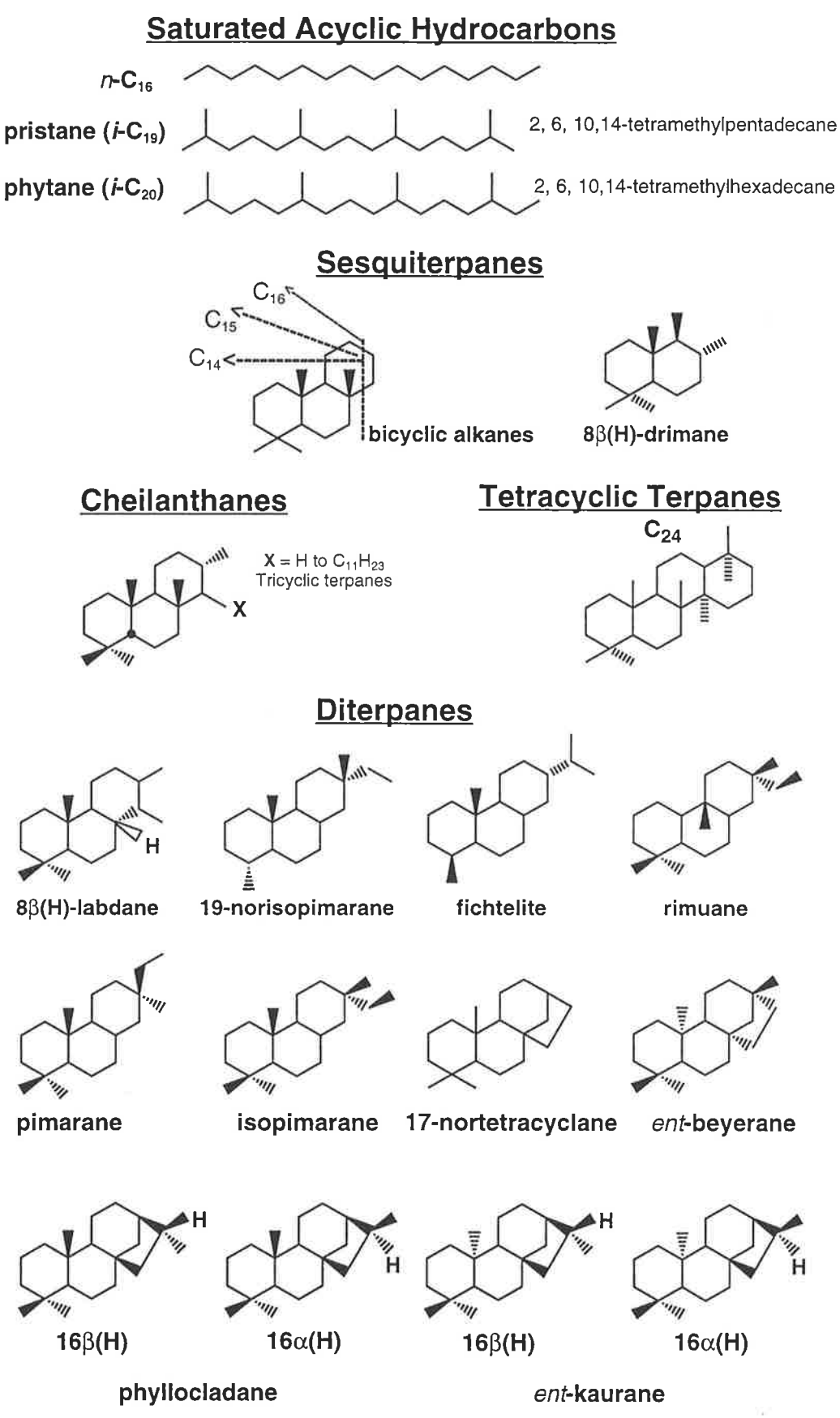

Figure 2.1 Structures of *n*-alkane, isoprenoid, sesquiterpenoid, diterpenoid, tri- and tetracyclic terpenoid biomarkers identified in this study.

2.2.2 *Terpanes*

Drimanes, cheilanthanes and tetracyclic terpanes

Drimanes are C_{14} - C_{16} bicyclic sesquiterpanes (Fig. 2.1) (Alexander et al., 1984a). Homologues up to C_{24} were also reported in a Chinese boghead coal (Wang and Simoneit, 1990). Cheilanthanes are tricyclic terpanes (TT) with distributions ranging from C_{19} up to C_{45} (Fig. 2.1) (Connan et al., 1980; Moldowan et al., 1983). Isomerization in the tricyclic terpanes occurs at the C-13 and C-14 positions and all the possible isomers ($\beta\alpha$, $\alpha\alpha$, $\alpha\beta$, and $\beta\beta$) are found in sediments, although with increasing maturity the $\beta\alpha$ isomer predominates (Chicarelli et al., 1988). Tetracyclic terpanes belong to the 17,21-secohopane series which extends from C_{24} to C_{27}, and probably up to C_{35}, with the C_{24} homologue (Fig. 2.1) being the most common in sediments and petroleum (Aquino Neto et al., 1983).

Diterpanes

The naturally-occurring diterpenoid hydrocarbons (diterpenes) include bicyclics, tricyclics and tetracyclics which can be grouped into 20 main skeletal classes, as reviewed by Devon and Scott (1972). Of these classes, six are commonly reported as alkanes in sediments and crude oils, namely abietane, pimarane, kaurane, phyllocladane, beyerane (or podocarpane) and labdane (Noble et al., 1985a,b; Simoneit et al., 1986). The C_{15} - C_{24} bicyclic diterpanes identified in the Athabasca tar sand belong to the labdane series (Dimmler et al., 1984). However, the C_{20} homologue is the most common bicyclic diterpane and, indeed, is the only C_{20} bicyclic diterpane identified in Australian oils, sediments and coals (Noble et al., 1985b). Tricyclic diterpanes include C_{19} 4β(H)-19-norisopimarane, C_{19} fichtelite, C_{20} rimuane, C_{20} pimarane and C_{20} isopimarane, whereas the tetracyclic diterpanes include C_{19} 17-nortetracyclane, C_{20} *ent*-beyerane, C_{20} phyllocladanes and C_{20} *ent*-kauranes (Fig. 2.1).

Hopanes, homohopanes and moretanes

The 17α(H)-hopanes are pentacyclic triterpanes consisting of four six-membered rings (A-D), one five-membered ring (E) and a side-chain containing up to 8 carbon atoms attached to the C-21 position in the E-ring (Van Dorsselaer et al., 1977). This results in hopanes containing between 27 and 35 carbon atoms (Fig. 2.2). Hopanes with more than 30 carbon atoms are called *homohopanes* (C_{31}-C_{35}). In this case, the prefix indicates the number of additional methylene groups (e.g. C_{33} trishomohopane). Homohopanes have an asymmetric (chiral) centre at C-22 resulting in pairs of diastereomers (22R and 22S) for each homologue. Configurational isomerisation in hopanes also occurs because of

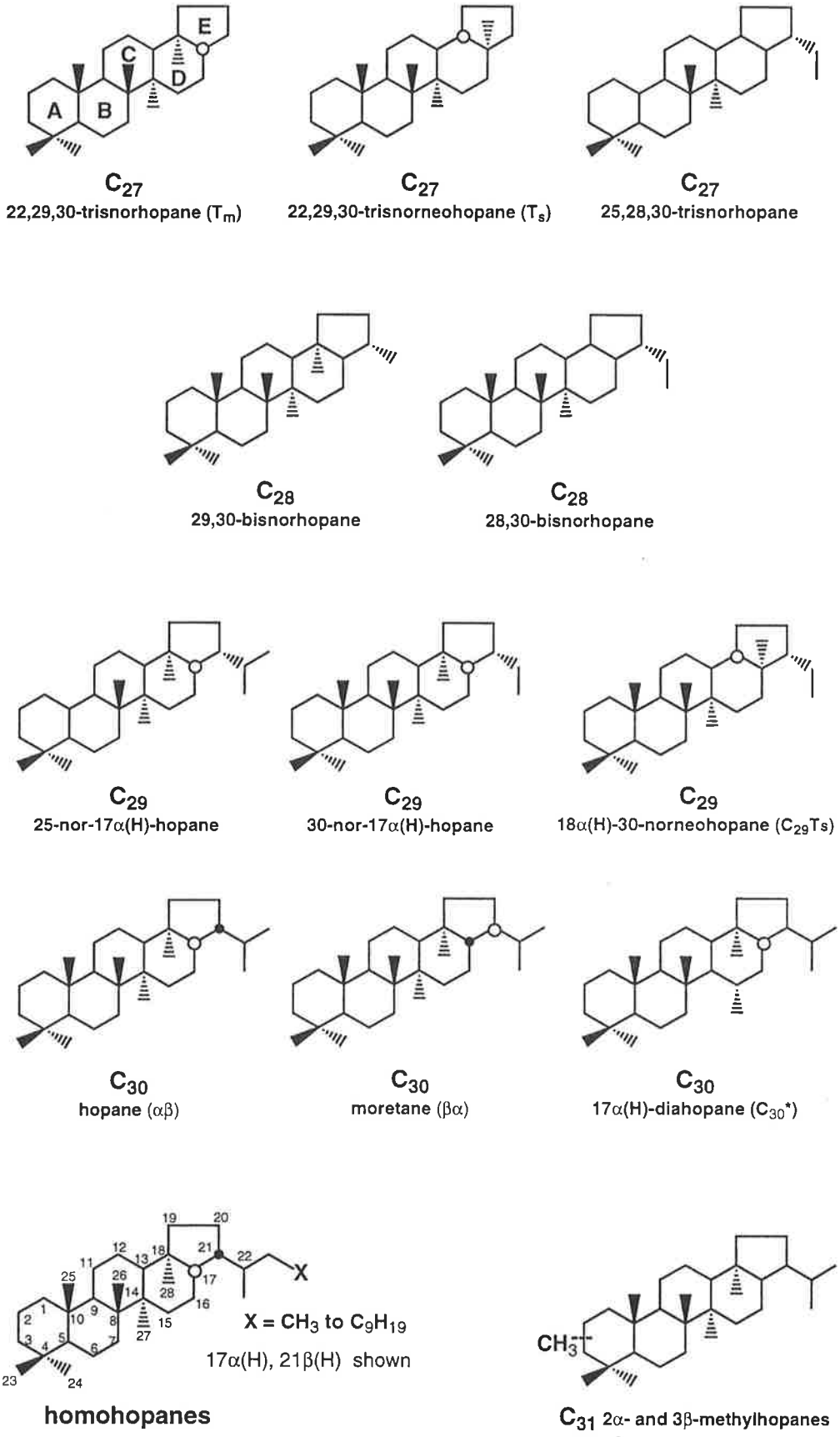

Figure 2.2 Structures of hopanoid biomarkers identified in this study.

asymmetric centres at the ring junctions, with the C-17 and C-21 positions being the most important locations (Fig. 2.2). If the hydrogen atoms at these locations are above the plane of the ring system, β notation is used whereas α notation is applied when the hydrogen atom in question is below the rings. All the hopanoid stereoisomeric series [17α(H),21α(H)-, 17β(H),21α(H)-, 17α(H),21β(H)-, and 17β(H),21β(H)-hopanes] are known (Peters and Moldowan, 1993). Compounds with the αβ configuration are the most thermodynamically stable hopanes and those with the ββ configurations are the least stable; the latter being the preferred biological configuration. The βα isomers are called *moretanes*.

Norhopanes

Hopanoid compounds containing less than 30 carbon atoms are called *norhopanes (desmethylhopanes)*. A prefix is used to indicate how many carbon atoms are missing. For example, 30-norhopane (or 30-nor-17α(H)-hopane) has a methyl group (CH_3) missing from the C-30 position; and 28,30-bisnorhopane (BNH) has methyl groups missing at both the C-28 and C-30 positions (Table 2.1, Fig. 2.2). The most common norhopanes are C_{28} 29,30-BNH and 28,30-BNH; and C_{27} 17α(H)-22,29,30-trisnorhopane (T_m) and 25,28,30-trisnorhopane (TNH) (Peters and Moldowan, 1993).

Diahopanes and Neohopanes

Diahopanes and neohopanes are rearranged hopanes in which a methyl group has migrated from one position on the ring system to another. In the case of the diahopanes, the migration is from the C-14 to the C-15 position, whereas for the neohopanes, it is from the C-18 to the C-17 position (Fig. 2.2). The most common neohopanes are C_{27} 18α(H)-22,29,30-trisnorneohopane (T_s) and its C_{29} analogue 18α(H)-30-norneohopane (C_{29} T_s), whereas the 17α(H)-diahopanes are represented by a larger number of homologues in the range C_{29}-C_{34} (Summons et al., 1988a,b; Moldowan et al., 1991; Peters and Moldowan, 1993).

Methylhopanes

Methylhopanes are hopanes with an extra methyl group attached to the A-ring (Fig. 2.2). The most common methylhopanes are the 2α- and 3β-methyl-17α(H),21β(H)-hopanes (Summons and Jahnke, 1992).

Table 2.1 Molecular fossils identified in this study using diagnostic *parent-to-daughter* transitions (MRM GCMS). (Structures of key molecular fossils[#] are presented in Figures 2.1 - 2.4)

Compounds	**MRM GCMS (Parent-daughter) transition**	**Peak label**
SESQUITERPANES		
	M^+ m/z	
C_{14} Bicyclane and rearranged drimanes?	194→123	C_{14}, R1, R2
C_{15} Bicyclanes (drimanes)	208→123	C_{15}
C_{16} Bicyclanes (homodrimanes)	222→123	C_{16}
C_{16} Bicyclanes (methyldrimanes)	222→137	C_{16}
C_{17} Methylhomodrimanes	236→137	C_{17}
CHEILANTHANES & C_{24} TETRACYCLIC TERPANE		
C_{19} Cheilanthane	262→191	C_{19}
C_{20} Cheilanthane	276→191	C_{20}
C_{21} Cheilanthane	290→191	C_{21}
C_{22} Cheilanthane	304→191	C_{22}
C_{23} Cheilanthane	318→191	C_{23}
C_{24} Cheilanthane	332→191	C_{24}
C_{25} Cheilanthane	346→191	C_{25}
C_{26} Cheilanthane (S+R)	360→191	C_{26} (S+R)
C_{30} Cheilanthane (S+R)	416→191	C_{30} (S+R)
C_{24} Tetracyclic terpane	330→191	C_{24}Tetra
DITERPANES		
Bicyclic		
C_{20} 8β(H)-Labdane	278→123	Labdane
Tricyclic		
C_{19} 19-Norisopimarane	262→233	19-Noriso
C_{19} Fichtelite	262→247	Fichtelite
C_{20} Rimuane	276→247	Rimuane
C_{20} Pimarane	"	Pimarane
C_{20} Isopimarane	"	Isopimarane
Tetracyclic		
C_{20} *ent*-Beyerane	274→245	Beyerane
C_{20} Phyllocladane (16α+16β)	274→259	Phylloclad
C_{20} *ent*-Kaurane (16α+16β)	"	Kaurane

Table 2.1 (Continued)

Compounds	MRM GCMS (Parent-daughter) transition	Peak label
HOPANES		
C_{27} 18α(H)-22,29,30-Trisnorneohopane	370→191	T_s
17α(H)-22,29,30-Trisnorhopane	"	T_m
17α,18α,21β(H)-25,28,30-Trisnorhopane	"	25,28,30
C_{28} 29,30-Bisnorhopane	384→191	29,30
28,30-Bisnorhopane	"	28,30
C_{29} 25-Nor-17α(H)-hopane@	398→177	C_{29} 25–NH
30-Nor-17α(H)-hopane	398→191	C_{29} αβ
18α(H)-30-Norneohopane ($C_{29}T_s$)	"	$C_{29}T_s$
30-Normoretane	"	C_{29} βα
17α(H)-Diahopane (30-nordiahopane?)	"	C_{29}*
C_{30} 25-Nor-17α(H)-hopanes (S+R)@	412→177	C_{30} 25–NH
Hopane	412→191	C_{30} αβ
Moretane	"	C_{30} βα
17α(H)-Diahopane	"	C_{30}*
C_{31} Hopanes (S+R)	426→191	αβ 22S, αβ 22R
Moretane (one peak)	"	C_{30} βα
17α(H)-Diahopanes (S+R)	"	C_{31}*
2α-Methylhopane	426→205	2α Me
3β-Methylhopane	"	3β Me
C_{32} Hopanes (S+R)	440→191	αβ 22S, αβ 22R
Moretane (S+R)	"	C_{32} βα
17α(H)-Diahopanes (S+R)	"	C_{32}*
C_{33} Hopanes (S+R)	454→191	αβ 22S, αβ 22R
Moretane (S+R)	"	C_{33} βα
17α(H)-Diahopanes (S+R)	"	C_{33}*
C_{34} Hopanes (S+R)	468→191	αβ 22S, αβ 22R
Moretane (S+R)	"	C_{34} βα
17α(H)-Diahopanes (S+R)	"	C_{34}*
C_{35} Hopanes (S+R)	482→191	αβ 22S, αβ 22R
Moretane (S+R)	"	C_{35} βα
17α(H)-Diahopanes (S+R)	"	C_{35}*

@ also called C_{29} and C_{30} demethylated hopanes.

Table 2.1 (Continued)

Compounds	MRM GCMS (Parent-daughter) transition	Peak label
STERANES		
C_{27} 5α,14α,17α(H)-cholestane 20S	372→217	ααS
5α,14α,17α(H)-cholestane 20R	"	ααR
5α,14β,17β(H)-cholestane 20S	"	ββS
5α,14β,17β(H)-cholestane 20R	"	ββR
5α,13β,17α(H)-diacholestane 20S	"	βαS
5α,13β,17α(H)-diacholestane 20R	"	βαR
5α,13α,17β(H)-diacholestane 20S	"	αβS
5α,13α,17β(H)-diacholestane 20R	"	αβR
C_{28} 5α,14α,17α(H)-24-methylcholestane 20S	386→217	ααS
5α,14α,17α(H)-24-methylcholestane 20R	"	ααR
5α,14β,17β(H)-24-methylcholestane 20S	"	ββS
5α,14β,17β(H)-24-methylcholestane 20R	"	ββR
5α,13β,17α(H)-dia-24-methylcholestane 20S	"	βαS
5α,13β,17α(H)-dia-24-methylcholestane 20R	"	βαR
5α,13α,17β(H)-dia-24-methylcholestane 20S	"	αβS
5α,13α,17β(H)-dia-24-methylcholestane 20R	"	αβR
C_{29} 5α,14α,17α(H)-24-ethylcholestane 20S	400→217	ααS
5α,14α,17α(H)-24-ethylcholestane 20R	"	ααR
5α,14β,17β(H)-24-ethylcholestane 20S	"	ββS
5α,14β,17β(H)-24-ethylcholestane 20R	"	ββR
5α,13β,17α(H)-dia-24-ethylcholestane 20S	"	βαS
5α,13β,17α(H)-dia-24-ethylcholestane 20R	"	βαR
5α,13α,17β(H)-dia-24-ethylcholestane 20S	"	αβS
5α,13α,17β(H)-dia-24-ethylcholestane 20R	"	αβR
C_{30} 5α,14α,17α(H)-24-*n*-propylcholestane 20S	414→217	ααS
5α,14α,17α(H)-24-*n*-propylcholestane 20R	"	ααR
5α,14β,17β(H)-24-*n*-propylcholestane 20S	"	ββS
5α,14β,17β(H)-24-*n*-propylcholestane 20R	"	ββR
5α,13β,17α(H)-dia-24-*n*-propylcholestane 20S	"	βαS
5α,13β,17α(H)-dia-24-*n*-propylcholestane 20R	"	βαR

Table 2.1 (Continued)

Compounds	MRM GCMS (Parent-daughter) transition	Peak label
METHYLSTERANES		
C_{28} 2α-methyl-5α,14α,17α(H)-cholestane 20R	386→231	20R ααα 2α Mest
3β-methyl-5α,14α,17α(H)-cholestane 20R	"	20R ααα 3β Mest
4α-methyl-5α,14α,17α(H)-cholestane 20R	"	20R ααα 4α Mest
C_{29} 2α-methyl-5α,14α,17α(H)-24-methylcholestane 20R	400→231	20R ααα 24(Me)-2α(Me)
3β-methyl-5α,14α,17α(H)-24-methylcholestane 20R	"	20R ααα 24(Me)-3β(Me)
4α-methyl-5α,14α,17α(H)-24-methylcholestane 20R	"	20R ααα 24(Me)-4α(Me)
C_{30} 2α-methyl-5α,14α,17α(H)-24-ethylcholestane 20R	414→231	20R ααα 24(Et)-2α(Me)
2α-methyl-5α,14α,17α(H)-24-ethylcholestane 20S	"	20S ααα 24(Et)-2α(Me)
3β-methyl-5α,14α,17α(H)-24-ethylcholestane 20R	"	20R ααα 24(Et)-3β(Me)
3β-methyl-5α,14α,17α(H)-24-ethylcholestane 20S	"	20S ααα 24(Et)-3β(Me)
4α-methyl-5α,14α,17α(H)-24-ethylcholestane 20R	"	20R ααα 24(Et)-4α(Me)
4α,23,24-trimethyl-5α,14α,17α(H)-cholestane 20R	"	dinosteranes@

@ Identification of 4α,23,24-trimethyl-5α,14α,17α(H)-cholestanes (dinosteranes) is tentative and GCMSMS 414 → m/z 98 transition is needed to verify their presence (Summons et al., 1987).

References used: Philp (1985), Noble et al. (1985a,b), Alexander et al. (1988), Peters and Moldowan (1993).

2.2.3 Steranes

Regular steranes

The steranes (also called cholestanes) are cyclic alkanes consisting of three six-membered rings (A-C), one five-membered ring (D) and a branched side-chain containing from eight to eleven carbon atoms (Fig. 2.3). The regular sterane series includes C_{26} (norcholestane), C_{27} (cholestane), C_{28} (24-methylcholestane), C_{29} (24-ethylcholestane) and C_{30} (24-*n*-propylcholestane) compounds, with the C_{26} homologue being the least reported. Various steroid stereoisomers exist. Important locations for isomerisation in steranes are at the C-5, C-14, C-17 and C-20 positions. Stereoisomers of the regular steranes are 5α(H),14α(H),17α(H), 20R (abbreviated ααα*R*, or simply αα*R*); 5α(H),14α(H),17α(H),20S (ααα*S*); αββ*R* and αββ*S* (Fig. 2.3).

Diasteranes

Diasteranes (or diacholestanes) are rearranged steranes in which methyl groups are located at ring positions C-5 and C-14, instead of C-10 and C-13 as in steranes (Fig. 2.3). All four isomers [13β,17α(H),20R abbreviated βα*R*; 13β,17α(H),20S (βα*S*); αβ*R*; and αβ*S*] are commonly reported for the C_{27}-C_{29} diasterane series.

Methyl steranes

Methylation in steranes may occur at the C-2, C-3 or C-4 positions in the A-ring (Peters and Moldowan, 1993). The 4-methyl steranes are the most commonly studied (e.g. Summons et al., 1987). These compounds can be grouped into two families: (1) *dinosteranes* which are C_{30} 4α-methyl steranes with side-chain methylation at positions C-23 and C-24 (4α,23,24-trimethylcholestanes), and (2) C_{28}-C_{30} 4α-methyl steranes in which the C_{29} and C_{30} homologues are substituted at C-24 (Fig. 2.3).

2.2.4 Aromatic hydrocarbons

Two major classes of aromatic hydrocarbons that occur widely in petroleum are the naphthalenes (2-ring, or diaromatic) and phenanthrenes (3-ring, or triaromatic) and their alkylated derivatives (Fig. 2.4). Particular alkylphenanthrenes identified include the monomethyl-substituted phenanthrenes (1-, 2-, 3- and 9- isomers), various dimethylphenanthrenes, and 1-methyl-7-isopropylphenanthrene, i.e. retene (Radke and Welte, 1983; Alexander et al., 1988). Dimethylnaphthalenes (DMN: Radke et al., 1982;

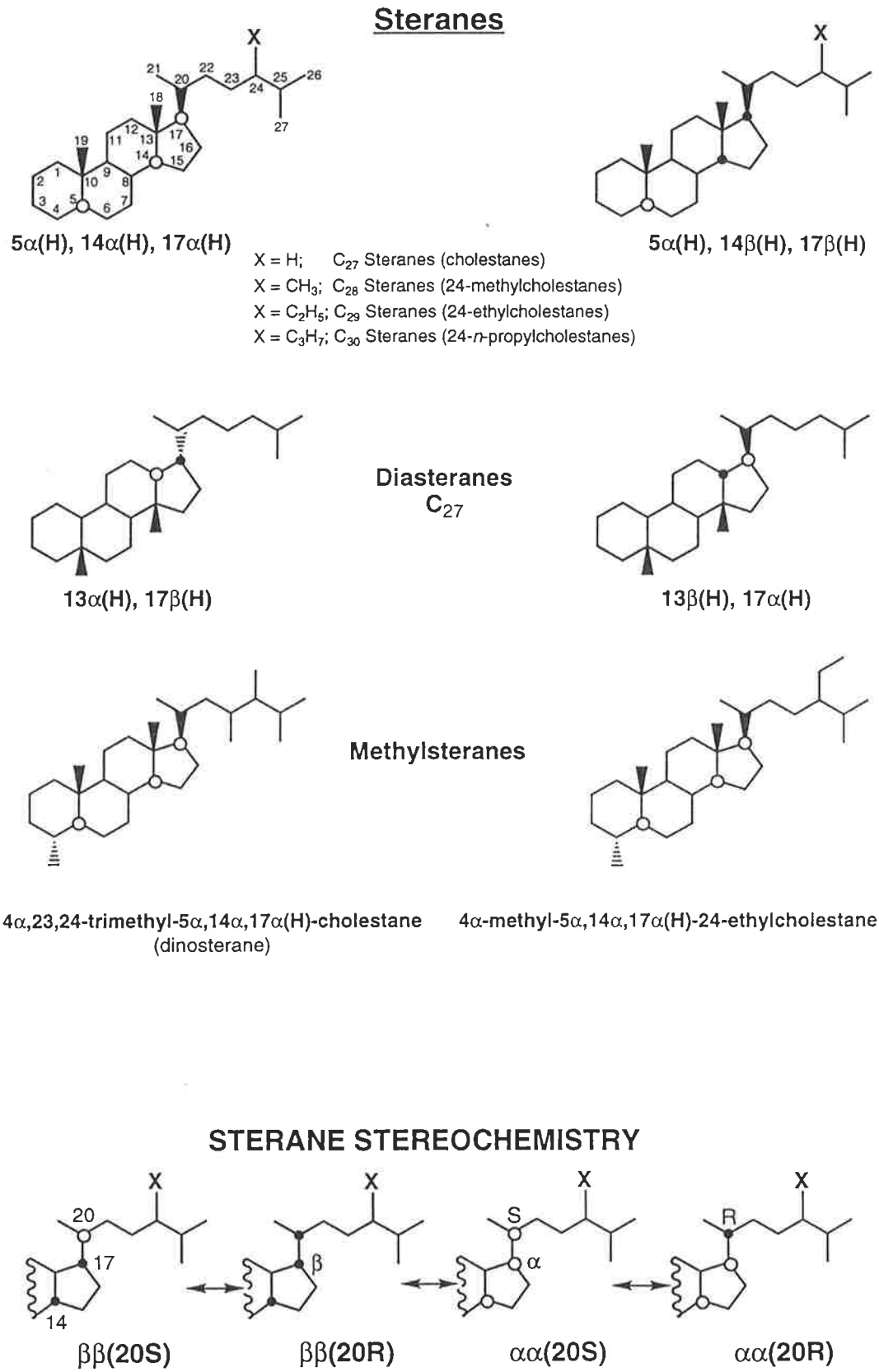

Figure 2.3 Structures of sterane, diasterane and methylsterane biomarkers identified in this study.

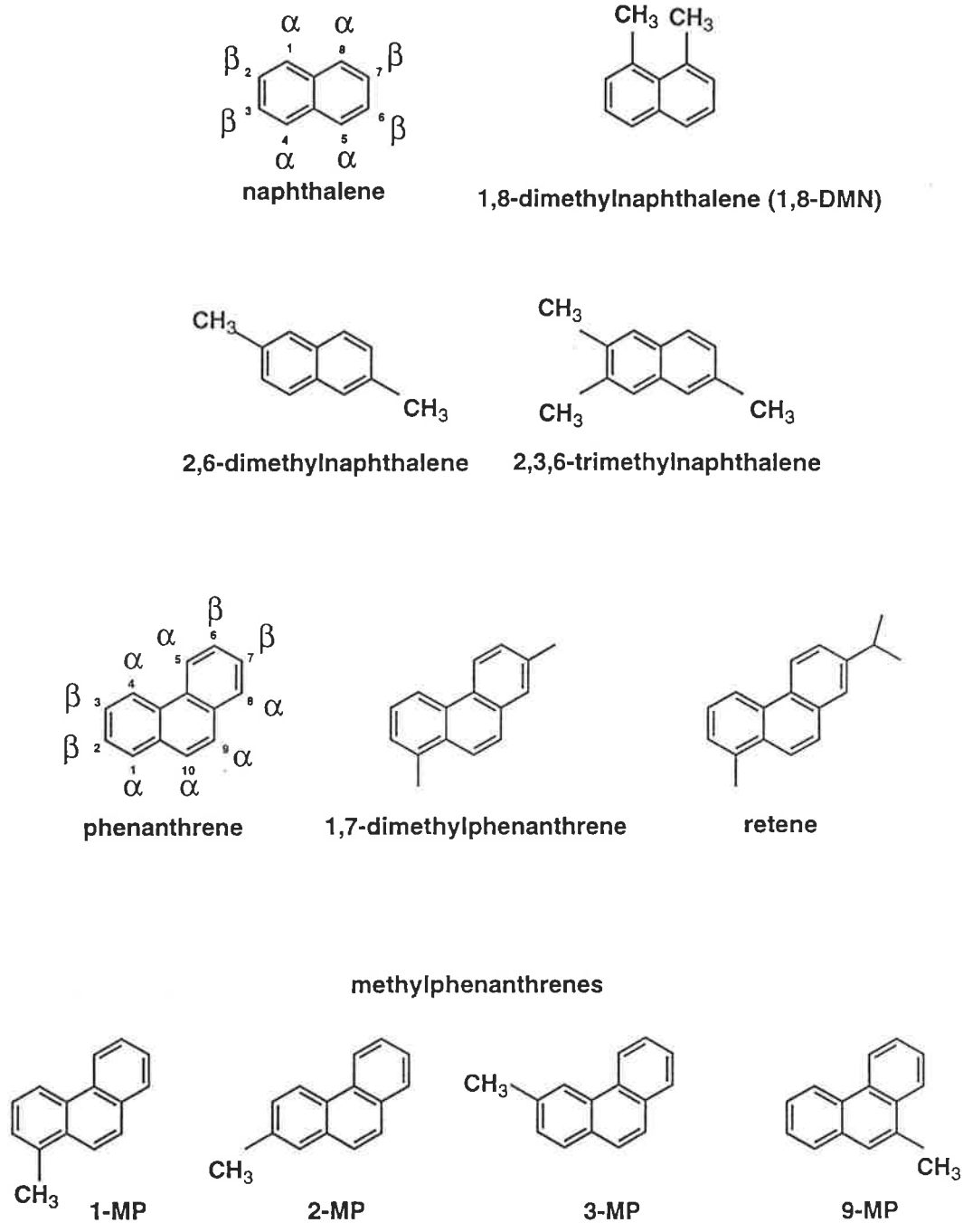

Figure 2.4 Structures of aromatic biomarkers identified in this study.

Alexander et al., 1983, 1985) and trimethylnaphthalenes (TMN: Alexander et al., 1985) are among the alkylnaphthalene compounds of interest.

2.3 Analysis and identification (see also Table 2.1)

The identification and quantification of biomarkers can be achieved using a range of analytical methods. The most effective tools are gas chromatography (GC) and gas chromatography-mass spectrometry (GCMS). These methods are characterised by their high sensitivity and selectivity which enable differentiation and detection of organic compounds at ppb levels (Brassell, 1992). Compounds introduced onto the GC column will fractionate between a mobile gas phase (typically hydrogen or helium) and a stationary liquid phase lining the interior wall of the column. Temperature programming of the column allows the more volatile components of lower-molecular-weight to elute first, followed by compounds of successively higher-molecular-weight and lower volatility. These eluting compounds are then detected by a flame ionization detector (FID), and finally passed to a computer to be presented as gas chromatograms.

Although the GC is a useful technique for detecting certain compounds such as *n*-alkanes and acyclic isoprenoids, it is not adequate to identify the more complex molecules such as steranes and triterpanes. However, this can be achieved by the coupling of a gas chromatograph to a mass spectrometer (GCMS), which provides diagnostic mass spectra for each component eluting from the GC. Here, data can be presented as individual mass spectra, or as reconstructed ion chromatogram (RIC; also called total ion current TIC) representing the sum of all the recorded mass spectra. In most applications, however, acquisition of full-scan GCMS data is not required. Instead, selected ions of interest are detected and presented as mass chromatograms (or mass fragmentograms). This mode of detection is called selected ion monitoring (SIM-GCMS) or multiple ion detection (MID-GCMS). In this method, the most abundant ion in the mass spectrum (base peak) of each compound type (e.g. m/z 217 for steranes and m/z 191 for hopanes) is used for monitoring particular compound classes.

Recently, a new advance (gas chromatography / mass spectrometry / mass spectrometry 'GCMSMS') has been introduced which enables the ionized molecules (parent ions) to be fragmented, in a field-free region, into smaller charged masses (daughter ions) which can then be detected by the second mass spectrometer (Peters and Moldowan, 1993). Metastable reaction monitoring (MRM, also called multiple reaction monitoring) can provide parent-daughter relationships similar to those of GCMSMS. Here, decomposition of molecular ions in a field-free region of a magnetic sector instrument produces an unfocused metastable ion which can be enhanced by the introduction of argon into this

field-free region and then detected by a mass spectrometer. The only disadvantage of this technique is that it cannot detect daughter ions which have very low masses (e.g. m/z 98 of dinosterane) (Brassell, 1992). For more details about the GCMSMS and MRM GCMS techniques, the reader is referred to chapter 2 of Peters and Moldowan (1993). The methods used to analyse and identify biomarkers in the present study are summarised in this section.

2.3.1 Normal alkanes and isoprenoids

The *n*-alkanes appear as regularly-spaced peaks in the saturates gas chromatogram, with pristane eluting immediately after *n*-C_{17} and phytane after *n*-C_{18}. Both the *n*-alkanes and isoprenoids are normally detected by GC but they also can be measured by GCMS using the mass chromatograms m/z 85 (*n*-alkanes) and m/z 183 (pristane and phytane). Another, but less common, isoprenoid is the botryococcane ($C_{34}H_{70}$) which elutes just before *n*-C_{29} on the GC chromatogram. Diagnostic mass fragments of botryococcane are m/z 238, 239, 294 and 295 (Peters and Moldowan, 1993).

2.3.2 Terpanes

Drimanes can be detected by SIM-GCMS using m/z 123 mass chromatograms. In this study, drimanes were detected by the MRM GCMS metastable transitions m/z 194→123 (C_{14} bicyclanes and rearranged drimanes), m/z 208→123 [C_{15} drimanes and bicyclanes], m/z 222→123 (C_{16} homodrimanes), m/z 222→137 (C_{16} methyldrimanes) and m/z 236→137 (C_{17} methylhomodrimanes) (Table 2.1).

Cheilanthanes are measured on m/z 191 mass chromatograms using SIM-GCMS. Alternatively, GCMSMS or MRM GCMS may be used to monitor the following parents of m/z 191 (Table 2.1): M^+ = m/z 262 (C_{19} TT), m/z 276 (C_{20}TT), m/z 290 (C_{21}TT), m/z 304 (C_{22}TT), m/z 318 (C_{23}TT), m/z 332 (C_{24}TT), m/z 346 (C_{25}TT), m/z 360 (C_{26}TT), and m/z 416 (C_{30}TT). In the same manner, the M^+330→m/z 191 transition is used for detecting C_{24} tetracyclic terpanes.

The various diterpanes can be identified by SIM-GCMS using their common diagnostic fragment ion (m/z 123). In this study, 8β(H)-labdane was monitored by the MRM GCMS-transition M^+ 278→m/z 123, whereas the tricyclic diterpanes were detected using M^+ 262→m/z 233 or m/z 247, and M^+ 276→m/z 247 transitions. The tricyclic diterpanes are best detected on the M^+ 274→ m/z 245 (*ent*-beyerane) and m/z 259 (phyllocladane and *ent*-kaurane). These transitions are listed in Table 2.1.

Hopanes are commonly measured on the m/z 191 mass chromatogram using SIM-GCMS. More reliable identification and quantification can be obtained by monitoring parent-to-daughter (M+→m/z 191) transitions using GCMSMS or MRM GCMS. The latter technique was employed in the present study. The MRM GCMS transitions used for identification are listed in Table 2.1. These transitions are: M+ 370→m/z 191 for the identification of C_{27} hopanes [18α(H)-22,29,30-trisnorneohopane (T_s), 17β(H)-22,29,30-trisnorhopane (T_m) and 17α(H)-25,28,30-trisnorhopane]; M+ 384→m/z 191 for C_{28} hopanes (29,30-bisnorhopane and 28,30-bisnorhopane); M+ 398→m/z 177 and M+ 412→m/z 177 for C_{29}- and C_{30}- 25-norhopanes, respectively; and M+ 398→m/z 191 for C_{29} hopanes [30-norhopane, 18α(H)-30-nornehopane, 30-normoretane and diahopane]. C_{30}-C_{35} hopanes, moretanes and diahopanes were detected using their respective molecular ion (M+ 412, 426, 440, 454, 468 and 482)→m/z 191 transitions. Since methylhopanes have an additional methyl group attached to the A-ring, they can conveniently be measured on m/z 205 or using M+ 426→m/z 205 transition.

2.3.3 Steranes

The C_{27}-C_{29} steranes (both regular and rearranged) are routinely measured on m/z 217 mass chromatograms using SIM-GCMS. Better resolution can be obtained by monitoring parent to daughter transitions (M+→m/z 217) with GCMSMS or MRM GCMS, where M+ corresponds to molecular ions at m/z 372, m/z 386, m/z 400 and m/z 414 for the C_{27}, C_{28}, C_{29} and C_{30} steranes, respectively (Table 2.1). As m/z 259 is the principal fragment ion of diasteranes, this mass chromatogram (m/z 259) can also be used to measure diasteranes. The methylsteranes (2α-, 3β- and 4α-) are monitored using m/z 231 and 232 mass chromatograms or, better still, the M+→m/z 231 transition, where M+ corresponds to molecular ions at m/z 386, m/z 400 and m/z 414 for C_{28}, C_{29} and C_{30} methyl steranes, respectively. Because of the large number of possible methylsterane isomers and coelution of some of the dinosterane isomers with 4α-methyl-24-ethylcholestanes, even when MRM GCMS is used (Peters and Moldowan, 1993), their identification, in this study, is considered tentative. The transition M^+ 414→m/z 98 (which cannot be acquired using MRM GCMS) is needed to verify the presence of the dinosteranes (Summons et al., 1987).

2.3.4 Aromatic hydrocarbons

Aromatic compounds can readily be detected using either GC of a di- and triaromatics fraction (after high performance liquid chromatography), or with GCMS of the total aromatic fraction by monitoring specific molecular ions. In the latter technique,

Table 2.2 Aromatic-based maturity parameters applied in this study

Dimethylnaphthalene ratio .....*Alexander et al. (1985, 1988)*

DNR-1 = (2,6-DMN+2,7-DMN)/(1,5-DMN)

Trimethylnaphthalene ratio .....*Alexander et al. (1985, 1988)*

TNR-1 = (2,3,6-TMN)/(1,4,6-TMN+1,3,5-TMN)

Methylphenanthrene indices (MPI-1 and MPI-2).....Radke and Welte (1983)

MPI-1 = 1.5 x (2-MP+3-MP)/(P+1-MP+9-MP)

MPI-2 = 3 x (2-MP)/(P+1-MP+9-MP)

Methylphenanthrene Distribution Factor .....*Kvalheim et al. (1987)*

MPDF-1 = (2-MP+3-MP)/(1-MP+2-MP+3-MP+9-MP)

Calculated vitrinite reflectance (R_Cr) .....*Radke and Welte (1983)*

R_Cr = 0.6 (MPI-1)+0.4 , when R_o<1.35%, or

= -0.6 (MPI-1)+2.3 , when R_o>1.35%

Calculated vitrinite reflectance (R_Cb) .....*Boreham et al. (1988)*

R_Cb = 0.7 (MPI-1)+0.22 , when R_o<1.7%, or

= -0.55 (MPI-1)+3.0 , when R_o>1.7%

Calculated vitrinite reflectance (R_Ck) .....*Kvalheim et al. (1987)*

R_Ck = -0.166+2.242 x (MPDF-1)

N.B. Key to abbreviations used in this table and in Table 5.4, along with their diagnostic mass fragmentograms

Abbreviation		Compound	SIM-GCMS
DMN	=	Dimethylnaphthalene	m/z 156
DNR	=	Dimethylnaphthalene ratio	m/z 156
1,5-DMN	=	1,5-dimethylnaphthalene	m/z 156
2,6-DMN	=	2,6-dimethylnaphthalene	m/z 156
2,7-DMN	=	2,7-dimethylnaphthalene	m/z 156
TMN	=	Trimethylnaphthalene	m/z 170
TNR	=	Trimethylnaphthalene ratio	m/z 170
1,3,5-TMN	=	1,3,5-trimethylnaphthalene	m/z 170
1,4,6-TMN	=	1,4,6-trimethylnaphthalene	m/z 170
2,3,6-TMN	=	2,3,6-trimethylnaphthalene	m/z 170
P	=	Phenanthrene	m/z 178
MP	=	Methylphenanthrene	m/z 192
1-MP	=	1-methylphenanthrene	m/z 192
2-MP	=	2-methylphenanthrene	m/z 192
3-MP	=	3-methylphenanthrene	m/z 192
9-MP	=	9-methylphenanthrene	m/z 192
DMP	=	Dimethylphenanthrene	m/z 206
1,7-DMP	=	1,7-dimethylphenanthrene	m/z 206
X	=	(1,3-DMP)+(3,9-DMP)+(2,10-DMP)+(3,10-DMP)	m/z 206
Retene	=	1-methyl-7-isopropylphenanthrene	m/z 219

dimethylnaphthalenes (2,6-, 2,7-, and 1,5-DMN) are measured on m/z 156; trimethylnaphthalenes (2,3,6-, 1,4,6-, and 1,3,5-TMN) on m/z 170; phenanthrene on m/z 178; methylphenanthrenes (1-, 2-, 3-, and 9-MP) on m/z 192; dimethylphenan-threnes (1,3-, 3,9-, 2,10-, and 3,10-DMP) on m/z 206; and retene on m/z 219 mass chromatograms (Table 2.2).

2.4 Biomarkers as source and environmental indicators

2.4.1 Normal alkanes and isoprenoids

Normal alkane profiles skewed toward the lower molecular weight range ($\leq n$-C_{22}, with a maximum at C_{15} or C_{17}) characterise most algae and bacteria whereas distributions of longer chain alkanes (n-C_{23+}, with a maximum at C_{23}, C_{25}, C_{27}, or C_{29}) are usually of terrestrial higher plant origin (Eglinton and Hamilton, 1963; Youngblood and Blumer, 1973). A particular example is the fossil or cyanophyte *Gloeocapsamorpha prisca* alga (common in the Ordovician) which shows predominant n-$C_{15\text{-}20}$ alkanes (Rullkotter et al., 1986). Exceptions are the freshwater algae *Botryococcus braunii* and *Pediastrum*, characteristic of many Type I kerogens, which also produce C_{23+} n-alkanes with a maximum at C_{29} (Metzger et al., 1991).

Pristane and phytane are ubiquitous in sediments and oils of all ages. These two isoprenoids are formed partly by the geochemical diagenesis of the phytol chain of chlorophyll (Didyk et al., 1978). Other sources of pristane and phytane include archaebacterial lipids, tocopherols, and certain zooplankton (ten Haven et al., 1987). Bray and Evans (1961) introduced a formula (carbon preference index, CPI) to express the predominance of either odd or even-carbon-numbered n-alkanes over the C_{24} to C_{34} range:

$$CPI = \frac{1}{2} \times \left(\frac{C_{25} + C_{27} + C_{29} + C_{31} + C_{33}}{C_{24} + C_{26} + C_{28} + C_{30} + C_{32}} + \frac{C_{25} + C_{27} + C_{29} + C_{31} + C_{33}}{C_{26} + C_{28} + C_{30} + C_{32} + C_{34}} \right)$$

Another formula (odd : even preference, OEP) was introduced by Scalan and Smith (1970) to express the relative abundance of odd versus even carbon-numbered n-alkanes at specific carbon numbers, as shown by the following two examples:

$$OEP_{(1)} = \frac{C_{21} + 6C_{23} + C_{25}}{4C_{26} + 4C_{28}}, OEP_{(2)} = \frac{C_{25} + 6C_{27} + C_{29}}{4C_{22} + 4C_{24}}$$

The CPI and OEP expressions give similar results. Thus, CPI and OEP values > 1 indicate predominance of odd carbon-numbered *n*-alkanes over their even carbon-numbered counterparts, whereas CPI and OEP < 1 intimates a predominance of even carbon-numbered homologues. The former distribution (OEP and CPI > 1) is typical of land plant cuticular waxes, whereas the latter (OEP and CPI < 1) characterises certain (but not all) algae and bacteria. For example, Dembicki et al. (1976) and Vandenbroucke et al. (1976) reported a predominance of even carbon-numbered *n*-alkanes in sediments rich in algal remains, whereas Powell and McKirdy (1973b) noticed a marked predominance of odd carbon-numbered homologues in sediments rich in land plant waxes. In very reducing environments, the reduction of fatty acids and alcohols, including phytanic acid and phytol, is favoured over decarboxylation reactions, resulting in an even carbon number preference among the *n*-alkanes and abundant phytane (Maxwell et al., 1973). Therefore, *n*-alkanes with an OEP < 1 are normally associated with low pristane/ phytane ratios (pr/ph < 1), whereas those with an OEP >1 are associated with the predominance of pristane over phytane (Welte and Waples, 1973).

Normal alkane and isoprenoid distributions are influenced by lithological variations. CPI values less than unity tend to be associated with carbonate and hypersaline (evaporite) sediments (ten Haven et al., 1985), whereas values > 1 characterise many shaley source rocks deposited in lacustrine or marine environments (Peters and Moldowan, 1993). The pristane/phytane ratio may be used as an indicator of the redox potential of the depositional environment. It is thought that reducing to anoxic and/or hypersaline conditions convert phytol mainly to phytane, resulting in low pristane/phytane ratios (pr/ph < 1) (Fu Jiamo et al., 1986, 1990; ten Haven et al., 1987), whereas terrestrial organic matter deposited under oxidising conditions is characterised by high pristane/ phytane (pr/ph > 3) ratios (Powell and McKirdy, 1973b). Pristane/*n*-heptadecane (pr/*n*-C_{17}) and phytane/*n*-octadecane (ph/*n*-C_{18}) ratios are other useful environmental parameters. Low values (pr/*n*-C_{17} < 0.5) are often associated with open-marine sediments whereas higher values (pr/*n*-C_{17} > 1) characterise peat swamps (Lijmbach, 1975).

Distributions of *n*-alkanes and isoprenoids are also sensitive to maturity variations. The CPI of *n*-alkanes is always > 1 in immature sediments containing terrestrial organic matter and decreases with increasing maturity due to thermal cracking of the longer-chain compounds. Allan and Douglas (1977) studied the *n*-alkane distributions of coal macerals and showed that an inverse relationship exists between vitrinite reflectance (R_O) and CPI. Anomalously high CPI values are associated with immature sediments. As R_O increases the CPI decreases, approaching unity at the onset of oil generation. Thermal maturation also causes free radical decarboxylation of fatty acids (Tissot and Welte, 1984). This, and

the aforementioned cracking of long *n*-alkyl groups, skews the resulting *n*-alkane distribution to lower carbon numbers.

Immature samples are also characterised by high isoprenoid abundances relative to *n*-alkanes (Powell and McKirdy, 1973b). With increasing thermal maturity the ratio of isoprenoids to *n*-alkanes, represented by pr/*n*-C_{17} and ph/*n*-C_{18}, decreases (Ishiwatari et al., 1977; Claypool et al., 1978; Rashid, 1979; Alexander et al., 1981; Bjoroy et al., 1983). This is probably controlled by the different rates at which *n*-alkanes and isoprenoids are released from the kerogen matrix, with *n*-alkanes being liberated faster. Lower thermal stability of branched alkanes and, hence, their greater liability to be destroyed, compared with *n*-alkanes may be another reason for the decreasing trend of isoprenoid to *n*-alkane ratios with increasing temperature and burial depth (Kinghorn, 1983). Although the pr/ph ratio is primarily an oxicity parameter, it increases with increasing maturity up to the onset of oil generation (Powell and McKirdy, 1973b; Rashid, 1979; Alexander et al., 1981; ten Haven et al., 1987).

2.4.2 Terpanes

Hopanes originate from bacteriohopanetetrol and other hopanoids in the membrane lipids of prokaryotic organisms (bacteria and cyanobacteria) and hence are ubiquitous in oils and sediments (Ourisson et al., 1982). Variations in the relative distribution of the C_{27}-C_{35} hopanes, therefore, must be related to different bacterial inputs and depositional environments. This can be summarised as follows:

1. The C_{29} and C_{30} 17α(H)-hopanes are the dominant triterpanes. Some workers (Zumberge, 1984; Connan et al., 1986; Clark and Philp, 1989) have noticed high values (>1) for the C_{29}/C_{30} hopane ratio in carbonate and evaporite source rocks, due to an additional input of the C_{29} homologue of the 30-nor-17α(H)-hopane series (Subroto et al., 1991) which is common in these lithologies. Others (e.g. Brooks, 1986) relate this fact to enhanced inputs of terrestrial organic matter. Low C_{29} hopane concentrations (C_{29}/C_{30} hopane <1) in petroleums may imply their derivation from shale source rocks.

2. The 17α(H)-homohopanes normally decrease in abundance from the C_{31} homologue onwards. High values of the homohopane index [C_{35}/(C_{31}-C_{35})-homohopane] are indicative of an anoxic depositional environment (Peters and Moldowan, 1991), and are commonly associated with carbonate (McKirdy et al., 1983) or evaporite sediments (ten Haven et al., 1988; Clark and Philp, 1989). The homohopane index decreases with increasing maturity while a related parameter %C_{31} homohopane increases (Peters and Moldowan, 1991).

3. Other indicators of the redox potential of the depositional environment are 28,30-bisnorhopane (BNH) and its C_{27} analogue 25,28,30-trisnorhopane (TNH); their presence in high abundance is strong evidence of anaerobic bacterial activity in highly reducing to anoxic settings (Grantham et al., 1980; Mello et al., 1990). These compounds (BNH and TNH) are present in the source rock as free hydrocarbons (Moldowan et al., 1984; Noble et al., 1985c) and their absolute concentrations and relative abundance (BNH/TNH) can be employed to relate oils to their source rocks (Tannenbaum et al., 1986b). Although the presence or absence of BNH and TNH in oil and rock samples is controlled by the type of bacterial input and/or depositional environment as explained, the absolute concentrations of these compounds, and their abundance relative to 17α(H)-hopanes, tend to decrease with increasing maturity due to their dilution by hydrocarbons released catagenetically from the kerogen (Moldowan et al., 1984).

4. Other hopanoid bacterial markers are the 2α- and 3β-methyl-17α(H),21β(H)-hopanes which are derived from methylotrophic bacteria (Bisseret et al., 1985; Summons and Jahnke, 1992). These methylhopanes (particularly the 2α-isomers) are commonly found in carbonate rocks (Summons and Walter, 1990).

5. The 17α(H)-diahopane (C_{30}*) is thought to be a product of the oxidation of bacterial hopanoid precursors in the D-ring and their subsequent rearrangement by clay catalysis (Peters and Moldowan, 1993). Volkman et al. (1983a) and Philp and Gilbert (1986) noted the presence of C_{30}* in oils of terrestrial source affinity. Therefore, high diahopane/hopane and high C_{30}*/$C_{29}T_s$ ratios appear to be characteristic of shales deposited under oxic-suboxic depositional conditions. However, both ratios can also increase with increasing thermal maturity due to the relative thermal stabilities of the compounds in question [17α(H)-diahopanes > $C_{29}T_s$ > 17α(H)-hopane] (Peters and Moldowan, 1993).

Precise structures have not yet been assigned to the drimanes (bicyclic sesquiterpanes) found in petroleum and so their origin is largely unknown (Peters and Moldowan, 1993). Similarities between their distributions and those of the hopanes led Alexander et al. (1984a) to conclude their derivation from hopanes via microbial activity during the early stages of diagenesis. Philp (1994) suggests that microbes present within oxic, higher-plant-rich environments are the main, and probably the only, contributor of drimanes. This may explain their abundance in coal facies and their absence in marine or lacustrine sediments (Price et al., 1987). Noble et al. (1986) suggest that rearrangement of the drimanes parallels that of the steranes; both are suppressed in evaporite/carbonate environments (see also Palacas et al., 1984).

The origin of the tricyclic terpanes is not well understood. They may have a prokaryotic (Ourisson et al., 1982) or algal (*Tasmanites*) origin (Volkman et al., 1989). Zumberge (1983) suggested that C_{19} and C_{20} homologues are produced by transformation reactions of some of the sester- and triterpanes upon maturation while Peters and Moldowan (1993) argued that a higher plant origin was likely for some of these homologues. Philp et al. (1989) found high abundances of C_{19}-C_{30} tricyclic terpanes in oils of brackish source affinity and low concentrations in oils derived from freshwater lacustrine source rocks. Because of the high thermal stability of the tricyclics, the C_{19}-C_{30} tricyclic terpanes/17α(H)-hopane ratio is found to increase with maturity (Peters and Moldowan, 1993) although this ratio is primarily a source parameter (Seifert and Moldowan, 1978).

The C_{24} tetracyclic terpane has been suggested as a marker for carbonate (Palacas et al., 1984) and hypersaline (evaporite) environments (Connan et al., 1986), although this compound has also been detected in terrestrially-sourced oils (Philp and Gilbert, 1986). The tetracyclic terpanes are similar to the cheilanthanes in that both compound types are resistant to thermal stress and biodegradation and, hence, they can be used in correlating severely biodegraded and highly mature oils with their respective source rocks (Aquino Neto et al., 1983).

Bicyclic diterpanes of the labdane series in the Athabasca tar sand were assigned a microbial origin (Dimmler et al., 1984). Nevertheless, Philp et al. (1983), Noble et al. (1985b) and Alexander et al. (1987) exclusively relate C_{20} labdane and other diterpanes in Australian oils and sediments to higher plant resins. Both the tricyclic and tetracyclic diterpanes have been suggested as biological markers for leaf resins of the gymnosperm conifer families Podocarpaceae, Araucariaceae and Cupressaceae (Noble et al., 1985a,b). On the Australian continent, remains of these conifer families proliferate during the Jurassic (Alexander et al., 1988). Pimarane (Fig. 2.1) may be derived from both gymnosperms and angiosperms (Peters and Moldowan, 1993). Compounds with the phyllocladane structure (Fig. 2.1) are abundant in the Podocarpaceaen genera *Podocarpus, Dacrydium* and *Phyllocladus*. Tricyclic diterpanes in general, and isopimarane, norisopimarane and rimuane in particular, are also related to the aforementioned genera (especially *Dacrydium*: Alexander et al., 1987). Kaurane precursors, on the other hand, occur in the conifer families Araucariaceae (including the genus *Agathis*), Podocarpaceae and Taxodiaceae. Ferns and certain species of the angiosperm families Labiatae, Phyllocladaceae, Compositae also contain large amounts of kauranes and phyllocladanes (Thomas, 1969). The less common tetracyclic diterpane *beyerane* is abundant in the families Araucariaceae, Cupressaceae and Podocarpaceae (Alexander et al., 1987 and references therein). The other common tetracyclic diterpane is the C_{19} 17-nortetracyclane which is formed by geochemical transformation of other C_{20} compounds. Simoneit (1986) detected diterpanes (including kaurane and pimarane) in

marine organisms, albeit in minor concentrations. Although phyllocladane and kaurane in an oil may be quoted as age-specific markers of Permian or younger source affinity (Noble et al., 1985a,b), the presence of these compounds in Upper Carboniferous coals suggests their derivation also from early conifers (the *Voltziales*) (Schulze and Michaelis, 1990).

2.4.3 Steranes

Steranes originate from eukaryotes (organisms with nucleated cells, like algae and higher plants). As such, the ratio of regular steranes/17α(H)-hopanes indicates the relative contributions of eukaryotic *versus* prokaryotic organic matter to the depositional environment (Seifert and Moldowan, 1978). Ratios ≥ 1 are indicative of marine organic matter and in particular of planktonic and/or benthic algae (Moldowan et al., 1985) whereas low values suggest terrestrial (or microbially reworked) organic matter (Tissot and Welte, 1984). This ratio can also be used to help distinguish petroleums derived from shale (high sterane/hopane) and carbonate (low sterane/hopane) source rocks (Connan et al., 1986; Moldowan et al., 1985).

The relative abundance of the C_{27}, C_{28}, and C_{29} regular steranes is commonly used to identify different organic matter inputs (Huang and Meinshein, 1979) and source-rock organic facies (Palmer, 1984), and in oil-oil and oil-source correlation (Mackenzie et al., 1983; Peters et al., 1989). To establish the C_{27}-C_{28}-C_{29} sterane ternary plot, the 5α,14α,17α 20R isomer of the corresponding steranes can be used, although some workers (e.g. Moldowan et al., 1985) prefer to use the sum of the four stereoisomers (ααα*R*, ααα*S*, αββ*R* and αββ*S*). The latter procedure minimises problems caused by selective depletion of the ααα*R* epimer with increasing maturity (Mackenzie, 1984) and biodegradation (McKirdy et al., 1983). High abundance of C_{27} and C_{28} steranes in a crude oil is commonly ascribed to an algal contribution (Huang and Meinshein, 1979), usually of marine origin (Peters and Moldowan, 1993), whereas high C_{29}/C_{27} ratio (>1) is usually interpreted as a higher plant marker (e.g. Czochanska et al., 1988) and/or shale matrix (Hughes, 1984). However, there are some problems with this approach (Volkman, 1988). For example, the ethylcholestane-dominant sterane signatures of certain Precambrian sediments and oils (Grantham, 1986) and of some carbonate source rocks and their related oils (Rullkotter et al., 1986), and the abundance of C_{29} sterols in diatoms (Volkman et al., 1981) suggest that land plants are not the only source of C_{29} steranes. Grantham and Wakefield (1988) noticed that the ratio of C_{28} /C_{29} steranes is low in Paleozoic and older marine oils and that there is a steady increase in the abundance of C_{28} steranes in younger oils, most noticeably from the Jurassic onwards. They

attributed this phenomenon to an increase in the diversity of marine phytoplankton (algae) during the Jurassic, Cretaceous and Tertiary periods.

Diasteranes are formed during diagenesis by rearrangement reactions thought to be catalysed by clay minerals (Rubinstein et al., 1975). Therefore, high diasterane concentrations and high diasterane/sterane ratios in oils are indicators of clay-rich (shale) source rocks, whereas low diasterane abundances, and hence low diasterane/sterane ratios, indicate clay-lean source rocks (carbonates) deposited under anoxic conditions (McKirdy et al., 1983; Hughes, 1984). However, this conclusion is not universally true and there are several examples of high diasterane abundances in clay-poor carbonates (Clark and Philp, 1989; Moldowan et al., 1992) and phosphates (Al-Arouri, 1992). If dealing with oils or sediments from similar organic facies, the diasterane/sterane ratio can also be used as a maturity indicator (Peters et al., 1990). Because diasteranes are thermally more stable and more resistant to biodegradation than are steranes, the diasterane/sterane ratio increases with maturity (Seifert and Moldowan, 1978; Goodarzi et al., 1989) and with the extent of biodegradation (Peters and Moldowan, 1993).

Epimeric C_{30} 4-desmethyl steranes (24-*n*-propylcholestanes or simply C_{30} steranes: Fig. 2.3) are found in most oils and sediments of marine origin, and are completely absent from terrestrial and lacustrine sediments. These compounds are related to the *n*-propylcholesterols synthesised by marine *Chrysophyte* algae and found in marine invertebrates which feed on the algae (Raederstorff and Rohmer, 1984; Moldowan et al., 1985). Therefore, high values of the C_{30}-sterane index (C_{30}/C_{27} to C_{30} steranes) in crude oils are a strong indication of their marine source affinity (Peters et al., 1989).

The origin of the methyl steranes found in sediments and oils is still ambiguous. The 4-methyl steranes are derived mainly from dinoflagellates (Wolff et al., 1986; Summons et al., 1987), but also from prymnesiophyte algae (e.g. the genus *Pavlova*: Volkman et al., 1990) and the methanotrophic bacterium *Methylococcus capsulatus* (Bird et al., 1971). Dinosterane (Fig. 2.3) is derived from marine dinoflagellates (Withers, 1983) which first became abundant during the Triassic (Summons et al., 1987; Goodwin et al., 1988). This explains the high abundance of this compound in oils and sediments of Triassic and younger age (Summons et al., 1987; Thomas et al., 1989). On the other hand, 4α-methyl-24-ethylcholestane occurs in both marine and lacustrine sediments. Its presence, in the absence of dinosterane, is indicative of the latter environment (Summons et al., 1987). The 2α- and 3β-methyl steranes usually occur in much higher abundance than their 4α-counterparts. Their distributions are different from those of the 4α-methyl steranes, which is consistent with their suggested bacterial affinity (Summons and Capon, 1988).

2.4.4 Aromatic source parameters

Alkylnaphthalenes and alkylphenanthrenes are ubiquitous in both aquatic and terrestrial organic matter (Radke, 1987). However, oil-oil and oil-source correlations can be made on the basis of the presence or absence of certain isomers. For example, resins from various higher plant families can be differentiated on the basis of their bi-, tri- and tetracyclic diterpenoids (Thomas, 1969). Upon burial, these compounds undergo a series of transformations that result in varying proportions of saturated and aromatic products depending on the depositional and diagenetic histories of the original material. As such, the natural resin input can be inferred by examining the saturated and aromatic diterpenoid hydrocarbons of the rock or oil samples. Alexander et al. (1988, 1992) used biomarkers of the *post-Triassic*-conifer family Araucariaceae to distinguish oils derived from the Permo-Triassic Cooper Basin from those derived from the overlying Jurassic-Cretaceous Eromanga Basin. They found that various araucariacean (*Agathis*) aromatic biomarkers [*viz.* 1,2,5-trimethylnaphthalene (TMN); 1,7-dimethylphenanthrene (DMP), 1-methylphenanthrene and retene: Fig. 2.4] are particularly abundant in the Jurassic sediments of the Eromanga Basin, but absent from Permo-Triassic sediments of the Cooper Basin. Values larger than 1.0 (Alexander et al., 1988) or 1.25 (Boreham, 1995) for the 1-MP/9-MP ratio, and larger than about 1.5 for the 1,2,5-TMN/1,3,6-TMN ratio indicate a Jurassic source affinity (Alexander et al., 1988). The inferred source can be confirmed using a plot of log (retene/9-MP) *versus* log (1,7-DMP/X; where X is the chromatographically unresolved mixture of 1,3-, 3,9-, 2,10-, and 3,10-DMP). On this plot, a pre-Jurassic source is demonstrated if the retene/9-MP ratio is < 0.3 (Alexander et al., 1988) or < 0.4 (Boreham, 1995) and the 1,7-DMP/X ratio is < 0.8 (Alexander et al., 1988).

Other aromatic source indicators include monoaromatic and triaromatic steroids and aryl isoprenoids (Peters and Moldowan, 1993). However, these compounds are not discussed here because no attempt was made to detect them in the oil or source rock samples examined in the present study.

2.5 Biomarkers as maturity indicators

Among the geochemical methods commonly used to assess the thermal maturity of sedimentary organic matter and petroleum source rocks are vitrinite reflectance (R_O), Rock-Eval pyrolysis (T_{max}, Production Index *PI*) and biomarker data (Peters and Moldowan, 1993). However, biomarkers are as yet the only means of assessing the expulsion maturity of an oil and its maturation history. These data can then be used, with other geological information in the thermal modelling of sedimentary basins in order to evaluate the extent and timing of hydrocarbon generation from the source rocks of

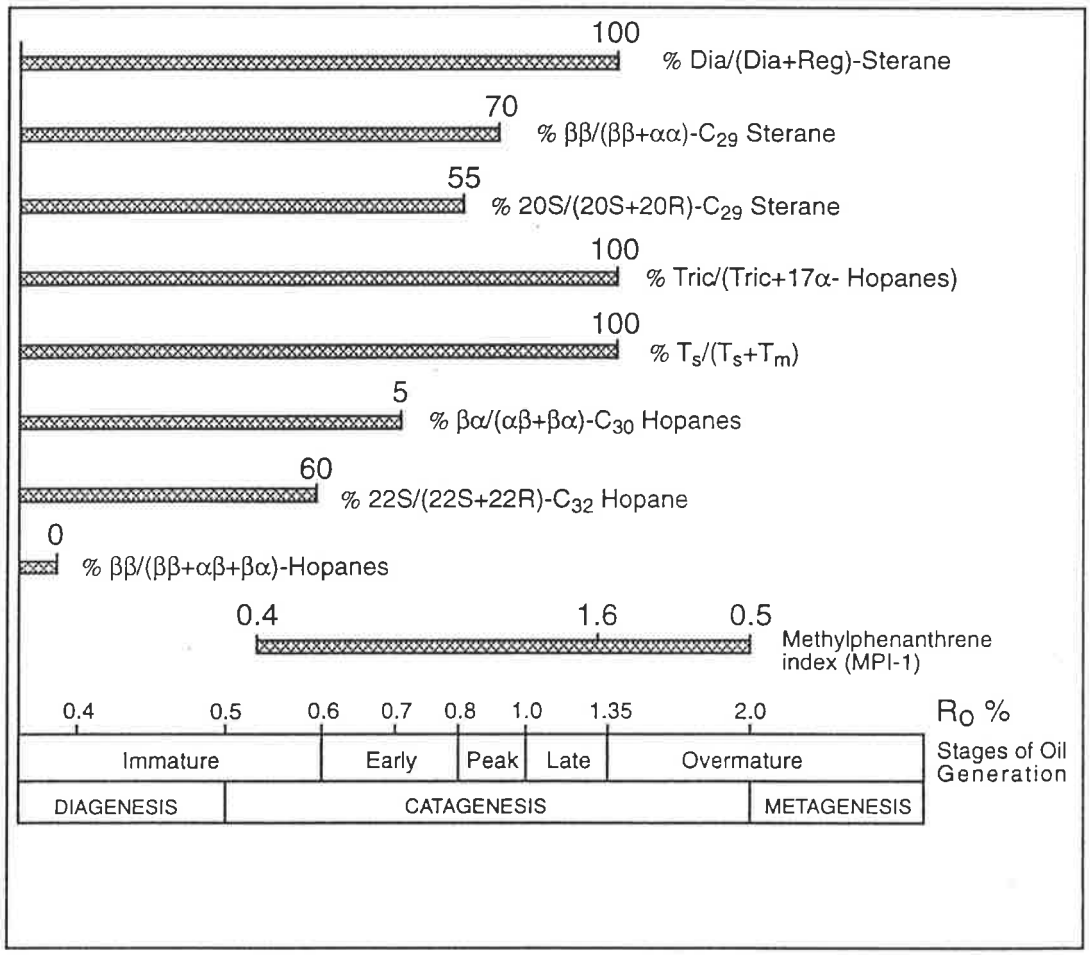

Figure 2.5 Correlation of various biomarker maturity parameters used in the present study with vitrinite reflectance and stages of petroleum generation (modified after Peters and Moldowan, 1993 and Killops and Killops, 1993).

interest.Various biomarkers undergo isomerisation (including epimerization) and aromatization reactions which attain equilibrium at different maturity levels. While the usefulness of some parameters (e.g. %20S-C_{29} steranes) is restricted to low maturity levels, others (e.g. $T_s/(T_s+T_m)$, tricyclics/17α(H)-hopanes) can be used for assessment of highly mature samples (Fig. 2.5). The following is a summary of the standard maturity parameters based on terpane, sterane and aromatic molecular fossils.

2.5.1 Terpane maturity parameters

%22S/(22S+22R)-Homohopanes

The most common homohopanes used for calculation of the %22S/(22S+22R) ratio are C_{31} and/or C_{32} homologues. The biological 22R configuration in these homohopanes is converted, upon maturation, to a mixture of 22R and 22S diastereomers. Thermodynamic equilibrium (57 to 62%: Seifert and Moldowan, 1986) is reached at the early phase of oil generation and no increase in this value can be achieved with further maturation (Peters and Moldowan, 1993). While this rule is commonly applied, caution should be exercised when dealing with carbonates (Moldowan et al., 1992), evaporites (ten Haven et al., 1986) or phosphates (Al-Arouri, 1992) wherein mature hopane distributions are noticed even the sediments are immature.

C_{30} Moretane/hopane

The biological 17β(H),21β(H)-hopanoid (ββ-hopane) is unstable and once deposited it transforms into the more stable isomers βα-moretane and αβ-hopane, with the latter predominating. The moretane to hopane (βα-/αβ-hopane) ratio decreases with increasing maturity from about 0.8 in immature sediments to about 0.15-0.05 in mature rock and oil samples (Seifert and Moldowan, 1980; Mackenzie et al., 1980). This ratio can be influenced by the organic matter type or its depositional environment, most obviously in hypersaline settings where moretanes are abnormally abundant (Rullkotter and Marzi, 1988).

$C_{29}T_s/C_{29}$ hopane and $T_s/(T_s+T_m)$

The $C_{29}T_s/C_{29}$ hopane ratio increases with maturity because of the greater thermal stability of $C_{29}T_s$ (Hughes et al., 1985; Kolaczkowska et al., 1990). Similarly, T_s is relatively more stable than T_m and, therefore, a general trend of increasing T_s/T_m [or

$T_S/(T_S+T_m)$] ratio is noticed with increasing maturity (Seifert and Moldowan, 1978; Kolaczkowska et al., 1990). However, this ratio is also source-dependent (Moldowan et al., 1986). High values are associated with shale-derived oils, whereas anoxic carbonates and related oils show anomalously low T_S/T_m values (McKirdy et al., 1983, 1984).

Tricyclic terpanes/17α(H)-hopanes

When dealing with different organic facies of comparable maturity, variations in the tricyclic terpanes/17α(H)-hopanes ratio are obviously source-related (Seifert and Moldowan, 1978; Seifert et al., 1980). However, this ratio increases dramatically with advancing maturation, as is noticed in oil and rock samples of widely different maturity levels (Aquino Neto et al., 1983) and during hydrous pyrolysis experiments (Peters et al., 1990). Complications arise when using this ratio as a maturity parameter for heavily biodegraded oils. It increases dramatically as biodegradation proceeds because the tricyclics are much more highly resistant to bacterial attack than are hopanes (Seifert and Moldowan, 1979).

2.5.2 Sterane maturity parameters

Epimerization and isomerisation in the regular steranes are well studied reactions which have been widely used in evaluating the thermal maturity of oils and source rocks. Epimerization takes place in the side chain at the C-20 position, whereas isomerisation occurs in the ring system at the C-14 and C-17 positions (Fig. 2.3).

%20S/(20S+20R) Steranes

The sterane isomerisation ratio [%20S/(20S+20R) or simply %20S] is a highly sensitive parameter for the immature to mature levels (Peters and Moldowan, 1993). Any of the regular steranes [5α(H),14α(H),17α(H)-C_{27}, C_{28} or C_{29}] can be used to measure this ratio. This ratio increases with maturity (because of the higher thermal stability of the 20S epimer) until an equilibrium between the biological epimer (20R) and the geological epimer (20S) is reached [52-55% (Seifert and Moldowan, 1986), or 50% (Gallegos and Moldowan, 1992)] at the onset of oil generation. Based on hydrous pyrolysis experimentations on a range of vitrinite kerogen, Abbott et al. (1990) show that the sterane isomerisation ratio is not controlled by direct chiral isomerisation in the saturated hydrocarbon structure. Nevertheless, this ratio is very reliable for estimating the onset of oil window, particularly if used in conjunction with vitrinite reflectance; and if variations due to facies changes (Moldowan et al., 1986), weathering (Clayton and King, 1987) and biodegradation (McKirdy et al., 1983) are accounted for. Weathering can decrease the

abundance of the ααα 20S epimers whereas bacteria may selectively remove the ααα 20R epimers. As is the case for the %22S homohopanes parameter, immature evaporite sediments give mature sterane patterns (ten Haven et al., 1986).

The same ratio (%20S) can be calculated for the 13β(H),17α(H)-diasteranes. Equilibrium here is also achieved at the onset of oil generation but at a slightly higher value (20S = 60%: Mackenzie et al., 1980).

%ββ/(ββ+αα) Steranes

One of the most commonly reported maturity parameters is the ratio of the 14β(H),17β(H)- to the total of 14α(H),17α(H)- and 14β(H),17β(H)-(20S+20R) steranes [ββ/(ββ+αα) or simply %ββ]. This ratio can be calculated for any of the C_{27}, C_{28} and C_{29} sterane homologues, although the latter is the most commonly measured (e.g. Seifert and Moldowan, 1986). Again, caution should be applied when studying samples from carbonate (McKirdy et al., 1983) or hypersaline sediments (ten Haven et al., 1986; Rullkotter and Marzi, 1988); both give %ββ higher than expected (when checked against other maturity parameters such as %20S). Many combinations of maturity parameters can be plotted against each other, such as the biomarker maturation-migration index (BMAI) of Seifert and Moldowan (1981), to better constrain oil and source rock maturity. This plot (5α,14β,17β-20R / 5α,14α,17α-20R *versus* 5α,14α,17α-20S / 5α,14α,17α-20R) has also been used to estimate relative migration distances where the oils plotting far from the BMAI-curve for source rocks are those which have experienced longer migration distances than those plotting at, or closer to, the first-order kinetic conversion curve (Seifert and Moldowan, 1981; Vincent et al., 1985; Zhao-An and Philp, 1987).

2.5.3 Aromatic maturity parameters

The thermal maturity of oils and source rocks can also be calculated using certain internal isomer ratios of their aromatic hydrocarbons. A number of these aromatic parameters are used to supplement the maturity data obtained from the saturated biomarkers. They are particularly useful in the later stages of catagenesis. Aromatic maturity parameters include those based on aromatic steroids (Mackenzie, 1984), monoaromatic hopanoids (He Wei and Lu Songnian, 1990), porphyrins (Sundararaman et al., 1988), alkylbiphenyls (Cumbers et al., 1987), alkylphenanthrenes (Radke and Welte, 1983) and alkyl naphthalenes (Alexander et al., 1985). Of these parameters, those based on alkyl-substituted naphthalenes and phenanthrenes are the most commonly used for maturity

assessment because of their wider dynamic range, and hence are the ones applied in the present study.

The methylphenanthrene index (MPI; Table 2.2), proposed by Radke and Welte (1983), is based on the internal distribution of phenanthrene (P) and the methylphenanthrenes (MP) in coals and Type III organic matter. There are five possible isomers of methylphenanthrene, namely 1-, 2-, 3-, 4-, and 9-MP, with the 4-isomer being the least abundant (< 1% total MPs: Garrigues and Ewald, 1983). Dewar reactivity numbers show that methylphenanthrenes (as well as the di- and trimethylnaphthalenes) with a methyl group adjacent to a ring junction (α-notation: Fig. 2.4) are kinetically less stable than those with a methyl group located one carbon further from the junction (β-notation: Fig. 2.4). In other words, the lesser stability of the former compounds (e.g. 1,8-DMN and 1-MP: Fig. 2.4) is due to the close proximity of the methyl group to a hydrogen atom or another methyl group, which results in stronger steric interaction. As such, the 1- and 9-methylphenanthrenes are less stable than their 2- and 3-methyl counterparts (Radke, 1987). Therefore, the concentrations of 1-MP and 9-MP decrease relative to the thermodynamically favoured 2-MP and 3-MP, as maturity increases (Radke and Welte, 1983; Radke, 1987). Measured vitrinite reflectance (R_O) shows a good correlation with MPI for $R_O > 0.4$ (Boreham et al., 1988) or > 0.7% (Radke and Welte, 1983), giving rise to equations for calculated vitrinite reflectance (R_C) (Table 2.2). An MPI range of 0.45-1.5 defines the zone of oil generation (≈ 0.6-1.3% R_O). At 1.3% R_O a reversal occurs in the trend of increasing MPI. This results in two possible values of R_C for each MPI measurement, which limits the use of methylphenanthrene indices especially if no independent data are available. Furthermore, variations in organic matter type and facies can influence the aromatic isomer patterns (Radke et al., 1986; Radke, 1987; Budzinski et al., 1995) and, in particular, the alkylphenanthrene distributions. These authors found that the 2- and 3-MP isomers predominate over their 1- and 9-MP counterparts in marine-influenced organic matter and in highly mature Type I and II kerogens, relative to Type III kerogen of equivalent maturity. Kvalheim et al. (1987) found that phenanthrene abundance is the most susceptible to such source effects and, therefore, they proposed another parameter, the methylphenanthrene distribution factor (MPDF-1: Table 2.2), which does not include phenanthrene, for use in calculating vitrinite reflectance.

Changes in the distributions of dimethylnaphthalenes (Radke et al., 1982; Alexander et al., 1983, 1984b, 1985) and trimethylnaphthalenes (Alexander et al., 1985) with increasing maturity have also been described and compared with other maturity parameters such as R_O, Rock-Eval T_{max}, %20S-sterane, and MPI. A general decrease was observed in the relative abundances of αα-dimethylnaphthalenes and αβα- and ααβ-trimethylnaphthalenes (Fig. 2.4) with increasing maturity. This was associated by a remarkable increase in the relative abundances of ββ-DMN and βββ-TMN because of

their higher stability. Therefore, when plotting the dimethylnaphthalene ratio (DNR-1) versus the trimethylnaphthalene ratio (TNR-1), as suggested by Alexander et al. (1988), the relative maturity of oils and sediments can be established and more accurate correlations made between oils and their source rocks.

2.6 Effects of biodegradation on biomarkers

Before interpreting biomarker data to determine the source affinity and maturity of an oil, it is crucial to recognise what changes (if any) have been caused by biodegradation in the reservoir. Biodegradation of petroleum by aerobic and, to a lesser extent, anaerobic bacteria occurs when suitable conditions (contact with oxygenated, nutrient-rich water; temperature < 80°C; H_2S-free oil) prevail in the reservoir. Therefore, the occurrence of a biodegraded oil implies that the host reservoir has come in contact with surface water at some stage in its history after oil generation (e.g., Volkman et al., 1983a,b).

Biodegradation can be recognised by diagnostic changes in the oil's physical properties (e.g. low API gravity and pour point) and in its chemical characteristics (Connan, 1984). Some of these bulk chemical changes are higher sulphur contents and enhanced proportions of cyclic alkanes and polar (NSO) compounds. More accurate recognition of the degradational changes can be achieved by studying the biomarker content of the oil. The various classes of biomarkers respond differentially to biodegradation because of their differing resistance to microbial attack (Fig. 2.6). Normal alkanes are the first group of compounds to be degraded, followed by acyclic isoprenoids, steranes, hopanes, diasteranes, and finally aromatic hydrocarbons (Volkman et al., 1983a,b; Moldowan et al., 1992; Chossen et al., 1992). Based on the relative abundances of these biomarker classes, several scales have been erected to describe the severity of biodegradation of an oil (Volkman et al., 1983a,b; Moldowan et al., 1992; Peters and Moldowan, 1993).

A naphthene hump or unresolved complex mixture (UCM) in the GC trace of the saturated hydrocarbons represents undifferentiated branched and cyclic alkanes. Such a pronounced UCM may be a sign of immaturity (Powell and McKirdy, 1973a). However, this unresolved envelope becomes more prominent with increasing oxidation of organic matter during weathering (Clayton and Swetland, 1978; Bjoroy et al., 1983; Forsberg and Bjoroy, 1983) and/or biodegradation (Connan, 1984). Normally, the shorter-chain compounds are the first to be removed by bacteria (Connan, 1984). Selective bacterial removal of *n*-alkanes results in increased pr/*n*-C_{17} and ph/*n*-C_{18} ratios (Leytheauser, 1973; Clayton and Swetland, 1978). Later work (Peters and Moldowan, 1993) has shown that pr/ph ratio also increases with biodegradation.

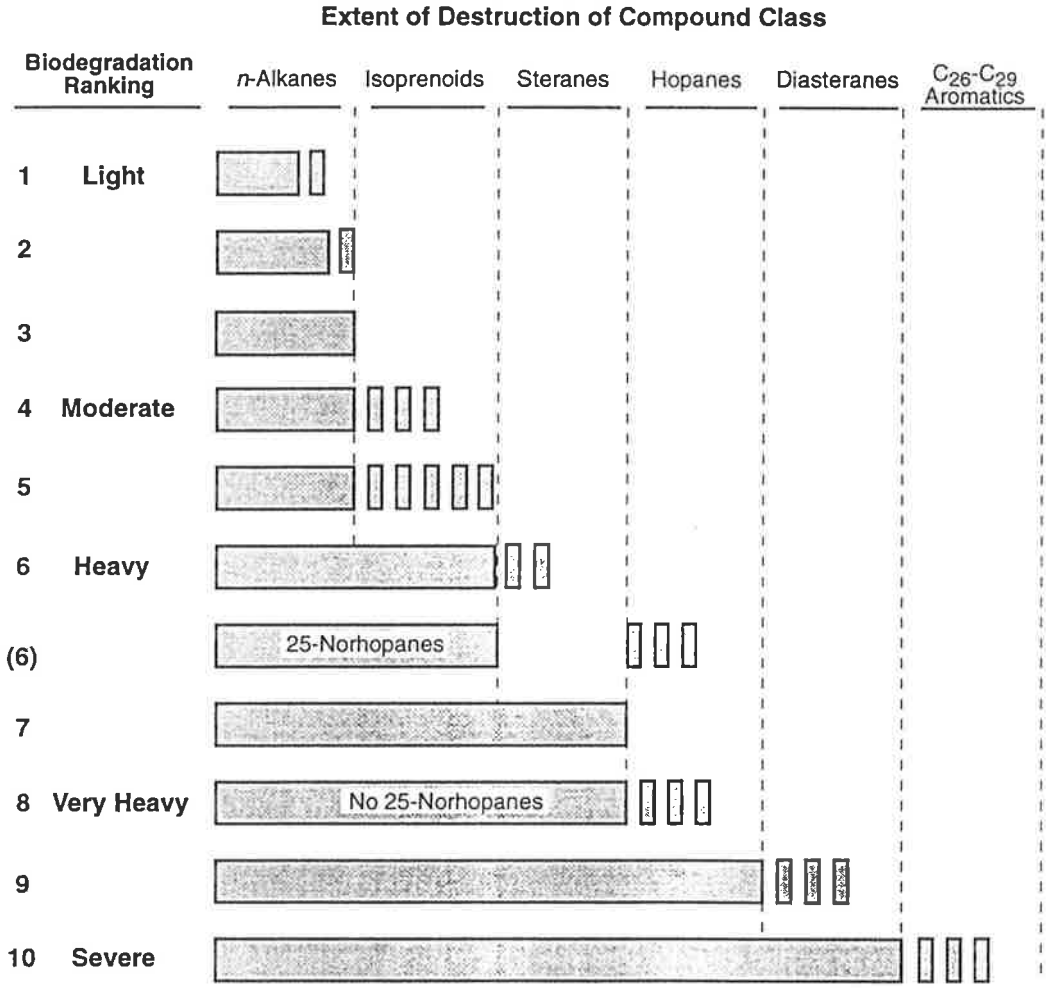

Figure 2.6 Biodegradation scale (after Peters and Moldowan, 1993).

As a general rule, compounds with the biological epimeric configuration are selectively attacked by bacteria, rather than their more stable "geological" isomers. Thus, for example, the biological ααα-sterane isomers are preferentially removed before their αββ counterparts, while the S configuration is more resistant than the R isomer (McKirdy et al., 1983; Volkman et al., 1983a). This results in 20S/(20S+20R) ratios larger than the equilibrium value (~56%) (Peters and Moldowan, 1993). In the middle stages of bacterial attack, hopanes, steranes and diasteranes with lower-molecular-weight are more susceptible than their higher-molecular-weight homologues (Fig. 2.6). The 25-norhopanes become abundant due to the bacterial removal of the methyl group at C-10 from the regular hopanes. However, as biodegradation proceeds to higher levels, even these residual 25-norhopanes will be removed and the previously intact hopane homologues will be removed faster (Fig. 2.6). Although steranes are known to undergo biodegradation before hopanes, the reverse does occur; and where this has happened, the affected hopanes are converted to 25-norhopanes (Peters and Moldowan, 1991). Just as diasteranes are more resistant than steranes (Seifert and Moldowan, 1979; McKirdy et al., 1983), so too diahopanes are also more resistant than their regular counterparts. Other compounds which are resistant to biodegradation are gammacerane, cheilanthanes, oleanane, and bicadinanes (Peters and Moldowan, 1993).

The impact of water washing on saturated biomarkers is not well known. However, Radke (1987) noticed that oils, suspected to have been water-washed, have elevated MPI-1 values due to the depletion of phenanthrene, whereas their methylphenanthrenes are unaffected. Because the effect of water washing is greater on the lower-molecular-weight aromatics, C_1 to C_3 naphthalenes are more readily removed from the oil than are phenanthrenes (Radke, 1987).

CHAPTER THREE

SAMPLES AND ANALYTICAL TECHNIQUES

3.1 Samples

3.1.1 Sediments

Seventy three samples of potential source rock (core and cuttings), ranging in age from Early Permian to Middle Jurassic, were chosen from 43 exploration wells distributed throughout the southern Taroom Trough. Figure 1.2 shows the geographical locations of the wells sampled for source rocks, and Figure 1.3 shows the stratigraphic levels of these samples. Lithologies selected for analysis were mainly mudstones and coals (see also Table 4.1). Particular attention was paid to the Middle Triassic Snake Creek Mudstone which was sampled in 40 wells.

3.1.2 Petroleum

Eleven oils and one condensate from reservoirs of Permian to Jurassic age in the Surat and Bowen Basins were chosen for purpose of oil-source correlation (Figs. 1.2 and 1.3; Table 5.1). These petroleum samples were supplied by exploration companies, as follows: Bridge Petroleum Ltd. (Roswin North-1, Taylor-11, Taylor-12A, Tinker-4 and Merroombile-1), Oil Company of Australia N.L. (Martini-1, Waratah-1, Riverslea-1, Washpool-1, Cogoon River West-1 and Wilga-2) and Command Petroleum Holdings N.L. (Bellbird-1).

3.2 Preparation of source rock samples

Preparation techniques were directed towards obtaining clean rock samples, free of drilling mud and mud additives, cavings and indeterminate fine material. Core samples were wire-brushed, washed with organic-free water and then dried. Cuttings samples were washed with water and wet-sieved through 2mm and 74μm (200 mesh) screens. The < 2mm > 200 mesh size fraction was considered indigenous, but double-checked for contamination under a binocular microscope. Representative portions of the core and cuttings samples were finely milled to powder (~ 200 mesh) for geochemical analyses; whereas the remaining portions were kept for petrographic examination.

3.3 Analysis

The analytical techniques employed in this study are summarised in Figure 3.1. Details of the individual analyses are as follows:

3.3.1 Total organic carbon and Rock-Eval pyrolysis

Screening analyses including determination of total organic carbon (TOC) content and Rock-Eval pyrolysis were undertaken for all 73 core and cuttings samples. These standard analyses were performed at AGSO (Canberra) using a Leco carbon analyser and a Girdel IFP-Fina Mark II instrument (Model 59). Guidelines outlined in Peters (1986) were followed in interpreting the Rock-Eval data.

3.3.2 Organic petrography (white light and fluorescence microscopy)

The rock samples were mounted in araldite resin blocks. Grinding was started with #400 and #600 grit carborundum paper, followed by successive polishing with 1 μm diamond paste on Lamplan 450 cloth and with 0.25μm diamond paste on Buehler Microcloth™. Finally, the polished blocks were cleaned on Selvyt cloth using ethanol. Petrographic analysis were then accomplished using a *Leitz Ortholux II* microscope under reflected white light and UV-excitation using Leitz oil immersion objectives (magnification of the nocular lenses is X12.5 whereas the objective magnification is X32, X50 or X120). A *Wild Photoautomat MPS* camera was used for photography. Maceral analysis was performed in accordance with the Australian Standard AS 2856 (Standards Association of Australia, 1986).

3.3.3 Scanning electron microscopy (SEM)

To further illustrate the nature of the organic matter in some samples, SEM was utilised. The specimen was mounted onto an aluminum stub, labelled, coated with a thin layer of gold and examined with a Philips 1000 SEM housed in the University of Adelaide Optical Centre.

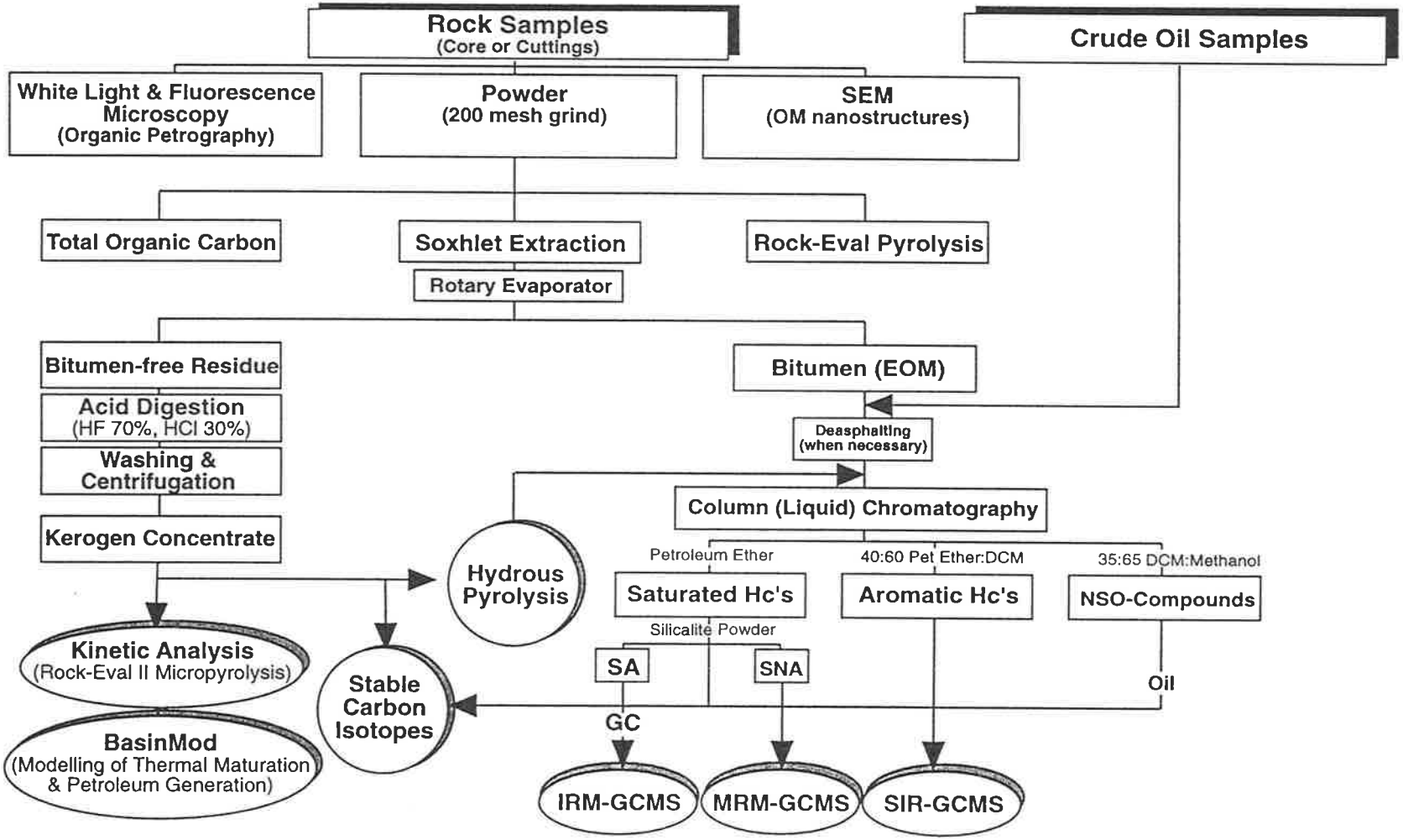

Figure 3.1 Flow chart of the analytical techniques applied in this study.

3.3.4 Soxhlet extraction, liquid chromatography and isolation of hydrocarbon fractions

Bitumen, or extractable organic matter (EOM), was extracted from the rock samples (up to 50 grams) using an azeotropic solvent mixture (dichloromethane:methanol, 93:7) in a Soxhlet apparatus, for 72 hours (Padley et al., 1991). Some of the extracts and the oils were deasphalted. Extracts were added to the top of a silica gel/alumina column (40 or 60 cm long) and saturated hydrocarbons, aromatic hydrocarbons and polars (NSO compounds) were successively eluted with petroleum ether (80 mL), petroleum ether/dichloromethane (40:60, 80 mL) and dichloromethane:methanol (35:65, 80 mL), respectively.

To concentrate biomarkers in the oils and some extracts, the saturated hydrocarbons were further separated into *n*-alkanes (silicalite-adduct; SA) and branched-cyclic hydrocarbons (silicalite non-adduct; SNA) using silicalite powder (West et al., 1990). Simply, saturated hydrocarbons (10 mg) were transfered to the top of a Pasteur pipette filled with silicalite powder (~1 g) and plugged with glass wool. After 10 minutes, the silicalite non-adduct (SNA) fraction containing branched/cyclic hydrocarbons was eluted in pentane. The *n*-alkane (SA) fraction was isolated by liquid-liquid extraction into hexane after dissolution of the zeolite in 30% hydrofluoric acid.

3.3.5 Gas chromatography

Gas chromatography (GC) was carried out on the saturated hydrocarbon fractions of both the extracts and the kerogen pyrolysates (section 3.3.8). A *Varian 3400* GC fitted with an OV101 fused silica column (25m x 0.25mm i.d.) was used. The oven was programmed from 60 °C to 300 °C at 4 °C/min and held at the final temperature until all compounds eluted. Hydrogen was used as the carrier gas. Data handling and reduction were controlled by MacLab software available in the Organic Geochemistry Laboratory, Department of Geology and Geophysics, University of Adelaide.

3.3.6 Metastable reaction-monitoring (MRM) gas chromatography-mass spectrometry

The SNA fractions were analysed in the multiple reaction monitoring (MRM) mode at AGSO's Isotope and Organic Geochemistry Laboratories (Canberra) using a VG Analytical AutoSpec-UltimaQ mass spectrometer fitted with a Carlo Erba 8060 gas chromatograph and an A200S Autosampler, and controlled by a VG OPUS data system. The GC was equipped with a 50m x 0.2mm i.d., crosslinked methylsilicone capillary column (HP Ultra-1, film thickness = 0.33 μm).

Samples in hexane were injected (splitless mode) onto the column at 28 °C. The oven was held at 50 °C for 2 minutes, then temperature was raised to 150 °C at 15 °C/min, then to 310 °C at 3 °C/min, and held isothermal for 28 minutes. Hydrogen was employed as the carrier gas. Ions were generated by electron impact (EI+) with an accelerating voltage of 8kV. The mass spectrometer was used in the multiple reaction monitoring (MRM) mode. The total analysis time was 90 minutes with a cycle time of 1.82s. The selected parent-to-daughter pairs, which included one pair (M^+ 389 → 234) for the predeuterated internal standard [3-CD_3-5α(H)-cholestane], are shown in Table 2.1. This deuterated-sterane standard was used for quantification of the biomarkers. The standard (100 ng) was first added to hexane (25 μL). The resulting standard solution was then mixed with hexane (25 μL) containing either extract saturates (0.5 mg) or pyrolysate saturates (1 mg). One μL of the aliquot was injected, on-column, into the MRM GCMS.

3.3.7 Kerogen isolation

Kerogen concentrates were obtained from six representative SCM rock samples. The Soxhlet-extracted rock powder (Section 3.3.4) was exhaustively macerated with hydrochloric and hydrofluoric acids to remove the mineral matter. This was followed by centrifugation and/or flotation in dichloromethane to concentrate the kerogen. Rock-Eval pyrolysis of the kerogen concentrate (10-20 mg) was undertaken and the results were compared with those obtained on the corresponding whole-rock sample.

3.3.8 Sealed-tube hydrous pyrolysis and fractionation of pyrolysates

This experiment was carried out at AGSO's Isotope and Organic Geochemistry Laboratories (Canberra) following the procedure of Boreham and Powell (1991). Briefly, the isolated kerogen (~50 mg) was placed in a 150 mm x 6 mm i.d. Vycor tube. After addition of distilled water (20 μL) to the sample, the tube was evacuated to 10^{-3} torr and sealed with a hydrogen/air flame while immersed in liquid nitrogen. The tubes were then placed inside a GC oven at 340 °C for 72 hours. The pyrolysates were fractionated, as for the EOM, into saturated hydrocarbons, aromatic hydrocarbons and NSO compounds by standard liquid chromatography on activated silica. Saturates were further separated into normal (silicalite-adduct, SA) and branched/cyclic alkanes (silicalite non-adduct, SNA) using silicalite powder, as for the extract's saturates. The SA was analysed by gas chromatography, whereas MRM GCMS was used to analyse the SNA, as discussed in Section 3.3.6

3.3.9 Stable carbon isotope analysis

The oil fractions (i.e. saturated hydrocarbons, aromatic hydrocarbons, and NSO-containing compounds), kerogen concentrates and rock extract and kerogen pyrolysate fractions (saturates and aromatics) were analysed for their stable carbon isotopic composition. Kerogen (2 mg) was sealed in a quartz tube and oxidized over Copper oxide at 950°C. The liberated carbon dioxide was analysed using a Europa Scientific isotope-ratio mass spectrometer in the Department of Geology and Geophysics, University of Adelaide. The carbon isotopic composition is expressed using the delta notation:

$$\delta^{13}C=(^{13}C/^{12}C_{sample} / {}^{13}C/^{12}C_{standard} -1) \times 1000$$

Results are expressed as parts per thousand (per mil, ‰) relative to the PeeDee Belemnite (PDB) standard.

3.3.10 Gas chromatography-isotope-ratio mass spectrometry

The isotopic compositions of individual *n*-alkanes of two end-member SCM samples (extracts and their corresponding kerogen pyrolysates) were determined using AGSO's isotope-ratio-monitoring gas chromatograph-mass spectrometer (IRM GCMS). The specifications and operating conditions of the instrument were as reported in Boreham (1994) and Boreham et al. (1994). In summary, it consists of a Varian 3400 gas chromatograph connected to a Finnigan MAT 252 isotope-ratio mass spectrometer via a micro-volume combustion system. The GC was equipped with a PoraPlot Q fused silica column (10 m x 0.53 mm i.d.). The gas was injected (50 µL) using a gas-tight syringe into a heated split injector (split ratio 1:50). The column temperature was maintained at 30 °C for 2 minutes then temperature programmed to 200 °C at 10 °C/min and held at the final temperature for 20 minutes. The individual gaseous hydrocarbons were quantitatively converted to carbon dioxide and water in the combustion reactor (CuO, 950 °C) and, following removal of water, the isotopic composition of carbon dioxide was measured. Delta (δ) values were determined using the manufacturer's software which corrected for background contributions, partial separation of isotopic species on the chromatographic column, and contributions of ^{17}O.

3.3.11 Chemical kinetic analysis

Kinetic measurements were conducted, at AGSO and by Geotech (Perth), using a Rock-Eval II programmed micropyrolysis instrument (Delsi Instruments) interfaced to a stand-

alone PC-based data aquisition system. Soxhlet-extracted (dichloromethane: methanol, 93:7; 72 hours), crushed (<100 μm), kerogen concentrates (~100mg) were subjected to kinetic analysis. Analyses were performed in duplicate at four different heating rates (*viz.* 5, 15, 25, 50 °C/min) for each sample. Initial and final isotherms were 300 °C (5 min) and 550 °C (1 min), respectively. Kinetic parameters (*A* and *E*) were obtained using the Kinetics™ software which performs an iterative non-linear regression analysis of reaction rate data using a discrete distributed activation energy model (Braun and Burnham, 1987; Burnham et al., 1987, 1988).

CHAPTER FOUR

SOURCE ROCK GEOCHEMISTRY AND PETROGRAPHY

4.1 Introduction

Data on the bulk organic geochemistry and petrography of potential source rocks (Permian, Triassic and Jurassic) in the southern Taroom Trough are presented and discussed in this chapter. Source-richness was measured by means of total organic carbon (TOC) content, Rock-Eval genetic potential (S1+S2) and extractable C_{15+} hydrocarbon yield (saturates + aromatics, ppm) (Tables 4.1 and 4.2; Fig. 4.1). Source rock quality (kerogen type) and depositional environment was inferred from a combination of Rock-Eval hydrogen index (Table 4.1; Figs. 4.2 and 4.8); normal and isoprenoid alkane distributions (Table 4.2; Figs. 4.3, 4.5 and 4.6); and maceral composition (Table 4.4; Plates I-VI). Special attention was paid to the Triassic Snake Creek Mudstone (SCM), it being the main target of this research project. Finally, source rock maturation level was determined from Rock-Eval T_{max} and production index (Table 4.1; Figs. 4.4 and 4.7); various alkane maturity parameters (Table 4.2; Figs. 4.3, 4.5, 4.6, 4.9 and 4.10) and vitrinite reflectance data, where available (Table 4.3; Fig. 4.4).

Further information on the origin and depositional environment and maturity of the organic matter preserved in these source rocks (particularly the SCM) was obtained from their saturated (terpane and sterane) and aromatic biomarker distributions, but these data are discussed in Chapter 5.

4.2 Source-richness

The Back Creek Group (BCG) mudstones, examined in four wells (Cockatoo Creek-1, Burunga-1, Meeleebee-1 in the northern part of the study area, and Flinton-1 in the south: Fig. 1.2), have fair to very good total organic richness (TOC = 0.7-3.7%) and a poor hydrocarbon genetic potential (S1+S2 < 2 kg h'c/tonne rock: Table 4.1a). However, the TOC (%) *versus* Hydrocarbons (ppm) crossplot (Fig. 4.1), which illustrates source-rock richness, shows that the BCG at best has hydrocarbon contents typical of a fair oil source. Its oil-proneness decreases with increasing maturity as shown by samples #13, 14, 15 from Cockatoo Creek-1 (see also next section).

Table 4.1(a) Rock-Eval pyrolysis and TOC data, Permian and Jurassic source rocks, southern Taroom Trough

Sample No.	Well Name	Depth (m)	Formation	Lithology	Sample Type	TOC (%)	T_{max} (°C)	S1	S2	S3	PI	HI	OI
1	Burunga-1	393.42	Evergreen Fm	Mudstone	C	2.91	439	0.03	2.03	1.56	0.01	70	54
11	"	868.7-872	BWG (BCM)	Carb. shale	Cut	44.7	435	8.60	82.7	18.6	0.09	185	41
12	"	1094.23	" "	Carb. shale	Cut	28.8	434	11.0	72.2	4.45	0.13	251	15
9	"	1482.34	Gyranda Fm	Mudstone	C	0.15	[373]	0.00	0.01	0.00	0.00	7	0
10	"	1642.23	"	"	C	0.71	448	0.07	0.27	0.00	0.21	38	0
8	"	1642.66	"	"	C	0.70	444	0.06	0.24	0.00	0.20	34	0
7	"	1963.03	"	"	C	0.85	461	0.08	0.25	0.00	0.25	29	0
6	"	2123.30	BCG (Flat Top Fm)	"	C	0.96	460	0.18	0.42	0.00	0.30	44	0
5	"	2590.83	"	"	C	2.64	485	0.13	0.59	0.00	0.18	22	0
4	"	2617.94	"	"	C	2.74	480	0.14	0.61	0.00	0.19	22	0
3	"	2773.93	"	"	C	2.25	493	0.12	0.64	0.00	0.16	28	0
2	"	2957.88	" (Barfield Fm)	"	C	3.63	507	0.09	0.87	0.00	0.09	24	0
18	Cockatoo Creek-1	1430.57	BWG (BCM)	Carb. shale	C	9.86	451	0.85	11.9	0.00	0.07	120	0
17	"	2484.15	BCG (Flat Top Fm)	Mudstone	C	0.69	[400]	0.00	0.04	0.00	0.00	6	0
16	"	2725.42	" (Barfield Fm)	"	C	3.65	493	0.41	1.29	0.02	0.24	35	1
15	"	3132.25	" "	"	C	1.98	493	0.02	0.18	0.00	0.10	9	0
14	"	3335.40	" "	"	C	0.74	493	0.00	0.04	0.00	0.00	5	0
13	"	3466.85	" "	"	C	1.35	505	0.00	0.04	0.00	0.00	3	0
23	Flinton-1	1676-1680	WCM	Coal	Cut	65.2	424	22.2	305.1	16.1	0.07	468	25
22	"	2423.46	Rewan Group	Siltstone	C	0.06	[412]	0.00	0.00	0.00	0.00	0.0	0
21	"	2574.26	BWG (BCM)	Carb. siltst.	C	5.05	431	2.00	14.6	0.79	0.12	290	16
20	"	2682-2688	" (BCM)	Coal	C	50.0	443	10.4	120.7	4.39	0.08	241	9
19	"	2748.32	BCG	Siltstone	Cut	0.97	[434]	0.05	0.08	0.28	0.38	8	29
32	Meeleebee-1	302-305	WCM	Coal	Cut	68.0	423	0.22	259.8	27.6	0.04	382	41
31	"	309.1	"	Mudstone	C	2.95	428	0.24	10.66	0.51	0.02	361	17
30	"	309.5	"	Coal	C	66.8	423	19.7	285.2	19.9	0.06	427	30
29	"	789.3	Precipice Sst	Mudstone	C	2.06	431	0.17	8.40	0.12	0.02	408	6
28	"	1122-1125	BCM?	Coal	Cut	71.2	431	12.6	160.3	13.9	0.07	225	20
27	"	1141.3	BWG	Mudstone	C	1.97	443	0.15	1.41	0.09	0.10	72	5
26	"	1183-1186	"	Carb. shale	Cut	39.3	432	4.85	81.91	5.98	0.06	208	15
25	"	1247.26	"	Siltstone	C	1.04	434	0.16	0.53	7.96	0.24	51	765
24	"	1361.70	BCG	Mudstone	C	1.86	431	0.12	0.33	0.00	0.27	18	0

Table 4.1(b) Rock-Eval pyrolysis and TOC data, Snake Creek Mudstone, southern Taroom Trough

Sample No.	Well Name	Depth (m)	Lithology	Sample Type	TOC (%)	T_{max} (°C)	S1	S2	S3	PI	HI	OI
33	Amoolee-1	2463-2487.2	Mudstone	Cut	2.33	439	0.17	4.25	0.19	0.04	182	8
			"	M	3.20	438	0.17	5.45	0.44	0.03	170	14
			"	S	0.38	436	0.03	0.25	0.00	0.11	65	0
34	Dulacca-1	1877.6-1905	"	Cut	2.19	436	0.25	2.39	0.92	0.08	132	42
			"	M	1.25	432	0.14	1.83	0.09	0.07	154	7
35	Flinton-1	2347-2371.3	"	Cut	2.52	434	0.23	4.20	0.36	0.05	167	14
			"	M	2.55	438	0.17	5.45	0.22	0.03	214	9
			"	S	0.14	[442]	0.05	0.05	0.00	0.50	36	0
36	Sussex D-1	2374.4-2390	"	Cut	1.83	438	0.16	3.19	1.60	0.05	174	87
			"	M	1.74	433	0.13	2.65	0.07	0.05	152	4
37	Teelba-1	2051.3-2076	"	Cut	1.38	436	0.10	1.67	0.53	0.06	120	38
			"	M	1.27	432	0.09	1.29	0.00	0.07	102	0
38	Tiggrigie Creek-1	1203-1233	"	Cut	1.47	436	5.15	2.64	0.88	0.66	180	60
			"	M	1.63	437	3.37	2.91	0.53	0.54	179	33
39	Bellbird-1	224-2262	"	Cut	1.12	436	0.08	0.98	0.08	0.08	88	7
			"	M	1.44	435	0.05	0.56	0.17	0.08	39	12
40	Bengalla-1	1563.6-1579	"	Cut	1.32	438	0.13	1.91	0.70	0.06	145	53
			"	M	1.44	437	0.13	2.06	0.50	0.06	143	35
41	Glenhaughton-1	585.2-609.6	"	Cut	1.07	439	0.04	0.96	0.44	0.04	90	41
			"	M	1.42	440	0.04	1.35	0.59	0.03	95	42
			"	S	0.40	436	0.00	0.28	0.00	0.03	70	0
42	Inglestone-1	2718-2748	"	Cut	1.63	435	0.19	3.41	0.03	0.05	209	2
43	Apple Tree-1	1844-1859.3	"	Cut	1.48	436	0.04	1.48	0.56	0.03	100	38
			"	M	0.85	436	0.05	0.37	0.33	0.12	44	39
			"	S	0.32	439	0.01	0.13	0.00	0.07	41	0
44	Booberanna-1	2155-2170.2	"	Cut	1.59	435	0.08	1.77	0.33	0.04	111	21
			"	M	1.22	435	0.05	1.41	1.48	0.03	116	122
45	Cabawin-1	2255.5-2271	"	Cut	1.83	439	0.18	2.19	1.10	0.08	120	60
			"	M	1.26	439	0.09	1.22	0.92	0.07	97	73
			"	S	0.11	[442]	0.02	0.03	0.00	0.40	25	0
46	Muggleton-1	1417-1436	"	Cut	1.39	436	0.09	1.42	2.02	0.06	102	145
			"	M	1.37	435	0.06	1.18	3.14	0.05	86	229
47	Snake Creek-1	1521-1534.4	"	C	3.38	429	0.59	5.57	0.00	0.10	165	0
48	Red Cap-1	2155-2178.1	Siltstone	C	0.66	438	0.04	0.40	0.40	0.09	61	61
49	Borah Creek-3	1613	Mudstone	C	2.08	434	0.28	1.93	1.10	0.13	93	53
50	Taylor-8	1978-2002	"	C	1.94	437	0.18	2.54	0.00	0.07	131	0
51	Taylor-13	1990.4-2010	"	C	1.82	436	0.03	1.90	0.00	0.02	104	0

Table 4.1(b) Rock-Eval pyrolysis and TOC data, Snake Creek Mudstone, southern Taroom Trough (continued)

Sample No	Well Name	Depth (m)	Lithology	Sample Type	TOC (%)	T_{max} (°C)	S1	S2	S3	PI	HI	OI
52	Weeyan-1	1878.5-1883.8	"	C	1.45	438	0.14	1.81	1.00	0.07	125	69
53	Borah Creek-3	1614	"	C	2.54	434	0.40	5.67	0.39	0.07	223	15
54	Beardmore-2	1834.9-1853.2	"	C	1.50	435	0.04	1.11	0.00	0.04	74	0
55	Causeway-1	1984.2-2002.8	"	C	1.33	437	0.06	1.06	1.80	0.05	80	135
56	Taroom-14	550-591.7	"	C	1.86	437	0.07	2.08	0.55	0.03	112	30
57	Taroom12-12A	620.5-636	"	C	1.47	436	0.05	1.59	2.88	0.03	108	196
58	Tinker-2	2078.3-2100.4	"	C	1.64	436	0.16	3.97	0.00	0.04	242	0
59	Waroon-1	2080	"	C	2.26	431	0.33	1.78	5.37	0.16	79	238
60	Waroon-3	2075.2-2098	"	C	1.75	439	0.13	2.11	1.01	0.06	121	58
61	Fairymount-3	2026.2-2041.9	"	C	1.83	440	0.13	2.00	0.39	0.06	109	21
62	Fairymount-4	2018.6-2034.2	"	C	1.79	439	0.11	1.95	0.39	0.05	109	22
63	Glenearn North-1	1838.7-1839.8	"	C	1.63	433	0.26	2.58	0.00	0.09	158	0
64	Borah Creek-4	1487.4-1494.7	"	C	1.68	439	0.45	4.43	1.12	0.09	264	67
65	Namarah-2	2191-2213	Siltstone	C	0.12	[433]	0.00	0.03	0.00	0.00	25	0
66	McGregor-1	1848.2-1854.5	Mudstone	C	2.92	436	0.07	2.07	2.29	0.03	71	78
67	Hollow Tree-1	1802.9-1804.4	"	C	1.73	435	0.02	1.99	0.00	0.01	115	0
68	Rednook-1	2184.5-2205	"	C	1.26	438	0.06	1.05	0.00	0.05	83	0
69	Rocky Glen-1	2000-2018.5	"	C	1.48	437	0.08	1.46	1.61	0.05	99	109
70	Renlim-1	1884-1898	Siltstone	C	0.72	426	0.00	0.13	0.00	0.00	18	0
71	Newington-2	1487.4-1494.7	Mudstone	C	2.00	434	0.58	2.84	0.00	0.17	142	0
72	Yellowbank Nth-1	1860-1863	"	C	1.84	438	0.09	1.97	0.53	0.04	107	29
73	Harbour-1	1965-1980.5	"	C	1.65	439	0.09	1.83	0.38	0.05	111	23

Cut = Whole rock cuttings; C = Whole rock core; M = Mudstone fraction, S = Sandstone/siltstone fraction
BCG = Back Creek Group, BWG = Blackwater Group, BCM = Baralaba Coal Measures, WCM = Walloon Coal Measures

Rock-Eval parameters (Peters, 1986):
S1 = mg h'c/g rock = the amount of free hydrocarbons which can be distilled from one gram of rock.
S2 = mg h'c/g rock = the amount of hydrocarbons (plus resins and asphaltenes) released thermally from the kerogen.
S3 = mg CO_2/g rock = the amount of carbon dioxide released thermally from the kerogen.
HI = Hydrogen Index = (S2/TOC) x 100 (mg h'c/g TOC)
OI = Oxygen Index = (S3/TOC) x 100 (mg CO_2/g TOC)
PI = Production Index = S1/(S1+S2)
T_{max} (°C) = The pyrolysis temperature at which the maximum amount of S2 hydrocarbons is generated. Square brackets indicate unreliable T_{max} measurements because of very low S2 value.
TOC = Total organic carbon (wt%).

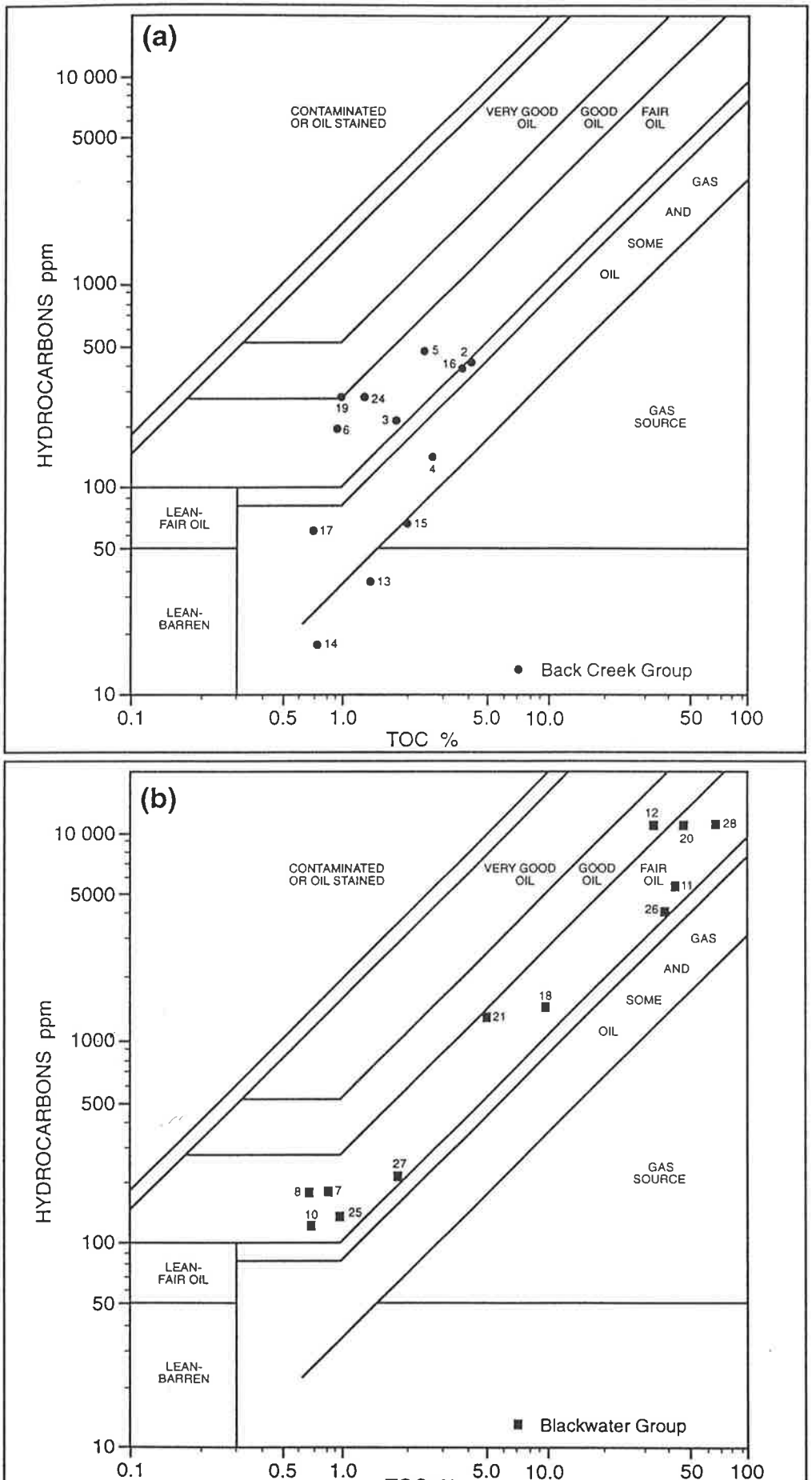

Figure 4.1 Source-rock-richness plots: (a) Back Creek Group, and (b) Blackwater Group (including Gyranda Formation), southern Taroom Trough.

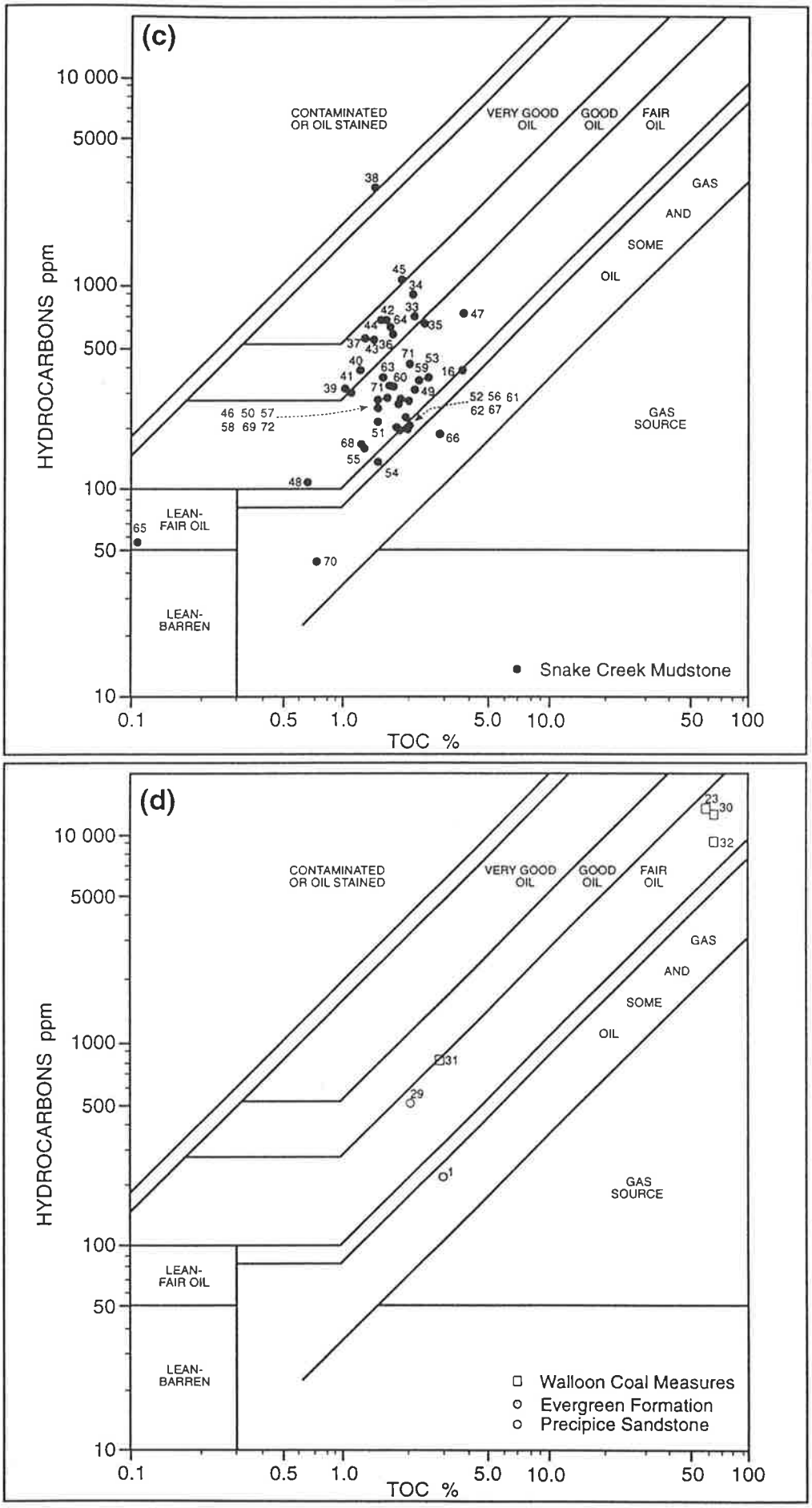

Figure 4.1 Source-rock-richness plots: (c) Triassic Snake Creek Mudstone, and (d) Jurassic Precipice Sandstone, Evergreen Formation and Walloon Coal Measures.

Coals of the Baralaba Coal Measures (BCM), represented by samples #20 and 28, have very good organic richness (TOC = 50-71%, S1+S2 = 131-173 kg h'c/tonne: Table 4.1). Other carbonaceous sediments in the Blackwater Group (BWG) also have good to very good organic carbon contents (TOC = 1-45%) with genetic potential ranging from poor to very good (S1+S2 = 0.7-91 kg h'c/tonne). They are rich enough to be fair to good oil-source rocks (Fig. 4.1b).

The vast majority of the 41 SCM samples examined (Table 4.1b) have good to very good organic richness (TOC = 1.1-3.5%) and hydrocarbon contents indicative of fair to very good source potential for oil (Fig. 4.1c). Siltstone intervals in the SCM from three wells are too lean (TOC ≤ 0.7%) to be effective source rocks. Throughout the Taroom Trough (notably at Snake Creek-1, Amoolee-1, Flinton-1, Inglestone-1, Tinker-2 and Borah Creek-3 and -4), the SCM exhibits fair to good genetic potential (S1+S2 = 4-6 kg h'c/tonne: Table 4.1b). The SCM in Tiggrigie Creek-1 (sample #38; S1+S2 = 7.8 kg h'c/tonne: Table 4.1b) is, most likely, stained by oil which was used in the drilling process (C. Boreham, pers. comm. 1994). This is indicated by a low TOC value combined with a high extract yield and production index (TOC = 1.47%; EOM = 5928 ppm; PI = 0.7: Tables 4.1b and 4.2; Fig. 4.1c). Nearly half of its organic carbon is extractable (EOM = 403 mg/g TOC) which is inconsistent with its low T_{max} value (436°C).

Mudstone from the Evergreen Formation (sample #1; TOC = 2.9%, S1+S2 = 2.1 kg h'c/tonne) has very good gas potential, whereas that from the Precipice Sandstone (sample #29; TOC = 2.1%, S1+S2 = 8.6 kg h'c/tonne) also has a very good organic richness and a fair oil potential (Table 4.1a, Fig. 4.1d). The greatest extractable hydrocarbon yields were obtained from the Middle Jurassic Walloon Coal Measures (WCM) and associated carbonaceous siltstone. The WCM samples (#23, 30, 32: TOC = 65-68%) have very high potential hydrocarbon yields (S1+S2 = 270-327 kg h'c/tonne: Table 4.1a). A carbonaceous mudstone within the WCM (sample #31: TOC = 3%, S1+S2 = 11.2 kg h'c/tonne) is sufficiently rich in hydrocarbons to be a good oil source (Fig. 4.1d).

4.3 Kerogen type and maturity

4.3.1 Back Creek Group

Based on T_{max} data, the BCG in the northern part of the southern Taroom Trough is overmature and is currently within the gas window (Fig. 4.2a). A T_{max} of 493°C is representative of this overmaturity in Cockatoo Creek-1 (Table 4.1a) and is compatible

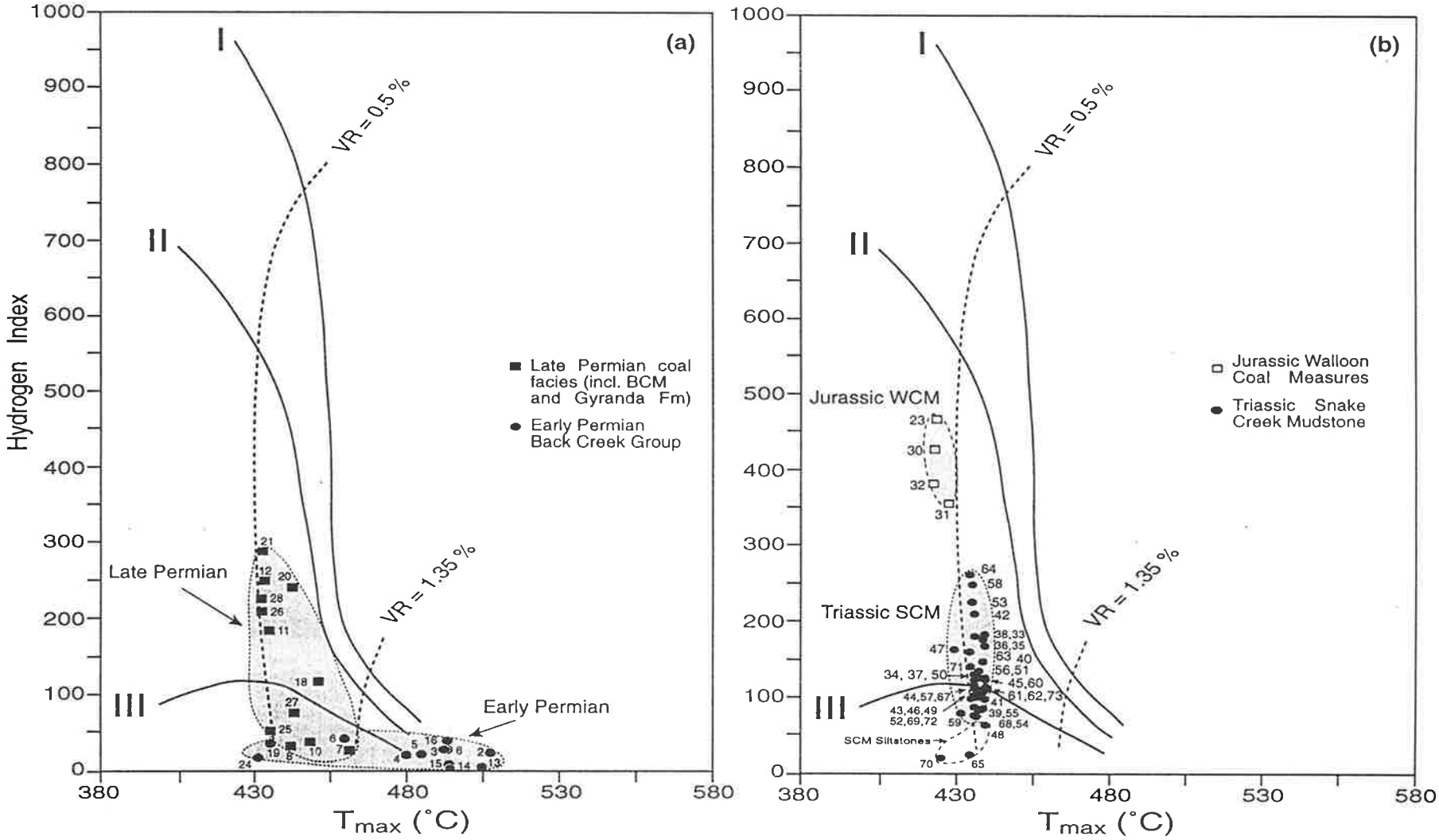

Figure 4.2 HI-T_{max} plot for (a) Permian Back Creek and Blackwater Groups and (b) Triassic Snake Creek Mudstone and Jurassic Walloon Coal Measures.

with vitrinite reflectance values of 1.5-2.3% (QPED, 1994), very low values of hydrogen index (HI = 3-44), poor genetic potential (S1+S2 = 0-1.7 kg h'c/tonne: Table 4.1a), and minimal C_{15+} hydrocarbon yields (2-11 mg/g TOC: Table 4.2). These data imply that the bulk of the available hydrocarbons have been generated and have subsequently migrated out of these rocks. Thermal maturation modelling of these well sections shows that hydrocarbon generation and expulsion from the BCG culminated in the Triassic (see Chapter 8).

Low pristane/*n*-C_{17} ($\leq$ 0.6) and phytane/*n*-C_{18} ($\leq$ 0.2) values in the BCG alkanes from Cockatoo Creek-1 and Burunga-1 (Table 4.2; Fig. 4.3) all indicate organic matter of high maturity (*cf.* Claypool et al., 1978). Notwithstanding the slight predominance of odd-over-even carbon-numbered *n*-alkanes (OEP) in two samples (e.g. in samples #4 and 15: Fig. 4.3), the striking features are the absence of OEP and (except in sample #2) their unimodal *n*-alkane distributions which maximise in the lower molecular weight range (C_{17} - C_{21}) and decline smoothly towards higher molecular weight *n*-alkanes. This type of profile can be interpreted as further evidence of overmaturity in poor quality, predominantly terrestrial, organic matter (*cf.* Allan and Douglas, 1977; Radke et al., 1980). A marine influence, possibly associated with carbonate deposition, is indicated by an even carbon-number predominance among the C_{15}-C_{20} *n*-alkanes, and by low pristane/phytane ratios (pr/ph $\leq$ 1.2) in the lower part of the sequence at Cockatoo Creek-1 (samples #13, 14 and 15: Fig. 4.3). Based on the non-waxy nature of most of *n*-alkane distributions, much of the BCG organic matter is inferred to be of algal/bacterial origin (Eglinton and Hamilton, 1963). Organic petrological investigation of the BCG revealed remnant acritarchs and phytoplankton in the Flat Top Formation (Plate VI c, e, and f). However, the only recognisable macerals in the underlying and more mature Barfield Formation are highly reflecting vitrinite and inertinite (Plate VI a, b, and d). This anomaly is most likely due to the overmaturity of these rocks, making their source input extremely difficult to identify, either from their alkane distributions or by reflected light microscopy. Most of the BCG section in Cockatoo Creek-1 and Burunga-1 lies beyond the medium-volatile bituminous stage and, therefore, all its liptinites will have been converted to rank-inertinite and micrinite (Plate VI). The low Rock-Eval pyrolysis yield, represented by low HI values (Table 4.1a) as discussed above, is consistent with overmature organic matter of low reactivity. Hence, thermal maturation has most likely obscured the original maceral composition, and resulted in *n*-alkane distributions maximising in the lower molecular weight range (Fig. 4.3).

A steady decrease in the T_{max} values upwards through the BCG (as well as the overlying BWG) is noticed in Burunga-1 (Fig. 4.4). The lowermost sample examined (at 2958 m depth) has a T_{max} = 507°C whereas the uppermost BCG (at 2123 m depth) has a T_{max} value of 460°C indicating that the bulk of the section is within the gas generation

Table 4.2 Extract yield and composition, southern Taroom Trough

Sample No.	TOC %	EOM ppm	EOM mg g^{-1}TOC	SATURATES ppm	SATURATES % EOM	AROMATICS ppm	AROMATICS %EOM	NSO ppm	NSO %EOM	ASPHALTENE ppm	ASPHALTENE %EOM	HYDROCARBONS ppm	HYDROCARBONS mgg^{-1}TOC	HYDROCARBONS %EOM	Sat Arom	*n*-alkane maximum	Pr *n*-C$_{17}$	Ph *n*-C$_{18}$	Pr Ph	CPI*
Permian and Jurassic source rocks																				
Burunga-1																				
1	2.91	1132	39	114	10.1	107	9.5	410	36.2	501	44.2	221	8	19.6	1.1	C_{25},C_{27}	0.6	0.3	2.5	2.7
11	44.70	26897	60	241	9.0	2776	10.3	18422	68.5	3287	12.2	5188	12	19.3	0.1	C_{14},C_{23}	0.8	0.1	5.8	1.9
12	28.80	34542	120	7326	21.2	4393	12.7	18674	54.1	4149	12.0	11719	41	33.9	1.7	C_{23}	0.8	0.1	6.3	1.3
9	0.15	242	161	24	9.9	28	11.6	123	50.8	66	27.7	52	35	21.5	0.9	C_{18}	0.3	0.1	1.9	1.6
10	0.71	742	105	34	4.6	139	18.7	485	65.4	84	11.3	173	24	23.3	0.2	C_{18}	0.6	0.2	2.3	1.3
8	0.70	516	74	66	12.8	126	24.4	159	30.8	165	32.0	192	27	37.2	0.5	C_{19}	1.4	0.2	5.3	1.4
7	0.85	652	77	79	12.1	113	17.3	250	38.3	210	32.3	192	23	29.4	0.7	C_{18}	0.5	0.4	2.8	1.5
6	0.96	952	99	52	5.5	148	15.6	330	34.7	422	44.2	200	21	21.1	0.4	C_{18}-C_{20}	0.3	0.1	2.2	1.1
5	2.64	558	21	373	66.9	114	20.4	61	10.9	10	1.8	487	18	87.3	3.3	C_{17}	1.0	0.1	8.6	n.d
4	2.74	569	21	34	6.0	127	22.3	149	26.2	259	45.5	161	6	28.3	0.3	C_{17}	0.3	0.1	1.9	1.4
3	2.25	629	28	73	10.1	140	19.4	186	25.8	230	44.7	213	10	29.5	0.5	C_{18}	0.3	0.1	2.7	1.6
2	3.63	769	21	56	7.3	350	45.5	307	39.9	56	7.3	406	11	52.8	0.2	C_{18}	0.3	0.2	1.3	1.2
Cockatoo Creek-1																				
18	9.86	7981	81	471	5.9	979	12.3	5211	65.3	1320	16.5	1450	15	18.2	0.5	C_{23},C_{25}	1.3	0.2	6.9	1.4
17	0.69	326	47	28	8.6	37	11.4	155	47.6	106	32.4	95	9	20.0	0.8	C_{18}	0.5	0.2	1.6	1.2
16	3.65	1021	28	39	3.8	368	36.0	568	55.6	46	4.6	470	11	39.8	0.1	C_{18}	0.6	0.2	2.6	1.1
15	1.98	270	14	7	2.6	64	23.7	112	41.5	87	32.2	71	4	26.3	0.1	$C_{20\text{-}21}$	0.4	0.2	1.2	1.5
14	0.74	136	18	4	2.9	14	10.3	61	44.9	57	41.9	18	2	13.2	0.3	C_{18}	0.3	0.1	0.9	1.6
13	1.35	134	10	5	3.7	31	23.5	46	34.3	52	38.9	36	3	26.8	0.2	C_{20}	0.2	0.1	0.9	1.2
Flinton-1																				
23	65.20	61608	95	11430	18.6	7933	12.9	26183	42.5	16062	26.0	19363	30	31.5	1.4	C_{25}	1.9	0.7	2.3	1.6
22	0.06	241	402	1	0.4	6	2.5	223	92.5	11	4.6	7	12	2.9	0.2	C_{18}	0.3	0.2	1.2	1.2
21	5.05	7396	147	331	4.5	1036	14.0	4214	60.0	1815	21.5	1369	27	18.5	0.3	C_{17}	0.2	0.2	1.2	1.1
20	50.00	44942	90	3071	6.8	7392	16.5	17895	39.8	16584	36.9	10463	21	23.3	0.4	C_{19}	0.8	0.1	6.1	1.0
19	0.97	767	79	95	12.4	196	25.6	388	50.6	88	11.4	291	30	38.0	0.5	C_{17}-C_{19}	0.7	0.3	3.4	1.1
Meeleebee-1																				
32	68.00	66119	97	3583	5.4	5389	8.2	16712	25.3	40435	61.1	8972	13	13.6	0.7	C_{20}	1.1	2.6	0.6	1.2
31	2.95	2152	73	475	22.1	336	15.6	646	30.0	695	32.3	811	28	37.7	1.4	C_{25}	0.7	0.1	5.3	1.7
30	66.80	70095	105	5908	8.4	8187	11.7	26041	37.2	29958	42.7	14095	21	20.1	0.7	C_{25}	1.3	0.2	5.5	1.6
29	2.06	1541	75	303	19.7	217	14.1	621	40.3	400	25.9	520	25	33.8	1.4	C_{29}	0.8	0.1	5.9	1.4
28	71.20	54258	76	3939	7.3	8640	15.9	21823	40.2	19856	36.6	12579	18	23.2	0.5	C_{17}	0.5	0.1	4.2	1.0
27	1.97	1903	97	40	2.1	191	10.0	1632	85.8	40	2.1	231	12	12.1	0.2	C_{17}	1.0	0.3	3.7	1.0
26	39.30	27476	70	1134	4.1	2825	10.3	10998	40.0	12519	45.6	3959	10	14.4	0.4	C_{15}-C_{17}	1.0	0.2	5.6	1.0
25	1.04	1281	123	48	3.8	105	8.2	1033	80.6	95	7.4	153	15	12.0	0.5	C_{16}-C_{18}	1.1	0.4	2.5	1.0
24	1.86	1172	63	81	6.9	204	17.4	792	67.6	95	8.1	285	15	24.3	0.3	C_{19}	0.6	0.2	2.1	1.1

Table 4.2 Extract yield and composition, southern Taroom Trough (continued)

Sample No.	TOC %	EOM ppm	EOM mg g^{-1}TOC	SATURATES ppm	SATURATES % EOM	AROMATICS ppm	AROMATICS %EOM	NSO ppm	NSO %EOM	ASPHALTENE ppm	ASPHALTENE %EOM	HYDROCARBONS ppm	HYDROCARBONS mgg^{-1}TOC	HYDROCARBONS %EOM	Sat/Arom	*n*-alkane maximum	Pr/*n*-C$_{17}$	Ph/*n*-C$_{18}$	R_{22}^{S} Index	Pr/Ph	CPI*	Organic Facies†
Snake Creek Mudstone																						
Algal-rich facies																						
34	2.19	2300	105	629	27.3	259	11.3	926	40.3	486	21.1	888	41	38.6	2.4	C_{17-18}	0.7	0.2	1.5	4.5	1.9	A
37	1.38	1575	114	356	22.6	193	12.3	752	47.8	274	17.3	549	40	34.9	1.8	C_{17}	0.8	0.2	1.4	5.2	1.6	A
38	1.47	5928	403	2195	37.0	582	9.8	1944	32.8	1207	20.4	2777	189	47.0	3.8	C_{19}	0.9	0.2	n.d	3.6	n.d	A
39	1.12	2052	183	200	9.8	125	6.1	674	32.9	1053	51.2	325	29	15.9	1.6	C_{18}	0.8	0.2	0.8	4.2	2.0	A
40	1.32	3799	288	191	5.0	192	5.1	908	23.9	2508	66.0	383	29	10.1	1.0	C_{17}	0.8	0.2	0.9	3.9	1.3	A
41	1.07	1597	149	164	10.3	139	8.7	747	46.8	547	34.2	303	28	19.0	1.2	C_{17}	0.8	0.2	1.5	3.5	1.2	A
43	1.48	2240	151	172	7.7	366	16.3	1166	52.1	536	23.9	538	36	24.0	0.5	C_{18}	0.9	0.3	1.2	2.7	1.4	A
44	1.59	2331	147	444	19.1	264	11.3	763	32.7	860	36.9	708	45	30.4	1.7	C_{17-19}	0.9	0.3	0.6	3.8	1.9	A
46	1.39	2037	147	175	8.6	110	5.4	818	40.2	934	45.8	285	21	14.0	1.6	C_{17}	0.8	0.3	0.9	3.5	1.3	A
47	3.38	2971	88	168	5.7	554	18.6	1789	60.2	460	15.5	722	21	24.3	0.3	C_{18}	0.4	0.11	1.0	3.0	1.1	A
50	1.94	962	56	131	13.6	153	15.9	577	60.0	101	10.5	284	15	29.5	0.9	C_{19}	0.3	0.09	1.0	3.9	1.0	A
52	1.82	719	40	110	15.3	112	15.6	350	48.7	147	20.4	222	12	30.9	1.0	C_{17}	0.4	0.10	0.9	4.4	1.2	A
58	1.64	854	52	131	15.3	159	18.6	494	57.9	70	8.2	290	18	33.9	0.8	C_{18}	0.2	0.04	1.0	4.7	1.2	A
59	2.26	3101	137	74	2.4	281	9.1	1726	55.7	1020	32.8	355	16	11.5	0.3	C_{18}	0.2	0.06	1.0	1.7	1.2	A
60	1.75	1004	57	166	16.6	152	15.1	673	67.0	13	1.3	318	18	31.7	1.1	C_{18-19}	0.4	0.11	0.9	4.0	1.2	A
63	1.63	1337	82	169	12.6	186	13.9	501	37.5	481	36.0	355	22	26.5	0.9	C_{15}	0.1	0.05	0.9	3.1	1.2	A
Bacteria-rich facies																						
56	1.86	783	42	103	13.2	95	12.1	462	59.0	123	15.7	198	11	25.3	1.1	C_{21}	0.3	0.07	1.0	4.4	1.1	B
62	1.79	848	47	89	10.5	110	13.0	598	70.5	51	6.0	199	11	23.5	0.8	C_{21}	0.3	0.08	1.0	4.5	1.1	B
68	1.26	641	51	78	12.2	93	14.5	337	52.6	133	20.7	171	14	26.7	0.8	C_{21}	0.3	0.07	1.0	3.1	1.1	B
70	0.72	173	24	16	9.3	30	17.3	88	50.9	39	22.5	46	6	26.6	0.8	C_{21}	0.5	0.17	0.9	3.0	1.5	B
73	1.65	733	44	182	24.8	143	19.5	289	39.4	119	16.2	325	20	44.3	1.3	C_{21}	0.2	0.06	0.9	3.3	1.4	B
Higher plant-rich facies																						
33	2.33	2205	95	374	17.0	313	14.2	990	44.9	528	23.9	687	30	31.2	1.2	C_{25},C_{27}	0.9	0.3	1.1	4.1	1.7	C
35	2.52	2647	105	334	12.6	306	11.6	1419	53.6	588	22.2	640	25	24.2	1.1	C_{25},C_{27}	0.9	0.2	0.8	4.6	1.5	C
48	0.66	563	85	47	8.3	59	10.5	115	20.4	342	61.8	106	13	15.3	0.8	C_{25},C_{27}	0.4	0.16	0.9	1.5	1.3	C
54	1.50	532	36	55	10.3	83	15.6	359	67.5	35	6.6	138	9	25.9	0.7	C_{25},C_{27}	0.4	0.09	0.9	2.9	1.4	C
65	0.12	251	209	18	7.2	39	15.5	143	57.0	51	20.3	57	48	22.7	0.5	C_{29}	0.9	0.23	1.0	1.9	1.1	C
66	2.92	732	25	88	12.0	92	12.6	532	72.7	20	2.7	180	6	24.6	1.0	C_{27}	0.6	0.13	0.9	3.4	1.4	C
67	1.73	984	57	96	9.8	118	12.0	638	64.8	132	13.4	214	12	21.8	0.8	C_{27}	0.6	0.14	0.9	3.3	1.3	C
71	2.00	1529	44	18	1.2	392	25.6	1041	68.1	78	5.1	410	12	26.8	0.1	C_{29}	0.1	0.08	1.0	1.0	1.4	C
72	1.84	972	53	119	12.3	151	15.5	562	57.8	140	14.4	270	15	27.7	0.8	C_{23},C_{27}	0.5	0.11	0.7	2.0	1.2	C

Table 4.2 Extract yield and composition, southern Taroom Trough (continued)

Sample No.	TOC %	EOM ppm	EOM mg g^{-1}TOC	SATURATES ppm	SATURATES % EOM	AROMATICS ppm	AROMATICS %EOM	NSO ppm	NSO %EOM	ASPHALTENE ppm	ASPHALTENE %EOM	HYDROCARBONS ppm	HYDROCARBONS mgg^{-1}TOC	HYDROCARBONS %EOM	Sat Arom	*n*-alkane maximum	Pr n-C_{17}	Ph n-C_{18}	R_{22}§ Index	Pr Ph	CPI*	Organic Facies†
Mixed facies																						
36	1.83	1513	83	318	21.0	264	17.5	734	48.5	197	13.0	582	32	38.5	1.2	C_{17},C_{27}	0.8	0.2	0.8	4.8	1.5	A/C
42	1.63	3732	229	217	5.8	473	12.7	1533	1.1	1509	40.4	690	42	18.5	0.5	C_{18},C_{27}	0.9	0.3	0.9	3.5	1.6	A/C
45	1.83	2498	135	221	8.9	845	33.8	1020	40.8	412	16.5	1066	58	42.7	0.3	C_{17},C_{25}	0.6	0.2	0.9	3.1	1.4	A/C
49	2.08	1026	49	61	6.0	256	25.0	577	56.1	132	12.9	317	15	31.0	0.2	C_{18},C_{27}	0.6	0.15	1.0	3.3	1.1	A/C
51	1.45	621	43	91	14.7	126	20.3	326	52.4	78	12.6	217	15	35.0	0.7	C_{21-22}	0.3	0.09	0.9	2.5	1.1	A/B
53	2.54	1386	55	192	13.9	169	12.2	390	28.1	635	45.8	361	14	26.1	1.1	C_{19},C_{27}	0.8	0.14	1.0	4.6	1.3	A/C
55	1.33	434	33	76	17.6	91	21.1	243	60.0	24	1.3	167	13	38.7	0.8	C_{19},C_{21}	0.2	0.06	0.9	3.6	1.2	A/B
57	1.47	870	59	142	16.3	140	16.1	514	59.1	74	8.5	282	19	32.4	1.0	C_{19},C_{27}	0.4	0.09	0.9	4.4	1.3	A/C
61	1.83	786	43	93	11.8	103	13.1	541	68.8	49	6.2	196	11	24.9	0.8	C_{19},C_{21}	0.2	0.07	1.0	2.8	1.1	A/B
64	1.68	1786	106	262	14.7	355	19.9	1042	58.3	127	7.1	617	37	34.6	0.7	C_{18},C_{27}	0.7	0.11	0.9	5.6	1.1	A/C
69	1.48	688	47	102	14.8	167	24.3	260	37.8	159	23.1	269	18	39.1	0.6	C_{19},C_{21},C_{27}	0.4	0.11	0.9	4.0	1.2	ABC

* CPI for *n*-alkanes in the range C_{24}-C_{34}

† Organic facies classification based mainly on *n*-alkane and maceral distributions

§ R_{22} index = $2xC_{22}/(C_{21}+C_{23})$.....(ten Haven et al., 1985, 1988)

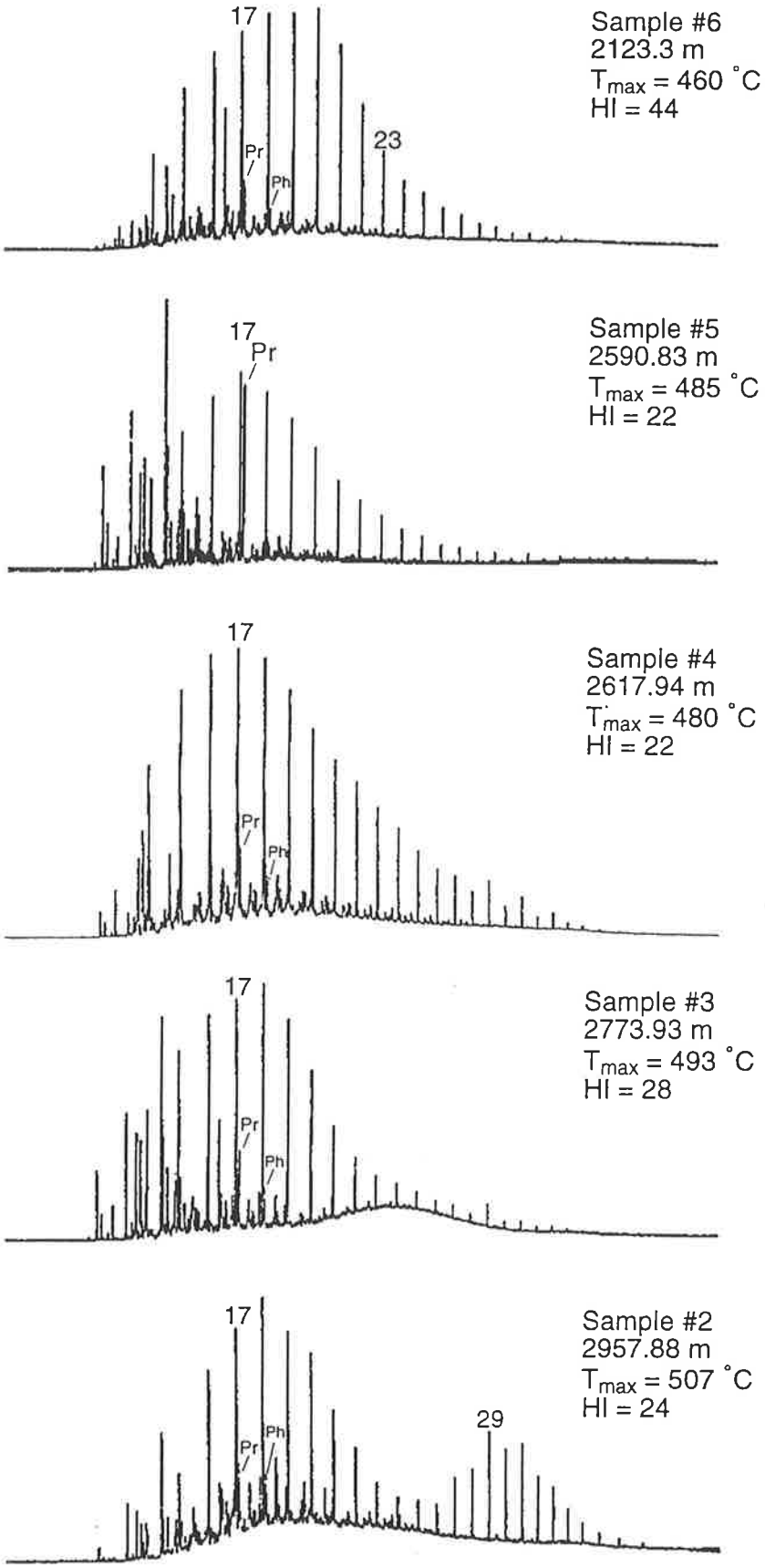

Figure 4.3 (a) Alkane distributions of Back Creek Group extracts, Burunga-1.

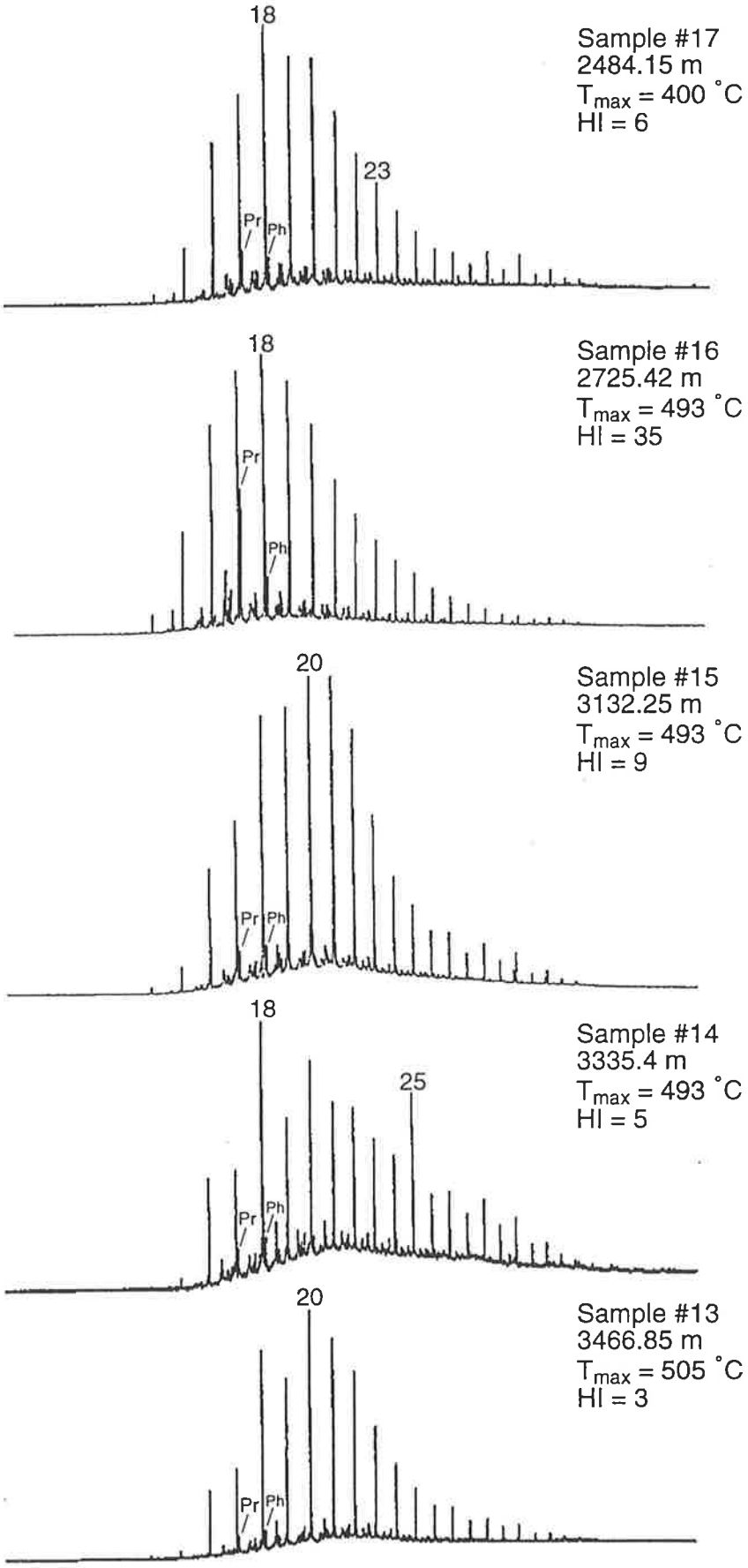

Figure 4.3 (b) Alkane distributions of Back Creek Group extracts, Cockatoo Creek-1. T_{max} value of sample #17 is unreliable (refer to Table 4.1).

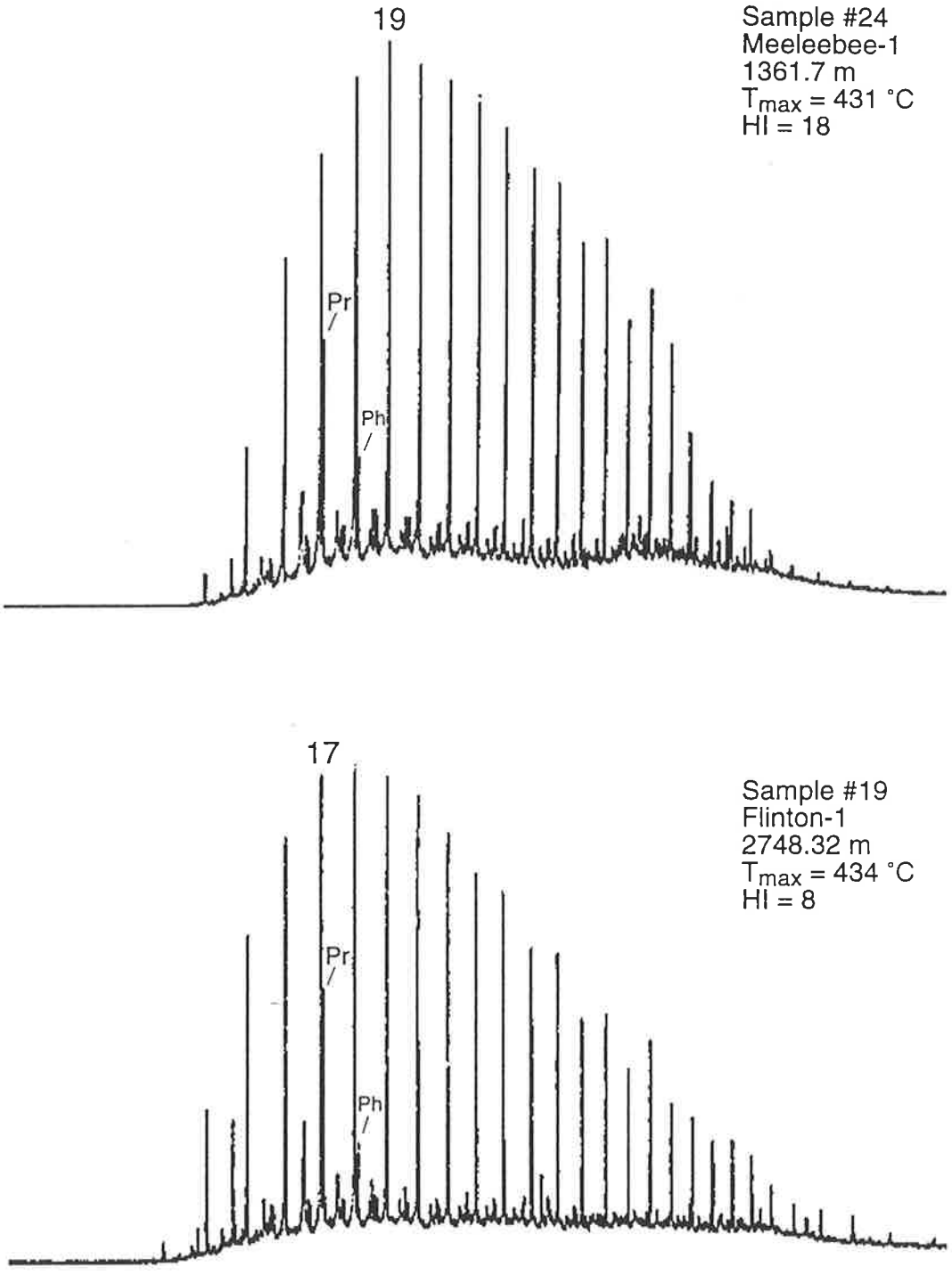

Figure 4.3 (c) Alkane distributions of Back Creek Group extracts in the western (Meeleebee-1) and southern (Flinton-1) Taroom Trough.

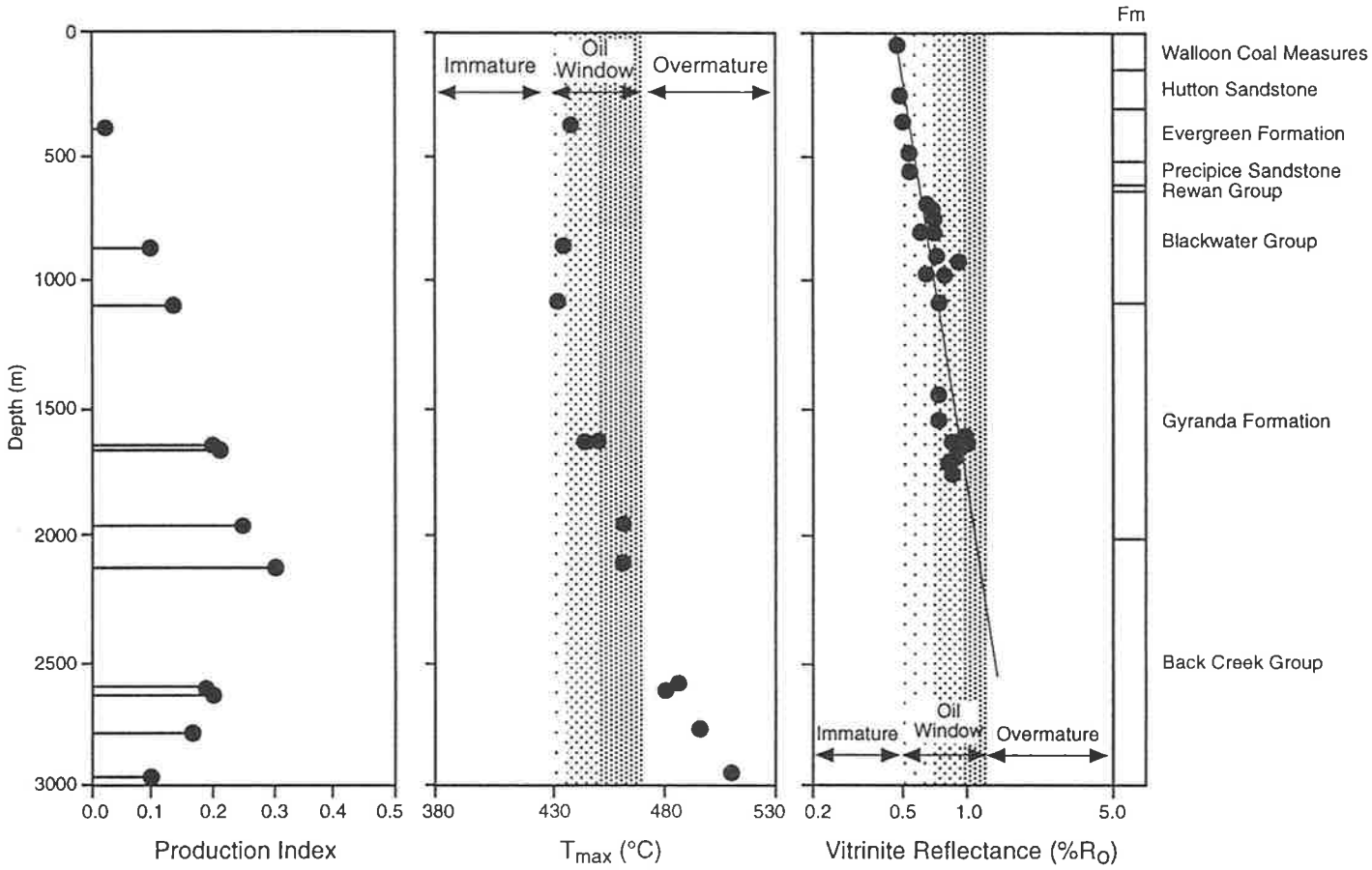

Figure 4.4 Evolution of selected maturity parameters with depth in Burunga-1. The Back Creek Group is late mature to overmature, whereas the Gyranda Formation is within the oil generation window.

window, with the upper part of the section having appropriate maturity for oil generation. At Scotia-1, just north of Burunga-1, gas is bleeding from the Gyranda Formation, whereas oil traces were observed in fractures within tuffaceous sandstone of the Back Creek Group, and in fractured basement.

Farther south along the axis of the Taroom Trough, the BCG in Flinton-1 (Fig. 1.2) exhibits a lower maturity level (within the oil window: R_O = 0.87%, T_{max} = 434°C, PI = 0.16) and, also, an enhanced input of land plant organic matter. This is indicated by the higher relative abundance of C_{23+} *n*-alkanes (sample #19, Fig. 4.3). The same phenomenon is noticed at the base of the BCG section in Burunga-1 where sample #2 shows a bimodal *n*-alkane distribution indicative of two major organic matter populations, algal/bacterial and land plant (Fig. 4.3). This is consistent with the fact that the BCG is a mosaic of marine and non-marine facies. However, the same maturity-dependent feature of decreasing abundance of higher molecular weight *n*-alkanes (*cf.* Tissot and Welte, 1984) and lower isoprenoid concentrations (*cf.* Alexander et al., 1981) is evident with increasing depth in all Permian sections examined, whether they be on the eastern (Cockatoo Creek-1, Burunga-1) or western (Meeleebee-1) flanks, or in the southern part (Flinton-1), of the Taroom Trough (Fig. 4.3).

The production indices of the BCG in Flinton-1 and Meeleebee-1 (PI = 0.16 and 0.27, respectively) are consistent with their location within the oil window. Meanwhile, the PI values for the BCG farther north at Cockatoo Creek-1 and in the lower BCG at Burunga-1 are between 0.01 and 0.24, with most of the values being less than 0.1 in Cockatoo Creek-1 (Table 4.1). These PI values are lower than expected for the indicated range of thermal maturity ($R_O \geq 1.55\%$), probably due to expulsion of the generated hydrocarbons out of these rocks (see also Chapter 8).

With decreasing sediment overburden and thickness of the Permian rocks to the west, the top of the BCG at 1361 m depth in Meeleebee-1 has attained a lower maturity level corresponding to the initial stage of oil generation (T_{max} = 431°C, PI = 0.26: Table 4.1a). However, the HI-T_{max} plot (Fig. 4.2a) shows that this mudstone, like all the other, more mature BCG samples, contains gas-prone Type III-IV kerogen (HI < 45).

4.3.2 Blackwater Group

Blackwater Group samples seem to plot within one distinct zone on the HI-T_{max} diagram (Fig. 4.2a). The lower part of the BWG shows a close association with the underlying BCG in terms of the similarity of their organic matter type (Type III-IV) and level of maturity (samples #6, 7, 8, 10, 25 and 27). Also, the Gyranda Formation at

Burunga-1 exhibits *n*-alkane distributions which maximise in the lower molecular weight range (C_{15}-C_{20}), and are similar to those of the underlying BCG (Fig. 4.5a). Where present, the BCM (uppermost BWG) offers an excellent source for both oil and gas (HI = 120-290). A bimodal naphthene hump or unresolved complex mixture (UCM) is prominent in the alkane chromatograms of two BWG mudstones from Meeleebee-1 (samples #25 and 27: Fig. 4.5b) and of a siltstone from the uppermost BWG in Flinton-1 (sample #21: Fig. 4.5c). This feature is generally absent, or much more muted, in the northern samples (Fig. 4.5a), consistent with their higher maturity. Predominant UCM is normally associated with less mature sediments (Powell and McKirdy, 1973a). The corresponding *n*-alkane distributions are controlled by both maturity and depositional facies. The less mature BCM exhibits predominance of pristane over phytane and/or *n*-C_{17}, associated with an *n*-alkane maximum at C_{23} or C_{25} (Fig. 4.5). This may also reflect increased inputs of higher plant materials. Better quality Type II/III organic matter occurs in the BWG at Burunga-1 (samples #11 and 12) and Meeleebee-1 (samples #26 and 28) and in the southern part of the Taroom Trough at Flinton-1 (samples #20 and 21) (Fig. 4.2a). These organic facies are rich in cutinite, resinite and liptodetrinite, with rare sporinite (Hawkins et al., 1992).

The BWG in the northern part of the study area is currently mature and within the oil window. In Burunga-1, T_{max} values of 444-461°C and production indices of 0.20-0.25 are typical of this maturity state. Even the BCM (uppermost BWG) is at the onset of oil window (T_{max} = 435°C, PI = 0.09-0.13). In Cockatoo Creek-1, the BCM is mature (T_{max} = 451°C) and the underlying section of the BWG is overmature. Farther north, this formation is mature enough to be generating wet gas, as indicated by vitrinite reflectance values of 1.49-1.61% in Glenhaughton-1 (Thomas et al., 1982; Hawkins et al., 1992). Petrographic examination of the BCM in Cockatoo Creek-1 revealed abundant resinite, sporinite, cutinite, liptodetrinite and desmocollinite with lesser amounts of telocollinite, gelovitrinite, fusinite and micrinite (see also Hawkins et al., 1992). The fluorescence of the liptinites (and in particular resinite) is subdued (Plate VI g and h), probably due to expulsion of much of their hydrocarbons. The BWG is initially mature on the western flank of the Taroom Trough in Meeleebee-1 (samples #25, 26 and 27) and at the southern end of the trough in Flinton-1 (samples #20 and 21) (Fig. 4.2).

4.3.3 Snake Creek Mudstone

All the SCM samples, representative alkane profiles of which are shown in Figure 4.6, contain initially mature (T_{max} = 429-440 °C) Type III or Type II/III kerogen (Fig. 4.2b). Although the available vitrinite reflectance data set (measured, or interpolated

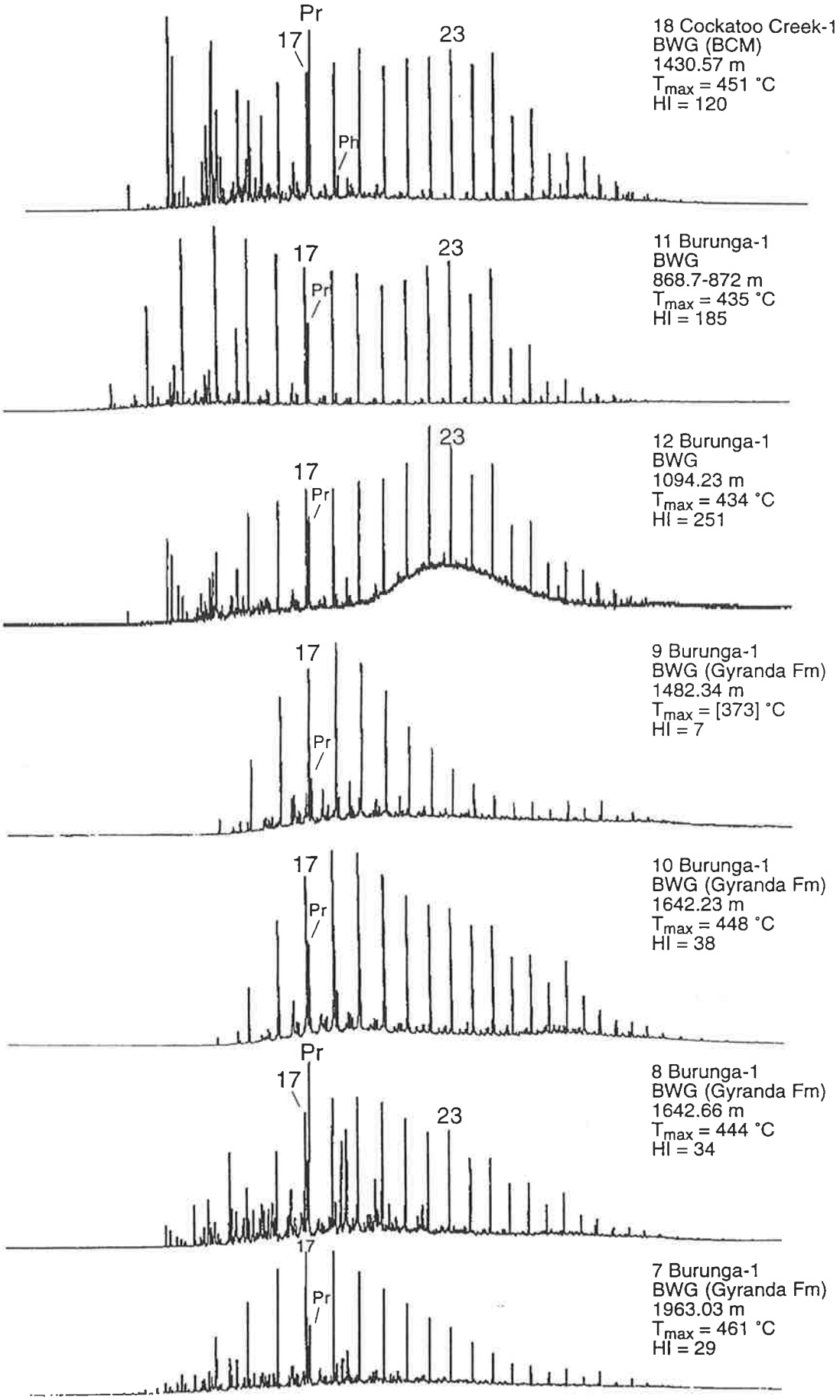

Figure 4.5 (a) Alkane distributions of the Late Permian Blackwater Group (BWG; including Baralaba Coal Measures 'BCM' and Gyranda Formation) in the northern part of the study area. T_{max} of sample #9 is unreliable.

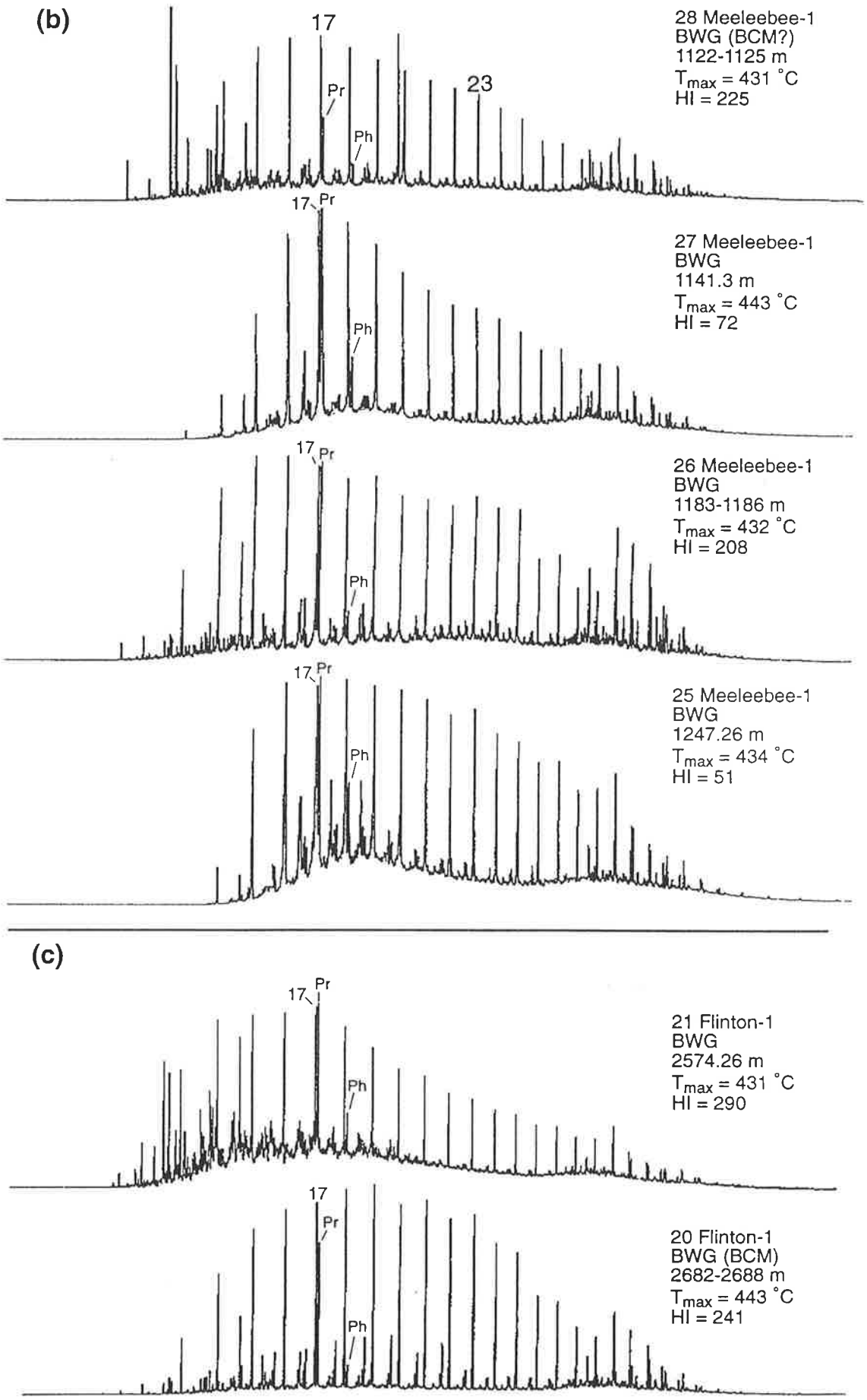

Figure 4.5 Alkane distributions of Blackwater Group extracts in the (b) western (Meeleebee-1) and (c) southern (Flinton-1) Taroom Trough.

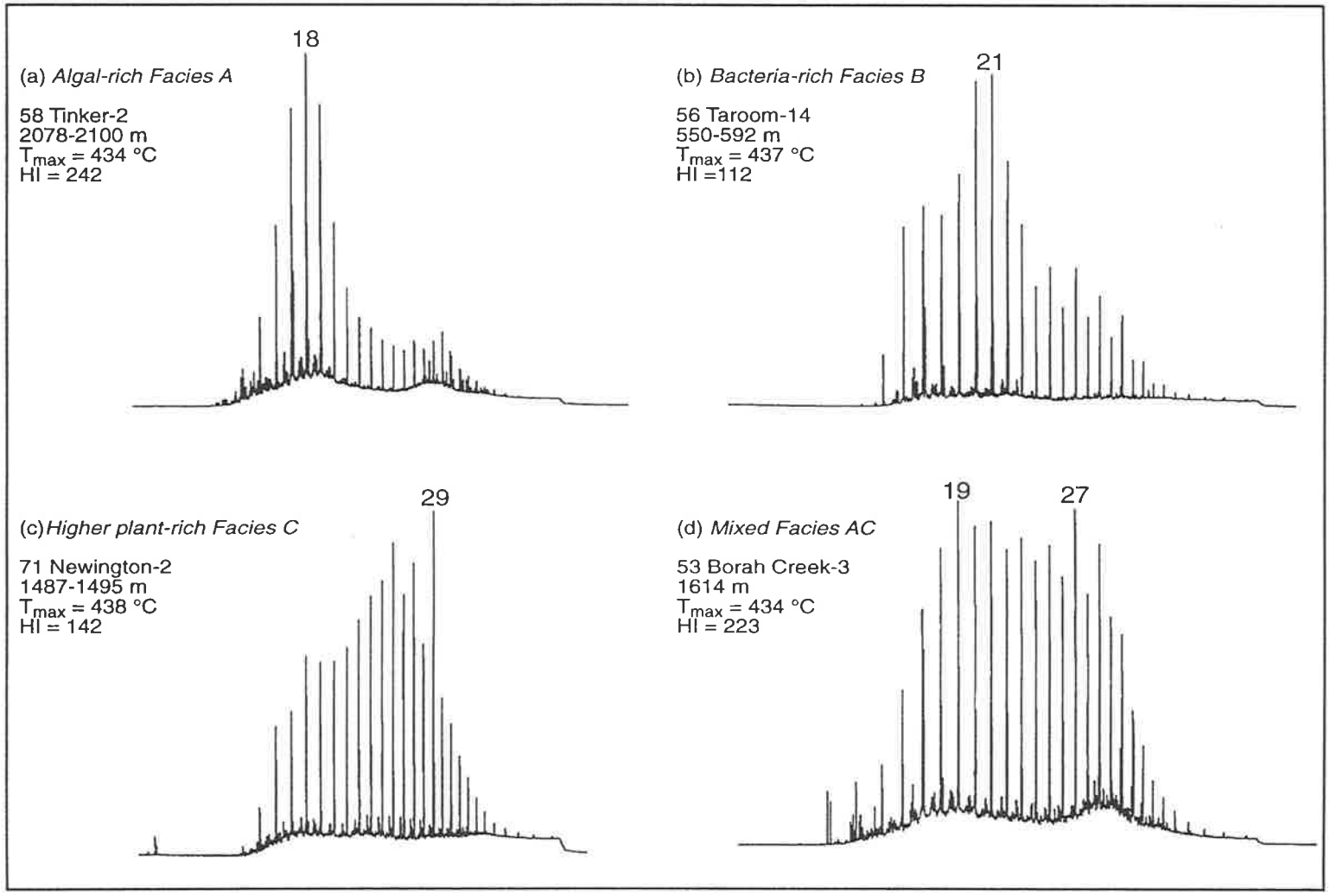

Figure 4.6 Representative alkane distributions of the Snake Creek Mudstone organic facies.

from the depth-reflectance profiles in 21 wells, Table 4.3) is small, it does indicate that this unit has passed the generation threshold for Type III kerogen (R_O = 0.7%) over the axial part of the trough, with the maximum reflectance in the vicinity of Inglestone-1 (Fig. 4.7). This maximum maturation level corresponds to the early mature stage of hydrocarbon generation for Type II/III kerogen.

The alkane profile of the SCM extract from Tiggrigie Creek-1 (PI = 0.54-0.66: Table 4.1b) is similar to that of mature oil, with a unimodal *n*-alkane profile maximising at *n*-C_{19} and the absence of C_{23+} *n*-alkanes. This is probably caused by contamination with the oil-based mud used in the drilling of this well. Similarly, high production index values (PI = 0.63-0.86) have been reported previously for the SCM, Moolayember Formation, Precipice Sandstone and Clematis Group, and attributed to contamination by oil additives (QPED, 1994).

Figure 4.8 is a contour map of hydrogen index data for the SCM in the southern Taroom Trough. It shows that this formation has its highest hydrocarbon-generating potential (HI > 200) in the southwestern part of the study area in the vicinity of Borah Creek-3 and -4, Tinker-2, Inglestone-1 and Flinton-1. Outside this 'sweet spot' the SCM has hydrogen indices in the range HI = 39-182. Where the formation is sandy/silty with TOC contents less than 1%, the HI drops to less than 20 (Table 4.1b). Low hydrogen indices for the SCM in some areas appear to be related to its higher content of vitrinite and, in particular, inertinite (Section 4.4.2). Furthermore, the HI in such continental facies is usually underestimated (Powell and Boreham, 1991). The different organic facies of the SCM (Fig. 4.6), and petrographic evidence of petroleum generation from these source rocks, are discussed in detail in Sections 4.4 and 4.5, respectively.

4.3.4 Jurassic mudstone and coal facies

The Early and Middle Jurassic units (Precipice Sandstone, Evergreen Formation and Walloon Coal Measures: Fig. 1.3) are immature all over the Surat Basin. Mudstone of the Precipice Sandstone in Meeleebee-1 shows low maturity (T_{max} = 431°C; PI = 0.02: Table 4.1a). Their C_{23+} *n*-alkanes display a marked odd-over-even carbon preference (CPI = 1.4: Table 4.2; Fig. 4.9a). Similar signs of immaturity are evident in the Evergreen Formation at Burunga-1 (CPI = 2.9: Fig. 4.9b). The vitrinite reflectance map of the Evergreen Formation (Thomas et al., 1982) demonstrates its immaturity in the northeastern side of the study area, with higher maturity (R_O = 0.7%) attained in the central part of the Taroom Trough and on the Roma Shelf. The WCM samples examined reveal low maturity ($T_{max} \leq 428$ °C, equivalent to $\leq$ 0.5% R_O). Their alkane profiles (Fig. 4.10) show a high concentration of pristane relative to *n*-C_{17} (pr/*n*-C_{17} = 1.1-1.9) and

Table 4.3 Measured and interpolated* vitrinite reflectance data for the Snake Creek Mudstone in 21 exploration wells, southern Taroom Trough

Well Name	Depth (m)	Vitrinite Reflectance (%)	
Amoolee-1	2463-2487.2	0.73	Measured
Apple Tree-1	1844-1859.3	0.68	Interpolated
Bellbird-1	224-2262	0.81	Interpolated
Bengalla-1	1563.6-1579	0.71	Interpolated
Booberanna-1	2155-2170.2	0.75	Measured
Cabawin-1	2255.5-2271	0.67	Interpolated
Dulacca-1	1877.6-1905	0.67	Interpolated
Flinton-1	2347-2371.3	0.79	Interpolated
Glenhaughton-1	585.2-609.6	0.74	Interpolated
Ingleston-1	2718-2748	0.89	Measured
Maintop-1	528-536	0.67	Interpolated
McGregor-1	1848.2-1854.5	0.56	Measured
Muggleton-1	1417-1436	0.75	Interpolated
Rednook-1	2184.5-2205	0.82	Interpolated
Snake Creek-1	1521-1534.4	0.72	Interpolated
Snake Creek-4	1506.7	0.73	Measured
Sussex Downs-1	2374.4-2390	0.70	Interpolated
Taroom-12-12A	620.5-636	0.68	Interpolated
Taroom-14	550-591.7	0.76	Measured
Teelba-1	2051.3-2076	0.80	Interpolated
Tiggrigie Creek-1	1203-1233	0.80	Interpolated

* Vitrinite reflectance interpolated from depth-reflectance profiles (data source: QPED, 1995)

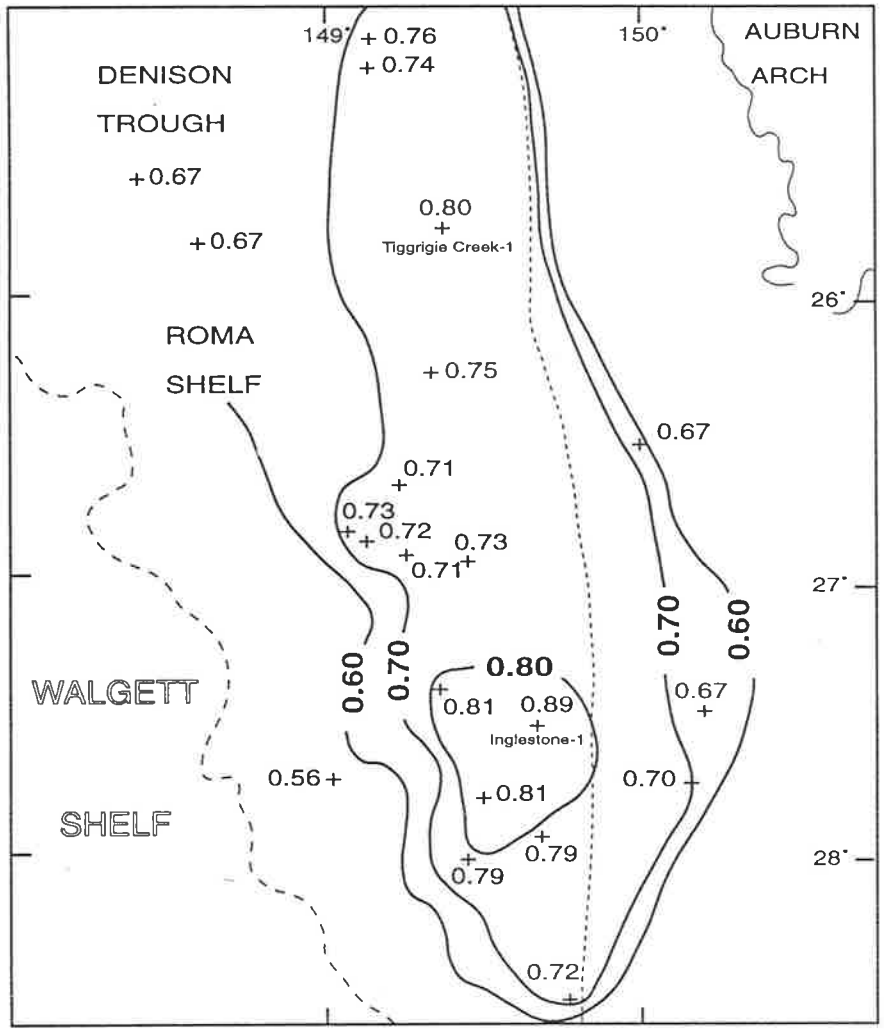

Figure 4.7 Vitrinite reflectance map of the Snake Creek Mudstone showing higher maturity towards the trough axis.

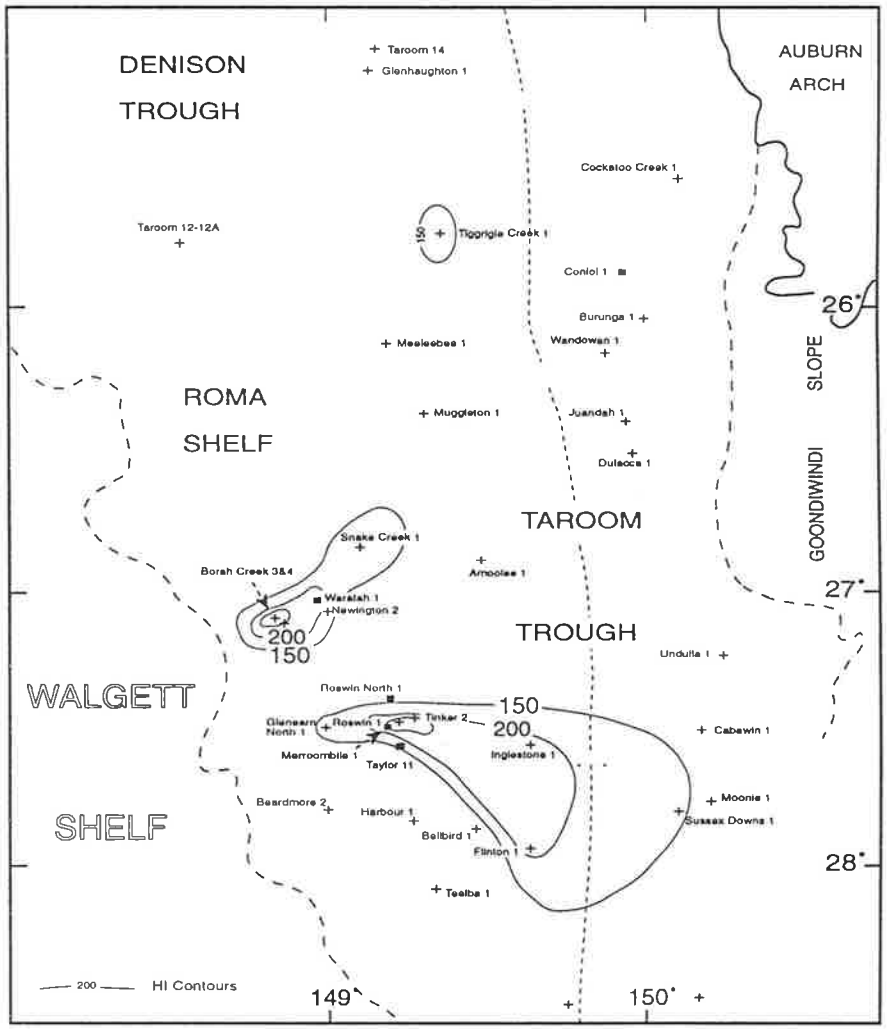

Figure 4.8 The hydrogen index map of the Snake Creek Mudstone showing the highest hydrocarbon-generating potential in Borah Creek field, Roswin-1 and Tinker-2 wells.

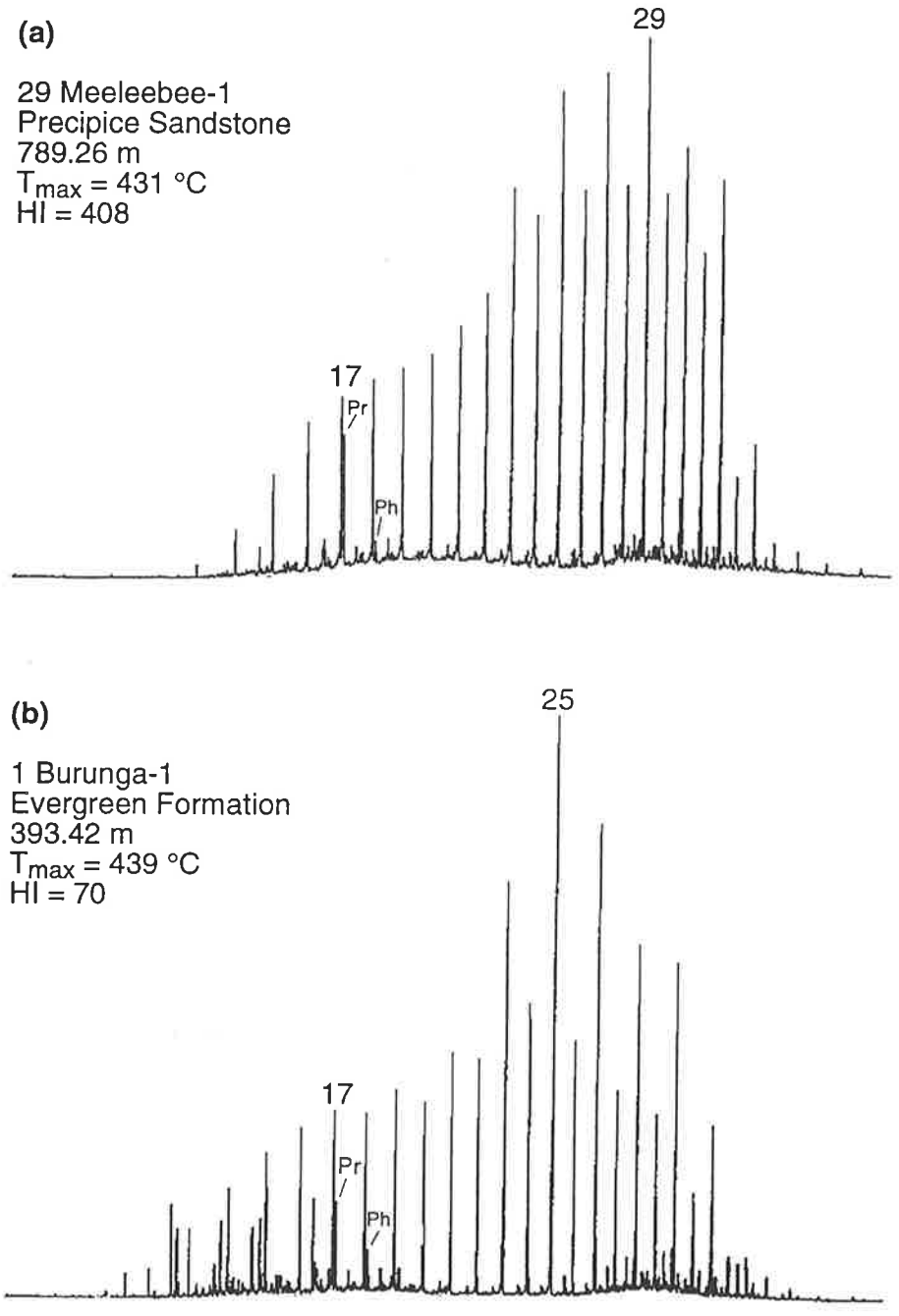

Figure 4.9 Immature alkane distributions of the Early Jurassic (a) Precipice Sandstone in Meeleebee-1, and (b) Evergreen Formation in Burunga-1.

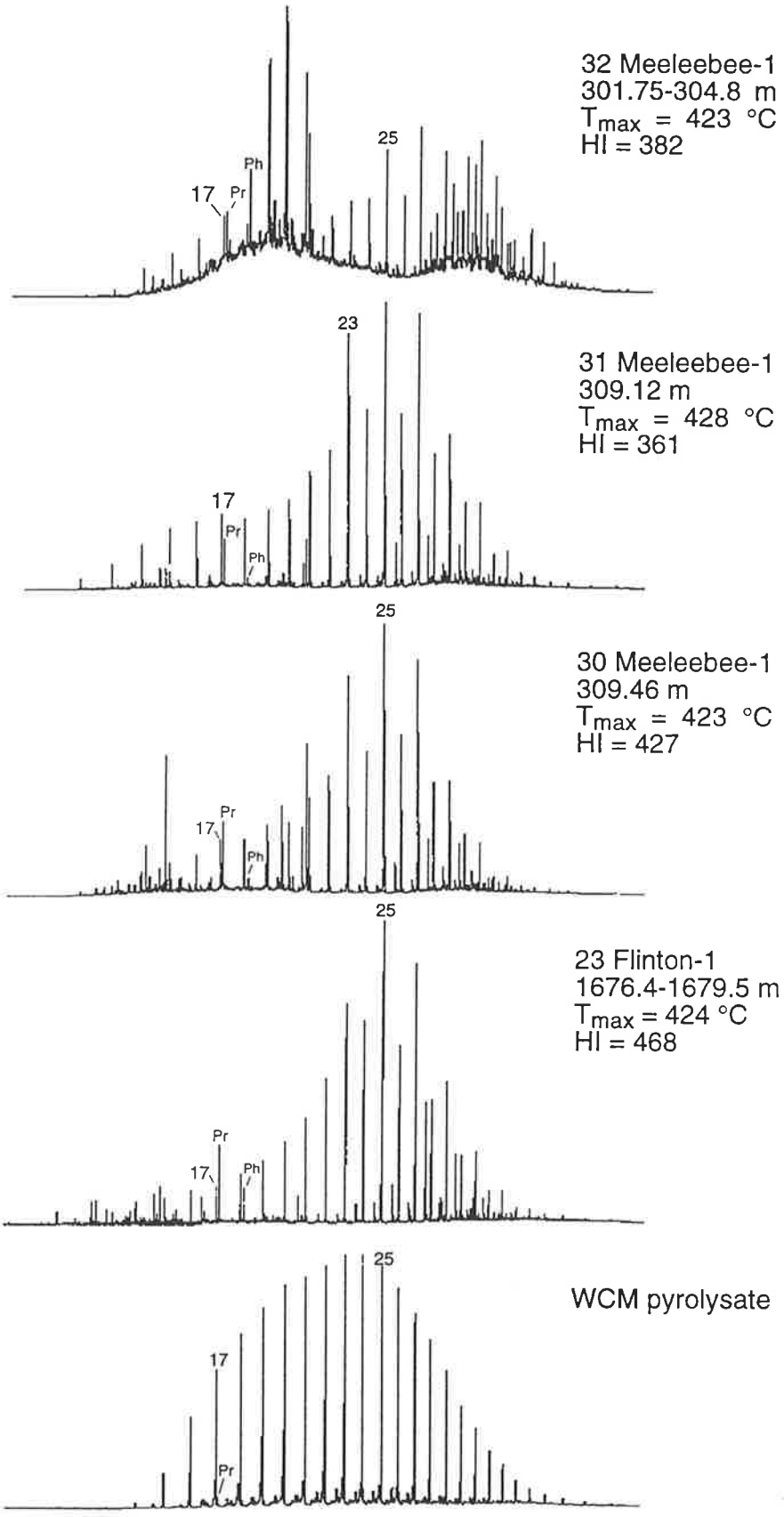

Figure 4.10 Immature alkane distributions of the Middle Jurassic Walloon Coal Measures (WCM) extracts. Alkane chromatogram of a WCM pyrolysate (sample courtesy Dr. C. Boreham) is also included for comparison.

abundant high molecular weight *n*-alkanes with a pronounced odd/even predominance (CPI up to 1.7). The uppermost portion of the WCM at Meeleebee-1 has a bimodal *n*-alkane distribution (maxima at *n*-C_{20} and *n*-C_{27}) and a prominent bimodal naphthenic hump. The position of the WCM samples on the HI *versus* T_{max} plot (Fig. 4.2b) testifies to their immature Type II kerogen. Thomas et al. (1982) obtained similar results for the WCM from Cabawin-1.

4.4 Organic facies of the Snake Creek Mudstone

4.4.1 Alkane profiles

Higher plants, algae and bacteria all have contributed considerably to the Snake Creek palaeolacustrine environment, with the relative contribution of each being difficult to assess. However, most samples exhibit *n*-alkane profiles with one maximum; either in the low molecular weight range (C_{15} - C_{19}), the medium molecular weight range (C_{20} - C_{22}), or in the higher molecular weight range (C_{23} - C_{29}). Accordingly, three organic facies can be recognised (1) algal-rich facies (*Facies A*), (2) bacteria-rich facies (*Facies B*), and (3) higher plant-rich facies (*Facies C*). A fourth facies (*Mixed Facies*) can be identified where inputs from algae, bacteria and land plants are roughly equal (Fig. 4.6). These four facies are discussed below.

Algal-rich facies (Facies A)

This facies is liptinite-rich and in most cases alginite constitutes a considerable portion of the liptinite fraction (Table 4.4). Both lamalginite and telalginite are present. Phytoplankton of unknown taxonomic affinity are abundant, whereas *Botryococcus*-like algae occur in trace concentrations. This organic matter assemblage is consistent with a freshwater lacustrine setting. Its alkane distribution is dominated by lower molecular weight *n*-alkanes (*n*-C_{15} - *n*-C_{19}) with a maximum at any of the alkanes in this range (Fig. 4.6a). This facies is represented by samples from Dulacca-1, Teelba-1, Tiggrigie Creek-1, Bellbird-1, Bengalla-1, Glenhaughton-1, Apple Tree-1, Booberanna-1, Muggleton-1, Snake Creek-1, Taylor-8, Weeyan-1, Tinker-2, Waroon-1, Waroon-3 and Glenearn North-1: Table 4.2). Such predominance of lower molecular weight compounds is usually related to abundant algal organic matter (Eglinton and Hamilton, 1963). It is interesting to note that the SCM source rocks deposited in a *brackish and less oxic* environment (Dulacca-1, Teelba-1, Glenhaughton-1, Apple Tree-1, Section 5.4.2) all belong to this facies. These conditions are favourable for the production and preservation of autochthonous eukaryotic algal organic matter. Thus, higher alginite

Table 4.4 Maceral distributions, Snake Creek Mudstone, southern Taroom Trough

Sample	Well	Type of OM	% OM of whole rock	Maceral Groups		
				%Liptinite	%Vitrinite	%Inertinite
Algal-rich facies*						
34	Dulacca-1	DOM	3.4	29#	59	12
37	Teelba-1	DOM	3.8	26#	61	13
38	Tiggrigie Creek-1	DOM	4.6	60	30	10
39	Bellbird-1	DOM	2.1	18#	67	15
40	Bengalla-1	DOM	2.3	21#	57	22
41	Glenhaughton-1	DOM	3.9	52	26	22
43	Apple Tree-1	DOM	3.4	18#	55	12
44	Booberanna-1	DOM/Coal bands	4	20#	43	37
46	Muggleton-1	DOM	3.5	41	50	9
47	Snake Creek-1	DOM	6.8	41	44	15
50	Taylor-8	DOM	2.4	66	23	11
52	Weeyan-1	DOM	2.7	52	26	22
58	Tinker-2	DOM	4	67	2	31
59	Waroon-1	DOM	4.4	22#	51	27
60	Waroon-3	DOM/Coal bands	3.5	72	25	3
63	Gleanern North-1	DOM	5	60	24	16
Bacteria-rich facies*						
56	Taroom-14	DOM	3	48	40	12
62	Fairymount-4	DOM	4.8	41	39	20
68	Rednook-1	DOM	3	51	33	16
70	Renlim-1	DOM	1	20	50	30
73	Harbour-1	DOM	3	64	28	8
Higher plant-rich facies*						
33	Amoolee-1	DOM/Coal bands	6.4	66	33	1
35	Flinton-1	DOM/Coal bands	6	37	40	25
48	Red Cap-1	DOM/Coal bands	2.5	24	60	16
54	Beardmore-2	DOM	2	58	30	12
65	Namarah-2	DOM	0.2	10	75	15
66	McGregor-1	DOM	3	71	20	9
67	Hollow Tree-1	DOM	3.7	61	29	10
71	Newington-2	DOM	5.5	1	90	9
72	Yellowbank Creek-1	DOM	2.6	52	37	11
Mixed facies*						
36	Sussex Downs-1	DOM	4	17	71	12
42	Inglestone-1	DOM/Coal bands	4.7	65	25	10
45	Cabawin-1	DOM	2.3	57	39	4
49	Borah Creek-3(1)	DOM	5	12	57	31
51	Taylor-13	DOM	2.4	66	26	8
53	Borah Creek-3(2)	DOM	4	45	30	25
55	Causeway-1	DOM	3.4	32	25	43
57	Taroom-12-12A	DOM	2	62	24	14
61	Fairymount-3	DOM	3.6	33	47	20
64	Borah Creek-4	DOM	5.6	56	30	14
69	Rocky Glen-1	DOM	3	58	23	16

* Organic facies classification is based mainly on *n*-alkane distributions (Section 4.4.1, Table 4.2) which may, or may not, reflect the corresponding maceral distributions (Section 4.4.3).

These samples are not algal-rich and their 'algal' *n*-alkane profile is due to something else (see Section 4.4.3). DOM = dispersed organic matter; Coal bands = discrete coal seams observable under the microscope

Table 4.4 Maceral distributions, Snake Creek Mudstone, southern Taroom Trough (continued)

Maceral Group	Liptinite								
Maceral	Spor	Cut	Res	Lip	Tel	Lam	Fluor	Exsud	Bitum
Sample									
34	6	9	12	-	1B	-	1	-	-
37	1	5	4	13	-	-	3	-	-
38	2	17	4	4	11*	15a,d	-	-	7
39	2	5	-	5	4	-	2	-	-
40	-	10	-	8	3	-	-	-	-
41	5	26	-	3	15*	3a	-	-	-
43	-	10	6	-	-	-	2	-	-
44	12	2	1	3	1B*	1	-	-	-
46	1	11	-	11	15*	3	-	-	-
47	12	21	1	3	3B	1	-	-	-
50	13	21	17	4	3	8	-	-	-
52	8	7	7	19	4*	7	-	-	-
58	5	20	2	7	10B*	15	1	2	5
59	2	17	2	-	-	-	1	-	-
60	29	28	-	9	3	3	-	-	-
63	20	8	2	20	4	6	-	-	-
56	17	13	3	10	3	-	2	-	-
62	4	4	4	11	11	6	1	-	-
68	27	17	7	-	-	-	-	-	-
70	10	-	-	-	6	4	-	-	-
73	3	11	-	17	25	8	-	-	-
33	7	31	3	5	10*	10a,d	-	-	-
35	1	10	8	7	2B	-	-	-	9
48	4	20	-	-	-	-	-	-	-
54	10	5	3	25	-	5	5	-	-
65	-	-	-	10	-	-	-	-	-
66	23	17	-	25	5	-	1	-	-
67	22	16	3	11	3	2	1	3	-
71	-	-	-	1	-	-	-	-	-
72	12	27	-	8	-	4	1	-	-
36	-	3	-	8	6	-	-	-	-
42	5	7	7	18	12	14	1	1	-
45	9	-	3	22	6*	9a	-	-	8
49	3	5	-	2	2B	-	-	-	-
51	8	8	17	23	-	4	2	-	4
53	7	30	-	-	8*	-	-	-	-
55	3	3	6	15	-	5	-	-	-
57	14	14	-	23	-	9	2	-	-
61	6	-	3	22	-	-	2	-	-
64	-	49	-	-	5*	-	1	1	-
69	9	11	3	33	-	3	2	-	-

Spor = Sporinite; Cut = Cutinite; Res = Resinite; Lip = Liptodetrinite; Tel = Telalginite; Lam = Lamalginite; Fluor = Fluorinite; Exsud = Exsudatinite; Bitum = Bituminite; * = includes amorphous organic matter and phytoplanktons of unknown affinity; a = acritarchs; d = dinoflagellates; B = *Botryococcus*-like algae

Table 4.4 Maceral distributions, Snake Creek Mudstone, southern Taroom Trough (continued)

Maceral Group	Vitrinite				Inertinite					Pyrite
Maceral	Telo	Texto	Desmo	Gelo	Fusin	Semi	Inerto	Mic	Mac	
Sample										
34	35#	-	9	15	-	-	3	-	9	<0.1
37	26#	24	11#	-	-	4	5	4	-	0.1
38	22	-	8	-	8	2	2	-	-	0.1
39	38	19	10	-	-	10	5	-	-	0.2
40	17	4	36	-	9	9	4	-	-	0.2
41	8#	5	13	-	-	13	5	4	-	0.2
43	29	-	14	12	15	-	9	-	3	0.2
44	8	10	8	17	10	8	5	3	11	-
46	9	12	29	-	-	-	9	-	-	<0.1
47	29	-	15	-	-	-	15	-	-	0.2
50	-	-	23	-	-	-	8	-	3	0.1
52	-	4	11	11	-	7	4	-	11	-
58	-	-	2	-	14	5	12	-	-	-
59	21	25	5	-	9	16	-	2	-	-
60	11#	-	14#	-	-	-	3	-	-	1.5
63	4#	-	20#	-	10	-	3	-	3	-
56	7	-	33	-	-	4	8	-	-	1
62	11	6	11	11	-	13	2	1	4	3
68	-	-	33	-	-	-	16	-	-	0.1
70	-	-	50	-	-	-	20	-	10	2
73	10	3	15	-	-	5	3	-	-	0.8
33	17	16	-	-	1	-	-	-	-	0.1
35	25	-	13	-	17	-	8	-	-	<0.1
48	40	8	12	-	4	8	-	4	-	<0.05
54	-	5	25	-	-	5	-	-	7	<0.1
65	-	-	75	-	-	-	15	-	-	-
66	-	-	15	5	-	2	7	-	-	0.1
67	4	10	15	-	-	5	5	-	-	-
71	36	-	54	-	-	4	3	2	-	-
72	11#	14	12	-	-	-	3	8	-	-
36	38	15	18	-	-	-	5	-	7	<0.1
42	5	-	20	-	3	-	2	5	-	0.5
45	13#	13	13	-	-	-	4	-	-	<0.1
49	20#	8	29#	-	-	10	5	16	-	0.2
51	-	18	8	-	8	-	-	-	-	0.1
53	5	-	25	-	-	-	20	5	-	0.1
55	-	6	19#	-	-	20	6	5	12	<0.1
57	9	-	15	-	-	-	9	-	5	-
61	-	6	28#	13#	-	6	-	3	-	0.1
64	10	-	18	2	9	-	5	-	1	1
69	3	7	13	-	-	10	4	-	2	0.2

Telo = Telocollinite; Texto = Texto-ulminite; Desmo = Desmocollinite;
Gelo = Gelovitrinite; Fusin = Fusinite; Semi = Semifusinite; Inerto = Inertodetrinite;
Mic = Micrinite; Mac = Macrinite; # = Fluorescent vitrinite

contents are typically associated with highly fluorescing telocollinitic/desmocollinitic groundmass (Table 4.4).

Bacteria-rich facies (Facies B)

Heterotrophic bacteria consume pre-existing organic materials, including the remains of algae and higher plants. This bacterial degradation can influence the chemical and isotopic characteristics of the bulk organic matter (Kelts, 1988). Such bacteria can be a major contributor of lipids to the preserved organic matter. In some lakes, the primary production of organic matter by photosynthetic bacteria may exceed algal production. For example, the production rate of the green sulphur bacterium *Chlorobacteriaceae* is estimated to be about 25 times more than that of phytoplankton (Kelts, 1988).

A major bacterial contribution to the SCM is reflected in the GC traces of five samples, as abundant *n*-C_{20-22} alkanes with a maximum at *n*-C_{21}. These samples, assigned to Facies B, are: Taroom-14, Fairymount-4, Rednook-1, Renlim-1 and Harbour-1 (Table 4.2). The gas chromatogram of the SCM in Renlim-1 is shown in Figure 4.6b to represent the *n*-alkane distribution of this facies. Under the scanning electron microscope these samples are seen to contain substantial amounts of coccoid and rod-shaped bacteria (Plate II a and b). Relatively high concentrations of granular and framboidal pyrite (~ 1-3% of the whole rock: Table 4.4) in many of these samples suggest that some of the bacteria were sulphate-reducers (e.g. *Desulphovibrio desulphuricans*). When *n*-alkanes exhibit two maxima, one in the lower molecular weight range and the other in the medium molecular weight range, the contributions from algae and bacteria are inferred to have been similar and, therefore, the organic facies is designated AB (Taylor-13, Causeway-1, Fairymount-3: Table 4.2).

Higher plant-rich facies (Facies C)

A dominance of C_{23+} *n*-alkanes (Table 4.2), which is characteristic of Facies C (Fig. 4.6), is observed along the southern and southwestern edges of the Taroom Trough in three areas, namely: 1) Red Cap-1 and Namarah-2; 2) McGregor-1, Hollow Tree-1, Beardmore-2 and Yellowbank Creek North-1; and 3) Newington-2 (Table 4.2). This is interpreted to indicate an enhanced input of terrestrial detritus in more proximal lacustrine settings. Abundant long chain alkanes with a maximum at C_{23}, C_{25}, C_{27} or C_{29} are normally attributed to higher plants (Youngblood and Blumer, 1973).

4.4.2 Maceral distributions

The composition of the SCM kerogen as determined by Rock-Eval analysis (Fig. 4.2) is confirmed by microscopic examination of its macerals. The SCM source rocks contain dispersed organic matter (DOM) of mixed origin. Coal and carbonaceous mudstone are occasionally interlaminated. Rapid lateral and vertical variations in DOM content and maceral distribution are observed. The DOM content ranges between 0.2 and 7% (average 4%: Table 4.4).

Characterising the different organic facies and maceral distributions is of particular interest for exploration since each maceral has a unique chemical composition and consequently a different ability to generate hydrocarbons. This can help in predicting the quality and amount of generated petroleum. For example, resinite-rich facies generate mainly terpenoid hydrocarbons, even at very low thermal maturity (Snowdon, 1980, 1991; Teerman et al., 1987). Cutinite contains mainly long-chain polymethylene moieties which upon maturation produce long-chain *n*-alkanes (Mukhopadhyay and Hatcher, 1994). Similarly, alginite is composed mainly of long-chain paraffinic macromolecules, whereas sporinite comprises sporopollenin formed by polymerization of unsaturated fatty acids or alcohols (Nip et al., 1989). In coal, alginite can generate more than twice the amount of gas derived from sporinite, whereas the latter generates twice the amount of gas that comes from vitrinite (Levine, 1987). Vitrinite is derived from lignin biopolymers (Mukhopadhyay et al., 1991) and, with increasing maturity, its polyaromatic ring structure evolves towards that of inertinite (Mukhopadhyay and Hatcher, 1994). As a result, alginite- and cutinite-rich facies have the highest potential to generate waxy paraffinic oils, whereas sporinite- and resinite-rich facies are more likely to generate light oils and condensates of naphthenic composition (Mukhopadhyay and Hatcher, 1994). Both liptodetrinite and bituminite can generate a range of crude oil types, depending on the identity of their precursor materials.

Structured higher plant remains are present in all samples, together with varying amounts of amorphous organic matter (AOM) and phytoplankton (Table 4.4). No sharp line can be drawn between the humic (vitrinite/inertinite)-rich and sapropelic (liptinite)-dominant depositional settings for the SCM since these organic matter populations are distributed irregularly along the southern Taroom Trough. Vitrinite comprises 23-67% of DOM in Facies A, and 20-75% in Facies C. Therefore, on the basis of their DOM, there is no obvious systematic difference between the proposed SCM organic facies. In other words, liptinite is not the dominant maceral group in all Facies A samples, and vitrinite is not the dominant maceral group in all samples from Facies C (see also Section 4.4.3). The best correlation between the maceral and alkane

distributions is noticed for the two end-member SCM facies, represented by sample #58 (Table 4.4, Fig. 4.6, Plate I) for Facies A; and sample #71 for Facies C (Table 4.4, Fig. 4.6, Plate III). In sample #58 (Tinker-2), dominant liptinite (67% of DOM) and rare vitrinite (2% of DOM) is associated with an *n*-alkane maximum at C_{18}, whereas in the latter sample (#71 Newington-2) the dominant vitrinite (90% of DOM: Table 4.4) is reflected by maximum at *n*-C_{29} (Fig. 4.6). Vitrinite occurs mainly as detrovitrinite (desmocollinite) and/or telovitrinite, but texto-ulminite and gelovitrinite are also present in many samples. Inertinite ranges from being almost absent (e.g. in Amoolee-1) to the dominant maceral group (e.g. in Causeway-1). The inertinite population includes a considerable amount of inertodetrinite and semifusinite. Fusinite and macrinite were observed in several samples.

The majority of the SCM samples contain abundant liptinite, comprising mainly cutinite/liptodetrinite with rare to common sporinite. Alginite is present as acritarch or dinoflagellate remains, *Botryococcus*-like algae, other phytoplankton and AOM of unknown affinity (Plate I, Table 4.4). Samples from Borah Creek-3(2), Borah Creek-4, Tinker-2, which exhibit the highest hydrogen indices (HI >200: Table 4.1b) and bear close affinity to Type II kerogen, all contain abundant alginite. On the other hand, the liptinite-poor samples (e.g. Newington-2: liptinite < 1%; Table 4.4) have lower HI values and their kerogen is Type III (Fig. 4.2b). However, many liptinite-rich samples have low hydrocarbon potentials (e.g. McGregor-1: liptinite = 71%; HI = 71; Tables 4.1b and 4.4). Such poor correlation between low HI and liptinite-rich kerogen with a high H/C atomic ratio has been previously noticed by Sentfle et al. (1986) and Powell et al. (1991) who attributed it to the heterogeneous nature of such terrestrial facies. This discrepancy has also been observed in the marine facies of the Early Cretaceous Bulldog Shale in the southwestern Eromanga Basin and has been ascribed to partial oxidation of hydrogen-rich liptinite during and after sedimentation (McKirdy et al., 1986). Similar preferential oxidation may also explain the low HI values for some of the liptinite-rich samples of the SCM source rocks.

Local depressions in the SCM palaeolake-floor were sites of greater preservation efficiency as indicated by higher alginite, phytoplankton and AOM contents (as at Harbour-1, Tiggrigie Creek-1, Inglestone-1 and Tinker-2; and to a lesser extent in Amoolee-1, Glenhaughton-1, Muggleton-1, Fairymount-4 and Cabawin-1: Table 4.4). Pyrite concentrations in many samples indicate anaerobic bacterial activity in suboxic or locally anoxic sediments. Under these conditions, algal and bacterial lipids would be selectively concentrated in the form of AOM. The associated intact liptinites generally exhibit high fluorescence intensity, indicating deposition in quiet environments close to their site of growth (*cf.* Beeston, 1987). It should be mentioned, however, that the algal contents of some of these rocks may have been increased by marine incursions, as

indicated by the presence of acritarchs (Tiggrigie Creek-1, Amoolee-1) and/or C_{30} desmethyl steranes (Flinton-1, Cabawin-1, Muggleton-1, Glenhaughton-1: see Chapter 5).

4.4.3 Maceral versus alkane distributions

No regular change in organic facies within the SCM is evident across the southern Taroom Trough. The identification of different organic facies based on their *n*-alkane distributions is not supported by their maceral distribution although in some samples a positive correlation exists between these two parameters. For example, in most cases the organic matter of Facies A is relatively alginite-rich (e.g. samples #38, 41, 45, 46, 58, 62 and 73: Table 4.4 and Plate I), in accordance with the proposition that the C_{15}-C_{20} *n*-alkanes are algal-related. The presence of acritarchs in some of these samples (e.g. at Glenhaughton-1, Cabawin-1) reflects a marine influence which also is evidenced by the presence of C_{30} desmethyl steranes (Section 5.4.3). On the other hand, in Facies C, a positive correlation was observed between the waxiness of the alkane distributions (represented by dominant C_{23+} *n*-alkanes) and higher plant precursors. Where *n*-alkanes are skewed towards the *n*-C_{23+} range, abundant vitrinite as well as cutinite, sporinite and/or liptodetrinite are present (Plate III).

Some samples show a poor correlation between their chemical (*n*-alkane) and petrographic (maceral) distributions. For example, although sample #33 (Amoolee-1) is liptinite (mainly alginite)-rich, its alkane distribution is dominated by C_{23+} *n*-alkanes. This is not unusual since some of these C_{23+} *n*-alkanes may have an algal source, such as the freshwater chlorophyte *Botryococcus braunii* (Metzger et al., 1991). Acritarchs are also present in the SCM in Amoolee-1 but their signature does not figure prominantly in the *n*-alkane profile, probably because of their low abundance. In this case, the marine influence could not be confirmed by the molecular evidence since no GCMS trace (414 → m/z 217) was obtained for this particular sample. Moreover, although alginite is very rare or occurs in trace concentrations in some other samples (e.g. #34, 37, 39, 40, 56 and 59: Table 4.4), their *n*-alkanes are still dominated by C_{15}-C_{20} homologues (Table 4.2). This suggests that these low molecular weight *n*-alkanes can be derived from liptinites other than alginite, or even from the vitrinite itself. Behar and Vandenbroucke (1987) have provided evidence that vitrinite contains substantial aliphatic moieties which, upon diagenesis, can yield significant amounts of normal hydrocarbons (Powell et al., 1991). Of particular importance is the vitrinite-maceral desmocollinite which may contain considerable concentrations of bacterial lipids (Powell et al., 1991) or other microbial remains (Taylor et al., 1988), which have a low molecular weight *n*-alkane signature. Such poor correlation between geochemical and petrographic composition is not

unexpected and it appears to be the rule rather than the exception in many Australian coals and carbonaceous shales (Powell et al., 1991; Boreham and Powell, 1994; Powell and Boreham, 1994). Many liptinite-poor kerogens in these terrestrial facies produce significant amounts of hydrocarbons dominated by *n*-alkanes below C_{17}, whereas many liptinite-rich samples give smaller amounts of pyrolysable *n*-alkanes than do the liptinite-poor ones. Although the origin of these low molecular weight *n*-alkanes in such cases is uncertain (Powell et al., 1991), they may be derived from the polyethylene-like polymer in plants (Nip et al., 1986) or a contribution from unknown micro-organisms during early diagenesis (Powell et al., 1991). Finally, algal remains, although minimal, are still capable of dominating the *n*-alkane profile at the maturity levels attained by the SCM.

Whatever the explanation, it is clear that intertonguing of freshwater-brackish and terrestrial-aquatic palaeoenvironments has led to the accumulation of mixed organic matter assemblages having diverse alkane signatures.

4.5 Petrographic evidence of oil generation in the SCM

As most of the SCM section sampled has passed the first coalification jump (T_{max} = 429-440 °C; R_O = 0.67-0.89%: Tables 4.1 and 4.3), petroleum generation may be expected to have commenced in this unit. As discussed above, the SCM has two end-member organic facies. The first is sapropelic and rich in either phytoplankton or sporinite/cutinite. The second, is humic and rich in vitrinite and inertinite. The sapropelic facies was deposited in mildly oxidising conditions, with local anoxic subenvironments (gyttja-type). Given this compositional diversity of the SCM organic matter, and particularly its liptinite fraction, hydrocarbon generation is likely to have begun over a range of maturities. Certainly, some liptinites and vitrinites within the SCM have passed their oil generation threshold (0.6% R_O for sporinite and cutinite, and 0.5% R_O for desmocollinite: Cook, 1982). Resinite and suberinite can begin expelling their hydrocarbon contents at a much lower maturation level than do cutinite and sporinite (Teichmuller and Durand, 1983). At this low maturity level (R_O < 0.6%) such organic matter can generate significant amounts of light oil and condensate (Cook, 1982; Snowdon and Powell, 1982). Moreover, for such mixed organic facies, the hydrocarbon products can be expected to be heterogeneous.

Microscopic observations (Plates IV and V) confirm that hydrocarbon generation from the SCM organic matter has indeed started. A high generating potential is indicated for the SCM liptinites by their strong fluorescence. Good preservation is also indicated by the presence of sporogenite (the internal contents of spore and pollen) in several

samples (Plate III d). However, subdued liptinite fluorescence is observed in some samples, in association with flattened sporinite, probably as a result of the generation and expulsion of some of their hydrocarbons into the surrounding matrix (giving it a hazy fluorescence, e.g. Plate III f). Cutinite expelling its hydrocarbons into the surrounding medium is also common in many samples (Plates II f, III c and e).

Extensive micrinitisation was observed in a few samples. It has been suggested that micrinite is a secondary degradation product of the liptinite macerals bituminite and resinite (e.g. Stach et al., 1982), or of vitrinite (Cook and Struckmeyer, 1986), through disproportionation reactions which yield a hydrogen-rich mobile phase (liquid petroleum) and a hydrogen-poor residuum (micrinite). Therefore, the presence of micrinite indicates previous hydrocarbon generation. However, care must be taken when dealing with micrinite since it is polygenetic and, therefore, its presence does not necessarily imply generation of hydrocarbons. Shibaoka (1978, 1983) regarded micrinite as a porigelinite-related, cavity-filling, primary inertinite maceral, whereas Faraj et al. (1993) provide geochemical evidence that micrinite is in fact a clay mineral and not a maceral.

Nevertheless, the association of micrinite (which starts to form at ~ 0.5% R_O: Mukhopadhyay and Hatcher, 1994) with brown fluorescing desmo- and telocollinite (Plate V a, b, and f), and other secondary liptinites such as exsudatinite (Plates IV c and d; V e, g, and h), fluorinite and bituminite (Plates II e, III b, and IV h), is testimony to the generation of hydrocarbons from both liptinite and perhydrous vitrinite in the SCM. Vitrinite fluoresces when it is hydrogen-rich, indicating good oil-generating ability. Alternatively, vitrinite may fluoresce when its micropores are impregnated by liquid hydrocarbons generated from associated liptinites (Mukhopadhyay and Hatcher, 1994). Exsudatinite/oil-cuts are present in telocollinite fractures and fusinite cell lumens (e.g. Plate V e, g, and h). Oil haze surrounds cutinite, resinite, fluorinite and alginite (Plates IV and V), whereas oil droplets have mobilised and migrated into the surrounding rock matrix (Plate IV d). Early work by Blackburn (1936) showed that protoplasm of the alga *Botryococcus braunii* contains oil which, upon diagenesis, can be converted into petroleum (Beeston, 1987). Fluorinite (the essential oils of plants) is present in some samples (Plates IV b and f, V c).

Many coal and petroleum geologists (e.g. Stach et al., 1982; Powell et al., 1978) relate the genesis of these secondary liptinites to active hydrocarbon generation and migration, so that they may be regarded as relict liquid petroleum. Cook and Struckmeyer (1986) considered the presence of exsudatinite and oil cut in coal and DOM to be an indicator of free oil, whereas fluorinite can, sometimes, be regarded as non-migrated oil. In fact, some of the observed exsudatinite/oil droplets and fluorinite were in motion (live oil!)

when examined under the microscope (Plate IV d). In many SCM samples, fluorinite is seen dissolving in the mounting medium to form oil haze (Plate V c). This phenomenon should not be considered unusual since the embedding polyester resin can act as a solvent for the generated hydrocarbons (Teichmuller and Durand, 1983).

Resinite is also abundant in many SCM samples. Resinite can be derived from resins or copals (so called terpene resinite); wax, fat and essential oils (lipid resinite); or from secondary exsudates (secondary resinite) (Mukhopadhyay and Hatcher, 1994). Bituminite occurs sporadically in some samples, most noticeably in the bacteria-rich facies (Plate II e). The association of bituminite with severly biodegraded liptinite has previously been reported (e.g. Mukhopadhyay et al., 1985) pointing to the role of bacterial degradation in the formation of bituminite. This 'biological' bituminization, plus the aforementioned 'thermal' bituminization of liptinite and perhydrous vitrinite which starts at about 0.65% R_O, can generate substantial amounts of petroleum-like hydrocarbons (Ottenjann, 1988).

Petrographic analysis by Smyth and Mastalerz (1991) of Triassic sediments (including that of the SCM) in five Australian sedimentary basins revealed that, although their organic matter is vitrinite- and inertinite-rich, it contains sufficient liptinite to be oil-prone. In particular, their cutinite and suberinite are expected to yield waxy oil (Powell et al., 1991). Even the vitrinite, particularly desmocollinite, has a higher specific yield of *n*-alkanes than some sporinite- and resinite-rich liptinites which are predominantly naphthenic (Powell et al., 1991). Finally, waxes (invisible coatings on spores, pollen, algae and cuticles) are richer in hydrogen (H/C atomic ratio ≈ 2) than all of the macerals (van Krevelen, 1961; Hunt, 1991) and have the potential to be major contributors to the generated oil.

In conclusion, given the level of maturity attained, primary migration of hydrocarbons is likely to have occurred within the SCM source rocks. Fluorinite, resinite, sporogenite and alginite all have most likely been mobilised, in the form of exsudatinite, and thus contributed to the oil reserves of the Bowen/Surat Basin.

4.6 Summary

The BCG is mature (in the southern part of the study area) to overmature (in the north) and contains gas-prone Type III/IV kerogen. Better quality Type II/III kerogen with good to very good potential for oil and gas is preserved in the overlying BWG (particularly its uppermost part, the BCM) and in the SCM. Both formations have appropriate maturity for hydrocarbon generation over the major part of the southern

Taroom Trough. Source rocks of the SCM can be assigned to four principal organic facies on the basis of their *n*-alkane profiles, although there is a poor correlation between *n*-alkane signature and maceral assemblage. All facies show microscopic evidence of active hydrocarbon generation, with the best source potential developed on the southwestern edge of the trough.

PLATE I

TRIASSIC SNAKE CREEK MUDSTONE

Algal-rich Facies A

(a) Phytoplankton with their cell contents replaced by yellow to greenish yellow fluorescing carbonates; and the outer cell walls replaced by dark brown fluorescing bituminite. Tiggrigie Creek-1, 1203-1233 m, (625X).

(b) Telalginite. Tiggrigie Creek-1, 1203-1233 m, (400X).

(c) Unicellular acritarch ?*Visbysphaera* (ac) showing the central body and the outer wall separated by the pericoel. Also shown are *Botryococcus*-related algae. Sections parallel to bedding. Amoolee-1, 2463-2487.2 m, (625X).

(d) A well-preserved dinoflagellate theca (left) and dinoflagellate cyst (right). Amoolee-1, 2463-2487.2 m, (1563X).

(e) Lamalginite (dinoflagellates with their flagellae intact) in a fluorescing groundmass of comminuted organic matter and/or dispersed bituminite. Tiggrigie Creek-1, 1203-1233 m, (1563X).

(f) Colony of *Botryococcus*. Tinker-2, 2078.3-2100.4 m, (1563X).

(g) Lamalginite (la) associated with pyrite framboids (py). Muggleton-1, 1417-1436, (625X).

(h) Compressed *Botryococcus*-related telalginite. Harbour-1, 1965-1980.5 m, (1563X).

N.B. All photos are taken under the ultraviolet excitation (fluorescence mode).

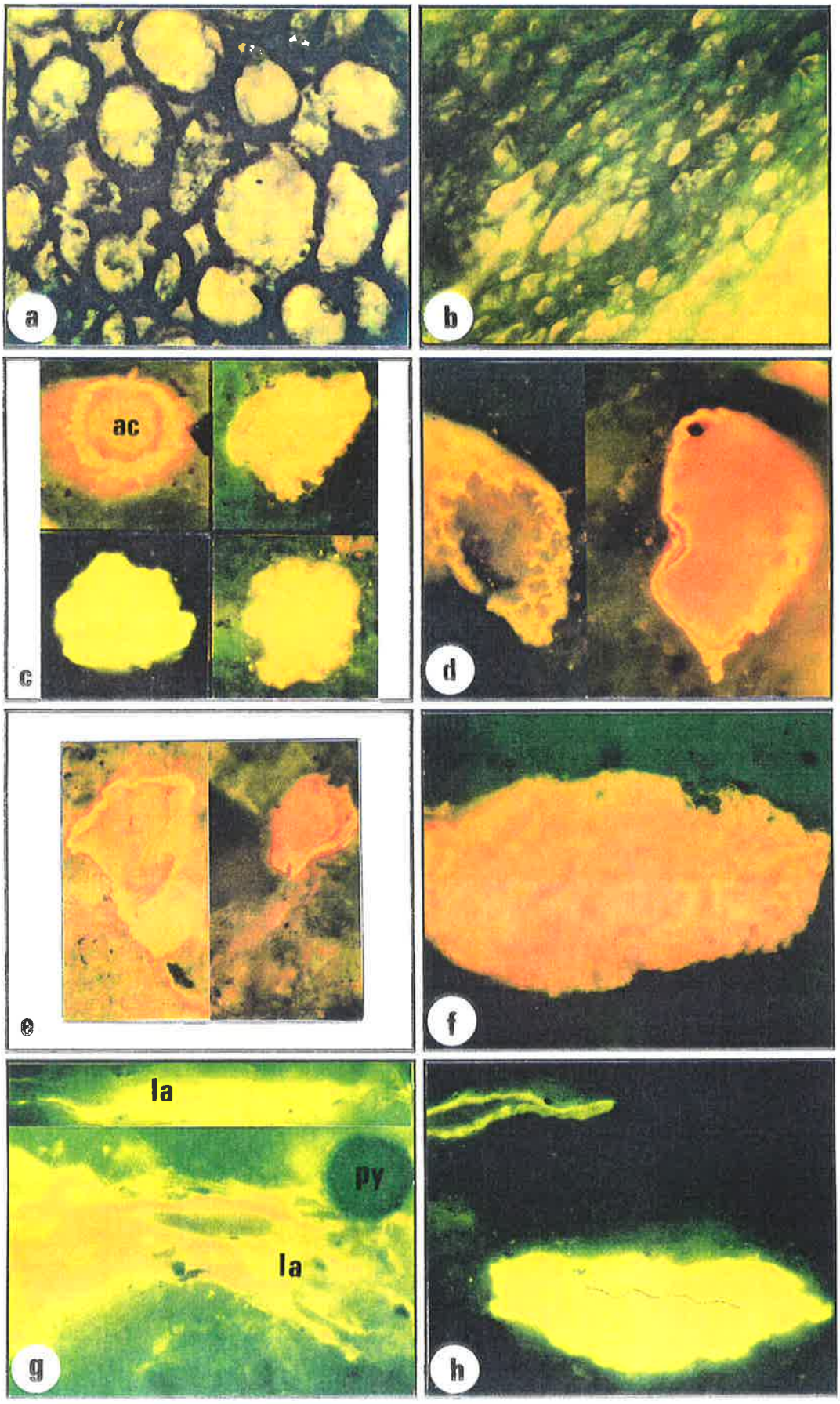
a
b
ac
c
d
e
f
la
py
la
g
h

PLATE II

TRIASSIC SNAKE CREEK MUDSTONE

Bacteria-rich Facies B

(**a** and **b**)

Coccoid (cb) and bacillar (bb) bacteria on probable algal substrate. Fairymount-4, 2018.6-2034.2 m, SEM photomicrographs.

(**c**) Bands of gelovitrinite (gv) alternating with microlaminae of pyrite-rich calcareous shale, indicating anaerobic decay by sulphate-reducing bacteria such as *Desulphovibrio desulphuricans*, in local suboxic environment. Fairymount-4, 2018.6-2034.2 m, incident white light (625X).

(**d**) Concentration of framboidal pyrite fully replacing organic matter. Renlim-1, 1884-1898 m, incident white light (1563X).

(**e**) Brown fluorescing bituminite (bm) associated with dull fluorescing lamalginite (la) and telalginite (ta). Black shreds are desmocollinite (dc). This amorphous bituminite might be a degradation product of algal, faunal, herbaceous aquatic plant and bacterial remains. Cabawin-1, 2255.5-2271 m, fluorescence mode (1563X).

(**f**) Well-preserved large (>5mm long) cutinite phytoclast which has started releasing its labile components in the form of exsudatinite flecks. Tinker-2, 2078.3-2100.4 m, fluorescence mode (320X).

(**g**) Resinite, Jurassic Walloon Coal Measures. Meeleebee-1, 309.5m, fluorescence mode (320X).

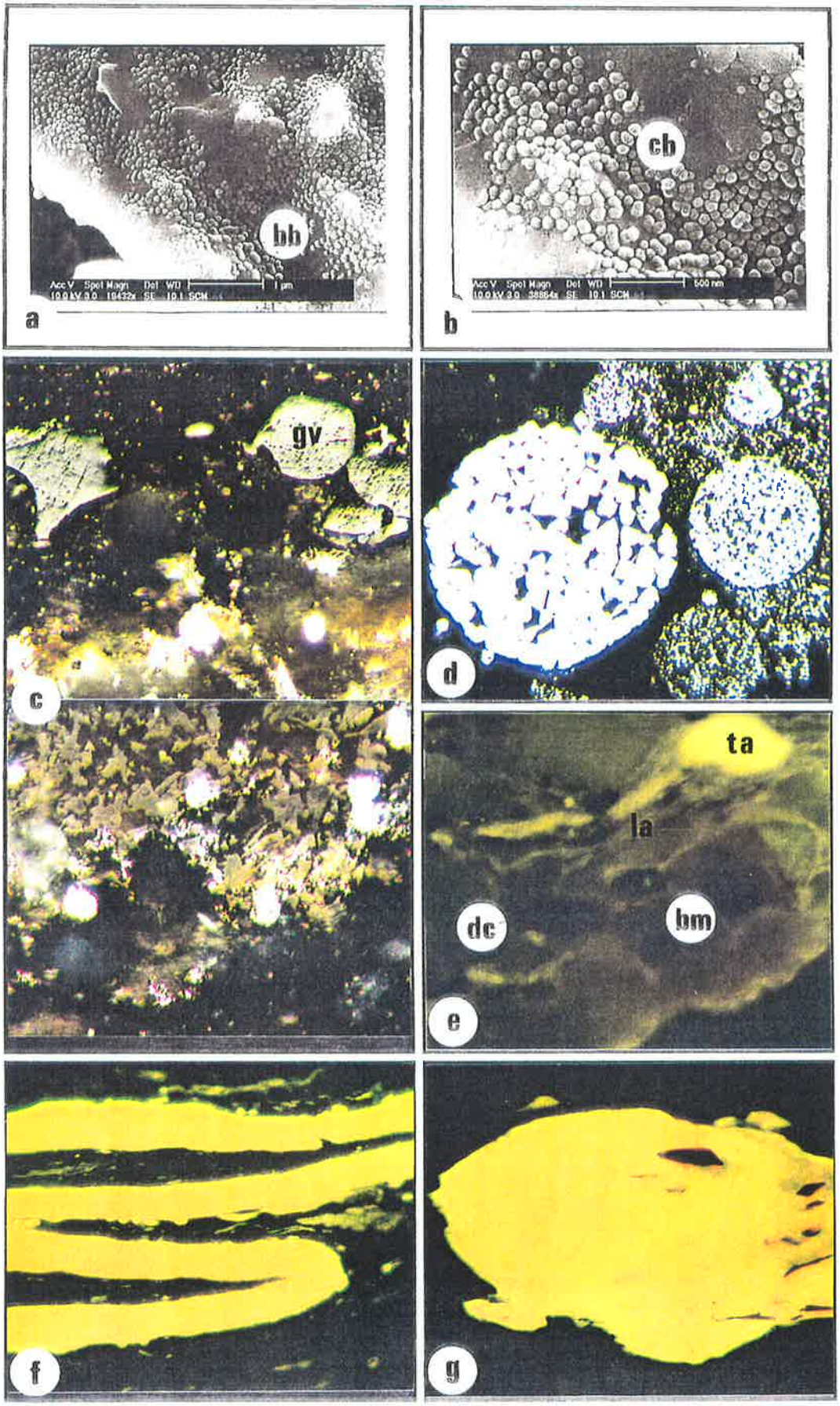
bb
a
cb
b
gv
c
d
ta
la
dc
bm
e
f
g

PLATE III

TRIASSIC SNAKE CREEK MUDSTONE

Higher plant-rich Facies C

(a) Megaspore (sp), resinite globules (r) and cutinite. McGregor-1, 1848.2-1854.5 m, fluorescence mode (625X).

(b) *Reinschospore* (rs) and megaspore (sp) with their labile contents being released as globular differentiated exsudatinite. Bituminite (bm) is also associated. Flinton-1, 2347-2371.3 m, fluorescence mode (625X).

(c) A section parallel to bedding showing cuticular cells and epidermis (cu) losing its structure during diagenetic gelification. Amoolee-1, 2463-2487.2 m, fluorescence mode (400X).

(d) A wide range of near-perfectly preserved sporinite (macro- and mega-spores) of different ornamentation:
- spongy exine with papillate sculptured margins (ms) indicative of partial oxidation (Taroom 12-12A, 620.5-636 m),
- smooth spore (ss) and pollen (p) of undifferentiated wall structure (Flinton-1, 2347-2371.3 m). Sporogenite (inner content) is preserved in most of these pollens and spores, fluorescence mode (400X)

(e) Cutinite. Amoolee-1, 2463-2487.2 m, fluorescence mode (400X).

(f) Well-preserved, complex form of megaspores with serrated wall structure. Tinker-2, 2078.3-2100.4 m, fluorescence mode (625X).

(g) Fusinite. Causeway-1, 1984.2-200.8 m, incident white light (320X).

(h) Telocollinite band (v) grading into macrinite (mac), gelovitrinite (gv) and inertodetrinite. Booberanna-1, 2155-2170.2 m, incident white light (400X).

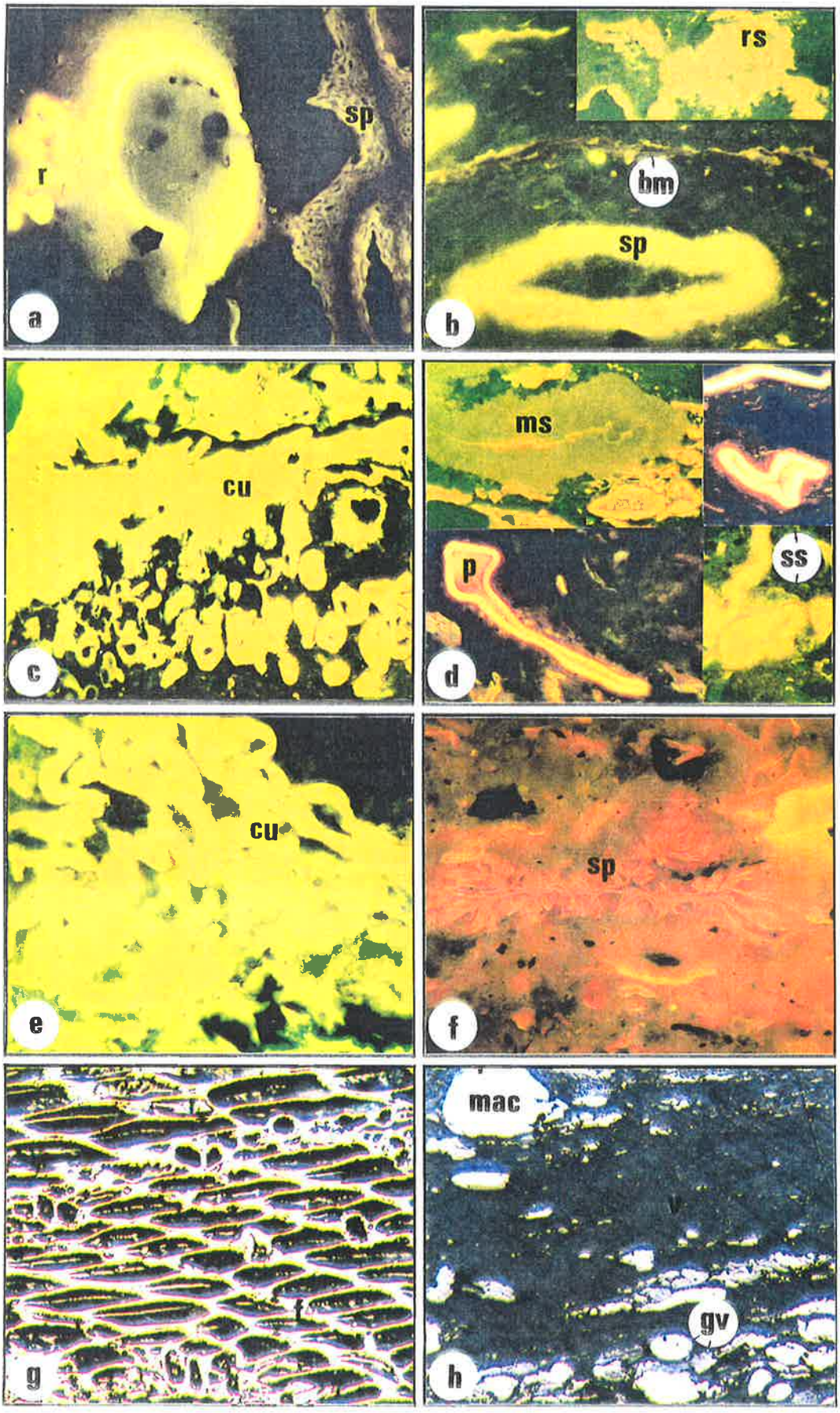
a
r
sp
b
rs
bm
sp
c
cu
d
ms
p
ss
e
cu
f
sp
g
h
mac
gv

PLATE IV

Optical evidence of hydrocarbon generation in the Snake Creek Mudstone

(a) Fluorinite showing colour zonation ranging from bright yellow in the centre to yellowish green and green towards the rim. Inglestone-1, 2718-2748 m, fluorescence mode (400X).

(b) Globules of fluorinite. Apple Tree-1, 1844-1859.3 m, fluorescence mode (400X).

(c) Exsudatinite. Borah Creek-4, 1487.42-1494.74 m, fluorescence mode (625X).

(d) Oil droplets (ol) in the mineral matrix and exsudatinite (ex) filling cavities in desmocollinite. Tinker-2, 2078.3-2100.4 m, fluorescence mode (1563X). These oil droplets and exsudatinite were in motion when examined under the microscope.

(e) Bitumen stringers and exsudatinite as viewed under incident white light (top) and uv-excitation (middle and bottom). Taylor-13, 1990.4-2010 m (625X).

(f) Fluorinite and resinite aggregates. Flinton-1, 2347-2371.3 m (400X).

(g) Bituminite strands (bm) associated with alginite (yellow). Borah Creek-3, 1468 m, incident white light (625X).

(h) Same field as (g), fluorescence mode.

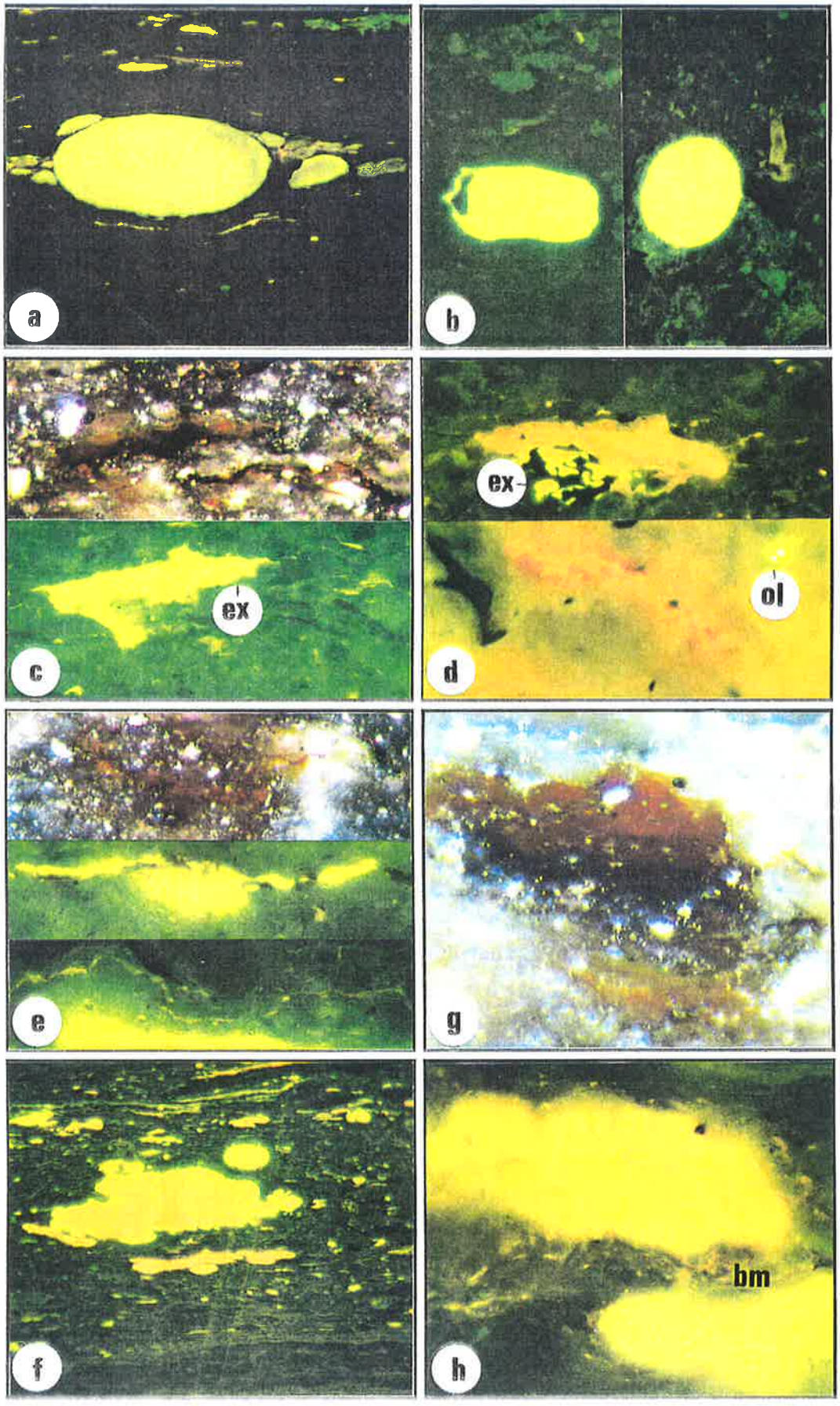
a
b
ex
c
ex
ol
d
e
g
f
bm
h

PLATE V

Optical evidence of hydrocarbon generation in the Snake Creek Mudstone
(continued)

(a) Probable oil stain of anomalously low reflectance (top). The dull greenish brown fluoresence (bottom) is possibly due to mixing with bituminite. Incident white light (top) and uv-excitation (bottom). Glenhaughton-1, 585.2-609.6 m (320X).

(b) Lamellae of bituminite associated with fluorinite flecks (bottom) and fluorescent telocollinite (fv). Teelba-1, 2051.3-2076 m, fluorescence mode (1563X).

(c) Oil haze (oh) 'solubilising' from fluorinite globules into the mounting resin medium (er). Teelba-1, 2051.3-2076 m, fluorescence mode (320X).

(d) Fluorescent vitrinite (dark brown) probably due to show-through of the underlying highly fluoresing alginite. Teelba-1, 2051.3-2076 m, fluorescence mode (1563X).

(e) Exsudatinite (ex) filling fusinitised cell lumens under the incident white light (top) and uv-excitation (bottom). Tinker-2, 2078.3-2100.4 m (400X).

(f) Fluorescent vitrinite (fv), white light (top) and uv-excitation (bottom). Tinker-2, 2078.3-2100.4 m (320X).

(g) Exsudatinite (dark grey) filling cell cavities in fusinite. Tiggrigie Creek-1, 1203-1233 m, incident white light (1563X).

(h) Same field as (g), fluorescence mode.

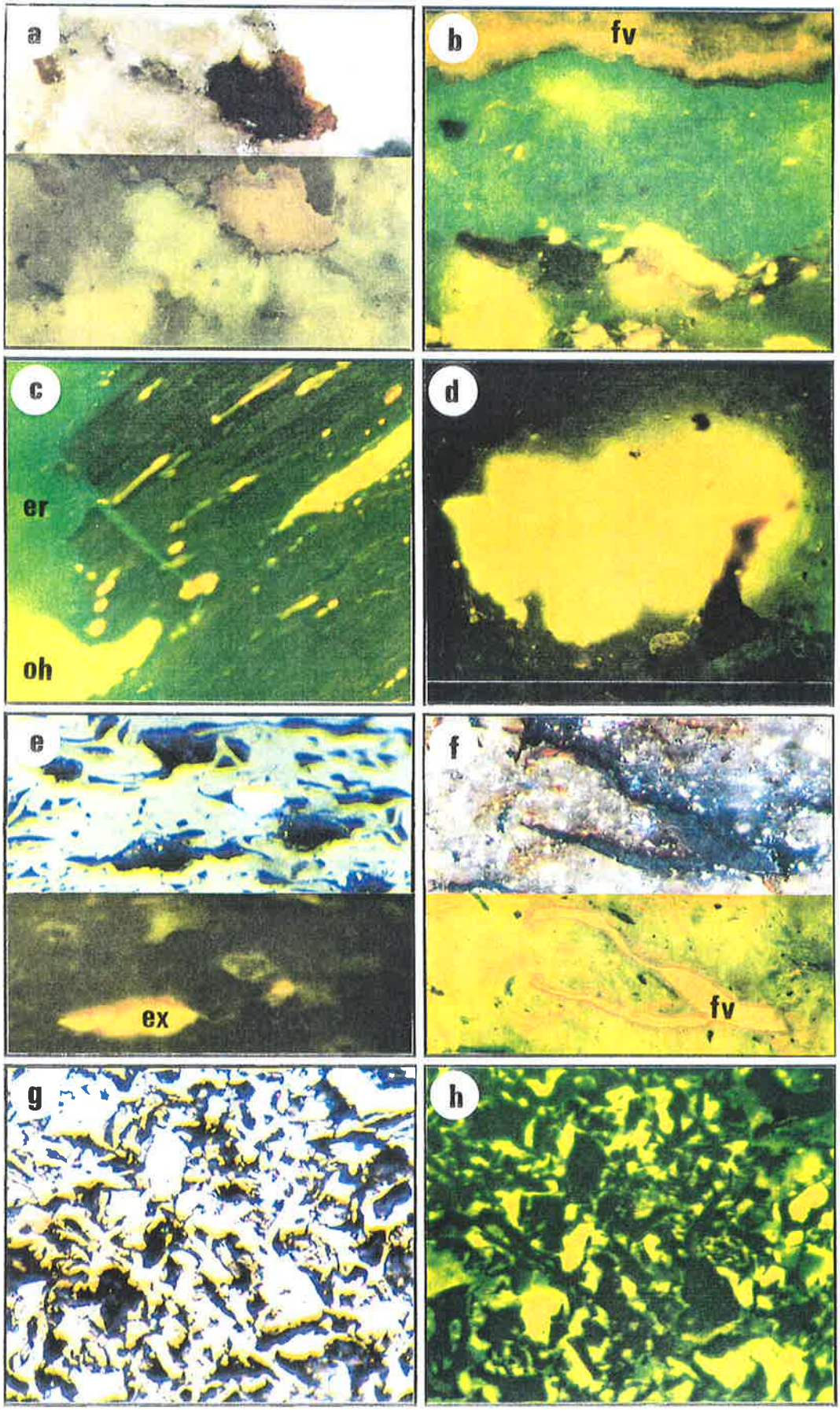
a
b
fv
c
er
oh
d
e
ex
f
fv
g
h

PLATE VI

PERMIAN ORGANIC FACIES

Marine-influenced Back Creek Group

(a and **b)**

Carbopyrite with framboidal pyrite completely replacing texto-ulminite, sporinite and other organic matter. Micrinitisation is also extensive. Cockatoo Creek-1, 3466.9 m, incident white light (625X).

(c) Phytoplankton, Flat Top Formation. Burunga-1, 2123.3m, fluorescence mode (1563X).

(d) Sclerotinite (sc) associated with micrinitised organic matter and pyrite framboids, Barfield Formation. Cockatoo Creek-1, 3335.4 m, incident white light (625X).

(e) Unicellular phytoplankton, Flat Top Formation. Burunga-1, 2123.3 m, fluorescence mode (1563X).

(f) Biodegraded phytoplankton, Flat Top Formation. Cockatoo Creek-1, 2725.42 m, fluorescence mode (1563X).

Coal/carbonaceous Blackwater Group

(g) Non-fluorescing flattened *sporinite*(top; incident white light) with dull fluorescing resinite (r) due to the high level of maturity, Baralaba Coal Measures. Cockatoo Creek-1, 1430.57 m (400X).

(h) Dull fluorescing resinite, Baralaba Coal Measures. Burunga-1, 1094.23 m, fluorescence mode (625X).

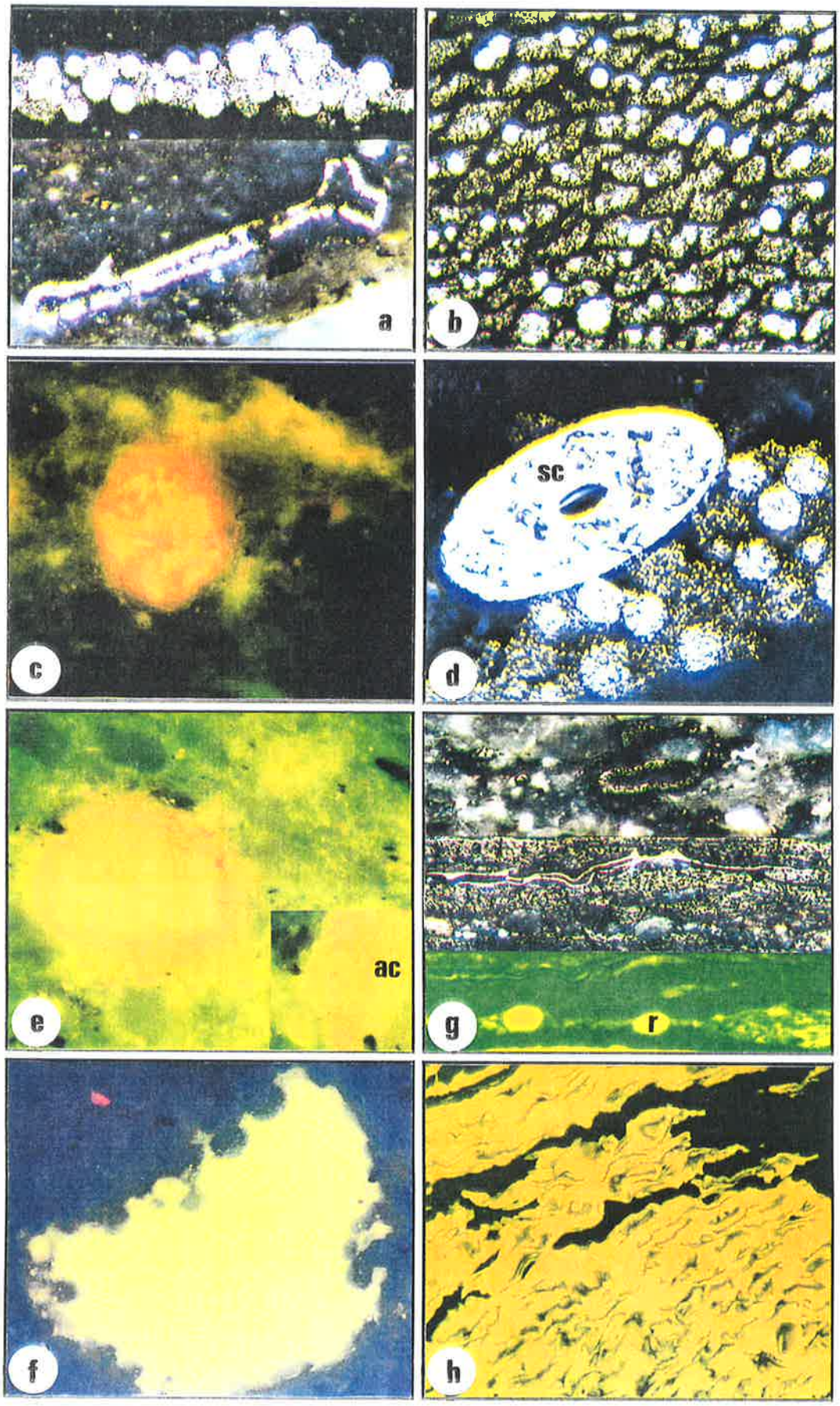
a
b
c
sc
d
ac
e
g
r
f
h

CHAPTER FIVE

BIOMARKER CHARACTERISATION OF PERMIAN AND TRIASSIC SOURCE ROCKS

5.1 Introduction

Molecular parameters of the diverse set of saturated and aromatic hydrocarbons identified in selected Permian and Triassic source rocks of the southern Taroom Trough are presented in this chapter. The maturity data, based on isomer ratios of hopanes and steranes and methyl-substituted di- and triaromatic hydrocarbons (Tables 5.1, 5.3a and 5.4), are discussed first. The origin and depositional environment of the organic matter preserved in these sediments are reconstructed from their source-sensitive biomarker signatures (Tables 5.2 and 5.3b; Figs. 5.1-5.8).

5.2 Molecular maturity parameters

5.2.1 Hopanes and steranes

Permian source rocks

The C_{31} hopane 22S/(22S+22R) ratio in the Permian samples examined has attained equilibrium (59-61%, average 60%: Table 5.1). Seifert and Moldowan (1986) observed that the 22R-to-22S conversion reaction reaches its end point (equilibrium) at a 22S/(22S+22R) value of 57 to 62% corresponding to the onset of oil generation (Fig. 2.5). According to the C_{29} sterane 20S/(20S+20R) ratio, the BWG in the west (at Meeleebee-1) is somewhat less mature (20S < 46%) while in the north (at Cockatoo Creek-1) it has passed the oil generation threshold (20S = 52%, sample #18). The more mature BCG samples generally give higher ratios (20S = 50-55%). The sterane isomerisation reaches an equilibrium (20S = 50%) at the onset of oil generation (Gallegos and Moldowan, 1992). This ratio can decrease at high levels of thermal maturity (Lewan et al., 1986; Peters et al., 1990) which may explain the decreased value (20S = 43%) in the lowermost samples examined from the overmature BCG section at the Cockatoo Creek-1 (Table 5.1).

Distinct maturity differences also can be noticed between the mature BCG and the less mature BWG in terms of the ratios T_s/T_m, C_{30} moretane/hopane and the %ββ C_{29} sterane where they are, respectively, 0.35-0.94, ≤0.11 and 44-56% in the former; and

Table 5.1 Biomarker maturity parameters of source rocks and oils, southern Taroom Trough

Parameter *	1	2	3	4	5	6	7
	Hopanes			Steranes			
Ratio	%22S	Mor / Hop	Ts / Tm	%20S	% ββ	20S / 20R	αββ / ααα20R
Sample No. & Well Name							
Snake Creek Mudstone							
35 Flinton-1	60.3	0.20	0.05	37.3	39	0.60	1.03
41 Glenhaughton-1	62.5	0.11	0.24	49.5	43	0.98	1.49
45 Cabawin-1	58.5	0.13	0.17	40.3	45	0.67	1.34
46 Muggleton-1	65.5	0.12	0.09	48.6	41	0.95	1.34
47 Snake Creek-1	59.7	0.22	0.08	45.8	33	0.84	0.90
48 Red Cap-1	58.8	0.13	0.27	49.3	41	0.97	1.34
49 Borah Creek-3(1)	59.5	0.16	0.13	46.7	42	0.88	1.37
53 Borah Creek-3(2)	59.5	0.11	0.28	44.7	41	0.81	1.24
57 Taroom-12-12A	60.3	0.13	0.22	41.3	33	0.70	0.85
58 Tinker-2	59.9	0.15	0.07	43.8	37	0.78	1.03
59 Warroon-1	59.3	0.13	0.20	50.5	37	1.02	1.20
63 Glenearn North-1	57.8	0.14	0.39	31.0	33	0.45	0.70
64 Borah Creek-4	60.3	0.13	0.14	49.5	40	0.98	1.29
65 Namarah-2	56.4	0.07	0.25	45.5	38	0.84	1.71
67 Hollow Tree-1	58.2	0.24	0.11	25.6	32	0.34	0.62
70 Renlim-1	44.2	0.22	0.05	22.2	35	0.29	0.70
71 Newington-2	61.3	0.20	0.14	47.7	39	0.91	1.23
72 Yellowbank Creek North-1	59.7	0.26	0.07	33.0	34	0.49	0.77
Permian Source Rocks							
Blackwater Group							
27 Meeleebee-1	60.9	0.20	0.07	45.8	34	0.85	0.96
26 Meeleebee-1	61.4	0.15	0.03	40.5	33	0.68	0.81
18 Cockatoo Creek-1	60.6	0.12	0.02	51.8	40	1.08	2.26
Back Creek Group							
24 Meeleebee-1	60.7	0.11	0.36	53.2	47	1.14	1.91
19 Flinton-1	59.3	0.07	0.65	54.9	56	1.22	2.77
10 Burunga-1	59.7	0.09	0.35	52.0	52	1.09	2.30
6 Burunga-1	59.0	0.11	0.78	51.1	55	1.05	2.49
16 Cockatoo Creek-1	59.8	0.10	0.85	43.0	47	1.01	1.82
13 Cockatoo Creek-1	59.0	0.10	0.95	42.9	44	0.75	1.38
Bowen/Surat Basin Oils							
1 Taylor-12A	62.5	0.07	0.64	58.4	58	1.41	3.33
2 Taylor-11	64.3	0.05	1.28	61.1	61	1.57	3.99
3 Tinker-4	60.6	0.04	1.32	59.6	63	1.47	4.21
4 Roswin North-1	58.9	0.12	0.83	54.6	51	1.20	2.30
5 Washpool-1	58.7	0.08	1.22	60.1	61	1.51	3.93
6 Wilga-2	58.7	0.12	0.82	61.6	60	1.61	2.93
7 Waratah-1	60.5	0.09	0.37	55.8	52	1.26	2.46
8 Martini-1	58.4	0.08	0.84	56.6	55	1.30	2.81
9 Riverslea-1	52.9	0.14	0.60	52.6	55	1.11	2.59
10 Cogoon River West-1	57.4	0.09	0.72	53.7	54	1.16	2.50
11 Bellbird-1	58.1	0.06	0.89	59.0	60	1.44	3.66
12 Merroombile-1	57.0	0.07	0.84	59.5	54	1.47	2.84

* Refer to Table 5.3 (a) for explanation of parameters used. Individual parameters and their dynamic ranges are defined in Section 2.5 and Figure 2.5.

≤0.07, 0.12-0.20 and 33-40% in the latter. It is well established that, as maturity increases, T_s/T_m increases (Seifert and Moldowan, 1978), βα/αβ hopane decreases (Seifert and Moldowan, 1980) and %ββ increases (Seifert and Moldowan, 1986).

Snake Creek Mudstone

Consistent with the Rock-Eval maturity parameters of the SCM, the following maturity-sensitive biomarker data emphasise its marginal maturity across the major part of the trough: C_{31} hopane 22S = 56–66%; T_s/T_m = 0.05–0.39; C_{30} moretane/hopane = 0.07–0.3; C_{29} sterane 20S = 26-51%; and C_{29} sterane ββ ≤ 45%. Amongst those SCM samples analysed for their biomarkers, the one in Renlim-1 is the least mature (C_{29} sterane 20S = 22% and C_{31} hopane 22S = 44%: Table 5.1). The isomerisation rate at the C-20 position in steranes is generally slower than that at the C-22 position in hopanes. Thus, for the SCM extracts, the range of C_{31} hopane 22S values (44-66%) corresponds to lower values of C_{29} sterane 20S (22-51%: Table 5.1).

5.2.2 Di- and triaromatic hydrocarbons

Several different aromatic maturity parameters were measured for selected Permian and Triassic source rocks (Table 5.4). These parameters include the dimethylnaphthalene (DNR-1) and trimethylnaphthalene (TNR-1) ratios of Alexander et al. (1985), the methylphenanthrene index (MPI-1) of Radke and Welte (1983) and the methylphenanthrene distribution factor (MPDF-1) of Kvalheim et al. (1987). Values of calculated vitrinite reflectance (R_c) were derived from the latter two parameters using the calibrations of Radke and Welte (1983), Boreham et al. (1988) and Kvalheim et al. (1987).

Of these parameters, the $\%R_c$ of Radke and Welte (1983) gave the best estimate of maturity, when compared to the T_{max} values of the source rocks. This correlation has been previously observed in Bowen/Surat Basin sediments (Boreham, 1995). The calculated vitrinite reflectance for the initially-mature to mature SCM (R_cr = 0.5 - 0.9%) is clearly differentiated from those of the BCG ($R_cr \approx 2.0\%$). The low R_cr value of 0.62%, obtained for a carbonaceous shale of the BWG (sample #18) with a T_{max} value of 451°C, is caused by an anomalously high abundance of phenanthrene. Such high phenanthrene concentrations were also observed in European coals (Kvalheim et al., 1987). The MPDF-derived R_ck value of 1.15% is more reasonable and consistent with the regional pattern of thermal maturity.

Maturity differences between the Permian and Triassic sediments are also indicated by their respective di- and trimethylnaphthalene distributions (Table 5.4). The Permian section has dimethylnaphthalene ratios (DNR-1 = 19-20) that are higher than those of the SCM (DNR-1 < 15). This is also obvious when comparing the trimethylnaphthalene distributions of the BWG (TNR-1 = 2) and the SCM (TNR-1 = 0.7-0.9). The trimethylnaphthalene ratios measured from the two BCG samples (TNR-1 = 0.4-0.5) are, however, unexpectedly low. Such low values most likely reflect differences in the original source material.

5.3 Source-specific biomarker parameters of the Permian sediments

5.3.1 Hopanes and steranes

Marked variations are evident in the biomarker distributions of the Permian facies (Table 5.2). The most striking differences appear when comparing the freshwater coal facies of the BWG (samples #18, 26 and 27) with the marine-influenced section of the BCG (samples #16 and 13) (Table 5.2, Figs. 5.1 and 5.2). A diagnostic feature of the marine influence in the BCG is the presence of C_{30} desmethyl sterane (C_{30}/C_{29} sterane = 0.01-0.12: Table 5.2, Fig. 5.1c). This is accompanied by higher abundances of the C_{27} and C_{28} steranes relative to C_{29} sterane (C_{27} $\alpha\alpha\alpha$R/C_{29} $\alpha\alpha\alpha$R sterane = 0.9 - 1.0: Table 5.2; Fig. 6.6). The same marine-influenced section of the BCG displays evidence of increased anoxicity which is indicated by higher abundances of C_{34} and C_{35} homohopanes (e.g. C_{35}/C_{33} homohopane is up to 0.4 in sample #16: Table 5.2). Furthermore, steranes exhibit their highest abundance relative to the hopanes (hop/ster = 1.1-1.6) in the BCG sections at Cockatoo Creek-1 and Burunga-1 (Table 5.2). Such elevated concentrations of steranes relative to hopanes (*cf.* Moldowan et al., 1985), enhanced proportions of C_{27} and C_{28} steranes (*cf.* Huang and Meinshein, 1979) and, in particular, the presence of C_{30} sterane (*cf.* Peters et al., 1989) all are consistent with a marine algal input to the BCG mudstones.

The presence of C_{30} tricyclic terpane (C_{30}TT/hopane = 0.01-0.11: Fig. 5.1a, Table 6.2) in association with C_{30} desmethyl sterane (see above) is noticed for the BCG samples. This association has previously been observed for other sets of oil and rock samples from the Bowen/Surat Basin (Boreham, 1994), suggesting that both biomarkers may originate from the same type of alga (Boreham, 1995). Low pristane/phytane ratios (0.9 $\leq$ pr/ph $\leq$ 2.8: Table 4.2) for all but two samples indicate that anoxic to suboxic conditions prevailed during deposition of the major part of the BCG.

Table 5.2 Biomarker source parameters of Permo-Triassic sediments and oils, southern Taroom Trough

Parameter *	8	9	10	11	12	13	14	15	16	17
Ratio	25NH Hop	30NH Hop	29,30BNH Hop	28,30BNH Hop	2+3MeH Hop	2MeH 3MeH	C_{29}Ts 30NH	C_{30}diah Hop	C_{35}HH C_{33}HH	Hop Ster
Sample No. & Well Name										
Snake Creek Mudstone										
Facies A (Algal-rich)										
41 Glenhaughton-1	0.01	1.15	0	0.118	0.03	1.89	0.15	0	0.12	1.70
46 Muggleton-1	0	1.16	0	0.052	0.02	1.59	0.01	0	0.10	2.40
47 Snake Creek-1	0.01	0.80	0.04	0.130	0.06	1.05	0.08	0.19	0.09	7.40
58 Tinker-2	0	1.37	0	0	0.06	0.39	0.10	0.04	0.04	5.20
59 Warroon-1	0.04	1.00	0.03	0.192	0.04	1.86	0.11	0.09	0.11	4.40
63 Glenearn North-1	0.03	0.68	0	0.112	0.02	0.74	0.23	0.05	0.13	3.70
Facies B (Bacteria-rich)										
70 Renlim-1	0.01	0.80	0	0.300	0	1.25	0.15	0.03	0.06	4.20
Facies C (Higher plant-rich)										
35 Flinton-1	0.01	1.62	0	0.058	0.06	2.00	0.02	0	0.14	2.40
48 Red Cap-1	0.02	1.00	0.01	0.049	0.04	2.09	0.14	0.04	0.18	5.30
65 Namarah-2	0.01	1.47	0.01	0.030	0.09	2.07	0.17	0.04	0.19	3.10
67 Hollow Tree-1	0	0.91	0	0.252	0.03	0.92	0.15	0.04	0.06	3.90
71 Newington-2	0.01	1.00	0.01	0.021	0.05	0.97	0.07	0.08	0.10	6.50
72 Yellowbank Creek North-1	0.01	1.45	0	0.079	0.03	1.49	0.01	0.02	0.07	7.20
Mixed Facies (AC)										
45 Cabawin-1	0	1.07	0	0.022	0.04	2.59	0.10	0	0.17	2.20
49 Borah Creek-3(1)	0.02	1.31	0	0.045	0.05	1.84	0.13	0.04	0.11	5.90
53 Borah Creek-3(2)	0.01	0.94	0	0.025	0.04	1.43	0.18	0.05	0.08	8.20
57 Taroom-12-12A	0.01	0.77	0	0.045	0.02	1.07	0.17	0.06	0.08	6.70
64 Borah Creek-4	0.02	1.21	0	0.035	0.04	1.44	0.14	0.07	0.09	9.40
Permian Source Rocks										
Blackwater Group										
27 Meeleebee-1	0	1.58	0	0.164	0.04	3.52	0	0.04	0.05	3.70
26 Meeleebee-1	0	1.49	0	0.069	0.07	2.64	0	0.04	0.04	10.30
18 Cockatoo Creek-1	0	1.18	0	0.000	0.03	8.21	0	0.04	0.04	5.00
Back Creek Group										
24 Meeleebee-1	0.01	0.61	0.01	0.067	0	2.75	0.15	0.16	0.10	6.30
19 Flinton-1	0.01	0.66	0	0.022	0.03	1.45	0.19	0.17	0.12	2.10
10 Burunga-1	0.01	0.76	0	0.020	0.05	5.03	0.13	0.10	0.08	1.10
6 Burunga-1	0.02	1.07	0.02	0.060	0.04	3.01	0.21	0.17	0.10	1.30
16 Cockatoo Creek-1	0.03	1.07	0.03	0.055	0.06	1.16	0.23	0.07	0.35	1.60
13 Cockatoo Creek-1	0.04	1.05	0.02	0.062	0.06	3.35	0.27	0.06	0.14	1.60
Bowen/Surat Basin Oils										
1 Taylor-12A	0.02	0.83	0.01	0.064	0.06	3.43	0.10	0.19	0.06	2.10
2 Taylor-11	0.02	0.74	0.02	0.031	0.07	20.82	0.14	0.20	0.08	1.40
3 Tinker-4	0.01	0.61	0.01	0.017	0.01	3.03	0.13	0.22	0.16	1.50
4 Roswin North-1	0.01	0.66	0	0.018	0.05	4.57	0.19	0.11	0.09	6.50
5 Washpool-1	0.30	0.69	0	0.079	0.16	5.49	0.25	0.46	0.15	0.70
6 Wilga-2	1.10	0.89	0	0.146	0.26	8.78	0.37	0.54	0.13	0.62
7 Waratah-1	0.02	0.72	0	0.087	0.09	8.91	0.08	0.11	0.14	1.70
8 Martini-1	0.09	0.72	0.03	0.098	0.10	5.61	0.18	0.37	0.07	1.20
9 Riverslea-1	0.20	0.81	0.02	0.135	0.10	6.95	0.30	0.37	0.12	1.20
10 Cogoon River West-1	0.07	0.70	0.01	0.087	0.09	8.72	0.16	0.24	0.09	2.00
11 Bellbird-1	0.02	0.71	0.01	0.044	0.05	2.99	0.15	0.33	0.14	1.70
12 Merroombile-1	0.02	0.79	0.04	0.061	0.11	5.89	0.07	0.17	0.37	1.50

* Refer to Table 5.3 (b) for explanation of parameters used

Table 5.2 Biomarker source parameters of Permo-Triassic sediments and oils, southern Taroom Trough (continued)

Parameter *	18			19	20	21	22	23
Ratio	Steranes							
	$C_{27}R$	$C_{28}R$	$C_{29}R$	$C_{27}R/C_{29}R$	C_{27}/C_{29}	C_{28}/C_{29}	$C_{30}R/C_{29}R$	C_{29}dia/ster
Sample No. & Well Name								
Snake Creek Mudstone								
Facies A (Algal-rich)								
41 Glenhaughton-1	30	23	47	0.64	0.84	0.62	0.036	0.95
46 Muggleton-1	36	18	46	0.77	0.86	0.48	0.011	0.87
47 Snake Creek-1	17	23	60	0.28	0.28	0.41	0	1.01
58 Tinker-2	36	15	49	0.74	0.92	0.43	0	0.48
59 Warroon-1	17	20	63	0.27	0.33	0.38	0	0.99
63 Glenearn North-1	23	16	61	0.38	0.41	0.35	0	0.59
Facies B (Bacteria-rich)								
70 Renlim-1	27	16	57	0.48	0.98	0.59	0	0.74
Facies C (Higher plant-rich)								
35 Flinton-1	20	26	54	0.37	0.44	0.53	0.034	0.59
48 Red Cap-1	25	19	56	0.41	0.38	0.31	0	0.54
65 Namarah-2	39	19	42	0.42	0.40	0.32	0	0.48
67 Hollow Tree-1	18	17	65	0.27	0.34	0.29	0	0.40
71 Newington-2	28	25	47	0.43	0.40	0.25	0	0.65
72 Yellowbank Creek North-1	20	18	62	0.33	0.40	0.34	0	0.41
Mixed Facies (AC)								
45 Cabawin-1	27	20	53	0.52	0.66	0.45	0.015	0.91
49 Borah Creek-3(1)	24	18	58	0.41	0.53	0.42	0	1.16
53 Borah Creek-3(2)	21	17	62	0.35	0.46	0.38	0	1.34
57 Taroom-12-12A	4	19	77	0.05	0.08	0.33	0	0.67
64 Borah Creek-4	18	19	63	0.29	0.34	0.33	0	1.09
Permian Source Rocks								
Blackwater Group								
27 Meeleebee-1	10	8	82	0.13	0.16	0.15	0	1.15
26 Meeleebee-1	4	9	87	0.04	0.05	0.16	0	0.60
18 Cockatoo Creek-1	3	7	90	0.04	0.05	0.08	0	0.69
Back Creek Group								
24 Meeleebee-1	21	12	67	0.32	0.39	0.24	0.014	1.88
19 Flinton-1	37	16	47	0.79	0.91	0.41	0.068	2.56
10 Burunga-1	17	13	70	0.24	0.28	0.22	0.016	1.16
6 Burunga-1	31	18	51	0.61	0.57	0.36	0.059	0.61
16 Cockatoo Creek-1	39	23	38	1.03	0.90	0.59	0.119	0.71
13 Cockatoo Creek-1	39	20	41	0.94	0.82	0.51	0.065	0.87
Bowen/Surat Basin Oils								
1 Taylor-12A	23	15	62	0.37	0.18	0.23	0	1.74
2 Taylor-11	31	15	54	0.59	0.35	0.29	0	1.21
3 Tinker-4	25	15	60	0.42	0.20	0.21	0	1.29
4 Roswin North-1	18	9	73	0.25	0.25	0.07	0	2.13
5 Washpool-1	13	13	74	0.18	0.09	0.20	0	1.41
6 Wilga-2	12	13	75	0.16	0.10	0.21	0	1.40
7 Waratah-1	10	12	78	0.12	0.09	0.16	0	1.90
8 Martini-1	14	18	68	0.20	0.14	0.27	0	1.25
9 Riverslea-1	9	15	76	0.13	0.09	0.24	0	0.99
10 Cogoon River West-1	12	12	76	0.15	0.10	0.19	0	1.49
11 Bellbird-1	16	16	68	0.23	0.19	0.30	0	1.10
12 Merroombile-1	31	12	57	0.54	0.42	0.38	0	1.20

* Refer to Table 5.3 (b) for explanation of parameters used

Table 5.2 Biomarker source parameters of Permo-Triassic sediments and oils, southern Taroom trough (continued)

Parameter *	24	25	26	27	28	29	30
Ratio	Methylsteranes						
	C_{28}	C_{29}	C_{30}	4Mest / C_{29} st	2+3Mest / C_{29} st	4αS / 3βS	dino / 3βS
Sample No. & Well Name							
Snake Creek Mudstone							
Facies A (Algal-rich)							
41 Glenhaughton-1	25.8	29.7	44.5	0.10	0.23	0.58	0.10
46 Muggleton-1	28.8	39.8	31.4	0.04	0.11	0.50	0.15
47 Snake Creek-1	23.0	14.3	62.3	0.11	0.25	0.74	0.05
58 Tinker-2	17.9	21.2	60.9	0.06	0.18	0.41	0.04
59 Warroon-1	18.7	19.8	61.5	0.14	0.19	0.49	0.14
63 Gleneam North-1	14.3	20.9	64.8	0.06	0.10	0.94	0.09
Facies B (Bacteria-rich)							
70 Renlim-1	15.2	37.0	47.8	0.12	0.16	0.55	0.50
Facies C (Higher plant-rich)							
35 Flinton-1	12.0	29.3	58.7	0.15	0.37	0.32	0.13
48 Red Cap-1	15.4	16.8	67.8	0.21	0.30	0.96	0.05
65 Namarah-2	15.3	36.6	48.9	0.21	0.28	0.49	0.05
67 Hollow Tree-1	19.8	21.9	58.3	0.06	0.17	0.71	0.43
71 Newington-2	23.4	24.6	52.0	0.12	0.19	0.78	0.07
72 Yellowbank Creek North-1	15.1	19.0	65.9	0.10	0.17	0.68	0.32
Mixed Facies (AC)							
45 Cabawin-1	23.9	35.6	40.5	0.05	0.36	0.28	0.14
49 Borah Creek-3(1)	16.5	22.9	60.6	0.15	0.24	0.57	0.12
53 Borah Creek-3(2)	16.6	18.3	65.1	0.15	0.16	0.51	0.16
57 Taroom-12-12A	14.1	11.9	74.0	0.10	0.14	0.69	0.03
64 Borah Creek-4	13.7	17.1	69.2	0.14	0.21	0.65	0.07
Permian Source Rocks							
Blackwater Group							
27 Meeleebee-1	36.8	36.9	26.3	0.01	0.22	0.12	0
26 Meeleebee-1	34.4	41.6	24.0	0.01	0.24	0.17	0
18 Cockatoo Creek-1	35.0	39.5	25.5	0.01	0.23	0.20	0
Back Creek Group							
24 Meeleebee-1	13.0	16.4	70.6	0.05	0.28	1.32	0
19 Flinton-1	29.2	16.3	62.5	0.03	0.26	1.21	0
10 Burunga-1	33.1	25.8	41.1	0.03	0.18	0.31	0
6 Burunga-1	23.5	29.6	46.9	0.13	0.29	0.63	0
16 Cockatoo Creek-1	0	27.7	72.3	0.06	0.30	1.64	0
13 Cockatoo Creek-1	0	40.0	60.0	0.04	0.32	0.69	0
Bowen/Surat Basin Oils							
1 Taylor-12A	14.0	17.0	69.0	0.07	0.44	0.39	0
2 Taylor-11	38.5	16.1	45.4	0.01	0.50	0.50	0
3 Tinker-4	25.5	15.0	59.5	0.01	0.38	0.45	0
4 Roswin North-1	10.3	13.2	76.5	0.15	0.20	0.98	0.16
5 Washpool-1	20.0	39.4	40.6	0.03	0.40	0.40	0
6 Wilga-2	47.1	17.8	35.1	0.02	0.36	0.30	0
7 Waratah-1	49.6	29.8	20.6	0.01	0.27	0.29	0
8 Martini-1	30.1	21.3	48.6	0.01	0.35	0.28	0
9 Riverslea-1	40.8	31.4	27.8	0.02	0.32	0.30	0
10 Cogoon River West-1	36.6	22.0	41.4	0	0.27	0.42	0
11 Bellbird-1	17.4	44.1	38.5	0.01	0.50	0.47	0
12 Merroombile-1	11.2	11.2	77.6	0	0.66	0.30	0.10

* Refer to Table 5.3 (b) for explanation of parameters used

Table 5.3 (a) Key to maturity-dependent biomarker parameters listed in Table 5.1

Parameter		Ratio	MRM Transitions
1. **%22S**	=	%22S/(22S+22R)-C_{31} homohopane = 100 x 17α,21β(H) 22S homohopane / 17α,21β(H) 22(S+R) homohopane	426→191
2. **Mor / Hop**	=	C_{30} moretane / C_{30} hopane = 17β,21α(H)-hopane / 17α,21β(H)-hopane	412→191
3. **T_s / T_m**	=	C_{27} 18α(H)-22,29,30-trisnorneohopane / C_{27} 17α(H)-22,29,30-trisnorhopane	370→191
4. **%20S**	=	% 20S/(20S+20R)-C_{29} sterane = 100 x 5α,14α,17α(H)-24-ethylcholestane 20S / 5α,14α,17α(H)-24-ethylcholestane 20(S+R)	400→217
5. **%ββ**	=	%ββ/(ββ+αα)-C_{29} sterane = 5α,14β,17β(H)-24-ethylcholestane 20(S+R) / [5α,14β,17β(H)-24-ethylcholestane 20(S+R) + 5α,14α,17α(H)-24-ethylcholestane 20(S+R)]	400→217
6. **20S / 20R**	=	5α,14α,17α(H)-24-ethylcholestane 20S / 5α,14α,17α(H)-24-ethylcholestane 20R	400→217
7. **αββ / ααα20R**	=	5α,14β,17β(H)-24-ethylcholestane 20R / 5α,14α,17α(H)-24-ethylcholestane 20R	400→217

Table 5.3 (b) Key to source-specific biomarker parameters listed in Table 5.2

Parameter		Ratio	MRM Transitions
8. **25NH / Hop**	=	C_{29} 17α(H),21β(H)-25-norhopane / C_{30} 17α(H),21β(H)-hopane	398→177 412→191
9. **30NH / Hop**	=	C_{29} 17α(H),21β(H)-30-norhopane / C_{30} 17α(H),21β(H)-hopane	398→191 412→191
10. **29,30BNH / Hop**	=	29,30-bisnorhopane / C_{30} 17α(H),21β(H)-hopane	384→191 412→191
11. **28,30BNH / Hop**	=	28,30-bisnorhopane / C_{30} 17α(H),21β(H)-hopane	384→191 412→191
12. **2+3MeH / Hop**	=	C_{31} (2α+3β)-methylhopane / C_{30} 17α(H),21β(H)-hopane	426→205
13. **2MeH / 3MeH**	=	2α-methylhopane / 3β-methylhopane	398→191
14. **$C_{29}T_s$ / 30NH**	=	18α(H),21β(H)-30-norneohopane / C_{29} 17α(H),21β(H)-30-norhopane	398→191 412→191
15. **C_{30} diah/ Hop**	=	C_{30} 17α-diahopane / C_{30} 17α(H),21β(H)-hopane	398→191 412→191
16. **C_{35}HH / C_{33}HH**	=	C_{35} / C_{33} homohopanes	454→191 482→191
17. **Hop / Ster**	=	Hopane/Sterane;	M+→191; where M+ = m/z 370 (C_{27}), m/z 384 (C_{28}), m/z 398 (C_{29}), m/z 412 (C_{30}), m/z 426 (C_{31}), m/z 440 (C_{32}), m/z 454 (C_{33}), m/z 468 (C_{34}).
Hopane	=	$\Sigma C_{27\text{-}34}$ hopanes and moretanes = C_{27} trisnorhopanes (T_s+T_m) + C_{28} bisnorhopanes (28,30-BNH + 29,30-BNH) + C_{29} (30-NH+moretane) + C_{30} (hopane+moretane) + $C_{31\text{-}34}$ (homohopanes+homomoretanes)	
Sterane	=	$\Sigma C_{27\text{-}29}$ [5α,14α,17α(H)-20(S+R) + 5α,14β,17β(H)-20(S+R)] steranes	372→217 386→217 400→217

Table 5.3 (b) Key to source-specific biomarker parameters listed in Table 5.2 (continued)

Parameter	Ratio	MRM Transitions
18. C_{27} : C_{28} : C_{29}	5α,14α,17α(H)-cholestane 20R	372→217 386→217 400→217
19. C_{27} R / C_{29} R	= 5α,14α,17α(H)-cholestane 20R / 5α,14α,17α(H)-24-ethylcholestane 20R	372→217 400→217
20. C_{27} / C_{29} st	= [5α,14α,17α(H)-cholestane 20(S+R) + 5α,14β,17β(H)-cholestane 20(S+R)] / [5α,14α,17α(H)-24-ethylcholestane 20(S+R) + 5α,14β,17β(H)-24-ethylcholestane 20(S+R)]	372→217 400→217
21. C_{28} / C_{29} st	= [5α,14α,17α(H)-24-methylcholestane 20(S+R) + 5α,14β,17β(H)-24-methylcholestane 20(S+R)] / [5α,14α,17α(H)-24-ethylcholestane 20(S+R) + 5α,14β,17β(H)-24-ethylcholestane 20(S+R)]	386→217 400→217
22. C_{30} R/ C_{29} R	= 5α,14α,17α(H)-24-*n*-propylcholestane 20R / 5α,14α,17α(H)-24-ethylcholestane 20R	400→217 414→217
23. C_{29} dia/ ster	= 5α,13β,17α(H)-dia-24-ethylcholestane 20(S+R) / [5α,14α,17α(H)-24-ethylcholestane 20(S+R) + 5α,14β,17β(H)-24-ethylcholestane 20(S+R)]	400→217
24. C_{28} 4α-methyl sterane	= Ratio of 4α-methyl-5α,14α,17α(H)-cholestane 20R to total C_{28}-C_{30} 4α-methylcholestanes	386→231

Table 5.3 (b) Key to source-specific biomarker parameters listed in Table 5.2 (continued)

Parameter	Ratio	MRM Transitions
25. **C_{29} 4α-methyl sterane**	= Ratio of 4α-methyl-5α,14α,17α(H)-24-methylcholestane 20R to total C_{28}-C_{30} 4α-methylcholestanes	400→231
26. **C_{30} 4α-methyl sterane**	= Ratio of (4α-methyl-5α,14α,17α(H)-24-ethylcholestane 20R + 4α,23,24-trimethyl-5α,14α,17α(H)-cholestane 20R) to total C_{28}-C_{30} 4α-methylcholestanes	414→231
27. **4 Mest / C_{29} st**	= C_{30} 4α-methyl cholestane 20R / 5α,14α,17α(H)-24-ethylcholestane 20R	386→231 400→231 414→231 400→217
28. **2+3 Mest / C_{29} st**	= (2α+3β)-methyl-5α,14α,17α(H)-24-ethylcholestane 20R / 5α,14α,17α(H)-24-ethylcholestane 20R	400→217 414→231
29. **4αS / 3βS**	= 4α-methyl-5α,14α,17α(H)-24-ethylcholestane 20S / 3β-methyl-5α,14α,17α(H)-24-ethylcholestane 20S	414→231
30. **dino / 3βS**	= 4α,23R,24S-trimethyl-5α,14α,17α(H)-cholestane 20R / 3β-methyl-5α,14α,17α(H)-24-ethylcholestane 20S	414→231

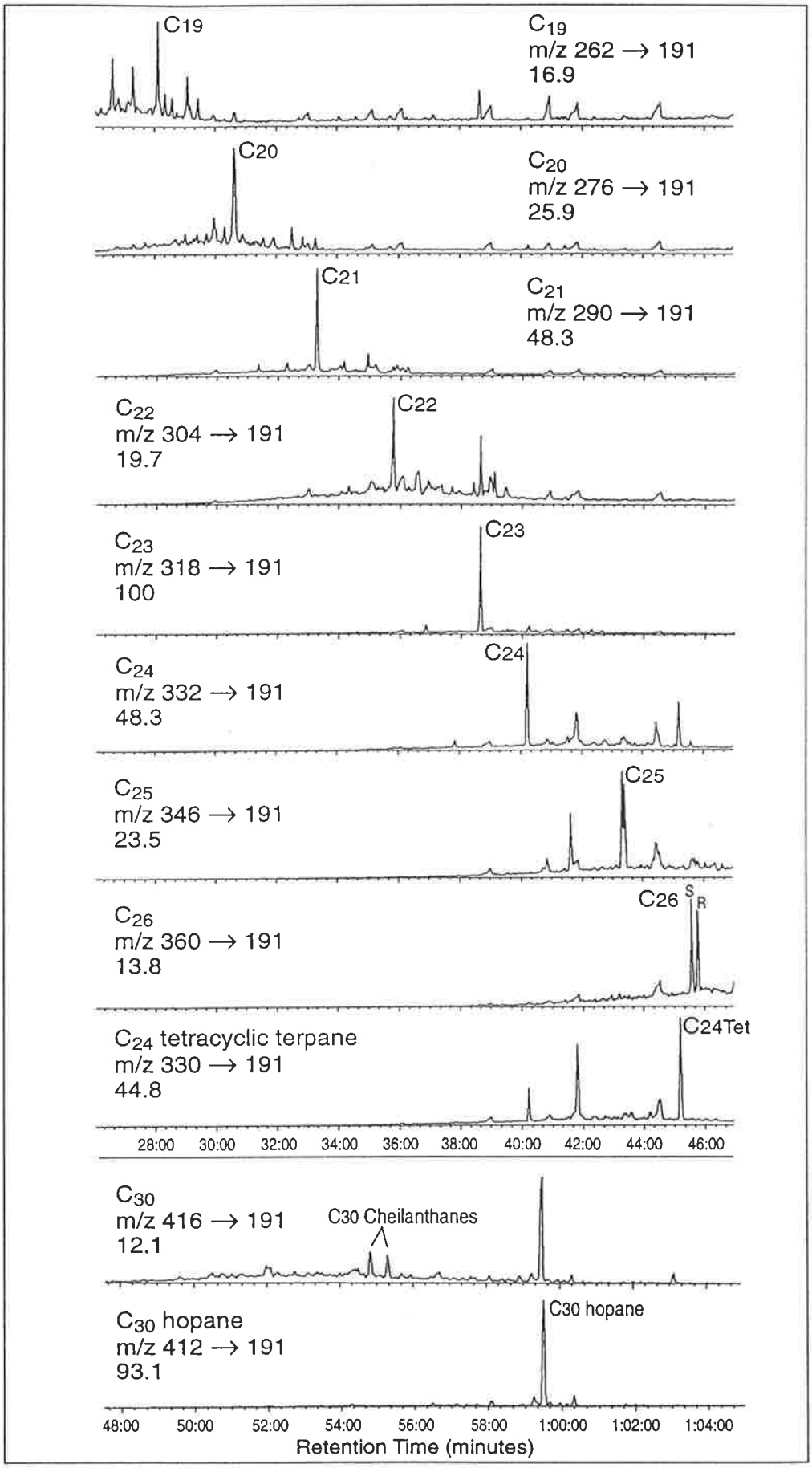

Figure 5.1 (a) MRM chromatograms showing the distributions of cheilanthanes and C_{24} tetracyclic terpane in calcareous mudstone of the Back Creek Group, Cockatoo Creek-1 (sample #13). The intensity for each trace is normalised against C_{30} hopane.

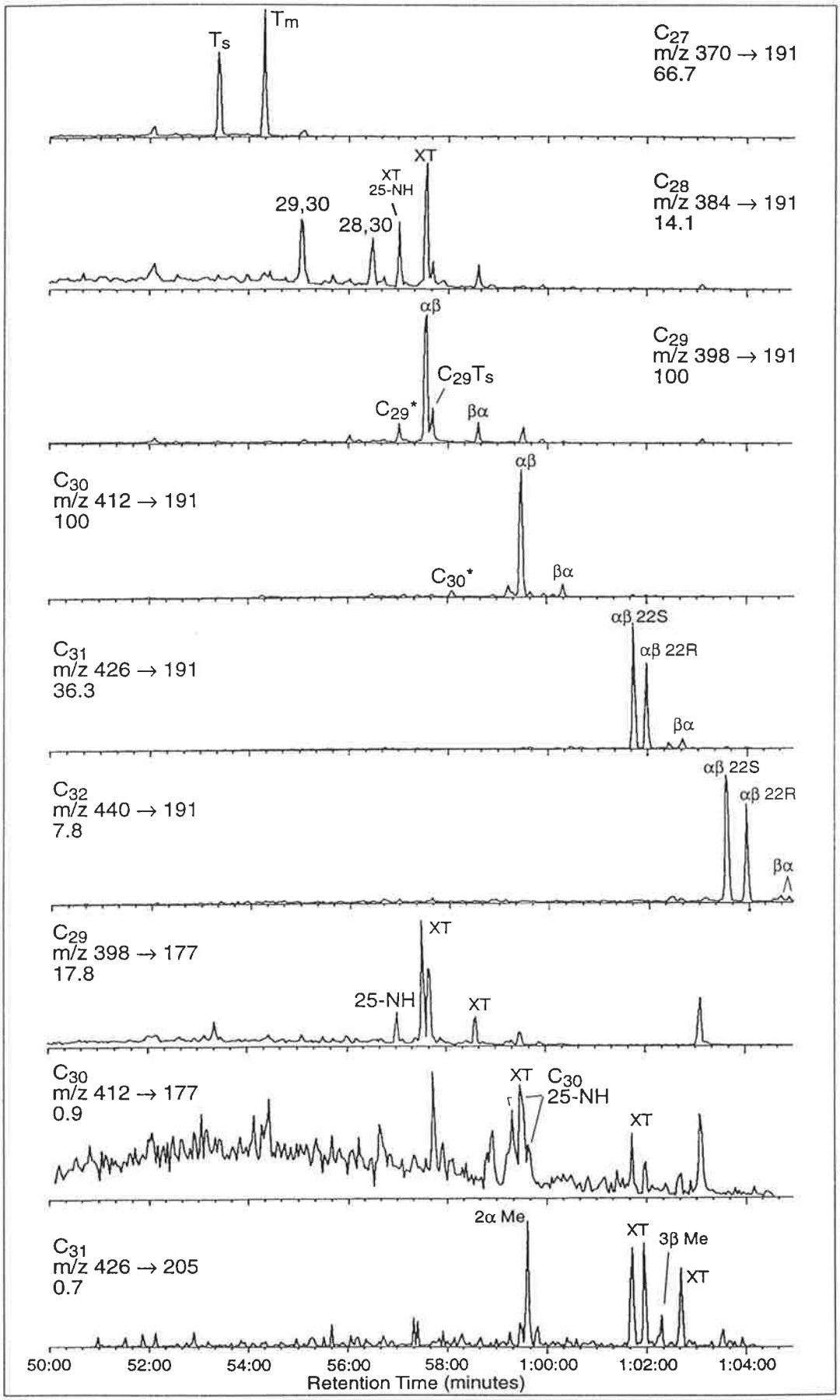

Figure 5.1 (b) MRM chromatograms showing the distributions of hopanes, norhopanes and methylhopanes in calcareous mudstone of the Back Creek Group, Cockatoo Creek-1 (sample #13). The intensity for each trace is normalised against the highest peak in the hopanes and steranes.

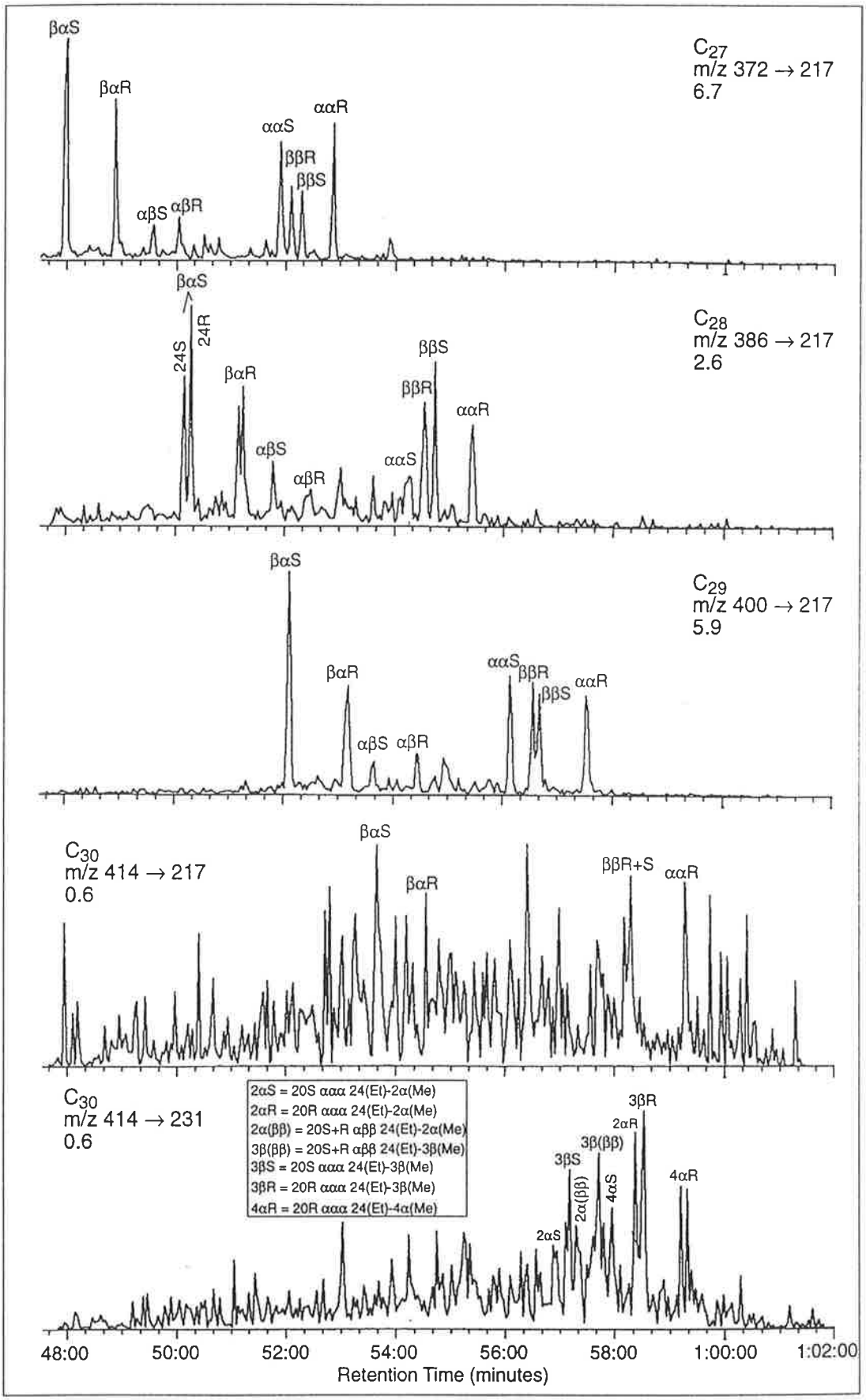

Figure 5.1 (c) MRM chromatograms showing the distributions of steranes ($M^{+\cdot} \rightarrow$ m/z 217) and methylsteranes ($M^{+\cdot} \rightarrow$ m/z 231) in calcareous mudstone of the Back Creek Group, Cockatoo Creek-1 (sample #13). The intensity for each trace is normalised against the highest peak in the hopanes and steranes.

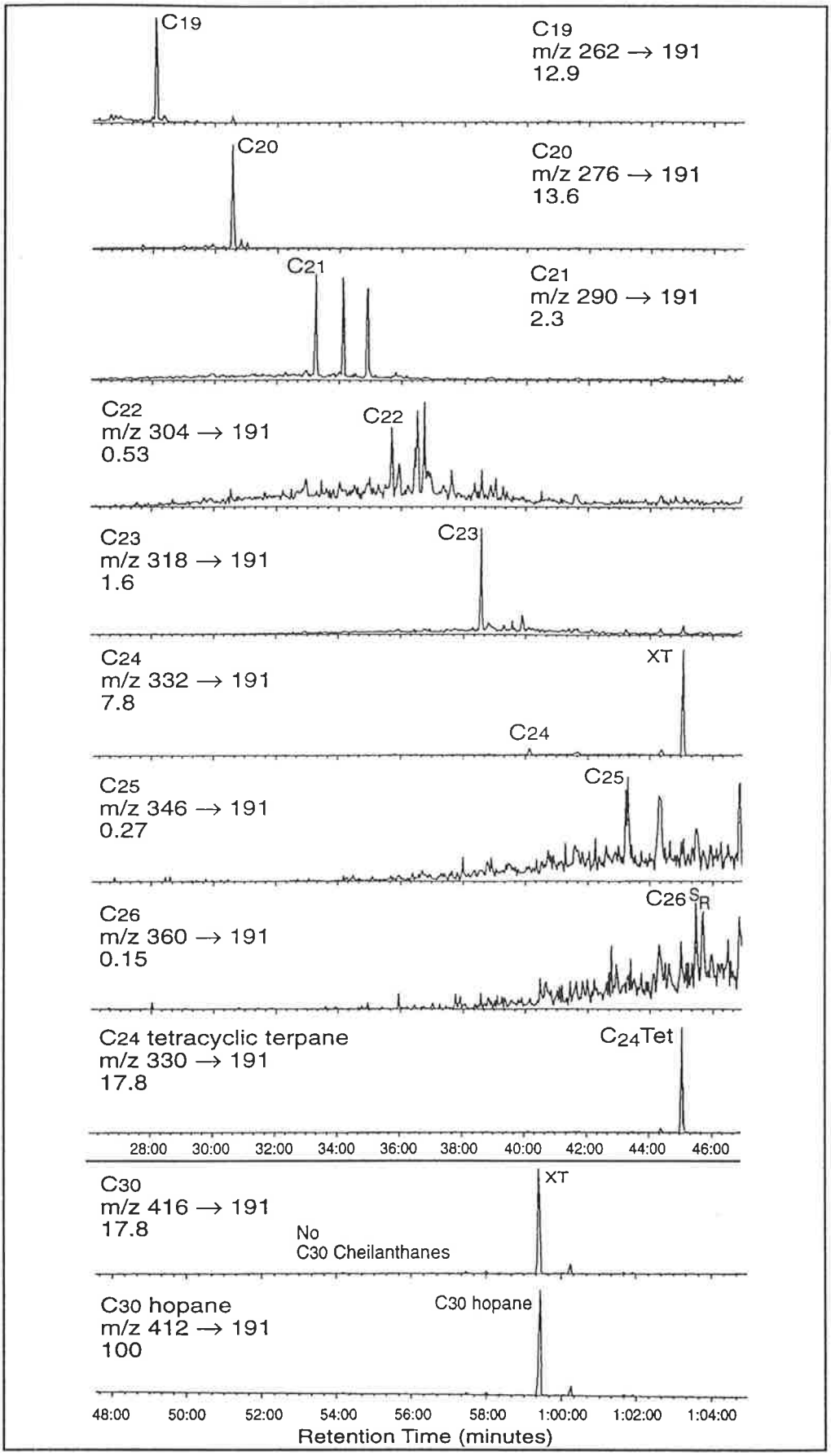

Figure 5.2 (a) MRM chromatograms showing the distributions of cheilanthanes and C_{24} tetracyclic terpane in carbonaceous shale of the Baralaba Coal Measures, Blackwater Group, Cockatoo Creek-1 (sample #18). The intensity for each trace is normalised against C_{30} hopane.

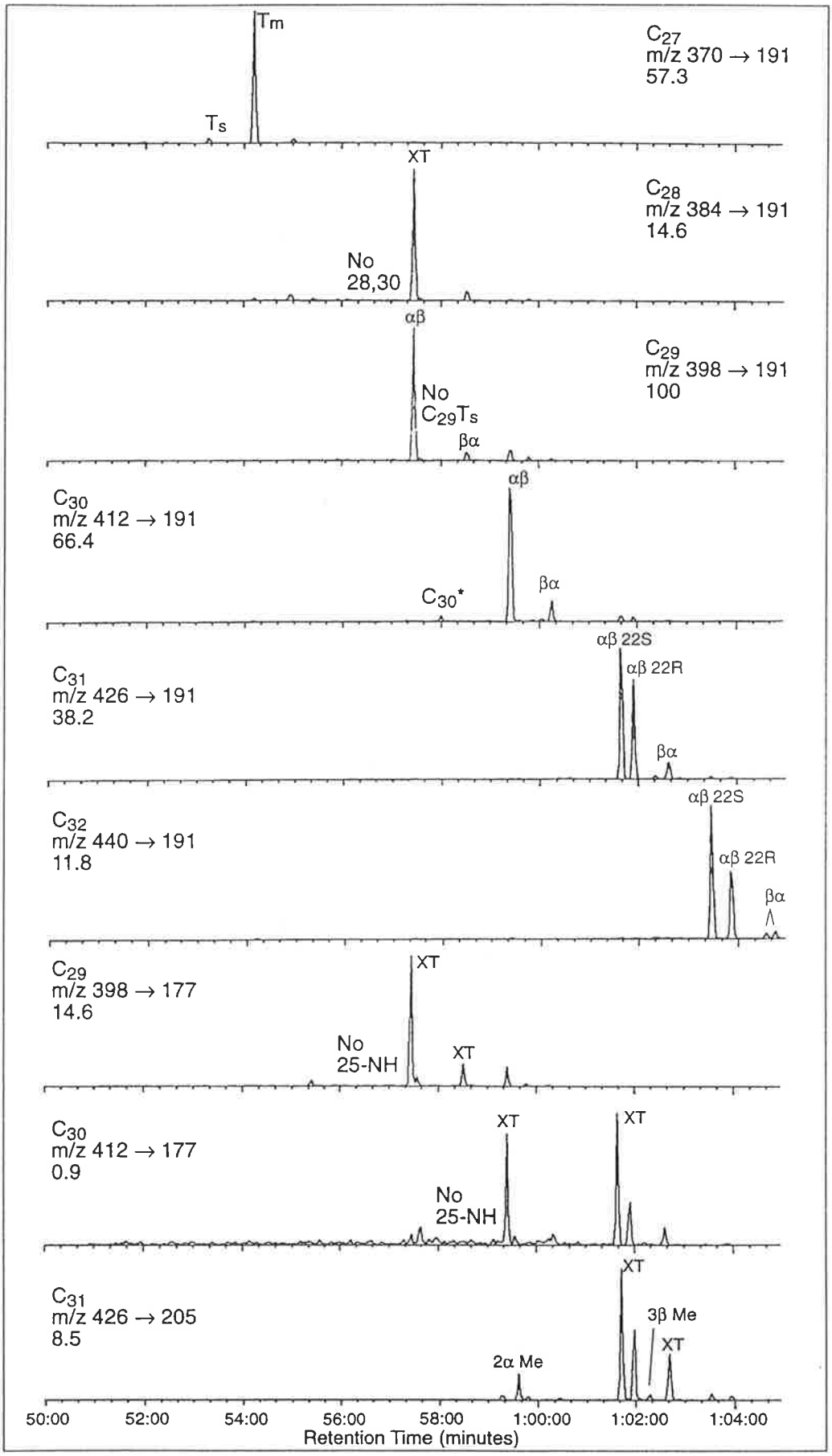

Figure 5.2 (b) MRM chromatograms showing the distributions of hopanes, norhopanes and methylhopanes in carbonaceous shale of the Baralaba Coal Measures, Blackwater Group, Cockatoo Creek-1 (sample #18). The intensity for each trace is normalised against the highest peak in the hopanes and steranes.

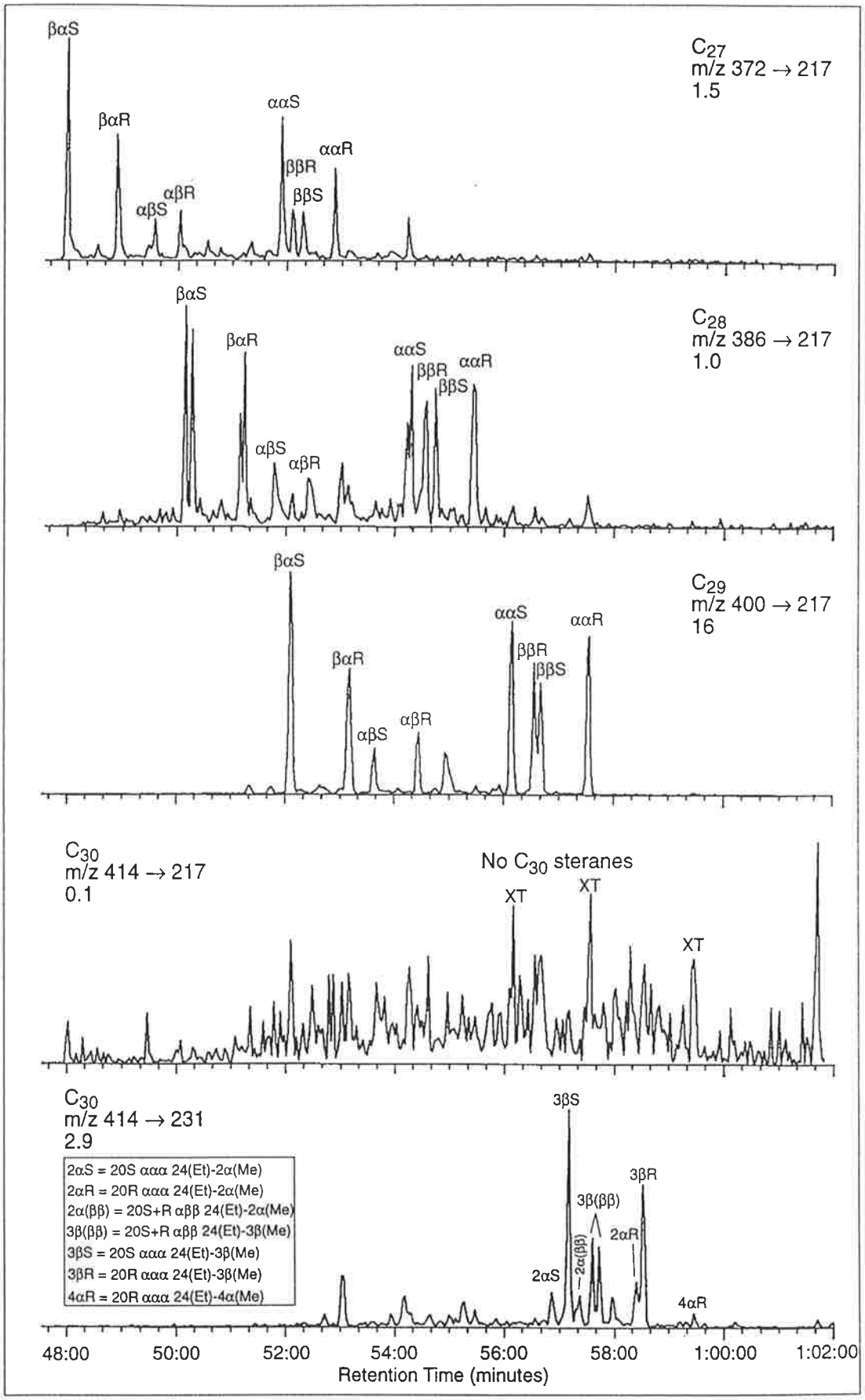

Figure 5.2 (c) MRM chromatograms showing the distributions of steranes ($M^{+\cdot} \rightarrow$ m/z 217) methylsteranes ($M^{+\cdot} \rightarrow$ m/z 231) in carbonaceous shale of the Baralaba Coal Measures, Blackwater Group, Cockatoo Creek-1 (sample #18). The intensity for each trace is normalised against the highest peak in the hopanes and steranes.

On the other hand, the sediments of the coal-bearing BWG are devoid of C_{30} desmethyl steranes (Fig. 5.2c, Table 5.2) and C_{30} tricyclic terpanes (Fig. 5.2a, Table 6.2). These features, together with the near absence of the higher homohopane series (C_{35}/C_{33} homohopanes $\leq$ 0.05: Table 5.2), hopane/sterane ratios up to 10.3, and the predominance of the C_{29} steranes among the C_{27}-C_{29} regular steranes (C_{27} $\alpha\alpha\alpha$20R/C_{29} $\alpha\alpha\alpha$20R sterane = 0.04: Table 5.2), are testimony to land-plant remains deposited in a freshwater setting (*cf.* Huang and Meinshein, 1979; Tissot and Welte, 1984; Luo Binjie et al., 1988).

The near absence of 4α-methyl steranes, and complete absence of dinosterane, in the BCG (e.g. Fig. 5.1c) and BWG (e.g. Fig. 5.2c) samples is consistent with their Permian age. Despite rare occurrences of dinoflagellate fossils in Paleozoic sediments (Tappan,1980), dinosterane has only been reported in Mesozoic and Cenozoic oils and sediments (Summons et al., 1987, 1992; Thomas et al., 1993). Plotting the relative abundances of the C_{28}, C_{29} and C_{30} 4α-methyl-5α,14α,17α(H)-steranes on a ternary diagram (*cf.* Fu Jiamo et al., 1990; Boreham et al., 1994) demonstrates the variability of the algal input into the Permian sediments (Fig. 6.7b). The BCG samples exhibit dominance of C_{30} 4α-methyl steranes over their C_{28} and C_{29} counterparts, and complete absence of C_{28} compounds in the calcareous mudstones (Table 5.2). This may be related to slightly higher salinity and/or algal inputs that are different from those of the BWG. The increased marine algal input (as indicated by the presence of C_{30} sterane, see above) to the BCG sediments might have been a factor in increasing their C_{30} 4α-methyl sterane concentrations. On the other hand, carbonaceous shales of the BWG contain less C_{30} 4α-methyl steranes, whereas their C_{29} 4α-methyl steranes are equally abundant with, or dominant over, the C_{28} homologues (Table 5.2). In the case of Chinese lacustrine sediments of Cretaceous-Tertiary age, such compositional variations in the 4α-methyl steranes have been attributed to different species of dinoflagellate (Fu Jiamo et al., 1990). Although a similar explanation may hold for the Triassic samples of the Bowen Basin (Section 5.4.1), it is more likely that such differences in the Permian sediments are related to variable inputs of algal species other than dinoflagellates, due to their scarcity in sediments older than Triassic, as mentioned above. Variations in the 4α-methyl sterane composition of the BCG and BWG sediments may also be explained by differences in the paleosalinity of their depositional environments. Fu Jiamo et al. (1990) show that sediments deposited under more saline conditions are enriched in C_{29} and C_{30} 4α-methyl steranes and depleted in C_{28} homologues, compared with those from frehwater and brackish lacustrine settings. As such, the 4α-methyl composition ($C_{28} \approx C_{29}$, low C_{30}: Table 5.2) of the BWG carbonaceous shales is consistent with their deposition in a freshwater environment.

The highest abundances of 4α-methyl-24-ethylsteranes relative to 3β-methyl-24-ethylsteranes (4αS/3βS = 1.2-1.6: Table 5.2) are found in calcareous mudstones of the BCG, consistent with their deposition under reducing conditions (*cf.* Dahl et al., 1994). On the other hand, all other carbonaceous shales of the BCG and BWG are depleted in 4α-methyl steranes (3β > 2α > 4α; 4αS/3βS = 0.1-0.7), with the BWG showing the lowest concentrations (4αS/3βS = 0.1-0.2: Table 5.2, Fig. 5.2c). Such predominance of 3β-methyl steranes is commonly associated with sediments deposited under more oxic conditions (Dahl et al., 1994). Nevertheless, the ubiquitous presence of 2α- and 3β-methyl steranes in all samples is consistent with their presumed bacterial affinity. Summons and Capon (1988, 1991) suggested that these methylsteranes are formed by alkylation of desmethylsteranes at the 2- and 3- positions via a diagenetic process. The resulting 2- and 3-methyl steranes are then incorporated into the bacteria and selectively preserved in their membranes (Dahl et al., 1992).

The presence of C_{28} 28,30-bisnorhopane in the BCG sediments is further evidence of an anaerobic bacterial input to a less oxic depositional environment (*cf.* Grantham et al., 1980). However, this is not unique to the BCG, and some BWG samples also show enhanced concentrations of these compounds (Table 5.2), indicating that although the environment was predominantly oxic, suboxic conditions prevailed locally. The additional presence of 2α- and 3β-methylhopanes suggests that some of the bacterial input was from aerobic methylotrophs (*cf.* Bisseret et al., 1985).

Trace amounts of 25-norhopanes (e.g. 25NH/C_{30} hopane = 0.01-0.04) and C_{28} 29,30-bisnorhopane (29,30BNH/C_{30} hopane = 0.01-0.03) were detected in the BCG, whereas they are completely absent in the BWG (Table 5.2, Figs 5.1b and 5.2b). Also absent is $C_{29}T_s$, and the diahopanes occur in trace amounts (C_{30} diah/hop = 0.04: Table 5.2, Figs. 5.1b and 5.2b). Diahopanes (C_{30}*-C_{34}*) and $C_{29}T_s$ have been reported in sediments deposited under more oxic to suboxic conditions and/or containing terrestrial organic matter (Philp and Gilbert, 1986; Peters and Moldowan, 1993), and their concentrations increase with increasing maturity (Moldowan et al., 1991). Applying these observations to the Permian source rocks of the Bowen Basin shows that maturity is the principal factor controlling their occurrence and relative abundance. Although the BWG was deposited under more oxic conditions (with absolutely no marine influence), the higher maturation levels of the BCG resulted in its higher concentrations of both C_{30}* and $C_{29}T_s$ because of their greater stability (see also Fig. 6.4a).

5.3.2 Alkylnaphthalenes and alkylphenanthrenes

Alexander et al. (1988) used the Araucariaceae (*Agathis*)-specific biomarkers 1,2,5-trimethylnaphthalene (TMN), 1,7-dimethylphenanthrene (DMP), 1-methylphenanthrene and retene to distinguish between oils derived from the Permo-Triassic Cooper Basin and those derived from the overlying Jurassic-Cretaceous Eromanga Basin. The three Permian samples in Table 5.4 plot within (or immediately adjacent to) the Permian quadrants of the source affinity diagrams conceived by Alexander et al. (1988) (Figs. 6.10a and b).

Methylphenanthrene (MP) distributions are primarily maturity-related. Nevertheless, they also are influenced by organic matter variations (Radke et al., 1986; Budzinski et al., 1995). For the present suite of rock samples (Table 5.4), 2-MP and 3-MP predominate over 1-MP and 9-MP only in the marine-influenced Permian section represented by sample #16. This is compatible with previous observations (Radke et al., 1986) regarding the predominance of 2-MP and 3-MP in highly mature Type I and II kerogens. On the other hand, all other terrestrial sediments examined have MP distributions dominated by the 1- and 9- substituted compounds (Table 5.4).

5.4 Depositional environment and molecular source parameters of the SCM

Variations in organic facies reflect differences in the original biota, their depositional environment and the diagenetic processes the preserved organic matter undergoes during and after deposition. Based on *n*-alkane and biomarker compositions, two main lacustrine environments can be recognised within the SCM depositional setting. The first is freshwater and oxic, and the other is brackish and suboxic. A marine influence on the SCM lake is seen locally in the northwest and southeast margins of the southern Taroom Trough. These findings are discussed in detail in the following sections.

5.4.1 Molecular signatures common to all SCM samples

The SCM source rocks contain Type III or, in some cases, Type II/III kerogen (Section 4.3.3) which is inferred to be of mixed origin and deposited in a fresh to brackish water lacustrine environment (*cf.* Tissot and Welte, 1984; Yang Wanli et al., 1985). This inference is supported by the following biomarker characteristics which are common to all SCM samples:

Table 5.4 Aromatic-based maturity and source parameters of selected source rocks and oils, southern Taroom Trough

Parameter *	Maturity Parameters							Source Parameters			
	DNR-1	TNR-1	MPI-1	MPDF-1	R_cr %	R_cb %	R_ck %	Retene / 9-MP	1,7-DMP / X	1-MP / 9-MP	1,2,5-TMN / 1,3,6-TMN
Sample											
Triassic SCM											
70 Renlim-1	14.81	0.81	0.26	0.30	0.56	0.4	0.51	0.078	0.457	1.175	1.660
47 Snake Creek-1	5.24	0.63	0.37	0.47	0.62	0.48	0.90	0.065	0.355	0.724	0.437
P47 Snake Creek-1 (Pyrolysate)	1.89	0.87	0.48	0.41	0.67	0.56	0.75	0.126	0.513	0.603	1.950
64 Borah Creek-4	4.07	0.73	0.19	0.37	0.51	0.35	0.65	0.174	0.234	0.724	1.445
Permian sediments											
18 Cockatoo Creek-1 (BWG)	19.00	1.98	0.37	0.59	0.62	0.48	1.15	0.032	0.468	0.830	1.514
6 Burunga-1 (BCG)	nd	0.36	0.48	0.44	2.01	2.74	0.82	nd	2.692	0.891	1.585
16 Cockatoo Creek-1 (BCG)	20.00	0.48	0.59	0.83	1.95	2.68	1.70	0.007	0.282	0.692	0.047
Bowen/Surat oils											
11 Bellbird-1	3.28	0.80	0.37	0.48	0.62	0.48	0.91	0.191	0.363	0.646	0.617
4 Roswin North-1	8.15	0.96	0.38	0.51	0.63	0.49	0.97	0.062	0.398	0.692	1.514
5 Wilga-2	7.31	0.60	0.60	0.52	0.75	0.64	1.00	0.093	0.339	0.617	0.447
6 Washpool-1	6.55	0.54	0.60	0.45	0.75	0.63	0.84	0.355	0.331	0.692	0.562

* Abbreviations, definitions and mass fragmentograms used for the identification of alkylnaphthalenes and alkylphenanthrenes are listed in Table 2.2
nd = not determined

1. Pristane is dominant over phytane (pr/ph = 1.5-5.6: Table 4.2) in all but one sample, and *n*-heptadecane and *n*-octadecane are dominant over pristane and phytane (pr/*n*-C_{17} = 0.1-0.9; ph/*n*-C_{18} = 0.04-0.3: Table 4.2). This indicates deposition under fluctuating oxic/suboxic conditions (Didyk et al., 1978) or under 'mildly oxidising conditions' (Powell, 1986). Powell and McKirdy (1973b) suggested that high pristane/phytane ratios (pr/ph ≥ 3) are a characteristic feature of terrestrial organic matter deposited in oxic environments. Pristane and phytane are equally abundant (pr/ph = 1) in the SCM at Newington-2 (sample #71: Table 4.2). It is not unusual, however, to find relatively low pristane/phytane ratios in lacustrine facies and many of the Chinese freshwater sediments and freshwater-derived oils have such low values (Luo Binjie et al., 1988; Fu Jiamo et al., 1990).

2. Consistently, these terrestrial (oxic to suboxic) environments are also characterised by the predominance of odd-numbered *n*-alkanes (1< CPI ≤2: Table 4.2). However, the CPI decreases with increasing maturity and fluctuates about unity at the onset of the oil window (Allan and Douglas, 1977). Therefore, these CPI values may have been lowered by this maturity effect and may not represent the original signature. Similarly, the pr/*n*-C_{17} and ph/*n*-C_{18} values recorded for the SCM samples have probably also been lowered by maturation.

3. The terrestrial nature of the organic matter in the SCM is also reflected by the predominance of the C_{29} homologue among the C_{27}-C_{30} steranes (C_{27}/C_{29} ster =0.1-1.0 and C_{28}/C_{29} ster = 0.3-0.6: Fig. 5.3c; Table 5.2). The complete absence of the marine indicator C_{30} desmethyl steranes (Fig. 5.3c) in the major part of this unit is testimony to a lacustrine depositional setting (*cf.* Moldowan et al., 1985). These rocks are also characterised by moderate to high diasterane abundances (C_{29} dia/ster = 0.4–1.3); moderate to high hopane/sterane ratios (1.7–9.4); and $C_{31}>C_{32}>C_{33}>>C_{34}>>C_{35}$ hopanes. The highest relative concentrations of the diasteranes (C_{29} dia/ster >1) are associated with higher abundances of 17α(H)-diahopanes (C_{30}*-C_{34}*) and norneohopane ($C_{29}T_s$), most noticeably in Borah Creek-3 and -4, indicating deposition of the terrestrial organic matter in a clay-rich, oxic to suboxic environment. Some of the bacterial input was of methylotrophic origin, as indicated by the presence of 2α- and 3β-methyl-17α(H),21β(H)-hopanes (*cf.* Summons and Jahnke, 1992) in these lacustrine source rocks (Fig. 5.3b).

4. The 4α-methyl steranes, as well as their 2α and 3β homologues, occur in much higher abundance than do their desmethyl counterparts (Fig. 5.3c), emphasising the non-marine nature of the SCM organic matter. The majority of the Triassic samples show abundances of 4α-methyl steranes (C_{30} 4α-methyl/C_{29} sterane = 0.04-0.2: Table 5.2) greater than most of the Permian sediments (C_{30} 4α-methyl/C_{29} sterane = 0.01-

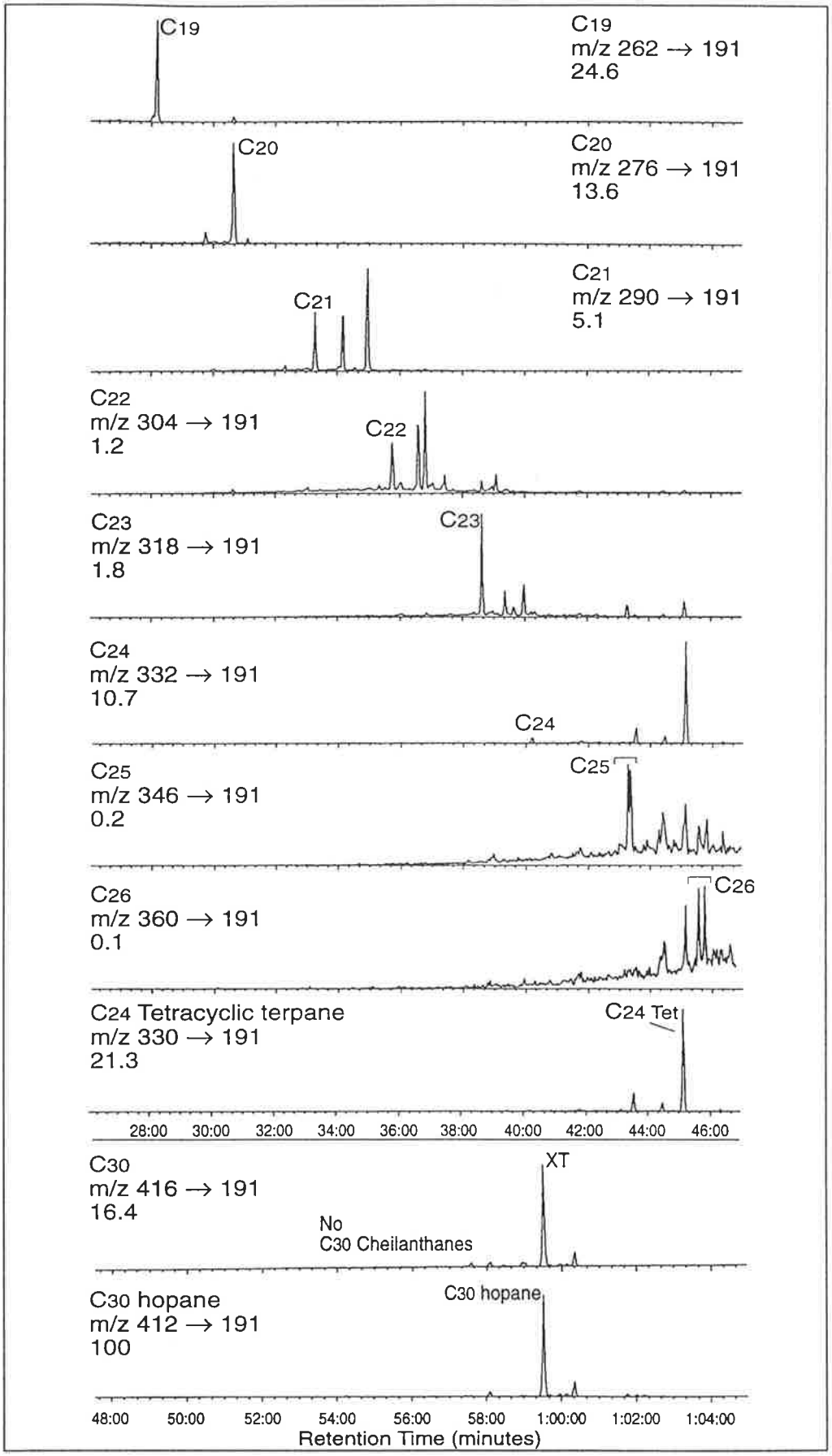

Figure 5.3 (a) MRM chromatograms showing the distributions of tricyclic terpanes and C_{24} tetracyclic terpane in the Snake Creek Mudstone, Tinker-2 (sample #58).

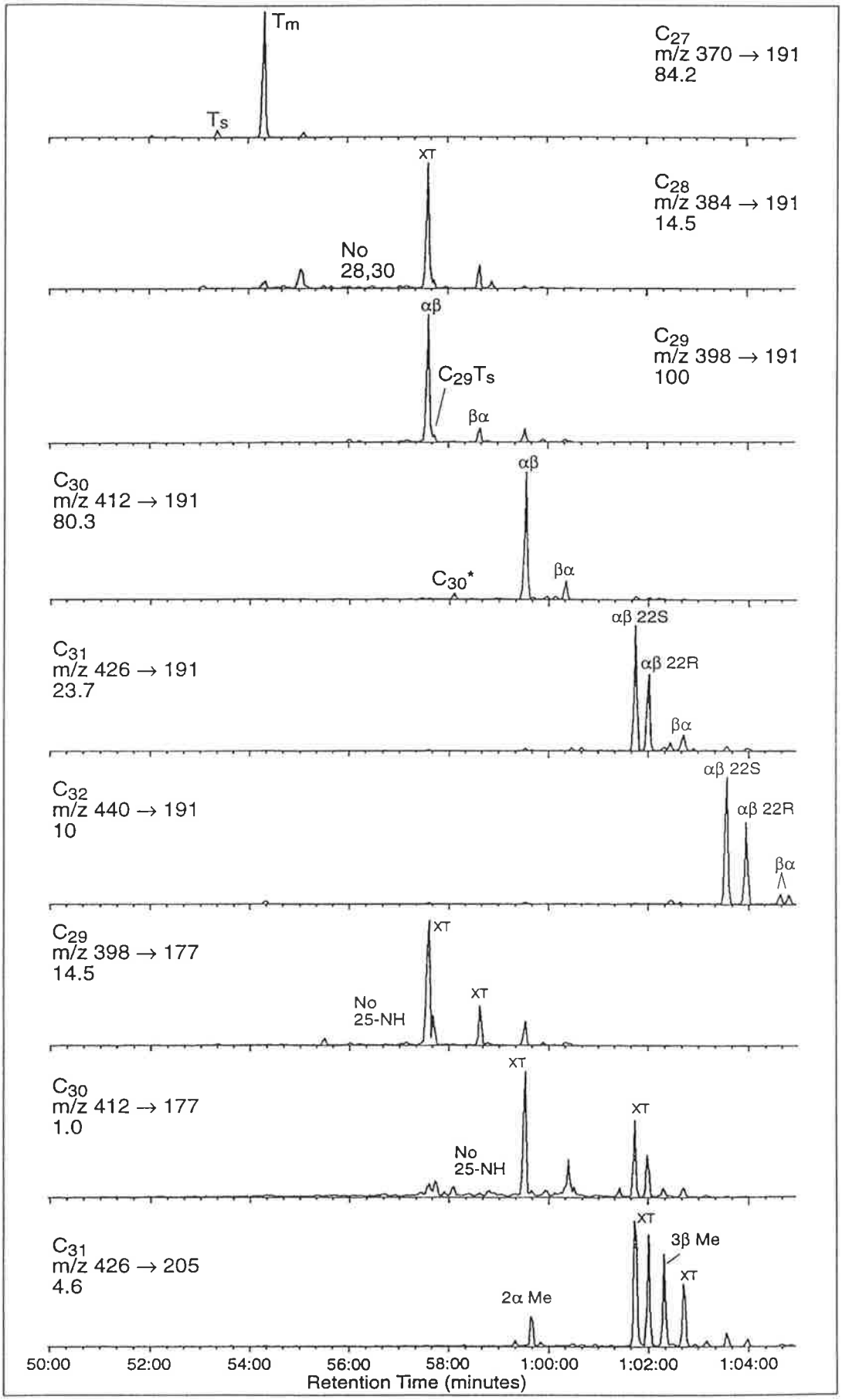

Figure 5.3 (b) MRM chromatograms showing the distributions of hopanes, norhopanes, and methylhopanes in the Snake Creek Mudstone, Tinker-2 (sample #58).

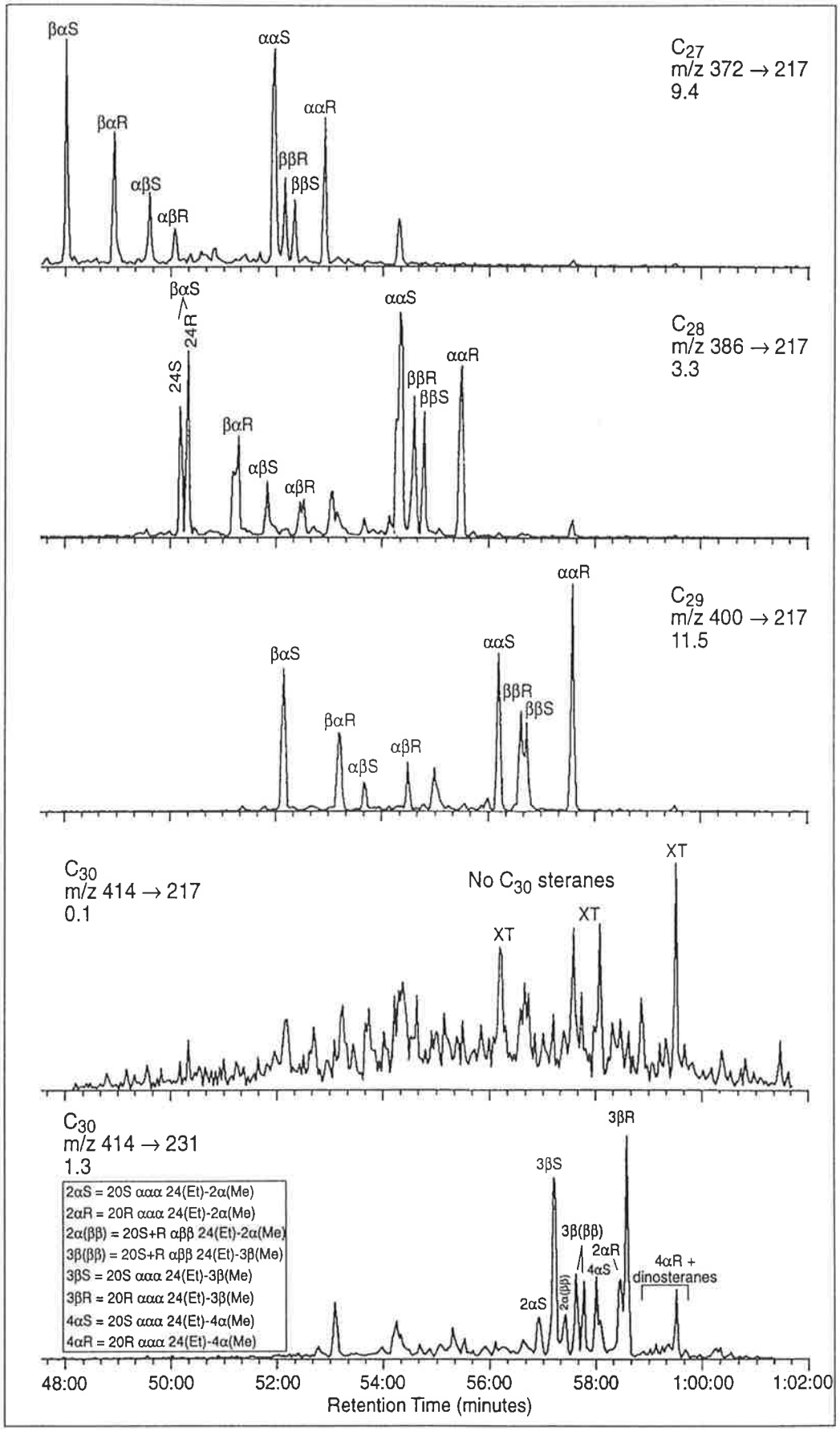

Figure 5.3 (c) MRM chromatograms showing the distributions of steranes ($M^{+\cdot} \rightarrow$ m/z 231) and methylsteranes ($M^{+\cdot} \rightarrow$ m/z 231) in the Snake Creek Mudstone, Tinker-2 (sample #58).

0.06). This may be caused by the additional contribution of 4α-methyl components (including dinosterane) from a wider range of algae (including dinoflagellates which first became abundant during the Triassic: Summons et al., 1987; Thomas et al., 1993). A similar explanation may account for the greater abundances of C_{30} 4α-methyl sterane relative to the C_{28} and C_{29} homologues (Fig. 6.7b, Table 5.2) (*cf.* Fu Jiamo et al., 1990) in the SCM source rocks.

5. Methylsterane distributions in the Triassic source rocks (3β > 4α > 2α: e.g. Figs. 5.3c, 5.5c, 5.7c) are also remarkably different from those of the carbonaceous shales of the BWG (3β > 2α > 4α: e.g. Fig. 5.2c). This, again, can be explained by the greater diversity of Triassic algal (including dinoflagellate) populations which contain 4α-methyl sterols (Robinson et al., 1984; Volkman et al., 1990; Summons and Capon, 1991). Such differences in methylsterane distributions between Triassic and Permian sediments have proven valuable in distinguishing oils sourced by the SCM and those generated from Permian organic matter (Section 6.3.3.5).

5.4.2 Freshwater vesus brackish lacustrine environments

As mentioned above, two main depositional environments can be recognised for the Snake Creek Mudstone. The oxygenated freshwater setting was widely distributed and covers the major part of the southern Taroom Trough, whereas the brackish and less oxic environment developed locally around Teelba-1 (in the southern part of the study area); Dulacca-1 and Apple Tree-1 (in the central part); and Glenhaughton-1 (in the north).

Freshwater environment

The following is the molecular evidence of organic matter deposited in a freshwater environment under oxic conditions. Biomarker fingerprints of the SCM in Tinker-2 are depicted in Figure 5.3 to represent this oxygenated freshwater environment.

1. There is a complete absence of C_{30} tricyclic terpanes (Table 5.2) associated with very low concentrations of C_{19} to C_{26} homologues in all but one sample ($C_{19\text{-}26}TT/C_{30}$ hopane ≈ 0.2-2: Table 6.2). This is an indication of deposition in a freshwater environment. Oils of freshwater source affinity are normally characterised by the absence, or very low concentrations, of tricyclic terpanes (Philp et al., 1989).

2. The homohopane concentrations decrease with increasing molecular weight (C_{31}>C_{32}>C_{33}>>C_{34}>>C_{35}). The C_{35} homologue is either absent or occurs in very low concentrations (C_{35}/C_{33} homohopanes < 0.2: Table 5.2). This is consistent with a freshwater, or sometimes mixed fresh/brackish, depositional environment (*cf.* Fu Jiamo et al., 1988).

3. The variable abundance of 28,30-bisnorhopane can give a clue to the redox potential of the depositional environment (Grantham et al., 1980). The complete absence of this compound and its C_{27} homologue 25,28,30-trisnorhopane in Tinker-2 (Fig. 5.3b) indicates that oxic conditions prevailed during deposition. On the contrary, these compounds are detected in trace concentrations in the other SCM samples, most noticeably those from Hollow Tree-1, Warroon-1 and Renlim-1 (Fig. 5.7b; Table 5.2), suggesting mildly oxidising conditions or bacterial reworking in locally anoxic subenvironment (*cf.* Mello et al., 1990).

4. Abundant drimanes, particularly rearranged drimanes, in this environment, as represented by the SCM at Snake Creek-1 (Fig. 5.6a) are also consistent with oxic depositional conditions. Philp (1994) suggests that drimanes are produced by microbes present within *oxic* environments rich in higher plants.

5. Rearranged hopanes are detected in all samples except those from Glenhaughton-1, Muggleton-1, Cabawin-1 and Flinton-1 (see below), although only in trace concentrations (C_{30} diahopane/hopane = 0.03 - 0.2: Table 5.2). The highest diahopane abundance is observed in the Snake Creek-1 sample. The presence of diahopanes can be attributed to the oxicity of the depositional environment and/or the richness of the source rock in clays (Peters and Moldowan, 1993). The latter alternative is consistent with the appreciable abundance of rearranged steranes (C_{29} dia/ster = 0.4 - 1.3: Table 5.2).

6. High hopane/sterane ratios (hop/ster = 3.1-9.4: Table 5.2). This strongly suggests that the eukaryotic contribution (algae and higher plants) was much less than that of prokaryotes (Seifert and Moldowan, 1978). In addition, such high values are common in suboxic to oxic freshwater environments (*cf.* Tissot and Welte, 1984).

Brackish environment

The SCM source rock samples from Teelba-1, Dulacca-1, Apple Tree-1 and Glenhaughton-1 were deposited in a more saline (brackish) lacustrine setting. This is indicated by their *n*-alkane and biomarker distributions. The *n*-alkane distribution of the

SCM in Glenhaughton-1, as a representative of the suboxic/brackish setting, is depicted in Figure 5.4. This and the other *n*-alkane profiles exhibit a local maximum at docosane, i.e. *n*-C_{22} (Fig. 5.4). ten Haven et al. (1985, 1988) introduced a new parameter called "*R_{22} index*" which is the ratio of docosane (multiplied by 2) to the sum of heneicosane plus tricosane. They found that values larger than unity for this parameter are associated with, and therefore probably caused by, higher salinity and less oxic depositional conditions. Applying this concept to these four SCM samples (R_{22} index = 1.2 - 1.5: Table 4.2) suggests that they were deposited under brackish, suboxic conditions. In other areas, deposition of the SCM occurred in a freshwater environment (R_{22} index = 0.6 - 1: Table 4.2).

The biomarker fingerprints of the Glenhaughton-1 SCM extract are presented in Figures 5.5 and 5.6b. They have the following features:

1. Lowest hopane/sterane ratio (hop/ster = 1.7: Table 5.2). Comparing different lacustrine settings, Duncan and Hamilton (1988) found that the deeper water, more distal facies have the lowest hopane/sterane ratios. Such environments are normally characterised by higher salinity and consequently less oxicity.

2. Highest abundance of C_{19} to C_{26} tricyclic terpanes (C_{19-26}TT/C_{30} hopane = 3.6: Fig. 5.5a; Table 6.2), indicative of a brackish environment. Oils derived from brackish source rocks are characterised by high abundances of tricyclic terpanes, whereas low concentrations are more indicative of freshwater affinity (Philp et al., 1989).

3. Among the C_{19}-C_{26} cheilanthanes, the C_{21} and C_{23} homologues are the most prominent with the latter compound and C_{30} hopane being equally abundant (Fig. 5.5b). This, together with the presence of C_{30} cheilanthane and C_{24} tetracyclic terpane, is testimony to the deposition of their precursor prokaryotes in suboxic, calcareous mudstones (*cf.* Palacas et al., 1984; Connan et al., 1986; Philp et al., 1989). Less oxic, or possibly reducing, depositional conditions are also indicated by the presence of 28,30-bisnorhopane and, to a lesser extent, its C_{27} homologue 25,28,30-trisnorhopane (Fig. 5.5b). This contention is supported by the complete absence of 17α(H)-diahopanes (C_{30}*-C_{35}*) (Fig. 5.5b); a series of compounds formed by clay-catalysed rearrangement of bacterial hopanoids under oxic conditions (Peters and Moldowan, 1993). Therefore, their absence in this sample implies less oxic conditions and/or a low clay content. The presence of C_{27}-C_{29} diasteranes (Fig. 5.5c) is not necessarily at odds with this interpretation because many clay-lean sediments (e.g. carbonates) contain abundant diasteranes (Clark and Philp, 1988). Another explanation for diasterane formation in carbonates is that there only needs to be a small amount of clay minerals present to catalyse the rearrangement, and caly-richness may not, therefore, be important. Other workers (Moldowan et al., 1986) have suggested that the presence of diasteranes, in certain clay-poor samples, was due to high pH

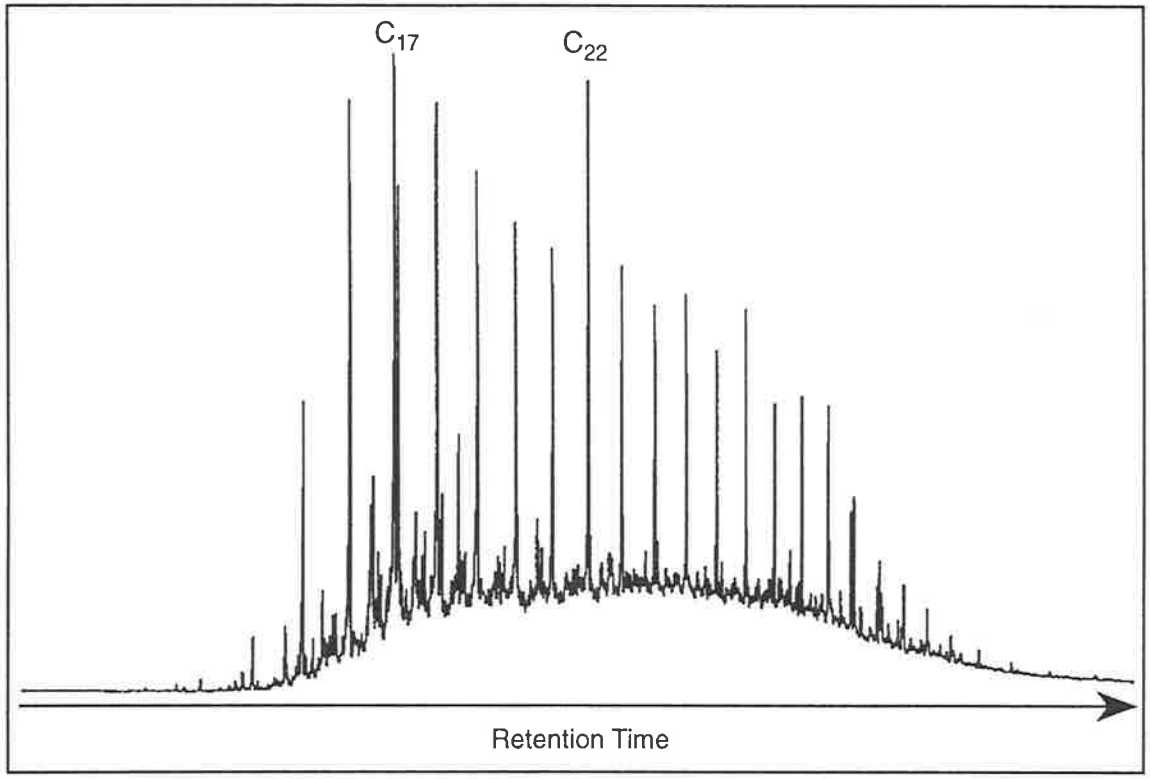

Figure 5.4 Gas chromatogram showing the alkane distribution in the Snake Creek Mudstone, Glenhaughton-1.

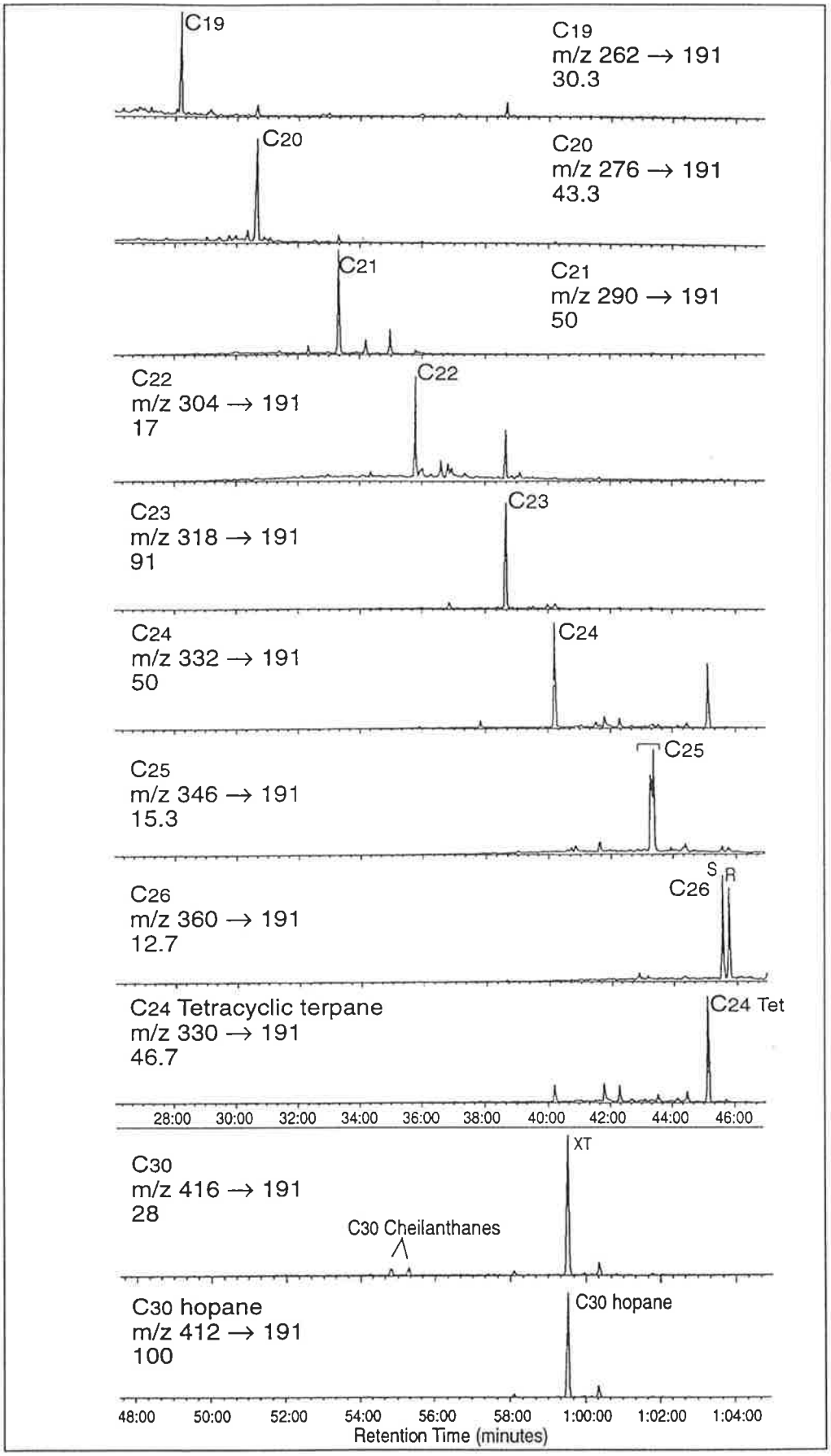

Figure 5.5 (a) MRM chromatograms showing the distributions of tricyclic terpanes and C_{24} tetracyclic terpane in the Snake Creek Mudstone, Glenhaughton-1. C_{21} and C_{23} cheilanthanes predominate over C_{19} and C_{20} homologues; C_{23} cheilanthane ≈ C_{30} hopane; and C_{30} cheilanthane is present.

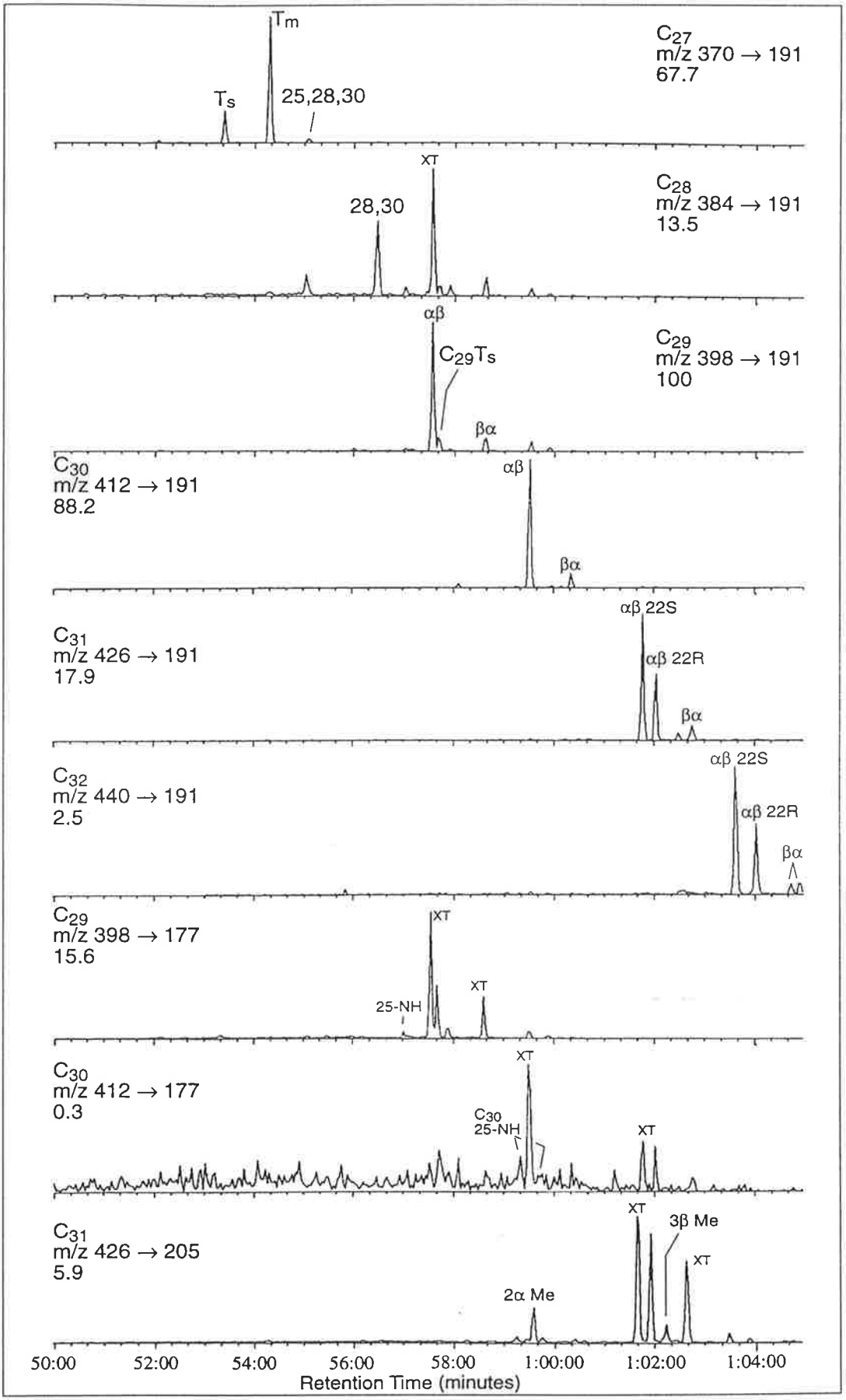

Figure 5.5 (b) MRM chromatograms showing the distributions of hopanes, norhopanes, and methylhopanes in the Snake Creek Mudstone, Glenhaughton-1 (sample #41).

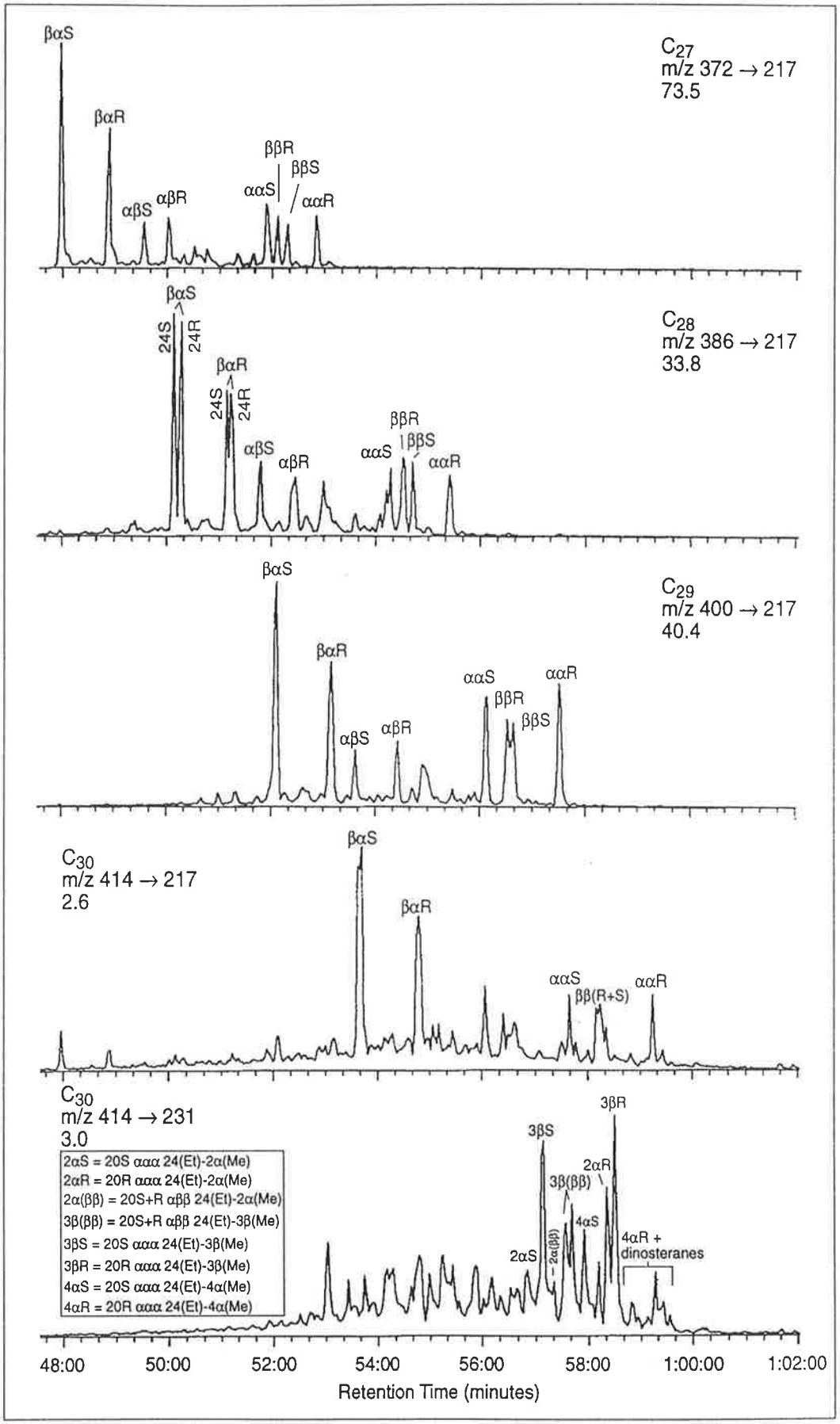

Figure 5.5 (c) MRM chromatograms showing the distributions of steranes ($M^+ \rightarrow$ m/z 217) and methylsteranes ($M^+ \rightarrow$ m/z 231) in the Snake Creek Mudstone, Glenhaughton-1 (sample #41).

during deposition brought about by oxic conditions. This later explanation is, however, not favoured here and is at odds with the presence of bisnorhopane in this particular sample.

4. A high relative abundance of C_{29} hopane (30NH/C_{30} hopane >1: Fig. 5.5b) is consistent with increased salinity. Clark and Philp (1989) noticed the predominance of 30-norhopane over its C_{30} homologue in carbonates and evaporites.

5. Low relative concentrations of drimanes and other C_{14} and C_{15} bicyclic sesquiterpanes (Fig. 5.6b), and particularly the very low concentrations of rearranged drimanes (R1, R2), are consistent with the environment being more calcareous and less oxic. Rearranged drimanes are known to be abundant in clay-rich sediments, and suppressed in evaporite and carbonate environments (Palacas et al., 1984; Noble et al., 1986). On the other hand, C_{16} and C_{17} bicyclic terpanes (homodrimanes and methylhomodrimanes) are abundant in this calcareous SCM facies (Fig. 5.6b). Such a clay-poor environment is likely to be deficient in iron and other metals and, therefore, the sulphide produced by sulphate-reducing bacteria will remain free for incorporation into the residual organic matter during diagenesis (Tissot and Welte, 1984; Orr, 1986). Such enrichment of sulphur in sedimentary organic matter is a function of environmental conditions during the early stages of diagenesis (Francois, 1987) and is not related to the biochemical organic sulphur present in living biomass (Philp et al., 1992). Sulphur incorporation appears to occur immediately after deposition via anaerobic microbial activity, or through chemical reactions with sulphur-rich sediments such as evaporites (Philp et al., 1992). Valisolalao et al. (1984) identified hopanoids containing thiophene rings in immature sediments. In the hopanoid side-chain, the C-S bond is weak and can easily be broken during diagenesis, yielding free hopanoids and homodrimanes. It appears, therefore, that abundant homodrimanes are characteristic of calcareous mudstones deposited under less oxic, and probably more saline, conditions.

6. The highest sterane concentrations relative to hopanes (hop/ster = 1.7), associated with the highest abundance of C_{28} steranes (C_{28}/C_{29} steranes = 0.62: Table 5.2). Although this may primarily be a result of an additional marine algal contribution (Section 5.4.4), it is also possible that less oxic and more saline conditions enhanced the preservation potential of the algal input.

5.4.3 Comments on the biomarker signatures of the SCM organic facies

It appears that the majority of the SCM organic facies (identified on the basis of their *n*-alkane distributions: Section 4.4.1) were deposited under oxic conditions in freshwater environments. All the facies have biomarker signatures quite similar to those depicted in Figure 5.3. However, as discussed in the previous section, samples from Teelba-1, Dulacca-1, Glenhaughton-1 and Apple Tree-1 (Fig. 1.2) showed *n*-alkane distributions

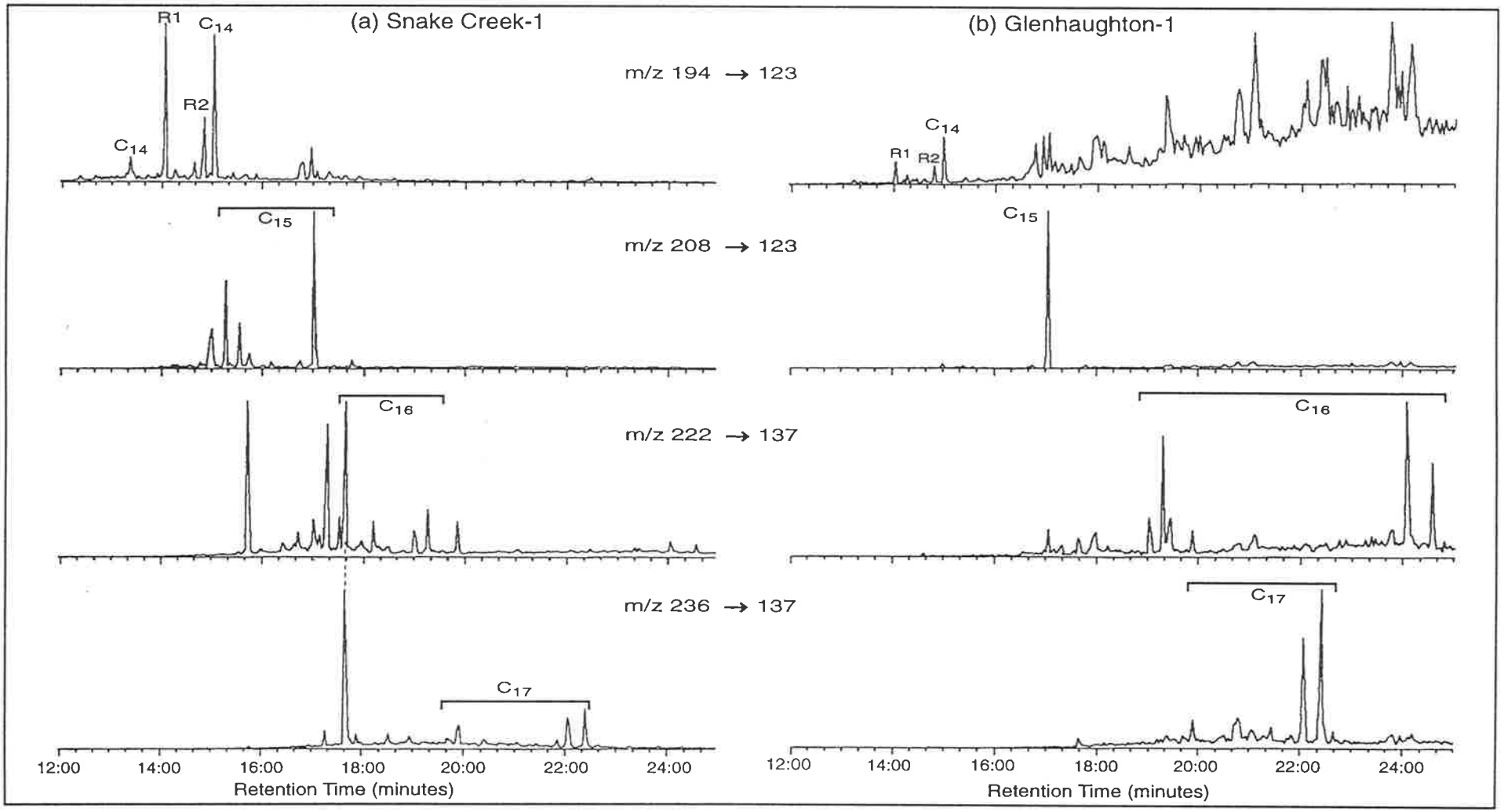

Figure 5.6 MRM chromatograms showing the distributions of sesquiterpanes in the Snake Creek Mudstone at (a) Snake Creek-1, and (b) Glenhaughton-1. In Glenhaughton-1, rearranged (R1, R2) and $C_{14\text{-}15}$ drimanes are in low abundance, whereas C_{16+} homodrimanes are abundant.

(n-C_{22} > 1) indicative of deposition in a brackish and suboxic environment. These four samples belong to Facies A (Table 4.2) and, therefore, can be considered a special subfacies (Facies A'). When a representative of this sample set (*viz.* Glenhaughton-1) was analysed for its biomarkers, distinctive fingerprints (testimony to brackish/suboxic depositional conditions) were demonstrated (Fig. 5.5), as discussed in the previous section.

Distributions of C_{27} through C_{30} steranes in sediments and petroleums are commonly used as indicators of the original organic matter precursors. C_{27} steranes are derived mainly from plankton, whereas C_{29} sterols, the biological precursors of C_{29} steranes, are abundant in higher plants (Huang and Meinschein, 1979; Moldowan et al., 1985). Although the terrestrial nature of the organic matter preserved in the SCM sediments is clearly evident from the predominance of C_{29} steranes, subtle variations can be observed between different facies. For example, the C_{27}/C_{29} sterane ratio is generally higher in samples from Facies A and Facies B (0.3-1.0), and lower in Facies C (0.3-0.4: Table 5.2). Similarly, a majority of the Facies C samples contain less C_{28} steranes (C_{28}/C_{29} sterane ≤ 0.3; range 0.3-0.5) than do Facies A and Facies B (C_{28}/C_{29} sterane ≥ 0.4; range 0.4-0.6). These variations in the sterane distributions are consistent with greater planktonic contributions to the latter facies (A and B), compared with Facies C which received greater inputs of land-plant sterols. The relatively high abundance of C_{28} sterane (C_{28}/C_{29} sterane = 0.53: Table 5.2) in the SCM at Flinton-1 is probably related to its additional marine algal input, as indicated by the presence of C_{30} desmethyl steranes (Section 5.4.4). Another exception is the low C_{27} sterane content (C_{27}/C_{29} sterane = 0.28) of the Snake Creek-1 sample. However, it is not uncommon to find such low C_{27} (and consequently high C_{29}) sterane abundances in lacustrine facies. Volkman (1986) showed that C_{27}, C_{28}, and C_{29} steranes can be derived from both algal and terrestrial plant sources. Furthermore, oxidation of organic matter during deposition can selectively remove sterols from algal and other lipid-rich precursors, giving rise to selective preservation of higher plant components, rich in C_{29} sterols (Volkman et al., 1987).

The bacteria-rich Facies B (represented by the SCM at Renlim-1) exhibits hopane fingerprints (Fig. 5.7b) which differ slightly from those of other facies. Here, extensive bacterial reworking of organic matter (and consequently enhanced bacterial input) is evidenced by the presence of relatively high concentrations of 28,30-bisnorhopane and its C_{27} homologue 25,28,30-trisnorhopane (28,30BNH/C_{30} hopane = 0.3: Table 5.2). Abundant 28,30-bisnorhopane is thought to be derived from sulphate-reducing bacteria (Schoell et al., 1992). These bacteria thrive on algal and land plant precursors where anoxic sediments are overlain by an oxic water column (Williams, 1984). The compound 25,28,30-trisnorhopane, detected in Facies B (Fig. 5.7b), is also present in

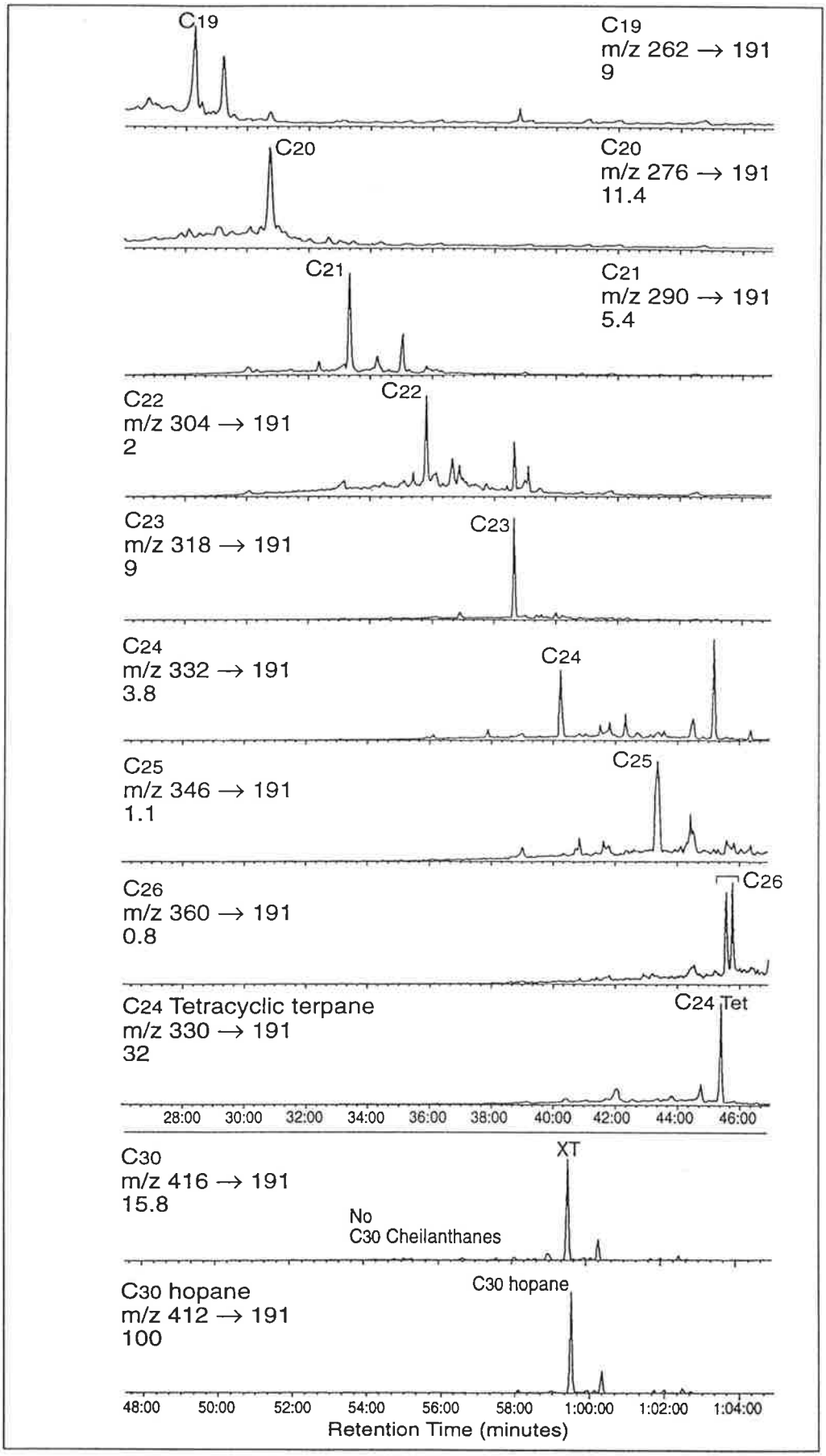

Figure 5.7 (a) MRM chromatograms showing the distributions of tricyclic terpanes and C_{24} tetracyclic terpane in the Snake Creek Mudstone, Renlim-1 (sample #70). The intensity for each trace is normalised against C_{30} hopane.

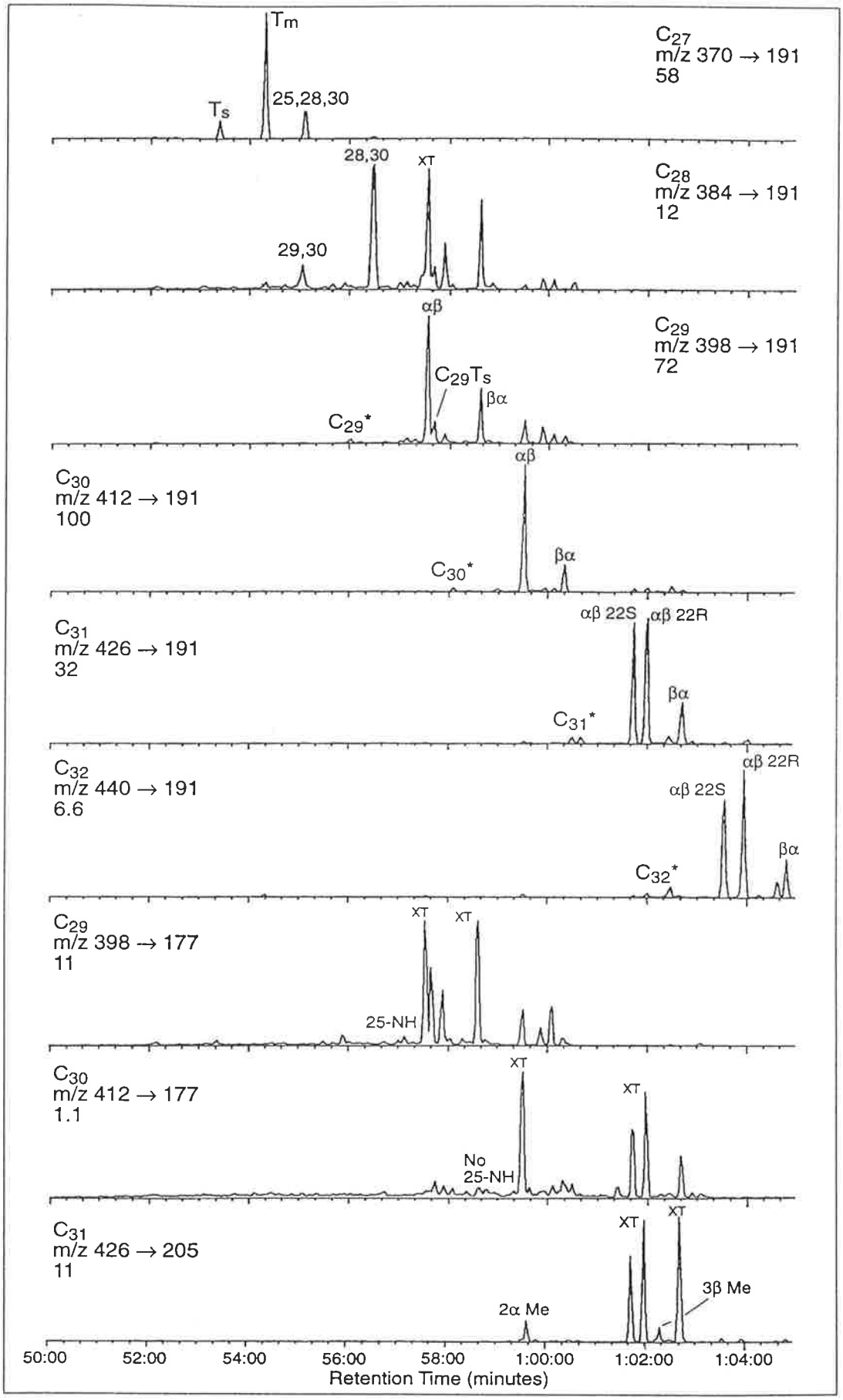

Figure 5.7 (b) MRM chromatograms showing the distributions of hopanes, norhopanes and methylhopanes in the Snake Creek Mudstone, Renlim-1 (sample #70). The intensity for each trace is normalised against the highest peak in the hopanes and steranes.

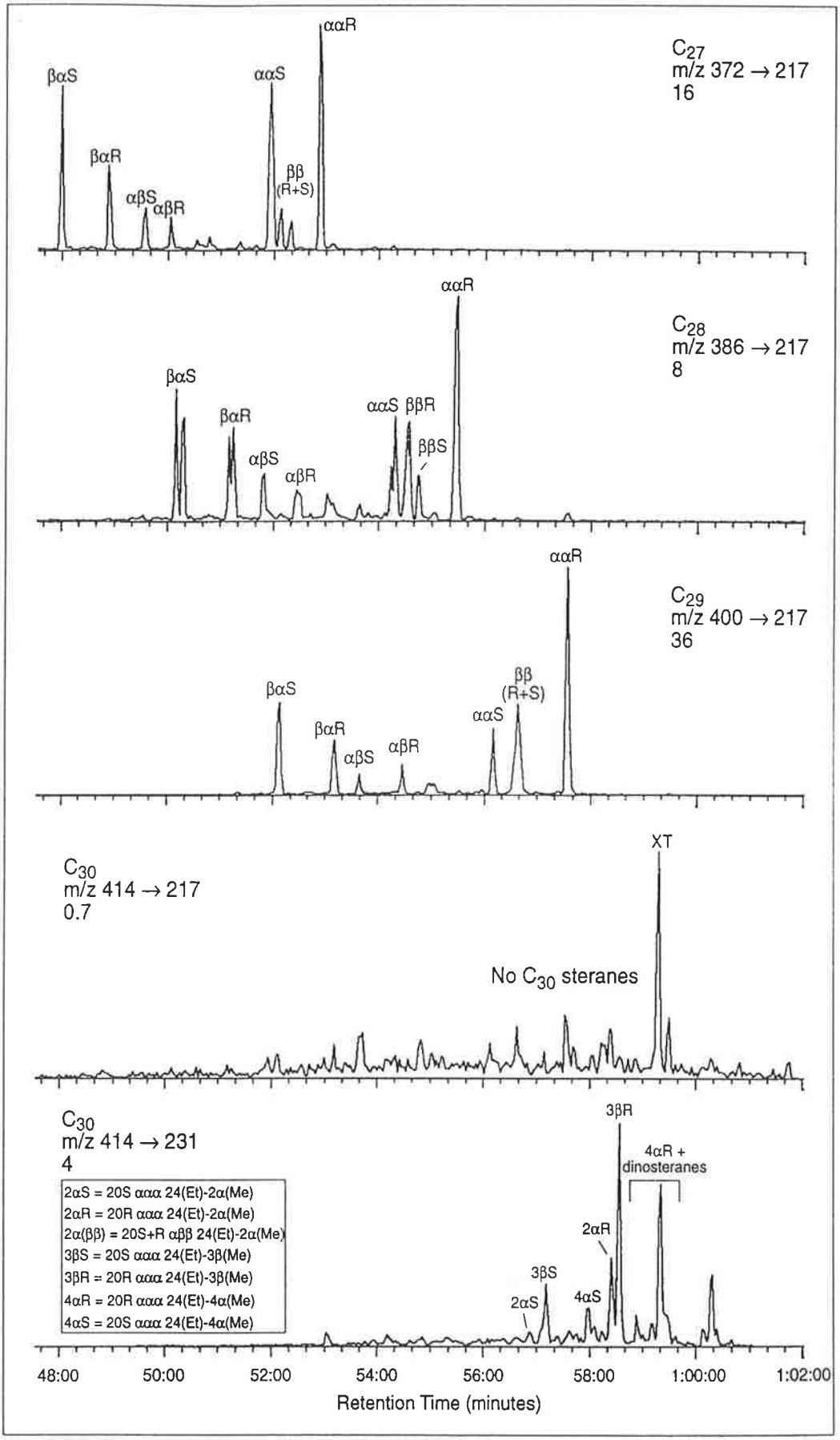

Figure 5.7 (c) MRM chromatograms showing the distributions of steranes ($M^+ \rightarrow$ m/z 217) and methylsteranes ($M^+ \rightarrow$ m/z 231) in the Snake Creek Mudstone, Renlim-1 (sample #70). The intensity for each trace is normalised against the highest peak in the hopanes and steranes.

some samples of Facies A (e.g. Fig. 5.5b), indicating that suboxic conditions prevailed locally during deposition of the SCM (*cf.* Peters and Moldowan, 1993). On the other hand, the sterane distributions in Facies B (Fig. 5.7c) are quite similar to those of other facies (e.g. compare with Fig. 5.3).

5.4.4 Marine influence on the SCM lake

Marine incursions to the Snake Creek palaeolake are confined to the northwest (Glenhaughton-1, Muggleton-1) and southeast (Cabawin-1 and Flinton-1) margins of the southern Taroom Trough. This finding is based on the following parameters:

1. Presence of C_{30} desmethyl steranes (Fig. 5.8). This group of compounds is used as a definitive indication of marine algal input (Moldowan et al., 1985; Peters et al., 1989). The presence of C_{30} 4α-methyl steranes (including dinosteranes) in subordinate abundance relative to the C_{30} desmethyl steranes also may imply a marine input.

2. The additional contribution of organic matter from marine algae (probably *Chrysophyte*) has affected the relative proportions of hopanes and steranes. These samples exhibit the highest concentrations of steranes relative to hopanes (hop/ster = 1.7 - 2.4: Table 5.2).

3. This marine algal input has also increased the abundance of C_{27}, and particularly C_{28}, steranes in these samples (e.g. C_{28}/C_{29} steranes ≈ 0.5 - 0.6). Dahl et al. (1994) found a positive correlation between the percentages of C_{28} (and C_{30}) steranes in rock extracts and the abundance of marine organic matter in the associated kerogen. High abundances of C_{27} and/or C_{28} homologues are also consistent with the calcareous nature of the host rock (Hughes, 1984). The calcareous nature of these samples is also reflected in their complete lack of diahopanes (Table 5.2). As sea water is calcareous (rich in dissolved $CaCO_3$), the carbonate content of the Snake Creek Mudstone increased during marine incursions. It is also noticed that these marine-influenced source rocks have abundant C_{29} hopane (30-NH/C_{30} hopane = 1.2-1.6: Table 5.2). Such C_{29} hopane abundance is usually associated with carbonate or evaporite sediments (Zumberge, 1984; Connan et al., 1986). However, other samples are shaley (e.g. samples #49 and 64 with C_{29} diasterane/sterane > 1: Table 5.2) and they too display C_{29}/C_{30} hopane ratios larger than unity. The abundance of C_{29} hopane in such terrestrial facies may be largely related to major inputs from higher plants (*cf.* Brooks, 1986).

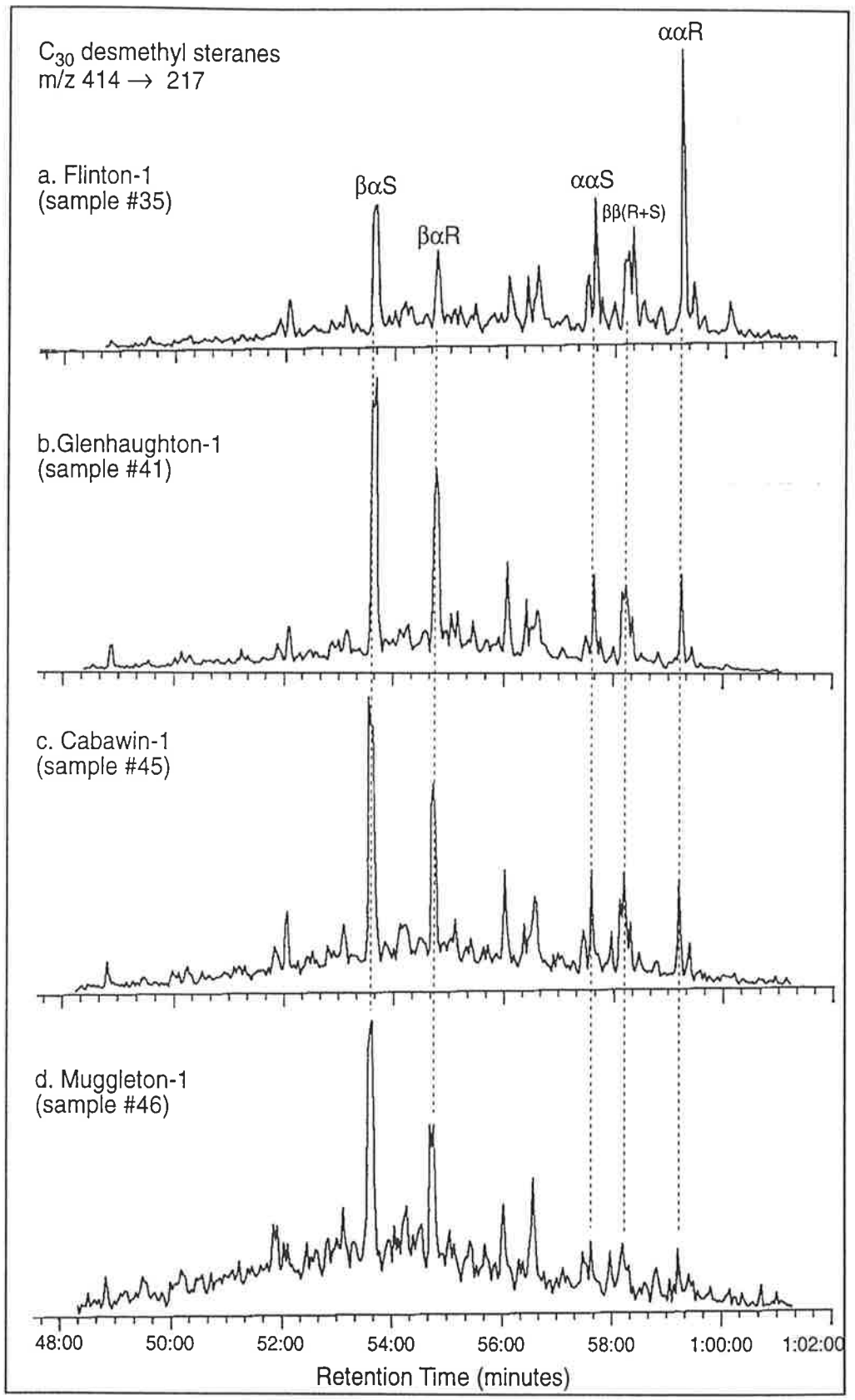

Figure 5.8 MRM chromatograms (414 → m/z 217) showing the distributions of C_{30} desmethyl steranes in the Snake Creek Mudstone from (a) Flinton-1, (b) Glenhaughton-1, (c) Cabawin-1 and (d) Muggleton-1.

5.5 Summary

Saturated and aromatic molecular maturity parameters confirm that the Permian source rocks have passed the oil generation threshold over the major part of the southern Taroom Trough and are currently overmature in the north, whereas the Triassic SCM is marginally mature across the basin. Carbonaceous shales in the lower part of the Permian BCG show molecular evidence of marine incursions (associated with carbonate deposition) and suboxic to reducing conditions associated with increased salinity. The Permian coal-bearing BWG contains mainly land-plant remains deposited in a freshwater environment under predominantly oxic conditions.

The proposed SCM organic facies (based on their *n*-alkane distributions) are substantiated, to some extent, by their polycyclic biomarker distributions. The algal-rich Facies A and the bacteria-rich Facies B are characterised by lower concentrations of C_{29} sterane and greater relative abundances of C_{27} and C_{28} steranes, whereas the higher plant-rich Facies C generally contains less C_{28} and more C_{29} steranes. Facies B is characterised by high abundances of 28,30-bisnorhopane and 25,28,30-trisnorhopane. Most of the SCM source rocks appear to have been deposited under predominantly oxic conditions in a freshwater setting. A special subfacies of Facies A was deposited under brackish and less oxic conditions. These two main lacustrine environments are characterised by their diagnostic molecular fingerprints. The oxygenated freshwater setting was widely distributed and covers the major part of the southern Taroom Trough, whereas the brackish/suboxic environment developed locally in different parts of the basin (*viz.* in the vicinity of Teelba-1, Dulacca-1, Apple Tree-1 and Glenhaughton-1). A marine influence on the Snake Creek palaeolake is confined to the northwest (Glenhaughton-1, Muggleton-1) and southeast (Cabawin-1 and Flinton-1) margins of the southern Taroom Trough.

Generally speaking, the SCM source rocks are characterised by higher abundances of 4α-methyl steranes, compared with the Permian carbonaceous shales. Variations in drimane distributions in different facies suggest that abundant homodrimanes and methylhomo-drimanes are characteristic features of calcareous mudstones deposited under less oxic, and probably more saline, conditions. These molecular variations proved to be highly useful in distinguishing Triassic oils from the Permian hydrocarbons.

CHAPTER SIX

PETROLEUM GEOCHEMISTRY AND OIL - SOURCE CORRELATION

6.1 Introduction

The sources of the oil and gas accumulations in the Surat and Bowen Basins are still being debated. Thomas et al. (1982) considered the Permian rocks of the Taroom Trough to be the only, or most evident, source for the oils. This implies long lateral and vertical migration paths, the likelihood of which is doubted by many workers (e.g. Hawkins et al., 1992). McKirdy (1984) and Philp and Gilbert (1986) suggested the existence of additional effective source rocks in the area. Most recently, Boreham (1995) analysed over 70 oil and condensate samples and concluded that all but one have their source in the Permian coal facies. Sixty-one oil and gas discoveries, out of a total of 94 made in the Taroom Trough, are located within the Roma Shelf region (Hawkins et al., 1992).

6.2 Recognition of oil families

6.2.1 Basic geochemical characteristics of oils

The alkane chromatograms of the eleven oils and one condensate from the southwestern Taroom Trough and southern Roma Shelf examined in this study (Fig. 6.1) indicate that they were sourced primarily from algal and land plant organic matter deposited in oxic environments. Table 6.1 summarises their basic characteristics. All the oils have highly paraffinic alkane distributions with high pristane/phytane ratios (pr/ph = 4-6) and smooth, unimodal *n*-alkane profiles, most maximising below *n*-C_{20}. No odd or even predominance is evident in the *n*-alkanes of any oil or the condensate. Their *MPI-derived* calculated vitrinite reflectance values (R_C = 0.62-0.75%: Table 5.4) suggest reasonably similar maturities at the time of primary migration. Some oils, such as that in Waratah-1, display higher concentrations of waxy hydrocarbons, probably reflecting the effect of different source facies on the hydrocarbon product. This implies that any differences in the alkane distributions of the oils are most likely related to subtle variations in organic facies rather than markedly different maturation levels at the time of expulsion. Hence, higher concentrations of lower molecular weight alkanes in the Taylor-11, Taylor-12A and Roswin North-1 oils and the Merroombile-1 condensate

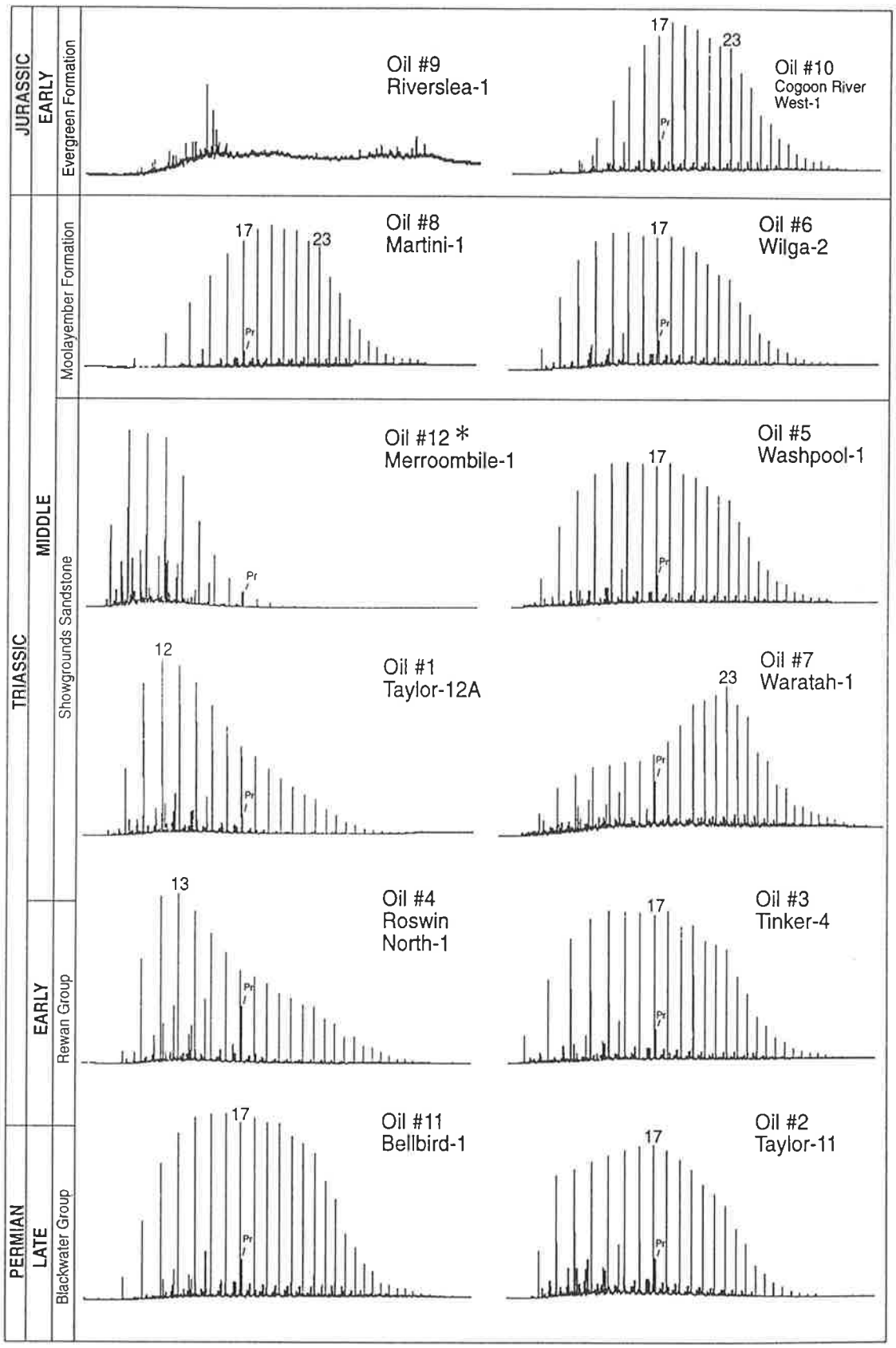

Figure 6.1 Alkane distributions of oils and a condensate (*) from the southern Taroom Trough.

Table 6.1 API gravity, bulk chemical composition and selected alkane ratios of oils from the southern Taroom Trough

Sample	Well Name	DST	Depth (m)	H'c Type	API gravity	Saturates %	Aromatics %	NSO %	Asphaltene %	Pr n-C_{17}	Ph n-C_{18}	Pr Ph
Family 1												
1	Taylor-12A	1	1979.1-1991	Oil	52.0	88.5	7.4	3.8	0.3	0.2	0.1	5.5
4	Roswin North-1	1	2138-2160	Oil	65.1	88.7	5.8	5.3	0.2	0.6	0.1	5.6
12	Merroombile-1	1	2023-2035	Condensate	65.3	90.5	3.9	5.5	0.1	0.8	0.1	6.0
Family 2												
2	Taylor-11	1	1022.3-2033	Oil	46.6	83.1	5.7	5.1	6.1	0.2	0.1	5.0
3	Tinker-4	1	2103.1-2142	Oil	43.5	81.3	9.4	4.9	4.4	0.2	0.1	4.3
5	Washpool-1	-	1600-1601	Oil	-	82.3	12.0	5.3	0.4	0.2	0.1	4.8
6	Wilga-2	-	1487-1489	Oil	-	83.2	10.5	4.8	1.5	0.2	0.1	4.2
7	Waratah-1	-	1635-1638	Oil	-	87.0	8.0	2.3	2.7	0.6	0.1	4.0
8	Martini-1	-	1638-1681	Oil	-	87.0	6.5	3.1	3.4	0.2	0.1	4.0
9	Riverslea-1	-	1507-1522	Oil	-	76.8	12.4	3.2	7.6	nd	nd	nd
10	Cogoon River West-1	-	1419-1438	Oil	-	88.7	8.0	2.8	0.5	0.2	0.1	4.3
11	Bellbird-1	4	2416-2420	Oil	40.0	81.2	6.4	5.3	7.1	0.2	0.1	4.0

nd = not determined due to the removal of n-alkanes and acyclic isoprenoid by biodegradation

(Fig. 6.1) are attributable to source rocks which had higher algal/bacterial contributions to their kerogen.

High saturated/aromatic hydrocarbon ratios (sat/arom = 6-23: Table 6.1), accompanied by high pristane/phytane and low phytane/*n*-C_{18} ratios (pr/ph = 4-6, ph/*n*-C_{18} = 0.1: Table 6.1), are typical of oils derived from coal and/or coaly organic matter (e.g. Powell and McKirdy, 1973b; Clayton, 1994). However, none of the coal or carbonaceous shale samples examined in the present study has such high values and, indeed, most of them have saturate/aromatic ratios <1.0 (Table 4.2). Low saturate/aromatic ratios (<1.0) in coal extracts, and much higher values in the oils generated from coal, seem to be the rule rather than the exception. Clayton et al. (1991) found very low saturate/aromatic ratios (<0.5) in extracts of coals from the San Juan Basin and very high ratios (>10) in the associated oils. Higher amounts of saturates relative to aromatics in the oil, compared to its source rock bitumen, may be interpreted as either fractionation during primary migration from the source rock (Leythaeuser et al., 1984) or that oils can undergo further maturation after expulsion, giving rise to elevated concentrations of saturated hydrocarbons (Clayton et al., 1991).

6.2.2 Oil-to-oil correlation based on bulk geochemistry

On the basis of the bulk compositional data in Table 6.1 and Figure 6.1, two different oil families can be recognised. Family 1 includes two very light (52-65°API), non-waxy oils from Taylor-12A and Roswin North-1, and the condensate from Merroombile-1. Each has a unimodal *n*-alkane distribution with a maximum around *n*-C_{12-14} and a steadily-decreasing abundance of higher molecular weight alkanes.

Family 2 includes the oils from Taylor-11, Tinker-4, Washpool-1, Wilga-2, Martini-1, Cogoon River West-1 and Bellbird-1, which are of lower API gravity (40-47°). Although their reservoir formations differ and range in age from Permian to Jurassic, all Family 2 oils have a dome-like *n*-alkane profile peaking around *n*-C_{18}. Oils of this family are relatively waxy and, hence, they may be compared with oils from Moonie-1, Duarran-1, Rockwood North-1, Sunnybank-2 and Alton-1 (Hawkins et al., 1992; Boreham, 1995). The more waxy Waratah-1 oil has an *n*-alkane distribution maximising at *n*-C_{23} reflecting possible removal of its low molecular weight alkanes by water washing (McKirdy, 1984). The Riverslea-1 oil is clearly biodegraded as indicated by the bacterial removal of its *n*-alkanes and isoprenoids (Fig. 6.1). Therefore, due to the alteration of their alkane profiles by water washing (Waratah-1) and/or biodegradation (Riverslea-1), these oils cannot be assigned to either of the aforementioned families.

Detailed characterisation of their polycyclic biomarkers is needed before their genetic affinity can be established.

6.2.3 Oil-to-source correlation based on n-alkanes

The alkane distributions of the Back Creek Group section from Cockatoo Creek-1 (Fig. 4.3b) are of no use for the purpose of oil-to-source correlation, because of its overmaturity (see also Hawkins et al., 1992). However, those of the less mature sections (within the oil window) in Flinton-1 and Meeleebee-1 (Fig. 4.3c) may be compared with some confidence to oils from Family 2.

Although they are mature, none of the coal facies extracts from the Baralaba Coal Measures (samples #11, 12, 18: Table 4.1, Fig. 4.5a) correlates with any of the oils analysed in this study. However, saturated hydrocarbon extracts from the lower part of the Blackwater Group (Figs. 4.5a and 4.5c) show some similarities to the oils from Family 2. On the basis of a similar alkane distribution, Thomas et al. (1982) suggested that the Cabawin-1 oil was generated locally from the Blackwater Group which is currently in the peak oil generation window. On the other hand, Philp and Gilbert (1986) concluded that this oil originated in the underlying Back Creek Group. Their conclusion was based on the presence of possible marine biomarkers (tricyclic terpanes) in the Cabawin oil which would correlate only with marine intercalations in the basal Back Creek Group. However, Boreham (1995) has reanalysed the Cabawin oil and argued for its non-marine origin.

The SCM in Muggleton-1 (Fig. 6.2) displays some similarities to the Family-1 oils (Taylor-12A and Roswin North-1). Alkane profiles of SCM extracts from Flinton-1 (R_O = 0.79%) and Amoolee-1 (R_O = 0.73%) (Fig. 6.2) suggest that a slightly more mature SCM section would yield oil comparable to the Waratah-1 crude; all are of waxy character showing unimodal *n*-alkane distributions with a maximum at *n*-C_{23} to *n*-C_{27}. Dahl et al. (1994) demonstrated that such organic facies which are rich in higher plant remains and deposited under relatively oxic conditions generate light oils and condensates at a lower maturity than source rocks containing marine-derived organic matter. No oil *n*-alkane profile proved to be similar to those of the Jurassic extracts or their pyrolysed counterparts (Fig. 4.10; see also Powell and Boreham, 1991).

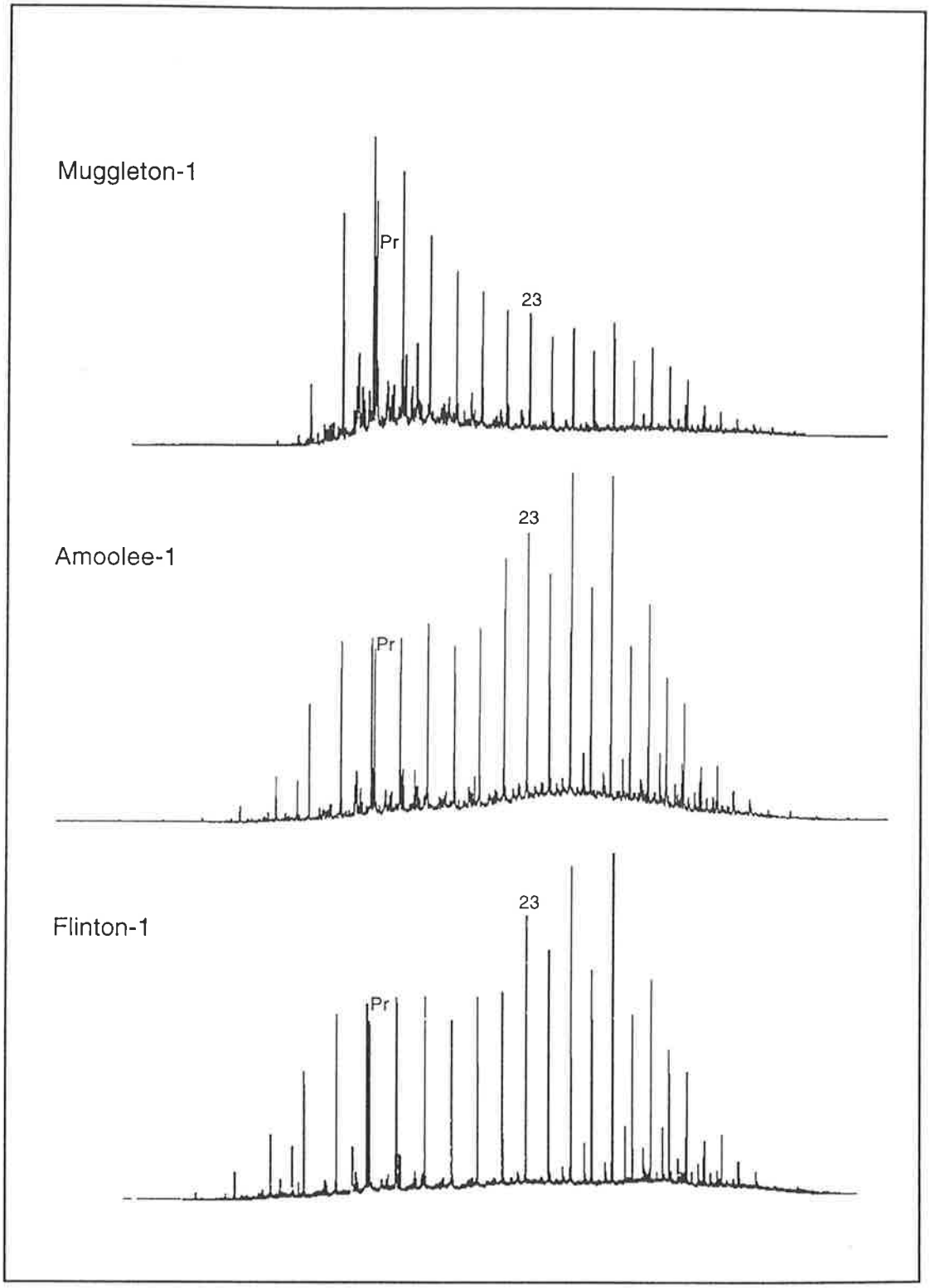

Figure 6.2 Alkane chromatograms of the Snake Creek Mudstone extracts from Muggleton-1, Amoolee-1 and Flinton-1.

6.3 Biomarker geochemistry

On the basis of the triterpane and sterane distributions of a suite of Taroom Trough oils, McKirdy (1984) suggested lacustrine and deltaic sediments from the lower Jurassic Evergreen Formation, Middle Triassic Moolayember Formation and Permian Blackwater Group as their potential sources. He also proposed the marine-influenced Back Creek Group as a likely source for condensates from Namarah-1 (reservoired in Devonian-Permian basement), Waggamba-1 (BWG), Warroon-1 (Showgrounds Sandstone) and Broadway-1 (Evergreen Formation). However, the major source for the oils in this area is considered by others (Thomas et al., 1982; Boreham, 1995) to be the Permian coal-bearing strata of the BWG, with a very minor contribution by the marine rocks of the BCG.

To elucidate the expulsion maturity and source affinity of the oils, their saturated (Tables 5.1 and 5.2) and aromatic (Table 5.4) biomarker contents were examined. Examples of the MRM chromatograms acquired for the oils are presented in Figures 6.3, 6.4, 6.8 and 6.10-6.13. Before any oil-to-oil or oil-to-source correlations can be made, the impact of biodegradation on the biomarker and isotopic compositions of the oils must be assessed since the original source and maturity fingerprints can be strongly affected by bacterial alteration in the reservoir.

6.3.1 Biodegradation

Three oils, among the twelve studied here, show the effects of bacterial alteration, demonstrated either in their alkane chromatogram (Riverslea-1: Fig. 6.1) or in their polycyclic alkane distributions (Wilga-2 and Washpool-1: Figs. 6.3 and 6.4).

6.3.1.1 Effect on n-alkanes and isoprenoids

Biodegradation in Riverslea-1 was first noticed by McKirdy (1984) and confirmed later by Philp and Gilbert (1986) and Boreham (1995). Although the effect of biodegradation on this oil is demonstrated by removal of its *n*-alkanes and acyclic isoprenoids (Fig. 6.1), its polycyclic biomarker content remains intact or has been only slightly affected. McKirdy (1984) and Philp and Gilbert (1986) described the extensive biodegradation of this oil and of the adjacent Conloi-1 (Evergreen) and Yapunyah-1 (Moolayember) oils. Biodegradation seems to be most intense in the shallow Triassic and Jurassic reservoirs on the Roma Shelf where conditions are suitable for aerobic bacteria (Thomas et al., 1982; McKirdy, 1984).

6.3.1.2 Effect on hopanes and steranes

The 17α(H)-hopanes have been partially converted to 25-norhopanes (NH) in Riverslea-1, Washpool-1 and Wilga-2 (C_{29} 25-NH/hop = 0.2, 0.3 and 0.7, respectively). This is clearly shown for the latter two oils in the 398→m/z 177 and 412→m/z 177 chromatograms (Figs. 6.3b and 6.4b).

For the Bowen Basin sediments (Triassic and Permian) variations in the ratios C_{30} diahopane/C_{30} hopane and 20S/20R C_{29} sterane are primarily maturity-controlled, whereas in oils such variations can be accounted for by both biodegradation and maturity. However, insignificant variations in the maturity levels between the oils (R_c = 0.62-0.75%: Table 5.4, see Section 6.3.2.2), dictate that the diahopane enrichment evident in some samples was caused mainly by biodegradation. This is because the hopanes and ααα 20R steranes are more susceptible to biodegradation than are diahopane and ααα 20S steranes, respectively (Peters and Moldowan, 1993). A higher abundance of the C_{30} diahopane (C_{30}*/C_{30} hopane up to 0.54: Fig. 6.5a, Table 5.2) is noticed in the oils from Wilga-2 (oil #6: Fig. 6.3b) and Washpool-1 (oil #5: Fig. 6.4b), again suggesting preferential removal of the C_{30} hopane.

This preferential removal of hopanes has resulted in enhanced concentrations of the more resistant diahopanes, 18α(H)-30-norneohopane ($C_{29}T_s$/C_{30} hopane is up to 0.4 in Wilga-2 oil: Table 5.2) and 2α- and 3β-methyl-17α(H),21β(H)-hopanes (2+3MeH/C_{30} hopane is up to 0.3). Furthermore, the concentration of the *total hopanes (C_{27}-C_{34})* relative to *total steranes (C_{27}-C_{29})* is lowered as a result of preferential biodegradation of the former in the Wilga-2 and Washpool-1 oils (hop/ster = 0.6-0.7: Table 5.2). Moreover, the highest abundances of trisnorhopane (25,28,30-TNH) relative to bisnorhopane (28,30-BNH) are found in these biodegraded oils, suggesting that the former is derived from the latter.

Interestingly, biodegradation had no obvious effect on the S and R epimer distributions of either the steranes or the hopanes. The ααα 20S/ααα 20R sterane ratios show no marked differences between the most biodegraded oils and the rest of the oils in Table 5.2. The same is true for hopanes where the 22S/(22S+22R) ratio is very similar for all the oils. Indeed, the Riverslea-1 crude has the lowest %22S value of ~53 (Table 5.2), emphasising that its S and R epimer distributions have not been affected by biodegradation (see also Boreham, 1995).

All of these observations suggest that, at least in this set of oils, hopanes were more readily degraded than steranes. No preferential removal of regular steranes compared to diasteranes is observed for any of the aforementioned biodegraded oils, although they

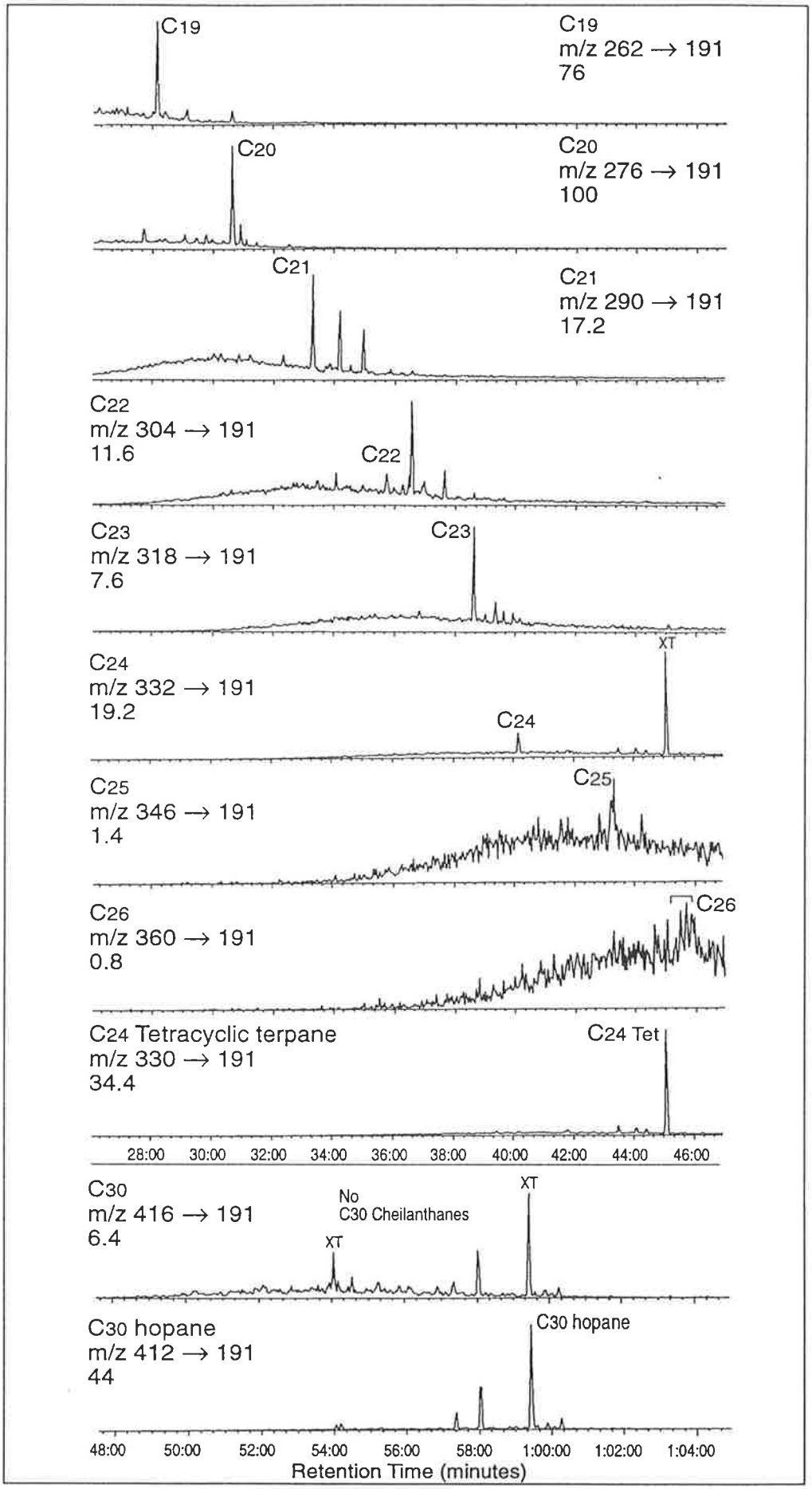

Figure 6.3 (a) MRM chromatograms showing the distributions of tricyclic terpanes and C_{24} tetracyclic terpane in the Wilga-2 oil (sample #6). The intensity for each trace is normalised against C_{30} hopane.

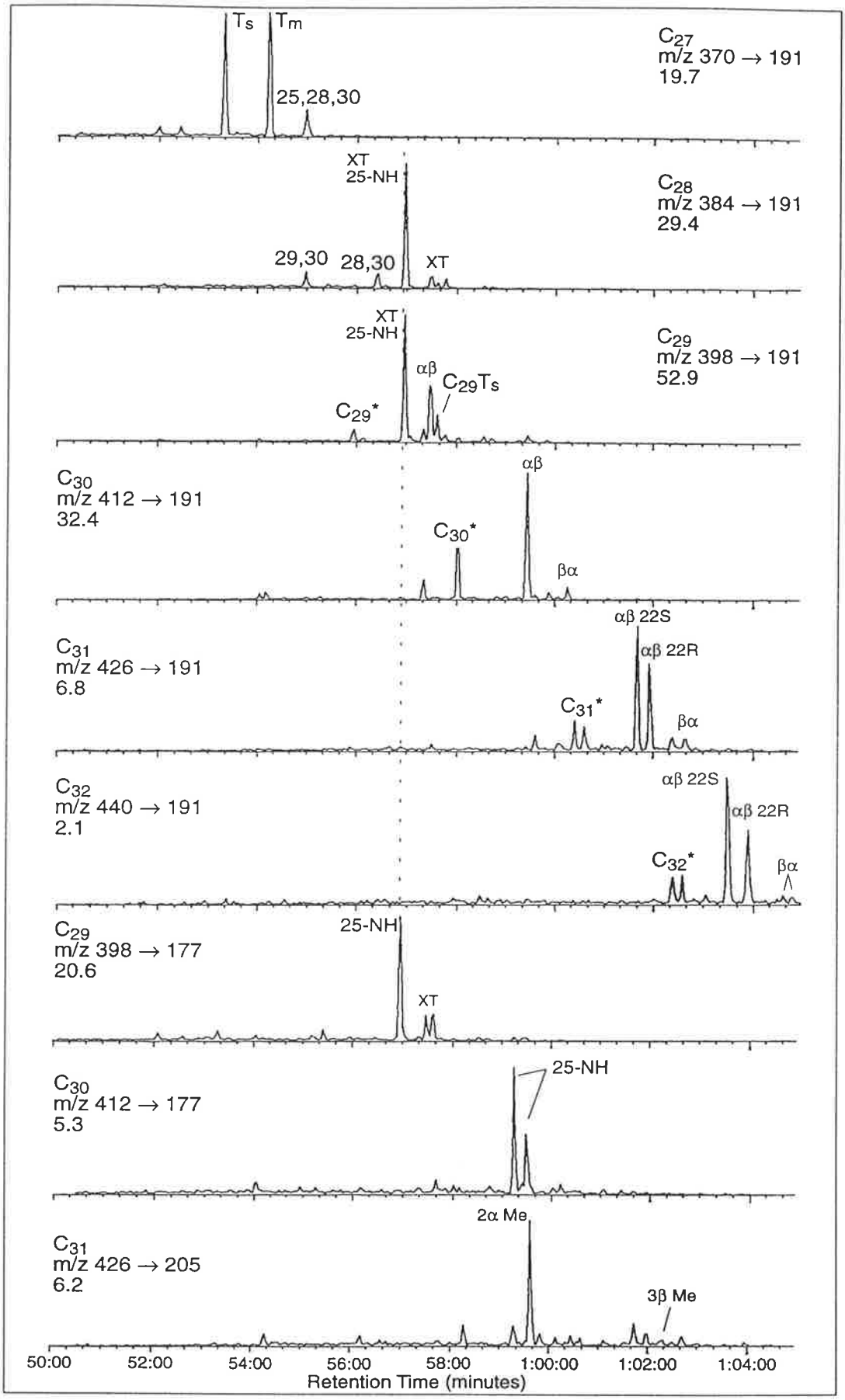

Figure 6.3 (b) MRM chromatograms showing the distributions of hopanes, diahopanes, norhopanes and methylhopanes in the Wilga-2 oil (sample #6). The intensity for each trace is normalised against the highest peak in the hopanes and steranes.

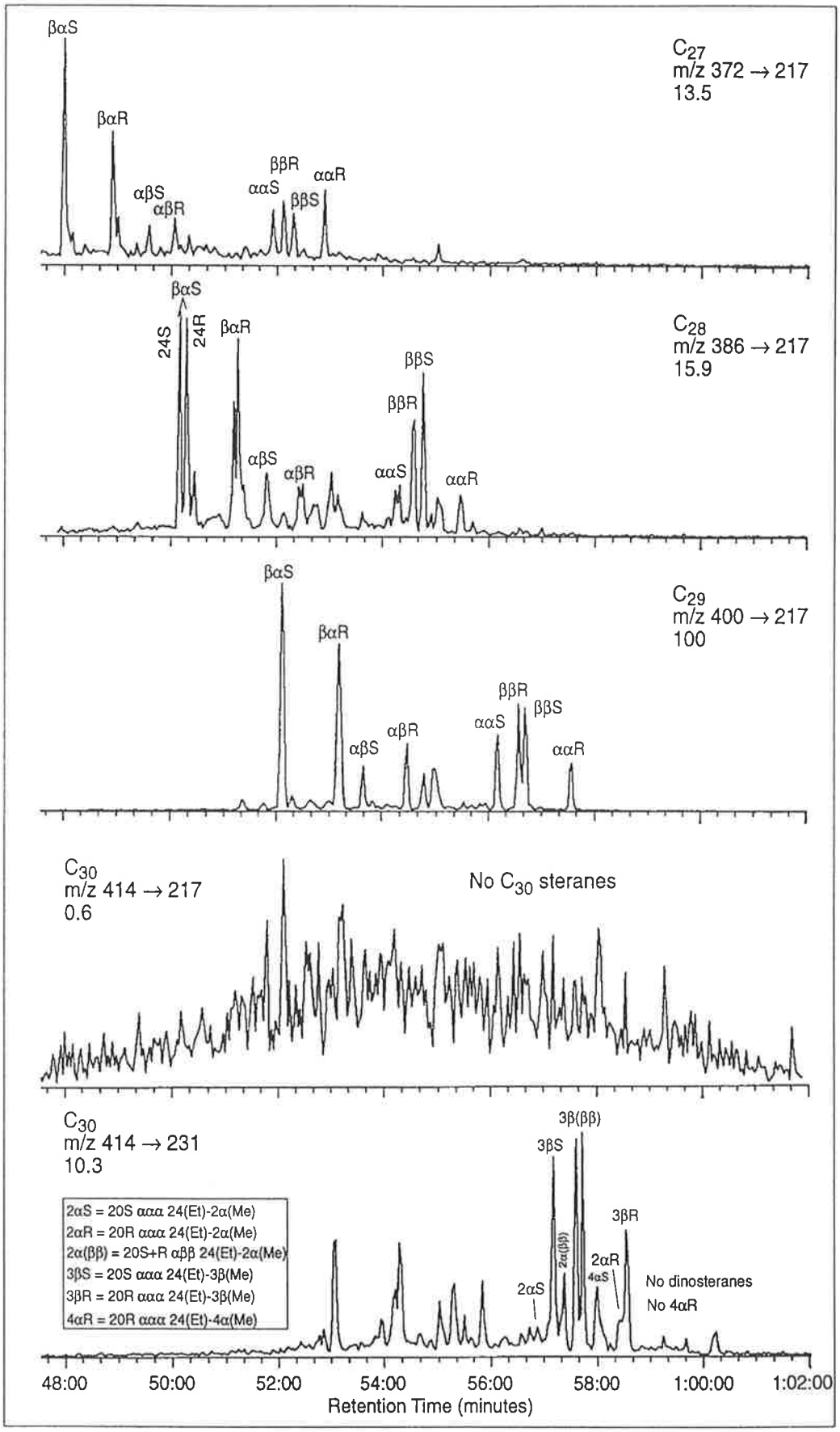

Figure 6.3 (c) MRM chromatograms showing the distributions of steranes ($M^{+\cdot} \rightarrow$ m/z 217) and methylsteranes ($M^{+\cdot} \rightarrow$ m/z 231) in the Wilga-2 oil (sample #6). The intensity for each trace is normalised against the highest peak in the hopanes and steranes.

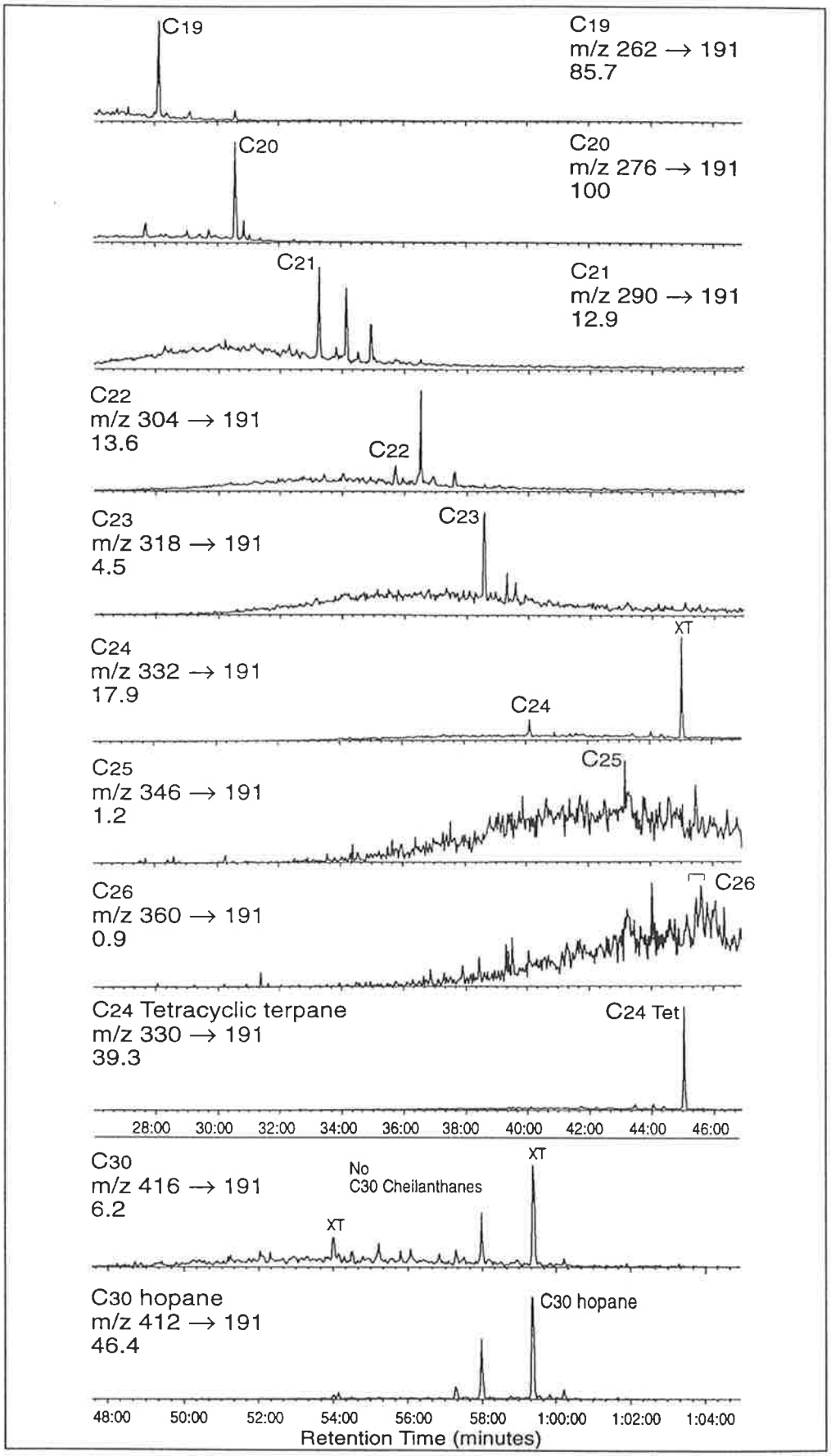

Figure 6.4 (a) MRM chromatograms showing the distributions of tricyclic terpanes and C_{24} tetracyclic terpane in the Washpool-1 oil (sample #5). The intensity for each trace is normalised against C_{30} hopane.

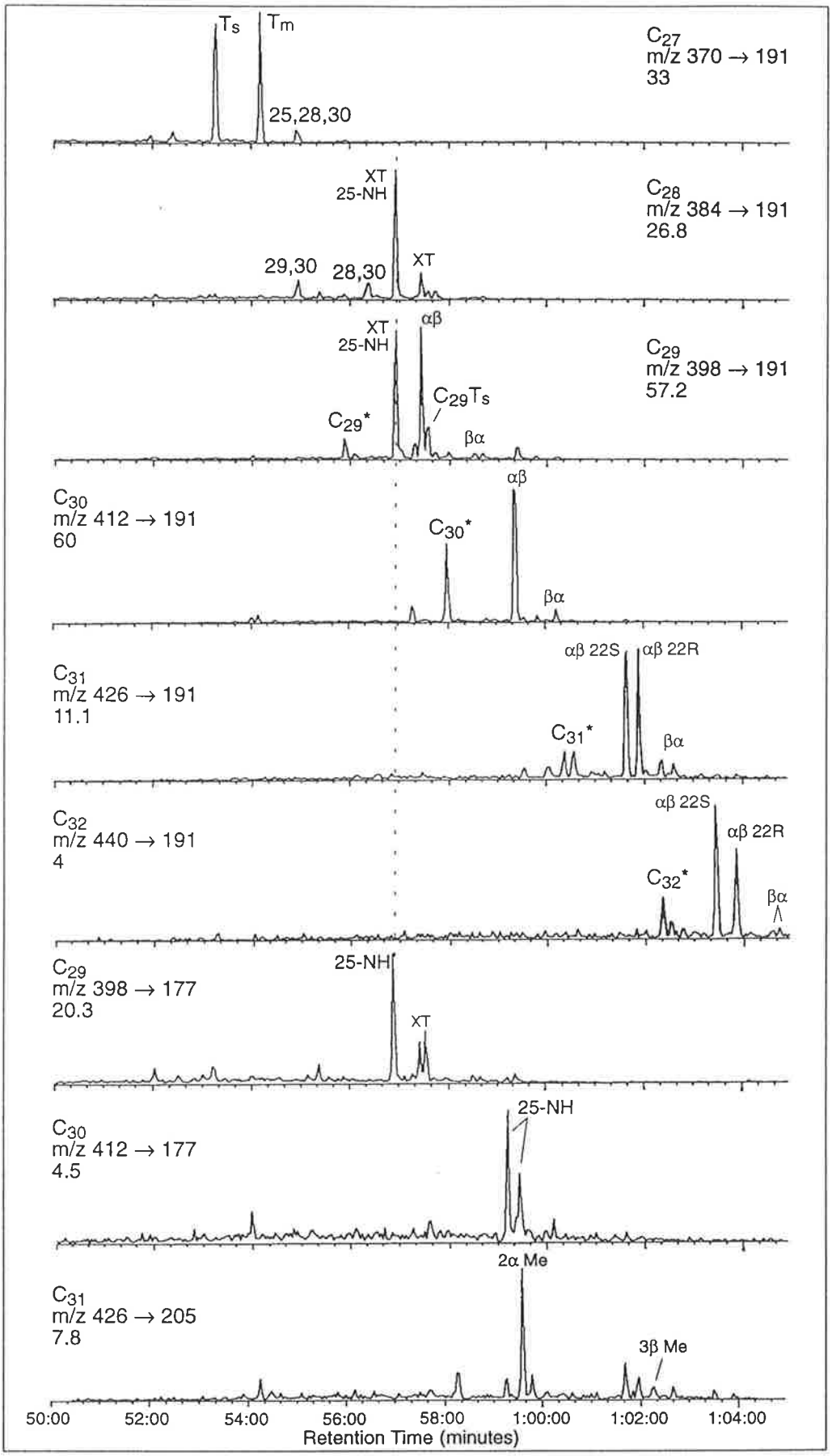

Figure 6.4 (b) MRM chromatograms showing the distributions of hopanes, diahopanes, norhopanes and methylhopanes in the Washpool-1 oil (sample #5). The intensity for each trace is normalised against the highest peak in the hopanes and steranes.

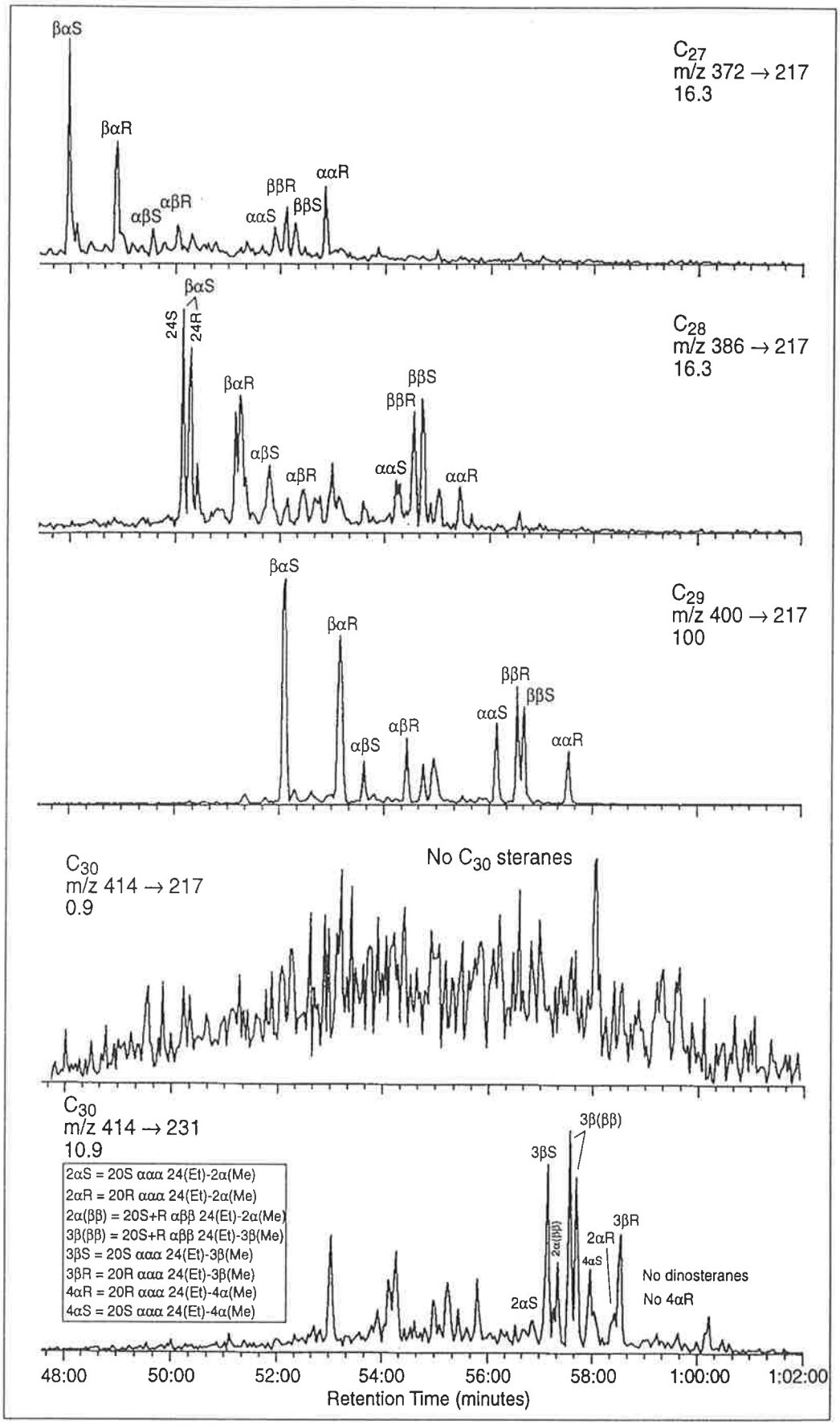

Figure 6.4 (c) MRM chromatograms showing the distributions of steranes ($M^+ \rightarrow$ m/z 217) and methylsteranes ($M^+ \rightarrow$ m/z 231) in the Washpool-1 oil (sample #5). The intensity for each trace is normalised against the highest peak in the hopanes and steranes.

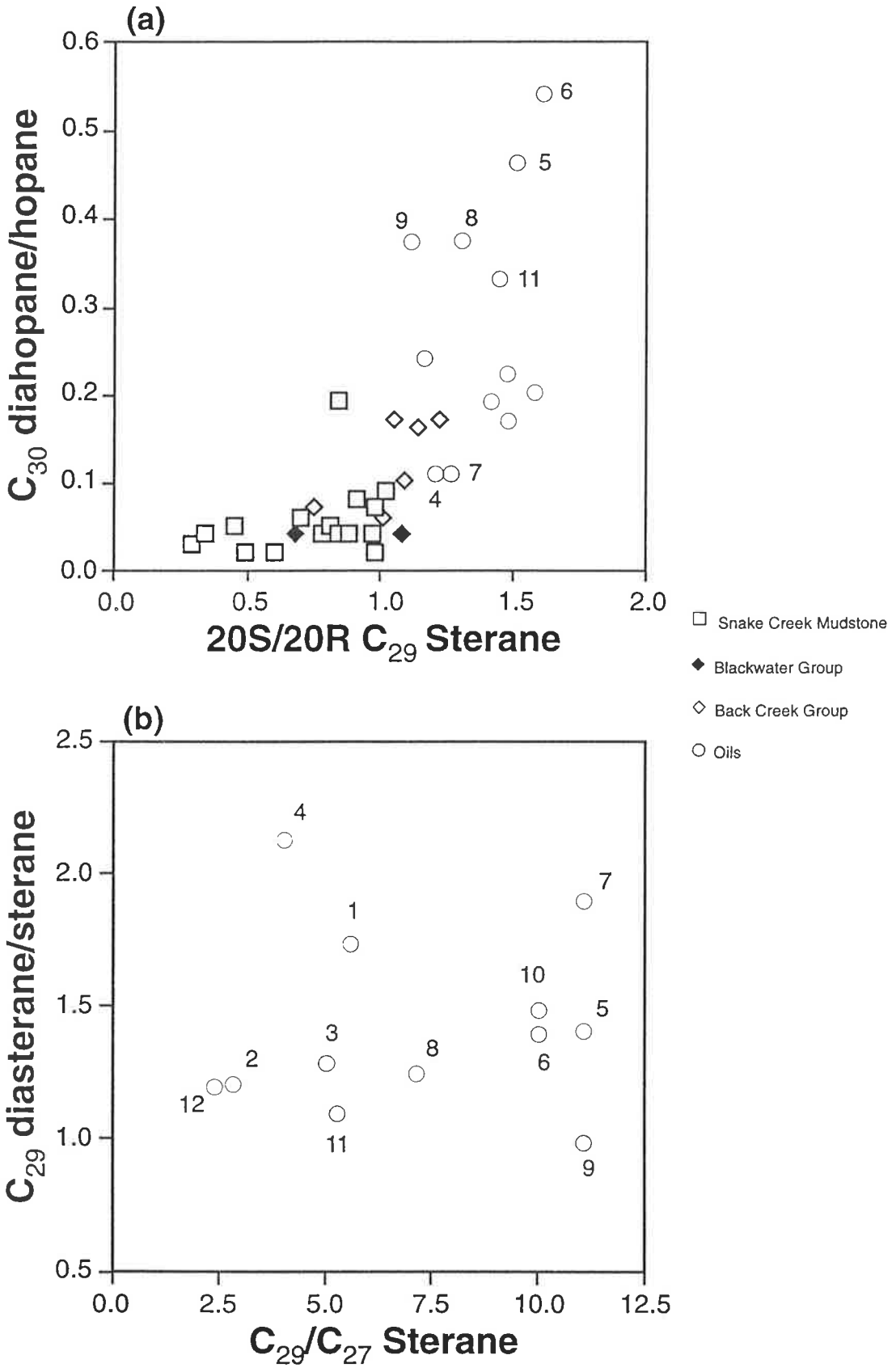

Figure 6.5 Crossplots of (a) C_{29} 20S/20R sterane *versus* C_{30} diahopane/hopane and (b) C_{29}/C_{27} steranes *versus* C_{29} diasterane/sterane for sediments and oils from the southern Taroom Trough.

do have high C_{29}/C_{27} sterane ratios (Fig. 6.3c, 6.4c and 6.5b). This latter feature is consistent with the conclusion of Peters and Moldowan (1993) that C_{27}, rather than C_{29}, steranes are favoured by bacteria during biodegradation.

That the alkane chromatogram of the Riverslea-1 oil should show clear evidence of biodegradation, but not those of the Wilga-2 and Washpool-1 crudes, may be explained by recharging of the latter reservoirs by an unaltered oil (*cf.* Volkman et al., 1983b). This is common for many of the Bowen/Surat Basin petroleums (Boreham, 1995). On the Peters and Moldowan (1993) scale of biodegradation (Fig. 2.6) these three oils (Wilga-2, Washpool-1 and Riverslea-1) can be ranked as mildly to moderately (4-5) biodegraded. Water washing might have played a role in removing the lower molecular weight *n*-alkanes in Waratah-1 oil (#7: Fig. 6.5b).

The 25-norhopanes are thought to result from the bacterial removal of the 25-methyl group from the regular 17α(H)-hopanes at an early (Chosson et al., 1992) or late (Palmer, 1993) stage of *in-reservoir* biodegradation. However, the presence of these 25-norhopanes and 28,30-BNH, among many other norhopanes, in source rock extracts led Noble et al. (1985c) and Chosson et al. (1993) to suggest a much earlier origin for these norhopanes, probably through syndepositional bacterial reworking of the precursor organic matter. The Permian and the Triassic sediments in this study also show considerable concentrations of the C_{29} 25-NH and C_{28} 28,30-BNH (Table 5.2). This is consistent with a bacterial source for these norhopanes. The C_{28} 28,30-BNH may be derived from anaerobic chemoautotrophic bacteria (Schoell et al., 1992) although its further concentration during bacterial reworking of organic matter is a possible alternative (see also Boreham, 1995).

6.3.1.3 Effect on carbon isotopic composition

Although variations in the carbon isotopic composition ($\delta^{13}C$) of saturated and aromatic hydrocarbons in crude oils are primarily source- and maturity-related, processes such as biodegradation and migration may account for the observed slight isotopic variability among the oils examined here. These secondary processes can result in heavier isotopic signatures in the hydrocarbon fractions (Schoell, 1984). The Bellbird oil (#11) is isotopically the lightest among the Permian-sourced oils, whereas other Permian oils reservoired in Triassic and Jurassic formations have heavier carbon isotopic compositions, attesting to longer vertical and lateral migration distances. The isotopically heaviest oil is the Riverslea-1, consistent with removal of isotopically-light *n*-alkanes (Boreham et al., 1995) during biodegradation (Section 6.3.1.2). However, the other biodegraded crudes (#5 and #6) do not show this effect on their isotopic

compositions. This is a further evidence that the Washpool-1 and Wilga-2 reservoirs have been recharged by unaltered oils. The distinctly lighter carbon isotopic compositions of the Triassic oils (#4 and #13) are probably related to their local generation from a Triassic source rock containing kerogen with a light isotopic signature (see Section 6.4).

6.3.2 Biomarker maturity parameters

6.3.2.1 Hopanes and steranes

The ratios of 22S to 22R C_{31} hopanes for all but one of the oils examined show mature signatures (22S = 57-64%: Table 5.1). The Riverslea-1 oil has a slightly lower value (53%), although the reason for this is not apparent. The ratio 20S/(20S+20R) C_{29} sterane (%20S) for the oils ranges between 55 and 62% which best matches those of the Permian sediments (50-55%: Table 5.1, Fig. 6.6). All the oils have very low moretane concentrations (C_{30} $\beta\alpha/\alpha\beta$ hopane $\leq$ 0.14) with the BCG values (C_{30} $\beta\alpha/\alpha\beta$ hopane $\leq$ 0.11) being closest to those of the oils. The less mature BWG and SCM extracts exhibit somewhat higher moretane abundances (0.12-0.20 and 0.11-0.26, respectively) consistent with low %$\beta\beta$ sterane values in both formations (C_{29} sterane $\alpha\beta\beta/(\alpha\alpha\alpha+\alpha\beta\beta) \leq 48\%$). The biomarker maturity-migration index (BMAI) plot (Fig. 6.6) illustrates the relative maturity levels for the Triassic and Permian oils and sediments. The BCG displays the best match with the oils. The oils also show a relatively high abundance of the more stable trisnorhopane T_s (T_s/T_m = 0.40-1.32: Table 5.1). In three oils (Tinker-4, Taylor-11 and Washpool-1) T_s predominates over the T_m. Accordingly, these same oils have both the highest relative concentrations of the more stable $\beta\beta$ steranes ($\beta\beta \geq 61\%$) and the lowest moretane abundances (C_{30} $\beta\alpha/\alpha\beta$ hopane $\leq$ 0.08).

6.3.2.2 Aromatic maturity parameters

The maturity of the oils at the time they were expelled from their source rocks can be estimated from their methylphenanthrene indices (MPI-1 and the corresponding calculated R_c: Radke and Welte, 1983). The oils examined were expelled early and at reasonably similar maturity levels, 0.62 and 0.75% R_c (Table 5.4). Although slightly lower values were obtained for the Roswin North-1 and Bellbird-1 oils, they are within the R_c range calculated by Boreham (1995) for a larger set of Bowen/Surat oils. He concluded that generation of liquid petroleum in the Taroom Trough started at 0.65% R_c and continued to 1.05% R_c. Philp and Gilbert (1986) examined twelve oils from the

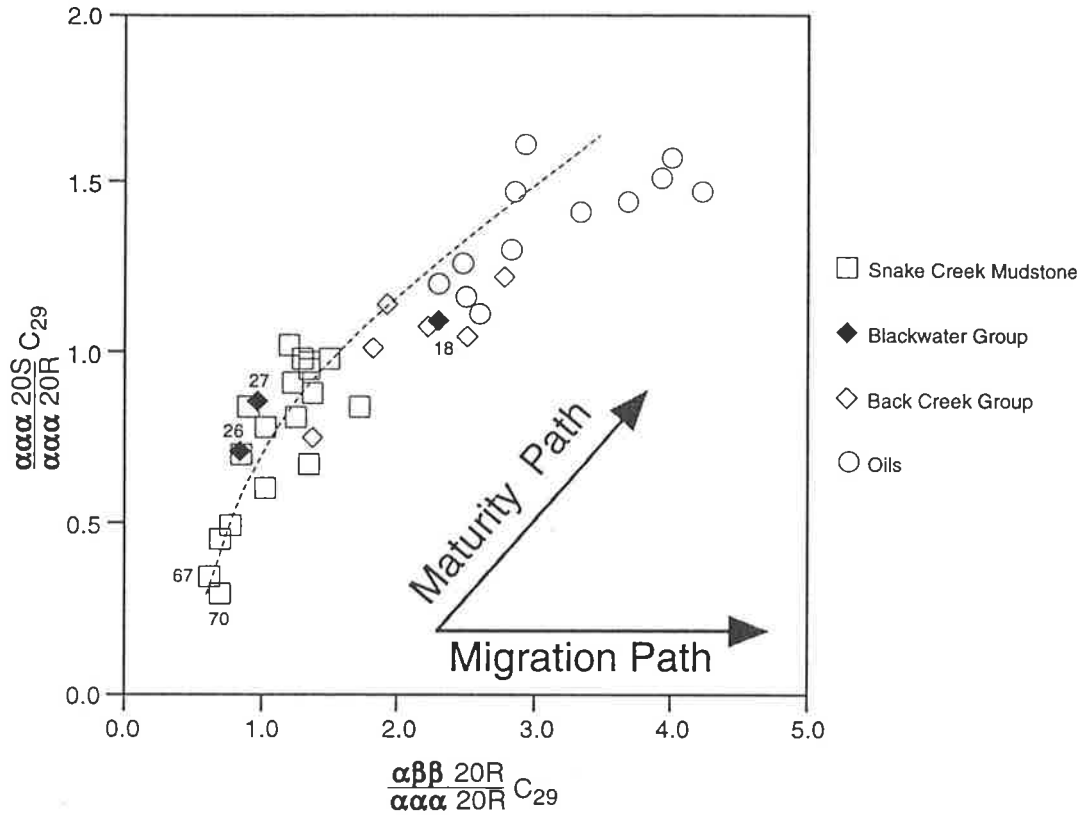

Figure 6.6 Biomarker maturation-migration (BMAI) plot for oils from the southern Taroom Trough. Data for Permian and Triassic sediments are included for comparison.

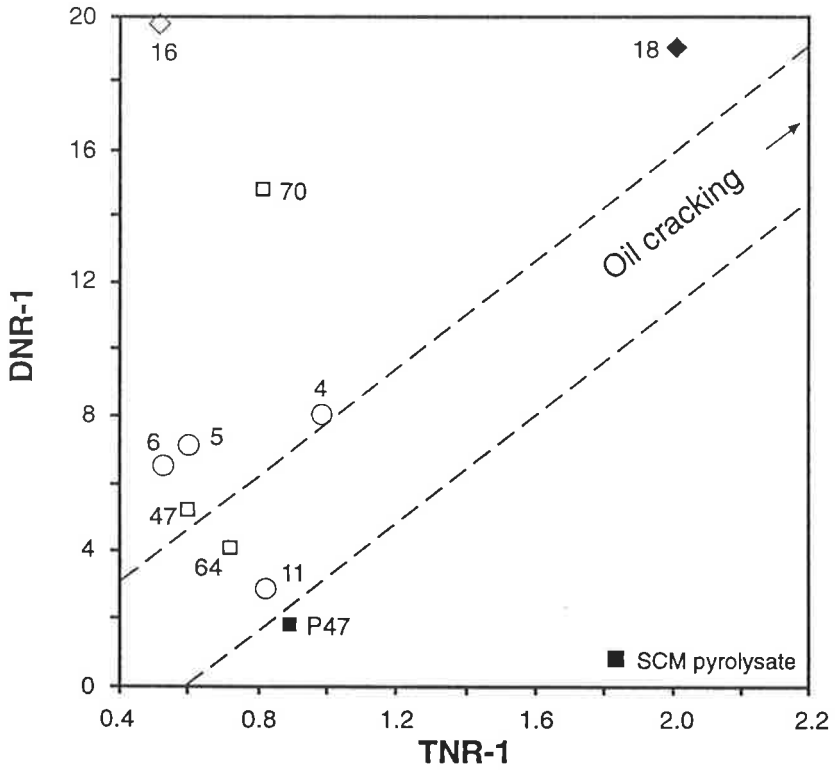

Figure 6.7 TNR-1 *versus* DNR-1 crossplot for selected sediments and oils from the southern Taroom Trough.

Taroom Trough area and found that all have the same level of maturity, except for the Conloi oil (in the north) which is most mature (1.2% R_C: see also Boreham, 1995) and the Yapunyah oil (in the southwest) which is the least mature (0.7% R_C).

The relative maturity of the oils (as well as the source rocks) can also be evaluated using isomeric ratios of the dimethylnaphthalenes (DNR-1) and the trimethylnaphthalenes (TNR-1) (Table 5.4). The limited number of Triassic and Permian oils examined appear to have been generated at similar maturity levels (Fig. 6.7) which, in this case, appear to differ markedly from those of the two Permian rock extracts from Cockatoo Creek-1 for which data are available.

6.3.3 Biomarker source parameters

6.3.3.1 Drimanes (bicyclic sesquiterpanes)

All the oils examined here are enriched in C_{14}-C_{15} bicyclic alkanes, including rearranged drimanes, at the expense of their C_{16+} homologues (Fig. 6.8). C_{16+} bicyclic alkanes are either absent or present as minor components. Noble et al. (1986) suggest that rearrangement of the drimanes parallels that of the steranes; both are suppressed in evaporite/carbonate environments (see also Palacas et al., 1984). Thus, the presence of rearranged drimanes in all the Taroom Trough oils attests to their origin from coal and/or shale source rocks.

The origin of these less-commonly-used compounds is largely unknown (Peters and Moldowan, 1993). Alexander et al. (1984) and Philp (1994) suggest their derivation from hopanes via aerobic microbial activity during the early stages of diagenesis within oxic, higher plant-rich environments. Palacas et al. (1984) noticed low abundances of drimanes and rearranged drimanes in evaporites and carbonates, whereas Price et al. (1987) reported abundant drimanes in coal-bearing sediments.

The distributions of these bicyclic sesquiterpanes in the present suite of Permo-Triassic source rock samples from the southern Taroom Trough are as follows. C_{16} and C_{17} bicyclic alkanes (homodrimanes and methylhomodrimanes) are exclusively abundant in calcareous mudstones of the BCG, whereas in carbonaceous shales of the BWG (samples #18, 26 and 27) they are either absent or, rarely, occur as minor components (Fig. 6.8a). Instead, C_{14}-C_{15} bicyclic alkanes, including rearranged drimanes (R1, R2), are the most abundant components in coal-bearing strata of the BWG (Fig. 6.8a). Similar observations were made when comparing carbonaceous shales and calcareous

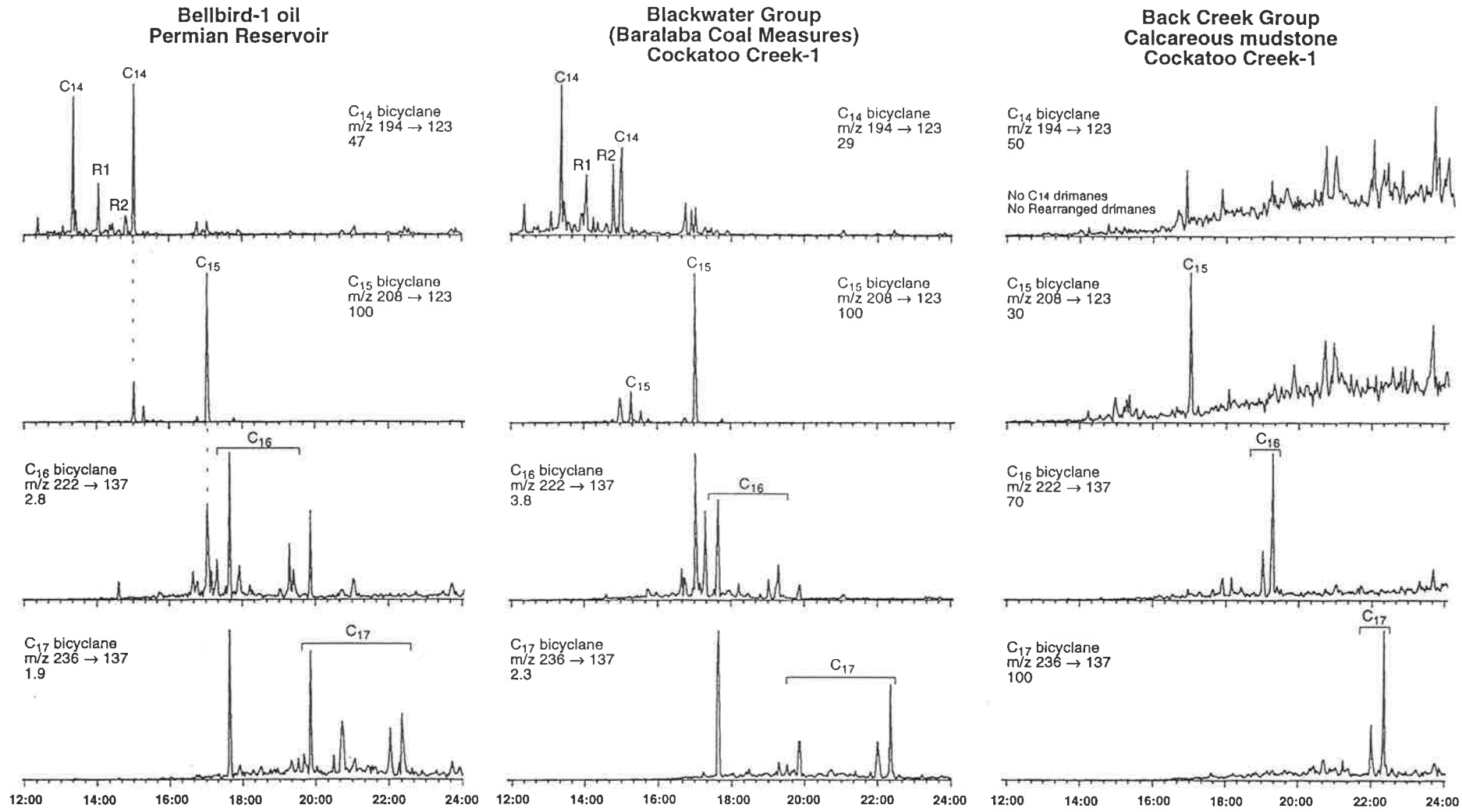

Figure 6.8 (a) MRM chromatograms showing the distributions of sesquiterpanes (C_{14}-C_{17} compounds) in Bellbird-1 oil (#11), Blackwater Group (sample #18) and Back Creek Group (sample #13) extracts, Cockatoo Creek-1.

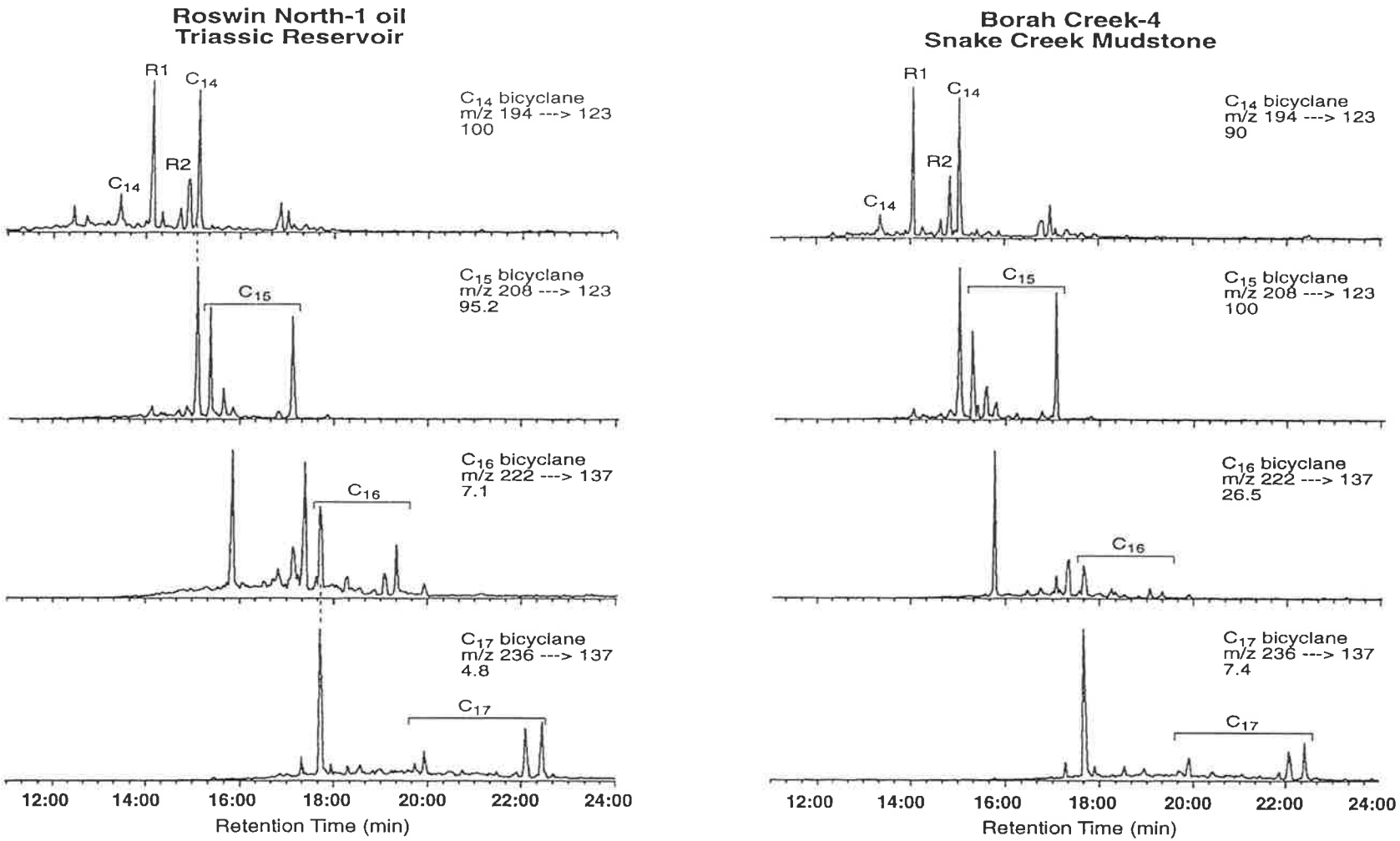

Figure 6.8 (b) MRM chromatograms showing the distributions of sesquiterpanes (C_{14}-C_{17}) in the Roswin North-1 oil (#4) and the Snake Creek Mudstone (Borah Creek-4).

mudstones of the SCM (Fig. 6.8b, see also Figure 5.6 and Section 5.4.2). No eudesmane is found in any oil or sediment studied from the Taroom Trough (Fig. 6.8).

A positive correlation exists between the C_{14-16+} bicyclic alkane distributions in the Roswin North-1 oil and shales of the SCM; all have abundant C_{14}-C_{15} rearranged and regular bicyclic alkanes while C_{16+} homologues are nearly absent (Fig. 6.8b). All the other Permian oils have sesquiterpane distributions similar to that exhibited by the Bellbird-1 oil (Fig. 6.8a). It has long been debated whether the oil pools in the Taroom Trough have been sourced from the coal-bearing facies of the BWG or from the marine-influenced mudstones of the BCG. Sesquiterpane distributions from this set of samples provide a definitive answer to this debate and prove that the Permian oils examined have their source in the carbonaceous shale facies of the BWG.

6.3.3.2 Tricyclic terpanes (C_{19}-C_{26} and C_{30} cheilanthanes)

A series of C_{19-26} tricyclic terpanes (TT) were detected, in varying abundances, in the Permo-Triassic sediments and oils from the Taroom Trough (e.g. Figs. 5.1a, 5.2a, 5.3a, 5.5a, 5.7a, 6.11a and 6.13a). Their abundances relative to 17α(H)-C_{30} hopane are presented in Table 6.2. Their highest relative and absolute abundances were found in the oils and the Lower Permian BCG mudstones. However, the Roswin North-1 oil contains low concentrations of tricyclic terpanes relative to C_{30} hopane ($C_{19-26}TT/C_{30}$ hop < 0.2). This latter value best matches those of the SCM shales (Table 6.2).

The origin of these biomarkers is not well understood. Connan et al. (1980) and Ourisson et al. (1982) suggest a prokaryotic origin while Volkman et al. (1989) argue that they may be of marine algal origin. In the present suite of Permo-Triassic source rock samples tricyclic terpanes appear to follow a certain pattern according to lithofacies. The carbonaceous shales (of the Permian and some of the SCM samples) show the lowest relative concentrations of the cheilanthanes ($C_{19-26}TT/C_{30}$ hopane ≤1.2: Table 6.2, e.g. Fig. 5.2a), whereas the highest relative and absolute abundances of cheilanthanes were found in the calcareous mudstone facies (3.4-5.5: Table 6.2, e.g. Fig. 5.1a). Although the TT/17α(H)-hopane ratio is believed to increase with maturity (Peters and Moldowan, 1993), its variation in this set of samples is more source-related. Indeed, coals from the same formation (BWG; samples #18 and 26), with clearly different maturation levels (T_{max} = 451°C and 432 °C, respectively), have the same TT/C_{30} hopane value (0.3). On the other hand, the mudstone facies in Flinton-1 (sample #19) shows much higher abundances of the tricyclic terpanes (TT/C_{30} hop = 3.6: Table 6.2) although it is less mature (T_{max} = 434°C).

Table 6.2 Abundance of the C_{19}-C_{26} and C_{30} cheilanthanes and C_{24} tetracyclic terpane relative to C_{30} hopane

Ratio	C_{19}	C_{20}	C_{21}	C_{22}	C_{23}	C_{24}	C_{25}	C_{26}	C_{30}	C_{24}Tetra	C_{19}-C_{26}	$\frac{C_{19+20}}{C_{21+23}}$
Sample												
Snake Creek Mudstone												
35 Flinton-1	0.28	0.28	0.09	0.02	0.09	0.05	0.03	0.02	0	0.25	0.84	3.11
41 Glenhaughton-1	0.31	0.59	0.55	0.16	0.91	0.51	0.31	0.22	0.03	0.48	3.55	0.6
45 Cabawin-1	0.48	0.61	0.04	0.07	0.49	0.21	0.09	0.07	0	0.42	2.05	2.06
46 Muggleton-1	0.32	0.38	0.27	0.04	0.03	0.01	0.01	0.01	0	0.25	1.06	2.33
47 Snake Crrek-1	0.23	0.40	0.08	0.02	0.04	0.01	0.01	0.01	0	0.14	0.79	5.25
48 Red Cap-1	0.96	0.07	0.08	0.02	0.09	0.05	0.04	0.03	0	0.09	1.33	6.06
49 Borah Creek-3(1)	0.23	0.29	0.17	0.35	0.13	0.05	0.03	0.02	0	0.22	1.27	1.73
53 Borah Creek-3(2)	0.09	0.12	0.07	0.01	0.35	0.15	0.10	0.07	0	0.1	0.96	0.5
57 Taroom 12-12A	0.05	0.05	0.05	0.01	0.02	0.01	0.01	0.01	0	0.06	0.2	1.43
58 Tinker-2	0.23	0.16	0.03	0.01	0.02	0.01	0	0	0	0.23	0.46	7.8
59 Warroon-1	0.14	0.16	0.10	0.02	0.12	0.06	0.04	0.03	0	0.17	0.66	1.36
63 Glenearn North-1	0.07	0.08	0.04	0.01	0.04	0.01	0.01	0.01	0	0.07	0.26	1.88
64 Borah Creek-4	0.67	0.50	0.17	0.02	0.07	0.03	0.02	0.01	0	0.21	1.48	4.88
65 Namarah-2	0.09	0.20	0.05	0.07	0.04	0.23	0.05	0.14	0	0.36	1.61	0.44
67 Hollow Tree-1	0.03	0.04	0.04	0	0.02	1.00	0.01	0.01	0	0.06	0.17	1.17
70 Renlim-1	0.06	0.09	0.09	0.03	0.1	0.04	0.03	0.02	0	0.1	0.45	0.79
71 Newington-2	0.18	0.24	0.13	0.07	0.28	0.13	0.10	0.05	0	0.37	1.17	1.02
72 Yellowbank Creek North-1	0.05	0.08	0.08	0.01	0.06	0.02	0.02	0.01	0	0.14	0.32	0.93

Table 6.2 Abundance of the C_{19}-C_{26} and C_{30} cheilanthanes and C_{24} tetracyclic terpane relative to C_{30} hopane (continued)

Ratio	C_{19}	C_{20}	C_{21}	C_{22}	C_{23}	C_{24}	C_{25}	C_{26}	C_{30}	C_{24}Tetra	C_{19}-C_{26}	$\frac{C_{19+20}}{C_{21+23}}$
Sample												
Permian source rocks												
Blackwater Group												
18 Cockatoo Creek-1	0.12	0.13	0.02	0	0.01	0.01	0	0	0	0.15	0.3	8.33
26 Meeleebee-1	0.11	0.10	0.02	0.01	0.03	0.02	0.01	0	0	0.20	0.31	3.50
27 Meeleebee-1	0.31	0.42	0.19	0.05	0.15	0.06	0.05	0.02	0	0.27	1.24	2.15
Back Creek Group												
6 Burunga-1	1.10	1.34	0.87	0.25	1.04	0.59	0.22	0.13	0.06	0.61	5.53	1.28
10 Burunga-1	0.18	0.19	0.13	0.03	0.12	0.06	0.03	0.02	0.01	0.16	0.77	1.48
13 Cockatoo Creek-1	0.23	0.44	0.52	0.20	1.05	0.49	0.38	0.23	0.11	0.44	3.36	0.43
16 Cockatoo Creek-1	0.74	1.04	0.71	0.21	0.88	0.48	0.27	0.19	0.08	0.35	4.51	1.12
19 Flinton-1	0.38	0.52	0.82	0.10	0.79	0.58	0.30	0.07	0.01	0.31	3.56	0.56
24 Meeleebee-1	0.08	0.11	0.09	0.02	0.09	0.04	0.02	0.01	0.01	0.14	0.45	1.06
Oils												
1 Taylor-12A	2.91	2.62	0.30	0.13	0.19	0.16	0.06	0.11	0	0.56	6.47	11.29
2 Taylor-11	3.53	3.11	0.48	0.14	0.36	0.29	0.23	0.16	0	0.92	8.28	7.91
3 Tinker-4	1.37	1.14	0.14	0.07	0.09	0.07	0.05	0.03	0	0.38	2.97	10.91
4 Roswin North-1	0.07	0.06	0.02	0	0.02	0.01	0.01	0	0	0.07	0.19	3.25
5 Washpool-1	1.61	1.88	0.22	0.11	0.12	0.18	0.07	0.04	0	0.56	4.12	10.27
6 Wilga-2	1.99	2.68	0.43	0.14	0.19	0.14	0.07	0.05	0	0.77	5.69	7.53
7 Waratah-1	0.71	0.67	0.08	0.04	0.05	0.05	0.03	0.02	0	0.21	1.66	10.62
8 Martini-1	1.47	1.51	0.18	0.10	0.11	0.13	0.07	0.04	0	0.38	3.60	10.28
9 Riverslea-1	0.95	1.14	0.16	0.06	0.08	0.05	0.04	0.02	0	0.34	2.50	8.71
10 Cogoon River West-1	0.88	0.93	0.17	0.06	0.09	0.07	0.04	0.03	0	0.30	2.25	6.96
11 Bellbird-1	0.84	0.75	0.11	0.06	0.13	0.08	0.09	0.05	0	0.32	2.10	6.63
12 Merroombile-1	1.36	1.13	0.38	0.09	0.34	0.27	0.27	0.21	0	0.28	4.04	3.46

Not all tricyclic terpanes are derived from prokaryotes or algae. The C_{19} and C_{20} compounds may be derived from higher plants (Peters and Moldowan, 1993). In an attempt to elucidate the effect of different lithofacies (and, therefore, varying depositional conditions) on the cheilanthane distributions, C_{19+20} cheilanthanes were plotted against C_{21+23} homologues (Fig. 6.9a). A clear distinction can be made between different lithofacies. In the calcareous mudstones of the BCG (samples #6, 13, 16 and 19: Fig. 6.9a) and SCM (sample #41: $C_{19+20}/C_{21+23}TT = 0.6$, $C_{19-26}TT/C_{30}$ hop = 3.6: Table 6.2) the C_{21+23} cheilanthanes predominate over their C_{19} and C_{20} homologues and C_{30} hopane (Table 6.2; Figs. 5.1a and 5.5a). On the other hand, C_{19} and C_{20} homologues are the most prominent (up to 84% of the total cheilanthanes) in the carbonaceous shales of the BWG and SCM (Table 6.2, Fig. 6.9a; see also Fig. 5.2a). It seems reasonable to conclude that where C_{19} and C_{20} cheilanthanes are present without their higher homologues land plants are the source, while prokaryotes and algae are considered the source when the higher homologues, particularly C_{21} and C_{23}, predominate. This inference is also demonstrated by plotting the C_{19+20}/C_{21+23} tricyclic terpanes ratio *versus* the hopane/sterane ratio (Fig. 6.9b). From this diagram it can be concluded that prokaryotic and algal remains in the calcareous facies accumulated in suboxic to anoxic environments, whereas the carbonaceous shales were deposited under more oxic conditions.

These relationships in the present suite of oil samples from the Taroom Trough attest to their derivation largely from higher-plant-rich carbonaceous shales which were deposited in a predominantly oxic environment (Figs. 6.9a and b). All the oils have high abundances of tricyclic terpanes ($C_{19-26}TT/C_{30}$ hop = 1.6-8.3: Table 6.2), with the C_{19} and C_{20} members constituting the major proportion of the total cheilanthanes ($C_{19+20}TT$ = 63-86%). The Roswin North-1 oil is an exception where cheilanthanes are present only in trace concentrations ($C_{19-26}TT/C_{30}$ hop = 0.19: Table 6.2). This may imply generation from a less mature source rock. The association of higher abundances of tricyclics with more mature sediments was observed by Peters and Moldowan (1993). However, this observation does not always apply. For example, among the McKittrick oils from California the largest tricyclic terpanes/17α(H)-hopane ratio was found in the least mature oil, and the smallest in the most mature oil (Peters and Moldowan, 1993). Thus, Seifert and Moldowan (1978) ascribed variations of the tricyclic abundances in the McKittrick oils to source rather than maturity differences. In the present study, the Roswin North-1 oil and other oils examined were expelled from their source rocks at similar maturity levels (Section 6.3.2). The former oil, therefore, appears to have been generated from a different source rock. As mentioned above, many of the SCM samples also contain low concentrations of tricyclics, suggesting a possible genetic relationship with Roswin North-1 oil.

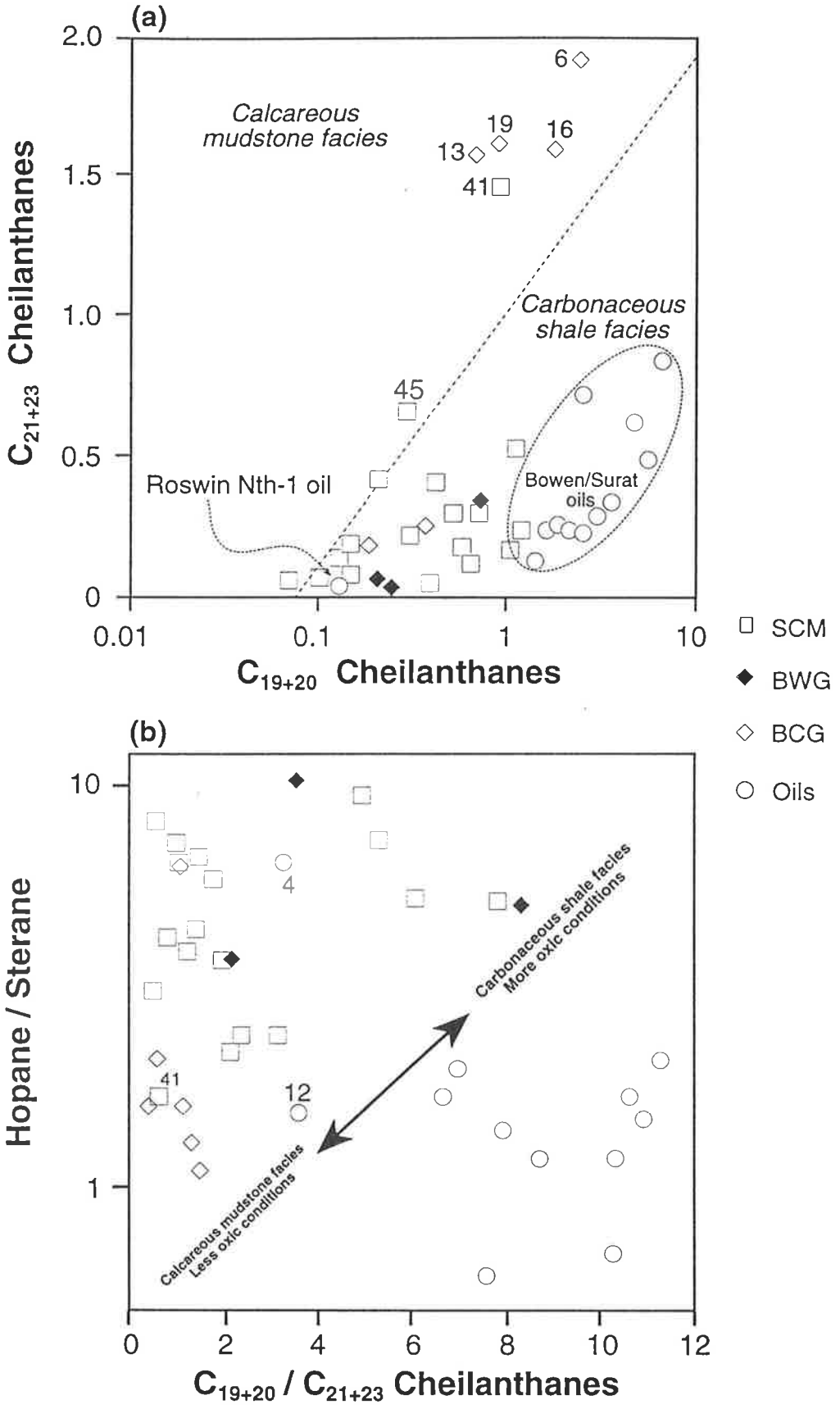

Figure 6.9 Crossplots of (a) C_{19+20} cheilanthanes *versus* C_{21+23} cheilanthanes and (b) C_{19+20}/C_{21+23} cheilanthanes ratio *versus* hopane/sterane ratio for sediments and oils from the southern Taroom Trough.

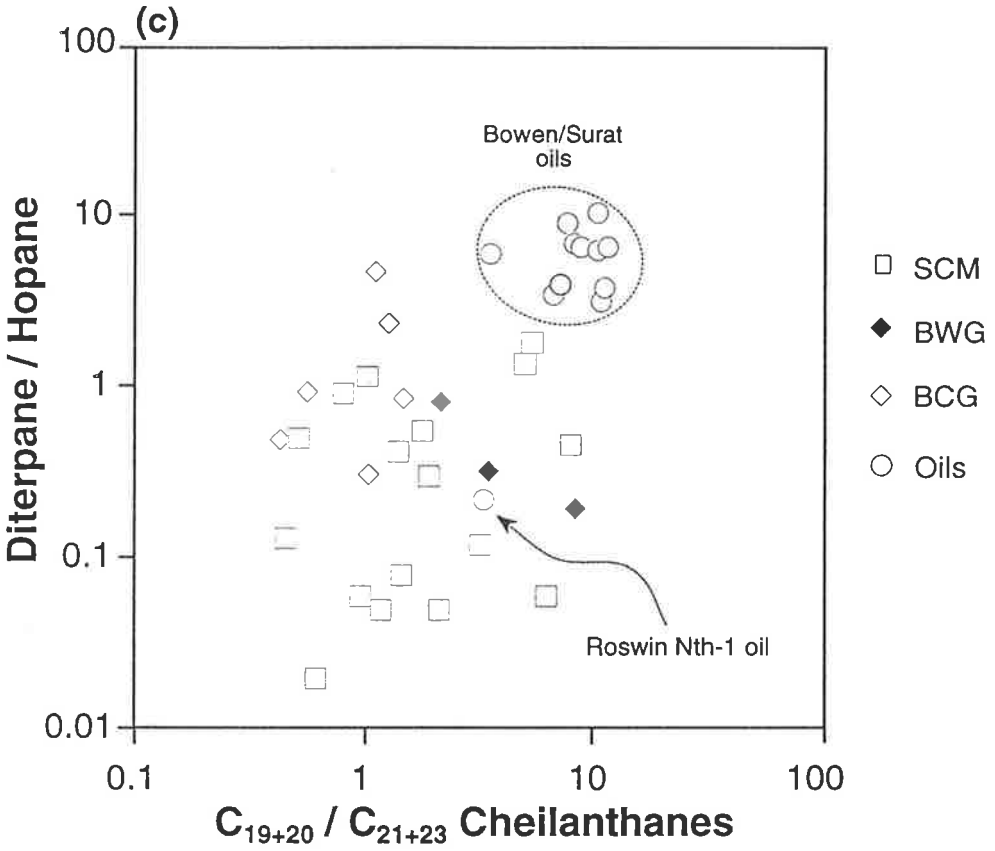

Figure 6.9 (c) Crossplot of C_{19+20}/C_{21+23} cheilanthanes ratio *versus* diterpane/C_{30} 17α(H)-hopane ratio for sediments and oils from the southern Taroom Trough.

6.3.3.3 Diterpenoid hydrocarbons

Diterpanes have been used successfully in oil-source correlation studies (R. Alexander et al., 1987, 1988). Distributions of the diterpenoid hydrocarbons in the Permo-Triassic oils and sediments examined from the southern Taroom Trough are presented in Table 6.3. These distributions vary widely between different facies within the same well. They also vary laterally within the same formation, reflecting different inputs of higher plant resins. The most striking observation is an inverse relationship between the TOC and diterpane/hopane values (Table 6.3). The same feature was noted in a suite of coals and shales from the Gippsland Basin (R. Alexander et al., 1987). One might expect to find the highest diterpane contents in the coals which normally receive greater amounts of land plant remains than do other sub-aquatic sediments. However, this inverse relationship can be explained by the development, within the peat swamp, of subenvironments suitable for bacteria to flourish. This gives rise to higher concentrations of bacterial lipids and, hence, lower diterpane/hopane ratios. Alexander et al. (1987) proposed the use of the diterpane/hopane ratio as an indicator of oxicity, with lower values being associated with oxic depositional environments. Thus, for the Permian section, the highest diterpane/hopane ratio (diterp/hop = 4.6) is found in BCG sample #13 (pr/ph = 0.9) postulated to have been deposited in a marine-influenced suboxic-anoxic environment, whereas the BWG carbonaceous shale sample #18 has the lowest value (diterp/hop = 0.2: Table 6.3). However, although this concept can be applied with some confidence to the sediment extracts, it does not apply to the oils (see below).

Such variations in the diterpane distributions and abundance relative to C_{30} hopane can be employed to distinguish oils from different sources. The oils and the condensate examined here contain large amounts of diterpenoid hydrocarbons relative to C_{30} hopane (diterp/C_{30} hop = 3.2-10.8: Table 6.3, Fig. 6.9c), whereas their pristane/phytane ratios indicate their origin from source rocks deposited in an oxic environment (pr/ph = 4-6: Table 4.1). These values most closely resemble those of the Permian source rocks, although diterpane/hopane ratios are slightly lower in the sediments (diterp/C_{30} hop = 0.3-4.6: Table 6.3). However, enhanced concentrations of diterpanes in the oils do not seem to be solely source-related (Fig. 6.9c). Instead, they may reflect geochromatographic fractionation during migration, which preferentially removes the higher-molecular-weight hopanes. The exception again is the Roswin North-1 oil which is relatively depleted in diterpanes (diterp/C_{30} hop = 0.2: Table 6.3, Fig. 6.9c). Such low values are observed for the BWG sample #18 and some of the SCM samples (Table 6.3). However, comparison of their diterpane distributions reveals great similarities between the SCM extract from Flinton-1 (Fig. 6.10a) and the Roswin North-1 oil (Fig. 6.10b); both show tricyclic diterpenoids predominating over the tetracyclic diterpanes,

Table 6.3 The relative abundances of diterpanes in Permian and Triassic sediments and oils, southern Taroom Trough

Ratio*	TOC	ΣDiterpanes	ΣTricyclic	ΣTetracyclic	Bicyclic	Tricyclic diterpanes					Tetracyclic diterpanes				16α(H)
					8β(H)-	19-Noriso-	Fichtelite	Rimuane	Pimarane	Isopimarane	17-Nortet-	*ent*-Beyerane	Phyllocladane#	*ent*-Kaurane#	16β(H)
	%	C_{30} hopane	diterpanes%	diterpanes%	Labdane%	pimarane%	%	%	%	%	racyclane%	%	%	%	Phyllocladane
Sample															
Snake Creek Mudstone															
35 Flinton-1	2.52	0.12	97	3	0	50	3	0	0	44	0	2	1	0	0.18
41 Glenhaughton-1	1.07	0.02	87	13	0	21	13	27	7	19	0	3	8	2	0.34
45 Cabawin-1	1.83	0.05	95	5	0	39	3	10	0	43	0	2	2		0.25
46 Muggleton-1	1.39	0.01	92	8	0	28	9	33	9	13	0	2	4	2	0.04
47 Snake Creek-1	3.38	1.84	49	51	0	10	11	14	5	9	2	10	31	8	0.50
48 Red Cap-1	0.66	0.06	63	37	0	13	16	14	9	11	0	5	27	5	0.51
49 Borah Creek-3(1)	2.08	0.55	63	37	0	16	18	10	8	11	5	5	19	8	0.36
53 Borah Creek-3(2)	2.54	0.51	72	28	0	12	11	22	10	17	2	6	16	4	0.59
57 Taroom-12-12A	1.47	0.08	75	25	0	5	48	12	4	6	4	5	10	6	0.45
58 Tinker-2	1.64	0.45	73	27	0	14	39	1	0	19	1	0	23	3	0.31
59 Warroon-1	2.26	0.42	62	38	0	18	18	9	5	12	4	9	18	7	0.43
63 Glenearn North-1	1.63	0.30	69	31	0	15	18	16	7	13	8	7	11	5	0.53
64 Borah Creek-4	1.68	1.37	55	45	0	11	21	10	5	8	13	8	18	6	0.42
65 Namarah-2	0.12	0.13	66	34	0	9	12	16	15	14	0	8	23	3	1.21
67 Hollow Tree-1	1.73	0.05	69	31	0	7	42	8	4	8	2	5	14	10	0.22
70 Renlim-1	0.72	0.77	64	36	0	23	11	15	1	14	5	15	14	2	1.51
71 Newington-2	2.00	1.13	60	40	0	12	16	19	9	4	7	7	17	9	0.20
72 Yellowbank Creek North-1	1.84	0.06	65	35	0	8	38	6	3	10	0	6	21	8	0.39
Permian source rocks															
Blackwater Group															
18 Cockatoo Ck-1	9.86	0.17	47	52	1	3	31	4	4	5	0	19	11	22	0.24
26 Meeleebee-1	39.3	0.30	67	33	0	19	13	3	0	32	3	10	9	11	0.20
27 Meeleebee-1	1.97	0.80	46	54	0	12	17	4	7	6	9	9	26	10	0.41
Back Creek Group															
6 Burunga-1	0.96	1.89	74	26	0	20	17	17	2	18	6	8	8	4	0.38
10 Burunga-1	0.71	0.76	60	40	0	12	12	10	10	16	10	9	13	8	0.24
13 Cockatoo Ck-1	1.35	0.49	71	28	1	13	12	15	12	19	0	12	13	3	0.60
16 Cockatoo Ck-1	3.65	4.56	84	16	0	17	4	21	21	21	0	3	11	2	0.60
19 Flinton-1	0.97	0.93	55	45	0	10	13	11	11	10	18	7	13	7	0.76
24 Meeleebee-1	1.86	0.30	47	53	0	10	16	8	6	7	6	9	30	8	0.43
Oils															
1 Taylor-12A		6.09	80	20	0	22	13	18	10	17	0	8	7	5	0.09
2 Taylor-11		6.86	72	28	0	9	11	22	13	17	3	9	13	3	0.31
3 Tinker-4		3.87	79	21	0	20	14	15	11	19	3	7	9	2	0.16
4 Roswin North-1		0.22	82	18	0	23	21	12	9	17	1	6	5	6	0.06
5 Washpool-1		6.42	69	31	0	13	13	21	9	13	5	8	13	5	0.21
6 Wilga-2		9.29	67	33	0	10	10	23	11	13	6	8	15	4	0.32
7 Waratah-1		3.22	74	26	0	13	10	22	12	17	5	9	10	2	0.32
8 Martini-1		10.75	60	39	1	11	13	14	10	12	2	12	18	7	0.29
9 Riverslea-1		6.70	58	42	0	11	12	16	8	11	6	12	17	7	0.24
10 Cogoon River West-1		4.03	62	38	0	14	14	14	7	13	5	11	16	6	0.28
11 Bellbird-1		3.45	66	34	0	17	9	10	7	13	3	10	13	8	0.25
12 Merroombile-1		6.19	69	31	0	23	11	11	9	15	5	9	12	5	0.29

* MRM transitions used to calculate the peak areas for each compound are listed in Table 2.1. All data are normalised against the total diterpanes

16α(H)+16β(H) isomers

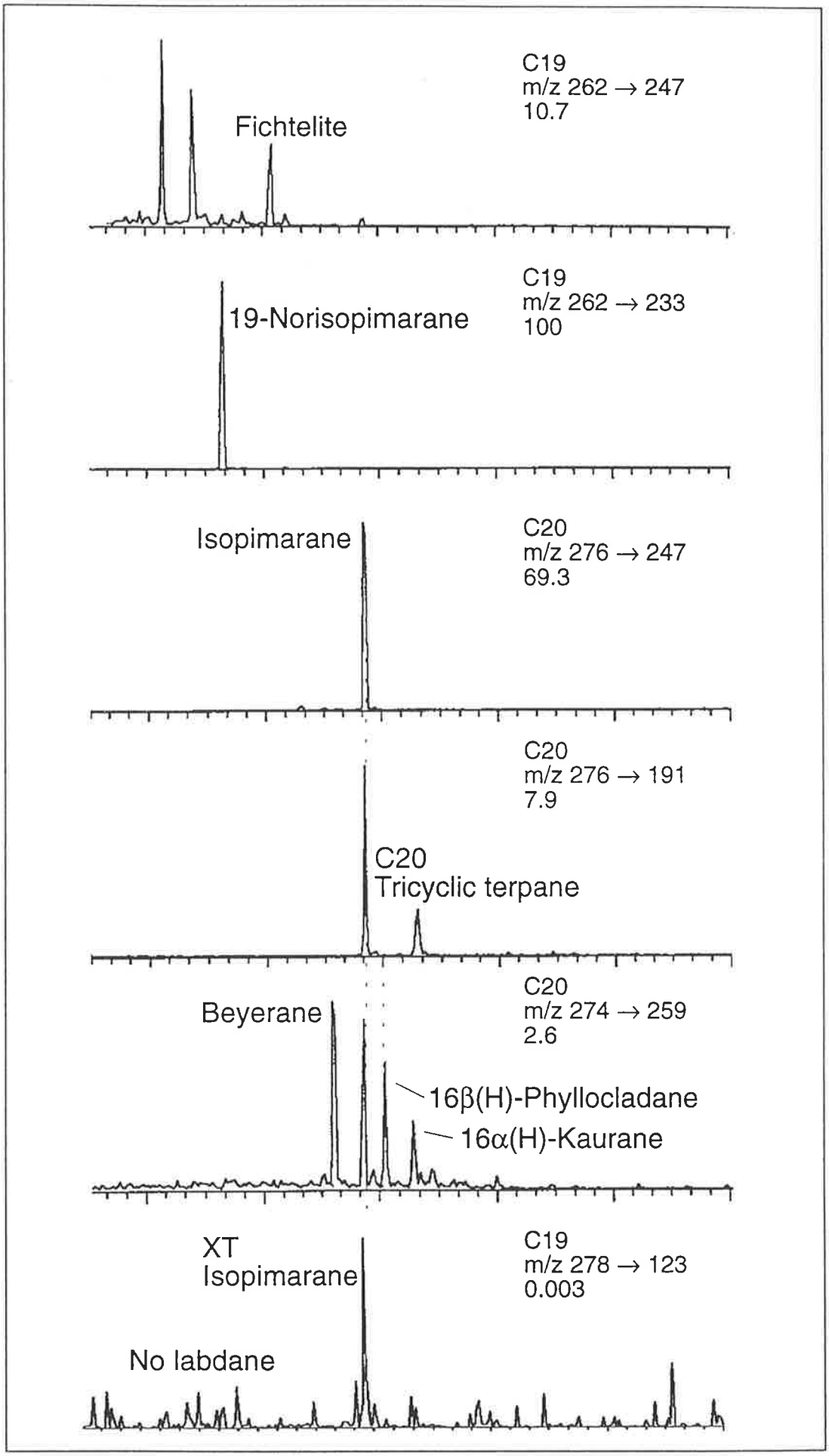

Figure 6.10 (a) MRM chromatograms of diterpanes in the Snake Creek Mudstone, Flinton-1 (sample #35). The diterpane distribution is similar to that of the Roswin North-1 oil (see Figure 6.10b).

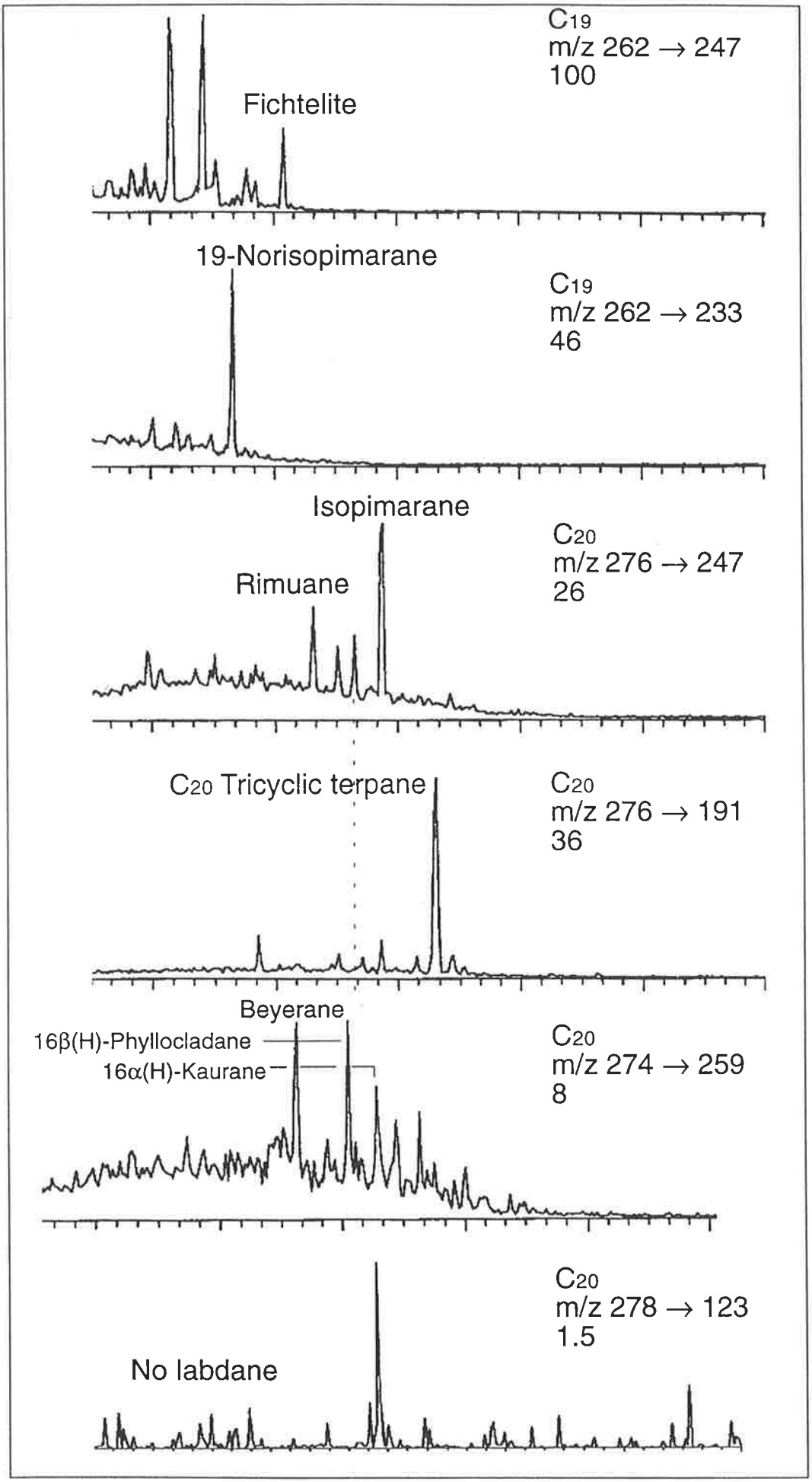

Figure 6.10 (b) MRM chromatograms of diterpanes in oil from Roswin North-1 (sample #4).

with the isopimarane and norisopimarane being the major individual compounds (Table 6.3). This is not the case for the BWG (sample #18) which lacks the isopimarane and norisopimarane and has, instead, much higher relative concentrations of *ent*-kaurane, *ent*-beyerane and fichtelite (Table 6.3).

The SCM source rocks are characterised by low relative abundances of diterpenoid hydrocarbons, in which tricyclics are dominant over the tetracyclics, and labdane is nearly absent. Of the tetracyclic diterpanes, phyllocladane is the most prominent in all samples (although *ent*-beyerane dominates in several samples, e.g. #35, 45 and 46). Fichtelite is the major tricyclic component in most samples, while in others either rimuane, isopimarane or norisopimarane predominates.

The contrasting abundances of sesquiterpanes, cheilanthanes and diterpanes in mudstones and carbonaceous shales can be summarised in Table 6.4. Distributions of these compounds in the Taroom Trough oils best resemble those of the carbonaceous shales, attesting to their genetic relationship.

Table 6.4 Composition of drimane, cheilanthane and diterpane distributions in Bowen/Surat oils and major source rock lithofacies

Biomarkers	Mudstones	Carbonaceous shales	Bowen/Surat oils
C_{14}-C_{15} sesquiterpanes	Absent	Abundant	Abundant
C_{16+} sesquiterpanes	Abundant	Nearly absent	Nearly absent
C_{19}-C_{20} cheilanthanes	Nearly absent	Abundant	Abundant
C_{21}-C_{30} cheilanthanes	Abundant	Low	Low
Diterpane/C_{30} hopane	High	Low	High

6.3.3.4 Hopanes and steranes

The hopane and sterane distributions of representative oils are shown in Figures 6.3, 6.4, 6.11, 6.12 and 6.13. The relationship C_{30}>C_{31}>C_{32}>C_{33}> C_{34}>C_{35} characterises the hopane distributions of all twelve oils. A common bacterial input to the Permo-Triassic sediments and oils is evident from the similarity in the relative proportions of their C_{27}-C_{29}-C_{30} and C_{30}-C_{31}-C_{32} αβ+βα-hopanes (Figs. 6.14a and b). Evidence for specific bacterial inputs to the oils' source rocks includes the presence of the C_{31} 2α-methyl and 3β-methyl-17α(H),21β(H)-hopanes (aerobic methylotrophic bacteria); 28,30-bisnorhopane (chemoautotrophic bacteria: Schoell et al., 1992); 29,30-bisnorhopane (unknown bacterial affinity; absent in some samples); and the 2α- and 3β-methylsteranes (of probable bacterial derivation: Summons and Capon, 1988).

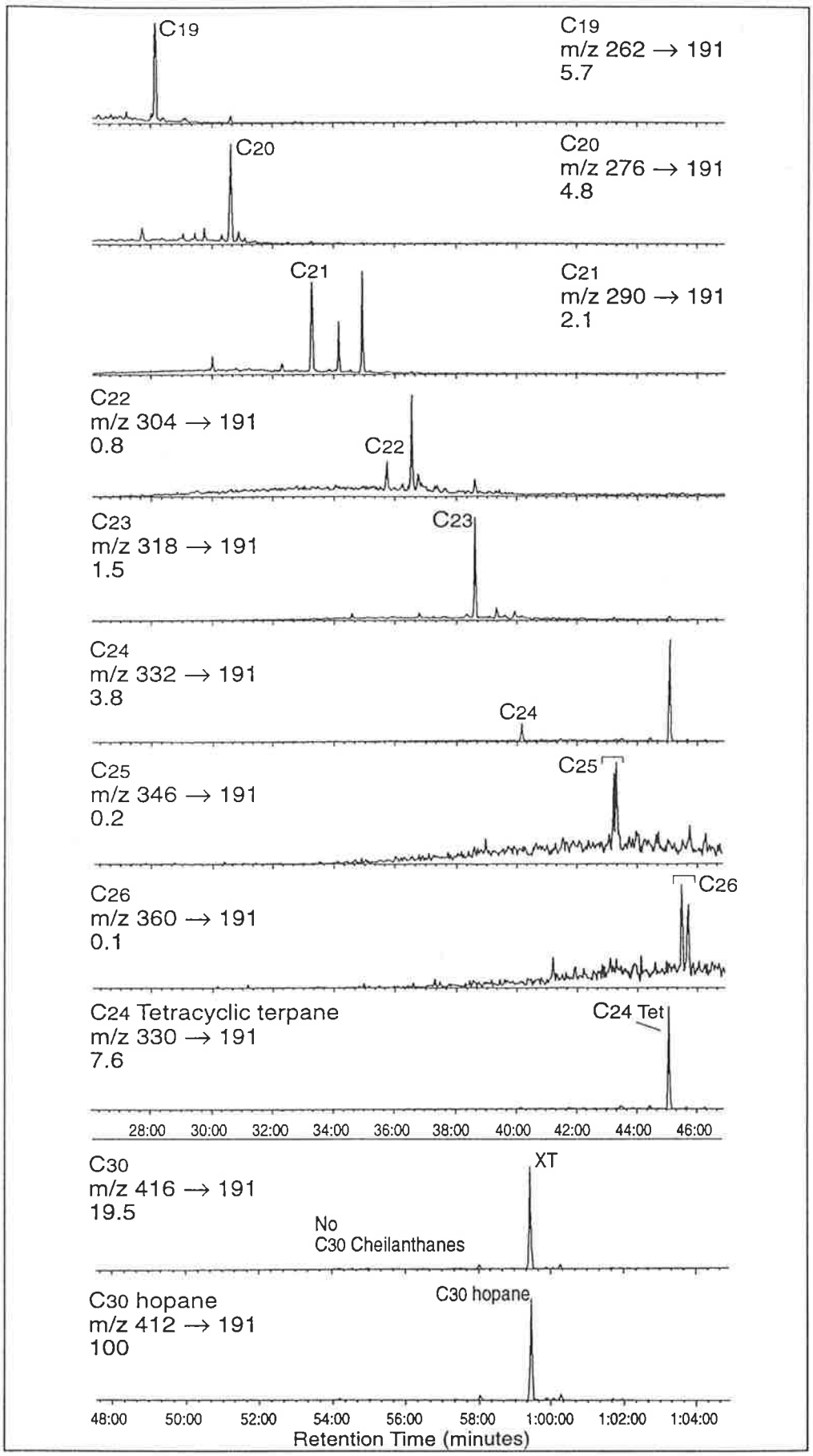

Figure 6.11 (a) MRM chromatograms showing the distributions of tricyclic terpanes and C_{24} tetracyclic terpane in the Roswin North-1 oil (sample #4).

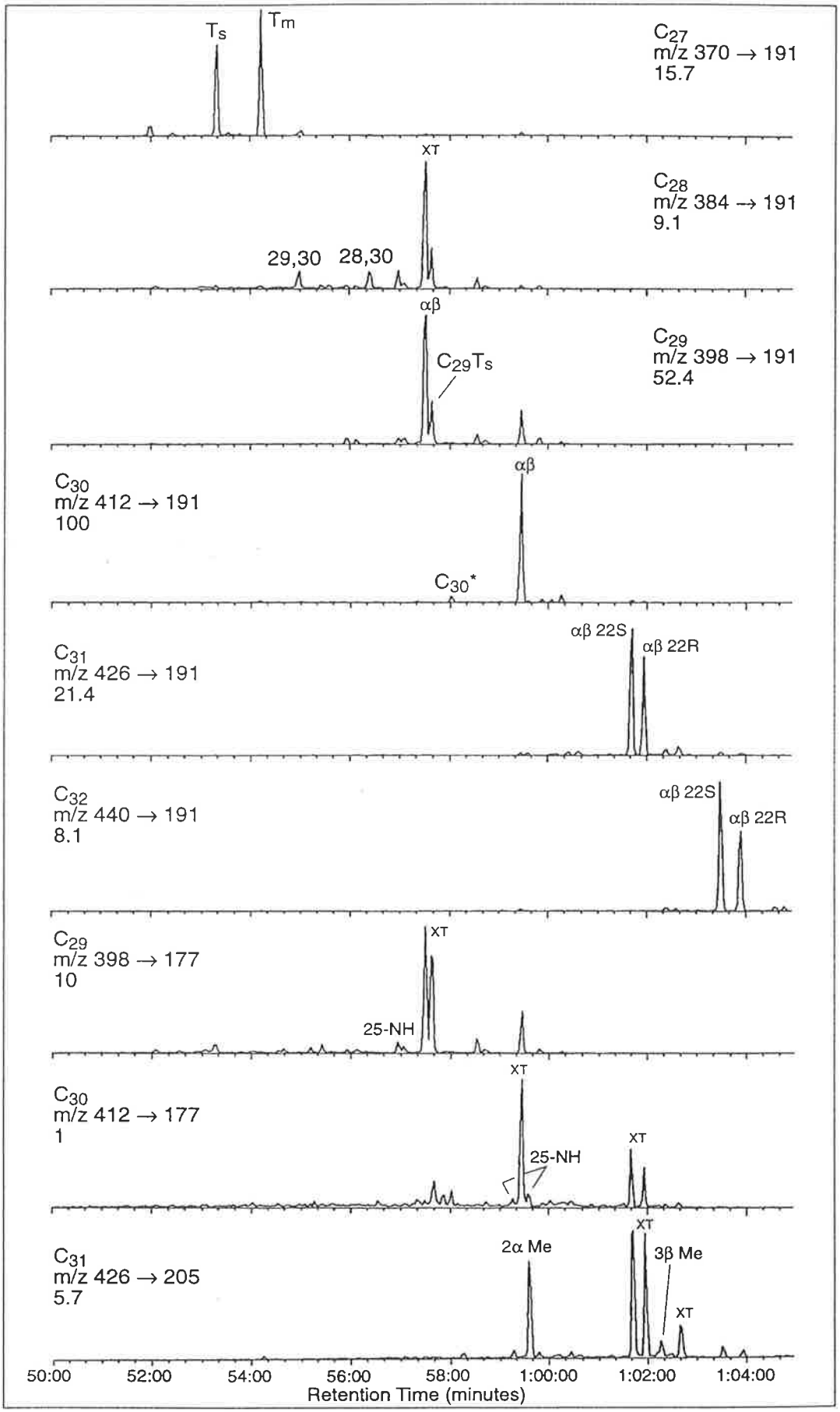

Figure 6.11 (b) MRM chromatograms showing the distributions of hopanes, norhopanes and methylhopanes in the Roswin North-1 oil (sample #4).

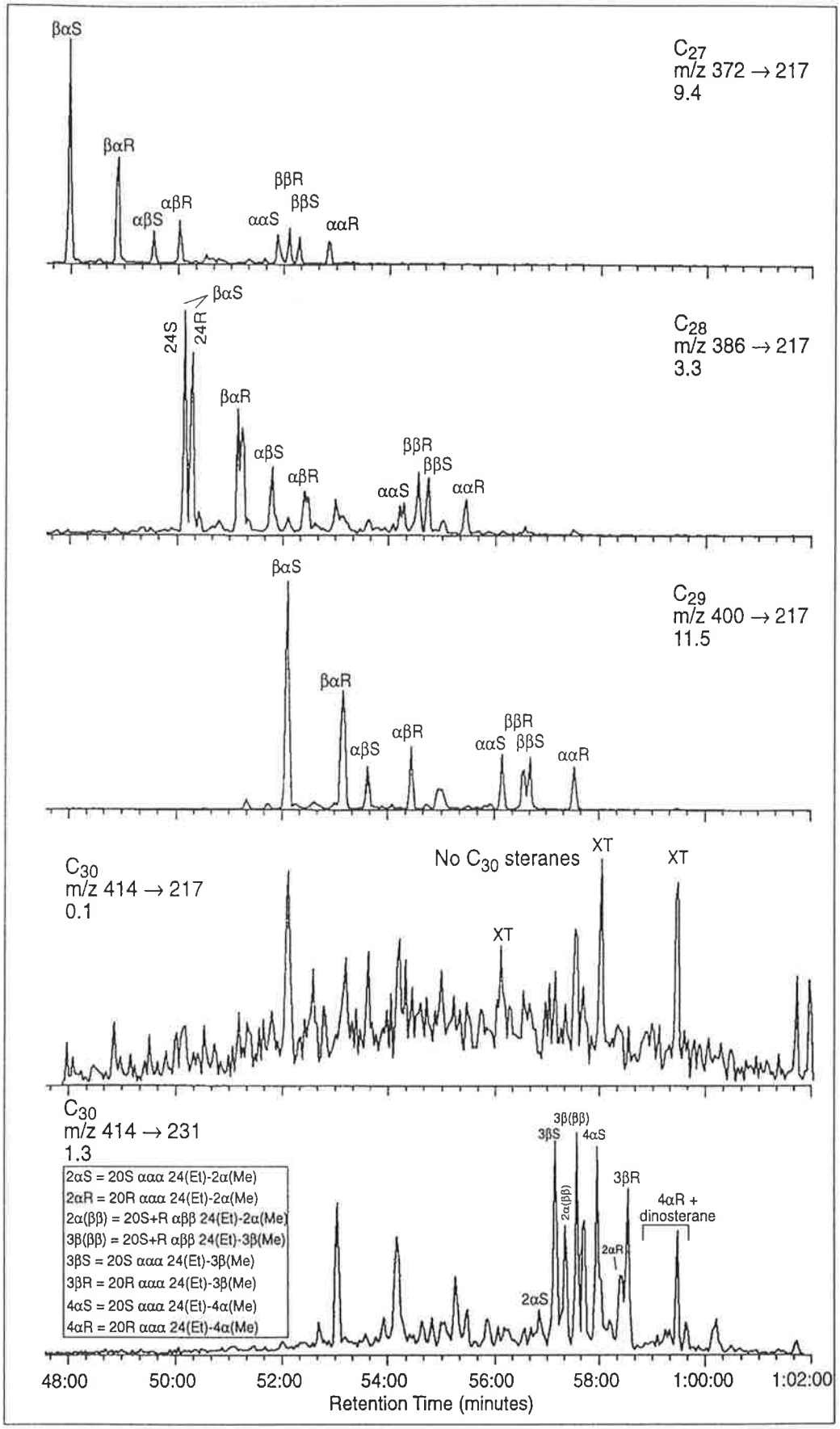

Figure 6.11 (c) MRM chromatograms showing the distributions of steranes ($M^{+\cdot} \rightarrow$ m/z 217) and methylsteranes ($M^{+\cdot} \rightarrow$ m/z 231) in the Roswin North-1 oil (sample #4).

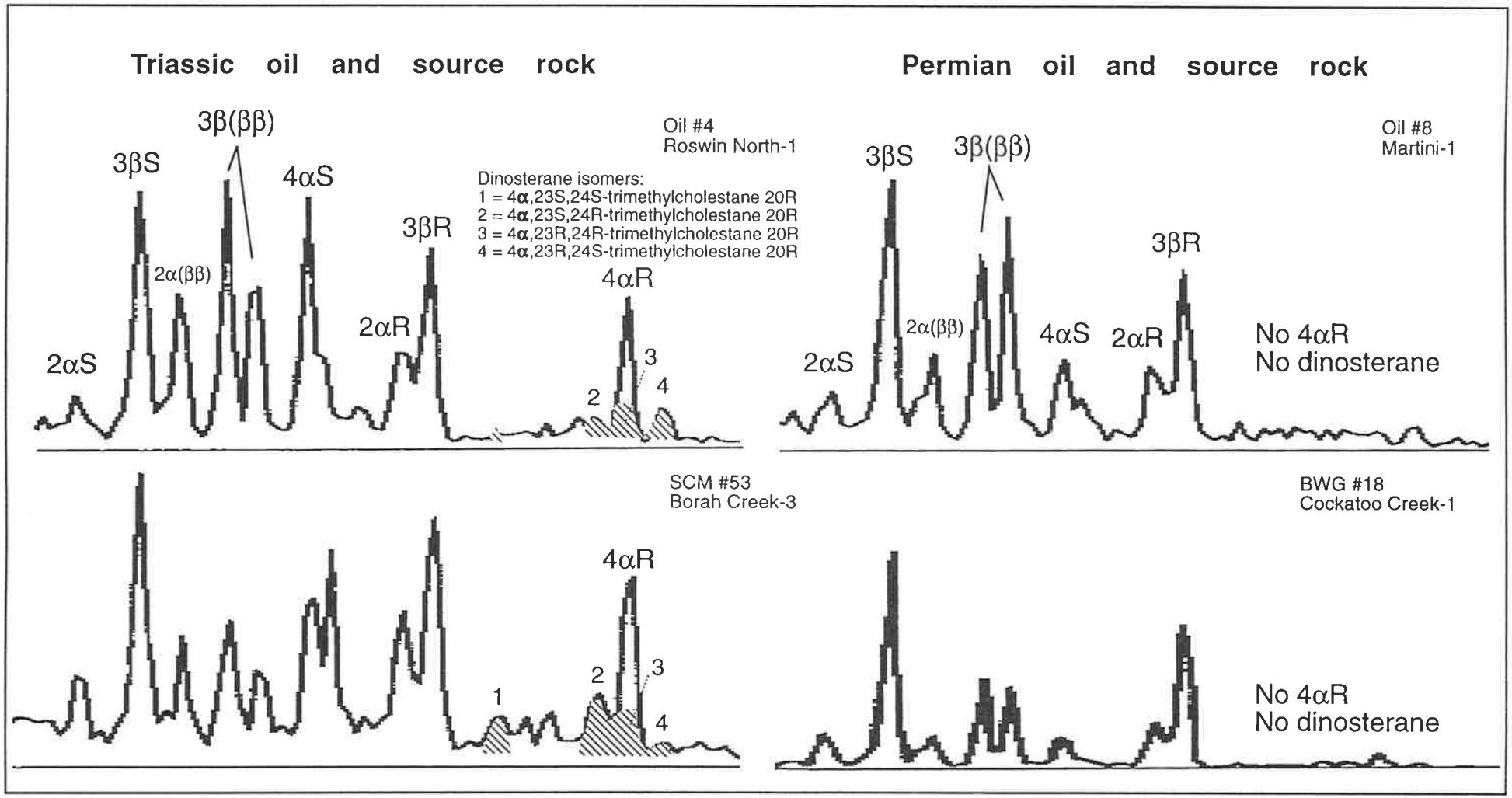

Figure 6.12 MRM chromatograms (414 → m/z 231) showing the positive correlation of methylsterane distributions in the Roswin North-1 oil and the Triassic SCM extract (sample #53). The other crudes (e.g. Martini-1 oil) have a different methylsterane distribution which best matches that of the Permian BWG extract (e.g. sample #18). For peak identification, see Figure 6.11 and Table 2.1.

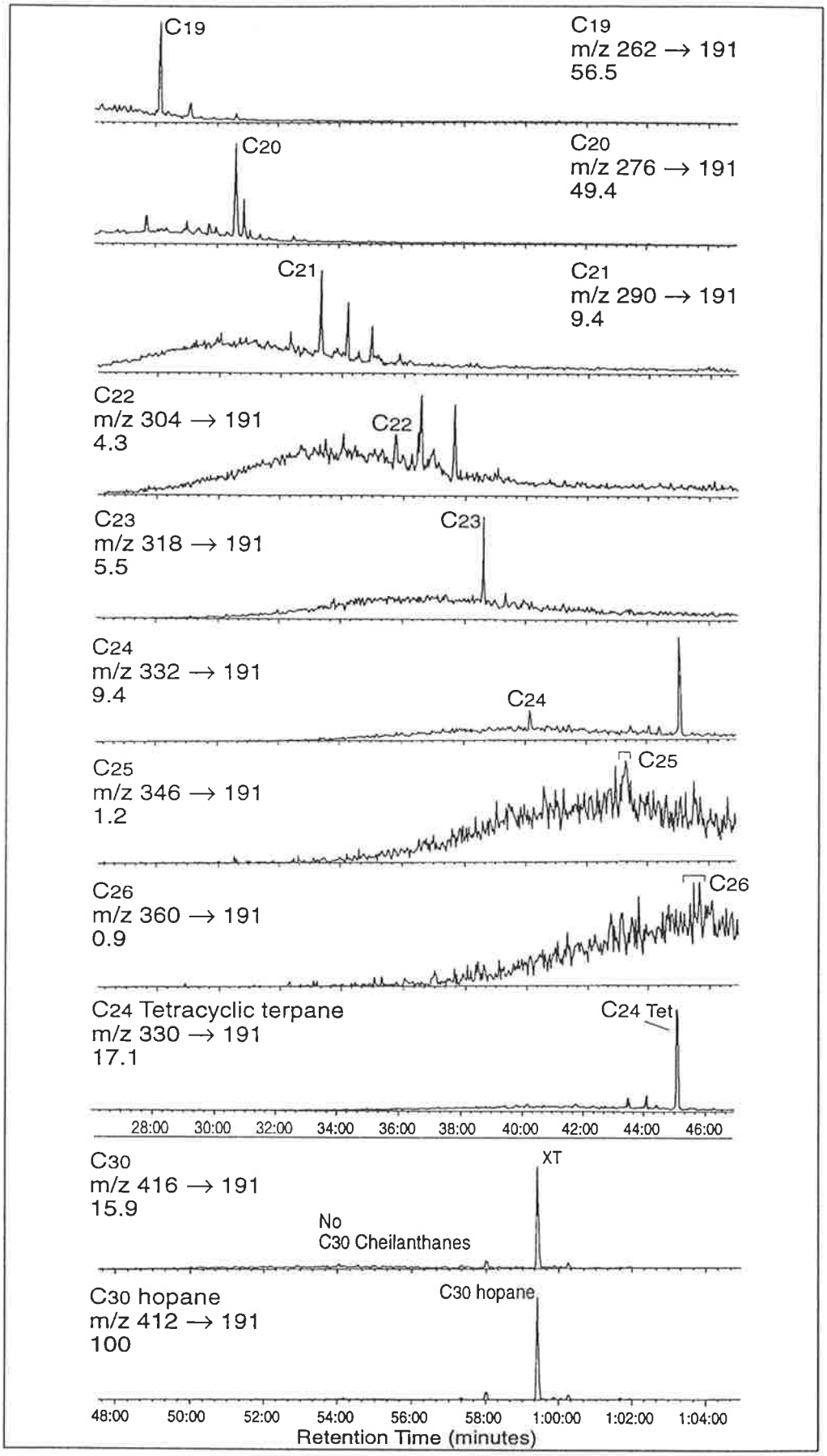

Figure 6.13 (a) MRM chromatograms showing the distributions of tricyclic terpanes and C_{24} tetracyclic terpane in the Waratah-1 oil (sample #7).

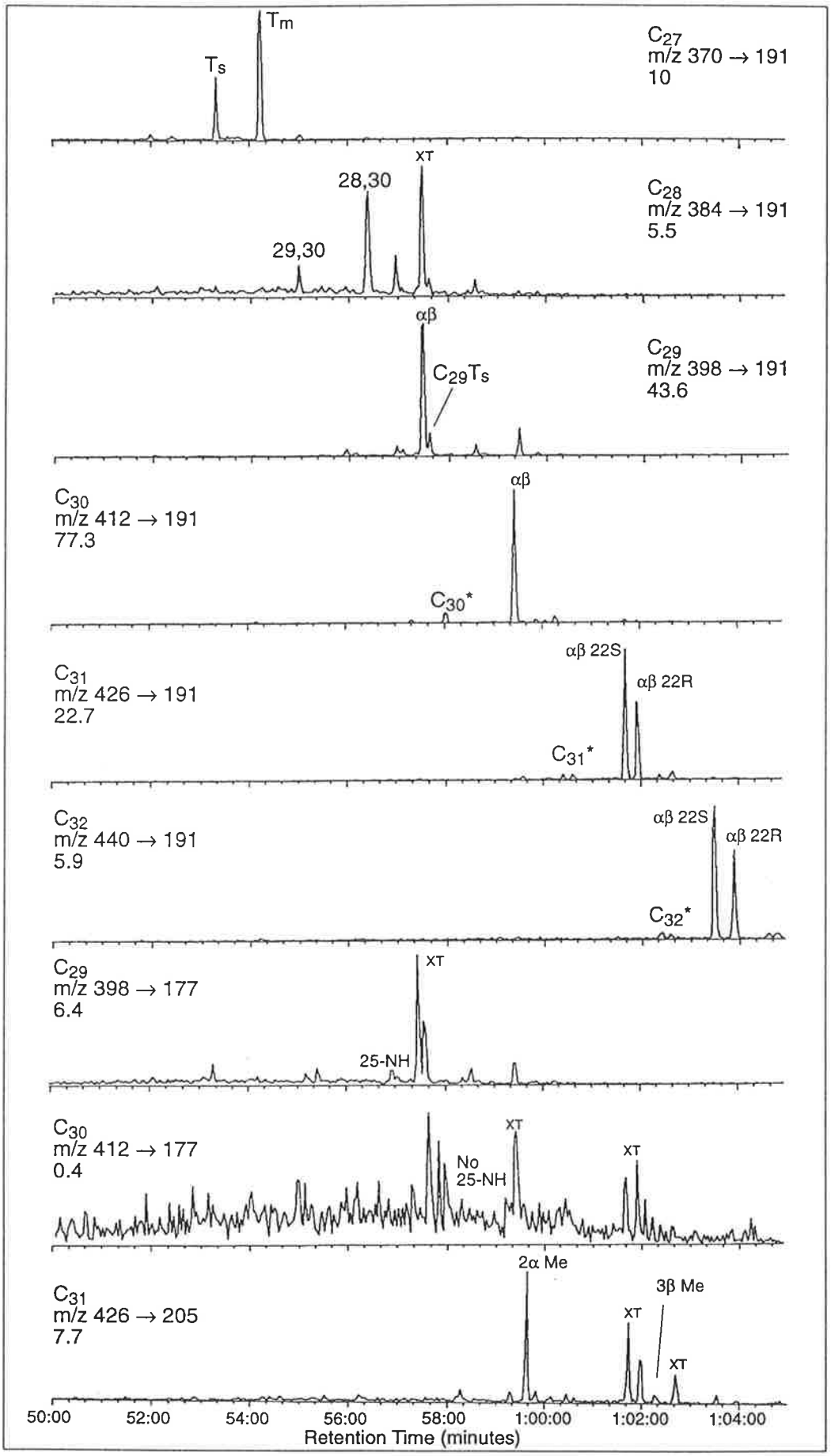

Figure 6.13 (b) MRM chromatograms showing the distributions of hopanes, norhopanes, and methylhopanes in the Waratah-1 oil (sample #7).

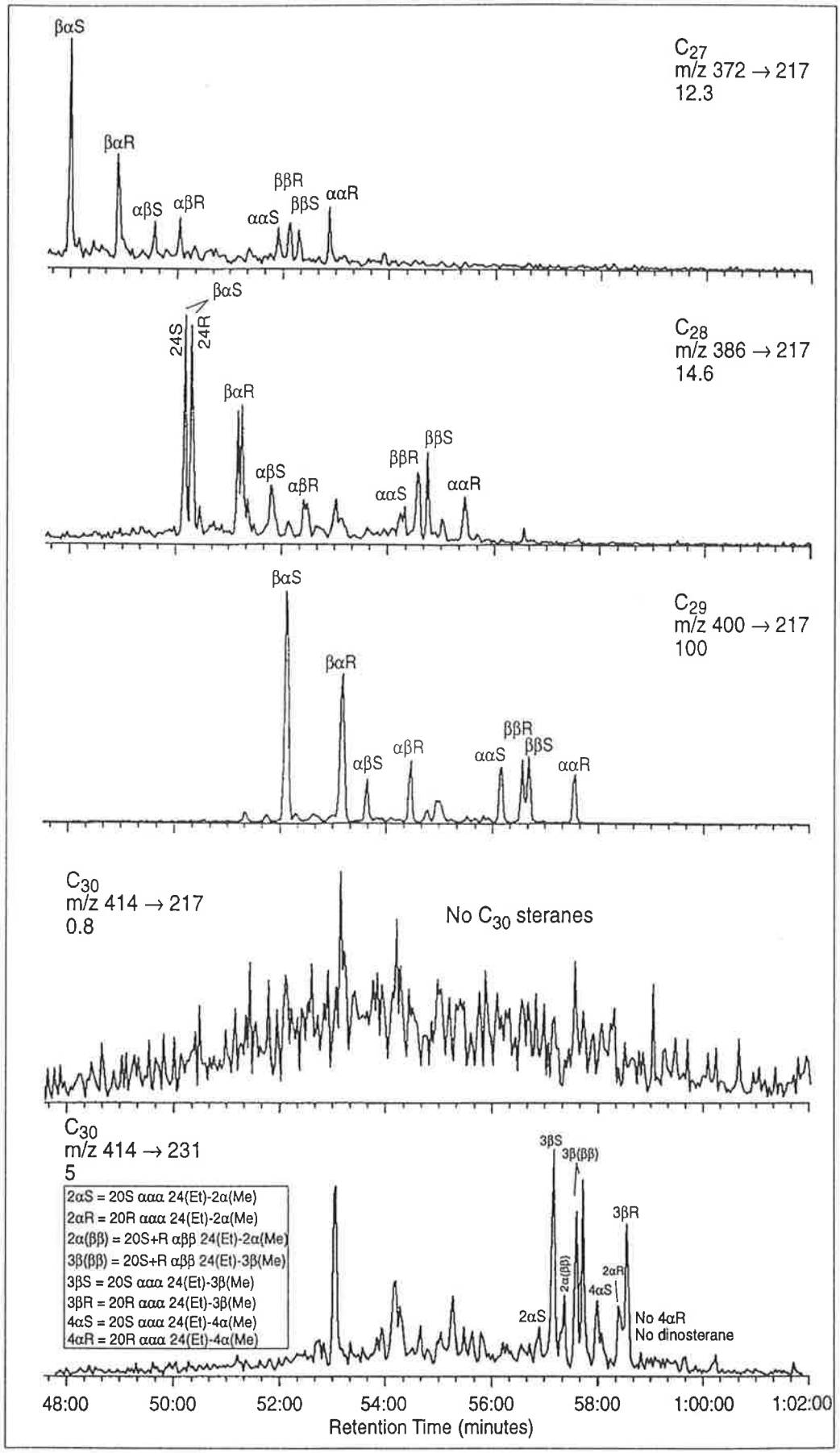

Figure 6.13 (c) MRM chromatograms showing the distributions of steranes ($M^{+\cdot} \rightarrow$ m/z 217) and methylsteranes ($M^{+\cdot} \rightarrow$ m/z 231) in the Waratah-1 oil (sample #7).

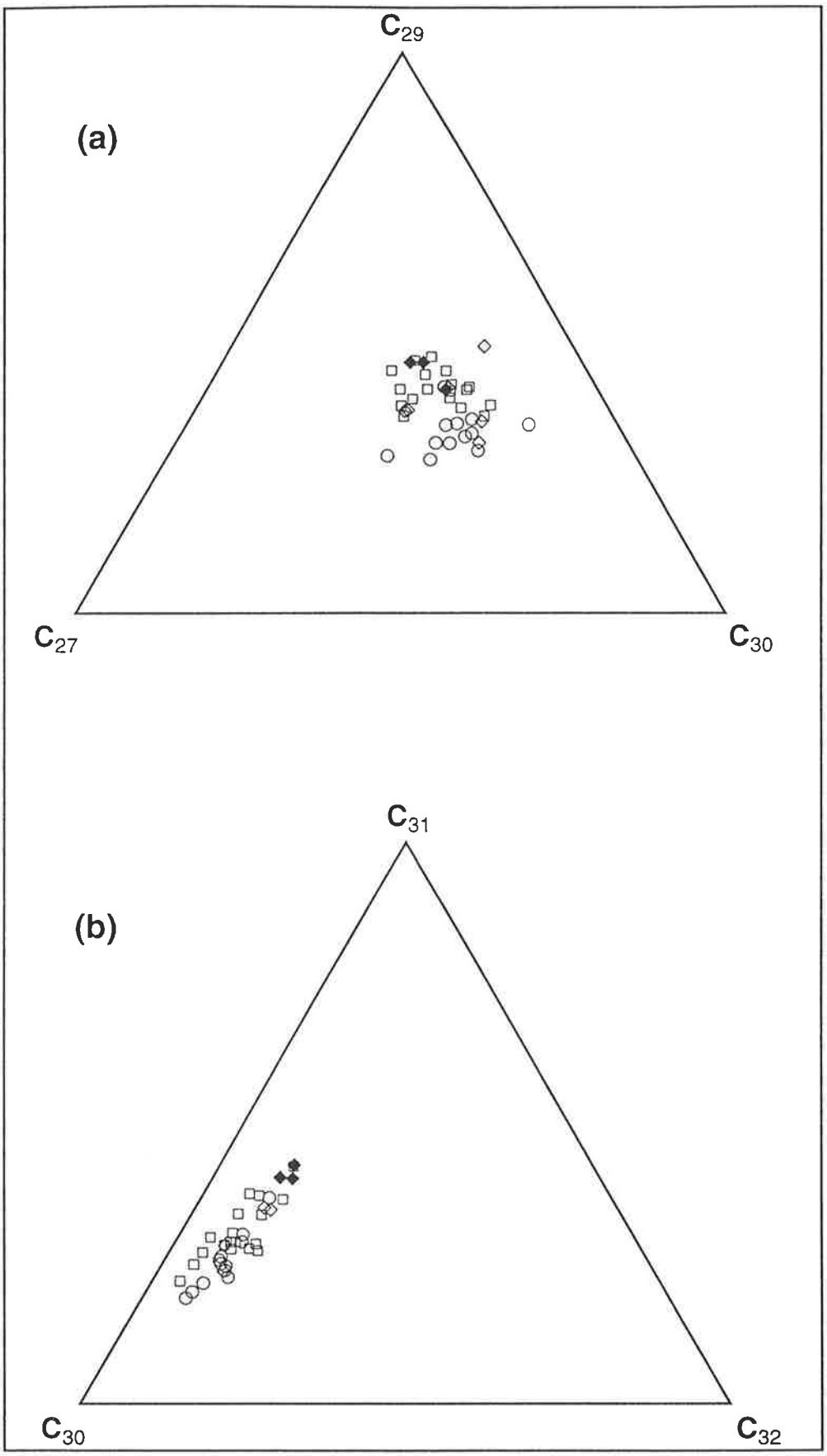

Figure 6.14 Ternary plots of (a) C_{27}-C_{29}-C_{30} hopanes and moretanes and (b) C_{30}-C_{31}-C_{32} homohopanes and homomoretanes in sediments and oils from the southern Taroom Trough. Symbols are as in Figure 6.5.

However, these bacterial biomarkers occur ubiquitously in the Permo-Triassic sediments examined (Table 5.2) and, therefore, they are of no help in correlating the oils to particular source rocks.

The oils not affected by biodegradation are characterised by a predominance of C_{29} steranes over the C_{27} and C_{28} homologues ($C_{29}>C_{28}\geq C_{27}$; C_{27}/C_{29} and C_{28}/C_{29} both < 0.6: Figs. 6.11c, 6.13c, 6.15 and 6.16a) and moderate to high hopane/sterane ratios ($\Sigma C_{27\text{-}34}$ hopanes/$\Sigma C_{27\text{-}29}$ steranes = 1.2-6.5: Table 5.2). A notable exception is the Roswin North-1 oil where $C_{27} >> C_{28}$ sterane. Grantham and Wakefield (1988) found that the C_{28}/C_{29} sterane ratio increases in marine oils from the mid-Paleozoic to the Tertiary. This age-related variation in the abundance of C_{28} and C_{29} steranes in oils is not applicable to the present study. The oils analysed here are terrestrially-derived and their potential source rocks are from a short geologic time span (Permian-Triassic). Therefore, any changes in the C_{28}/C_{29} data cannot be accounted for by age differences and, instead, they are caused by subtle variations in the eukaryotic biota contributing organic matter to the oils' source rocks.

On the pristane/phytane *versus* C_{29}/C_{27} sterane diagram (Fig. 6.15), all the oils plot in the upper right quadrant, attesting to their origin from land plant remains deposited in predominantly oxic depositional settings. On the basis of the relative abundances of 20R $\alpha\alpha\alpha$ C_{28}, C_{29} and C_{30} steranes (Fig. 6.16a) and C_{28}, C_{29} and C_{30} 4α-methyl steranes (Fig. 6.16b), the BWG carbonaceous shales appear to be poorly correlated to any of the oils examined. However, enhanced relative abundances of the lower molecular weight steranes (C_{27}, C_{28}) and methylsteranes (C_{28}, C_{29}) in the oils, relative to those in the BWG examined here may be accounted for by fractionation during migration of the oil, or that the effective source rocks are the more mature equivalents of the BWG carbonaceous shales. The latter explanation is favoured here since a shift to lower homologues is known to be maturity-related. More source-sensitive biomarkers (e.g. sesqui-, di- and tricyclic terpanes: Sections 6.3.3.1-6.3.3.4) showed that all but one of the oils (*viz.* Roswin North-1) have a close affinity with the carbonaceous shale facies of the BWG. These data also clearly prove that the Roswin North-1 oil has been sourced by the SCM, although this distinction is not demonstrated on the commonly-used sterane plot (Fig. 6.16a). However, interestingly, Family 1 oils (Section 6.2) exhibit the highest relative concentrations of C_{30} methyl steranes (oils #1, 4 and 12: Fig. 6.16b). This may be another, although subtle, indication of a common source for Family 1 oils.

Absence of the marine algal biomarker 24-*n*-propylcholestane (e.g. Figs. 6.3c, 6.4c, 6.11c, 6.13c; Table 5.2) further emphasises the terrestrial origin of the oils. As noticed by Boreham (1995) for other oils and sediments from the Bowen and Surat Basins,

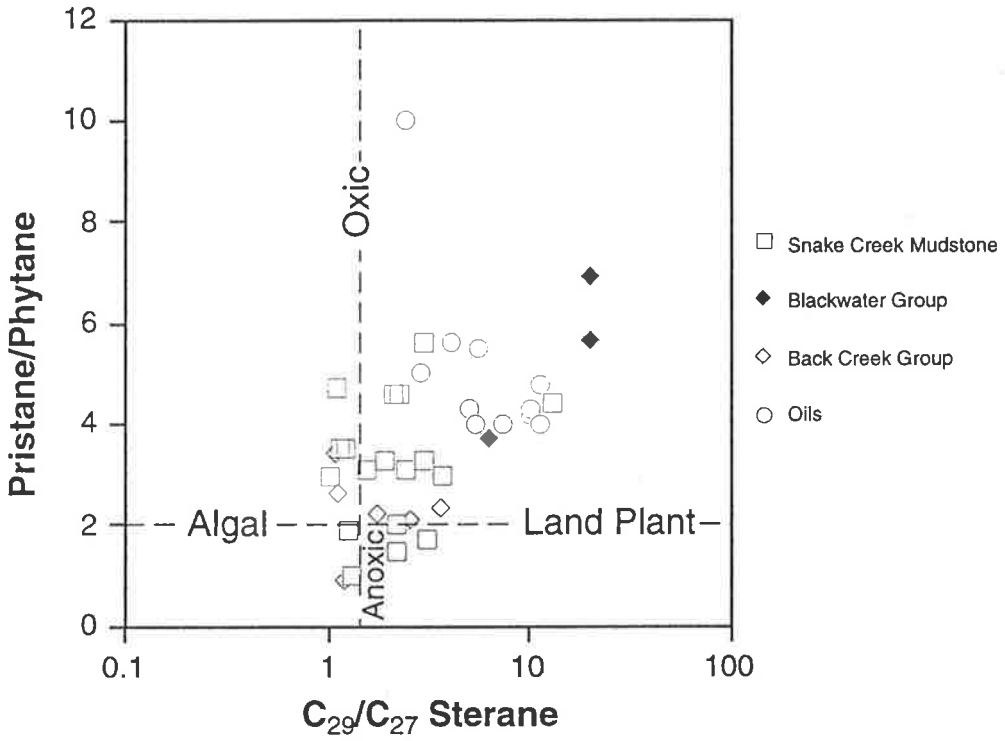

Figure 6.15 Crossplot of pristane/phytane *versus* C_{29}/C_{27} steranes for sediments and oils from the southern Taroom Trough.

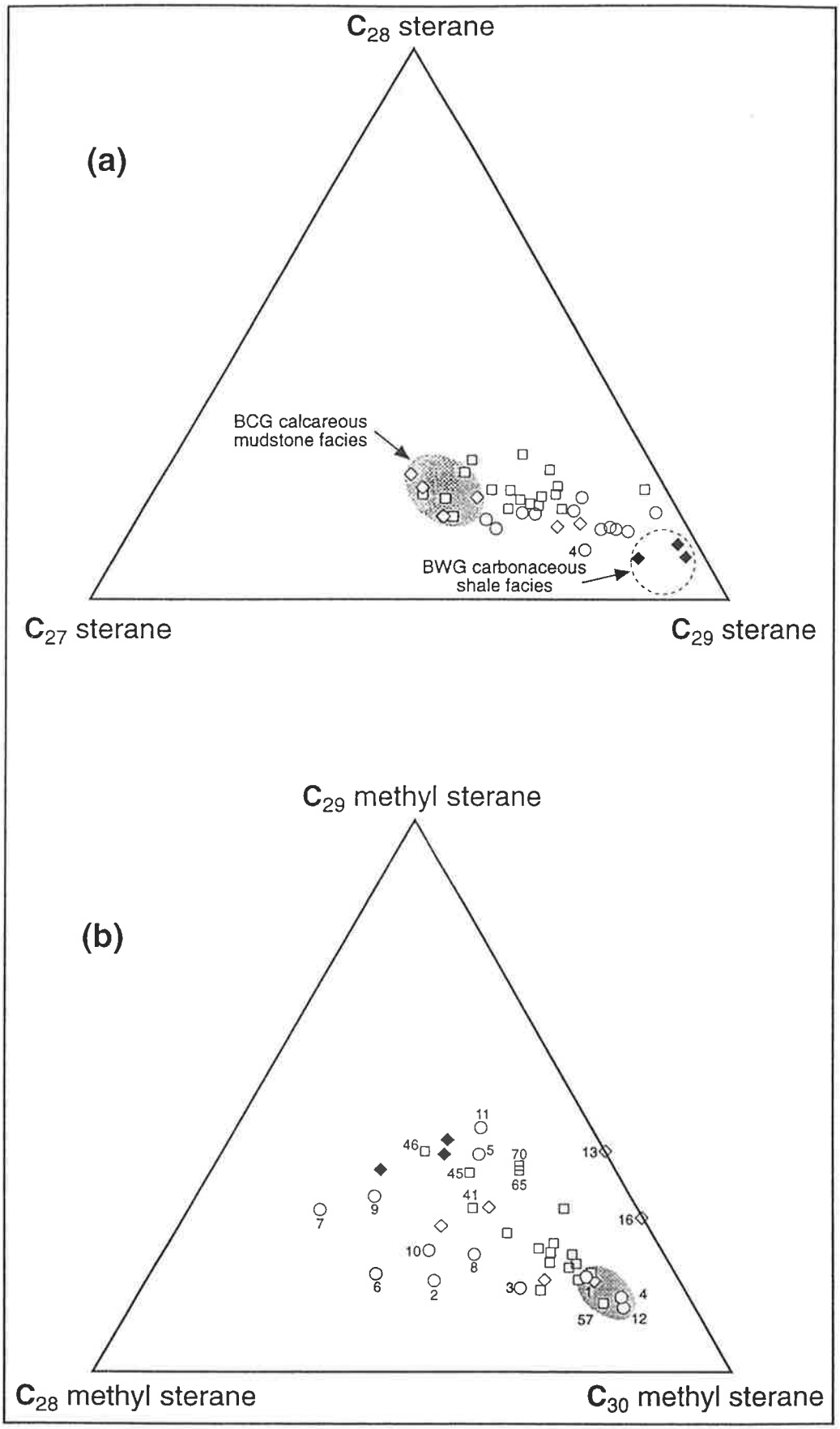

Figure 6.16 Ternary plots of (a) C_{27}-C_{28}-C_{29} ααα steranes and (b) C_{28}-C_{29}-C_{30} 4α-methyl-20R steranes in sediments and oils from the southern Taroom Trough. Symbols are as in Figure 6.5.

methylsteranes in the present set of Permo-Triassic oils are subordinate to their desmethyl counterparts. High concentrations of 2α- and 3β-methylsteranes relative to their 4α-methyl isomers is another feature that characterises most of the Bowen/Surat oils and the Permian sediments. All but two of the oils have low relative abundances of 4α-methylsteranes (e.g. 4αS/3βS = 0.3-0.5), and are devoid of dinosterane (Table 5.2). Similar methylsterane distributions were found in the carbonaceous shales of the Permian section. On the other hand, the Roswin North-1 oil has markedly higher abundances of 4α-methylsteranes, including tentatively identified dinosterane (4αS/3βS ≈ 1, dino/3βS ≈ 0.2: Fig. 6.12, Table 5.2). The Merroombile-1 condensate also contains dinosterane, although in lesser concentration (dino/3βS = 0.1: Table 5.2). Elevated abundances of 4α-methylsteranes are observed in many SCM samples (Table 5.2). This is further testimony to the origin of the Roswin North-1 oil from the Triassic SCM.

The oils exhibit moderate to high abundances of diasteranes relative to steranes (C_{29} dia/ster = 1.0-2.1: Table 5.2). This compositional feature is associated with high relative concentrations of diahopane (C_{30} diah/hop = 0.11-0.54) and 18α(H)-30-norneohopane ($C_{29}T_s$/30-NH = 0.07-0.37: Table 5.2) indicating deposition of the terrestrial organic matter in a clay-rich, oxic-suboxic environment (Peters and Moldowan, 1993). Although no obvious relationship can be shown to exist between the abundance of the C_{29} hopane (30-norhopane) and source rock lithology in the Bowen/Surat Basin (see also Boreham, 1995), the shaley character of the oils' source rocks is further emphasised by the low 30-norhopane/hopane ratio (30-NH/C_{30} hop < 0.9) and by the absence, or the very low concentration, of 29,30-bisnorhopane (29,30-BNH/C_{30} hop ≤ 0.04) in the oils. Clark and Philp (1989) noticed that 30-norhopane/hopane values larger than unity characterise carbonate source rocks.

6.3.3.5 Aromatic source parameters

The methylphenanthrene and trimethylnaphthalene distributions of selected oils (Table 5.4) are consistent with their presumed pre-Jurassic source affinity. In Figure 6.17 they plot in (or immediately adjacent to) the lower left quadrant of the two aromatic source affinity diagrams devised by Alexander et al. (1988) to distinguish oils of Jurassic and Permian origin in the Cooper/Eromanga Basin. Although the Roswin North-1 oil (sample #4) plots close to the other oils, it also shows a higher relative abundance of 1,2,5-TMN. This may be another, albeit subtle, indication of a different source for this oil (see next section).

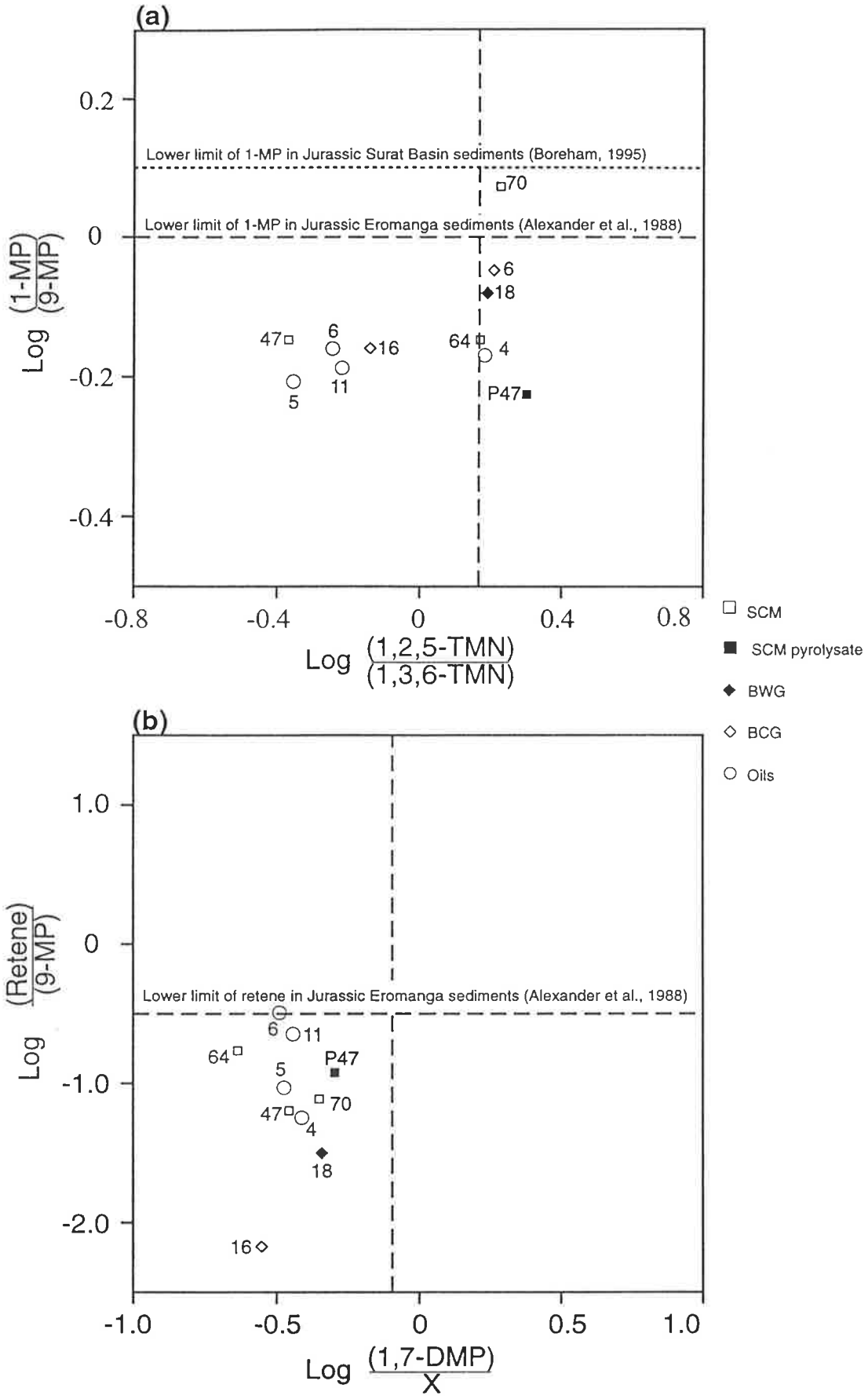

Figure 6.17 Aromatic hydrocarbon source plots for sediments and oils from the southern Taroom Trough. Vertical dashed lines in a and b are the lower limits, in Jurassic sediments and oils, of 1,2,5-trimethylnaphthalene and 1,7-dimethylphenanthrene, respectively. For definitions of the parameters used see Table 2.2.

6.4 Stable carbon isotopes

Stable isotopes have been a very useful tool in oil-oil and oil-source correlation studies. In addition, isotope geochemistry can be employed to evaluate secondary processes such as biodegradation and maturation, and to identify oil-prone organic facies and their depositional environments (Schoell, 1984; Sofer, 1991). In the present study, the stable carbon isotopic compositions of oil fractions (saturates, aromatics and NSO-compounds) were measured in order to help characterize the oils and to group them into different genetic families. For the purpose of oil-to-source correlation, the carbon isotopic composition of kerogens, extracts and pyrolysates from different Permo-Triassic organic facies were also studied. Compound-specific isotope analysis (CSIA) of individual *n*-alkanes in the extracts of two end-member SCM facies and their corresponding pyrolysates was also undertaken. Finally, the carbon isotopic composition of the bulk biomarker content (i.e. SNA fraction) was measured for selected SCM samples. The $\delta^{13}C$ values of crude oil fractions, rock extracts, kerogens and pyrolysates are presented in Table 6.5. The $\delta^{13}C$ values of individual *n*-alkanes in selected SCM extracts and pyrolysates are given in Table 6.6. These data are displayed diagramatically in Figures 6.18 - 6.21.

6.4.1 $\delta^{13}C$ of kerogens

Sofer (1984, 1991) stated that the isotopic composition of kerogen in a source rock is the most important factor controlling the isotopic composition of the oil generated from it. The Permian kerogens are isotopically heavier ($\delta^{13}C$ = -24.6 to -22.9‰: Table 6.5) than the Triassic kerogens ($\delta^{13}C$ = -28 to -26‰). Boreham (1995) made a similar observation, noting that kerogen from the Triassic Moolayember Formation was isotopically lighter than both Permian and Jurassic kerogens. The greater ^{13}C depletion in the Triassic organic matter may indicate changes in the redox potential and/or input biota (*cf.* Lewan, 1986) of the SCM lacustrine environment. A local isotopic anomaly, however, may not be appropriate since a Triassic isotopic depletion appears to be Australian-wide (Summons et al., 1995).

A mechanism which may account for the isotopically-heavier Permian kerogens is increased thermal maturity (*cf.* Conkright and Sackett, 1992). Thermal maturation results in loss of ^{12}C-enriched methane and concentration of ^{13}C in the residual kerogen, as noticed in natural systems (Simoneit et al., 1981) and modelled in laboratory pyrolysis experiments (Chung and Sackett, 1979; Peters et al., 1981). These studies show a maximum ^{13}C enrichment of 2‰ in the kerogen. However, an enrichment in ^{13}C

Table 6.5 Carbon isotopic compositions of kerogens and various oil, extract and pyrolysate fractions, southern Taroom Trough

Sample	$\delta^{13}C$ (PDB,per mil)								
	Kerogen	Extract / Oil					Kerogen pyrolysate			
		Sats	Arom	NSO	SA	SNA	Sats	Arom	SA	SNA
Jurassic coal										
30 WCM	-23.3	-25.2	nd							
Snake Creek Mudstone										
35 SCM	-26.0	-27.7	-26.5				-24.5	-26.5		
41 SCM	nd	-28.6	nd							
47 SCM	-26.2	-27.4	-27.0		-27.9	-27.1			-30.6	-24.2
53 SCM	-27.6	-30.3	-27.9				-31.0	-28.4		
58 SCM	-28.0	-31.6	-28.9				-32.0	-29.1		
64 SCM	-27.9	-26.8	-25.7							
71 SCM	-26.9	nd	nd		-28.1	-25.4			-30.0	nd
Permian source rocks										
Blackwater Group										
18 BWG	-24.4	-26.4	-25.0							
26 BWG	-24.2	-27.3	-24.6							
Back Creek Group										
2 BCG	-22.9	-25.6	-22.8							
6 BCG	-24.3	-25.9	-24.9							
10 BCG	-23.9	-26.7	-24.5							
14 BCG	-23.5	-26.0	-23.9							
15 BCG	-23.5	-26.5	-23.4							
16 BCG	-24.0	-25.8	-25.6							
19 BCG	-24.0	-26.2	-26.0							
24 BCG	-24.1	-28.1	-25.4							
Oils										
1 Taylor-12A		-23.9	-23.7	-24.9						
2 Taylor-11		-25.1	-24.9	nd						
3 Tinker-4		-25.0	-24.4	-25.3						
4 Roswin North-1		-27.0	-26.8	-26.9						
5 Washpool-1		-25.0	-24.3	-25.0						
6 Wilga-2		-24.6	-24.7	-25.0						
7 Waratah-1		-23.7	-23.6	nd						
8 Martini-1		-24.3	-23.8	-24.2						
9 Riverslea-1		-24.5	-23.7	-24.4						
10 Cogoon River West-1		-24.7	-24.1	-24.6						
11 Bellbird-1		-25.2	-25.0	-25.2						
Condensates										
12 Merroombile-1		-24.8	-24.9	nd						
13 Rednook-1*		-27.1	-27.4	nd						

* Data from Boreham (1995)
nd = not determined

of up to 10‰ in metamorphosed kerogens was observed by McKirdy and Powell (1974) and Hoefs and Frey (1976).

The combined effect of maturity and organic facies changes best explains the observed variations in $\delta^{13}C$ values for Triassic and Permian kerogens from the Taroom Trough. On a Stahl-type isotope curve (Fig. 6.18a), a clear separation is evident between the Permian and Triassic organic facies. Selective concentration of algal and bacterial lipids in mildly sub-oxic conditions would also give rise to a very negative carbon isotopic signature (*cf.* Lewan, 1986) such as that seen in sample #58. It is noteworthy that many of the Permian samples are overmature (R_O is up to 2.1%). Therefore, their remaining organic matter ("dead" kerogen) is characterised by heavier $\delta^{13}C$ signatures after loss of their isotopically lighter, labile fractions during oil expulsion. Whatever the reason for their ^{13}C enrichment, the Permian oils correlate well with the Permian source rocks (Fig. 6.18b).

Although the Permian kerogens are well-separated from the Triassic samples in Figure 6.18, the Jurassic and Permian kerogens are isotopically indistinguishable. A $\delta^{13}C$ value of -23.3‰ for the Jurassic WCM kerogen (sample #30) falls clearly within the field of the Permian samples (Fig. 6.18a). If maturity was the only factor affecting $\delta^{13}C$, then this immature Jurassic organic matter would be expected to have a much lighter carbon isotopic composition than those of the Permian and Triassic. The different kerogen type in the WCM sample (Fig. 4.2b) might partially explain its more positive $\delta^{13}C$ value.

6.4.2 $\delta^{13}C$ of extract fractions

The carbon isotopic composition of subfractions of the total extract can provide additional information for use in oil-source correlations. In general, extracts are isotopically lighter than their corresponding kerogens (Schoell et al., 1983; Schoell, 1984). In Figure 6.18, the SCM extract (and pyrolysate) subfractions are clearly separated not only from the Permian extracts but also from the Permian oils. The heavier values of the Permian extracts may partly reflect preferential loss of ^{12}C due to a kinetic isotope effect (Hoefs and Frey, 1976) associated with the generation and expulsion of oil from these more mature samples.

It is not unusual to encounter anomalous $\delta^{13}C$ values in the saturated hydrocarbons, because, once generated from the kerogen, they become more susceptible to secondary processes such as thermal cracking and fractionation. For the present suite of Permo-Triassic source rocks, their differentiation into distinct organic facies seems to be more reliable when using the carbon isotopic composition of the aromatics, rather than the

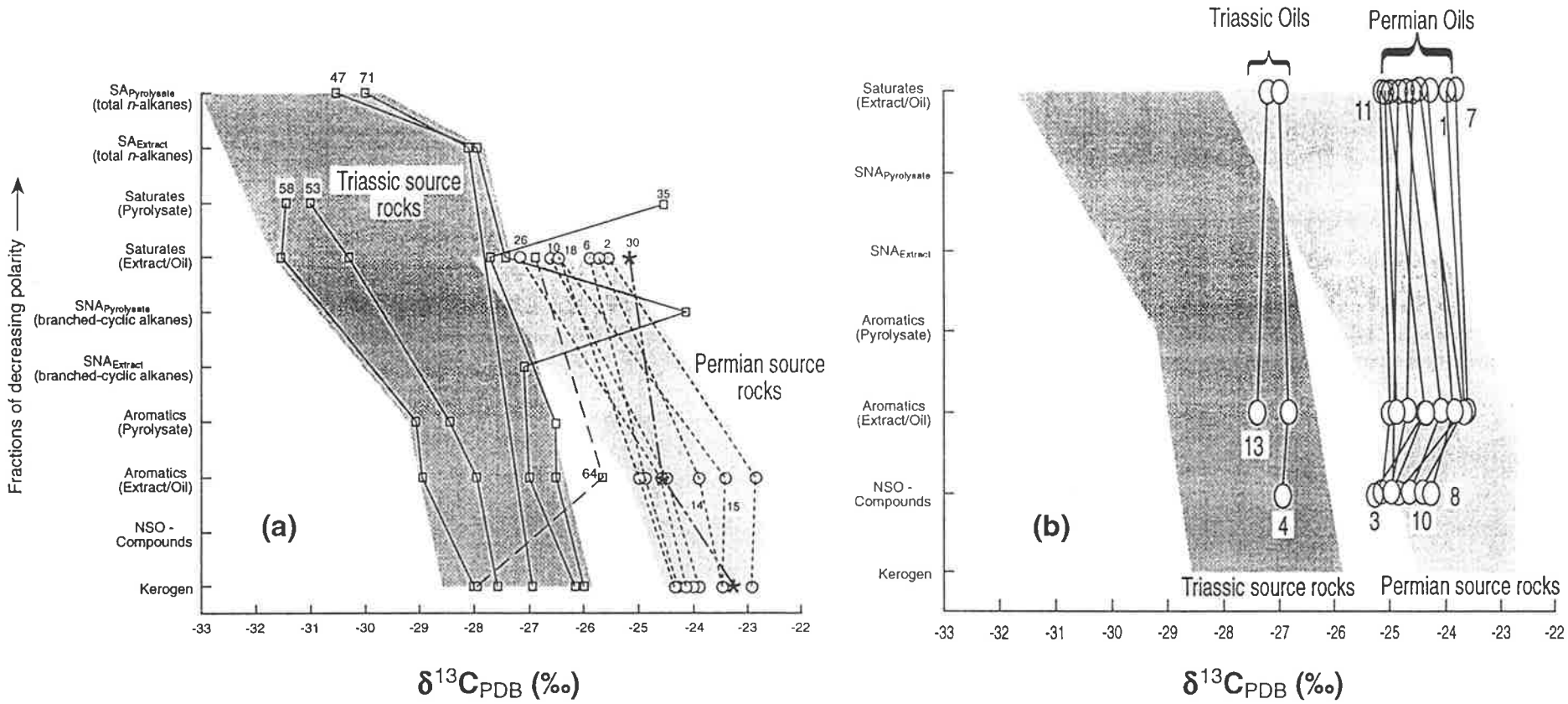

Figure 6.18 Stahl-type carbon isotope curves showing a good separation (a) between Permian and Triassic source rocks, and (b) between Triassic and Permian oils, southern Taroom Trough.

saturates. The $\delta^{13}C$ values of the Permo-Triassic kerogens and those of the aromatic fractions of respective extracts are very well correlated (Fig. 6.19). Schoell (1984) actually recommends using the carbon isotopic signature of the aromatics for correlation purposes. Sometimes (e.g. when the extract is contaminated) kerogen isotope data offer better resolution, making them the preferred isotope signature for use in correlation studies.

The Stahl-type isotope curve of one SCM extract (sample #64) looks slightly unusual compared to the other curves (Fig. 6.18a, see also Fig. 6.19). In this case, the aromatic fraction is enriched in ^{13}C by 2.2‰ relative to the kerogen. Such inconsistency in the isotopic composition between the kerogen and its corresponding aromatic hydrocarbons can be caused by oil staining (Peters and Moldowan, 1993). However, other geochemical data for this particular sample indicate that it is not stained. This evidence includes a low bitumen to TOC ratio (106 mg/g TOC) and a low S1 value (0.45 mg h'c/g rock), together with a low production index (PI = 0.09), a low T_{max} (434 °C) value (Table 4.2), and a barely-mature biomarker signature (T_s/T_m = 0.14; C_{29} sterane 20S = 50%: Table 5.1). Therefore, the observed 2.2‰ difference in the $\delta^{13}C$ value suggests that the extractable hydrocarbons in this case are primarily free lipids and not derived from the kerogen.

6.4.3 $\delta^{13}C$ of oil fractions

Assuming the aromatic fraction to be representative of the whole oil, twelve out of thirteen oils have very similar $\delta^{13}C$ values, averaging -24.3‰ (range -25.0 to -23.6‰: Table 6.5). One oil, Roswin North-1 (sample #4) and one condensate, Rednook-1 (sample #13) are isotopically lighter with $\delta^{13}C$ values of -26.9‰ and -27.4‰, suggesting their derivation from a different source rock. Genetic relationships between oils and their sources can be demonstrated using the Sofer (1984) plot (Fig. 6.20a). On this plot, the isotopic difference is clear between the Roswin North-1 oil and Rednook-1 condensate (hereafter referred to as *Triassic oils*), on the one hand, and the rest of the oil suite (hereafter referred to as *Permian oils*), on the other.

The separation between the Triassic oils and the Permian oils is also evident from the Stahl-type isotope curves (Fig. 6.18b) and pristane/phytane ratio *versus* $\delta^{13}C$ plot (Fig. 6.20b). These diagrams indicate that the Permian oils are genetically related and best match the Permian source rock extracts. The Triassic oils plot separately and can be tied to a Triassic (SCM) source. Lewan (1982) and Schoell (1984) indicated that the aromatic fraction is the most suitable for correlation purposes and attributed this to the fact that the aromatics are not much affected by secondary processes such as thermal

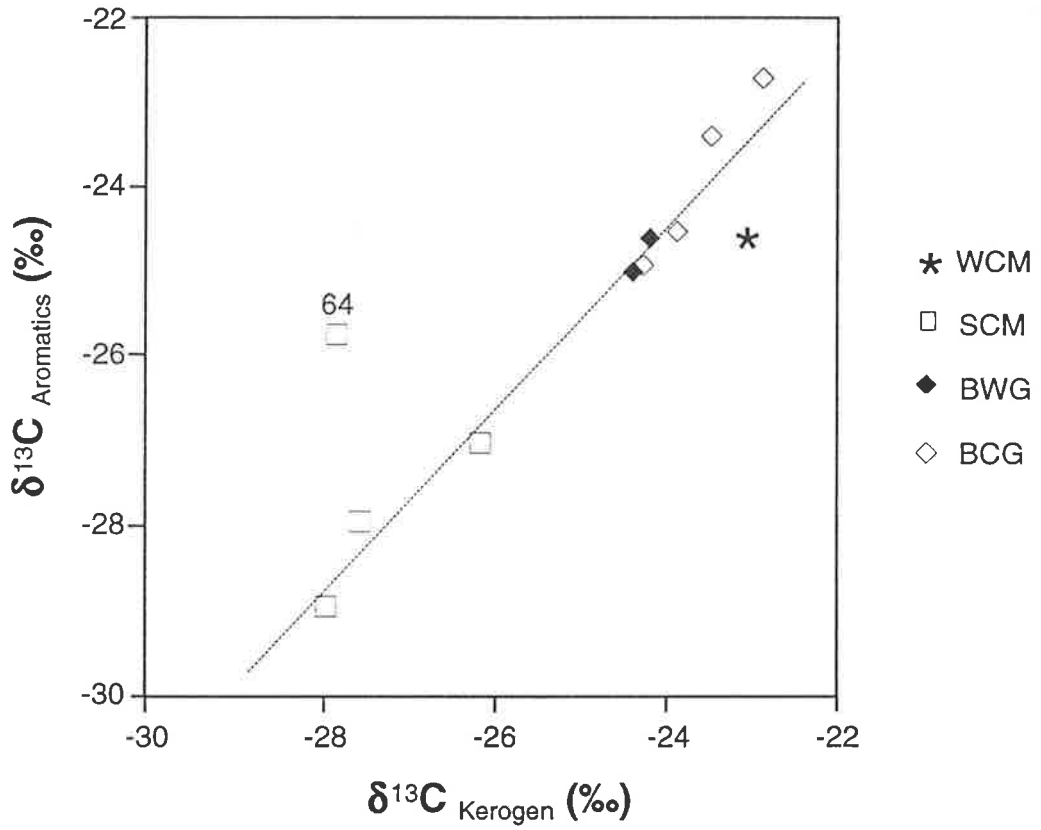

Figure 6.19 Relationship between the carbon isotopic compositions of kerogens and aromatic hydrocarbons in rock extracts, southern Taroom Trough. The line represents the best fit between these two parameters.

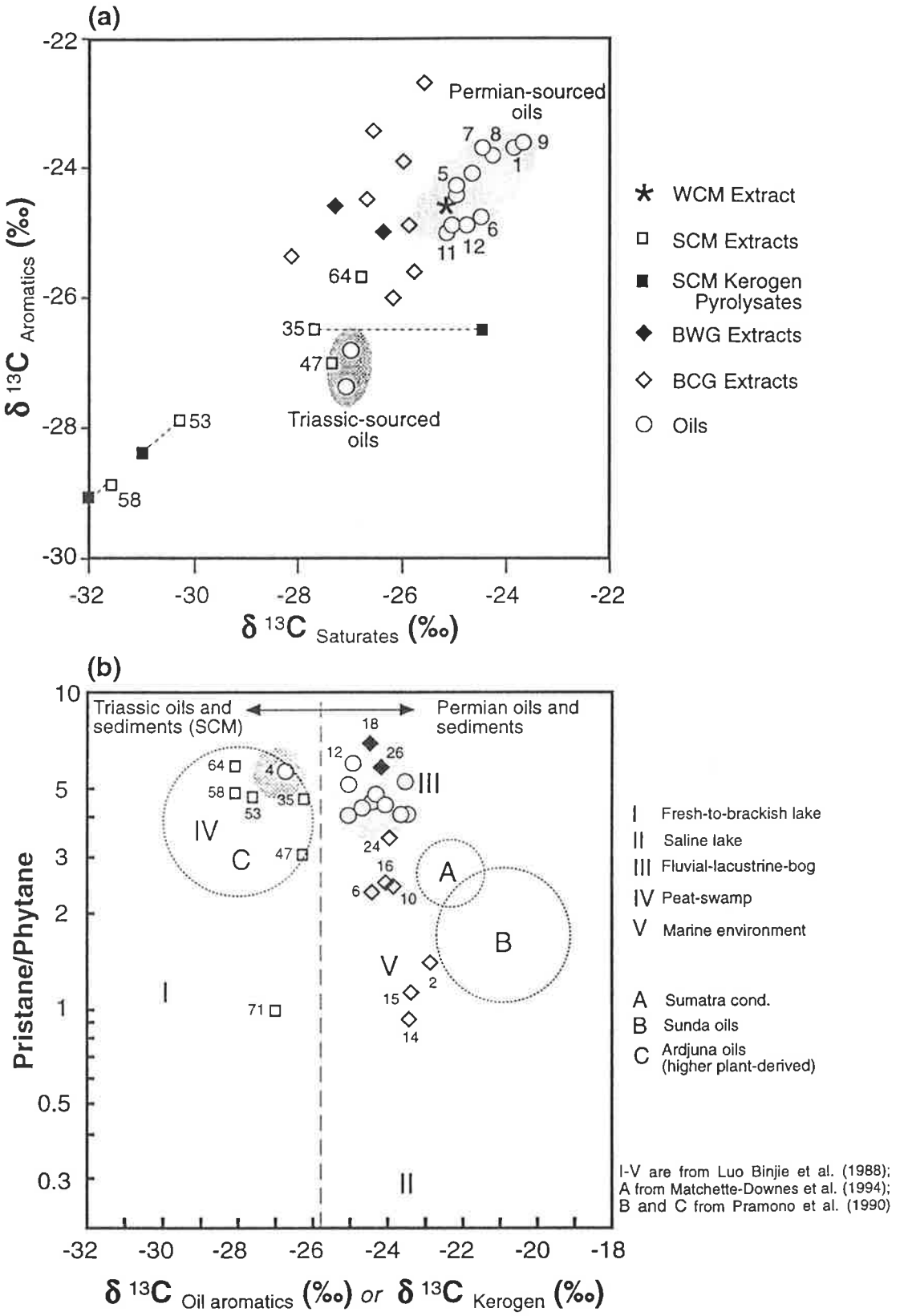

Figure 6.20 Crossplots of (a) carbon isotopic composition of saturated *versus* aromatic hydrocarbons, and (b) pristane/phytane ratio *versus* carbon isotopic composition for oils, rock extracts and kerogen pyrolysates, southern Taroom Trough.

alteration and biodegradation. Therefore, the $\delta^{13}C_{arom}$ value best mimics that of the precursor organic matter, as is also demonstrated on Figure 6.19. On this basis, oils and source rock extracts can be reliably distinguished. Normally, oils show $\delta^{13}C$ variations of up to 1.5‰ relative to their source rock bitumens (Peters and Moldowan, 1993) or kerogens of similar maturity. In fact, this is what is observed here for both of the Permian and Triassic oils when compared with their respective Permian and Triassic extracts and kerogens (Fig. 6.18b). The aromatic fractions of the oils clearly obey this *1.5%-maximum difference rule* when compared to the aromatics of their source rock bitumen.

The kerogen and extract-saturates fraction of a coal from the Jurassic Walloon Coal Measures (WCM) have carbon isotopic compositions falling within the range for Permian oils and source rocks (Figs. 6.18 and 6.20a). The possibility of a WCM source for these oils is, however, eliminated on the basis of its immaturity (Section 4.3.4).

As illustrated in Figure 6.18, and consistent with the findings of previous studies (Galimov, 1973; Stahl, 1978), kerogens are the most enriched in ^{13}C. Sub-fractions of the rock extracts (and SCM kerogen pyrolysates: see below) become isotopically lighter (enriched in ^{12}C) in order of decreasing polarity. A slight enrichment in ^{13}C is noticed for the saturates of the oils, most likely due to a higher content of ^{13}C-enriched light volatiles (Boreham, 1995) compared to the rock extracts.

Since thermal maturation tends to increase the ^{13}C concentration, it could be inferred that all eleven Permian oils have quite similar maturities which, in turn, are higher than those of the two Triassic oils. However, MPI measurements (Table 5.4) suggest that all the oils were expelled at a similar maturity level (R_C = 0.62-0.75%). Therefore, the observed differences in $\delta^{13}C$ values are best explained by primary source variations.

6.4.4 $\delta^{13}C$ of SCM kerogen pyrolysates

Carbon isotope analysis of kerogen pyrolysates is a powerful tool for oil-source correlations and organic facies studies. Bailey et al. (1990) employed this high-precision technology to solve oil correlation problems in North Sea basins and to demonstrate organic-facies variations in otherwise apparently homogenous source rocks. Using this technique, common problems such as non-indigenous shows and contaminant hydrocarbons can be recognised and avoided (Burwood et al., 1990; Bailey et al., 1990). Kerogen also may contain inert and gas-prone fractions that affect its carbon isotopic composition without being actively related to oil generation.

Sealed-tube hydrous pyrolysis of kerogen concentrates of various SCM organic facies (A, C and AC) gave oils (pyrolysates) with subfractions that are more depleted in ^{13}C than their parent kerogens (Fig. 6.18a). This is because the pyrolysates are thermally-labile fractions of the kerogen, and as such are normally composed of isotopically-lighter carbon (Simoneit et al., 1981). Pyrolysate sub-fractions of some samples (#35 saturate and #47 SNA) are markedly and inexplicably ^{13}C-enriched. Aromatics in the pyrolysates are isotopically more consistent in relation to their parent kerogens, with the former being 0.5-1.1‰ lighter. With decreasing polarity, the pyrolysate sub-fractions become isotopically lighter. For example, $\delta^{13}C$ for the pyrolysate saturates of samples #53 and 58 is 3-4‰ lighter than the parent kerogen. In SCM organic facies C (sample #35), saturated hydrocarbons of the pyrolysate are unusually enriched in ^{13}C ($\delta^{13}C$ = -24.5‰) compared to its solvent-extracted counterpart ($\delta^{13}C$ = -27.7‰). This may be due to kerogen heterogeneity. That the SA fraction ($\delta^{13}C$ = -30.6‰) of sample #47 is 6.4‰ lighter than the SNA ($\delta^{13}C$ = -24.2‰) suggests that the pyrolysate *n*-alkanes are derived from phytoplankton, whereas the SNA contains contributions from other sources such as higher plant lipids.

Recent work (Burwood et al., 1990) showed that there is a good correlation between the carbon isotopic composition of a source rock (measured on its kerogen pyrolysate) and its activation energy of petroleum generation. More positive carbon isotopic signatures are associated with lower activation energies, and vice versa. The lower the activation energy, the earlier petroleum expulsion starts (Tissot et al., 1987). This implies earlier hydrocarbon generation from the ^{13}C-enriched organic facies. The pyrolysates of the SCM organic facies at Tinker-2 (sample #58) and Borah Creek-3 (sample #53) are isotopically lighter than any oil in the area. Those from Flinton-1 (sample #35) and Snake Creek-1 (sample #47) are markedly heavier and, therefore, are able to generate petroleum earlier than those in Tinker-2 and Borah Creek-3. Interestingly, both the Sofer plot (Fig. 6.20a) and Stahl plot (Fig. 6.18) show a very good isotopic match between these rock extracts (#35 and 47) and the Triassic oils from Roswin North-1 and Rednook-1.

6.4.5 Compound-specific isotope analysis (CSIA) of individual n-alkanes

6.4.5.1 CSIA of saturated hydrocarbon fractions from rock extracts

Compound-specific isotope analysis of individual *n*-alkanes in two SCM extracts reveals subtle variations between the *algal facies* and the *higher-plant facies* (Table 6.6, Fig. 6.21). The algal facies has a maximum $\Delta\ \delta^{13}C$ of 1.3‰ for the $n\text{-}C_{15\text{-}25}$ range, with a mean $\delta^{13}C$ of -27.9‰ (range -28.93 to -27.2‰), consistent with a single source which

Table 6.6 Carbon isotopic composition of *n*-alkanes in SCM extracts and kerogen pyrolysates

Sample	*n*-Alkane carbon number															
	16	**17**	**18**	**19**	**20**	**21**	**22**	**23**	**24**	**25**	**26**	**27**	**28**	**29**	**30**	**31**
47 SCM *Extract*	-27.26	-27.20	-27.27	-27.45	-27.38	-27.58	-28.93	-28.42	-28.67	-28.57						
Pyrolysate	-29.33	-25.99	-30.32	-31.53	-32.45	-32.15	-31.71	-31.10	-31.12	-30.20	-30.17					
71 SCM *Extract*						-27.62	-27.58	-28.26	-28.37	-28.07	-28.41	-28.91	-27.99	-28.46	-27.43	-28.40
Pyrolysate	-27.79	-25.22	-29.13	-30.12	-31.73	-30.97	-31.54	-31.13	-31.34	-30.77						

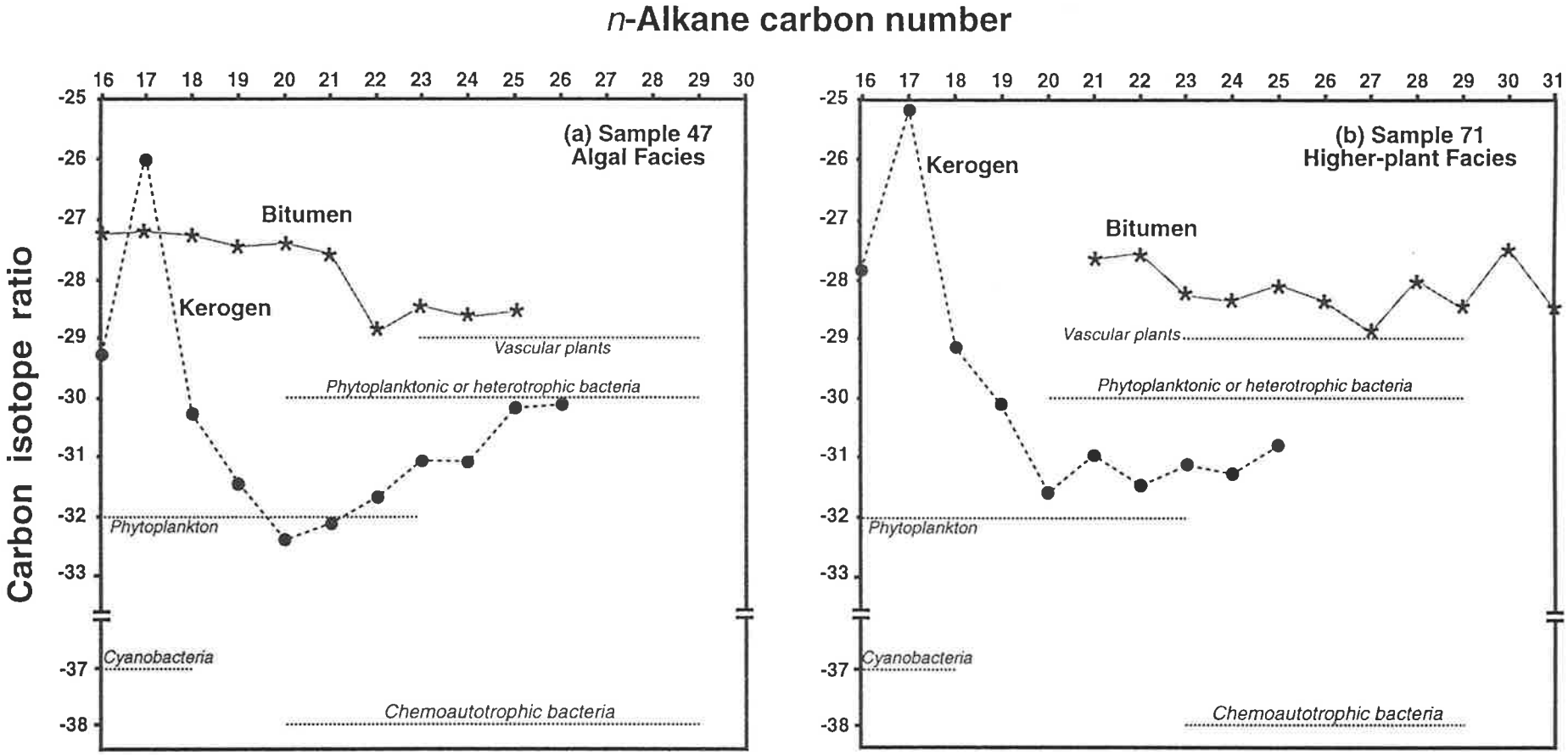

Figure 6.21 Carbon-isotopic composition of *n*-alkanes from saturated hydrocarbon fractions of kerogen pyrolysates and their corresponding rock extracts. $\delta^{13}C$ values of *n*-alkanes from different types of organic matter (summarised from Collister et al., 1994) are included for comparison.

is shown under the microscope to be phytoplankton. On the other hand, the higher-plant facies has a mean $\delta^{13}C$ of -28.1‰ (range -28.91 to -27.43‰) for the *n*-C_{21-31} range. Although the two *n*-alkane $\delta^{13}C$ ranges are similar, incorporation of land-plant waxes into the latter facies is evidenced by a saw-toothed isotopic profile in the C_{25+} region. For higher molecular weight *n*-alkanes (*n*-C_{23+}), Collister et al. (1992, 1994) found that $\delta^{13}C$ values of -29 to -27‰ are typical of vascular plants. Petrographically, this latter facies is dominated by vitrinite and inertinite, with lesser amounts of liptinite (mostly sporinite and cutinite).

6.4.5.2 CSIA of saturated hydrocarbon fractions from kerogen pyrolysates

The *n*-alkane $\delta^{13}C$ profiles of the pyrolysates differ markedly from those of the corresponding extracts (Fig. 6.21). Excluding *n*-C_{17}, the pyrolysate *n*-alkanes become isotopically more negative with increasing carbon number until *n*-C_{20} ($\delta^{13}C$ = -32.45‰ and -31.73‰), whereafter $\delta^{13}C$ increases gradually again. These variations may be interpreted in terms of variable sources for individual *n*-alkanes. Heavy isotopic values for *n*-C_{17} ($\delta^{13}C$ = -25.99‰ in sample #47 and -25.22‰ in sample #71) are consistent with its algal derivation (*cf.* Boreham et al., 1994).

Compared to the *n*-alkane $\delta^{13}C$ profile of the bitumen, the pyrolysate of sample #47 is offset to lighter isotopic values by 2.1‰ at *n*-C_{16}. Excluding *n*-C_{17}, the gap widens gradually to 5.1‰ at *n*-C_{20} before diminishing again to 1.6‰ at *n*-C_{25} (Fig. 6.21). A similar trend to progressive ^{13}C depletion is also demonstrated by sample #71, with the greatest ^{13}C depletion ($\delta^{13}C$ = -32 to -31‰) occurring for *n*-alkanes in the range C_{20-24}. This suggests a phytoplanktonic source for these *n*-alkanes. Phytoplanktonic *n*-alkanes in the Green River Formation have a mean $\delta^{13}C$ value of -32‰ over the range C_{16-23} (Collister et al., 1994).

The *n*-alkane $\delta^{13}C$ profiles of the two SCM-facies extracts and pyrolysates do not match those of any of the Permian oils analysed by Boreham et al. (1995), one of which is shown in Figure 6.22. None of the oils of Triassic origin (*viz.* Roswin North-1, Rednook-1) underwent CSIA and, therefore, a comparison could not be made between these oils and the SCM on the basis of their *n*-alkane $\delta^{13}C$ profiles.

There is one question which still needs to be addressed. Why do the SCM bitumens have *n*-alkane isotopic profiles indicative of land-plants, whereas their kerogen pyrolysates display dual algal and land-plant signatures ? A possible answer is that, at the low level of natural thermal maturity attained by these samples (T_{max} = 429-434°C; R_O ~ 0.5-0.6%), sporinite, cutinite and vitrinite are the only constituents to have

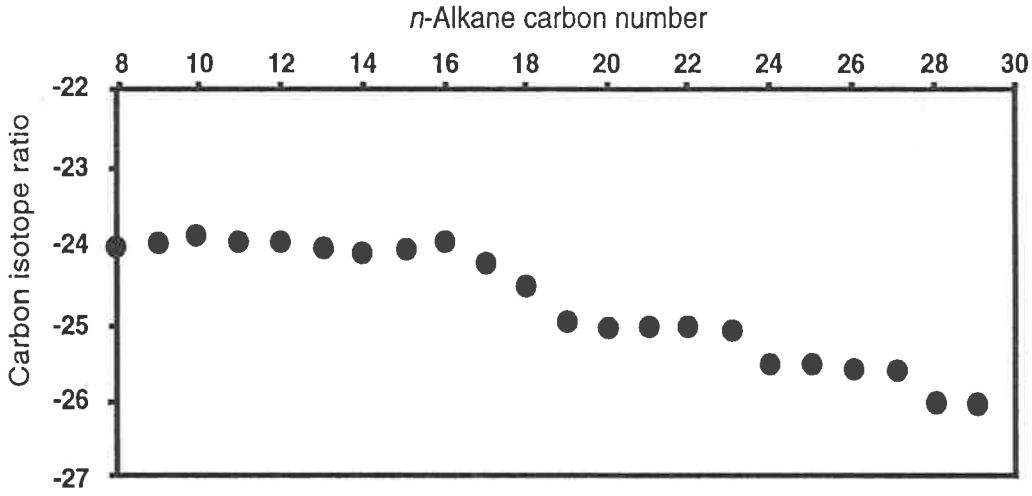

Figure 6.22 *n*-Alkane $\delta^{13}C$ profile of the Moonie oil, a representative Permian oil from the southern Taroom Trough (Boreham et al., 1995).

generated hydrocarbons. Cook (1982) and Snowdon and Powell (1982) demonstrated that vitrinite starts to generate oil at about 0.5% R_O (*cf.* 0.6% R_O for sporinite and cutinite). At a slightly higher thermal maturity (simulated here by pyrolyzing the kerogen at 340°C for 72 hours), *n*-alkanes released from phytoplankton dominate the pyrolysis products and consequently the *n*-alkane isotopic signature.

The overall conclusion from the aforementioned observations can be summarised as follows: (i) the extractable hydrocarbons are derived primarily from free lipids; (ii) kerogeneous lipids and biopolymers have not yet contributed significantly to the extractable organic matter because of the low thermal maturity of the host rock; and (iii) there has been preferential release of *n*-alkanes from phytoplankton (i.e. alginite) during artificial maturation. The likelihood that the extractable hydrocarbons are derived almost entirely from free lipids is supported by the pre-catagenic maturity ($T_{max} \leq 434$°C) of these SCM samples.

6.5 Summary

Biomarker and isotopic evidence suggests that the Triassic SCM has sourced the crude oils produced from the Showgrounds Sandstone at Roswin North-1 and Rednook-1. Although not indicated by their carbon isotopic signatures, the other Family 1 oils (Taylor-12A and Merroombile-1) may have a minor Triassic contribution. Facies A and Facies AC are the most likely source rocks within the SCM. These facies have their best hydrocarbon generating potential, and an appropriate thermal maturity, in the southwestern part of the Taroom Trough. The oils of Family 2, currently being produced from other fields in the area, are of Permian source affinity and most likely derived from carbonaceous shales of the Blackwater Group.

CHAPTER SEVEN

THE BEHAVIOUR OF BIOMARKERS DURING ARTIFICIAL AND NATURAL MATURATION OF SOURCE ROCKS

7.1 Introduction

This chapter examines the saturated biomarkers obtained upon sealed-tube hydrous pyrolysis of kerogens isolated from different organic facies of the Triassic Snake Creek Mudstone. The biomarker assemblage of each kerogen pyrolysate is compared with that of the corresponding whole-rock extract. Finally, the response of the principal diterpane classes to artificial and natural maturation is elucidated using a suite of Triassic and Permian sediments from the southern Taroom Trough. Particular attention is paid to the process of phyllocladane isomerisation.

7.1.1 Uses of hydrous pyrolysis

Hydrous pyrolysis is the best available method to simulate the process of petroleum generation (Winters et al., 1983; Lewan, 1994). Such studies allow calculation of kerogen conversion kinetic parameters which can then be used to predict the quality and quantity of hydrocarbons generated from a particular source rock. The biomarker fingerprints of the oil and various extracts are commonly used to correlate the oil to its source rock. Because the oil expelled as "pyrolysate" is similar to a natural crude oil (Hoering, 1984; Lewan et al., 1986) more rigorous "qualitative" correlation can be achieved with kerogen pyrolysates (e.g. Philp and Gilbert, 1985). Eglinton and Douglas (1988) have emphasised the importance of "quantitative" aspects of oil-source correlations. Whether the origin of the biomarkers in a petroleum is either the free bitumen or the kerogen in its source rock can be assessed by such a quantitative biomarker study (Eglinton and Douglas, 1988). Several studies have also documented the effects of hydrous pyrolysis on biomarker maturity (Lewan et al., 1986; Abbott et al., 1990; Peters et al., 1990) and source (Eglinton and Douglas, 1988) parameters.

7.1.2 Why hydrous pyrolysis at 340°C for 72 hours?

The starting material for hydrous pyrolysis (i.e. heating in the presence of water and in an oxygen-free atmosphere) can be unextracted whole source rock (Winters et al., 1983; Lewan et al., 1986) or a kerogen concentrate (Tannenbaum et al., 1986a; Eglinton and

Douglas, 1988; Boreham and Powell, 1991). Critical for the successful simulation of the petroleum generation process are the experimental conditions used, most importantly the temperature and duration of heating. Early work of anhydrous pyrolysis experiments yielded products very dissimilar to expected crude oils (e.g. deficient in diasteranes: Seifert, 1978; Mackenzie et al., 1981). Temperatures applied are normally in the range 260-365°C. Heating the source rock sample at 350°C for 72 h was found by Lewan (1985, 1994) to best approximate peak oil generation. Eglinton and Douglas (1988) found that the maximum yield of biomarker generation occurred when pyrolysing the kerogen at 330°C for 72 hrs. Similarly, Boreham et al. (1994) reported that pyrolysing kerogens at 330°C for 72 hrs yielded pyrolysates similar to an early mature crude oil. Peters et al. (1990) pyrolysed preextracted rock chips, with water, at selected temperatures in the range 260-360°C for 72 hrs. For kerogen concentrates, Boreham and Powell (1991) used temperatures of 310, 330, 350 or 380°C, for 72 h, whereas Boreham (personal communication, 1994) found that 340°C is probably the upper temperature limit before secondary cracking reactions become apparent in the closed system. Most recently, Abbott et al. (1995) studied the behaviour of 5α(H)-cholestane during hydrous and anhydrous closed-system pyrolysis and concluded that water is a crucial factor in mediating hydrocarbon degradation.

7.1.3 The present study

In the present study, sealed-tube hydrous pyrolysis (340°C for 72 h) was conducted on six SCM kerogen concentrates (see Section 3.3.8 for details). Bulk geochemical and isotopic data on the samples analysed are summarised in Table 7.1. Qualitative and quantitative variations in the biomarker content of the kerogen pyrolysates and their corresponding whole-rock extracts are documented in Tables 7.2-7.4 and Figures 7.1-7.4. The differential thermal response of the principal diterpane classes, including phyllocladane, is shown in Tables 7.5-7.6 and Figures 7.5-7.7.

7.2 Absolute concentrations of pyrolysis products

7.2.1 Quantitative yields of pyrolysates and saturated hydrocarbons

At the hydrous pyrolysis conditions employed (340°C/72 h), 5-11% of the SCM kerogen was converted to pyrolysates (Table 7.2). The amounts of saturated hydrocarbons liberated from the kerogens were 2- to 20-fold more (231-290 mg/g kerogen pyrolysate) than are present in the extracted bitumens (12-153 mg/g bitumen). The observed association of increasing saturated hydrocarbon concentrations with decreasing hopanes

Table 7.1 Rock-Eval pyrolysis and carbon isotope data on selected SCM source rocks and their respective kerogens

Parameter *	Sample Type	Organic Facies**	TOC (%)	T_{max} (°C)	S1	S2	S3	HI	OI	PI	$\delta^{13}C$ (‰, PDB)
Sample											
35 Flinton-1	W	C	2.5	434	0.23	4.2	0.4	167	14	0.05	
	K		63.6	439	8.64	196.8	16.2	309	25	0.04	-26.0
47 Snake Creek-1	W	A	3.4	429	0.59	5.6	0	165	0	0.10	
	K		64.2	438	8.61	218.8	5.2	341	8	0.04	-26.2
53 Borah Creek-3	W	AC	2.5	434	0.40	5.7	0.4	223	15	0.07	
	K		60.6	439	16.48	222.1	6.3	367	10	0.07	-27.6
58 Tinker-2	W	A	1.6	434	0.16	4.0	0	242	0	0.04	
	K		64.1	438	11.18	289.2	3.1	451	5	0.04	-28.0
64 Borah Creek-4	W	AC	1.7	439	0.45	4.4	1.1	264	67	0.09	
	K		64.5	439	11.07	40.3#	2.7	63#	4	0.21	-27.9
71 Newington-2	W	C	2.0	434	0.58	2.84	0	142	0	0.17	
	K		65.2	437	38.02	264.4	7.2	405	11	0.13	-26.9

* Refer to Table 4.1 for explanation of the Rock-Eval parameters

** Based on *n*-alkane distributions (Table 4.2)

Unreliable data; W = Whole rock; K = Kerogen concentrate

Table 7.2 Sterane and hopane abundance and maturity parameters for the SCM extracts and corresponding kerogen pyrolysates

Parameter #						17	1	2	3	4	5	6	7
Ratio	Sample Type	Pyrolysates (% of kerogen)	Saturates (mg)*	Hopanes (µg)**	Steranes (µg)**	Hop / Ster	%22S	Mor / Hop	Ts / Tm	%20S	%ββ	20S / 20R	αββ / ααα20R
Sample													
35 Flinton-1	Ex		126.0	776.4	325.5	2.4	60.3	0.20	0.05	37.3	39	0.60	1.03
	Py	7.8	289.5	229.0	59.0	3.9	59.9	0.30	0.11	48.1	44	0.92	1.53
47 Snake Creek-1	Ex		57.0	565.3	76.7	7.4	59.7	0.22	0.08	45.8	33	0.84	0.90
	Py	7.8	231.0	125.0	34.7	3.6	62.7	0.19	0.11	49.5	49	0.98	1.87
53 Borah Creek-3	Ex		139.0	2110.0	256.9	8.2	59.5	0.11	0.28	44.7	41	0.81	1.24
	Py	5.7	250.0	78.4	21.6	3.6	61.4	0.13	0.15	47.2	49	0.89	1.84
58 Tinker-2	Ex		153.0	3489.3	676.5	5.2	59.9	0.15	0.07	43.8	37	0.78	1.03
	Py	11.3	232.1	77.2	19.8	3.9	59.5	0.17	0.15	55.3	47	1.24	1.98
64 Borah Creek-4	Ex		147.0	404.9	43.1	9.4	60.3	0.13	0.14	49.5	40	0.98	1.29
	Py	5.0	240.0	15.0	17.7	0.9	61.8	0.10	2.40	56.3	59	1.29	3.28
71 Newington-2	Ex		12.0	24.7	3.8	6.5	61.3	0.20	0.14	47.7	39	0.91	1.23
	Py	7.7	242.1	35.6	14.4	2.5	57.6	0.17	0.23	52.9	48	1.12	1.97

* Amount of saturates contained in 1g of bitumen or 1g of kerogen pyrolysate.
** µg of biomarkers per g of bitumen or per g of kerogen pyrolysate.
Ex = Extract; Py = Pyrolysate
# For key see Table 5.3 (a)

and steranes (see below) suggests that the bulk of the alkanes released from these SCM kerogens are straight-chain aliphatics. This is also evident from Figure 7.1 which shows that the alkanes of the pyrolysates are depleted in hopanes and steranes compared to their extracted counterparts. It is also possible that some of the polycyclics have been aromatised or even destroyed (R. Alexander, pers. comm., 1996).

7.2.2 Quantitative yields of hopanes and steranes

The absolute amounts of steranes and hopanes in the bitumens and kerogens are listed in Table 7.2. Although the pyrolysates are more enriched in saturated hydrocarbons than are the bitumens, the absolute concentrations of both the steranes and hopanes decreased on pyrolysis (an exception occurs for sample #71; see below). In the experiment of Eglinton and Douglas (1988), concentrations of steranes and hopanes were noticed to increase with increasing pyrolysis temperature, with maximum yields at 310°C for steranes and 330°C for hopanes. Beyond these temperatures biomarker concentrations decreased. The pyrolysate in the present study, however, was collected only at the final pyrolysis temperature (340°C) and, thus, changes in the sterane and hopane distributions at different temperatures could not be acquired.

The decrease in hopane concentration in the 340°C pyrolysate (relative to the extract) was more than that for steranes by up to about 11 times. The same phenomenon was reported by Eglinton and Douglas (1988) to occur at temperatures higher than 330°C where the released hopanes are thermally unstable. This may explain why the hopane/sterane ratios in the pyrolysates (0.9-3.9) are lower than in the bitumens (5.2-9.4). It is also likely that there are more steranes than hopanes bounded into the kerogen (G. Abbott, pers. comm., 1996), knowing that hopanes are very stable compounds in the absence of catalysts (R. Alexander, pers. comm., 1996).

The DOM in sample #71 is composed almost entirely of vitrinite (90%) with minor inertinite (9%) and very little liptinite (Table 4.4). Interestingly, this is the only kerogen sample which showed increasing concentrations of both hopanes and steranes in the pyrolysate (steranes increased about 4 times compared to 1.4 times for hopanes: Table 7.2). This is consistent with observations on the Kimmeridge kerogen that steranes can be released at lower temperatures than hopanes (Eglinton and Douglas, 1988). The results from the present study suggest further that optimal release of hopanes and steranes from vitrinitic kerogen requires higher temperatures than is the case for other kerogens. At the specified heating conditions (340°C/72 h) biomarkers were probably still being released from this vitrinite-rich kerogen, whereas the more liptinite-rich kerogens (samples #35-64) had already realised their maximum biomarker yield. This is best observed in the

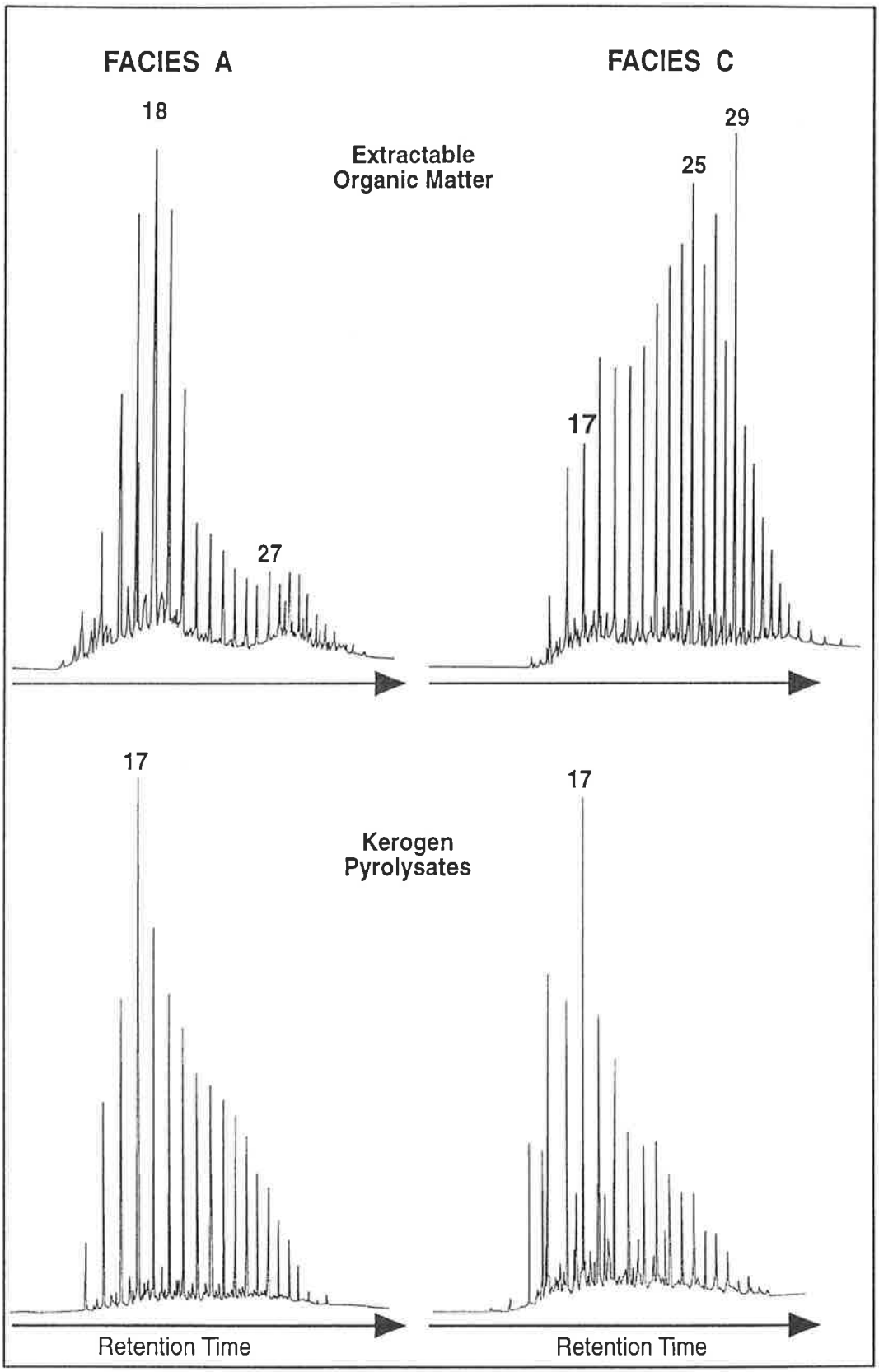

Figure 7.1 Gas chromatograms of saturated hydrocarbons in rock extracts and kerogen pyrolysates of two end-member SCM organic facies. Facies A and C are represented here by samples 47 and 71, respectively.

pyrolysate of the liptinite-rich kerogen sample #64 which has a hopane/sterane ratio of 0.9 compared to 9.4 in its bitumen (Table 7.2). This suggests that some liptinite-rich kerogens require lower temperatures in order to release their hopanes and steranes which, therefore, start to decline earlier, with the kerogen-bound hopanes decreasing faster.

7.2.3 Is the source of petroleum biomarkers free hydrocarbons or kerogen?

Biomarkers in oils derived from the vitrinite-rich facies (sample #71) are likely to be kerogen-related simply because the pyrolysate has a higher biomarker content than does the extract (Table 7.2). Oils generated from all the other SCM facies are expected to bear biomarker signatures that are essentially those of their bitumens because the latter are more enriched in biomarkers than are the pyrolysates. Thus, the relative contribution of the free bitumen to the biomarkers of any oil generated from such facies would be high. However, the biomarker input from the kerogen in this case may be somewhat underestimated because of the instability of both hopanes and steranes under the pyrolysis conditions employed herein.

7.3 Hopane and sterane isomerisation

Biomarker maturity parameters based on sterane and hopane isomerisation for the extracted bitumens and kerogen pyrolysates are listed in Table 7.2. In the bitumens, neither the 20S/(20S+20R) sterane ratio (37-50%) nor the ββ/(ββ+αα) sterane ratio (33-41%) has reached steady state. The equilibrium values of these two parameters are 52-55% (Peters et al., 1990) and 67-71% (Seifert and Moldowan, 1986), respectively. At the specified heating conditions (340°C/72 h), the monitored hopane and sterane isomers reach (or approach) their equilibrium status in some pyrolysates but not all. For example, the kerogen pyrolysate of sample #64 shows the most mature signature, comprising relatively high 20S/(20S+20R) and ββ/(ββ+αα) sterane ratios (56.3 and 59%, respectively) and the highest T_s/T_m and lowest βα/αβ hopane ratios (2.4 and 0.10, respectively). The pyrolysates of the other five SCM kerogens appear to be variously less mature (Table 7.2). These maturity differences may partly be due to slight maturity variations of the unheated samples, as suggested by the sterane distributions in the bitumens (Fig. 7.2). However, this is not supported by the Rock-Eval pyrolysis T_{max} data (434-439°C) obtained for the kerogens prior to heating (Table 7.1). Thus, it seems that the biomarkers in sample #64 are able to achieve isomer equilibrium earlier than those in other samples, the explanation of which is not clear at this stage.

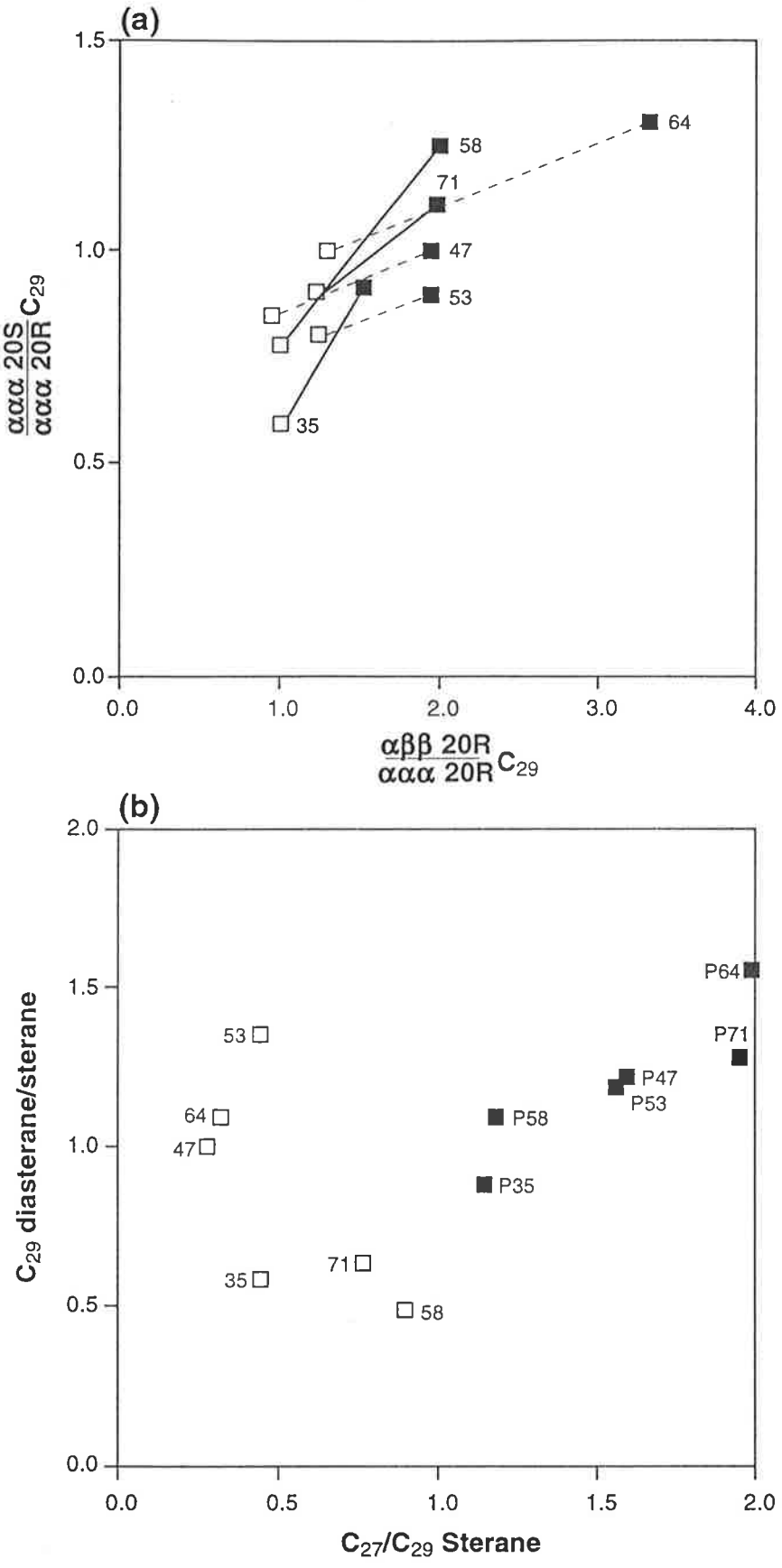

Figure 7.2 Crossplots of (a) biomarker maturation-migration index and (b) C_{27}/C_{29} steranes *versus* C_{29} diasterane/sterane ratios for the Snake Creek Mudstone extracts (□) and kerogen pyrolysates (■).

It is not unusual to find different hopane and sterane isomer ratios in different lithofacies of identical thermal maturity (Peters et al., 1990). Likewise, different types of kerogen may exhibit markedly variable thermal liabilities. Sulphur-rich Monterey kerogen, for example, displays unusually high rates of steroid isomerisation and aromatisation (Baskin and Peters, 1992). These and other studies (Strachan et al., 1989; Peters et al., 1990) have stressed the role of the rock matrix in controlling the level of hopane and sterane isomerisation/aromatisation rates. However, the present study shows that pyrolysing mineral-free preextracted kerogen concentrates of similar maturity but different maceral content can yield a wide range of epimerisation-isomerisation reaction rates. This suggests that the mineral matrix effect is not the only factor which can affect biomarker thermal maturity parameters. Another control is kerogen type. Neither lithological variations nor maturity differences could explain the observed variations in the diasterane/sterane ratios of the Monterey phosphatic and siliceous pyrolysates produced at the same temperature (Peters et al., 1990). However, this phenomenon can be explained by differences in maceral content detectable only at electron microscopic levels. These differences in organic matter may give rise to different hopanoid and steroid fingerprints in their extracts and pyrolysates as shown for the present SCM samples.

Unlike the analogous reaction in steranes, equilibrium is attained for homohopane epimerisation at C-22 in all of the SCM bitumens and kerogen pyrolysates. In each case the 22S/(22S+22R) value is at, or close to, 60%. Obviously, the 22R→22S isomerisation in these samples is faster than the other hopane and sterane reactions, supporting similar observations made by Peters et al. (1990) on the Monterey Formation.

7.4 Other rearrangement reactions

7.4.1 Diasteranes

Although diasteranes are less abundant than steranes in three of the SCM extracted bitumens (samples #35, 58, 71), the reverse is true in all but one of the pyrolysates (sample #35: Table 7.3). Moreover, although the diasterane/sterane ratio decreases slightly at C_{28} and C_{29} in the pyrolysate of one sample (#53), this ratio increases for the C_{27}-C_{29} homologues in all the other pyrolysates (Table 7.3). The increase of diasteranes relative to steranes in source rock and kerogen pyrolysates has been reported previously (Lewan et al., 1986; Peters et al., 1990) which is consistent with the general pattern of increasing steroid maturity in natural systems (Seifert and Moldowan, 1978). Peters et al. (1990) ascribed this to the faster generation rate of diasteranes from the kerogen structure. A more likely explanation is the greater stability of diasteranes relative to steranes (R. Alexander, pers. comm., 1996).

Table 7.3 Biomarker source parameters for the SCM extracts and kerogen pyrolysates

Parameter #		8	9	10	11	12	13	14	15	18			19	20	21	23	24	25	26
Ratio		Hopanes								Steranes							Methylsteranes		
	Sample Type	25NH Hop	30NH Hop	29.30BNH Hop	28.30BNH Hop	2+3MeH Hop	2MeH 3MeH	C29Ts 30NH	C30diah Hop	$C_{27}R$	$C_{28}R$	$C_{29}R$	$C_{27}R/C_{29}R$	C_{27}/C_{29}	C_{28}/C_{29}	C_{29}dia/ster	C_{28}	C_{29}	C_{30}
Sample																			
35 Flinton-1	Ex	0.01	1.62	0	0.058	0.06	2.00	0.02	0.02	20	26	54	0.37	0.44	0.53	0.59	12.0	29.3	58.7
	Py	0.01	2.60	0	0.018	0.05	3.10	0	0	47	19	34	1.40	1.15	0.55	0.88	40.4	32.9	26.7
47 Snake Creek-1	Ex	0.01	0.94	0.04	0.130	0.06	1.05	0.08	0.19	17	23	60	0.28	0.28	0.41	1.01	23.0	14.3	62.3
	Py	0	2.23	0.01	0.024	0.04	3.19	0.14	0.02	55	20	25	2.20	1.58	0.69	1.21	40.1	32.9	27.0
53 Borah Creek-3	Ex	0.01	0.94	0	0.025	0.04	1.43	0.18	0.05	21	17	62	0.35	0.46	0.38	1.34	16.6	18.3	65.1
	Py	0.02	2.50	0.02	0.025	0.04	3.24	0.13	0.05	52	20	28	1.89	1.56	0.72	1.17	37.3	37.8	24.9
58 Tinker-2	Ex	0	1.37	0	0	0.06	0.39	0.10	0.04	36	15	49	0.74	0.92	0.43	0.48	17.9	21.2	60.9
	Py	0	2.73	0.02	0	0.06	1.65	0.02	0.02	48	20	32	1.52	1.18	0.59	1.09	30.0	50.5	19.5
64 Borah Creek-4	Ex	0.02	1.21	0	0.035	0.04	1.44	0.14	0.07	18	19	63	0.29	0.34	0.33	1.09	13.7	17.1	69.2
	Py	0.04	1.83	0.03	0.118	0.11	3.99	0.39	0.09	63	15	22	2.82	1.97	0.6	1.55	38.8	32.2	29.0
71 Newington-2	Ex	0.01	1.19	0.01	0.121	0.05	0.97	0.07	0.08	28	25	47	0.43	0.40	0.25	0.65	23.4	24.6	52.0
	Py	0.03	2.50	0.01	0.038	0.06	4.05	0.08	0	62	14	24	2.58	1.94	0.68	1.28	45.8	23.7	30.5

Ex = Extract; Py = Pyrolysate
# For key see Table 5.3 (b)

7.4.2 Steranes and methylsteranes

As discussed in Section 5.4, the SCM extracts have C_{29}-dominant sterane distributions (see also Figure 7.3a). In the pyrolysates, there is a general shift to the lower molecular weight C_{27} 5α(H),14α(H),17α(H) steranes (Table 7.3). This is illustrated on the ternary plot of 20R- and 20S-5α(H),14α(H),17α(H) steranes (C_{27}, C_{28} and C_{29}) from rock extracts and kerogen pyrolysates (Fig. 7.3a). Boreham and Powell (1991) noticed a similar trend during artificial maturation of the Walloon Coal Measures, and ascribed it to a higher relative decomposition rate for C_{29} sterane and/or thermal cracking of its side-chain to produce the lower homologues. A similar trend towards lower-molecular-weight homologues in the C_{27}-C_{29} sterane series is also noticed for the C_{28-30} 4α-methyl steranes of the SCM pyrolysates (Table 7.3, Fig. 7.3b).

Both C_{27} sterane and C_{29} diasterane appear to increase relative to C_{29} sterane during hydrous pyrolysis (Fig. 7.2b, Table 7.3). Lewan et al. (1986) have already documented this phenomenon in artificially matured samples. In the study of Lewan and co-workers, the same sample was heated at different temperatures and, therefore, changes in the biomarker content with increasing heating temperature were related to the differing thermal stabilities of these compounds. In the present study, however, different samples were pyrolysed under identical conditions (340°C/72 hrs) which implies that any variations in biomarker assemblages must be related to different maturity levels of the initial (unheated) kerogens and/or to different kerogen facies with different thermal stabilities. A combination of both explanations is favoured here.

7.4.3 Tricyclic and tetracyclic terpanes

On pyrolysis, all tricyclic terpanes (TT) increased dramatically in their abundance by 10- to 40-fold compared to the extracted bitumens, as expressed by the ratio C_{19}-C_{26}TT/C_{30} hopane (Table 7.4). The tricyclics/17α(H)-hopane ratio increases during petroleum generation (Aquino Neto et al., 1983), during laboratory-simulated migration (Zhao-An and Philp, 1987) and during hydrous pyrolysis (Peters et al., 1990). This is partly because tricyclic terpanes can migrate, from the kerogen body, faster than 17α(H)-hopanes (Aquino Neto et al., 1983; Zhao-An and Philp, 1987) because of their smaller size (Peters et al., 1990). Higher tricyclics/17α(H)-hopane values in the pyrolysates are more likely related to the relative stabilities of these compounds. Similar reasoning may also explain the increased concentrations of the C_{24} tetracyclic terpane, relative to C_{30} hopane, in the pyrolysates (C_{24}Tetra/C_{30} hopane = 1.8-5.5, compared to 0.1-0.4 in the bitumens: Table 7.4).

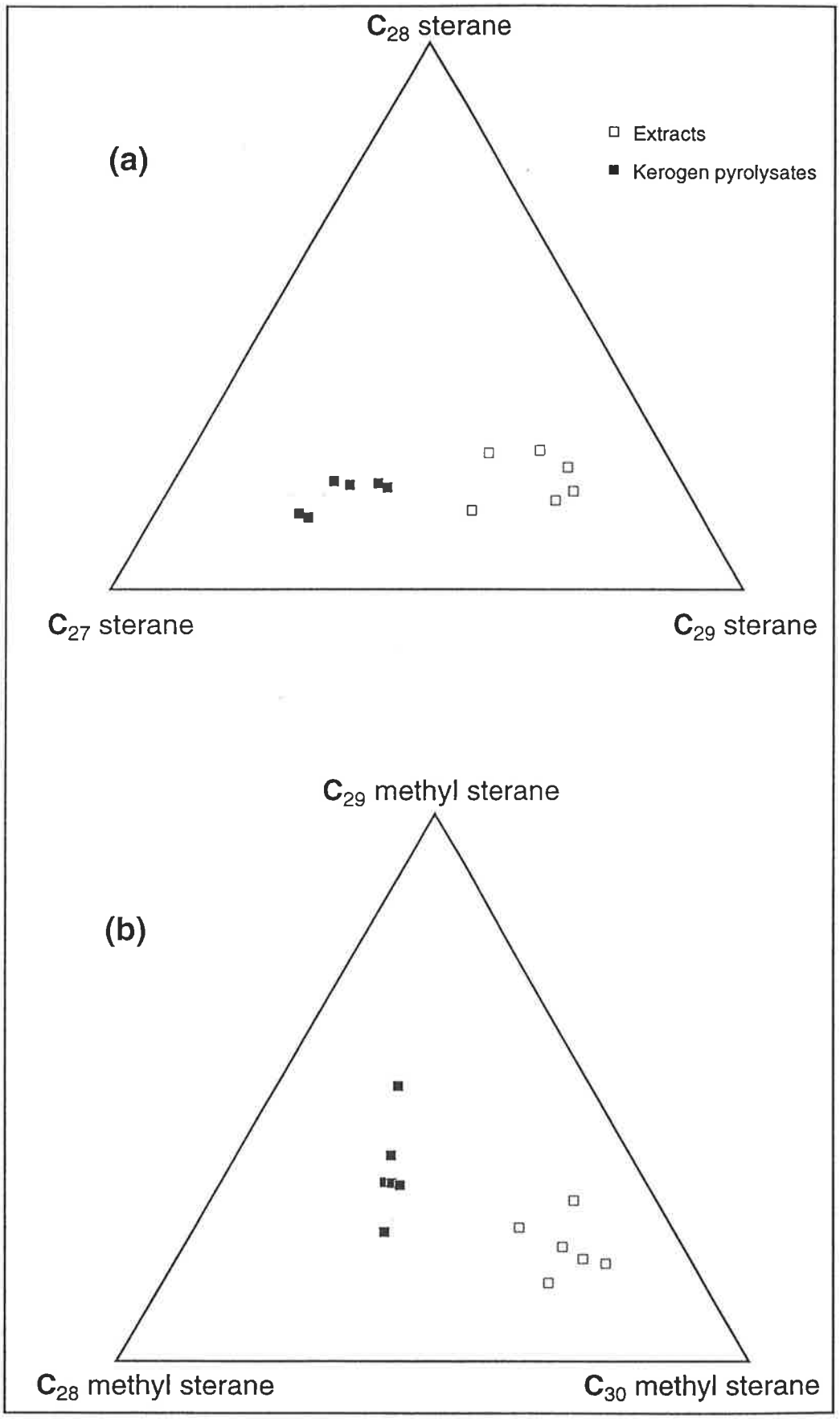

Figure 7.3 Effect of hydrous pyrolysis on (a) ααα C_{27}-C_{29} sterane and (b) C_{28}-C_{30} 4α-methyl sterane distributions in the Snake Creek Mudstone.

Table 7.4 Tricyclic and tetracyclic terpane abundances for SCM extracts and kerogen pyrolysates

Ratio *	Sample Type	C_{19}	C_{20}	C_{21}	C_{22}	C_{23}	C_{24}	C_{25}	C_{26}	C_{24}Tetra	C_{19}-C_{26}
Sample											
35 Flinton-1	Ex	0.28	0.28	0.09	0.02	0.09	0.05	0.03	0.02	0.25	0.84
	Py	3.12	2.64	0.61	0.22	0.82	0.26	0.17	0.17	1.80	8.00
47 Snake Creek-1	Ex	0.23	0.40	0.08	0.02	0.04	0.01	0.01	0.01	0.14	0.79
	Py	5.38	4.46	2.15	0.63	1.56	0.53	0.34	0.20	2.56	15.26
53 Borah Creek-3	Ex	0.09	0.12	0.07	0.01	0.35	0.15	0.10	0.07	0.10	0.96
	Py	9.03	8.10	4.15	1.13	3.14	1.39	0.54	0.38	3.15	27.86
58 Tinker-2	Ex	0.23	0.16	0.03	0.01	0.02	0.01	0	0	0.23	0.46
	Py	8.23	4.75	1.45	0.74	1.67	0.80	0.35	0.14	3.95	18.13
64 Borah Creek-4	Ex	0.67	0.50	0.17	0.02	0.07	0.03	0.02	0.01	0.21	1.48
	Py	1.38	3.14	3.64	1.27	7.56	2.93	1.89	1.61	5.51	23.42
71 Newington-2	Ex	0.18	0.24	0.13	0.07	0.28	0.13	0.10	0.05	0.37	1.17
	Py	5.70	6.08	4.26	2.78	4.69	1.84	0.87	0.53	3.51	26.74

Ex = Extract; Py = Pyrolysate

* Abundances are normalised against the C_{30} 17α(H)-hopane

The $C_{19}TT$ and $C_{20}TT$ dominate the tricyclic terpanes in the bitumens (Table 7.4). The same feature is noticed in the pyrolysates. However, an exception occurs for samples #53 and 71, where bitumens show relatively abundant $C_{23}TT$ whereas their kerogens released more $C_{19}TT$ and $C_{20}TT$. The reverse is true for sample #64 where kerogen released more $C_{23}TT$ and $C_{21}TT$.

7.4.4 Norhopanes, rearranged hopanes and methylhopanes

Hydrous pyrolysis produced no systematic changes to the concentrations of 25-norhopane, 29,30-bisnorhopane, $C_{29}T_s$ and C_{30} diahopane, relative to C_{30} hopane. This suggests that these ratios are maturity-independent. On the other hand, 30-norhopane has increased relative to C_{30} hopane, implying higher thermal stability of the former homologue. Both the extracts and pyrolysates are depleted in 28,30-bisnorhopane. This compound is known to occur in the bitumen as a free hydrocarbon, and is not bound to the kerogen structure (Peters et al., 1990). This may explain its higher relative abundance in some of the SCM bitumens, in particular samples #47 and 71, and their absence, or near absence, in the kerogens (Table 7.3).

In the pyrolysates, the proportion of C_{30} hopanes ($\alpha\beta+\beta\alpha$) has increased at the expense of the higher homologues C_{31} and C_{32} homohopanes (Fig. 7.4b) which, in turn, has decreased at the expense of the C_{27} (T_s+T_m) and C_{29} hopane members (Fig. 7.4a). The ratio of 2α- and 3β-methylhopanes/C_{30} hopane has not changed on pyrolysis. However, the 2α-/3β-methylhopanes ratio increased in the pyrolysates (1.7-4.1) relative to the bitumens (0.4-2.0).

7.5 Diterpenoids and phyllocladane isomerisation

7.5.1 Background and previous work

The naturally-occuring diterpenoid hydrocarbons include bicyclic, tricyclic and tetracyclic compounds. Diterpanes can be grouped into 20 main skeletal classes (Devon and Scott, 1972). Six of these classes, namely the labdanes, abietanes, pimarane, *ent*-kauranes, phyllocladanes and *ent*-beyerane (or podocarpane), are commonly reported in oils and sediments (Noble et al., 1985a,b; Simoneit et al., 1986). Different abundances and distributions of bi-, tri- and tetracyclic diterpanes are related to varying inputs of resins from gymnosperm conifers and/or certain angiosperms (Noble et al., 1985a, b). Their presence in Permian and younger sediments and oils was ascribed to various conifer families. However, earlier versions of conifers (the *Voltziales*) are expected to be the

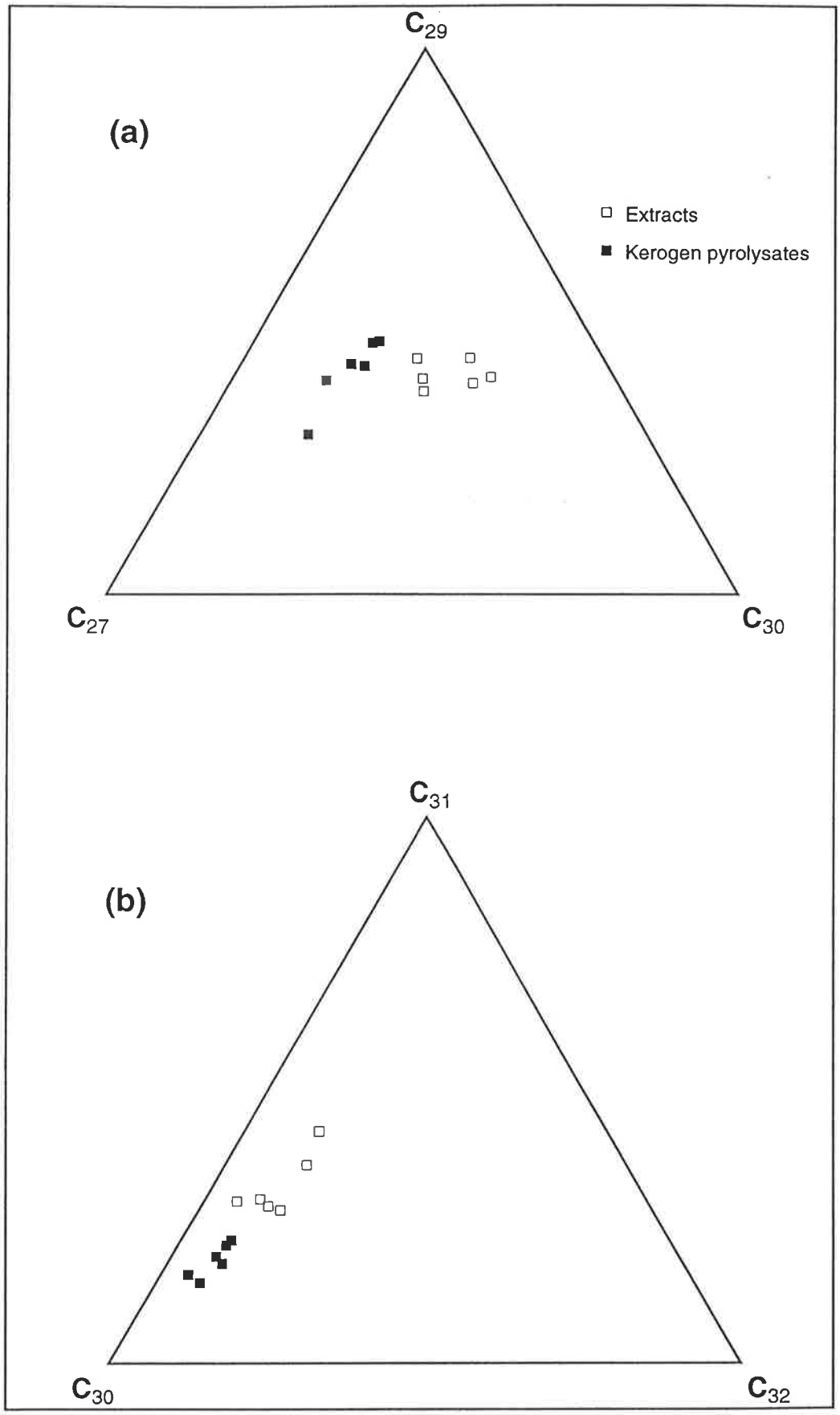

Figure 7.4 Effect of hydrous pyrolysis on the distributions of (a) C_{27}, C_{29} and C_{30} αβ+βα hopanes and (b) C_{30}-C_{32} αβ+βα homohopanes in the Snake Creek Mudstone.

source for terpenoid hydrocarbons, including phyllocladanes, found in Upper Carboniferous German coals (Schulze and Michaelis, 1990). In some cases, like the Athabasca tar sand, bicyclic diterpanes may be of microbial origin (Dimmler et al., 1984). Diterpane biomarker abundances and distributions display considerable stratigraphic variation through the Permian and Triassic succession in the Bowen Basin, and also can vary laterally within the same formation (Al-Arouri et al., 1995a). In addition, these distributions seem to respond readily to thermal stress, thereby reflecting the different thermal stabilities of individual diterpanes (Al-Arouri et al., 1995b).

In living plants, phyllocladane occurs as a monounsaturated hydrocarbon with a structure similar to that of 13β(H)-kaur-16-ene (Appleton et al., 1970). Upon burial, saturated phyllocladanes start to form. In lignites and brown coals, both 16α(H)- and 16β(H)-phyllocladane are present, with the former isomer predominating. Isomerisation at the C-16 position reaches equilibrium at a 16α(H)/16β(H) ratio of 0.3 (Noble et al., 1985b) or 0.25-0.30 (Alexander et al., 1987), just before the onset of oil generation. No change to this equilibrium value was observed to occur at higher maturities.

7.5.2 Diterpane abundance and distribution

The relative abundances of diterpanes in selected Permian and Triassic rock extracts and pyrolysates are summarised in Table 7.5. These diterpane distributions are controlled in the first instance by the extant conifer assemblage in the depositional basin, as is discussed elsewhere (Sections 6.3.3.3 and 6.3.3.4). The present section focuses on those features of the diterpane distribution that are attributable to differences in thermal maturity.

Kerogen pyrolysates show different patterns of diterpenoid abundance and distribution when compared to their less-mature, extracted-bitumen counterparts, suggesting differential thermal stability of different diterpane classes (Table 7.5, Fig. 7.5). Fichtelite increases in abundance relative to phyllocladane and kaurane, indicating that the former compound is thermally more stable. An exception occurs in Borah Creek-4 (sample #64) where fichtelite decreased in the kerogen pyrolysate. This sample is slightly more mature than the other SCM samples, with its kerogen-bound fichtelite being mature enough to transform, upon pyrolysis, into the more stable aromatic counterparts, such as retene and 1-methylphenanthrene. The increase in the relative concentrations of the more stable retene and 1,2,5-trimethylnaphthalene in the SCM kerogen pyrolysates (represented by sample #47) is shown in Figure 6.17.

The diterpane assemblage in the SCM from Flinton-1 is composed almost entirely of isopimarane and norisopimarane (94% of the total diterpanes) which, on pyrolysis,

Table 7.5 The relative abundances of diterpanes in Permian and Triassic source rock extracts and SCM kerogen pyrolysates

Ratio*	Sample Type	ΣDiterpanes / C_{30}hopane	ΣTricyclic diterpanes%	ΣTetracyclic diterpanes%	Bicyclic	Tricyclic diterpanes					Tetracyclic diterpanes			
					8β(H)-Labdane%	19-Noriso-pimarane%	Fichtelite %	Rimuane %	Pimarane %	Isopimarane %	17-Nortetra-cyclane%	*ent*-Beyerane %	Phyllocladane # %	*ent*-Kaurane # %
Sample														
Snake Creek Mudstone														
70 Renlim-1	Ex	0.77	64	36	0	23	11	15	1	14	5	15	14	2
35 Flinton-1	Ex	0.12	97	3	0	50	3	0	0	44	0	2	1	0
	Py	0.75	84	16	0	21	46	4	5	8	0	4	8	4
58 Tinker-2	Ex	0.45	73	27	0	14	39	1	0	19	1	0	23	3
	Py	0.12	88	12	0	10	51	11	10	6	0	3	6	3
53 Borah Creek-3	Ex	0.51	72	28	0	12	11	22	10	17	2	6	16	4
	Py	0.51	90	10	0	18	15	38	6	9	0	2	8	0
47 Snake Creek-1	Ex	1.84	49	51	0	10	11	14	5	9	2	10	31	8
	Py	0.12	92	8	1	20	30	16	15	10	0	3	4	1
71 Newington-2	Ex	1.13	60	40	0	12	16	19	9	4	7	7	17	9
	Py	0.09	81	19	0	14	19	18	18	12	0	7	9	3
64 Borah Creek-4	Ex	1.37	55	45	0	11	21	10	5	8	13	8	18	6
	Py	0.38	83	17	0	11	8	18	21	25	0	4	8	5
Permian source rocks														
Blackwater Group														
27 Meeleebee-1	Ex	0.80	46	54	0	12	17	4	7	6	9	9	26	10
26 Meeleebee-1	Ex	0.30	67	33	0	19	13	3	0	32	3	10	9	11
18 Cockatoo Creek-1	Ex	0.17	47	52	1	3	31	4	4	5	0	19	11	22
Back Creek Group														
24 Meeleebee-1	Ex	0.30	47	53	0	10	16	8	6	7	6	9	30	8
19 Flinton-1	Ex	0.93	55	45	0	10	13	11	11	10	18	7	13	7
10 Burunga-1	Ex	0.76	60	40	0	12	12	10	10	16	10	9	13	8
6 Burunga-1	Ex	1.89	74	26	0	20	17	17	2	18	6	8	8	4
16 Cockatoo Creek-1	Ex	4.56	84	16	0	17	4	21	21	21	0	3	11	2
13 Cockatoo Creek-1	Ex	0.49	71	28	1	13	12	15	12	19	0	12	13	3

* MRM transitions used to calculate the peak areas for each compound are listed in Table 2.1. All data are normalised against the total diterpanes
# 16α(H)+16β(H) isomers
Ex = Extract; Py = Pyrolysate

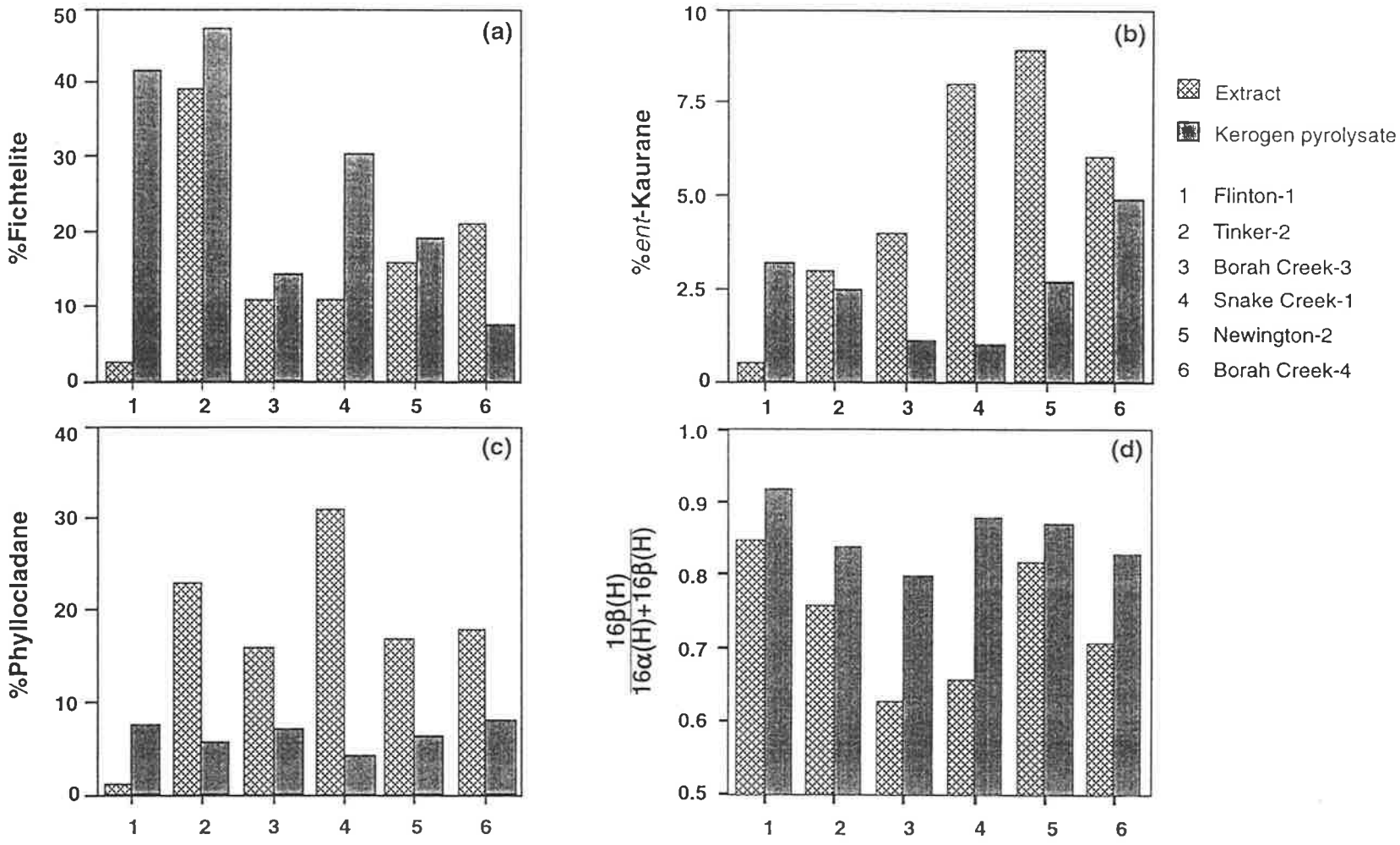

Figure 7.5 Effect of hydrous pyrolysis on the distributions of diterpanes (a-c) and (d) phyllocladane isomers at the C-16 position in the Snake Creek Mudstone. Data in a, b and c are normalised against the total diterpanes.

decreased dramatically in abundance while fichtelite increased. Livsey et al. (1984) reported similar observations and ascribed them to the greater thermal stability of fichtelite among the saturated diterpanes. Upon further maturation, some saturated diterpanes undergo aromatisation yielding retene and 1-methylphenanthrene (G. Alexander et al., 1987). It is not clear, however, why tetracyclic diterpanes in this particular sample become more abundant on pyrolysis (Fig. 7.5c). All the SCM samples listed in Table 7.5 were recovered from cores except that from Flinton-1 which is a cuttings sample. This sample may, therefore, contain contaminants from the overlying Jurassic formations which are rich in *Agathis* resin. In terms of diterpenoid abundance relative to the hopanes, the pyrolysates are depleted in four out of six samples when compared to the corresponding extracted bitumens (Table 7.5). This diminution in the pyrolysates can also be explained by aromatisation of the saturated diterpanes.

7.5.3 Phyllocladane isomerisation: Comparison with other maturity parameters

The phyllocladane isomerisation ratio (16β/16β+16α) is a maturity parameter that can be applied to sediments as old as Late Carboniferous (Schulze and Michaelis, 1990). Its value in selected sediments and oils from the Taroom Trough is compared with a range of other maturity parameters, including Rock-Eval T_{max}, vitrinite reflectance, *n*-alkane CPI and various sterane and hopane biomarker ratios (Table 7.6). Methylphenanthrene index (MPI-1) and the equivalent calculated vitrinite reflectance (Radke and Welte, 1983) values are also included for comparison.

In the Triassic and Permian sediments, T_{max} increases from 426°C in the least mature samples (Renlim-1) up to 505°C for the most mature section (Cockatoo Creek-1). The corresponding vitrinite reflectance measurements of these two samples are 0.48% and 2.0% R_O, respectively. Two well-known maturity parameters show reversals at later stages of catagenesis. These are the C_{29} sterane 20S/(20S+20R) ratio (Lewan et al., 1986; Strachan et al., 1989; Peters et al., 1990) and the MPI (Radke and Welte, 1983). For the present suite of samples, C_{29} sterane 20S/(20S+20R) is 22% in the least mature sample whereas for the artificially (SCM) and naturally (Permian) mature samples this ratio rises to about 50 to 55%. This latter range of values indicates equilibrium for these sterane isomers in the SCM pyrolysate and for samples currently in the oil window. However, samples currently in the gas window (those from Cockatoo Creek-1) show reversal of the trend of increasing S isomer with depth, with 20S/(20S+20R) values of 43% (Table 7.6). This 'natural' reversal supports the findings of Lewan et al. (1986) and Peters et al. (1990), based on laboratory heating experiments designed to mimic the later stages of catagenesis. With respect to MPI-1, the lowest values are recorded for the least (Renlim-1) and the most (Cockatoo Creek-1) mature samples. The maximum MPI-1

Table 7.6 Comparison of different maturity parameters with the extent of phyllocladane isomerisation at the C-16 position

Parameter	Sample Type	β/(α+β) Phyllocladane	HI	T_{max} (°C)	CPI	%22S	Mor / Hop	Ts / Tm	%20S	MPI-1#	$\%R_c$#	$\%R_m$
Sample												
Snake Creek Mudstone												
70 Renlim-1	Ex	0.40	18	426	1.5	44	0.22	0.05	22	0.26	0.56	0.48
35 Flinton-1	Ex	0.85	167	434	1.5	60	0.20	0.05	37	-	-	0.70
	Py	0.92	309	439	-	60	0.30	0.11	48	-	-	-
58 Tinker-2	Ex	0.76	242	436	1.2	60	0.15	0.07	44	-	-	-
	Py	0.84	451	438	-	60	0.17	0.15	55	-	-	-
53 Borah Creek-3	Ex	0.63	223	434	1.3	60	0.11	0.28	45	-	-	-
	Py	0.80	367	439	-	61	0.13	0.15	47	-	-	-
47 Snake Creek-1	Ex	0.66	165	429	1.1	60	0.22	0.08	46	0.37	0.62	-
	Py	0.88	341	438	-	63	0.19	0.11	50	0.48	0.67	-
71 Newington-2	Ex	0.82	142	434	1.4	61	0.20	0.14	48	-	-	-
	Py	0.87	405	437	-	58	0.17	0.23	53	-	-	-
64 Borah Creek-4	Ex	0.71	264	439	1.1	60	0.13	0.14	50	0.19	0.51	-
	Py	0.87	63	439	-	62	0.10	2.40	56	0.91	0.95	-
Permian source rocks												
Blackwater Group												
27 Meeleebee-1	Ex	0.71	72	443	1.0	61	0.20	0.07	46	-	-	-
26 Meeleebee-1	Ex	0.83	208	432	1.0	61	0.15	0.03	41	-	-	-
18 Cockatoo Creek-1	Ex	0.81	120	451	1.4	61	0.12	0.02	52	0.37	0.62	-
Back Creek Group												
24 Meeleebee-1	Ex	0.70	18	431	1.1	61	0.11	0.36	53	-	-	-
19 Flinton-1	Ex	0.57	29	434	1.1	59	0.07	0.65	55	-	-	0.90
10 Burunga-1	Ex	0.81	38	448	1.3	60	0.09	0.35	52	-	-	-
6 Burunga-1	Ex	0.73	44	460	1.1	59	0.11	0.78	51	0.48	2.01	-
16 Cockatoo Creek-1	Ex	0.60	35	493	1.1	60	0.10	0.85	43	0.59	1.95	1.90
13 Cockatoo Creek-1	Ex	0.60	3	505	1.2	59	0.10	0.95	43	-	-	2.01
Oils				API Gravity								
4 Roswin North-1	Oil	0.94	-	65.1	-	59	0.12	0.83	55	0.38	0.63	-
5 Washpool-1	Oil	0.83	-	-	-	59	0.08	1.22	60	0.60	0.75	-
6 Wilga-2	Oil	0.76	-	-	-	59	0.12	0.82	62	0.60	0.75	-
11 Bellbird-1	Oil	0.80	-	40.0	-	58	0.06	0.89	59	0.37	0.62	-

Ex = Extract; Py = Pyrolysate

MPI-1 (Methylphenanthrene Index) and vitrinite reflectance (R_c) calculated following Radke and Welte (1983)

(0.91, equivalent to 0.95% R_C) is recorded for 340°C pyrolysate of a liptinite-rich SCM kerogen (Borah Creek-4).

A similar 'reversal' trend is noticed for the phyllocladane β/(β+α) ratio in Figure 7.6. For the SCM pyrolysates and extracts (Figs. 7.5d and 7.7), the proportion of 16β(H)-phyllocladane (β/β+α) increased quickly with increasing maturation, reaching a maximum value of ~0.88 at about the oil generation threshold (T_{max} = 440°C, R_O~0.7%). This result confirms previous observations regarding the attainment of stereoisomeric equilibrium at C-16 within the early oil generation zone (Noble et al., 1985b; G. Alexander et al., 1987). In addition, the mature and overmature samples from the present study shed light on the previously undocumented behaviour of phyllocladane during the later stages of catagenesis (Fig. 7.7). Through the oil window, the β/(β+α) ratio declines steadily from 0.88 to 0.65, eventually attaining steady state at 0.6 ($T_{max} \geq$ 490°C) within the zone of dry gas generation.

Independent evidence, including MPI-1 values of 0.37-0.60 (0.62-0.75% R_C), suggests that the oils from Roswin North-1, Washpool-1, Wilga-2 and Bellbird-1 were generated during the early stages of the conventional oil window. Values of 0.76 to 0.94 for the β/(β+α) phyllocladane ratio are consistent with this inference (Fig. 7.7).

7.6 Summary

Examination of the saturated biomarkers obtained upon sealed-tube hydrous pyrolysis of kerogens isolated from different organic facies of the Snake Creek Mudstone suggests that Facies C would yield oil containing mainly kerogen-derived biomarkers, whereas oils derived from the other SCM facies are likely to inherit the biomarker signatures of their bitumens.

The present study demonstrates that biomarker maturity parameters of source rocks can be affected, not only by differences in the mineral matrix, but by variations in their kerogen type. Thus, caution should be exercised when comparing biomarker distributions from different organic facies.

The phyllocladane isomer ratio attains its maximum value (16β/16β+16α ~ 0.88) within the early stages of oil generation. During the later stages of catagenesis, however, the (β/β+α) ratio declines steadily from 0.88 to 0.65, eventually attaining steady state at 0.6 within the zone of dry gas generation.

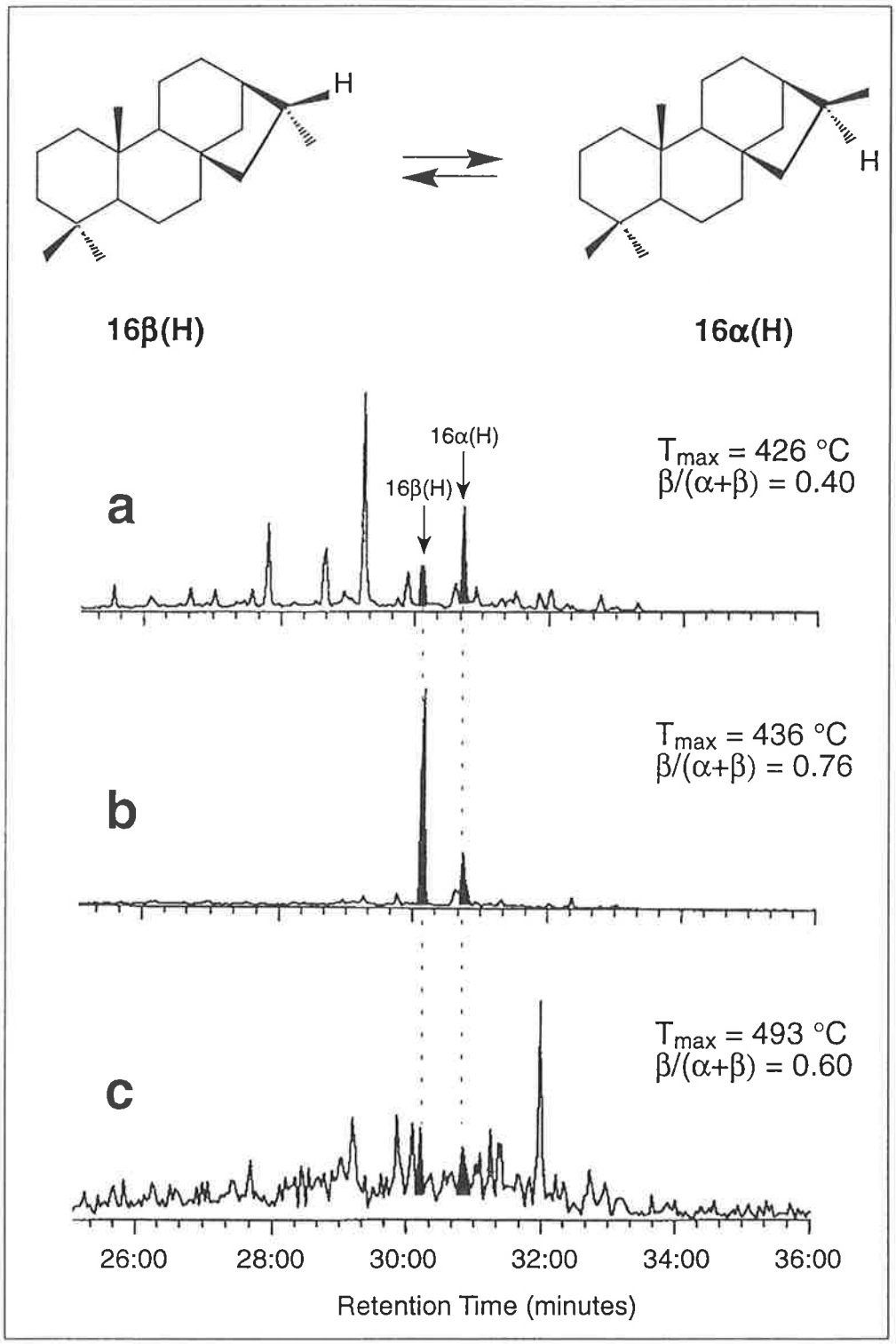

Figure 7.6 MRM chromatograms (274 → m/z 259) showing the relative abundance of 16α(H) and 16β(H) phyllocladane in extracts from the immature zone (a), oil window (b) and overmature zone (c) in the southern Taroom Trough.

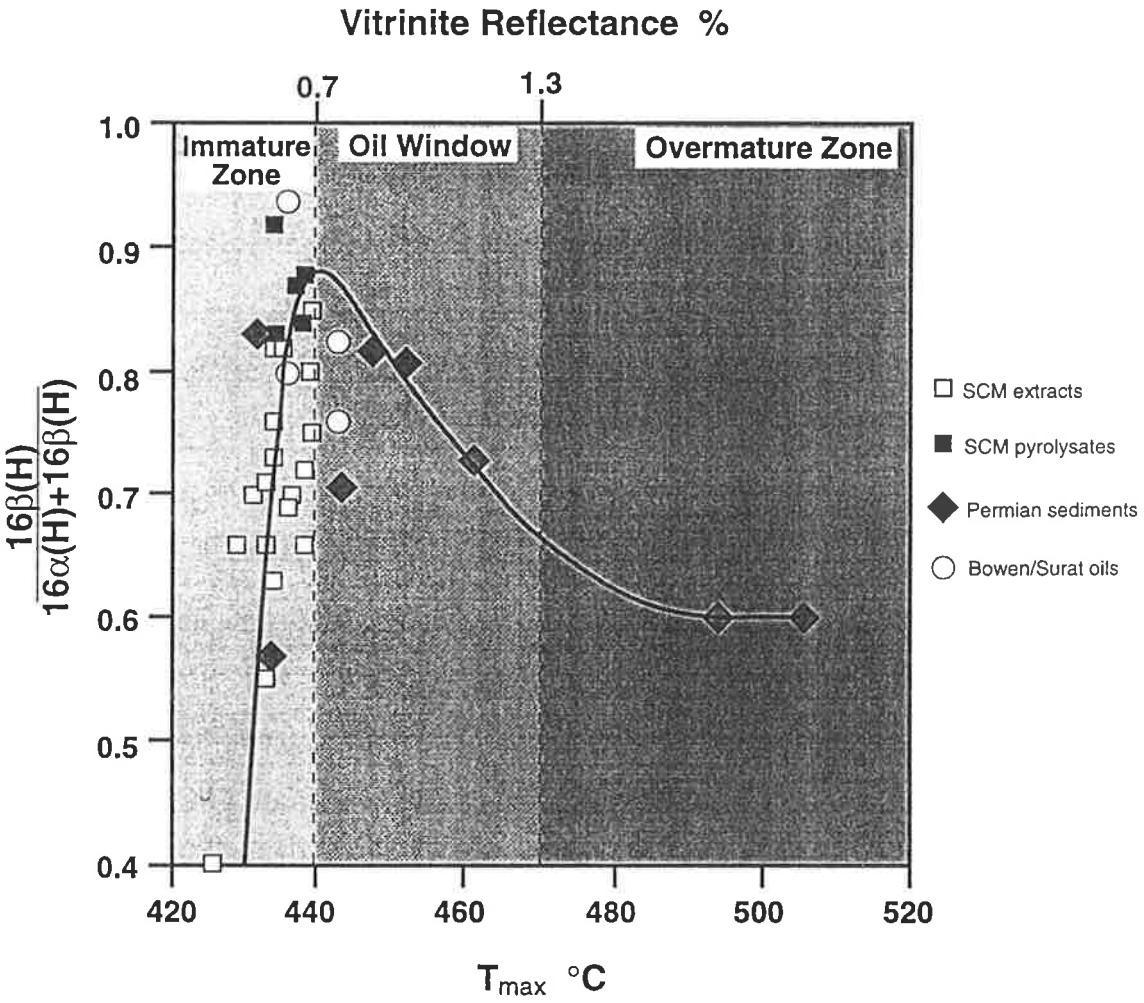

Figure 7.7 Correlation of phyllocladane isomerisation with T_{max} and vitrinite reflectance. Through the oil window, the $\beta/(\alpha+\beta)$ phyllocladane ratio declines steadily from 0.88 to 0.65, eventually attaining equilibrium at 0.6 within the dry gas generation zone. Vitrinite reflectance is measured (R_m) for the sediments and calculated (R_c) for the oils.

CHAPTER EIGHT

MODELLING OF THERMAL MATURATION AND HYDROCARBON GENERATION IN PETROLEUM SYSTEMS OF THE SOUTHERN TAROOM TROUGH

"If there is no petroleum generation in the subsurface, then all of the other necessary requirements of a petroleum system (e.g. structure, reservoir, seal) lose relevance."

Demaison and Huizinga (1991)

8.1 Introduction

Numerous oil and gas fields have been discovered along the eastern and western margins of the southern Taroom Trough. Over 500 exploration wells have resulted in about 100 discoveries, the largest being the Moonie/Cabawin oil fields to the east and Silver Springs/Renlim gas fields in the Roma Shelf-Wunger Ridge region to the west (Fig. 8.1) (Elliott and Brown, 1989; Hawkins et al., 1992). No significant discoveries have been made in the central and northeastern parts of the trough (Hawkins et al., 1992). The aim of this chapter is to investigate the maturation history of the southern Taroom Trough (Fig. 8.1) and, in particular, to elucidate the timing, type and amount of petroleum generation from its Permo-Triassic source rocks, with a view to explaining the observed distribution of its oil and gas reserves. The model presented here combines the current knowledge of basin evolution with a rigorous chemical kinetic treatment of petroleum generation from the Triassic Snake Creek Mudstone (SCM) and the Permian source rock facies, using the computer modelling program BasinMod®.

8.2 Petroleum systems of the southern Taroom Trough

A petroleum system, as defined by Magoon and Dow (1994, p.3) is "a pod of active source rock and all related oil and gas and includes all essential elements and processes needed for oil and gas accumulations to exist. The essential elements are the source rock, reservoir rock, seal rock, and overburden rock, and the processes include trap formation and the generation-migration-accumulation of petroleum. All essential elements must be placed in time and space such that the processes required to form a petroleum accumulation can occur." This means that when a source rock starts generating hydrocarbons, the petroleum system commences (Curiale, 1994). It is, therefore,

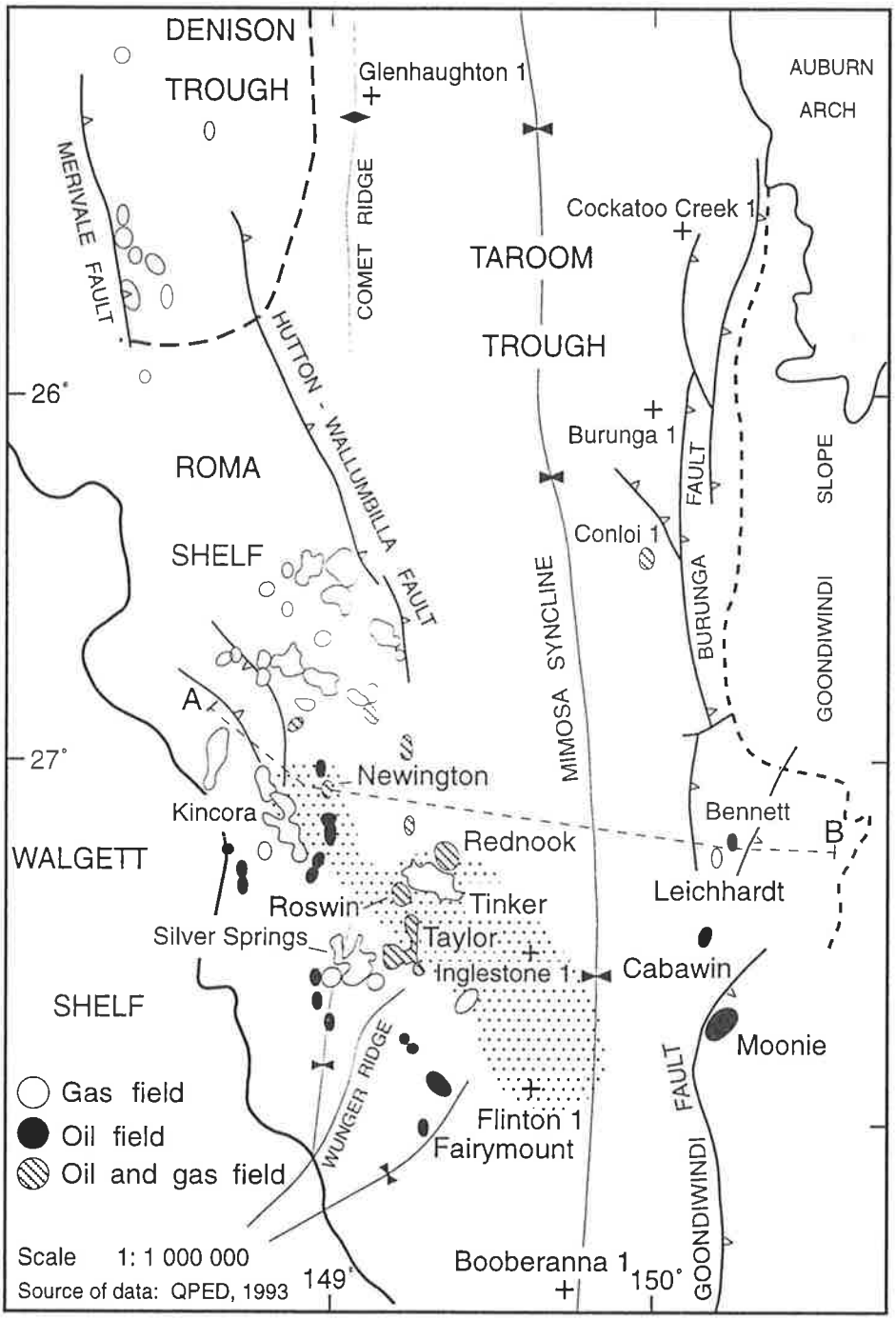

Figure 8.1 Major oil and gas fields and locations of the wells modelled in the southern Taroom Trough. The stipled area is the inferred areal extent of the Triassic 'SCM-Showgrounds' petroleum system where the SCM is mature and has high hydrocarbon generating potential. Also shown is location of the cross section A-B depicted in Figure 8.3.

obvious that locating the effective source rock units and establishing the timing of their hydrocarbon generation are crucial in any petroleum exploration program since, in most basins, the petroleum accumulations are commonly found over, or immediately adjacent to, hydrocarbon kitchens (Tissot and Welte, 1984).

The essential elements of the petroleum systems of the southern Taroom Trough are presented in Figure 8.2. Petroleum systems can be classified according to the kerogen type or the age of their source rock (Magoon, 1992). Based on the comprehensive geochemical investigations presented in Chapters 4-6 and on other publications (McKirdy, 1984; Hawkins et al., 1992; Boreham, 1995), a justifiable correlation can be established between oils from the Bowen/Surat Basins and Permo-Triassic source rocks (see next section). Magoon and Dow (1994) use the term 'known petroleum system' where an oil has been positively correlated with its source rock. Applying this concept to the Taroom Trough (Al-Arouri et al., 1997a), two 'known' petroleum systems can be identified, one Triassic-sourced (SCM-Showgrounds) and the other Permian-sourced (Blackwater-Precipice) (Figs. 8.1 and 8.3). The Triassic petroleum system has a very localised areal and stratigraphic extent implying relatively short migration distances. This system is developed in the southwestern part of the trough and encompasses the SCM source rock and its related oils in the Roswin North, Rednook and Merroombile fields, reservoired in the Showgrounds Sandstone. Both source and reservoir are of Middle Triassic age. As demonstrated in Chapter 4, it is in this part of the trough that the SCM shows its best potential for oil and gas generation (liptinite-rich, HI > 200). Primary migration of hydrocarbons within the SCM is indicated by petrographic observations of oil haze and oil droplets, associated with exsudatinite, fluorinite and bituminite (Section 4.5). A production index (PI) value of 0.5 in the intercalated sandstones of the SCM at Flinton-1 offers further evidence of a hydrocarbon charge, probably from the adjacent mudstone which has a considerable genetic potential (S1+S2 up to 5.6 kg/tonne rock: Table 4.1). Secondary migration of these hydrocarbons to the underlying Showgrounds Sandstone reservoir was probably facilitated by faulting, which is extensive in this part of the trough (Elliott and Brown, 1989). The Blackwater-Precipice petroleum system is laterally and stratigraphically more extensive, implying longer migration distances (Boreham, 1995) from the Permian 'kitchen' along the trough axis to reservoirs ranging in age from Permian to Jurassic (Fig. 8.2). Traps are located on the eastern and western margins of the southern Taroom Trough (Figs. 8.1 and 8.3).

8.2.1 Source rocks

The origin of petroleum in the Bowen/Surat Basins has been comprehensively investigated in the present study and by other workers, including Thomas et al. (1982),

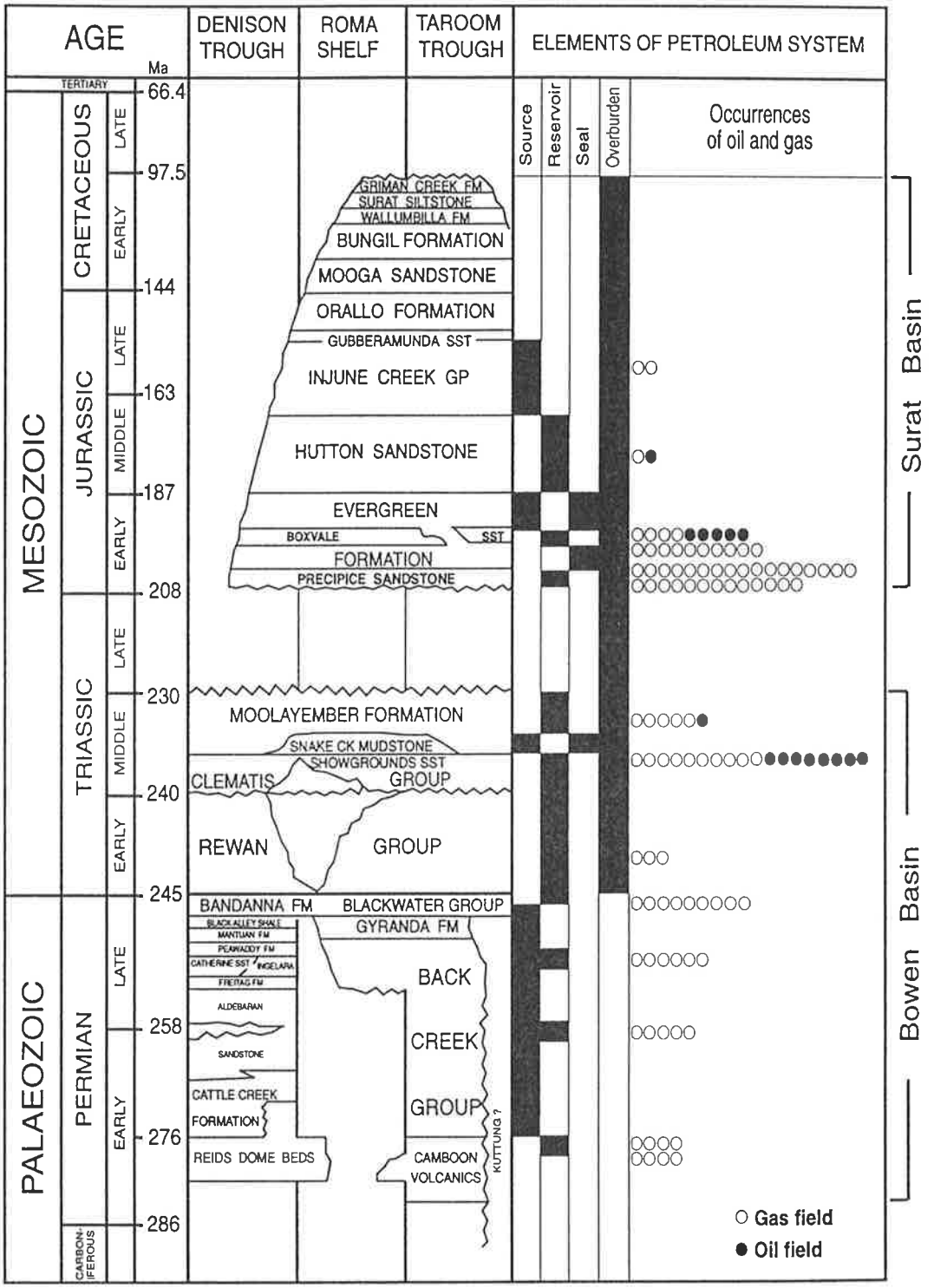

Figure 8.2 Hydrocarbon occurrences and the elements of the Taroom Trough petroleum systems. Also shown are the major Mesozoic unconformities.

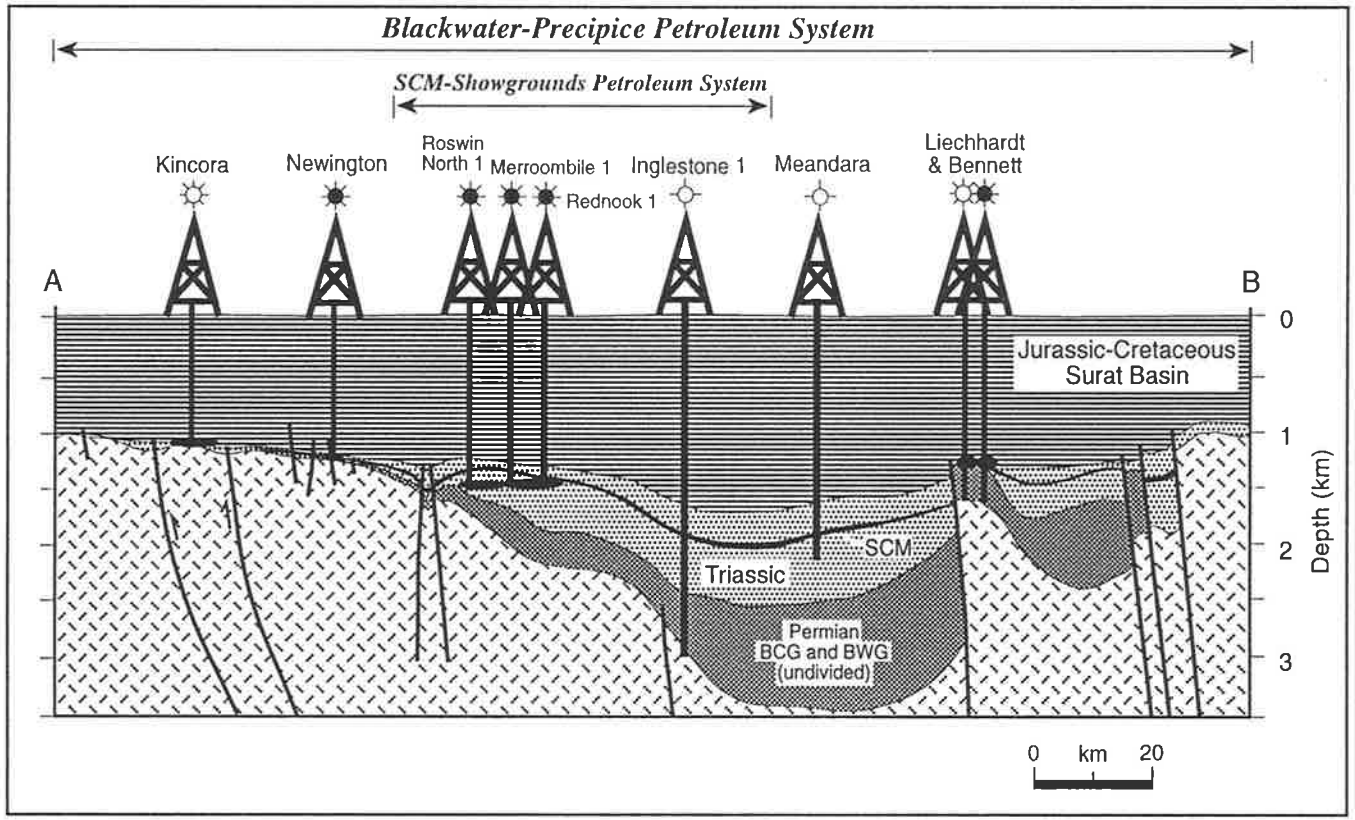

Figure 8.3 Cross-section of the central area of the southern Taroom Trough showing the distribution of its proposed petroleum systems. The 'SCM-Showgrounds' petroleum system is localised in the vicinity of Roswin North, Merroombile and Rednook fields, whereas the 'Blackwater-Precipice' petroleum system is of Permian source and has a wider stratigraphic and geographic extent throughout the trough. Black lenses are hydrocarbon accumulations. See Figure 8.1 for location of cross section.

McKirdy (1984), Philp and Gilbert (1986), Hawkins et al. (1992), Boreham (1995) and Carmichael and Boreham (1996). The *n*-alkane, isoprenoid alkane, sterane and triterpane biomarker distributions of crude oils suggest generation from coals or carbonaceous shales containing a mixture of higher plant, algal and bacterial remains that were deposited in a predominantly oxic environment (Chapter 6, see also McKirdy, 1984; Boreham, 1995). These are attributes of the organic-rich source rocks with high generating potential that are present throughout the whole Permian-Triassic-Jurassic succession. In other words, conventional biomarker signatures are not sufficient to confidently relate the oils to particular stratigraphic horizons. However, a Jurassic source for the oils is precluded by their alkylphenanthrene and trimethylnaphthalene distributions and their regional thermal maturity patterns (Chapter 6, see also Thomas et al., 1982; Boreham, 1995). Carbon isotope and other saturated biomarker (particularly sesquiterpane, diterpane and cheilanthane) data suggest Permian and Triassic sources for the oils (Chapter 6). Those from Rednook-1 (Boreham, 1995) and Roswin North-1 contain saturated and aromatic hydrocarbons that are isotopically light ($\delta^{13}C$ = -27‰) and can be tied to the Triassic SCM, whereas all the other oils are heavier (average $\delta^{13}C$ of the saturated and aromatic hydrocarbons = -24‰) and have a closer affinity with the Permian source rock facies.

8.2.2 Reservoir rocks and seals

The Middle Triassic Showgrounds Sandstone and the Early Jurassic Precipice and Boxvale Sandstones are the main reservoir rocks in the region (Fig. 8.2). These reservoirs are effectively sealed by impermeable, fine-grained sediments of the Snake Creek Mudstone and Evergreen Formation, respectively (Fig. 8.2). Other minor reservoir units include Carboniferous-Lower Permian fractured basement, tuffaceous sandstone of the Upper Permian BWG, the Middle Jurassic Hutton Sandstone and the Late Jurassic Injune Creek Group. Generally speaking, the western margin of the trough possesses reservoirs of high quality whereas widespread diagenetic modifications have reduced the porosity and permeability of reservoirs on the eastern side of the trough (Hawkins et al., 1992).

8.2.3 Traps

Hydrocarbon accumulations discovered in the region occur in stratigraphic and structural traps. An example of a hydrocarbon field in a stratigraphic trap is the Fairymount oil field, reservoired in the Showgrounds Sandstone (Elliott and Brown, 1989). The majority of the structural traps were formed by Late Triassic folding and faulting (e.g.

Kincora, and Silver Springs gas fields) (Elliott and Brown, 1989). In a few cases (e.g. Moonie oil field), there is evidence of Jurassic or Late Cretaceous reactivation of older structures.

8.3 Kinetic modelling of petroleum generation

8.3.1 Preview

The burial and thermal history of the source rock(s) within a basin must be reconstructed before any determination of the timing or amount of hydrocarbon genesis can be made (Fig. 8.4). By relating the onset of hydrocarbon generation to the timing of structural development, migration pathways can be delineated and the observed distribution of oil and gas in the region explained (e.g. Waples, 1994). Hydrocarbon formation in a basin is controlled by the kinetic properties and thermal histories of its source rock kerogens (e.g. Dahl and Augustson, 1993; Zhao and Lerche, 1993). Having constrained time and temperature (obtained from our thermal history reconstruction), use of laboratory-derived kinetics can then provide more accurate estimates of both the timing and extent of hydrocarbon generation in petroleum systems (Fig. 8.4).

Two types of kinetic analysis have been used in modelling hydrocarbon generation. A *bulk kinetics* approach describes the generation of total hydrocarbons (gas + oil) from kerogen (Tissot et al., 1987; Burnham and Sweeney, 1991), whereas a *compositional kinetics* model subdivides the hydrocarbon products into several groups (namely, C_1, C_2-C_5, C_6-C_{14} and C_{15+}: Ungerer et al., 1988; Forbes et al., 1991). Both kinetic models assume the process of hydrocarbon generation from kerogen to be a series of parallel first-order reactions, either based on discrete or continuous (usually Gaussian) distributions of activation energies (see Ungerer, 1993 for a review). Kerogens having different kinetics will respond differently to a given thermal history (e.g. Tissot and Welte, 1984). In other words, different types of organic matter require different burial and thermal conditions to reach the onset of petroleum generation (Tissot et al., 1987). This is basically due to the wide spectrum of activation energies (40 to 80 kcal/mol: Ungerer et al., 1986; Ungerer and Pelet, 1987) attributed to naturally-occurring kerogens. All basin-modelling software programs supply a basic set of at least three default kerogen types with their appropriate activation energy distributions for the chemical kinetics. Type II kerogens (particularly if sulphur-rich) have the lowest activation energies, and Type I kerogens the highest (e.g. Tissot and Welte, 1984; Burnham et al., 1987). Ideally, however, the kinetic parameters of the particular kerogen of interest should always be used (Comer, 1992; Espitalie et al., 1993; Waples, 1994).

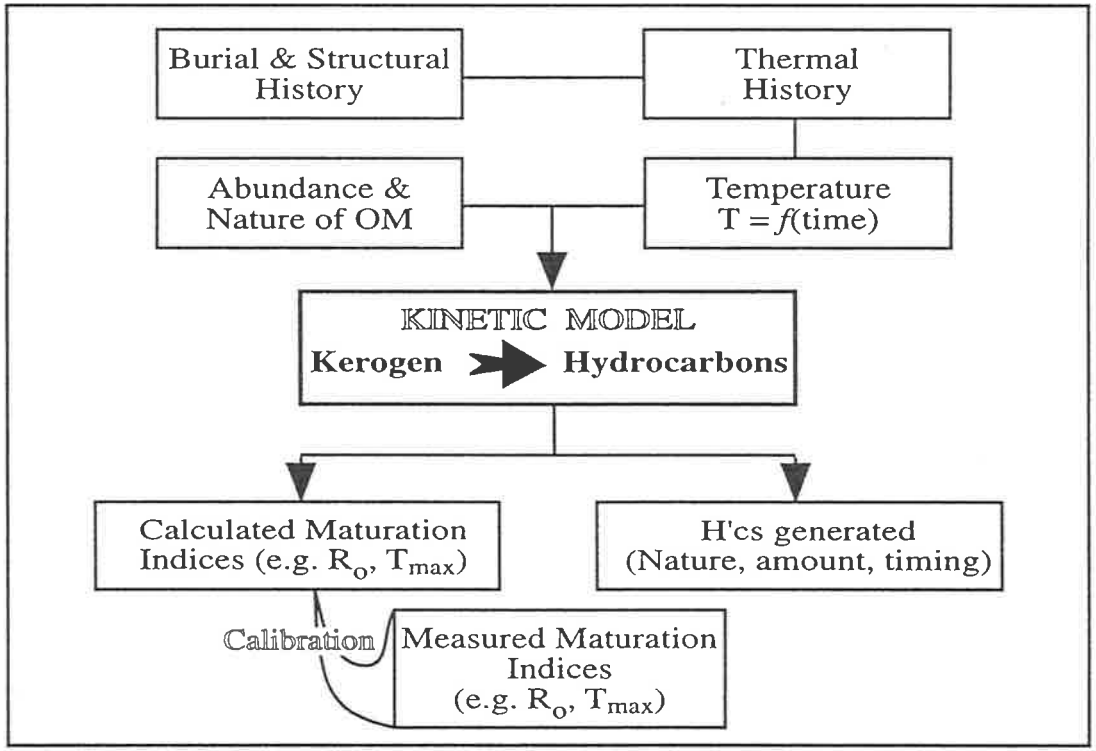

Figure 8.4 Inputs and outputs of the kinetic modelling of hydrocarbon generation (modified after Tissot et al., 1987).

8.3.2 Materials and methods

Oil-prone (liptinite-rich) and gas/condensate-prone (vitrinite-rich) mudstones, representative of the two end-member Triassic SCM organic facies and two Permian source rock samples were subjected to the kinetic analysis, as outlined in Section 3.3.11. The liptinite-rich samples will be referred to as organic Facies A and the vitrinite-rich ones as Facies C. Geological, lithological, lithostratigraphic (formation tops, thicknesses and ages), geothermal and vitrinite reflectance data were obtained from the Queensland Petroleum Exploration Database (QPED) and well completion reports. Subsidence modelling and kerogen conversion kinetics were used to model source rock maturation in the Taroom Trough using a commercially available computer program (BasinMod® version 4.2, Platte River Associates) at the National Centre for Petroleum Geology and Geophysics (Adelaide). This software incorporates the Lawrence Livermore National Laboratory (LLNL) program for kerogen conversion kinetics. The EASY%R_O-method was used to calculate vitrinite reflectance. The measured vitrinite reflectance data were then matched to calculated reflectance profiles, and were also compared to other independent maturity indicators, such as Rock-Eval T_{max}, production index (PI) and C_{29} sterane 20S/(20S+20R) ratio.

8.3.3 Results and data handling

The kinetics of bulk petroleum generation from the Permian facies and Triassic SCM organic facies were determined from a series of non-isothermal reactions of different durations (Table 8.1) following methods developed by Braun and Burnham (1987) and Burnham et al. (1987, 1988). These methods, widely employed for the determination of source rock kinetics, model kerogen decomposition using a set of parallel first-order reactions with a range of activation energies E and a common pre-exponential (frequency) factor A (Table 8.1). These chemical reactions are expressed in terms of the rate laws and the Arrhenius equation. The first-order rate law describes the dependence of reaction rate on the concentration of the starting material (kerogen), as shown by the following equation:

$$dC/dt = -kC \quad \text{.....(1)}$$

where C is the initial concentration of kerogen, t is time and k is the rate constant. The temperature dependence of the rate constant is defined by the empirical Arrhenius equation:

$$k = Ae^{-(E/RT)} \quad \text{.....(2)}$$

where k is the rate constant, A is the frequency factor, E is the activation energy, R is the gas constant (1.987 calories/mole/degree Kelvin), and T is the absolute temperature (°K). For a kinetic model using a set of n parallel first-order reactions, the n+1 variables

Table 8.1 Kinetic parameters determined for bulk generation of hydrocarbons from the Snake Creek Mudstone and Permian kerogens using discrete model, listed along with LLNL kinetics for the three standard kerogen types

	SCM Kerogen		Permian Kerogen		LLNL Model		
E (*kcal/mol*)	Facies A	Facies C	Facies A	Facies C	Type I	Type II	Type III
44	-	-	0.56	-	-	-	-
46	-	-	0.66	-	-	-	-
47	-	-	0.21	-	-	-	-
48	-	-	0.68	-	-	-	4
49	0.09	-	0.46	-	7	5	-
50	-	1.35	0.94	-	-	20	14
51	-	-	0.97	-	-	50	-
52	-	-	0.78	-	-	20	32
53	-	-	3.94	-	90	5	-
54	-	-	1.02	1	3	-	17
55	-	-	14.28	-	-	-	-
56	77.98	-	15.12	-	-	-	13
57	-	-	17.61	2	-	-	-
58	2.12	84.01	7.15	2	-	-	-
59	12.67	-	7.42	15	-	-	-
60	-	7.37	4.52	12	-	-	10
61	2.15	3.60	5.43	16	-	-	-
62	2.21	-	2.24	6	-	-	-
63	-	-	4.76	11	-	-	-
64	2.78	-	-	5	-	-	7
65	-	3.67	5.40	6	-	-	-
66	-	-	-	5	-	-	-
67	-	-	-	4	-	-	-
68	-	-	6.04	3	-	-	3
69	-	-	-	3	-	-	-
70	-	-	-	1	-	-	-
71	-	-	-	4	-	-	-
74	-	-	-	4	-	-	-
Frequency Factor (*A*) (m.y.$^{-1}$)	1.1E28	2.1E28	1.2E29	2.1E29	1.6E27	9.5E26	5.1E26
Reaction Constants							
Primary oil potential*	143	44	144	47	650	350	50
Primary gas potential*	99	98	99	103	70	65	110
Bulk H'c potential*	242	142	243	150	720	415	160

Oil cracking parameters@

A = 1.0 x 10^{12} s^{-1} = 3.2 x 10^{25} m.y.$^{-1}$

E = 54 kcal/mol

Gas fraction (oil to gas cracking efficiency) = 50%

* (mg/g TOC)

E = Activation energy (kcal/mol)

Values for each kerogen are the 'generated product' in percent or the fraction of total potential at a given value of E.

@LLNL (Lawrence Livermore National Laboratory) kinetics for Type I, II and III kerogens are from Burnham and Sweeney (1991).

(n x activation energies and a universal frequency factor) are determined from best-fits of calculated and experimental reaction rates (or cumulative yields) of the product derived from a minimum of three linear heating rates differing by one or two orders of magnitude. For a more detailed discussion of kinetic modelling, the reader is referred to Comer (1992) and Ungerer (1990, 1993). Figure 8.5 shows the contrasting activation energy distributions of the Triassic and Permian organic facies, along with their measured universal frequency factors. The total generative potential (HI, oil plus gas) is equal to the sum of the reaction potential at each individual activation energy (this is shown in Figure 8.5 as a percentage of the total). Further, the kinetic model used here assigns to each individual reaction potential a constant oil-to-gas ratio equivalent to the 5:11 split for the standard Type III kerogen for the Permian and Triassic Facies C, whereas a ratio of 14:10 (a mixture of 30% Type II and 70% Type III kerogens) was attributed to the Facies A of the Permian and Triassic sediments (Table 8.1). However, this is an approximation since a higher gas-to-oil ratio would be expected for the higher activation energies.

8.3.3.1 Chemical kinetics of hydrocarbon generation from the Triassic SCM organic facies

Both of the SCM organic facies (Figs. 5a and b) generate most oil at a single principal activation energy with minor contributions from five or six other reactions (Table 8.1). The principal activation energy of the vitrinitic kerogen (58 kcal/mol) accounts for 84% of its decomposition reactions, whereas that of the liptinite-rich kerogen (56 kcal/mol) is only slightly lower and represents a similarly high proportion (78%) of its hydrocarbon product. The higher activation energy of the former facies, however, is partially offset by a 2-fold increase in its frequency factor, confirming the strong positive correlation between A and E (Ungerer, 1990, 1993). Although these SCM kerogens are classified as Type II/III (Facies A) and Type III (Facies C) on the basis of their Rock-Eval characteristics (Section 4.3.3), their kinetic parameters (E and A) exhibit a considerable departure from those of the standard kerogen types (Table 8.1). With a major contribution of oil at 56 kcal/mol, hydrocarbon generation from the SCM Facies A occurs at a slightly lower maturation level than is the case for Facies C which releases most of its hydrocarbons at an activation energy of 58 kcal/mol.

8.3.3.2 Chemical kinetics of hydrocarbon generation from the Permian organic facies

Two major liquids-prone organic facies are recognised in the Permian succession. Facies A is considered to be oil-prone with average HI's > 200 while Facies C is gas- and condensate-prone having 150 < HI< 200 (Carmichael and Boreham, 1996). The broader

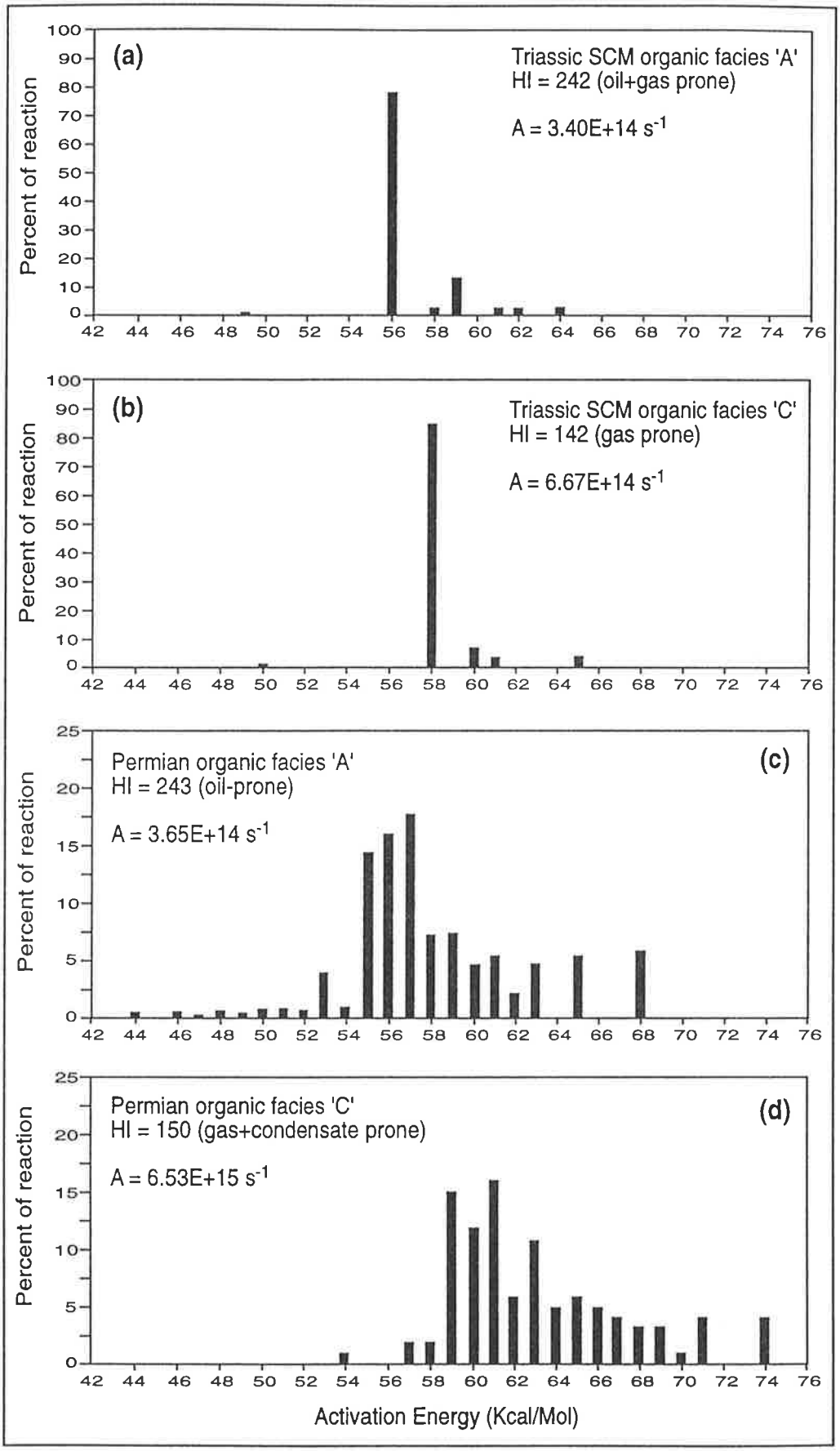

Figure 8.5 Activation energy distributions for kerogen decomposition and hydrocarbon generation from the Triassic Snake Creek Mudstone organic facies (a and b) and Permian source rock facies (c and d: Carmichael and Boreham, 1996).

spread of activation energies for the Permian source rock facies (Table 8.1, Fig. 8.5) results in markedly different hydrocarbon generative capabilities compared to the Triassic facies. Within the Permian source rocks, earlier generation from Facies A is clearly evident from its lower activation energies (range 44 - 68 kcal/mol for Facies A; *cf.* 54 - 74 kcal/mol for Facies C). More than half of Facies A kerogen was converted to hydrocarbons by reactions with activation energies between 44 and 57 kcal/mol, whereas over the same range of activation energies only 3% of Facies C kerogen was converted to hydrocarbons (Table 8.1, Fig. 8.5).

8.4 Application of thermal modelling to the southern Taroom Trough

Burial and thermal histories of the aforementioned Permian and Triassic source rocks were reconstructed for several well locations in the southern Taroom Trough. The wells chosen for modelling underwent different burial (and thermal) histories. The sections penetrated by Cabawin-1, Flinton-1 and Inglestone-1 represent the southern end of the trough, while those at Cockatoo Creek-1 and Burunga-1 reflect the maturation history of the northern part of the study area (Fig. 8.1).

8.4.1 Lithology and lithostratigraphy data

Lithologic and lithostratigraphic data for Inglestone-1 and Cockatoo Creek-1 are presented in Table 8.2. Petrophysical properties (compaction rates, thermal conductivities, and heat capacities) were calculated by the BasinMod program, based on the lithology mixes specified for each formation. As outlined earlier, two unconformities are evident; one between the Permo-Triassic Bowen Basin and the overlying Jurassic-Cretaceous Surat Basin and the other, a Late Cretaceous erosional surface. However, the nature of these unconformities (i.e. whether simply a hiatus or with associated uplift and erosion), and hence the amount of erosion involved, has proven difficult to establish (see below). Different burial history scenarios have been examined in trial-and-error comparisons of measured and calculated R_O, and the amounts of erosion shown in Table 8.2 represent the best-fit estimates.

8.4.2 Geothermal gradient

The corrected bottom-hole temperatures (BHT) for nine wells in the Taroom Trough are listed in Table 8.3. Present-day geothermal gradients are in the range 19-27°C/km. The present-day heat flow was calculated after the best fit was obtained between the

Table 8.2 (a) Stratigraphy and lithology data for the Inglestone-1 well

Formation	Event Name	Begin Age(Ma)	Formation Top (m)	Thickness (m)	Lithology (%)*				
					Sst	Slt	Shl	Lms	Kerogen
Cenozoic	Deposition	2	0	5.5					
-	Hiatus Tertiary	65	-	-					
-	Erosion Cretaceous	90	-	-1100					
-	Hiatus Cretaceous	95	-	-					
-	Dep. Cretaceous	102	-	1100					
Cretaceous	Deposition	144	5.5	981.5	10	25	55	9.7	0.3
Jurassic	Deposition	208	987	1280.1	55	34.5	10	0.1	0.4
-	Erosion Triassic	215	-	-50					
-	Hiatus Triassic	223	-	-					
-	Dep. Triassic	230	-	50					
Moolayember Fm	Deposition	234.5	2267.1	445.6	9	45	45	0.8	0.2
Snake Creek Mudstone	Deposition	237	2712.7	36.0	4.5	15	80	0.1	0.4
Rewan&Showgrounds	Deposition	245	2748.7	417.3	90	7.5	2.5	-	-
Blackwater Group	Deposition	250	3166	141.4	0.5	11.5	85	-	3
Back Creek Group	Deposition	276	3307.4	540.1	24	31	43.5	0.12	1.38
Basement	-	-	3847.5	-					

* Sst = Sandstone; Slt = Siltstone; Shl = Shale; Lms = Limestone

Table 8.2 (b) Stratigraphy and lithology data for the Cockatoo Creek-1 well

Formation	Event Name	Begin Age(Ma)	Formation Top (m)	Thickness (m)
-	Hiatus Cenozoic	65	-	-
-	Erosion Juras+Cretaceous	90	-	-2000
-	Hiatus Cretaceous	130	-	-
-	Dep. Juras+Cretaceous	185	-	2000
Evergreen	Deposition	189	5.4	98.2
Precipice Sst	Deposition	195	103.6	100.6
-	Erosion Triassic	215	-	-636
-	Hiatus Triassic	220	-	-
-	Dep. Moolayember	234.5	-	600
-	?Dep. SCM	237	-	36
Rewan Group	Deposition	245	204.2	807.8
Blackwater Group	Deposition	250	1012	1383.7
Back Creek Group	Deposition	280	2395.7	1287.3
Basement	-	-	3683	-

Table 8.3 Present-day geothermal and maturation gradients in wells in the southern Taroom Trough

Well Name	BHT (°C)	Total depth (m)	Geothermal gradient (°C/km)	Maturation gradient (%R_o/km)
Amoolee-1	-	-	-	0.15
Apple Tree-1	-	-	-	0.20
Bellbird-1	91.3	2620.0	27	0.26
Bengalla-1	-	-	-	0.34
Booberanna-1	66.7	2443.9	19	0.08
Burunga-1	82.8	3118.4	20	0.28
Cabawin-1	90.0	3588.7	20	0.15
Cockatoo Creek-1	108.0	3682.6	24	0.81
Dulacca-1	70.0	1968.4	25	0.15
Flinton-1	76.7	2780.7	20	0.18
Glenhaughton-1	86.7	2870.6	23	0.35
Inglestone-1	106.1	3869.0	22	0.27
Tiggrigie Creek-1	-	-	-	0.53

corrected BHT and calculated subsurface temperatures (based on the lithologies penetrated and their calculated thermal conductivities). The geothermal gradients are considered to be low (*cf.* Gretener, 1981). Modelling suggests that all units have experienced higher temperatures in the past. Comparison of the present-day geothermal gradients with the maturation gradients also indicates that the paleogeothermal gradient was higher in the northern part of the trough (represented here by Cockatoo Creek-1, Glenhaughton-1 and, to a lesser extent, Burunga-1). The increased paleotemperatures, accompanied by a higher paleogeothermal gradient, are likely to have been caused by uplift and erosion under a higher heat flow regime. There are two possible times when this could have occurred; Late Triassic and Late Cretaceous.

8.4.3 Vitrinite reflectance and maturation gradients

For all wells, a preliminary estimate of erosion was made by extrapolation of the maturation-depth profile above the present ground surface to an initial reference R_O value (0.2%: Dow, 1977). Although this method is not always valid (Gentzis and Goodarzi, 1991), it can give an estimated thickness of the eroded section. Application of this concept to wells in the Taroom Trough suggests a loss of section ranging from a few hundred metres in the south to about 2-3 km in the north at Cockatoo Creek-1 (Fig. 8.6) and Burunga-1 (Fig. 4.4). The maturation gradients range from 0.08 $\%R_O$/km in Booberanna-1 to 0.81 $\%R_O$/km in Cockatoo Creek-1 (Table 8.3) indicating that paleoheat flow varied across the study area. From the observed variation in maturation-depth profiles, it may be concluded that differential uplift and erosion has occurred across the basin. This has affected the thermal history of the southern Taroom Trough. Its influence on the timing of hydrocarbon generation in the southern and northern sectors of the trough is examined using more detailed modelling, illustrated in the following sections.

8.4.4 Modelling the northern part of the study area

Coalification in the northern part of the Taroom Trough has been the subject of much controversy (see Section 1.4.2 for discussion). Modelling of the burial and thermal histories of wells farther south (in the southern Taroom Trough) suggests a major Cretaceous event. This might have resulted solely from Cretaceous burial in the southern part of the study area (e.g. at Inglestone-1, Cabawin-1 and Flinton-1), or from a combination of Cretaceous burial and an increased heat flow farther north in the vicinity of Cockatoo Creek-1 and Burunga-1. This conclusion is consistent with apatite-fission-track-annealing studies (Marshallsea, 1988; Raza et al., 1995) which concluded

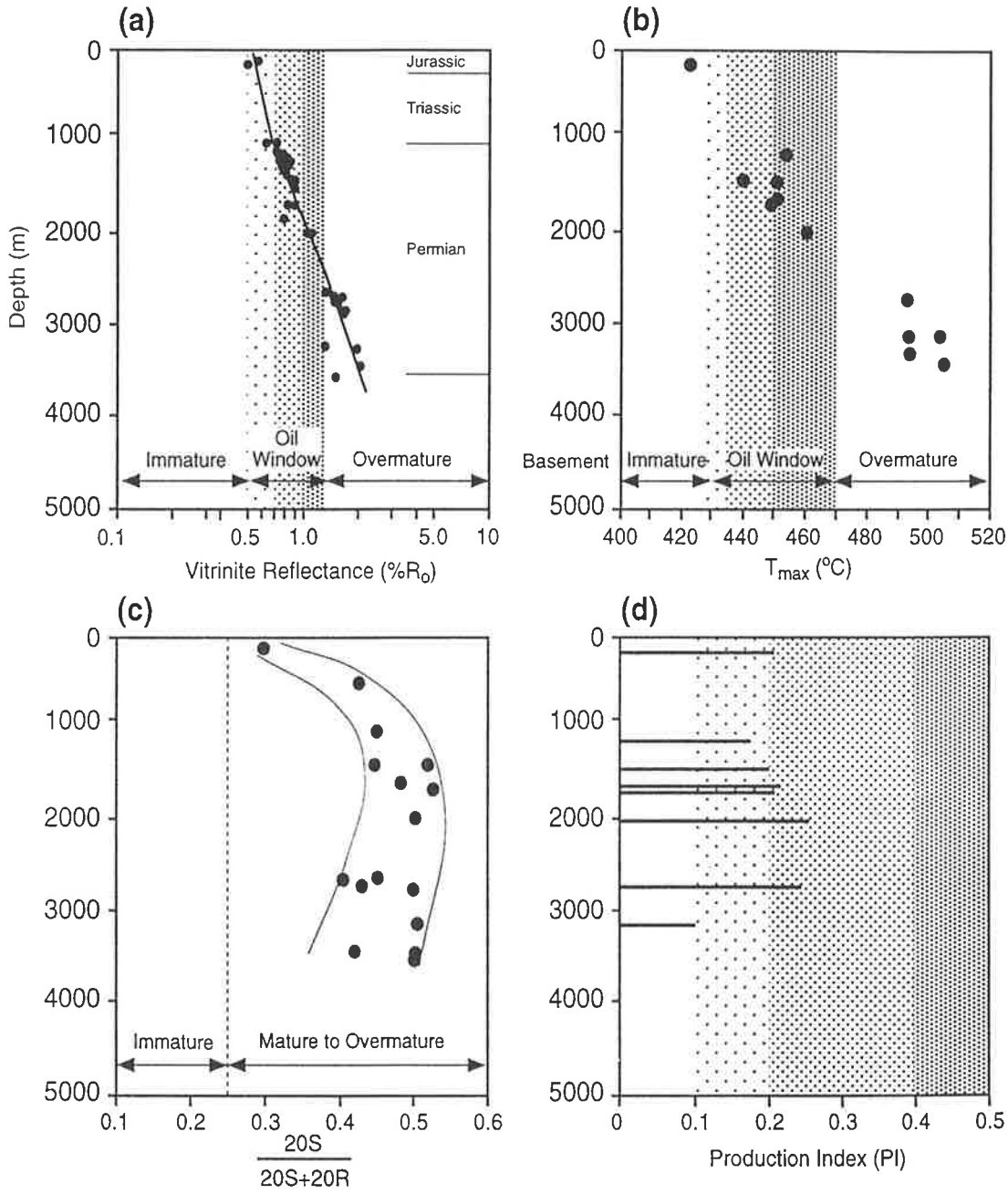

Figure 8.6 Measured maturity data integrated to constrain the burial and thermal histories in Cockatoo Creek-1. Near-mature to mature signatures [(a) R_O = 0.5-0.6%, (b) T_{max} = 425 °C, (c) 20S/(20S+20R) = 0.3, (d) PI = 0.21] for near-surface Jurassic sediments are consistent with a major erosional event during the Cretaceous. The continuous line in (a) is the vitrinite reflectance profile calculated using the EASY%R_O-method, whereas the solid circles are the measured R_O.

that the sediments in this area attained their maximum temperature during the Early Cretaceous. A high Permo-Triassic heat flow, first suggested by Beeston (1981, 1986), was probably also important. The vitrinite reflectance data, however, suggest that Cretaceous burial, with/or without higher heat flow, was the crucial factor which brought the sedimentary section to its maximum paleotemperature.

In the northern part of the study area, where the Bowen Basin is overlain by a very thin sequence of Surat Basin sediments, a combination of Triassic subsidence and uplift, followed by Jurassic subsidence and Cretaceous uplift was required to model the measured vitrinite reflectance data. Using the constraint of the present-day subsurface temperatures (palaeoheat flow = present-day heat flow = 37 mW/m^2), post-Early Cretaceous uplift and erosion of 1.5 to 2.0 km was needed to match the observed maturity in the Jurassic-Cretaceous section in Cockatoo Creek-1 and Burunga-1 (Figs. 8.7a and b). The Triassic unconformity represents an erosional loss less than, or equal to, that in the Cretaceous (see the different plausible scenarios in Figure 8.7a). Even an eroded section in excess of 4.0 km was insignificant to modelling the Permo-Triassic maturation gradient in Burunga-1, although Totterdell et al. (1992) suggested such a large thickness may have been present in this area based on the nearest non-eroded section immediately to the west. Other plausible, and possibly more realistic, alternatives to the 'Triassic erosion' scenario include: (1) rapid, deep Mesozoic subsidence followed by extensive Late Cretaceous erosion of about 3 km of sediments; and (2) a higher paleogeothermal gradient during the Permian and Triassic. A higher palaeogeothermal gradient might have been caused by elevated heat-flow, particularly during the Permian, and the fact that coal-shale lithologies have lower thermal conductivities than do the overlying sandy sediments. Thermal pulses may be assigned to major rift phases (McKenzie, 1978), after which the heat flow decays exponentially. However, Elliott (1993) disputes the initiation of the Taroom Trough during a rift phase. Clearly, there is a need for further evaluation of the proposed reconstructions.

The most realistic scenarios for modelling measured vitrinite reflectance data were: (1) post-Early Cretaceous uplift and erosion of about 3.0 km (within the additional constraints of a geothermal gradient unchanged from the present and a heat flow of about 37 mW/m^2); or (2) a Cretaceous heat flow pulse of about 45 mW/m^2 caused by igneous activity. This Cretaceous heating event can reduce the amount of post-Early Cretaceous erosion to less than 2.0 km. Both of these models assume that the maximum palaeotemperature was attained during the Cretaceous. In addition, the required Triassic event could have been either an hiatus or any amount of erosion less than, or equal to, the proposed Cretaceous erosion (scenarios 1, 2 and 3 in Figure 8.7a). Since the measured thermal indicators used in this study (R_O, T_{max}, %20S-sterane, and PI: Fig. 8.6, see also

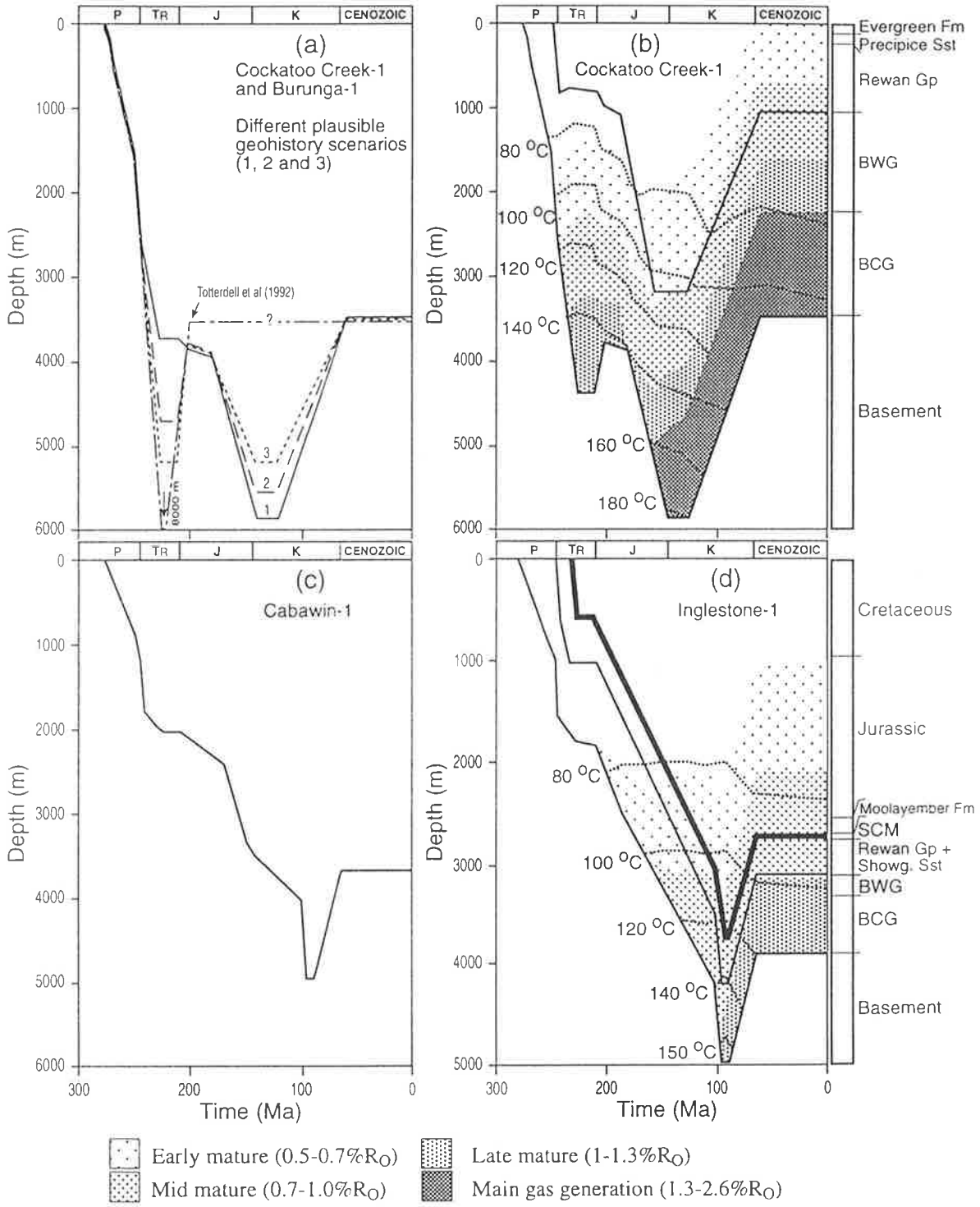

Figure 8.7 Burial and thermal history models of the southern Taroom Trough as represented by (a and b) Cockatoo Creek-1 in the north, and (c) Cabawin-1 and (d) Inglestone-1 in the south. Earlier generation (in the Triassic) is expected to have occurred in the north. Isotherms and maturation zones are shown in (b) and (d).

Figure 4.4) give the 'total thermal history', it was not possible to model the timing of the maximum palaeotemperature (whether Triassic or Cretaceous). However, all of these maturity parameters of the Jurassic sediments at the top of the well prove that a thermal event (higher paleotemperatures) occurred sometime post-Jurassic: firstly, because the outcropping, or near-surface, Jurassic remnants give near mature to mature signatures (R_O = 0.5-0.6%, T_{max} = 425°C, 20S/(20S+20R)-C_{29} sterane = 0.3, and PI = 0.21: Fig. 8.6) and, secondly, because there is no obvious break in the evolution of these parameters with depth (see also Figure 4.4).

8.4.5 Modelling the southern part of the study area

Cabawin-1 and Flinton-1

Maturation modelling of the Cabawin-1 well section by Hawkins et al. (1992, Fig. 15), which assumed no uplift or erosion throughout the burial history, resulted in a calculated vitrinite reflectance profile that plots well away from the measured one. Furthermore, the calculated vitrinite reflectance profile could not be matched with the measured data for any suggested amount of subsidence, uplift and erosion during the Triassic. A relatively uniform increase of reflectance with depth throughout the sequence suggests a stable heat flow since deposition. Finally, there is no evidence for initiation of the Taroom Trough during a rift phase (Elliott, 1993) which might otherwise have resulted in a higher heat flow. Modelling in Cabawin-1 (Fig. 8.7c) in the present study shows that the main event controlling the observed rank profile was Cretaceous burial. Subsidence and following Late Cretaceous uplift and erosion, with little or no Triassic uplift and erosion, were required to achieve a good match between the measured and calculated vitrinite reflectance. As a consequence, it is inferred that the basin fill in this area attained its maximum paleotemperature early in the Late Cretaceous (95-90 Ma).

The model for Flinton-1 (not shown) indicates a burial and thermal history very similar to that of the Cabawin-1 section. The Triassic unconformity in this area also proved to be no more than an hiatus which spanned the whole Late Triassic. Maximum burial temperatures (110-120°C for the SCM and 120-130°C for the Permian) were attained in the Late Cretaceous (95-90 Ma), about the time when the SCM entered the early mature phase of hydrocarbon generation (0.5-0.7% R_O). At present, this unit is mid-mature with a vitrinite reflectance value of 0.76%.

Inglestone-1

Different scenarios were able to provide a model fit of the geothermal history of this well section. Variable palaeoheat flow and different amounts of Triassic and Cretaceous erosion were adjusted to obtain a matching reflectance profile. However, the best fit necessitates either a Permo-Triassic heat flow (~39-40 mW/m^2) higher than the present-day heat flow (35 mW/m^2, calculated from BHT of 106.1°C: Table 8.3), or deep Mesozoic subsidence followed by Late Cretaceous (95-90 Ma) uplift and erosion of about 1.1 km of section (Fig. 8.7d). This yielded maximum palaeotemperatures of ~120-125°C for the SCM and of ~140-155°C for the Permian source rocks (Fig. 8.7d).

8.5 Implications for petroleum generation

The burial and thermal histories discussed above result in different hydrocarbon generation histories, and hence different prospectivities, for the southern and northern parts of the southern Taroom Trough.

8.5.1 Southern part of the study area

Cabawin-1

The Permian section at Cabawin-1 entered its early mature phase (0.5-0.7% R_O) in the latest Late Jurassic (150 Ma) and, since the latest Early Cretaceous (100 Ma), most of it has been in the middle of the oil window (0.70-1.0% R_O). The lowermost Back Creek Group is late mature (1.0-1.3% R_O). Oil and gas are currently produced from the Upper Permian BWG and gas is detected in the underlying fractured basement or Kuttung Formation (Fig. 8.2). Debate exists over whether the oil in this well originated in the BCG (Philp and Gilbert, 1986) or in some other Permian terrestrial source rocks (Boreham, 1995). Results presented in Chapter 4, together with other published data (Hawkins et al., 1992; Boreham; 1995; Carmichael and Boreham, 1996) suggest a mixed Type II/III kerogen in the BWG and Type III kerogen in the BCG. Therefore, the use of chemical kinetics of coal facies A (Table 8.1) for the former, and those of coal facies C for the latter, seems reasonable. When this is done, it is evident (Fig. 8.8) that the BWG kerogen has sourced the majority of the hydrocarbons in the Cabawin Field (about 211 mg h'c/g TOC, dominated by oil), whereas the contribution from the BCG kerogen was minor (70 mg h'c/g TOC, dominated by gas).

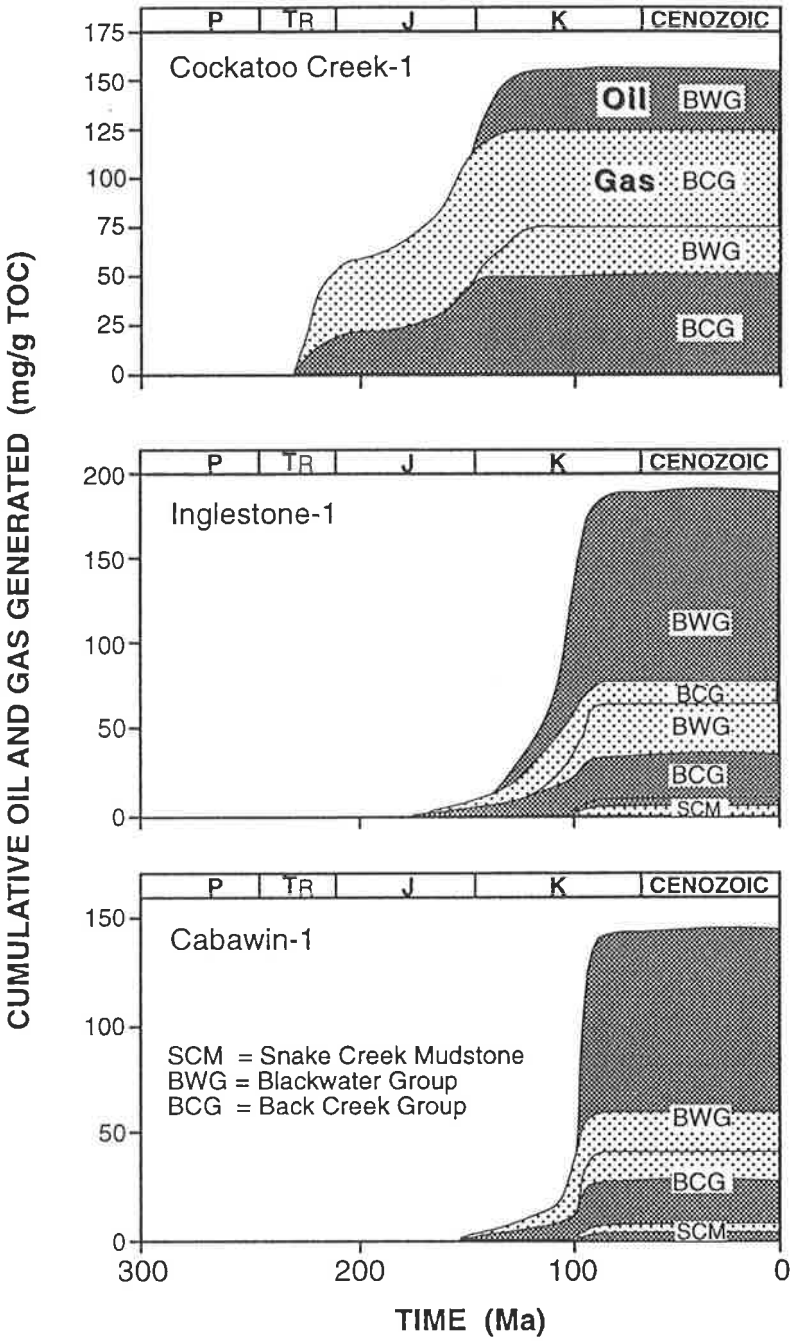

Figure 8.8 Cumulative hydrocarbon generation from Permo-Triassic source rocks different parts of the Taroom Trough. To simulate hydrocarbon generation from the Snake Creek Mudstone (SCM) in Inglestone-1 and Cabawin-1, measured kinetics for Facies A and Facies C, respectively, were applied. Kinetics measured on the Permian Facies A and Facies C were used for the Blackwater Group and Back Creek Group, respectively. No SCM is encountered in Cockatoo Creek-1 due to non-deposition or erosion.

The Moolayember Formation (including the SCM) has been in the early mature phase of its thermal evolution (0.67 $\%R_O$) since the latest Early Cretaceous. It has undergone no further maturation because of Late Cretaceous uplift and a Cenozoic hiatus. Nevertheless, this maturity level was sufficient for liptodetrinite and vitrinite (which are the dominant macerals in the SCM at this locality) to have started generating hydrocarbons. Based on Rock-Eval pyrolysis and petrographic observations, the SCM source rocks at Cabawin-1 contain Type III kerogen. A standard Type III kerogen is assumed (Burnham and Sweeney, 1991) to have an original hydrocarbon generative capacity of 160 mg h'c/ g TOC (Table 8.1). The hydrogen index of the SCM at Cabawin-1 is 120 mg h'c/g TOC (Table 4.1). Combining these data with the vitrinite reflectance of the unit (R_O = 0.67%) dictates that some of the labile kerogen fraction has already been converted to hydrocarbons. The production index (PI = 0.07) suggests only minor conversion, although expulsion of hydrocarbons into the associated sandstone beds (PI = 0.40) is evident. Minimal kerogen conversion (15 mg h'c/g TOC) is further indicated when using the kinetic parameters for standard Type III kerogen (Burnham and Sweeney, 1991). The amount of hydrocarbon generation was even less when the measured kinetics for this type of SCM kerogen (Facies C: Table 8.1) were used. In this case, only 10 mg h'c/g TOC (dominantly gas: Fig. 8.8, bottom) would have been generated. This represents only 5% of the original generative capacity and is probably not sufficient to form a commercially significant accumulation. Nevertheless, gas traces and shows which were detected in the Moolayember Formation and the overlying Precipice Sandstone and basal Evergreen Formation, may have been sourced partly by the SCM.

Inglestone-1

Because Inglestone-1 is located closer to the axis of the Taroom Trough, it is likely that the rate of sedimentation and subsidence in this locality was higher than that at Cabawin-1 or along the trough margins. Generation from Permo-Triassic source rocks began earlier, and the amounts of hydrocarbons generated were greater (Fig. 8.8, middle). Again, in the case of the Permian source rocks, the major contribution was from the Blackwater Group (255 mg h'c/g TOC, 75% of which is oil), with a lesser amount coming from the Back Creek Group (105 mg h'c/g TOC, dominated by gas).

To illustrate the effect of different chemical kinetics on the amount and type of hydrocarbon generation (oil *versus* gas) from the Snake Creek Mudstone, kerogens with different decompositional kinetics (Table 8.1) were compared when subjected to the same maturation history (Fig. 8.9). The SCM in this well contains mixed Type II/III kerogen of Facies A: Table 8.1). Use of default kinetics for the standard kerogens (Table

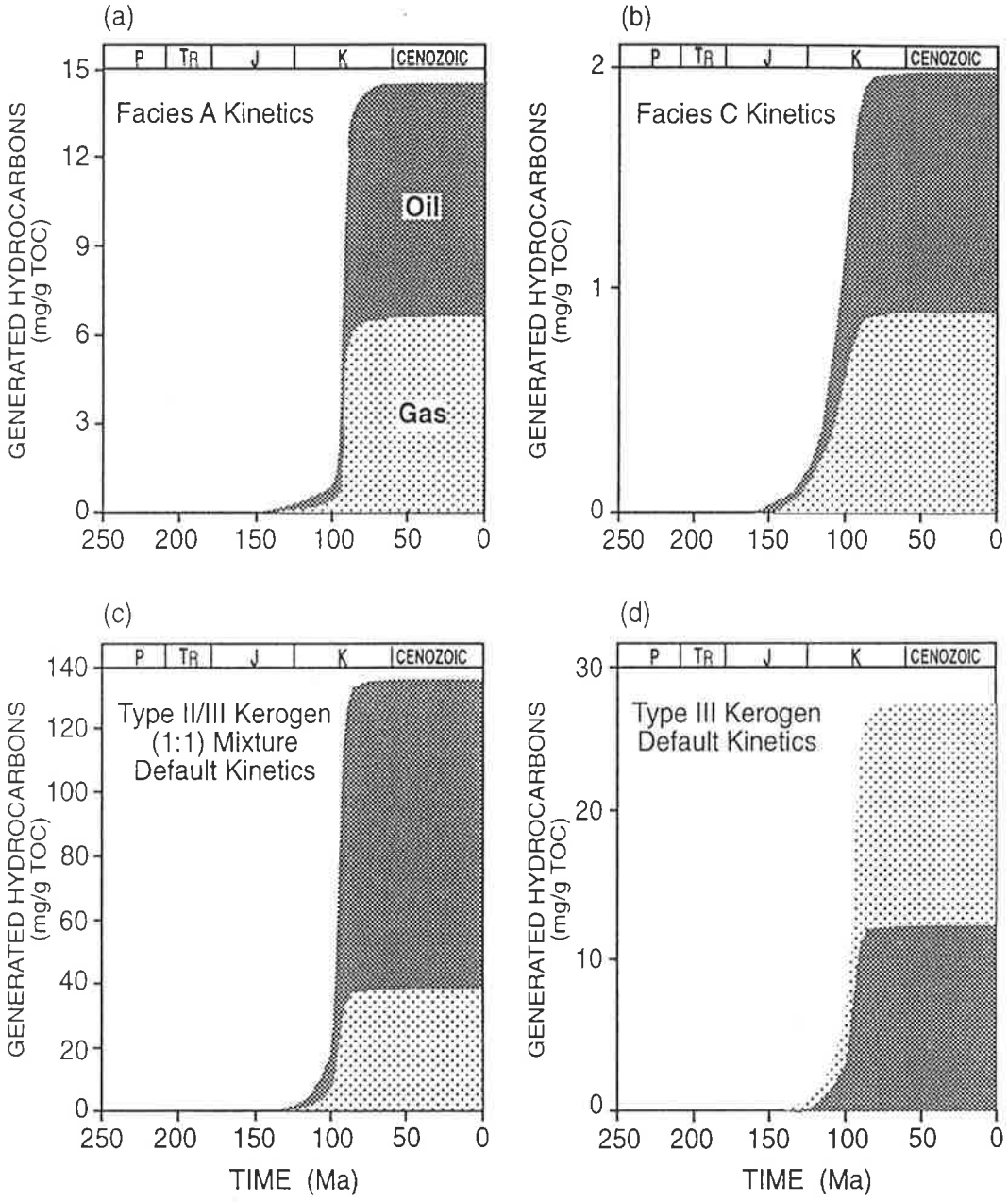

Figure 8.9 Comparison of the amount of hydrocarbons expected to have been generated from various Snake Creek kerogens when subjected to the same maturation history. Inglestone-1 is used as an example.

8.1) reveals considerable differences in the amount and type of product they generate (Figs. 8.9c and d). Type III kerogen gave about 40 mg h'c/g TOC (32% of which is oil), whereas Type II/III kerogen (30% Type II and 70% Type III) afforded a much higher hydrocarbon yield (172 mg/g TOC, of which 78% is oil).

By comparison with default kinetics, either end-member kerogens or combinations, the measured (or 'real') kinetics of SCM kerogens were less optimistic in their estimates of the amount of hydrocarbons generated. Under maturation conditions experienced by the Triassic section in Inglestone-1, generation of hydrocarbon from the SCM is minor, between 3 mg/g TOC (Facies C) and 21 mg/g TOC (Facies A). The latter amount (mainly oil) is about twice that generated from the same formation at Cabawin-1. This is partly due to the higher maturation level attained in Inglestone-1 (0.89% R_O versus 0.67% R_O in Cabawin-1) but mostly due to differences in kerogen type (Facies A in Inglestone-1 versus Facies C in Cabawin-1: Table 8.1). Hydrocarbons generated from the SCM in the vicinity of Inglestone-1, and in the deeper parts of the trough to the east (Figs. 8.1 and 8.3) where the SCM is expected to have attained higher maturity, most likely migrated updip to the west and northwest and contributed to the oil and gas currently produced from the Roswin North, Merroombile and Rednook fields (Fig. 8.3).

8.5.2 Northern part of the study area

The burial and thermal histories postulated for Cockatoo Creek-1 and Burunga-1 in the northern part of the study area suggest that the Permian source rocks started to generate hydrocarbons earlier (in the Triassic) than those in the southernmost part of the Taroom Trough (Figs. 8.7 and 8.8). Considerable amounts of hydrocarbons (400 mg/g TOC: Fig. 8.8, top) were generated from the Permian source rocks, about half of them by end of the Triassic when palaeotemperatures of 120-150°C (equivalent to the oil window: Mackenzie and Quigley, 1988) had been attained. In the Late Jurassic-Cretaceous, much of the Permian section entered the gas generation zone at temperatures in the range 150-180°C. Any hydrocarbons retained in the source rock would have been converted to gas and inert residue. This left an essentially exhausted overmature Permian section now able to generate only dry gas. Most of the BCG in Cockatoo Creek-1, where gas (predominantly methane) and water were recovered in DST 3 and 4, is now within the gas window. At Burunga-1, the BCG started generating hydrocarbons 230 Ma ago in the Middle Triassic. It is currently in the late mature stage, generating mainly gas and minor oil. This scenario is consistent with production index and other geochemical data from the same well (Fig. 4.4). For example, high T_{max} values (> 470°C) suggest that only gas is being generated over a major part of the BCG, with oil generation only from its uppermost part and from the overlying Gyranda Formation.

The expulsion of oil and gas from the BCG can be seen from the decreasing content of free hydrocarbons (and, hence, decreasing production index) at present-day depths >2100m (Fig. 4.4). This is probably caused by thermal cracking of locally-generated hydrocarbons to lighter fractions and gas, and their subsequent expulsion from the sandy matrix. The SCM is not encountered in Cockatoo Creek-1 and Burunga-1 due to non-deposition or erosion. A hypothetical SCM, here, may not have had enough time at the maximum temperature to reach the onset of hydrocarbon generation.

Hydrocarbon generation in this part of the trough predated the timing of the main deformational event (Triassic). Therefore, the considerable volumes of hydrocarbons generated in the north have, most likely, seeped to the surface or migrated updip to the south and west. A southward migration is compatible with a southerly increase in the liquids content of the gas and the findings of Philp and Gilbert (1986), based on migration-sensitive biomarkers, that oils in the southern part of the basin have migrated longer distances than those in the northern part. Further, a westerly migration direction is consistent with a decrease in oil maturity towards the margin of the basin (Boreham, 1995).

8.6 Summary

All units in the southern Taroom Trough attained maximum palaeotemperatures during the Late Cretaceous. These may have resulted solely from Cretaceous burial (in the south), or from a combination of Cretaceous burial and increased heat flow (in the north). The Cretaceous event could be interpreted as an erosional loss of 1.5 to 2 km of section, with/or without increased heat flow. Uplift and erosion has resulted in variable periods of maturation and thus different prospectivities along the Taroom Trough. In the southern part of the trough, the Triassic Snake Creek Mudstone entered the oil window in the latest Early Cretaceous, whereas the Permian Back Creek and Blackwater Groups started generating hydrocarbons during the Jurassic. These hydrocarbons migrated updip to the east and west where structural-stratigraphic traps had formed in response to Triassic compressional deformation. Kinetic modelling supports biomarker and other geochemical evidence that the oil and gas currently produced from the Bowen/Surat Basin reservoirs were sourced mainly from the Upper Permian BWG coal and carbonaceous shale facies, with lesser contributions from the BCG and SCM. Hydrocarbon outputs by the liptinite-rich Facies A of the SCM were slightly higher compared with the vitrinite-rich Facies C, although both were minor overall and probably not sufficient to form a commercially significant accumulation. In the north of the study area, early (Triassic) generation of hydrocarbons and subsequent (Jurassic-Cretaceous) burial resulted in an overmature Permian section able to generate only dry

gas. The bulk of its hydrocarbons have, most likely, seeped to the surface or migrated to the south and west where they are now mixed with a later hydrocarbon charge to form the oil and gas reserves of the southern Taroom Trough.

In conclusion, two petroleum systems were identified in the southern Taroom Trough. The Blackwater-Precipice petroleum system (Permian source) is of wide areal and stratigraphic extent. It includes the source rocks of the Back Creek and Blackwater Groups, which are mature to overmature throughout much of the Taroom Trough, and all related hydrocarbons produced from reservoirs of Permian to Jurassic age along the southeastern and southwestern margins of the trough. The SCM-Showgrounds petroleum system, on the other hand, involves Triassic source and reservoir rocks in a very localised area of the southwestern part of the trough. It encompasses the Roswin North, Rednook and Merroombile petroleum pools (reservoired in the Showgrounds Sandstone), and the Snake Creek Mudstone source rock in the vicinity of Inglestone-1 and the adjacent deeper parts of the trough. Elsewhere, the SCM is unlikely to have reached peak oil generation prior to the development of traps.

High prospectivity is indicated for the southern region where generation and migration of hydrocarbons (Jurassic-Cretaceous) post-dated trap formation (Triassic), as illustrated in the events chart for the Taroom Trough petroleum systems (Fig. 8.10). In the north, the bulk of generated hydrocarbons were expelled before the main deformation. Therefore, the considerable volumes of hydrocarbons generated in the north either seeped to the surface or migrated updip to the south and west (Al-Arouri et al., 1997b). Biomarker and gas compositional data suggest long migration distances for the petroleum reservoired on the basin margins.

The amounts of hydrocarbons estimated to have been generated from the Permo-Triassic source rocks of the Taroom Trough are exaggerated when 'default' kinetics are used instead of 'real' or measured source rock kinetics. These observations demonstrate the danger of using default kinetics for standard kerogen types to determine the quantity and type of hydrocarbon generation. Such estimates are, at best, only semi-quantitative.

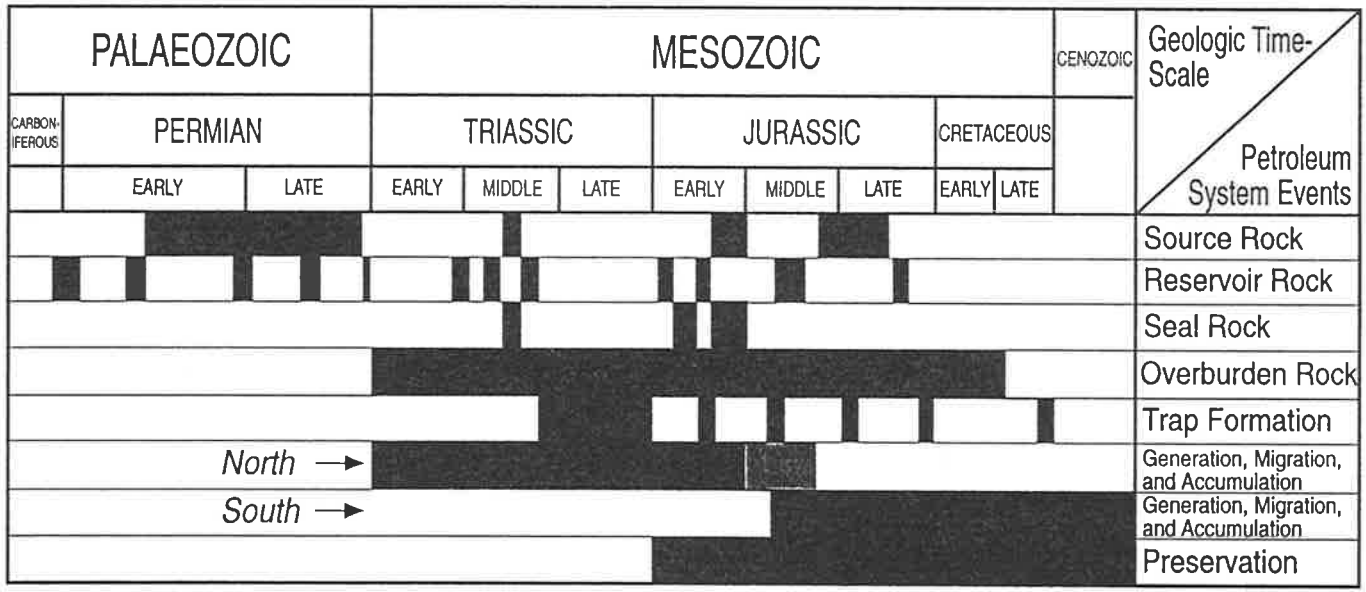

Figure 8.10 The Taroom Trough petroleum systems events chart showing the temporal relationship of their elements and processes. High prospectivity is exhibited by the southern region where generation and migration post-dated the timing of Triassic trap formation, whereas considerable amounts of hydrocarbons were generated in the north before the traps were formed. The hatched area indicates when gas was the only product.

CHAPTER NINE

CONCLUSIONS

The aims of the present study were to explain the observed distribution of oil and gas throughout the southern Taroom Trough, and to delineate those areas most prospective for further discoveries. Assessment of the relative contributions of Permian and Triassic source rocks to the oil reserves of the trough was based on an extensive organic geochemical investigation of liquid hydrocarbons and Permian (Back Creek Group, BCG; and Blackwater Group, BWG) and Triassic (Snake Creek Mudstone, SCM) source rocks. Oil-oil and oil-source correlations allowed different oil families and potential source rocks to be identified. These correlations were then complemented by modelling of the thermal history and a rigorous kinetic treatment of petroleum formation from Permian and Triassic organic facies in order to predict the timing and amount of hydrocarbon generation. The following are the principal conclusions of this investigation.

The Permian source rocks lie within the oil generation window over the major part of the southern Taroom Trough and are currently overmature in the north of the study area. The BCG is predominantly gas-prone. The upper part of the Permian section (BWG) offers better quality source rock with very good potential for oil and gas. These source rocks have appropriate maturity for hydrocarbon generation over the major part of the region. Carbonaceous shales in the lower part of the Permian BCG contain molecular evidence of marine incursions and suboxic to reducing conditions associated with increased salinity. The Permian coal-bearing BWG contains mainly land-plant remains deposited in a freshwater environment under predominantly oxic conditions.

A new effective source rock (the Triassic Snake Creek Mudstone) was identified. This rock unit was previously recognised only as a laterally-continuous seal which effectively forms a barrier to vertical migration from established Permian source rocks. The SCM comprises four main organic facies. These are (i) algal-rich Facies A, (ii) bacteria-rich Facies B, (iii) higher plant-rich Facies C, and (iv) mixed facies (AC or ABC). Most of the SCM source rocks appear to have been deposited under predominantly oxic conditions in a freshwater setting. A special subfacies of the algal-rich facies was deposited under brackish and less oxic conditions. These two lacustrine environments are distinguished by their diagnostic molecular fingerprints. The oxygenated freshwater setting was widely distributed and covers the major part of the southern Taroom Trough, whereas the brackish suboxic environment developed locally

in different parts of the basin (*viz.* around Teelba-1, Dulacca-1, Apple Tree-1 and Glenhaughton-1). An apparent marine influence on the Snake Creek palaeolake was detected only on the northwest (Glenhaughton-1, Muggleton-1) and southeast (Cabawin-1 and Flinton-1) margins of the southern Taroom Trough.

Two oil families were recognised within the set of oils analysed from the Taroom Trough. Family 1 includes the crude oils of Triassic source affinity that are produced from the Showgrounds Sandstone in the Roswin North and Rednook fields. Other Family 1 oils (Taylor-12A and Merroombile-1) may have a minor Triassic contribution. Facies A and Facies AC are the most likely source rocks within the SCM. These facies have their best hydrocarbon generating potential, and an appropriate thermal maturity, in the southwestern part of the Taroom Trough. Active hydrocarbon generation and primary migration within the SCM is indicated by petrographic observations of oil haze and oil droplets, associated with exsudatinite, fluorinite and bituminite. Where juxtaposed with carrier and reservoir rocks, this source rock unit might have contributed to the oil found in the underlying Showgrounds Sandstone. Sealed-tube hydrous pyrolysis and compound-specific isotope analysis of different SCM organic facies suggest that oils expelled from these source rocks, at the maturity level attained, are likely to be derived almost entirely from their bitumens. On the other hand, the oils of Family 2, currently being produced from other fields in the area, are of Permian source affinity and most likely derived from carbonaceous shales of the Blackwater Group. Variations in the drimane distributions of different Permo-Triassic lithofacies suggest that abundant homodrimanes and methylhomodrimanes are a characteristic feature of calcareous mudstones deposited under less oxic, and probably more saline, conditions. The absence of this class of sesquiterpanes in the present suite of Taroom Trough oils and condensates precludes the calcareous facies from being their source.

Careful examination of the behaviour of a wide range of molecular fossils during artificial and natural maturation of the Taroom Trough source rocks revealed that biomarker maturity parameters can be affected by variations in kerogen type as well as mineralogy. The attainment of stereoisomeric equilibrium at C-16 in the tetracyclic diterpenoid phyllocladane ($16\beta/16\beta+16\alpha \sim 0.6$) occurs within the zone of dry gas generation and not during the early stages of oil generation, as was previously assumed.

Maximum palaeotemperatures were attained in the southern Taroom Trough during the Late Cretaceous as a result of deep burial (in the south), or a combination of Cretaceous (± Triassic) burial and increased heat flow (in the north). This differential uplift and erosion has resulted in different periods of maturation and thus different prospectivities along the Taroom Trough. In the southern part of the study area, the Triassic Snake Creek Mudstone entered the oil window in the latest Early Cretaceous, whereas the

Permian Back Creek and Blackwater Groups started generating hydrocarbons during the Jurassic. These hydrocarbons migrated updip to the east and west where structural-stratigraphic traps had formed in response to Triassic compressional deformation. Kinetic modelling supports biomarker and other geochemical evidence that the oil and gas currently produced from sandstone reservoirs were sourced mainly from the carbonaceous shales of the Upper Permian BWG, with lesser contributions from the same rock type in the BCG. Hydrocarbon output by the SCM was minor but sufficient to produce a second petroleum system. In the north of the study area, early (Triassic) generation of hydrocarbons and subsequent (Jurassic-Cretaceous) burial resulted in an overmature Permian section, at present able to generate only dry gas.

Based on these geochemical and thermal modelling studies, two petroleum systems can be identified in the southern Taroom Trough. The Blackwater-Precipice petroleum system is of wide areal and stratigraphic extent. It includes the source rocks of the Back Creek and Blackwater Groups, which are mature to overmature throughout much of the Taroom Trough, and all related hydrocarbons produced from reservoirs of Permian to Jurassic age along the southeastern and southwestern margins of the trough. The Triassic SCM-Showgrounds petroleum system, on the other hand, involves Triassic source and reservoir rocks in a very localised area of the southwestern part of the trough. It encompasses the Roswin North, Rednook and Merroombile petroleum pools (reservoired in the Showgrounds Sandstone), and the Snake Creek Mudstone source rock in the vicinity of Inglestone-1 and the adjacent deeper parts of the trough. Elsewhere, the SCM is unlikely to have reached peak oil generation prior to the development of traps.

High prospectivity is indicated for the southern region where generation and migration of hydrocarbons (Jurassic-Cretaceous) post-dated trap formation (Triassic), whereas in the north the bulk of generated hydrocarbons were expelled before the main deformation. Therefore, the considerable volumes of hydrocarbons generated in the north have, most likely, seeped to the surface. Only late expulsion products which subsequently migrated southwards could have contributed to the petroleum reserves of the region. Biomarker and gas compositional data suggest long migration distances for the petroleum reservoired on the basin margins.

REFERENCES

Abbott G. D., Bennett B. and Petch G. S. (1995) The thermal degradation of 5α(H)-cholestane during closed-system pyrolysis. *Geochimica et Cosmochimica Acta* **59**(11), 2259-2264.

Abbott G. D., Lewis C. and Maxwell J. (1984) Laboratory simulation studies of steroid aromatization and alkane isomerization. *Organic Geochemistry* **6**, 31-38.

Abbott G. D., Wang G., Eglinton T., Home A. and Petch G. (1990) The kinetics of sterane biological marker release and degradation processes during hydrous pyrolysis of vitrinite kerogen. *Geochimica et Cosmochimica Acta* **54**, 2451-61.

Al-Arouri K. (1992) Organic geochemistry and petroleum source rock evaluation of phosphorite-oil shale succession in Jordan. M.Sc. Thesis. Department of Geology and Mineralogy, University of Jordan, 216p.

Al-Arouri K., McKirdy D. M. and Boreham C. J. (1995a) Sesqui-, di- and tricyclic terpanes in Permian and Triassic oils, coals and mudstones from the Bowen Basin, Queensland. *Proceedings of the 1995 Australian Organic Geochemistry Conference*. University of Adelaide, Australia, p.27-28.

Al-Arouri K., McKirdy D. M. and Boreham C. J. (1995b) Artificial maturation of Snake Creek Mudstone source rocks and phyllocladane isomerisation. *Proceedings of the 1995 Australian Organic Geochemistry Conference*. University of Adelaide, Australia, p.34.

Al-Arouri K., McKirdy D. M. and Boreham C. J. (1997a) Oil-source correlations as a tool in identifying the petroleum systems of the southern Taroom Trough, Australia. *The 18th International Meeting on Organic Geochemistry*, Maastricht, The Netherlands (accepted).

Al-Arouri K., McKirdy D. M., Boreham C. J. and Lemon N. M. (1997b) Modelling of thermal maturation and hydrocarbon generation in petroleum systems of the southern Taroom Trough, Australia. *American Association of Petroleum Geologists Bulletin.* (accepted).

Alexander G., Hazai I., Grimalt J. and Albaiges J. (1987) Occurrence and transformation of phyllocladanes in the brown coals from the Nograd Basin, Hungary. *Geochimica et Cosmochimica Acta* **51**, 2065-2073.

Alexander R., Kagi R.I. and Woodhouse G. W. (1981) Geochemical correlation of Windalia oil and extracts of Winning Group (Cretaceous) potential source rocks, Barrow Sub-basin, Western Australia. *American Association of Petroleum Geologists Bulletin* **65**, 235-250.

Alexander R., Kagi R.I. and Sheppard P. N. (1983) Relative abundance of dimethylnaphthalene isomers in crude oils. *Journal of Chromatography* **267**, 367-372.

Alexander R., Kagi R.I. and Sheppard P. N. (1984a) 1,8-Dimethylnaphthalene as an indicator of petroleum maturity. *Nature* **308**, 442-443.

Alexander R., Noble R. A. and Kagi R.I. (1984b) Identification of some bicyclic alkanes in petroleum. *Organic Geochemistry* **6**, 63-70.

Alexander R., Kagi R. I., Rowland S. J., Sheppard P. N. and Chirila T. V. (1985) The effects of thermal maturity on distributions of dimethylnaphthalenes in some ancient sediments and petroleums. *Geochimica et Cosmochimica Acta* **49**, 385-395.

Alexander R., Noble R. A. and Kagi R. J. (1987) Fossil resin biomarkers and their application in oil to source rock correlation, Gippsland Basin, Australia. *Australian Petroleum Exploration Association Journal* **27**(1), 63-72.

Alexander R., Larcher A. V., Kagi R. I. and Price P. L. (1988) The use of plant-derived biomarkers for correlation of oils with source rocks in the Cooper/Eromanga Basin system, Australia. *Australian Petroleum Exploration Association Journal* **28**(1), 310-24.

Alexander R., Larcher A. V., Kagi R. I. and Price P. L. (1992) An oil-source correlation study using age specific plant-derived aromatic biomarkers. In: *Biological Markers in Sediments and Petroleum* (J. M. Moldowan et al., eds.). Prentice Hall, Englewood Cliffs. N.J., p. 201-221.

Allan J. and Douglas A. G. (1977) Variations in the content and distribution of *n*-alkanes in a series of carboniferous vitrinites and sporinites of bituminous rank. *Geochimica et Cosmochimica Acta* **41**, 1223-1230.

Appleton R. A., McCrindle R. and Overton K. H. (1970) Diterpanes from the leaves of *Cryptomeria japonica*. *Phytochemistry* **9**, 581.

Aquino Neto F. R., Trendel J. M., Restle A., Connan J. and Albrecht P. A. (1983) Occurrence and formation of tricyclic and tetracyclic terpanes in sediments and petroleums. In: *Advances in Organic Geochemistry 1981* (M. Bjoroy et al., eds.). J. Wiley and Sons, Chichester, p.659-676.

Bailey, N. J. L., Burwood, R., and Harriman, G. E. (1990) Application of pyrolyzate carbon isotope and biomarker technology to organofacies definition and oil correlation problems in North Sea basins. *Organic Geochemistry* **16**, 1157-1172.

Baskin D. K.and Peters K.E. (1992) Early generation characteristics of a sulphur-rich Monterey kerogen. *American Association of Petroleum Geologists Bulletin* **76**, 1-13.

Beeston J. W. (1981) Coal rank variation in the Bowen Basin. *Geological Survey of Queensland*, Record 1981/48.

Beeston J. W. (1986) Coal rank variation in the Bowen Basin, Queensland. *International Journal of Coal Geology* **6**, 163-179.

Beeston J. W. (1987) Organic petrology of liptinites in the Denison Trough, Queensland. *Australian Petroleum Exploration Association Journal* **27**(1), 86-97.

Behar F. and Vandenbroucke M. (1987) Chemical modelling of kerogen. *Organic Geochemistry* **11**, 15-24.

Bird C. W., Lynch J. M., Pirt F. J., Reid W. W., Brooks C. J. W. and Middleditch B. S. (1971) Steroids and squalene in *Methylococcus capsulatus* grown on methane. *Nature* **230**, 473.

Bisseret P., Zundel M. and Rohmer M. (1985) Prokaryotic triterpenoids. 2: 2β-Methylhopan-oids from *Methylobacterium organophilum* and *Nostoc muscorum*, a new series of prokaryotic triterpenoids. *European Journal of Biochemistry* **150**, 29-34.

Bjoroy M., Mork A. and Vigran J. O. (1983) Organic geochemical studies of the Devonian to Triassic succession on Bjornoya and the implications for the Barent Shelf. In: *Advances in Organic Geochemistry 1981* (M. Bjoroy et al., eds.). J. Wiley and Sons, New York, p.49-59.

Blackburn K. B. (1936) Botryococcus and the algal coals. Part 1. A reinvestigation of the alga *Botryococcus Braunii* Kutzing. *Transactions of the Royal Society of Edinburgh* **58**, 841-854.

Boreham C. J. (1994) Origin of petroleum in the Bowen and Surat Basins: implications for source, maturation and migration. Canberra, AGSO record 1994/42.

Boreham, C. J. (1995) Origin of petroleum in the Bowen and Surat Basins: Geochemistry Revisited. *Australian Petroleum Exploration Association Journal* **35**(1), 579-612.

Boreham C. J. and Powell T. G. (1991) Variations in pyrolysate composition of sediments from the Jurassic Walloon Coal Measures, eastern Australia as a function of thermal maturation. *Organic Geochemistry* **17**(6), 723-733.

Boreham C. J. and Powell T. G. (1994) Petroleum source rock potential of coal and associated sediments: Qualitative and Quantitative Aspects. In: *Hydrocarbons from Coal* (B. E. Law and D. D. Rice, eds.). *AAPG Studies in Geology #38*, p.133-157.

Boreham C. J. Crick I. H. and Powell T. G. (1988) Alternative calibration of the methylphenanthrene index against vitrinite reflectance: Application to maturity measurements on oils and sediments. *Organic Geochemistry* **12**, 289-294.

Boreham C. J., Summons R. E., Roksandic Z., Dowling L. M. and Hutton A. C. (1994) Chemical, molecular and isotopic differentiation of organic facies in the Tertiary lacustrine Duaringa oil shale deposit, Queensland, Australia. *Organic Geochemistry* **21**(6/7), 685-712.

Boreham C. J., Dowling L. M. and Murray A. P. (1995) Biodegradation and maturity influence on *n*-alkane isotopic profiles in terrigenous sequences. In: *Organic Geochemistry: Developments and Applications to Energy, Environment and Human History* (J. O. Grimalt and C. Dorronsoro, eds.). Selected papers

from the 17th International Meeting on Organic Geochemistry 4th-8th September 1995, Donostia-San Sebastian, The Basque Country, Spain. Graphycems S.A., p.539-541.

Brassell S. C. (1992) Biomarkers in sediments, sedimentary rocks and petroleums: Biological origin, geological fate and applications (L. M. Pratt et al., eds.). *SEPM Short Course 27*, p.29-72.

Braun R. L. and Burnham A. K. (1987) Analysis of chemical reaction kinetics using a distribution of activation energies and simpler models. *Energy and Fuels* **1**, 153-161.

Bray E. E. and Evans E. D. (1961) Distribution of *n*-paraffins as a clue to recognition of source beds. *Geochimica et Cosmochimica Acta* **22**, 2-15.

Brooks P. W. (1986) Unusual biological marker geochemistry of oils and possible source rocks, offshore Beaufort-Mackenzie Delta, Canada. In: *Advances in Organic Geochemistry 1985* (D. Leythaeuser and J. Rullkotter, eds.). Pergamon, p.401-406.

Budzinski H., Garrigues Ph., Connan J., Devillers J., Domine D., Radke M. and Oudin J. L. (1995) Alkylated phenanthrene distributions as maturity and origin indicators in crude oils and rock extracts. *Geochimica et Cosmochimica Acta* **59**, 2043-2056.

Burnham A. K. and Sweeney J. J. (1991) Modelling the maturation and migration of petroleum. In: *Source and Migration Processes and Evaluation Techniques* (R. K. Merrill, ed.). AAPG Treatise of Petroleum Geology, p.55-63.

Burnham A. K., Braun R. L., Gregg H. R. and Samoun A. M. (1987) Comparison of methods for measuring kerogen pyrolysis rates and fitting kinetic parameters. *Energy and Fuels* **1**, 452-458.

Burnham A. K., Braun R. L., Gregg H. R. and Samoun A. M. (1988) Further comparison of methods for measuring kerogen pyrolysis rates and fitting kinetic parameters. In: *Advances in Organic Geochemistry 1987, Part II* (L. Mattavelli and L. Novelli, eds.), *Organic Geochemistry* **13**, 839-845.

Burwood R., Comet P. J., Jacob L. and Paulet (1990) Organofacies variation control on hydrocarbon generation: A lower Congo Coastal Basin (Angola) case history. *Organic Geochemisry* **16**, 325-338.

Carmichael D. and Boreham C. J. (1996) Source-rock evaluation in the southern Taroom Trough. *Geological Survey of Queensland Special Issue* (in press).

Chicarelli M. I., Aquino Neto F. R. and Albrecht P. (1988) Occurrence of four stereoisomeric tricyclic terpanes series in immature Brazilian shales. *Geochimica et Cosmochimica Acta* **52**, 1955-1959.

Chosson P., Connan J., Dessort D. and Lanau C. (1992) In vitro biodegradation of steranes and terpanes: A clue to understanding geological situations. In:

Biological markers in sediments and petroleum (J. M. Moldowan et al., eds.). Prentice Hall, Englewood Cliffs, N. J., p.320-349.

Chung, H. M. and Sackett, W. M. (1979) Use of stable carbon isotope compositions of pyrolytically derived methane as maturity indices for carbonaceous materials. *Geochimica et Cosmochimica Acta* **43**, 1979-1988.

Clark J. P. and Philp R. P. (1989) Geochemical characterization of evaporite and carbonate depositional environments and correlation of associated crude oils in the Black Creek Basin, Alberta. *Canadian Petroleum Geologists Bulletin* **37**, 401-416.

Claypool G. E., Love A. H. and Maughan E. K. (1978) Organic geochemistry, incipient metamorphism, and oil generation in black shale members of Phosphoria Formation, Western Interior United States. *American Association of Petroleum Geologists Bulletin* **62**, 98-120.

Clayton J. L. (1994) Composition of crude oils generated from coals and coaly organic matter in Shales. In: *Hydrocarbons from Coal* (B. E. Law and D. D. Rice, eds.). AAPG Studies in Geology #38, p.185-201.

Clayton J. L. and King J. D. (1987) Effects of weathering on biological marker and aromatic hydrocarbon composition of organic matter in Phosphoria shale outcrop. *Geochimica et Cosmochimica Acta* **51**, 2153-2157.

Clayton J. L. and Swetland P. L. (1978) Subaerial weathering of sedimentary organic matter. *Geochimica et Cosmochimica Acta* **42**, 305-312.

Clayton J. L., Rice D. D. and Michael G. E. (1991) Oil-generating coals of the San Juan Basin, New Mexico and Colorado, U.S.A. *Organic Geochemistry* **17**, 735-42.

Collister J. W., Summons R. E., Lichtfouse E. and Hayes J. M. (1992) An isotopic biogeochemical study of the Green River Oil Shale. In: *Advances in Organic Geochemistry 1991* (C. B. Eckardt et al., eds.). Pergamon Press, Oxford, p.265-276.

Collister J. W., Lichtfouse E., Hieshima G. and Hayes J. M. (1994). Partial resolution of sources of *n*-alkanes in the saline portion of the Parachute Creek Member, Green River Formation (Piceance Creek Basin, Colorado). *Organic Geochemistry* **21**(6/7), 645-659.

Comer J. B. (1992) Thermal Alteration. In: *Geochemistry of organic matter in sediments and sedimentary rocks* (L. M. Pratt et al., eds.). SEPM Short Course 27, p.73-100.

Conkright, M. E. and Sackett, W. M. (1992) Stable carbon isotope changes during the maturation of organic matter. In: *Organic Matter: Productivity, Accumulation, and Preservation in Recent and Ancient Sediments* (J. K. Whelan and J. W. Farrington, eds.). Columbia University Press, New York, p.403-414.

Connan J. (1984) Biodegradation of crude oils in reservoirs. In: *Advances in Petroleum Geochemistry, Vol. 1* (J. Brooks and D. H. Welte, eds.). Academic Press, London, p.299-335.

Connan J., Restle A. and Albrecht P. (1980) Biodegradation of crude oil in the Aquitaine basin. *Physics and Chemistry of the Earth* **12**, 1-17.

Connan J., Bouroullec J., Dessort D. and Albrecht P. (1986) The microbial input in carbonate-anhydrite facies of a sabkha palaeoenvironment from Guatemala: A molecular approach. *Organic Geochemistry* **10**, 29-50.

Cook A. C. (1982) Organic facies in the Eromanga Basin. In: *Eromanga Basin Symposium, summary papers* (P. S. Moore and T. J. Mount, compilers). Geological Society of Australia and Petroleum Exploration Society of Australia, Adelaide, p.234-57.

Cook A. C. and Struckmeyer H. (1986) The role of coal as a source rock for oil. In: *Second South-Eastern Australia Oil Exploration Symposium* (R. C. Glenie, ed.). Petroleum Exploration Society of Australia, Australia, p.419-432.

Cosgrove J. L. and Mogg W. G. (1985) Recent exploration and hydrocarbon potential of the Roma Shelf, Queensland. *Australian Petroleum Exploration Association Journal* **25**, 216-234.

Cumbers K. M., Alexander R. and Kagi R. I. (1987) Methylbiphenyl, ethylbiphenyl and dimethylbiphenyl isomer distributions in some sediments and crude oils. *Geochimica et Cosmochimica Acta* **51**, 3105-3111.

Curiale J. A. (1994) Correlation of oils and source rocks- a conceptual historical perspective. In: *The Petroleum Systems-From Source to Trap* (L. B. Magoon, and W. G. Dow, eds.). AAPG Memoir 60, p.251-260.

Czochanska Z., Gilbert T. D., Philp R. P. Sheppard C. M., Weston R. J., Wood T. A. and Woolhouse A.D. (1988) Geochemical application of sterane and triterpane biomarkers to a description of oils from the Taranaki Basin in New Zealand. *Organic Geochemistry* **12**, 123-135.

Dahl B. and Augustson J. H. (1993) The influence of Tertiary and Quaternary sedimentation and erosion on hydrocarbon generation in Norwegian offshore basins. In: *Basin Modelling: Advances and Applications* (A. G. Dore et al., eds.). Elsevier, Amsterdam, p.419-432.

Dahl J., Moldowan J. M., McCaffrey M. A. and Lipton P. A. (1992) A new class of natural products revealed by 3β-alkyl steranes in petroleum. *Nature* **355**, 154-157.

Dahl J., Moldowan J. M., Teerman S. C., McCaffrey M. A., Sundararaman P. and Stelting C. E. (1994) Source rock quality determination from oil biomarkers I: A new geochemical technique. *American Association of Petroleum Geologists Bulletin* **78**, 1507-1528.

de Jersey N. J. and Allen R. J. (1966) Jurassic source for oil of the Surat-Bowen Basin, Queensland. *American Association of Petroleum Geologists Bulletin* **50**, 2479-2481.

Demaison G. and Huizinga B. J. (1991) Genetic classification of petroleum systems. *American Association of Petroleum Geologists Bulletin* **75**, 1626-1643.

Dembicki H., Meinschein W. G. and Hattin D. E. (1976) Possible ecological and environmental significance of the predominance of even-carbon number C_{20}-C_{30} *n*-alkanes. *Geochimica et Cosmochimica Acta* **40**, 203-208.

Devon T. K. and Scott A. I. (1972) *Handbook of Naturally Occurring Compounds. Vol. II. Terpanes*. Academic Press, New York, 576p.

Didyk B. M., Simoneit B. R. T., Brassell S. C. and Eglinton G. (1978) Organic geochemical indicators of palaeoenvironmental conditions of sedimentation. *Nature* **272**, 216-222.

Dimmler A., Cyr T.D. and Strausz O.P. (1984) Identification of bicyclic terpenoid hydrocarbons in the saturate fraction of Athabasca oil sand bitumen. *Organic Geochemistry* **7**, 231-238.

Dow W. G. (1977) Kerogen studies and geological interpretations. *Journal of Geochemical Exploration* **7**, 79-99.

Draper J. J. and Beeston J. W. (1985) Summary of the hydrocarbon potential of the Reids Dome Beds, Denison Trough. *Queensland Government Mining Journal* **86**, 246-251.

Duncan A. D. and Hamilton R. F. M. (1988) Palaeolimnology and organic geochemistry of the Middle Devonian in the Orcadian Basin. In: *Lacustrine Petroleum Source Rocks* (A. J. Fleet et al., eds.). Geological Society Special Publication No. 40, p.173-201.

Eglinton T. I. and Douglas A. G. (1988) Quantitative study of biomarker hydrocarbons released from kerogens during hydrous pyrolysis. *Energy and Fuels* **2**, 81-88.

Eglinton G. and Hamilton R. J. (1963) The distribution of *n*-alkanes. In: *Chemical Plant Taxonomy* (T. Swain, ed.). Academic Press, New York, p.187-196.

Elliott L. (1989) The Surat and Bowen Basins. *Australian Petroleum Exploration Association Journal* **29**(1), 398-416.

Elliott L. (1993) Post-Carboniferous tectonic evolution of eastern Australia. *Australian Petroleum Exploration Association Journal* **33**(1), 215-236.

Elliott L. and Brown R. S. (1989) The Surat and Bowen Basins- a historical review. In: *Petroleum in Australia: The first century*. Australian Petroleum Exploration Association, Melbourne, p.120-138.

Espitalie J., Marquis F. and Drouet S. (1993) Critical study of kinetic modelling parameters. In: *Basin Modelling: Advances and Applications* (A. G. Dore et al., eds.). Elsevier, Amsterdam, p.233-242.

Exon N. F. (1974) The geological evolution of the southern Taroom Trough and the overlying Surat Basin. *Australian Petroleum Exploration Association Journal* **14**, 50-58.

Exon N. F. (1976) Geology of the Surat Basin in Queensland. *Bureau of Mineral Resources*, Australia, Bulletin 166.

Faraj B. S. M. and Mackinnon D. R. (1993) Micrinite in Southern Hemisphere sub-bituminous and bituminous coals: redefined as fine grained kaolinite. *Organic Geochemistry* **20**(6), 823-841.

Faraj B. S. M., Fielding C. R. and Mackinnon D. R. (1996) Cleat mineralization of Upper Permian Baralaba/Rangal Coal Measures, Bowen Basin, Australia. In: *Coalbed Methane and Coal Geology* (R. Gayer and I. Harris, eds.). Geological Society Special Publication No.97, p.151-164.

Fielding C. R., Falkner A. J., Kassan J. and Draper J. J. (1990) Permian and Triassic depositional systems in the Bowen Basin. In: *Proceedings of the Bowen Basin Symposium, Mackay, 1990*. Geological Society of Australia, Queensland Division, p.21-25.

Forbes P. L., Ungerer P. M. Kuhfuss A. B. Riis F. and Eggen S. (1991) Compositional modelling of petroleum generation and expulsion: Trial application to a local mass balance in the Smorbukk Sorfield, Haltenbanken area, Norway. *American Association of Petroleum Geologists Bulletin* **75**, 873-893.

Forsberg A. and Bjoroy M. (1983) A sedimentological and organic geochemical study of the Botneheia Formation, Svalbard, with special emphasis on the effects of weathering on the organic matter in shales. In: *Advances in Organic Geochemistry 1981* (M. Bjoroy et al., eds.). J. Wiley and Sons, New York, p.60-68.

Francois R. (1987) A study of sulphur enrichment in the humic fraction of marine sediments during early diagenesis. *Geochimica et Cosmochimica Acta* **51**, 17-27.

Fu Jiamo, Sheng Guoying, Peng Pingan, Brassell S. C. Eglinton G. and Jigang J. (1986) Peculiarities of salt lake sediments as potential source rocks in China. *Organic Geochemistry* **10**, 119-126.

Fu Jiamo, Sheng Guoying, and Liu D. (1988) Organic and geochemical characeteristics of major types of terrestrial source rocks in China. In: *Lacustrine Petroleum Source Rocks* (A. J. Fleet et al., eds.). Geological Society Special Publication No. 40, Blackwell, Oxford, p.279-289.

Fu Jiamo, Sheng Guoying, Xu Jiayou, Eglinton G., Gowar A. P., Jia Rongfen, Fan Shanfa and Peng Pingan (1990) Application of biological markers in the assessment of paleoenvironments of Chinese non-marine sediments. *Organic Geochemistry* **16**, 769-779.

Galimov, E. M. (1973) *Carbon Isotopes in Oil-Gas Geology*. Nedra, Moscow, 384 p.; National Aeronautics and Space Administration, Washington D. C. [Translation from Russian], 395p.

Gallegos E. J. and Moldowan J. M. (1992) The effect of hold time on GC resolution and the effect of collision gas on mass spectra in geochemical 'biomarker' research. In: *Biological Markers in Sediments and Petroleum* (J. M. Moldowan et al., eds.). Prentice Hall, Englewood Cliffs, N. J., p.156-181.

Garrigues P. and Ewald M. (1983) Natural occurrence of 4-methyl-phenanthrene in petroleums and recent marine sediments. *Organic Geochemistry* **5**, 53-56.

Gentzis T. and Goodarzi F. (1991) Thermal maturity and hydrocarbon potential of the sedimentary succession from the Hecla field in Sverdrup Basin, Arctic Canada. *International Journal of Coal Geology* **19**, 483-517.

Golin V. and Smyth M. (1986) Depositional environments and hydrocarbon potential of the Evergreen Formation, ATP 145P, Surat Basin, Queensland. *Australian Petroleum Exploration Association Journal* **26**(1), 156-171.

Goodarzi F., Brooks P. W. and Embry A. F. (1989) Regional maturity as determined by organic petrography and geochemistry of the Schei Point Group (Triassic) in the western Sverdrup Basin, Canadian Arctic Archipelago. *Marine and Petroleum Geology* **1**, 290-302.

Goodwin N. S., Mann A. L. and Patience R. L. (1988) Structure and significance of C_{30} 4-methyl steranes in lacustrine shales and oils. *Organic Geochemistry* **12**, 495-506.

Grantham P. J. (1986) The occurrence of unusual C_{27} and C_{29} sterane predominances in two types of Oman crude oil. *Organic Geochemistry* **9**, 1-10.

Grantham P. J. and Wakefield L. L. (1988) Variations in the sterane carbon number distributions of marine source rock derived crude oils through geological time. *Organic Geochemistry* **12**, 61-73.

Grantham P. J., Posthuma J. and Baak A. (1980) Triterpanes in a number of Far-Eastern crude oils. In: *Advances in Organic Geochemistry 1981* (M. Bjoroy et al., eds.). J. Wiley and Sons, New York, p.675-683.

Gretener P. E. (1981) Geothermics: using temperature in hydrocarbon exploration. *American Association of Petroleum Geologists Education Course Note Series #17*. Tulsa.

Hammond R. L. (1987) The Bowen Basin, Queensland, Australia: an upper crustal extensional model for its early history. In: *16th BMR Research Symposium, Bureau of Mineral Resources Geology and Geophysics.* Record 1987/51, p.131-139.

Harrington H. J. and Korsch R. J. (1985) Deformation associated with the accretion of the Gympie Terrane in eastern Australia. In: *Third Circum-Pacific Terrane*

Conference, extended abstracts (E. C. Leitch, ed.). Geological Society of Australia, Abstract No. 14, p.104-108.

Hatcher P. G., Lerch H. E., Kotra P. K. and Szeverenyi N. M. (1988) Pyrolysis/gas chromatography/mass spectrometry of a series of degraded woods and coalified logs that increase in rank from peat to subbituminous coal. *Fuel* **67**, 1069-1075.

ten Haven H. L., De Leeuw J. W. and Schenck P. A. (1985) Organic geochemical studies of a Messinian evaporitic basin, northern Appenines (Italy). I: Hydrocarbon biological markers for a hypersaline environment. *Geochimica et Cosmochimica Acta* **49**, 2181-2191.

ten Haven H. L., De Leeuw J. W. Peakman T. M. and Maxwell J. R. (1986) Anomalies in steroid and hopanoid maturity indices. *Geochimica et Cosmochimica Acta* **50**, 853-855.

ten Haven H. L., De Leeuw J. W., Rullkotter J. and Sinninghe Damste J. S. (1987) Restricted utility of the pristane/phytane ratio as a palaeoenvironmental indicator. *Nature* **330**, 641-643.

ten Haven H. L., De Leeuw J. W., Sinninghe Damste J. S., Schenck P. A., Palmer S. E. and Zumberge J. E. (1988) Applications of biological markers in the recognition of palaeohypersaline environments. In: *Lacustrine Petroleum Source Rocks* (A. J. Fleet et al., eds.). Geological Society Special Publication No. 40, p.123-130.

Hawkins P. J., Jackson K. S. and Horvath Z. (1992) Regional geology, petroleum geology, and hydrocarbon potential of the southern Taroom Trough, Bowen Basin, Queensland. *Queensland Geology* **3**, 42p.

He Wei and Lu Songnian (1990) A new maturity parameter based on monoaromatic hopanoids. *Organic Geochemistry* **16**, 1007-1013.

Hoefs, J. and Frey, M. (1976) The isotopic composition of carbonaceous matter in metamorphic profile from the Swiss Alps. *Geochimica et Cosmochimica Acta* **40**, 945-951.

Hoering T. C. (1984) Thermal reaction of kerogen with added water, heavy water and pure organic substances. *Organic Geochemistry* **5**, 267-278.

Huang W. Y. and Meinschein W. G. (1979) Sterols as ecological indicators. *Geochimica et Cosmochimica Acta* **43**, 739-745.

Hughes W. B. (1984) Use of thiophenic organosulfur compounds in characterizing crude oils derived from carbonate versus siliciclastic sources. In: *Petroleum Geochemistry and Source Rock Potential of Carbonate Rocks* (J. G. Palacas, ed.). AAPG Studies in Geology #18, p.181-196.

Hughes W. B., Holba A. G., Miller D. E. and Richardson J. S. (1985) Geochemistry of greater Ekofisk crude oils. In: *Geochemistry in Exploration of the Norwegian Shelf* (B. M. Thomas, ed.). Graham and Trotman, p.75-92.

Hunt J. M. (1991) Generation of gas and oil from coal and other terrestrial organic matter. *Organic Geochem*istry **17**(6), 673-680.

Ishiwatari R., Ishiwatari M., Kaplan I. R. and Rohrback B. G. (1977) Thermal alteration experiments on organic matter from recent marine sediments in relation to petroleum genesis. *Geochimica et Cosmochimica Acta* **41**, 815-828.

Jackson K. S., Hawkins P. J. and Bennett A. J. R. (1980) Regional facies and geochemical evaluation of the southern Denison Trough, Queensland. *Australian Petroleum Exploration Association Journal* **20**(1), 143-158.

Kelts K. (1988) Environments of deposition of lacustrine petroleum source rocks: an introduction. In: *Lacustrine Petroleum Source Rocks* (A. J. Fleet et al., eds.). Geological Society Special Publication No. 40, p.3-26.

King J. D., Yang J. and Pu F. (1994) Thermal history of the periphery of the Junggar Basin, Northwestern China. *Organic Geochem*istry **21**(3/4), 393-405.

Kinghorn R. R. F. (1983) An introduction to the physics and chemistry of petroleum. J. Wiley and Sons, Chichester, 420p.

Kolaczkowska E., Slougue N. E., Watt D. S., Marcura R. E. and Moldowan J. M. (1990) Thermodynamic stability of various alkylated, dealkylated, and rearranged 17α- and 17β-hopane isomers using molecular mechanics calculations. *Organic Geochemistry* **16**, 1033-1038.

Korsch R. J., Wake-Dyster K. D. and Johnstone D. W. (1990) Deep seismic profiling across the Bowen Basin. In: *Proceedings of the Bowen Basin Symposium, Mackay, 1990.* Geological Society of Australia, Queensland Division, p.10-14.

Kvalheim O. M., Christy A. A., Telnaes N. and Bjorseth A. (1987) Maturity determination of organic matter in coals using the methylphenanthrene distribution. *Geochimica et Cosmochimica Acta* **51**, 1883-1888.

Levine J. R. (1987) Influence of coal composition on the generation and retention of coalbed natural gas. In: *Proceedings of the 1987 Coalbed Methane Symposium*, Tuscaloosa, Alabama, p.15-18.

Lewan, M. D. (1985) Evaluation of petroleum generation by hydrous pyrolysis experimentation. Philosophical Transactions of the Royal Society **315**(A), 123-134.

Lewan, M. D. (1986) Stable carbon isotopes of amrphous kerogens from Phanerozoic sedimentary rocks. *Geochimica et Cosmochimica Acta* **50**, 1583-1591.

Lewan M. D. (1994) Assessing natural oil expulsion from source rocks by laboratory pyrolysis. In: *The Petroleum Systems-From Source to Trap* (L. B. Magoon and W. G. Dow, eds.). AAPG Memoir 60, p.201-210.

Lewan M. D., Bjoroy M. and Dolcater D. L. (1986) Effects of thermal maturation on steroid hydrocarbons as determined by hydrous pyrolysis of Phosphoria Retort shale. *Geochimica et Cosmochimica Acta* **50**, 1977-1988.

Leythaeuser D. (1973) Effects of weathering on organic matter in shales. *Geochimica et Cosmochimica Acta* **37**, 113-120.

Leythaeuser D., Mackenzie A. S., Schaefer R. G. and Bjoroy M. (1984) A novel approach for recognition and quantification of hydrocarbon migration effects in shale-sandstone sequences. *American Association of Petroleum Geologists Bulletin* **68**, 196-219.

Limbach G. W. M. (1975) On the origin of petroleum. In: *Proceedings of the 9th World Petroleum Congress, Vol. 2.* Applied Science Publishers, London, p.357-369.

Livsey A., Douglas A. G. and Connan J. (1984) Diterpenoid hydrocarbons in sediments from an offshore (Labrador) well. *Organic Geochemistry* **6**, 73-81.

Luo Binjie, Yang Xinghua, Lin Hejie and Zheng Goudong (1988) Characteristics of Mesozoic and Cenozoic non-marine source rocks in north-west China. In: *Lacustrine Petroleum Source Rocks* (A. J. Fleet et al., eds). Geological Society Special Publication No. 40, p.291-298.

Mackenzie A. S. (1984) Application of biological markers in petroleum geochemistry. In: *Advances in Petroleum Geochemistry, Vol. 1* (J. Brooks and D. H. Welte, eds.). Academic Press, London, p.115-214.

Mackenzie A. S. and Quigley T. M. (1988) Principles of geochemical prospect appraisal. *American Association of Petroleum Geologists Bulletin* **72**, 399-415.

Mackenzie A. S., Patience R. L., Maxwell J. R., Vandenbroucke M. and Durand B. (1980) Molecular parameters of maturation in the Toarchian shales, Paris Basin, France-I. Changes of the configuration of acyclic isoprenoid alkanes, steranes, and triterpanes. *Geochimica et Cosmochimica Acta* **44**, 1709-1721.

Mackenzie A. S., Lewis C. A. and Maxwell J. R. (1981) Molecular parameters of maturation in the Toarcian shales, Paris Basin, France-IV: Laboratory thermal alteration studies. *Geochimica et Cosmochimica Acta* **45**, 2369-2376.

Mackenzie A. S., Li Ren-Wei, Maxwell J. R., Moldowan J. M. and Seifert W. K. (1983) Molecular measurements of thermal maturation of Cretaceous shales from the Overthrust Belt, Wyoming, USA. In: *Advances in Organic Geochemistry 1981* (M. Bjoroy et al., eds.). J. Wiley and Sons, New York, p.496-503.

Magoon L. B. (1992) Identified petroleum systems within the United States. In: *The Petroleum System-Status of research and methods 1992* (L. B. Magoon, ed.). U.S. Geological Survey Bulletin **2007**, p.2-11.

Magoon L. B. and Dow W. G. (1994) The Petroleum System. In: *The Petroleum Systems-From Source to Trap* (L. B. Magoon and W. G. Dow, eds.). AAPG Memoir 60, p.3-24.

Mallett C. W., Hammond R. L. and Sullivan T. D. (1988) The implications for the Sydney Basin of upper crustal extension in the Bowen Basin. In: *Proceedings of the 22nd Newcastle symposium on advances in the study of the Sydney Basin.* Department of Geology, University of Newcastle, p.1-8.

Mallett C. W., Russell N. and McLennan T. (1990) Thermal history of the Bowen Basin. *Proceedings of the Bowen Basin Symposium, Mackay, 1990.* Geological Society of Australia, Queensland Division, p.15-20.

Marshallsea S. J. (1988) The thermal history of the Bowen Basin (Qld)-An apatite fission track study. Unpublished Ph.D. Thesis, University of Melbourne.

Matchette-Downes C. J., Fallick A. E., Karmajaya. and Rowland S. (1994) A maturity and palaeoenvironmental assessment of condensates and oils from the North Sumatra Basin, Indonesia. In: *Coal and coal-bearing strata as oil-prone source rocks?* (A. C. Scott and A. J. Fleet, eds.). Geological Society Special Publication No. 77, p.139-148.

Maxwell J. R., Cox R. E., Eglinton G., Pillinger C. T., Ackman R. G. and Hooper S. N. (1973) Stereochemical studies of acyclic isoprenoid compounds-II: The role of chlorophyll in the derivation of isoprenoid-type acids in a lacustrine sediment. *Geochimica Cosmochimica Acta* **37**, 297-313.

McKenzie D. P. (1978) Some remarks on the development of sedimentary basins. *Earth and Planetary Sciences Letters* **40**, 25-32.

McKirdy D. M. (1984) Geochemical correlation of crude oils: Surat/Bowen Basin, Queensland. Amdel Report F6657/85 for BHP Petroleum Pty. Ltd, Bridge Oil Ltd., Hartogen Energy Ltd., and Moonie Oil Company Ltd. 13p.

McKirdy D. M. and Powell T. G. (1974) Metamorphic alteration of carbon isotopic composition in ancient sedimentary organic matter: New evidence from Australia and South Africa. *Geology* **2**, 591-595.

McKirdy D. M., Aldridge A. K. and Ypma P. J. M. (1983) A geochemical comparison of some crude oils from Pre-Ordovician carbonate rocks. In: *Advances in Organic Geochemistry 1981* (M. Bjoroy et al., eds.). J. Wiley and Sons, New York, p.99-107.

McKirdy D. M., Kantsler A. J., Emmett J. K. and Aldridge A. K. (1984) Hydrocarbon genesis and organic facies in Cambrian carbonates of the Eastern Officer Basin, South Australia. In: *Petroleum Geochemistry and Source Rock Potential of Carbonate Rocks* (J. G. Palacas, ed.). AAPG Studies in Geology #18, p.13-31.

McKirdy D. M., Emmett J. K., Mooney B. A., Cox R. E. and Watson B. L. (1986) Organic geochemical facies of the Cretaceous Bulldog Shale, western Eromanga Basin, South Australia. In: *Contributions to the geology and hydrocarbon potential of the Eromanga Basin* (D. I. Gravestock et al., eds.). Geological Society of Australia Special Publication No. 12, p.287-304.

Mello M. R. Koutsoukos E. A. M., Hart M. B., Brassell S. C. and Maxwell J. R. (1990) Late Cretaceous anoxic events in the Brazilian continental margin. *Organic Geochemistry* **14**, 529-542.

Metzger P., Largeau C. and Casadevall E. (1991) Lipids and macromolecular lipids of the hydrocarbon-rich microalga *Botryococcus braunii*: Chemical structure and biosynthesis-Geochemical and biotechnological importance. In: *Progress in the Chemistry of Organic Natural Products* (W. Herz et al., eds.). Springer Verlag, New York, p.1-70.

Middleton M. F. (1982) Tectonic history from vitrinite reflectance. *Geophysical Journal of the Royal Astronomical Society* **68**, 121-132.

Middleton M. F. (1983) Coal rank trends in East Australian coal basins. CSIRO Division of Fossil Fuels, Institute of Energy and Earth Resources, Investigation Report 141, p.1-26.

Middleton M. F. and Hunt J. W. (1989) Influence of tectonics on Permian coal-rank patterns in Australia. *International Journal of coal Geology* **13**, 391-411.

Moldowan J. M., Seifert W. K. and Gallegos E. L. (1983) Identification of an extended series of tricyclic terpanes in petroleum. *Geochimica et Cosmochimica Acta* **47**, 1531-1534.

Moldowan J. M., Seifert W. K., Arnold E. and Clardy J. (1984) Structure proof and significance of stereoisomeric 28,30-bisnorhopanes in petroleum and petroleum source rocks. *Geochimica et Cosmochimica Acta* **48**, 1651-1661.

Moldowan J. M., Seifert W. K. and Gallegos E. L. (1985) Relationship between petroleum composition and depositional environment of petroleum source rocks. *American Association of Petroleum Geologists Bulletin* **69**, 1255-1268.

Moldowan J. M., Sundararaman P. and Schoell M. (1986) Sensitivity of biomarker properties to depositional environment and/or source input in the Lower Toarchian of S.W. Germany. *Organic Geochemistry* **10**, 915-926.

Moldowan J. M., Fago F. J., Carlson R. M. K., Young D. C., Duyne G. V., Clardy J., Schoell M., Pillinger C. T. and Watt D. S. (1991) Rearranged hopanes in sediments and petroleum. *Geochimica et Cosmochimica Acta* **55**, 3333-3353.

Moldowan J. M., Sundararaman P., Salvatori T., Alajbeg A. Gjukic B., Lee C. Y. and Demaison G. J. (1992) Source correlation and maturity assessment of selected oils and rocks from the Central Adriatic Basin (Italy and Yugoslavia). In: *Biological Markers in Sediments and Petroleum* (J. M. Moldowan et al., eds.). Prentice Hall, Englewood Cliffs, N. J., p.370-401.

Moran W. R. and Gussow W. C. (1963) The history of the discovery and geology of the Moonie oil field, Queensland, Australia. In: *Proceedings of the 6th World Petroleum Conference 1*, p.595-609.

Mukhopadhyay P. K. Hatcher P. G. (1994) Composition of Coal. In: *Hydrocarbons from Coal* (B. E. Law and D. D. Rice, eds). AAPG Studies in Geology #38, p.79-118.

Mukhopadhyay P. K., Hagemann H. W. and Gormly J. R. (1985) Characterization of kerogens as seen under the aspect of maturation and hydrocarbon generation. *Erdol und Kohle-Erdgas-Petrochemie* **38**(1), 7-18.

Mukhopadhyay P. K. Hatcher P. G. and Calder J. H. (1991) Hydrocarbon generation from deltaic and intermontane fluviodeltaic coal and coaly shale from the Tertiary of Texas and Carboniferous of Nova Scotia. *Organic Geochemistry* **17**, 765-784.

Murray C. G. (1985) Tectonic setting of the Bowen Basin. In: *Bowen Basin Coal Symposium.* Geological Society of Australia, Abstract No. 17, p.5-16.

Murray C. G. (1990) Tectonic evolution and metalogenesis of the Bowen Basin. In: *Proceedings of the Bowen Basin Symposium, Mackay, 1990.* Geological Society of Australia, Queensland Division, p.201-212.

Nip M., Tegalaar E. W., Brinkhuis H., de Leeuw J. W., Schenck P. A. and Holloway P. J. (1986) Analysis of recent and fossil plant cuticles by Curie point pyrolysis gas chromatography-mass spectrometry: recognition of a new, highly aliphatic and resistant biopolymer. *Organic Geochemistry* **10**, 769-788.

Nip M., de Leeuw J. W., Schenck P. A., Winding W., Meuzelaar H. L. C. and Crelling J. C. (1989) A flash pyrolysis and petrographic study of cutinite from the Indiana paper coal. *Geochimica et Cosmochimica Acta* **53**, 671-683.

Noble R, Knox J., Alexander R. and Kagi R. (1985a) Identifications of tetracyclic diterpanes hydrocarbons in Australian crude oils and sediments. *Journal of the Chemical Society Chemical Communications*, 32-33.

Noble R. A., Alexander R., Kagi. I. and Knox J. (1985b) Tetracyclic diterpenoid hydrocarbons in some Australian coals, sediments and crude oils. *Geochimica et Cosmochimica Acta* **49**, 2141-2147.

Noble R. A., Alexander R. and Kagi. I. (1985c) The occurrence of bisnorhopane, trisnorhopane, and 25-norhopanes as free hydrocarbons in some Australian shales. *Organic Geochemistry* **8**, 171-176.

Noble R. A., Alexander R., Kagi. I. and Knox J. (1986) Identification of some diterpenoid hydrocarbons in petroleum. *Organic Geochemistry* **10**, 825-829.

Orr W. L. (1986) Kerogen/asphaltene/sulfur relationships in sulfur-rich Monterey oils. *American Association of Petroleum Geologists Bulletin* **58**, 2295-2318.

Ottenjann K. (1988) Fluorescence alteration and its value for the studies of maturation and bituminization. *Organic Geochem*istry **12**(4), 309-322.

Ourisson G. Albrecht P. and Rohmer M. (1982) Predictive microbial biochemistry, from molecular fossils to prokaryotic membranes. *Trends in Biochemical Sciences* **7**, 236-239.

Padley D. Michaelsen B. H. and McKirdy D. M. (1991) *Organic geochemical procedures: A protocol of preparative geochemistry.* Organic Geochemistry Laboratory. Dpartment of Geology and Geophysics, The University of Adelaide, 24p.

Palacas J. G., Anders D. E. and King J. D. (1984) South Florida Basin-A prime example of carbonate source rocks in petroleum. In: *Petroleum Geochemistry and Source Rock Potential of Carbonate Rocks* (J. G. Palacas, ed.). AAPG Studies in Geology #18, p.71-96.

Palmer S. E. (1984) Hydrocarbon source potential of organic facies of the lacustrine Elko Formation (Eocene/Oligocene), Northeast Nevada. In: *Hydrocarbon Source Rocks of the Greater Rocky Mountain Region* (J. Woodward et al., eds.). Rocky Mountain Association of Geologists, Denver, p.491-511.

Palmer S. E. (1993) Effects of biodegradation and water washing on crude oil composition. In: *Organic Geochemistry: Principles and Applications* (M. H. Engel and S. A. Macko, eds.). Plenum Press, New York, p.511-533.

Peters K. E. (1986) Guidelines for evaluating petroleum source rocks using programmed pyrolysis. *American Association of Petroleum Geologists Bulletin* **70**, 318-329.

Peters K. E. and Moldowan J. M. (1991) Effects of source, thermal maturity, and biodegradation on the distribution and isomerization of homohopanes in petroleum. *Organic Geochemistry* **17**, 47-61.

Peters K. E. and Moldowan J. M. (1993) *The Biomarker Guide: Interpreting Molecular Fossils in Petroleum and Ancient Sediments.* Prentice Hall, Englewood Cliffs, N. J., 363p.

Peters K. E., Rohrback B. G. and Kaplan I. R. (1981) Geochemistry of artificially heated humic and sapropelic sediments-I: Protokerogen. *American Association of Petroleum Geologists Bulletin* **67**(II), 2137-2146.

Peters K. E., Moldowan J. M., Driscole A. R. and Demaison G. J. (1989) Origin of Beatrice oil by co-sourcing from Devonian and Middle Jurassic source rocks, Inner Moray Firth, U.K.. *American Association of Petroleum Geologists Bulletin* **73**, 454-471.

Peters K. E., Moldown J. M. and Sundararaman P. (1990) Effects of hydrous pyrolysis on biomarker thermal maturity parameters: Monterey Phosphatic and Siliceous members. *Organic Geochemistry* **15**(3), 249-265.

Philp R.P. (1985) *Fossil Fuel Biomarkers.* Methods in Geochemistry and Geophysics 23. Elsevier, New York, 294p.

Philp R. P. (1994) Geochemical characterstics of oils derived predominantly from terrigenous source materials. In: *Coal and coal-bearing strata as oil-prone source rocks?* (A. C. Scott and A. J. Fleet, eds.). Geological Society Special Publication No. 77, p.71-91.

Philp R.P. and Gilbert T. D. (1985) Source rock and asphaltene biomarker characterization by pyrolysis-gas chromatography-mass spectrometry-multiple ion detection. *Geochimica Cosmochimica Acta* **49**, 1421-1432.

Philp R. P. and Gilbert T.D. (1986) A geochemical investigation of oils and source rocks from the Surat Basin. *Australian Petroleum Exploration Asssociation Journal* **26**, 172-186.

Philp R. P., Gilbert T. D. and Friedrich J. (1982) Geochemical correlation of Australian crude oils. *Australian Petroleum Exploration Asssociation Journal* **22**(1), 188-199.

Philp R. P., Simoneit B. R. T. and Gilbert T.D. (1983) Diterpenoids in crude oils and coals of South Eastern Australia. In: *Advances in Organic Geochemistry 1981* (M. Bjoroy et al., eds.). J. Wiley and Sons, New York, p.698-704.

Philp R. P., Li Jinggui, and Lewis C. A. (1989) An organic geochemical investigation of crude oils from Shanganning, Jianghan, Chaidamu and Zhungeer Basins, People's Republic of China. *Organic Geochemistry* **14**, 447-460.

Philp R. P., Suzuki N. and Galvez-Sinibaldi (1992) Early-stage incorporation of sulfur into protokerogens and possible kerogen precursors. In: *Organic Matter: Productivity, Accumulation, and Preservation in Recent and Ancient Sediments* (J. K. Whelan and J. W. Farrington, eds.). Columbia University Press, New York, p.264-282.

Powell T. G. (1986) Petroleum geochemistry and depositional setting of lacustrine source rocks. *Marine and Petroleum Geology* **3**, 200-220.

Powell T. G. and Boreham C. J. (1991) Petroleum generation and source rock assessment in terrigenous sequences: an update. *Australian Petroleum Exploration Association Journal* **31**, 297-311.

Powell T. G. and Boreham C. J. (1994) Terrestrially sourced oils: where do they exist and what are our limits of knowledge?- a geochemical perspective. In: *Coal and coal-bearing strata as oil-prone source rocks?* (A. C. Scott and A. J. Fleet eds.). Geological Society Special Publication No. 77, p.11-29.

Powell T. G. and McKirdy D. M. (1973a) The effect of source material, rock type and diagenesis on the *n*-alkane content of sediments. *Geochimica et Cosmochimica Acta* **37**, 623-633.

Powell T. G. and McKirdy D. M. (1973b) Relationship between ratio of pristane to phytane, crude oil composition and geological environment in Australia. *Nature* **243**, 37-39.

Powell T. G., Foscolos A. E., Gunther P. R. and Snowdon L. R. (1978) Diagenesis of organic matter and fine clay minerals: a comparative study. *Geochimica et Cosmochimica Acta* **42**, 1181-1197.

Powell T. G., Boreham C. J., Smyth M., Russell N. and Cook A. C. (1991) Petroleum source rock assessment in non-marine sequences: pyrolysis and petrographic analysis of Australian coals and carbonaceous shales. *Organic Geochemistry* **17**, 375-394.

Power P. E. and Devine S. B. (1970) Surat Basin, Australia- subsurface stratigraphy, history and petroleum. *American Association of Petroleum Geologists Bulletin* **54**(12), 2410-2437.

Pramono H., Wu C. H. and Noble R. A. (1990) A new oil kitchen and petroleum bearing subbasin in the offshore Northwest Java Basin. In: *Proceedings of the Indonesian Petroleum Association, Nineteenth Annual Convention.* Indonesian Petroleum Association, Jakarta, p.253-278.

Price P. L., O'Sullivan T. and Alexander R. (1987) The nature and occurrence of oil in Seram, Indonesia. In: *Proceedings of the Indonesian Petroleum Association. Sixteenth Annual Convention, Vol. 1.* Indonesian Petroleum Association, Jakarta, p.141-173.

Radke M. (1987) Organic geochemistry of aromatic hydrocarbons. In *Advances in Petroleum Geochemistry, Vol. 2* (J. Brooks and D. Welte, eds.). Academic Press, New York, p.141-207.

Radke M. and Welte D. H. (1983) The Methylphenanthrene Index (MPI): A maturity parameters based on aromatic hydrocarbons. In: *Advances in Organic Geochemistry 1981* (M. Bjoroy et al., eds.). J. Wiley and Sons, Chichester, p.504-512.

Radke M., Schaefer R. G., Leythaeuser D. and Teichmuller M. (1980) Composition of soluble organic matter in coals: relation to rank and liptinite fluorescence. *Geochimica et Cosmochimica Acta* **44**, 1787-1800.

Radke M., Welte D. H. and Willsch H. (1982) Geochemical study on a well in the Western Canada Basin: Relation of the aromatic distribution pattern to maturity of organic matter. *Geochimica et Cosmochimica Acta* **46**, 1-10.

Radke M., Welte D. H. and Willsch H. (1986) Maturity parameters based on aromatic hydrocarbons: Influence of the organic matter type. *Organic Geochemistry* **10**, 51-63.

Raederstorff D. and Rohmer M. (1984) Sterols of the unicellular algae *Nematochrysopsis roscoffensis* and *Chrysotila lamellosa*: Isolation of (24E)-24-*n*-propylidenecholesterol and 24-*n*-propylcholesterol. *Phytochemistry* **23**, 2835-2838.

Rashid M. A. (1979) Pristane-phytane ratios in relation to source and diagenesis of ancient sediments from the Labrador Shelf. *Chemical Geology* **25**, 109-122.

Raza A., Hill K. C. and Korsch R. J. (1995) Mid-Cretaceous regional uplift and denudation of the Bowen-Surat Basins, Queensland and its relation to Tasman Sea rifting. In: *Proceedings of the Bowen Basin Symposium 1995* (I.W. Follington et al., eds.). Geological Society of Australia, Coal Geology Group, Brisbane, p.1-8.

Robinson N., Eglinton G., Brassell S. C. and Cranwell P. A. (1984) Dinoflagellate origin for sedimentary 4-methyl steroids and 5α(H) stanols. *Nature* **308**, 439-441.

Rubinstein I., Sieskind O. and Albrecht P. (1975) Rearranged steranes in a shale: Occurrence and simulated formation. *Journal of the Chemical Society, Perkin Transaction* **1**, 1833-1836.

Rullkotter J. and Marzi R. (1988) Natural and artificial maturation of biological markers in a Toarcian shale from northern Germany. *Organic Geochemistry* **13**, 639-645.

Rullkotter J., Meyers P. A., Schaefer R. G. and Dunham K. W. (1986) Oil generation in the Michigan Basin: A biological marker carbon and isotope approach. *Organic Geochemistry* **10**, 359-375.

Scalan R. S. and Smith J. E. (1970) An improved measure of the odd-even predominance in the normal alkanes of sediment extracts and petroleum. *Geochimica et Cosmochimica Acta* **34**, 611-620.

Schoell M. (1984) Stable isotopes in petroleum research. In: *Advances in Petroleum Geochemistry, Vol. 1* (J. Brooks and D. H. Welte, eds.). Academic Press, London, p.215-245.

Schoell M., Teschner M., Wehner H., Durand B. and Oudin J. L. (1983) Maturity related biomarker and stable isotope variations and their application to oil/source rock correlation in the Mahakam Delat, Kalimantan. In: *Advances in Organic Geochemistry 1981* (M. Bjoroy et al., eds.). J. Wiley and Sons, New York, p.156-163.

Schoell M., McCaffrey M. A., Fago F. J. and Moldowan J. M. (1992) Carbon isotopic compositions of 28,30-bisnorhopanes and other biological markers in a Monterey crude oil. *Geochimica et Cosmochimica Acta* **56**, 1391-1399.

Schulze T. and Michaelis W. (1990) Structure and origin of terpenoid hydrocarbons in some German coals. *Organic Geochemistry* **16**, 1051-1058.

Seifert W. K. (1978) Steranes and terpanes in kerogen pyrolysis for correlation of oils and source rocks.*Geochimica et Cosmochimica Acta* **42**, 473-484.

Seifert W. K. and Moldowan J. M. (1978) Applications of steranes, terpanes, and monoaromatics to the maturation, migration, and source of crude oils. *Geochimica et Cosmochimica Acta* **42**, 77-95.

Seifert W. K. and Moldowan J. M. (1979) The effect of biodegradation on steranes and terpanes in crude oils. *Geochimica et Cosmochimica Acta* **43**, 111-126.

Seifert W. K. and Moldowan J. M. (1980) The effect of thermal stress on source-rock quality as measured by hopane stereochemistry. *Physics and Chemistry of the Earth* **12**, 229-237.

Seifert W. K. and Moldowan J. M. (1981) Paleoreconstruction by biological markers. *Geochimica et Cosmochimica Acta* **45**, 783-794.

Seifert W. K. and Moldowan J. M. (1986) Use of biological markers in petroleum exploration. In: *Methods in Geochemistry and Geophysics 24* (R. B. Johns, ed.), p.261-290.

Seifert W. K., Moldowan J. M. and Jones R. W. (1980) Application of biological marker chemistry to petroleum exploration.In: *Proceedings of the Tenth World Petroleum Congress*, Bucharest, Romania. Sep. 1979. Paper SP8, Heyden, p.425-440.

Sentfle J. T., Larter S. R., Bromley B. W. and Brown J. H. (1986) Quantitative chemical characterisation of vitrinite concentrates using pyrolysis-gas chromatography: Rank variation of pyrolysis products. *Organic Geochemistry* **9**, 35-350.

Shiboaka M. (1978) Micrinite and exsudatinite in some Australian coals and their relation to the generation of petroleum. *Fuel* **57**, 73-77.

Shiboaka M. (1983) Genesis of micrinite in some Australian coals. *Fuel* **62**, 639-644.

Shiboaka M. and Bennett A. J. R. (1976) Effect of depth of burial and tectonic activity on coalification. *Nature* **259**, 385-386.

Simoneit B. R. T. (1986) Cyclic terpenoids of the geosphere. In: *Biological Markers in the Sedimentary Record* (R. B. Johns, ed.). Elsevier, New York, p.43-99.

Simoneit, B. R. T., Peters, K. E. and Kaplan, I. R. (1981) Thermal alteration of Cretaceous black shale by diabase intrusions in the Eastern Atlantic. II. Effects on bitumen and kerogen. *Geochimica et Cosmochimica Acta* **45**, 1581-1602.

Simoneit B. R. T., Grimalt J. O. Wang T. J. Cox R. E., Hatcher P. G. and Nissenbaum A. (1986) Cyclic terpenoids of contemorary resinous plant detritus and of fossil woods, ambers and coals. *Organic Geochemistry* **10**, 877-889.

Smyth M. (1988) Organic petrology of the Triassic Snake Creek Member in ATP 145P, Surat Basin, Queensland. A progress report for Bridge Oil limited, 18p.

Smyth M. and Mastalerz M. (1991) Organic petrological composition of Triassic source rocks and their clastic depositional environments in some Australian sedimentary basins. *International Journal of Coal Geology* **18**, 165-186.

Snowdon L. R. (1980) Resinite-a potential source rock in the Upper Cretaceous/Tertiary of Beaufort-Mackenzie Basin. *Canadian Society of Petroleum Geologists Memoir* **6**, 421-446.

Snowdon L. R. (1991) Oil from Type III organic matter: resinite revisited. *Organic Geochemistry* **17**, 743-747.

Snowdon L. R. and Powell T. G. (1982) Immature oil and condensate-modification of hydrocarbon generation model for terrestrial organic matter. *American Association of Petroleum Geologists Bulletin* **66**, 775-788.

Sofer Z. (1984) Stable carbon isotope composition of crude oils: application to source depositional environment and petroleum alteration. *American Association of Petroleum Geologists Bulletin* **68**, 31-49.

Sofer Z. (1991) Stable isotopes in petroleum exploration. In: *Source and Migration Processes and Evaluation Techniques* (R.K. Merrill, ed.). AAPG Treatise of Petroleum Geology, p.103-106.

Stach E., Mackows M. Th., Teichmuller M., Taylor G. H., Ghandra D. and Teichmuller R. (1982) *Stach's Textbook of Coal Petrology*, 3rd ed., Gebruder Borntraeger, Berlin, 546p.

Strachan M. G., Alexander R., Subroto E. A. and Kagi R. I. (1989) Source and heating rate effects on the C-20 epimerization of 24-ethylcholestane. *Organic Geochemistry* **14**, 423-432.

Standards Association of Australia (1986) Coal maceral analysis. Australian Standard AS2856.

Subroto E., Alexander R. and Kagi R. (1991) 30-Norhopanes: their occurrence in sediments and crude oils. *Chemical Geology* **93**, 179-192.

Summons R. E. and Capon R. J. (1988) Fossil steranes with unprecedented methylation in ring A. *Geochimica et Cosmochimica Acta* **52**, 2733-2736.

Summons R. E. and Capon R. J. (1991) Identification and significance of 3β-ethyl steranes in sediments and petroleum. *Geochimica et Cosmochimica Acta* **55**, 2391-2395.

Summons R. E. and Jahnke L. L. (1992) Hopenes and hopanes methylated in ring A: Correlation of the hopanoids from extant methylotrophic bacteria with their fossil analogues. In: *Biological Markers in Sediments and Petroleum* (J. M. Moldowan et al., eds.). Prentice Hall, Englewood Cliffs, N. J., p.182-194.

Summons R. E. and Walter M. R. (1990) Molecular fossils and microfossils of prokaryotes and protists from Proterozoic sediments. *American Journal of Science* **290**(A), 212-244.

Summons R. E., Volkman J. K. and Boreham C. J. (1987) Dinosterane and other steroidal hydrocarbons of dinoflagellate origin in sediments and petroleum. *Geochimica Cosmochimica Acta* **51**, 3075-3082.

Summons R. E., Brassell S. C., Eglinton G., Evans E., Horodyski R. J., Robinson N. and Ward D. M. (1988a) Distinctive hydrocarbon biomarkers from fossiliferous sediment of the Late Proterozoic Walcott Member, Chaur Group, Grand Canyon, Arizona. *Geochimica et Cosmochimica Acta* **52**, 2625-2637.

Summons R. E., Powell T. G. and Boreham C. J. (1988b) Petroleum geology and geochemistry of the Middle Proterozoic McArthur Basin, Northern Australia: III. Composition of extractable hydrocarbons. *Geochimica et Cosmochimica Acta* **52**, 1747-1763.

Summons R. E., Boreham C. J., Foster C. B., Murray A. P. and Gorter J. D. (1995) Chemostratigraphy and the composition of oils in the Perth Basin, Western Australia. *Australian Petroleum Exploration Association Journal* **35**(1), 613-632.

Sundararaman P., Biggs W. R., Reynolds J. G. and Fetzer J. C. (1988) Vanadylporphyrins, indicators of kerogen breakdown and generation of petroleum. *Geochimica et Cosmochimica Acta* **52**, 2337-2341.

Sweeney J. J.and Burnham A. K. (1990) Evaluation of a simple model of vitrinite reflectance based on chemical kinetics. *American Association of Petroleum Geologists Bulletin* **74**, 1559-1570.

Tannenbaum E., Ruth E. and Kaplan I. R. (1986a) Steranes and triterpanes generated from kerogen pyrolysis in the absence and presence of minerals. *Geochimica et Cosmochimica Acta* **50**, 805-812.

Tannenbaum E., Ruth E., Huizinga B. J. and Kaplan I. R. (1986b) Biological marker distribution in coexisting kerogen, bitumen and asphaltenes in Monterey Formation diatomite, California. *Organic Geochemistry* **10**, 531-536.

Tappan H. N. (1980) *The paleobiology of Plant Protists*. W. H. Freeman and Company, San Francisco, 1028p.

Taylor G., Liu S. Y. and Smyth M. (1988) New light on the origin of Cooper Basin oil. *Australian Petroleum Exploration Association Journal* **28**(1), 303-309.

Teerman S. C., Creeling J. C. and Glass G. B. (1987) Fluorescence spectral analysis of resinite macerals from coals of the Hanna Formation, Wyoming, USA. *International Journal of Coal Geology* **7**, 315-334.

Teichmuller M. and Durand B. (1983) Fluorescence microscopical rank studies on liptinites and vitrinites in peat and coals, and comparison with results of Rock-Eval pyrolysis. *International Journal of Coal Geology* **2**, 197-230.

Tissot B. P. and Welte D. H. (1984) *Petroleum Formation and Occurrence*, 2nd ed., Springer-Verlag, Berlin, 699p.

Tissot B. P., Pelet R. and Ungerer Ph. (1987) Thermal history of sedimentary basins, maturation indices, and kinetics of oil and gas generation. *American Association of Petroleum Geologists Bulletin* **71**, 1445-1466.

Thomas B. R. (1969) Kauri resins - modern and fossils. In: *Organic Geochemistry-Methods and Results* (G. Eglinton and M. T. J. Murphy, eds.). Springer-Verlag, Berlin, p.599-618.

Thomas B. M., Osborne D. G. and Wright A. J. (1982) Hydrocarbon habitat of the Bowen/Surat Basin. *Australian Petroleum Exploration Association Journal* **22**, 213-226.

Thomas J. B., Mann A. L., Brassell S. C. and Maxwell J. R. (1989) 4-Methyl steranes in Triassic sediments: Molecular evidence for the earliest dinoflagellates. In: *14th International Meeting on Organic Geochemistry*, Paris, Sept. 18-22, 1989, Abstract No. 177.

Thomas J. B., Marshall J., Mann A.L., Summons R.E. and Maxwell J. R. (1993) Dinosteranes (4,23,24-trimethylsteranes) and other biological markers in dinoflagellate-rich marine sediments of Rhaetian age. *Organic Geochemistry* **20**(1), 91-104.

Totterdell J. M., Wells A. T., Brakel A. T., Korsch R. J. and Nicoll M. G. (1992) Sequence stratigraphic interpretation of seismic data in the Taroom region, Bowen and Surat Basins, Queensland. Bureau of Mineral Resources, Australia. Record 1991/102, 61p.

Traves D. M. (1965) Petroleum in the Roma-Springsure area. In: *Proceedings of the 8th Commonwealth Mining and Metallurgy Congress* **5**, p.147-156.

Ungerer P. (1990) State of the art of research in kinetic modelling of oil formation and expulsion. *Organic Geochemistry* **16**, 1-25.

Ungerer P. (1993) Modelling of petroleum generation and expulsion-an update to recent reviews. In: *Basin Modelling: Advances and Applications* (A. G. Dore et al., eds.). Elsevier, Amsterdam, p.219-232.

Ungerer P. and Pelet R. (1987) Extrapolation of the kinetics of oil and gas formation from laboratory experiments to sedimentary basins. *Nature* **327**(6117), 52-54.

Ungerer P. Espitalie J. Marquis F. and Durand B. (1986) Use of kinetic models of organic matter evolution for the reconstruction of paleotemperatures: Application to the Gironville Well (France). In: *Thermal Modelling in*

Sedimentary Basins. Proc. 1st IFP Res. Conf., Carcans, June 1985. Technip, Paris, p.531-546.

Ungerer P. Behar F., Villalba M., Heum. O. R. and Audibert A. (1988) Kinetic modelling of oil cracking. *Organic Geochemistry* **13**, 857-868.

Valisolalao J. N., Perakis N., Chappe B. and Albrecht P. (1984) A novel sulfur containing C_{35} hopanoid in sediments. *Tetrahedron Letters* **25**, 1183-1186.

Vandenbroucke M., Albrecht P. and Durand B. (1976) Geochemical studies on organic matter from Douala Basin (Cameroon)-III: Comparison with the Early Toarchian shales, Paris Basin, France. *Geochimica et Cosmochimica Acta* **40**, 1241-1249.

Van Dorsselaer A., Albrecht P. and Ourisson G. (1977) Identification of novel 17α(H)-hopanes in shales, coals, lignites, sediments, and petroleum. *Bulletin de la Societe Chimique de France No. 1-2*, 165-170.

van Krevelen D. W. (1961) *Coal*. Elsevier, New York, 514p.

Vincent P. W., Mortimore I. R. and McKirdy D. M. (1985) Hydrocarbon generation, migration and entrapment in the Jackson-Naccowlah area, ATP 256P, southwestern Queensland. *Australian Exploration Association Journal* **25**(1), 62-84.

Volkman J. K. (1986) A review of sterol markers for marine and terrigenous organic matter. *Organic Geochemistry* **9**, 83-89.

Volkman J. K. (1988) Biological marker compounds as indicators of the depositional environments of petroleum source rocks. In: *Lacustrine Petroleum Source Rocks* (A. J. Fleet et al., eds.). Geological Society Special Publication No. 40, p.103-122.

Volkman J. K., Gillan F. T., Johns R. B. and Eglinton G. (1981) Sources of neutral lipids in a temperate intertidal sediment. *Geochimica et Cosmochimica Acta* **45**, 1817-1828.

Volkman J. K., Alexander R., Kagi R. I. and Woodhouse G. W. (1983a) Demethylated hopanes in crude oils and their application in petroleum geochemistry. *Geochimica et Cosmochimica Acta* **47**, 785-794.

Volkman J. K., Alexander R., Kagi R. I., Noble R. A. and Woodhouse G. W. (1983b) A geochemical reconstruction of oil generation in the Barrow Sub-basin of Western Australia. *Geochimica et Cosmochimica Acta* **47**, 2091-2106.

Volkman J. K., Farrington J. W. and Gagosian R. B. (1987) Marine and terrigenous lipids in coastal sediments from the Peru upwelling region at 15°S: Sterols and triterpane alcohols. *Organic Geochemistry* **11**, 463-477.

Volkman J. K., Banks M. R., Denwer K. and Aquino Neto F. R. (1989) Biomarker composition and depositional setting of Tasmanite oil shale from northern

Tasmania, Australia. In: *14th International Meeting on Organic Geochemistry*, Paris, Sept. 1989, Abstract No. 168.

Volkman J. K., Kearney P. and Jeffrey S. W. (1990) A new source of 4-methyl and 5α(H)-stanols in sediments: prymnesiophyte microalgae of the genus *Pavlova*. *Organic Geochemistry* **15**, 489-497.

Wake-Dyster K. D., Sexton M. J., Hohnstone D. W., Wright C. and Finlayson D. M. (1987) A deep seismic profile of 800 km length recorded in southern Queenslaand, Australia. *Geophysical Journal of the Royal Astronomical Society* **89**, 423-430.

Wang T. G. and Simoneit B. R. T. (1990) Organic geochemistry and coal petrology of Tertiary brown coal in the Zhoujing mine, Baise Basin, South China. 2. Biomarker assemblage and significance. *Fuel* **69**, 12-20.

Waples D. W. (1994) Maturity modelling: Thermal Indicators, Hydrocarbon Generation, and Oil Cracking. In: *The Petroleum Systems-From Source to Trap* (L. B. Magoon and W. G. Dow, eds.). AAPG Memoir 60, p.285-306.

Welte D. H. and Waples D. (1973) Uber die Bevorzugung geradzahliger *n*-alkane in sedimentagesteinen. *Natuwissenschaften* **6**, 516-517.

West N., Alexander R. and Kagi R. I. (1990) The use of silicalite for rapid isolation of branched and cyclic alkane fractions of petroleum. *Organic Geochemistry* **15**, 499-501.

Williams L. A. (1984) Subtidal stromatolites in Monterey Formation and other organic-rich rocks as suggested contributors to petroleum formation. *American Association of Petroleum Geologists Bulletin* **68**, 1879-1893.

Winters J. C., Williams J. A. and Lewan M. D. (1983) A laboratory study of petroleum generation by hydrous pyrolysis. In: *Advances in Organic Geochemistry 1981* (M. Bjoroy et al., eds.). J. Wiley and Sons, Chichester, p.524-533.

Withers N. (1983) Dinoflagellate sterols. In: *Marine Natural Products 5* (P. J. Scheuer, ed.). Academic Press, p.87-130.

Wolff G. A., Lamb N. A. and Maxwell J. R. (1986) The origin and fate of 4-methyl steroid hydrocarbons-I: 4-methyl steranes. *Geochimica et Cosmochimica Acta* **50**, 335-342.

Yang Wanli, Li Yong Kang and Gao Ruigi (1985) Formation and evolution of non-marine petroleum in Songliao Basin, China. *American Association of Petroleum Geologists Bulletin* **69**, 1112-1122.

Youngblood W. H. and Blumer M. (1973) Alkanes and alkenes in marine benthonic algae. *Marine Biology* **21**, 163-172.

Zhao-An and Philp R. P. (1987) Laboratory biomarker fractionations and implications for migration studies. *Organic Geochemistry* **11**, 169-175.

Zhao K. and Lerche I. (1993) Thermal maturation and burial history of the Multiwell Experiment Site, Piceance Basin, Colorado: application of thermal indicator tomography. In: *Basin Modelling: Advances and Applications* (A. G. Dore et al., eds.). Elsevier, Amsterdam, p.135-145.

Zumberge J. E. (1983) Tricyclic diterpane distributions in the correlation of Paleozoic crude oils from the Williston Basin. In: *Advances in Organic Geochemistry 1981* (M. Bjoroy et al., eds.). J. Wiley and Sons, New York, p.738-745.

Zumberge J. E. (1984) Source rocks of the La Luna (Upper Cretaceous) in the Middle Magdalena Valley, Colombia. In: *Petroleum Geochemistry and Source Rock Potential of Carbonate Rocks* (J. G. Palacas, ed.). AAPG Studies in Geology #18, p.127-133.